Journal of Applied Mechanics

(Contributions of the ASME Applied Mechanics Division)

Dynamic Stresses in Aircraft Landing . . . . . *Y. C. Fung* 449
Large Deflection Analysis for Combined Pressure and Heating . . . . . *M. L. Williams* 458
A New Approach to the Analysis of Large Deflections of Plates . . . . . *H. M. Berger* 465
Elastic-Stress Waves Produced by Pressure Loads on a Spherical Shell . *J. H. Huth and J. D. Cole* 473
A Study of the Speed of Sound in Porous Granular Media . . . . . *H. Brandt* 479
Linear Systems With Nonlinear Dynamic Vibration Absorbers . . . . . *F. R. Arnold* 487
Oscillations With Quadratic Damping Forces . . . . . *Karl Klotter* 493
Perturbation Methods Applied to Nonlinear Dynamics . . . . . *Richard Bellman* 500
Aerodynamic Interference of Cascade Blades in Synchronized Oscillation . . . . . *Chieh-Chien Chang and Wen-Hwa Chu* 503
A Study of the Stability of Plane Fluid Sheets . . . . . *W. W. Hagerty and J. F. Shea* 509
Integral Methods in Natural-Convection Flow . . . . . *Salomon Levy* 515
Plastic Deformations of a Free Ring Under Concentrated Dynamic Loading . . . . . *R. H. Owens and P. S. Symonds* 523
Torsion of Circular Shafts of Variable Diameter . . . . . *M. M. Abbassi* 530
Large Plastic Deformations of Circular Membranes . . . . . *N. A. Weil and N. M. Newmark* 533
Stress Distribution in Square Plates With Hydrostatically Loaded Central Circular Holes . . . . . *A. J. Durelli and J. Barriage* 539
Force at Point in the Interior of a Semi-Infinite Solid With Fixed Boundary . . . *Leif Rongved* 545
Free Vibrations of Thin Cylindrical Shells . . . . . *Yi-Yuan Yu* 547
Buckling of Laminated Columns . . . . . *L. G. Clark* 553
Thin Circular Conical Shells Under Arbitrary Loads . . . . . *N. J. Hoff* 557
On the Nonlinear Oscillations of Viscoelastic Plates . . . . . *A. C. Eringen* 563
Forced Vibration of a Clamped Rectangular Plate in Fluid Media . . . . . *G. C. K. Yeh and Johann Martinek* 568
Nonlinear Dynamic Coupling in a Beam Vibration . . . . . *P. H. McDonald, Jr.* 573
Some Solutions of the Timoshenko Beam Equations . . . . . *B. A. Boley and C. C. Chao* 579
Influence of Secondary Inertia Terms on Natural Frequencies of Rotating Beams . *J. L. Bogdanoff* 587
Discussion on previously published papers by *M. Kornhauser; A. P. Boresi; J. R. Schmittger; H. Zabrousky; C. F. Kettleborough; I. K. Silverman; T. C. Huang; S. I. Pai; H. T. Johnson; L. W. Hu and J. Marin; W. H. Hoppmann, 2nd; Martin Goland, P. D. Wichersham, and M. A. Dengler; and A. J. Durelli and C. H. Tsao* 592
Book Reviews 612

DECEMBER, 1955

VOL. 22, NO. 4

Transactions of The American Society of Mechanical Engineers

Journal of Applied Mechanics

Papers presented at the Semi-Annual Meetings of the ASME Applied Mechanics Division

EXECUTIVE COMMITTEE OF THE APPLIED MECHANICS DIVISION

[illegible], Secretary

[illegible], W. Prager

[illegible], Technical Editor

[illegible] (1956)

[illegible], Illinois

[illegible] (1956)

[illegible], Washington 25, D. C.

Ship Owner Committee

[illegible], Secretary

Published Quarterly by

The American Society of Mechanical Engineers

Office, Southwest Northampton Streets, Easton, Pa.

Publication Office of the Society, 29 West Thirty-Ninth Street, New York 18, N. Y.

Editorial Department

OFFICERS OF THE SOCIETY

[illegible], W. S. Messenger, President

[illegible], Treasurer

C. E. Davies, Secretary

[illegible], Assistant Treasurer

[illegible], Assistant Secretary

Publication Committee

Gustave A. Stetson, *Editor*

K. W. Czarnecki, *Mgr. Editor*

Statement: The [illegible] opinions advanced in papers or . . . printed in its publications (B13, Par. 4).

Published [illegible] Publication Office, [illegible] Northampton Streets, Easton, Pa. The editorial [illegible] 29 West Thirty-Ninth Street, New York 18, N. Y. [illegible] "Dynamic," New York. Price [illegible] to members [illegible] to all countries outside the United States [illegible] of subscription [illegible] to be effective on the mailing list. [illegible] of address [illegible] appeared in papers or . . . printed in [illegible] Entered as second-class matter [illegible] at the Post Office at Easton, Pa., under the act of August 24, 1912, [illegible] 14, 1925, at the Post Office at Easton, Pa., under the act of August 24, 1912. . . . [illegible] may be made [illegible] on condition that full credit be given [illegible]

The Analysis of Dynamic Stresses in Aircraft Structures During Landing as Nonstationary Random Processes[1]

By Y. C. FUNG,[2] PASADENA, CALIF.

The basic fact is recognized that throughout the service life of an airplane there occurs a variety of landing conditions and, consequently, it is subjected to transient dynamic loads of varied time histories. Accordingly, a statistical analysis is proposed. The landing-gear impact load is regarded as a nonstationary random process. In this paper the ensemble means and the correlation functions of landing impacts are defined and their experimental determination from flight or drop tests is illustrated. From these the mean response (displacement, bending moment, shear, or stress), the root mean square deviation from the mean, and higher statistical moments are computed. The results are used to find the most probable maximum stress (at any point in the structure) attained in a given number of landings, or the most probable total number of landings a given aircraft can withstand. A stress envelope can be derived which represents the distribution of the severest stress in the structure for a large number of landings. A design based on such an envelope, statistically, will have a uniform factor of safety over the entire aircraft with respect to landings.

Nomenclature

The following nomenclature is used in the paper:

$f^{(r)}$ = the rth external force
$h(x, t)$ = response of structure to a unit-impulse forcing function, giving response at a point x at time t after impulse is applied
m = total mass of airplane
m_n = generalized mass in the nth mode
$q_n(t)$ = generalized co-ordinates
q_{n0} = static deflection in nth mode
t, τ = time, sec
y = general notation for response
$u(x, t)$ = displacement (in a specified direction) at a point x at time t
$M(x, t)$ = bending moment at spanwise location x and at time t
$M_n(x)$ = bending moment at x due to a unit increase in q_n
N = total number of landings
P = probability
$Q_n(t)$ = generalized force in the nth mode
$R^n(t_1, t_2 \ldots t_n) = \overline{f(t_1)f(t_2)\ldots f(t_n)}$ = correlation function of order n
ϵ_n = damping coefficient
$\phi_n(x)$ = amplitude at point x of the nth normal mode of vibration, so normalized that the generalized mass corresponding to ϕ_n is equal to m
ω_n = circular frequency of the nth normal mode of vibration, radians per sec
$\xi_n^{(r)}$ = displacement at point of application of rth external force due to a unit change in q_n
$\sum_{n=0}^{\infty}{}'$ = summation in which terms associated with zero frequency ($\omega_n = 0$) are deleted

Introduction

We shall recognize the fundamental fact that throughout the service life of an airplane there occurs a variety of landing conditions and, consequently, it is subjected to transient loads of varied time histories. The prediction of dynamic stresses during landing, at any point in an airplane, is therefore at best a statistical process. The calculation of the most severe stress at a point in the structure and the estimation of the service life of an airplane with respect to landing are meaningful only if the results are stated in the statistical sense. The purpose of the paper is to outline a procedure in which the probabilistic feature is incorporated in the landing analysis.

The current developments in landing analysis will first be reviewed. In the past decade the importance of transient dynamic stresses in aircraft structures (particularly at the outer span of the wing or at the tail) caused by elastic vibrations during landing was recognized. Research in this field has taken two directions. In one approach the initial conditions (sinking speed, bank angle, conditions of the sea for a seaplane, conditions of the runway for a landplane, etc.) are studied (1).[3] A set of such initial conditions specifies, for a given airplane, a definite problem of dynamics (2, 3, 4). It is hoped that a statistical study of the initial conditions will enable a representative set of initial conditions to be determined which will be useful in structural design.

In another approach the form of the impact load-time histories, hereinafter called "applied-load curves," are assumed known; i.e., the forces transmitted by the landing gear to the main structure are specified for the purposes of stress analysis (5, 6, 7). The difficult calculation of the impact load-time histories from the initial conditions of landing is thus largely simplified. It is necessary to assume, in specifying the form of such applied-load curves, that a representative set of applied-load curves can be determined, and that the structure is insensitive to small variations in

[1] This paper is based on a report prepared by the author in February, 1954, while he was a consultant to Aercon, Inc., in connection with an Aercon research project sponsored by the Bureau of Aeronautics, U. S. Navy. The statements presented herein, however, do not necessarily represent the point of view of the Bureau.

[2] Associate Professor, California Institute of Technology.

Presented at the West Coast Conference of the Applied Mechanics Division, Monterey, Calif., September 12–13, 1955, of The American Society of Mechanical Engineers.

Discussion of this paper should be addressed to the Secretary, ASME, 29 West 39th Street, New York, N. Y., and will be accepted until January 10, 1956, for publication at a later date. Discussion received after the closing date will be returned.

Note: Statements and opinions advanced in papers are to be understood as individual expressions of their authors and not those of the Society. Manuscript received by ASME Applied Mechanics Division. Paper No. 55—APM-32.

[3] Numbers in parentheses refer to the Bibliography at the end of the paper.

the applied-load curves. Without satisfying these assumptions this simplified approach is useless.

A crucial problem, therefore, is whether an airplane is very sensitive to small variations in the exact impact load-time history or initial conditions. If it is, detailed calculations covering many special cases are necessary. If it is not, a few simplified calculations will be sufficient.

The answer to the sensitiveness question cannot be given without reference to the method of analysis. The sensitiveness varies in accordance with the variable on which attention is focused. As an example, consider a simple spring-mass-damper system subject to an impact load acting on the mass. One may be interested either in the displacement of the mass or in its acceleration. The choice between the displacement and acceleration, however, spells a great practical difference. If a large number of impact loads of the nature of landing impacts are considered, differing slightly in their time-history curves, it is found (8) that the maximum displacement of the mass is rather insensitive to the shape of the impact load-time history, whereas the maximum acceleration is very sensitive to small variations in it. Therefore, if an analysis is made for the maximum acceleration of the mass or the inertia load, it does not make sense to specify a single impact load-time history curve to represent a whole group of slightly different curves. If, on the other hand, the analysis is made for the maximum displacement of the mass, i.e., the maximum spring tension, a representative impact-load curve is meaningful.

Consider now the landing problem. Let the impact load-time histories be assumed known, but be allowed to vary statistically. When the method of normal co-ordinates is used, each mode acts like a simple oscillator. The maximum values of each generalized displacement may be chosen as a basis for practical analyses.

The severest response at any point in the structure is obtained by a superposition of responses in individual modes in the worst possible combination. It is known that when the duration of the applied load is short, in comparison with the period of oscillation of a mode, the peak response is reached after the applied load has transpired and thereafter that mode oscillates harmonically with no change in amplitude (if damping is neglected). Hence, if the duration of the applied load is small in comparison with the periods of all the significant normal modes, chances are great that the worst possible combination is simply the sum of the absolute values of the largest amplitudes of all the normal modes. This can be visualized by representing each harmonic oscillation by a rotating vector. When several vectors rotate with different speeds about a common origin (like the arms of a clock), there is always a possibility that they will coincide at some instant. This estimate may, however, tend to be overconservative when the effect of structural and aerodynamic damping is taken into consideration.

It is also known that when the duration of the applied load is long in comparison with the period of oscillation of a mode, that mode responds as if the applied load is a static one. Thus, when the fundamental-mode frequency is sufficiently high, the resultant response does not deviate much from the simple algebraic sum of the static responses in various modes.

The foregoing contingencies provide a simplified analysis of the landing problem. But one recognizes at once the existence of a more difficult situation, namely, the case in which the period of oscillation of the fundamental mode is sufficiently long, whereas those for other significant modes are sufficiently short in comparison with the duration of the applied load. In this case, it is necessary to consider the effect of damping and the phase relationship among various modes. The last item is sensitive to variations in the applied-load-time histories.

The vast literature on the subject of landing loads will not be discussed here. (A review and Bibliography are given by Pian and O'Brian, reference 18.) The method of normal co-ordinates to be used later is elucidated upon by von Karman and Biot (9) and details of its application to landing-loads analysis are fully discussed by Goland, Luke, and Kahn (6), and Bisplinghoff, Isakson, and Pian (10). A statistical approach was first proposed by Biot and Bisplinghoff (11), who use a summation of the absolute values of the peak responses in various normal modes to obtain the response of a composite structure. Unfortunately, modern aircraft wings and tails tend to fall outside the range of applicability of such a simple analysis.

The major objective of the paper is to provide a statistical analysis applicable to cases in which simplified analyses cannot be justified. The correlation function of the applied-load curves is introduced and is applied to obtain the root mean square of the response. Applications to design and flight testing will be discussed. It will become clear that although the data required for such an analysis are not currently collected in routine engineering testing, they are by no means difficult to obtain should the usefulness of such data be recognized.

Ensemble of Landing Impacts

A series of landings form an ensemble. A set of records of the landing-gear normal-load-time history forms an ensemble of impact load. A set of time histories of the bending moment at a station on the wing spar forms an ensemble of bending response at that station.

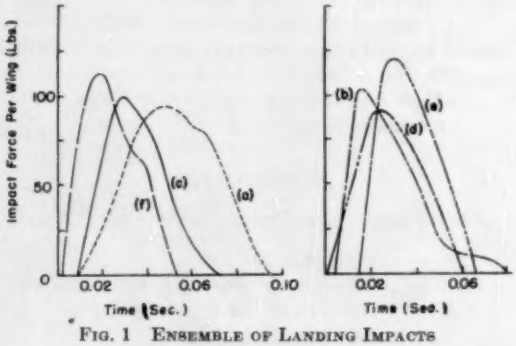

Fig. 1 Ensemble of Landing Impacts

Fig. 1 shows the experimental results of Ramberg and McPherson (12) on the landing-impact force of a simple model wing fitted with an oleo strut. The model was dropped from a carefully controlled height. The landing conditions were varied by changing the softness of the rubber mat on which the model was dropped, the initial spring loading, and the opening of pressure-relief ports in the damper. It is seen that considerable variation in the shape of the impact-force-time curves exist. Taking the records of Fig. 1 as an ensemble, a mean curve can be determined as shown on the left-hand side of Fig. 2. Each point on this mean curve is the mean value of the impact forces at each instant of time following contact of the landing gear with the ground. The individual impact curves in Fig. 1 can be represented by superpositions as shown in Fig. 2. An essential feature of the curves on the right-hand side of this figure is their irregularity. If one remembers the large number of factors involved, such irregularities are really not surprising.

The concept of "ensemble average" may be introduced as follows: Imagine that a large number of observations of a certain quantity are made under similar conditions. Let the records be numbered and denoted by $f_1(t), f_2(t), \ldots f_N(t)$. If the total number of records is N, the following averages may be formed

$$\overline{f(t)} = [f_1(t) + f_2(t) + \ldots + f_N(t)]/N \ldots\ldots [1]$$

$$\overline{[f(t) - m(t)]^2} = \frac{1}{N}\sum_{i=1}^{N}[f_i(t) - m(t)]^2 \quad [2]$$

where $m(t)$ is a specific function of time. Assume that $\overline{f(t)}$ and $\overline{[f(t) - m]^2}$ tend to definite limiting functions of time as $N \to \infty$. Then these limiting functions are ensemble averages of the random process $f(t)$. An ensemble average is indicated by a bar over the variable. If $m(t)$ is taken as the limit of $\overline{f(t)}$ as $N \to \infty$, called the *mean* of the random process $f(t)$, then $\overline{[f(t) - m(t)]^2}$ is called the mean square deviation of $f(t)$ from the mean. Similarly, the mean values of higher powers of the deviation $f(t) - m(t)$ may be defined.

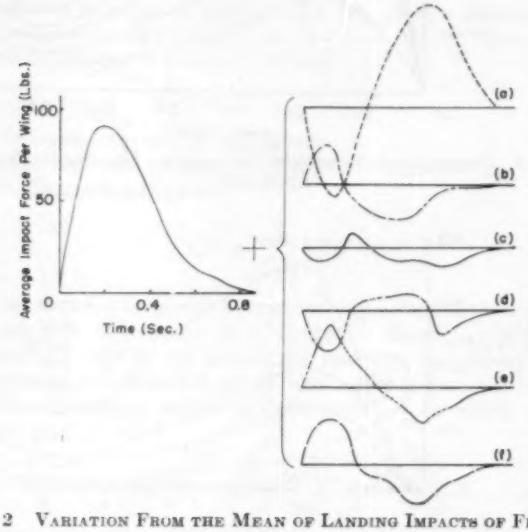

FIG. 2 VARIATION FROM THE MEAN OF LANDING IMPACTS OF FIG. 1

ENSEMBLE AVERAGES OF RESPONSE

The main problems in landing analyses are to find (*a*) the landing-impact force-time curve and (*b*) the stresses in airplane structures resulting from the landing-impact force. Consider the second problem and regard the impact force (force transmitted by the strut for a landplane or force acting on the hull or float for a seaplane) as a forcing function and the motion of the structure (or displacement, acceleration, bending moment, shear, etc.) as a response.

To fix ideas, let us consider a seaplane and let the resultant force acting on the hull be denoted by $f(t)$. A statistical study will define the probability distribution of $f(t)$ at each instant of time t, the time origin being taken at the instant of the hull's contact with water. One can define the "correlation function" $R(t, t')$ as follows

$$R(t, t') = \overline{f(t)f(t')} \quad [3]$$

the average being taken over the ensemble. In other words, from a set of hull-impact force-time histories, the product $f(t)f(t')$ is obtained on each record, t, t' being two instants of time, and an average is taken for each pair of t, t' among all the records. The limit when the number of records is large is the correlation function $R(t, t')$ which is a function of two parameters, t and t'. From the definition it is at once apparent that $R(t, t')$ is symmetric, i.e.

$$R(t, t') = R(t', t) \quad [4]$$

Let $y(x, t)$ represent the particular response of interest, which is a function of the space co-ordinates x and time t. Let $h(x, t)$ be the response of the structure to a unit impulse (delta function) acting at a given point; then, when the forcing function acting at that point is $f(t)$, the response is[4]

$$y(x, t) = \int_0^t h(x, t - \tau)f(\tau)d\tau \quad [5]$$

where it is assumed that $f(t) = 0$ if $t \leq 0$. Taking ensemble average gives

$$\overline{y(x, t)} = \int_0^t h(x, t - \tau)\overline{f(\tau)}\,d\tau \quad [6]$$

Similarly

$$y^2(x, t) = \int_0^t h(x, t - \tau)f(\tau)d\tau \int_0^t h(x, t - \tau')f(\tau')d\tau' \quad [7]$$

and

$$\overline{y^2(x, t)} = \int_0^t \int_0^t h(x, t - \tau)h(x, t - \tau')R(\tau, \tau')d\tau d\tau' \quad [8]$$

where the correlation $R(t, t')$ is defined by Equation [3]. It is clear that a very simple generalization is required to derive the following

$$\overline{(y - \bar{y})^2} = \int_0^t \int_0^t h(x, t - \tau)h(x, t - \tau') \times [R(\tau, \tau') - \overline{f(\tau)}\,\overline{f(\tau')}]d\tau d\tau' \quad [9]$$

More generally, we define the nth-order correlation function

$$R^{(n)}(t_1, t_2, \ldots, t_n) = \overline{f(t_1)f(t_2)\ldots f(t_n)} \quad [10]$$

Then the nth probability moment $\overline{y^n(x, t)}$ is given by

$$\overline{y^n(x, t)} = \int_0^t \cdots \int_0^t \prod_{i=1}^{n} h(x, t - \tau_i) \times R^{(n)}(\tau_1, \tau_2, \ldots \tau_n)d\tau_1 d\tau_2 \ldots d\tau_n \quad [11]$$

The successive moments $\overline{y^n(x, t)}$, $(n = 1, 2, \ldots)$ gives a complete description of the probability distribution of the response y at point x and time t. From such information the probability of exceeding a given stress level by a specific amount can be determined and is relevant to the problem of estimating the life of an aircraft with respect to landing.

The mean $\overline{f(t)}$ and the correlation functions $R^{(n)}(t_1, t_2, \ldots t_n)$ of the forcing function must be determined by experiments or by theoretical calculations on the basis of known probability distribution of the initial conditions of landing impacts. The response of the airplane to a unit impulse function, $h(x, t)$, can be calculated for each airplane by a number of well-known classical methods (9, 10).

A different expression for $\overline{y^n}$ can be derived by means of Fourier integrals. If $f(t)$ is written as

$$f(t) = \int_{-\infty}^{\infty} A(\omega)e^{i\omega t}d\omega$$

where

$$A(\omega) = \frac{1}{2\pi}\int_{-\infty}^{\infty} f(t)e^{-i\omega t}dt$$

then the response $y(x, t)$ is[5]

[4] Refer to (9), p. 402. For simplicity, we assume here that $f(t)$ is a single force acting on the seaplane. The resulting formulas can be generalized easily to include simultaneous action of a number of forces or to forces distributed over an area.

[5] Reference (9), p. 390.

$$y(x, t) = \int_{-\infty}^{\infty} \frac{A(\omega)}{Z(x, \omega)} e^{i\omega t} d\omega \ldots\ldots\ldots\ldots [12]$$

Where $Z(x, \omega)$ is the "impedance" of the system; i.e., $1/Z(x, \omega)$ is the steady-state response y to a unit forcing function $e^{i\omega t}$ of frequency ω. It is now necessary to define the ensemble averages $\overline{A(\omega)}$, $\overline{A(\omega_1)A(\omega_2)}$, etc., in the same way as before. Then

$$\overline{y^n(x, t)} = \int_{-\infty}^{\infty} \ldots \int \frac{\overline{A(\omega_1) \ldots A(\omega_n)}}{Z(x, \omega_1) \ldots Z(x, \omega_n)} \times e^{i(\omega_1 + \omega_2 + \ldots + \omega_n)t} d\omega_1 d\omega_2 \ldots d\omega_n \ldots [13]$$

Note also that if the correlation functions

$$\overline{y(x, t_1)\, y(x, t_2) \ldots y(x, t_n)}$$

of the response are desired, they can be obtained from Equation [11] by replacing

$$\prod_{i=1}^{n} h(x, t - \tau_i)$$

by

$$\prod_{i=1}^{n} h(x, t_i - \tau_i)$$

and changing integration limits successively to $t_1, t_2 \ldots t_n$; or from Equation [13] by replacing the term

$$\exp[i(\omega_1 + \omega_2 + \ldots + \omega_n)t]$$

by

$$\exp[i(\omega_1 t_1 + \omega_2 t_2 + \ldots + \omega_n t_n)]$$

In the following we shall consider a particular approach using normal co-ordinates to develop the function $h(x, t)$ into a series. The purpose of such a procedure is to make the analysis amenable for use without the aid of special computing devices such as those used in references (2, 3, 4). But first, an example of experimentally determined ensemble averages will be given.

Example, Correlation Function of a B-24D Airplane

A B-24D airplane has been subjected to extensive theoretical and experimental studies with respect to its vibration characteristics and landing loads. Westfall (13) gives the accelerations measured at the center of gravity and along the span of the wing as well as the landing-gear normal-load-time histories during landing impacts.

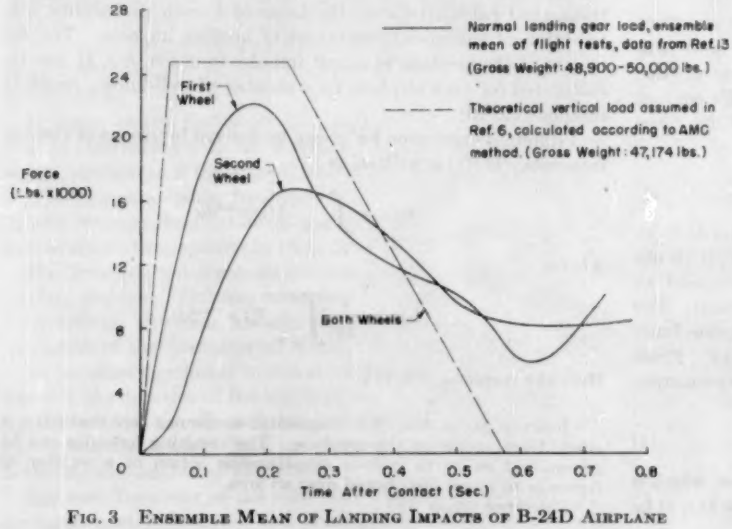
Normal landing gear load, ensemble mean of flight tests, data from Ref. 13 (Gross Weight: 48,900 - 50,000 lbs.)
Theoretical vertical load assumed in Ref. 6, calculated according to AMC method. (Gross Weight: 47,174 lbs.)
First Wheel
Second Wheel
Both Wheels
Force (Lbs. x 1000)
Time After Contact (Sec.)

Fig. 3 Ensemble Mean of Landing Impacts of B-24D Airplane

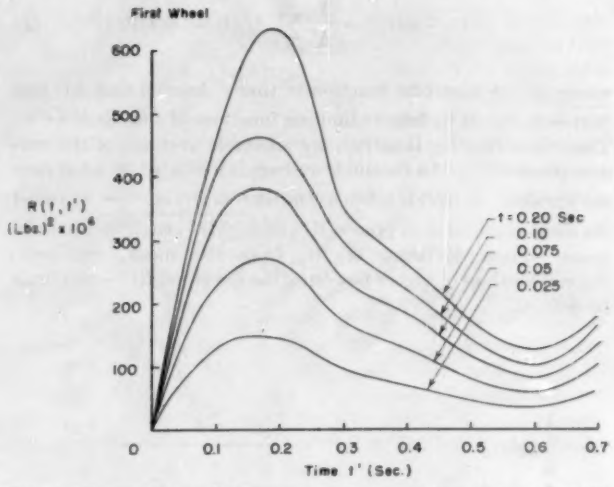

Fig. 4 Correlation Functions of Landing Impacts of B-24D Airplane

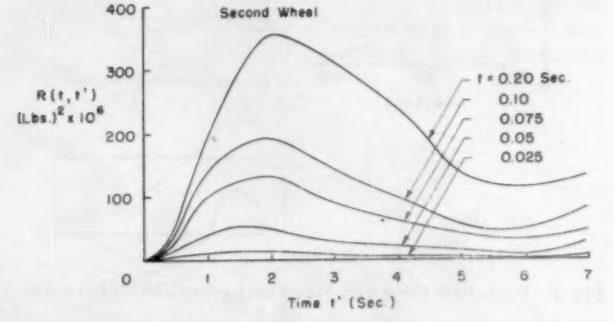

Fig. 5 Correlation Functions of Landing Impacts of B-24D Airplane

From the records in (13) the normal load per wheel can be obtained. The flight test data show that most landings are unsymmetrical. In the following the "first wheel" denotes the one that first touched the ground, or, if both wheels contacted the ground at apparently the same time, the one that gave the larger maximum impact load. From such data the ensemble means of the landing impacts are calculated, assuming that all the landings are equally probable. The results are plotted in Fig. 3. In the same figure is shown the "ideal" applied-load curve assumed in reference (6), which is calculated according to a method proposed by Wasserman (5). It is seen that the dotted curve encloses the measured mean curve over the main portion of the impact curve, but the leading-edge slope of the assumed curve is much too steep in comparison with the experimental curve. The time at which the peak load is reached in the theoretical curve is approximately one quarter of that which was measured. This time is significant in determining the peak responses (8).

The calculated values of the correlation function $R(t, t')$ for each wheel are plotted in Figs. 4 and 5. Note that if the mean load curve of Fig. 3 is denoted by $f(t)$, the correlation function

$R(t, t')$ resembles, but is not equal to, the product $f(t)f(t')$.

The available experimental data of the B-24 airplane would have furnished an excellent example to the statistical approach if the drag component of the landing-impact force were also recorded. The drag component contributes a significant share to the wing and tail acceleration response for the B-24 airplane, but unfortunately, correlation functions concerned with drag are yet unknown.

Expansion in Terms of Normal Co-Ordinates

The rigid-body motion and the elastic deformation of an airplane can be described by series expansions in terms of the natural vibration modes (without damping). Let these modes be denoted by $\phi_0(x)$, $\phi_1(x)$, $\phi_2(x) \ldots$, $\phi_n(x) \ldots$ which correspond to circular frequencies $\omega_0, \omega_1, \ldots \omega_n \ldots$, respectively. These modes will be arranged in such an order that

$$\omega_0 \leq \omega_1 \leq \ldots \leq \omega_n \leq \ldots$$

The lowest frequency ω_0 may be zero.

The displacement $u(x, t)$ at a point x in the structure at time t can be expressed as a series

$$u(x, t) = \sum_{n=0}^{\infty} q_n(t)\ \phi_n(x) \ldots\ldots\ldots\ldots [14]$$

If we assume that positive structural and aerodynamic damping exists and corresponds to a dissipation function which is a quadratic form in the generalized velocities, the expansion of Equation [14] converges for all finite values of time t, $(t > 0)$.

The equation of motion of the airplane can be written in the form (6, 9, or 10)

$$\ddot{q}_n + 2\epsilon_n\omega_n\dot{q}_n + \omega_n^2 q_n = \frac{Q_n(t)}{m_n}, \quad (n = 0, 1, 2 \ldots) \ldots [15]$$

In Equation [15], Q_n is the generalized force; it is related to the virtual work δW done by external forces (other than aerodynamic damping) when the elastic body is displaced through a virtual displacement δq_n, by the equation

$$\delta W = Q_n \delta q_n \quad (n = 0, 1, 2 \ldots) \ldots\ldots\ldots [16]$$

ϵ_n is the ratio of the actual damping to the critical damping in the nth mode. m_n is the generalized mass in the nth mode. It is convenient to normalize the modes $\phi_n(x)$ so that all m_n become equal to the total mass of the airplane m

$$m = m_n = \int \phi_n^2(x)dm \qquad (n = 0, 1, 2, \ldots) \ldots [17]$$

where dm is a mass element at the point (x), and the integration is taken over the entire mass of the airplane.

The generalized forces Q_n are calculated without difficulty according to the definition given by Equation [16]. Suppose that the structure is deflected in only the nth mode and let a unit q_n cause a linear displacement $\xi_n^{(r)}$ in the direction of the rth external force $f^{(r)}$ at its point of application, then

$$Q_n = \sum_r f^{(r)}\xi_n^{(r)} \ldots\ldots\ldots\ldots [18]$$

the summation being taken over all the individual forces. Determination of $\xi_n^{(r)}$ follows at once from normal mode shapes.

In the case where $Q_n(t)$ is a unit impulse function; i.e., $Q_n(t)$ tends to infinity as $t \to 0$ while its duration tends to zero in such a way that the area under the $Q_n(t)$ curve remains equal to unity, the solution of Equation [15] when $\epsilon_n^2 \ll 1$ is

$$q_n \doteq \frac{1}{m_n\omega_n} e^{-\epsilon_n\omega_n t} \sin \omega_n t \ldots\ldots\ldots [19]$$

The elastic displacement at a point x in response to a unit impulse function δf is, therefore, according to Equation [14]

$$h(x, t) = \sum_{n=0}^{\infty}{}' \frac{\delta Q_n}{m_n\omega_n} e^{-\epsilon_n\omega_n t} \sin \omega_n t\ \phi_n(x) \ldots\ldots [20]$$

where Σ' signifies that terms corresponding to rigid-body motions (for which $\omega = 0$) should be deleted from the summation, and δQ_n is the component of the unit impulse function in the nth mode to be computed from Equation [18]. Equation [20] gives the function h used in Equations [5] to [11] if y denotes the elastic displacement. Hence we derive from Equations [5] and [19] the well-known result

$$q_n(t) = \frac{1}{m_n\omega_n} \int_0^t e^{-\epsilon_n\omega_n(t-\tau)} \sin \omega_n(t - \tau)Q_n(\tau)d\tau \ldots [21]$$

Bending Moments

It will be shown that the transient stresses in a structure can be described by series similar to those of the preceding section. For example, consider a simple elastic beam. Let u of Equation [14] denote the flexural deflection of the beam. The bending moment at a spanwise location x is

$$M(x, t) = EI(x)\frac{\partial^2 u}{\partial x^2} = EI(x)\sum_{n=0}^{\infty}{}' q_n(t)\frac{d^2\phi_n(x)}{dx^2} \ldots [22]$$

where $EI(x)$ denotes the bending rigidity of the beam at x.

In order to avoid the differentiation of the normal modes $\phi_n(x)$ which are often given in the form of numerical tables, the bending moment

$$M_n(x) = EI(x)d^2\phi_n(x)/dx^2$$

in each mode can be computed from the inertia-force distribution, which is equal to $-\rho(x)\omega_n^2\phi_n(x)$, where $\rho(x)$ denotes the mass per unit length of the beam. Equation [22] can be written as

$$M(x, t) = \sum_{n=0}^{\infty}{}' q_n(t)M_n(x) \ldots\ldots\ldots [23]$$

Similar treatments can be made for shear or any stress components.

An alternate expression for $M(x, t)$ can be derived by reasoning that the bending moment arises as a resultant action of the external applied forces and the inertia forces

$$-\rho(x)\ddot{u} = -\sum \ddot{q}_n(t)\rho(x)\phi_n(x)$$

But the inertia force distribution $-\rho(x)\omega_n^2\phi_n(x)$ produces the bending moment $M_n(x)$. Hence the bending moment caused by the inertia forces is

$$[M(x, t)]_{\text{inertia}} = \text{moment due to rigid-body motion} + \sum_{n=0}^{\infty}{}' \frac{\ddot{q}_n(t)}{\omega_n^2} M_n(x) \ldots [24]$$

From the Equation of Motion [15], the last sum can be further written, in the case $\epsilon_n = 0$, as

$$\sum_{n=0}^{\infty}{}' \left[\frac{Q_n(t)}{m_n\omega_n^2} - q_n(t)\right] M_n(x) \ldots\ldots [25]$$

or as

$$\sum_{n=0}^{\infty}{}' q_{n0}\left[\frac{Q_n(t)}{Q_{n\max}} - \frac{q_n(t)}{q_{n0}}\right] M_n(x) \ldots\ldots [26]$$

where $Q_{n\,max}$ is the peak value of the forcing function $Q_n(t)$ and q_{n0} is the static deflection

$$q_{n0} = \frac{Q_{n\,max}}{\text{spring constant}} = \frac{Q_{n\,max}}{m_n\omega_n^2} \quad \ldots\ldots [27]$$

The total bending moment $M(x, t)$ is the sum of the foregoing and the static bending moment due to the external forces. Note that Equation [23] expresses the elastic moment in a structure accompanying the elastic deformation; the rigid-body motion therefore makes no contributions. On the other hand, Equation [24] expresses the moment due to inertia forces in which the rigid-body motion contributes a major share. The advantage of the latter procedure was first shown by D. Williams (14).

The Mean Response

The calculation of the mean response $\overline{y(x, t)}$ to the mean applied load $\overline{f(t)}$ is, according to Equation [6], identical with the calculation of conventional response history to a specific applied-load curve. Using normal co-ordinates, the response can be written as Equation [21]. It is necessary to evaluate the integral $q_n(t)$ of Equation [22] with $Q_n(t)$ replaced by $\overline{Q_n(t)}$. If $\overline{Q_n(t)}$ consists of a series of straight-line segments, a simple superposition described by Wasserman (7) is applicable. When $\overline{Q_n(t)}$ is not approximated by a series of straight-line segments the simplest way of evaluating the integral in Equation [22] seems to be the electrical analogy method described by Shapiro and Hudson (15).

The Mean Square Deviation of the Response

To determine the deviation from the mean response, we have to consider the quantity $\overline{(y - \bar{y})^2}$ as expressed by Equation [9]. The integral in Equation [9] can be transformed directly into a series in normal co-ordinates, but the following alternative derivation is simple. Since the response y is given by Equations [14] and [21], we have

$$y^2(x, t) = \sum_{n=0}^{\infty} q_n(t)\phi_n(x) \sum_{k=0}^{\infty} q_k(t)\phi_k(x) \quad \ldots\ldots [28]$$

Rearranging and taking ensemble average, we have

$$\overline{y^2(x, t)} = \sum_n \sum_k \overline{q_n(t)q_k(t)}\ \phi_n(x)\phi_k(x) \quad \ldots\ldots [29]$$

where

$$\overline{q_n(t)q_k(t)} = \frac{1}{m_n m_k \omega_n \omega_k} \int_0^t \int_0^t \exp\left[-\epsilon_n\omega_n(t-\tau) - \epsilon_k\omega_k(t-\tau')\right] \sin\omega_n(t-\tau) \sin\omega_k(t-\tau')\ \overline{Q_n(\tau)Q_k(\tau')}\, d\tau d\tau' \quad \ldots [30]$$

The function $\overline{Q_n(\tau)Q_k(\tau')}$ may be called a "generalized correlation function" associated with the nth and the kth modes. It is related to the correlation function $R(t, t')$ of Equation [3] as the generalized force $\overline{Q_n(t)}$ is related to the external forces $\overline{f(t)}$. If a number of individual forces acting on the body and $\xi^{(r)}$ is defined as in Equation [18], we have

$$\overline{Q_n(\tau)Q_k(\tau')} = \sum_r R^{(r)}(\tau, \tau')\xi_n^{(r)}\xi_k^{(r)} \quad \ldots\ldots [31]$$

where $R^{(r)}(\tau, \tau')$ is the correlation function of the rth force $f^{(r)}$.

If $\overline{(y - \bar{y})^2}$ is desired, it is only necessary to replace

$$\overline{q_n(t)q_k(t)} \text{ by } \left\{\overline{q_n(t)q_k(t)} - \overline{q_n(t)}\ \overline{q_k(t)}\right\}$$

and

$$\overline{Q_n(\tau)Q_k(\tau')} \text{ by } \left\{\overline{Q_n(\tau)Q_k(\tau')} - \overline{Q_n(\tau)}\ \overline{Q_k(\tau')}\right\}$$

in Equations [29] and [30].

The evaluation of $\overline{q_n(t)q_k(t)}$ is simplified in the undamped case ($\epsilon_n = \epsilon_k = 0$). Applying the mean-value theorem to the integral on the right-hand side of Equation [30] shows that

$$\overline{q_n(t)q_k(t)} = e^{-\epsilon_n\omega_n(t-a) - \epsilon_k\omega_k(t-b)} \left[\overline{q_n(t)q_k(t)}\right]_{\epsilon_n=\epsilon_k=0} \quad [32]$$

where a and b are two constants both less than t. In practice we may put a and b equal to zero and correct the effect of damping by simply altering the undamped response $\overline{q_n(t)q_k(t)}$ with $\epsilon_n = \epsilon_k = 0$, by a decay factor

$$e^{-(\epsilon_n\omega_n + \epsilon_k\omega_k)t}$$

When ϕ_n are replaced by M_n, as in Equations [23] and [24], the mean square of the bending moment is obtained.

Example. Consider an ensemble of impact loads of half-sine form

$$\left.\begin{aligned} f(t) &= a \sin(\pi t/t_0) && \text{for } 0 \le t \le t_0 \\ &= 0 && \text{for } t < 0 \text{ and } t > t_0 \end{aligned}\right\} \quad [33]$$

where the amplitude a is a random variable. Let an aircraft be acted upon by a single force $f(t)$ the point of application of which deflects an amount ξ_n when a unit change in the nth normal mode ($q_n = 1$) is made. Then the generalized force in the nth degree of freedom is

$$\left.\begin{aligned} Q_n(t) &= a\,\xi_n \sin(\pi t/t_0) && \text{for } 0 \le t \le t_0 \\ &= 0 && \text{for } t < 0, \quad t > t_0 \end{aligned}\right\} \quad [34]$$

The mean response $\overline{q_n(t)}$ is given by Equation [21]. In the absence of damping this gives

$$\left.\begin{aligned} \overline{q_n(t)} &= \bar{a}\,\xi_n A_n(t) \\ \overline{y(x, t)} &= \sum_n \overline{q_n(t)}\ \phi_n(x) \end{aligned}\right\} \quad \ldots\ldots [35]$$

where

$$\left.\begin{aligned} A_n(t) &= \frac{1}{m_n\omega_n^2} \frac{2}{\frac{T_n}{t_0} - \frac{4t_0}{T_n}} \left(\sin\omega_n t - \frac{2t_0}{T_n}\sin\frac{\pi t}{t_0}\right), \\ &\qquad (0 \le t \le t_0) \\ &= \frac{1}{m_n\omega_n^2} \frac{2}{\frac{T_n}{t_0} - \frac{4t_0}{T_n}} \left[(1 + \cos\omega_n t_0)\sin\omega_n t \right. \\ &\qquad \left. - \sin\omega_n t_0 \cos\omega_n t\right], \quad (t > t_0) \end{aligned}\right\} \quad [36]$$

with the notation $T_n = 2\pi/\omega_n$. Equations [36] become indeterminate when $t_0 = T_n/2$, in which case

$$\left.\begin{aligned} A_n(t) &= \frac{1}{2m_n\omega_n^2} (\sin\omega_n t - \omega_n t \cos\omega_n t), \\ &\qquad (0 \le t \le T_n/2) \\ &= -\frac{\pi}{2m_n\omega_n^2} \cos\omega_n t, \qquad (t > T_n/2) \end{aligned}\right\} \quad [37]$$

Forming the product Q_nQ_k and taking ensemble average, we obtain

$$\overline{Q_n(t)Q_k(t')} = \bar{a}^2\,\xi_n\xi_k \sin\frac{\pi t}{t_0}\sin\frac{\pi t'}{t_0}, \quad (0 \le t, t' \le t_0) \quad [38]$$

In the present case, the double integral in Equation [30] has no coupling, the following results are obtained at once

$$\overline{q_n(t)q_k(t)} = \overline{a^2}\xi_n\xi_k A_n(t)A_k(t) \quad [39]$$

$$= \frac{\overline{a^2}}{(\bar{a})^2}\,\overline{q_n(t)}\;\overline{q_k(t)} \quad [40]$$

$$\bar{y}^2 = \frac{\overline{a^2}}{(\bar{a})^2}(\bar{y})^2 \quad [41]$$

$$\overline{(y-\bar{y})^2} = \frac{\overline{a^2}-(\bar{a})^2}{(\bar{a})^2}(\bar{y})^2 \quad [42]$$

Higher statistical moments of y are obtained in like manner. They are proportional to the corresponding statistical moments of the amplitude a.

This example shows how simple it is to obtain the statistical moments of the response when the time history of the forcing function is of the same form for the entire ensemble except for the amplitude.

Relation to Initial Conditions

In the foregoing paragraphs the statistical nature of the elastic deformation of the aircraft is related to the statistics of the impact load-time history. Theoretically, the latter can be derived from statistics of the initial conditions at landing contact with ground.

Silsby (1) gives an analysis of measurements of contact conditions by means of a specially built motion-picture camera of 478 landings of present-day transport airplanes made during routine daylight operations in clear air at Washington National Airport. It was found that the probability distributions of the sinking speed, rolling velocity, bank angle, and horizontal speed at the instant before contact can be fitted reasonably well by the Pearson Type III distribution. Fig. 6 shows a sample of the fitted probability curve given by Silsby for the probability of equaling or exceeding a specific sinking speed. Table 1 gives the related statistical parameters for the sinking speed at landing contact. The influence of "gust" is apparent (see definition in reference 19). The influence of other parameters, such as wing loading, stalling speed, etc., would have to be determined by further observations.

The calculation of the impact load in the landing strut is complicated by the nonlinear characteristics of the wheel and oleo strut. But if each landing strut and tire together may be approximated by a linear spring, then the initial value problem can be analyzed simply. The solution has been given by Pian and O'Brian (18). As an example, let us consider an elastic airplane which is initially in static equilibrium under the action of lift and gravitational forces and has a sinking speed V_s at the instant of contact with ground. In this case the form of the impact force in the landing strut $f(t)$ resembles a half-sine wave for smaller values of t. The magnitude of $f(t)$ is usually influenced significantly by the elastic vibrations of the structure. Since the system is linear, $f(t)$ must be directly proportional to the sinking speed V_s.

Thus the example of preceding section is meaningful in symmetric landing if the landing gear can be approximated by a linear spring. If V_s is distributed like Pearson Type III, the response y will be of the same distribution with the same parameters as for V_s. All the statistical parameters of y as functions of position are proportional to the mean response $\bar{y}(x, t)$. Thus, in this very simple case, the statistical analysis is almost unnecessary. The severest landing load can be derived directly from the estimate of the severest sinking speed in the life of the airplane.

In the case of unsymmetric landing, the initial values of sinking speed V_s, bank angle θ_0, and rolling velocity $\dot{\theta}_0$ must be considered. The impact load $f(t)$ can be expressed as a linear function of V_s, θ_0, and $\dot{\theta}_0$. The probability distribution of $f(t)$ can then be determined from those of V_s, θ_0, and $\dot{\theta}_0$. It is important to note that the time histories of the ensemble of impact loads are no longer proportional to each other when unsymmetric landings are considered.

Applications to Design and Flight Testing

To answer questions such as the most severe stress y (at a given point in an airplane) that is likely to occur in a specific number of

TABLE 1 VALUES OF STATISTICAL PARAMETERS FOR SINKING SPEED V_s AT LANDING CONTACT[a]

Category	Gust condition	No. of landings	Maximum V_s, fps	Mean V_s, fps	Std. deviation, σ, fps	Coeff. of skewness, α
All airplanes	No gusts	207	3.4	1.22	0.57	0.66
	Gusts	271	4.5	1.50	0.76	0.79
	Total	478	4.5	1.38	0.70	0.76
Low wing loading (27–33 psf)	No gusts	47	2.4	0.95	0.48	0.82
	Gusts	45	2.3	1.02	0.46	0.75
	Total	92	2.4	0.98	0.47	0.79
Medium wing loading (47–51 psf)	No gusts	118	3.4	1.28	0.57	0.64
	Gusts	148	4.4	1.61	0.80	0.70
	Total	266	4.4	1.46	0.72	0.88
High wing loading (60–80 psf)	No gusts	42	2.5	1.32	0.60	0.20
	Gusts	78	4.5	1.58	0.73	0.51
	Total	120	4.5	1.49	0.69	0.53

[a] Reference (1).

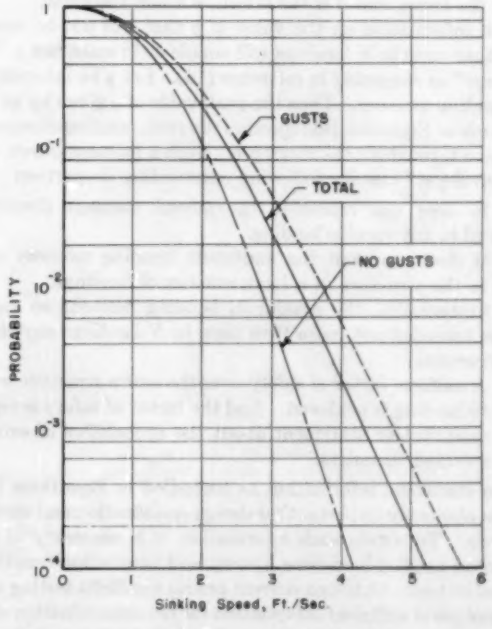

FIG. 6 PROBABILITY OF EQUALING OR EXCEEDING SINKING SPEED, FOR CONDITIONS OF GUSTS, NO GUSTS, AND TOTAL LANDINGS (1)

landings, it is necessary to know the probability that a certain value of y is exceeded. If the probability distribution of the response is known, the answer can be given immediately. For example, if it is possible to assume a normal distribution for the response, then the probability that the variable $y - \bar{y}$ will exceed k times the standard deviation

$$\sigma = [\overline{(y-\bar{y})^2}]^{1/2}$$

is, for large k

$$P = \text{prob}\,\{y - \bar{y} > k\sigma\} \doteq \frac{e^{-k^2/2}}{k\sqrt{2\pi}} \quad [43]$$

Thus the probability to exceed 3σ is about 0.0014. If the probability P is 0.01, k would have to be approximately 2.326; if P = 0.001, k would be 3.1.

If the probability for the response to exceed a given value y is P, then the probable number of landings N in which one will cause a response exceeding y is

$$N \doteq \frac{1}{P} \quad [44]$$

Thus y will be exceeded once in a thousand landings if P = 0.001. This number N obviously tells the probable life of the airplane with respect to landings.

For design purposes, it is desired to specify the value y so that the strength of the aircraft can be designed in anticipation of a total number of times N the aircraft is expected to land in its useful life. To do this, one computes $P = 1/N$ and determines the value y according to its probability distribution function. Thus, if y is normally distributed and N = 1000, then

$$y = \bar{y} + 3.1\sigma \quad [45]$$

If y is distributed like Pearson Type III (see Elderton, reference 20) and N = 750, then

$$y = \bar{y} + \sigma(3 + 1.33\alpha) \quad [46]$$

where $\bar{y}$ is the mean response, σ is the standard deviation of y about the mean, and α is the skewness about the mean.

Such information on the value of y that will not be exceeded more than once in N landings will enable us to construct a "stress envelope" as suggested in reference (16). Let y be interpreted as the bending moment. Then the peak value of y given by an equation such as Equation [46] specifies the peak bending-moment distribution throughout the structure. Such a moment curve, called an "envelope," has the following outstanding properties:

1 It does not represent the actual moment distribution achieved in any specific landing.

2 It does represent the maximum bending moment at any point in the structure in a large number of landings.

3 Statistically, the maximum bending moment so specified will be exceeded not more than once in N landings anywhere in the structure.

4 A uniform factor of safety over the entire structure with respect to landing is achieved. And the factor of safety is replaced by a quantitative statement about the probability of exceeding such specified moments.

The statistical information as embodied in Equations [44] to [46] is obviously important for design specification and structural analysis. To obtain such information, it is necessary to obtain the mean applied-load-time history and correlation functions of several orders. Although current practice in flight testing usually does not yield sufficient information for the determination of these functions, it is clear that conventional flight-test technique can give the desired information should the need be recognized.

For seaplane applications, the statistical approach will be ideally suited for the analysis of landing on rough water. It is well known that for a seaplane landing on rough water the most severe impact load and induced stresses usually do not occur on the first impact, but actually occur on the second or later impacts after the first rebound, even if the seaplane does not clear the water completely in the rebound. The unpredictable wave surface of the sea and the elastic vibration set in the structure by the first impact may cause severe dynamic stresses on successive impacts.

If a classical deterministic point of view were taken, a theoretical analysis of the rough-water landing would have to include all combinations of the conditions of the sea and the attitude of the seaplane, and also to consider all incidental variables such as when and where among the waves the successive impacts occur. The difficulty of such an analysis will be aggravated, the more flexible is the seaplane structure, because the effect of elastic vibration of the wing, tail, and hull on the impact load cannot be neglected. As the hydrodynamic impact is governed by nonlinear equations, the mathematical difficulty in such a general analysis is great. Up to date, there does not exist any reasonably complete rough-water landing analysis.

On the other hand, if the statistical approach is taken, the analysis can proceed in the usual manner. Some preliminary studies by Locke (17) on the correlation of the seaplane characteristics with the maximum vertical accelerations encountered in rough-water landings already have yielded successful results.

Conclusions

The foregoing analysis furnishes a way to determine the probable life of the structure with respect to landings and the distribution of the expected maximum stresses over the structure. If the correlation functions of the impact loads transmitted by the landing gears are known, the statistics of the elastic response of the wing, fuselage, and tail can be computed. The correlation functions of the impact loads can be obtained from the initial conditions at landing contact if the landing gear can be approximated by linear springs. Otherwise the statistics of the contact conditions (sinking speed, bank angle, etc.) cannot be used directly. In general, the correlation functions of the impact forces would have to be obtained from flight or drop tests.

Acknowledgment

The critical discussions and help of Dr. A. J. A. Morgan, president, Aercon, Inc., are gratefully acknowledged.

BIBLIOGRAPHY

1 "Statistical Measurements of Contact Conditions of 478 Transport-Airplane Landings During Routine Daytime Operations," by N. S. Silsby, NACA TN 3194, 1954.

2 "An Analytical Theory of Landing-Shock Effects on an Airplane Considered as an Elastic Body," by E. G. Keller, Journal of Applied Mechanics, Trans. ASME, vol. 66, 1944, pp. A-219–A-228.

3 "A Study of the Response of an Airplane Landing Gear Using the Differential Analyzer," by W. C. Hurty, *Journal of the Aeronautical Sciences*, vol. 17, 1950, pp. 756–764.

4 "The Solution of Aeroelastic Problems by Electric Analogue Computation," by J. Winson, *Journal of the Aeronautical Sciences*, vol. 17, 1950, pp. 385–395.

5 "Estimation of Vertical Loads in Landing Gears," by L. S. Wasserman, USAAF AMC Eng. Div. Memo Report TSEAC 5-4595-5-5, 1947.

6 "Prediction of Dynamic Landing Loads," by M. Goland, Y. Luke, and E. A. Kahn, AF Technical Report 5815, USAF Air Materiel Command, 1949.

7 "A Simplified Procedure for Computing Transient Responses of Linear Systems to Landing Gear Impulses," by L. S. Wasserman, Eng. Div. Memo Report TSEAC 5-4595-5-4, Air Materiel Command, 1947.

8 "On the Dynamic Amplification Spectra of Landing Impacts," by Y. C. Fung, report submitted to Bureau of Aeronautics,

U. S. Navy, on Contract No. NO as 53-348c by Aercon, Inc., Pasadena, Calif., January, 1954.

9 "Mathematical Methods in Engineering," by Th. von Karman and M. A. Biot, McGraw-Hill Book Company, Inc., New York, N. Y., 1940.

10 "Methods in Transient Stress Analysis," by R. L. Bisplinghoff, G. Isakson, and T. H. H. Pian, *Journal of the Aeronautical Sciences*, vol. 17, 1950, pp. 259–270.

11 "Dynamic Loads on Airplane Structures During Landing," by M. A. Biot and R. L. Bisplinghoff, NACA Wartime Report No. W-92, ARR 4H10, 1944.

12 "Experimental Verification of Theory of Landing Impact," by W. Ramberg and A. E. McPherson, *Journal of Research*, National Bureau of Standards, vol. 41, 1948, pp. 509–520.

13 "Accelerations Measured at Center of Gravity and Along Span of the Wing of a B-24D Airplane in Landing Impacts," by J. R. Westfall, NACA Wartime Report L-583, MR, 1944.

14 "Dynamic Loads in Aeroplanes Under Given Impulsive Loads With Particular Reference to Landing and Gust Loads on a Large Flying Boat," by D. Williams and R. P. N. Jones, British ARC, R and M 2221, 1945.

15 "The Measurement of Acceleration Pulses With the Multifrequency Reed Gages," by H. Shapiro and D. E. Hudson, JOURNAL OF APPLIED MECHANICS, Trans. ASME, vol. 75, 1953, pp. 422–426.

16 "Statistical Aspects of Dynamic Loads," by Y. C. Fung, *Journal of the Aeronautical Sciences*, vol. 20, 1953, pp. 317–330.

17 "A Statistical Study of Maximum Vertical Acceleration Encountered in Flying Boats in Rough Water Landings," by F. W. S. Locke, Jr., Report No. 1184, Research Division, Bureau of Aeronautics, U. S. Navy, 1952.

18 "Effect of Structural Flexibility on Aircraft Loading—Part 1. Ground-Loads," by T. F. O'Brian and T. H. H. Pian, Air Force Technical Report 6358, part 1, 1951.

19 "Manual of Surface Observations (WBAN)," anonymous, Circular N, Weather Bureau, U. S. Department of Commerce, 1951, p. 93.

20 "Frequency Curves and Correlation," by W. P. Elderton, C. and E. Layton, London, England, third edition, 1938

Large Deflection Analysis for a Plate Strip Subjected to Normal Pressure and Heating

By M. L. WILLIAMS,[1] PASADENA, CALIF.

Large deflection analysis is carried out to determine the deflections and membrane stresses for an infinite strip when subjected to pressure and temperature variations across the width of the strip with the end points fixed in space. Results are graphed for both clamped and simply supported edge conditions in the case of uniform temperature T_0, and uniform pressure p_0. The calculations also include the possible thermal buckling deflections. In the limit case of a membrane of width b and thickness h, subjected to this loading condition, the central deflection w_0 is determined from the simple relation

$$\left[(w_0/h)^2 - \frac{3}{8}(1+\nu)(b/h)^2\,\alpha T_0\right](w_0/h) = p_0 b^4/(256Dh)$$

A PROBLEM which frequently occurs in analyzing plates under normal pressure is the computation of the stresses and deflections when the deflection of the plate lies between the thick plate ($w/h \lesssim 1$) and membrane ($w/h \gg 1$) region. The difficulty is associated with the nonlinear build-up of stresses in the plane of the plate with increasing pressure or deflection. One of the cases which can be treated however is the case of an infinite strip or, in the terms of Timoshenko's summary and discussion[2] of Boobnov's and Way's work, cylindrical bending. Shaw, Pohle, and Perrone[3] also have discussed the infinite-strip case from a formulation in terms of Southwell's three displacement equations of equilibrium[4] and are led to similar results.

An extension of the problem, partially instigated by its occurrence in aircraft design, is proposed in order to treat the case of all combinations of normal pressure and heating (or cooling) of an infinite strip when the deflection lies in this particularly bothersome range. Calculations for the specific cases of both clamped and simply supported plates subjected to a uniform pressure and uniform temperature rise are presented.

An immediate consequence of the combined loading leads to an interesting point in that the governing equation changes type depending upon the magnitude of the middle-plane (compressive) stress induced by the heating with respect to the (tension) stress caused by the pressure. Therefore the case when the net stress is compressive, tending to cause buckling, also has been included. The results limit check the thick-plate and membrane theories as well as the plate-buckling stresses in the absence of all normal pressure.

Finally, the formulation has been based upon an energy approach in order to facilitate application to approximate solutions for related cases not included in this paper.

Formulation of Problem

Consider a strip of constant thickness h, with width b, extending in the y-direction and the length l extending toward infinity in the x-direction. Suppose that this strip is deflected out of its plane by a normal pressure $p(y)$ and heated (or cooled), uniformly through the thickness, by a temperature distribution $T(y)$. It is then proposed to calculate the deflections and stresses in the strip under the combined loading for certain boundary conditions at $y = \pm b/2$ when the membrane stresses in the middle plane are taken into account.

The potential energy in the system will be obtained and varied in such a way that differential equations for the deflection normal to the plane $w(y)$ and displacement of the middle surface in the direction of y, $v(y)$, will be obtained.

Inasmuch as the displacement u in the x-direction will be zero for the infinite strip,[5] $v(y)$ and $w(y)$ will be the only displacements with which at present we are concerned. The contributions to the total energy per unit length are summarized as follows:

Middle-surface or membrane-strain energy

$$U_m = \int_{-\frac{b}{2}}^{\frac{b}{2}} \frac{Eh}{2(1-\nu^2)}\left[\left(\frac{dv}{dy}\right)^2 + \frac{dv}{dy}\left(\frac{dw}{dy}\right)^2 + \frac{1}{4}\left(\frac{dw}{dy}\right)^4\right] dy \quad [1]$$

Bending-strain energy

$$U_b = \int_{-\frac{b}{2}}^{\frac{b}{2}} \frac{D}{2}\left(\frac{d^2w}{dy^2}\right)^2 dy \quad [2]$$

Energy contribution from the pressure loading

$$W_p = \int_{-\frac{b}{2}}^{\frac{b}{2}} p(y)\,w(y)\,dy \quad [3]$$

Energy contribution from heating[6]

[1] Associate Professor, California Institute of Technology.

[2] "Theory of Plates and Shells," by S. Timoshenko, McGraw-Hill Book Company, Inc., New York, N. Y., 1940, pp. 1–33.

[3] "The Non-Linear Deflection of Infinite Strip Plates," by F. S. Shaw, F. Pohle, and N. Perrone, Polytechnic Institute of Brooklyn, PIBAL Report No. 225, June, 1953.

[4] "Problems Relating to Large Transverse Displacements of Thin Elastic Plates," by J. R. Green and R. V. Southwell, Philosophical Trans. of the Royal Society of London, series A, vol. 239, 1945, pp. 539–578.

Presented at the West Coast Conference of the Applied Mechanics Division, Monterey, Calif., September 12–13, 1955, of The American Society of Mechanical Engineers.

Discussion of this paper should be addressed to the Secretary, ASME, 29 West 39th Street, New York, N. Y., and will be accepted until January 10, 1956, for publication at a later date. Discussion received after the closing date will be returned.

Note: Statements and opinions advanced in papers are to be understood as individual expressions of their authors and not those of the Society. Manuscript received by West Coast Committee of the ASME Applied Mechanics Division, May 2, 1955. Paper No. 55—APM-35.

[5] The case of constant strain may be similarly treated.

[6] See, for example, "Fundamental Principles and Methods of Thermo-Elasticity," by W. S. Hemp, *Aircraft Engineering*, April, 1954, p. 126, as specialized to two-dimensional problems.

$$W_t = \int_{-\frac{b}{2}}^{\frac{b}{2}} \frac{Eh\alpha\, T(y)}{1-\nu}\left[\frac{dv}{dy} + \frac{1}{2}\left(\frac{dw}{dy}\right)^2\right] dy \quad [4]$$

The potential energy of deformation per unit length V may be written

$$V = U_m + U_b - W_p - W_t \quad [5]$$

so there results

$$V = \int_{-\frac{b}{2}}^{\frac{b}{2}} \left\{ \frac{Eh}{2(1-\nu^2)}\left[\left(\frac{dv}{dy}\right)^2 + \frac{dv}{dy}\left(\frac{dw}{dy}\right)^2 + \frac{1}{4}\left(\frac{dw}{dy}\right)^4\right] + \frac{D}{2}\left(\frac{d^2w}{dy^2}\right)^2 - \frac{Eh\alpha\, T(y)}{1-\nu}\left[\frac{dv}{dy} + \frac{1}{2}\left(\frac{dw}{dy}\right)^2\right] - p(y)w(y)\right\} dy \quad [6]$$

It is convenient at this point to introduce dimensionless forms as follows

$$\left.\begin{aligned} \eta &= y/(b/2) & T(\eta) &= T_0 f(\eta) \\ \bar{w} &= w/b & p(\eta) &= p_0 g(\eta) \\ \bar{v} &= v/b & E(\eta) &= E_0 s(\eta) \end{aligned}\right\} \quad [7]$$

to obtain

$$V = \frac{b}{2}\int_{-1}^{1} \left\{ \frac{2hE_0 s(\eta)}{1-\nu^2}\left[\bar{v}'^2 + 2\bar{v}'\bar{w}'^2 + \bar{w}'^4\right] + \frac{2E_0 h^3 s(\eta)}{3(1-\nu^2)b^2}\bar{w}''^2 - \frac{2E_0 h\alpha T_0}{1-\nu}\, s(\eta)f(\eta)\left[\bar{v}' + \bar{w}'^2\right] - p_0 b g(\eta)\bar{w}\right\} d\eta \quad [8]$$

Setting up the variational functions in the usual fashion

$$\bar{v} = \bar{v}_0 + \epsilon_2 \overline{V} \quad [9]$$

$$\bar{w} = \bar{w}_0 + \epsilon_2 \overline{W} \quad [10]$$

substituting into Equation [8] and requiring

$$\left.\frac{\partial V}{\partial \epsilon_2}\right|_{\epsilon_2 = 0} = 0 \quad \text{and} \quad \left.\frac{\partial V}{\partial \epsilon_2}\right|_{\epsilon_2 = 0} = 0$$

yields the two differential equations governing v and w

$$\frac{d}{d\eta}\left\{\frac{4E_0 hs(\eta)}{1-\nu^2}\left[\frac{d\bar{v}}{d\eta} + \left(\frac{d\bar{w}}{d\eta}\right)^2\right] - \frac{2E_0 h\alpha T_0}{1-\nu} f(\eta)s(\eta)\right\} = 0 \quad [11]$$

$$\frac{d^2}{d\eta^2}\left[\frac{4h^2E_0}{3(1-\nu^2)b^2}\, s(\eta)\frac{d^2\bar{w}}{d\eta^2}\right] - \frac{d}{d\eta}\left[\left\{\frac{8E_0 h}{1-\nu^2}\, s(\eta)\left[\frac{d\bar{v}}{d\eta} + \left(\frac{d\bar{w}}{d\eta}\right)^2\right] - \frac{4E_0 h\alpha T_0}{1-\nu}\, s(\eta)f(\eta)\right\}\left\{\frac{d\bar{w}}{d\eta}\right\}\right] - p_0 b g(\eta) = 0 \quad [12]$$

Inasmuch as Equation [11] may be integrated once, there results[7]

$$\frac{4E_0 hs(\eta)}{1-\nu^2}\left[\frac{d\bar{v}}{d\eta} + \left(\frac{d\bar{w}}{d\eta}\right)^2\right] - \frac{2E_0 h\alpha T_0}{1-\nu} f(\eta)s(\eta) = 2N \quad [11a]$$

which can be substituted into Equation [12] effectively removing the nonlinearity and yielding the simple equation for the plate deflection when subjected to variable temperature and pressure across its width

$$\frac{d^2}{d\eta^2}\left[\frac{4E_0 h^3}{3(1-\nu^2)b^2}\, s(\eta)\frac{d^2\bar{w}}{d\eta^2}\right] - \frac{4N}{b}\frac{d^2\bar{w}}{d\eta^2} = p_0 g(\eta) \quad [12a]$$

The Membrane Case

It is convenient first to check the limit cases; for a membrane the bending rigidity is zero or in Equation [12a] $(h/b) \to 0$ leaving

$$-\frac{4N}{b}\frac{d^2\bar{w}}{d\eta^2} = p_0 g(\eta) \quad [12b]$$

whose solution is given as

$$-\bar{w}(\eta) = \frac{p_0 b}{4N}\int\int g(\eta)d\eta d\eta + A + B\eta \quad [13]$$

For the case of uniform pressure, $\bar{w}(\eta)$ must be an even function which implies $B = 0$; if further, for example, $\bar{w}(\pm 1) = 0$ for zero deflection on the boundary

$$\bar{w}(\eta) = \frac{p_0 b}{8N}(1-\eta^2) = \bar{w}(0)[1-\eta^2] \quad [14]$$

where

$$\bar{w}(0) = \frac{p_0 b}{8N} \quad \text{or} \quad N = \frac{p_0 b}{8\bar{w}(0)} \quad [15]$$

From Equation [14] $(d\bar{w}/d\eta)^2$ can be calculated easily and substituted into Equation [11a] yielding

$$\frac{d\bar{v}}{d\eta} = \frac{1+\nu}{2}\alpha T_0 f(\eta) + \frac{1-\nu^2}{16}\frac{p_0 b}{hE_0 s(\eta)}\frac{1}{\bar{w}(0)} - 4\bar{w}^2(0)\eta^2$$

From which, in this case where v must be an odd function, and for constant temperature[8]

$$\bar{v}(\eta) = \left[\frac{1+\nu}{2}\alpha T_0 + \frac{1-\nu^2}{16}\frac{p_0 b}{E_0 h}\frac{1}{\bar{w}(0)}\right]\eta - \frac{4}{3}\bar{w}^2(0)\,\eta^3 \quad [16]$$

and upon requiring $\bar{v}(\pm 1) = 0$ there results the equation determining N or, by Equation [15], $\bar{w}(0)$ the central deflection

$$[\bar{w}^2(0) - (3/8)(1+\nu)\alpha T_0]\,\bar{w}(0) = \frac{3(1-\nu^2)}{64}\frac{p_0 b}{E_0 h} \quad [17]$$

or in an alternative form with

$$\Pi \equiv \frac{3(1-\nu^2)}{64}\frac{p_0 b^4}{E_0 h^4} = \frac{1}{256}\frac{p_0 b^4}{Dh} \quad [18]$$

$$\Theta \equiv \frac{3(1+\nu)}{8}\left(\frac{b}{h}\right)^2 \alpha T_0 \quad [19]$$

Then the central deflection is given by

$$[(w/h)^2 - \Theta](w/h) = \Pi \quad [17a]$$

In the absence of any heating, Equation [17] yields the known solution for the membrane

$$\left.\frac{w_0}{h}\right|_{T_0 = 0} = \Pi^{1/3} = \sqrt[3]{\frac{3(1-\nu^2)}{64}\frac{p_0 b^4}{E_0 h^4}} \quad [17b]$$

and in the absence of normal pressure, the thermal deflection is obtained as

[7] This fact also could be deduced directly for small deflection analysis by specializing the equation of equilibrium, $\partial N_y/\partial y + \partial N_{xy}/\partial x = 0$, to this case where $N_{xy} = 0$. Thus N_y is a constant and proportional to the difference between elastic and thermal strains.

[8] Other temperature distributions may be similarly handled and amount to replacing the uniform temperature T_0 by its average value over the width of the plate.

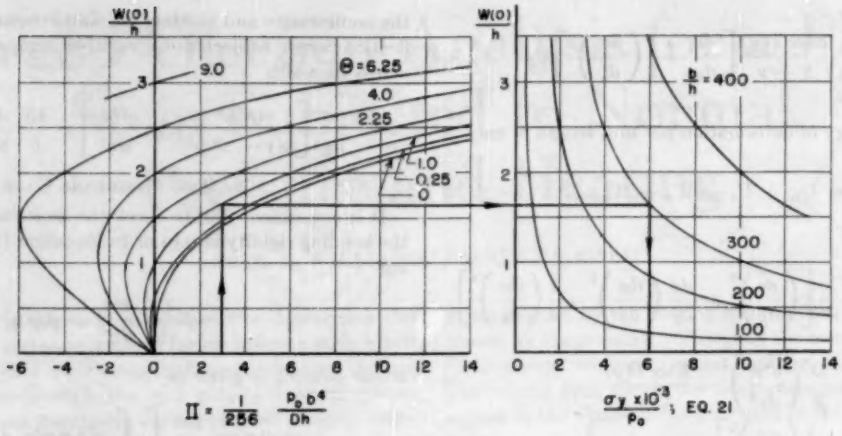

FIG. 1 MEMBRANE DEFLECTION AND STRESSES FOR COMBINED UNIFORM HEATING AND UNIFORM PRESSURE

$$\left.\frac{w_0}{h}\right|_{p_0=0} = \Theta^{1/2} = \frac{b}{h}\sqrt{\frac{3(1+\nu)}{8}\,\alpha T_0} \quad \ldots\ldots [17c]$$

The membrane deflection for combined uniform heating and uniform pressure is given in Fig. 1.

From a knowledge of the deflection functions, the membrane stress can be computed from the general two-dimensional relation

$$\sigma_y = \frac{E}{1-\nu^2}\left[\epsilon_y + \nu\epsilon_x\right] - \frac{E\alpha T}{1-\nu} \quad \ldots\ldots [20]$$

which for the case of an infinite strip becomes

$$\sigma_y = \frac{2E}{1-\nu^2}\left[\bar{v}' + \bar{w}'^2\right] - \frac{E\alpha T}{1-\nu} = \frac{N}{h} \quad \ldots\ldots [20a]$$

wherein the constant N is identified with the constant membrane stress σ_y by comparison with Equation [11a]. For the case where the pressure is also a constant, by Equations [15] and [17]

$$\sigma_y = \frac{1}{8}\frac{p_0 b}{\bar{w}(0)h} = \frac{8}{3}\frac{E}{1-\nu^2}\left[\bar{w}^2(0) - \frac{3}{8}(1+\nu)\,\alpha T_0\right] \quad \ldots [21]$$

which from Equation [17c] can be expressed

$$\sigma_y = \frac{8}{3}\frac{E_0}{1-\nu^2}\left[\bar{w}^2(0) - \bar{w}^2(0)\big|_{p_0=0}\right] \quad \ldots\ldots [21a]$$

indicating the expected fact that, in the absence of a pressure, no stress accompanies the thermal expansion. If there is no heating, the known result for the membrane stress is obtained

$$\sigma_y = \frac{8}{3}\frac{E_0}{1-\nu^2}\left[\frac{3(1-\nu^2)}{64}\frac{p_0 b}{E_0 h}\right]^{2/3} \quad \ldots\ldots [21b]$$

The membrane stress is also plotted as a function of temperature and pressure in Fig. 1.

THE THICK PLATE

In contrast to the limit results obtained for the membrane in which $(h/b) \to 0$, the other limit case when $(h/b) \to \infty$ yields the usual beam equation

$$\frac{d^2}{d\eta^2}\left[\frac{4E_0h^3}{3(1-\nu^2)b^3}\,g(\eta)\,\frac{d^2\bar{v}}{d\eta^2}\right] = p_0 g(\eta) \quad \ldots\ldots [12c]$$

where, for a constant-thickness plate, the temperature effect shows up only as a variable modulus.

In the case of constant temperature and pressure, elementary analysis yields the deflection for clamped edges

$$\bar{w}(\eta) = \frac{1-\nu^2}{32}\frac{p_0 b^3}{E_0 h^3}(1-\eta^2)^2 = \bar{w}(0)[1-\eta^2]^2 \quad \ldots [22]$$

$$\bar{v}(\eta) = 16\left[\frac{1-\nu^2}{32}\frac{p_0 b^3}{E_0 h^3}\right]^2\left[\frac{8}{105}\eta - \frac{1}{3}\eta^3 + \frac{2}{5}\eta^5 - \frac{1}{7}\eta^7\right] \quad \ldots\ldots [23]$$

and for simply supported edges

$$\bar{w}(\eta) = \frac{1-\nu^2}{32}\frac{p_0 b^3}{E_0 h^3}(5-\eta^2)(1-\eta^2) = \frac{1}{5}\bar{w}(0)\,[5-\eta^2][1-\eta^2] \quad \ldots\ldots [24]$$

$$\bar{v}(\eta) = 16\left[\frac{1-\nu^2}{32}\frac{p_0 b^3}{E_0 h^3}\right]^2\left[\frac{68}{35}\eta - 3\eta^3 + \frac{6}{5}\eta^5 - \frac{1}{7}\eta^7\right] \quad \ldots\ldots [25]$$

where the normal deflection is linear with pressure in contrast with the cubic dependence in the case of the membrane.

THE THIN PLATE

For plates whose membrane stresses cannot be neglected, it is necessary to integrate the complete Equation [12a] whose complexity is equivalent to that encountered in analyzing beams of varying flexural rigidity. In principle, however, the equation can still be handled quite easily.

In particular, for the case when the modulus is taken as constant over the width of the plate, Equation [12a] may be written

$$\frac{d^4\bar{w}}{d\eta^4} - 6\left(\frac{b}{h}\right)^2\frac{N(1-\nu^2)}{2E_0h}\frac{d^2\bar{w}}{d\eta^2} = \frac{3(1-\nu^2)}{4}\frac{p_0 b^3}{E_0 h^3}\,g(\eta)$$

or denoting for simplicity

$$\Lambda^2 \equiv 6\left(\frac{b}{h}\right)^2\frac{N(1-\nu^2)}{2E_0h} = \left(\frac{b}{2}\right)^2\frac{N}{D} \quad \ldots\ldots [26]$$

write

$$\frac{d^4\bar{w}}{d\eta^4} - \Lambda^2\frac{d^2\bar{w}}{d\eta^2} = 16\,\frac{h}{b}\,\Pi g(\eta) \quad \ldots\ldots [12d]$$

The characteristic solution for the deflection therefore is seen to

TABLE 1 QUANTITIES FOR TWO BOUNDARY CONDITIONS

	Clamped edges	Simply supported edges
γ_1	$1 - \frac{2 \coth \Lambda}{\Lambda}$	$1 - \frac{2}{\Lambda^2}$
γ_2	$\frac{2}{\Lambda \sinh \Lambda}$	$\frac{2}{\Lambda^2 \cosh \Lambda}$
$F^2(\Lambda)$	$1 + \frac{6}{\Lambda^2} - \frac{9 \coth \Lambda}{2\Lambda} - \frac{3}{2} \operatorname{csch}^2 \Lambda$	$1 - \frac{6}{\Lambda^2} + \frac{15}{2} \frac{\tanh \Lambda}{\Lambda^3} - \frac{3}{2} \frac{\operatorname{sech}^2 \Lambda}{\Lambda^2}$
$\frac{w(0)}{h}$	$\frac{8\Pi}{\Lambda^2}\left[1 + \frac{2(1 - \cosh \Lambda)}{\Lambda \sinh \Lambda}\right]$	$\frac{8\Pi}{\Lambda^2}\left[1 - \frac{2}{\Lambda^2}(1 - \operatorname{sech} \Lambda)\right]$
$\lim_{\Lambda \to 0} F^2(\Lambda)$	$\frac{2}{315}\Lambda^4$	$\frac{17}{105}\Lambda^4$
$\lim_{\Lambda \to \infty} F^2(\Lambda)$	1 (membrane case)	1 (membrane case)
$\lim_{\Lambda \to \infty} w(0)/h$	$\frac{8\Pi}{\Lambda^2} = \left[\Theta + \frac{1}{8}\Lambda^2\right]^{1/2} = \left[\Theta + \frac{\Pi}{w(0)/h}\right]^{1/2}$; by Equation [30]	

depend upon the sign of N (or Λ^2), which by Equation [11a] is determined by the amount of heating. For a fixed temperature rise sufficient to cause buckling but with no applied pressure, the membrane stress is compressive ($\Lambda^2 < 0$), giving trigonometric-type solutions. As the pressure is increased inducing tension, the net compressive stress is reduced, passing through zero ($\Lambda = 0$), and eventually resulting in a net tension ($\Lambda^2 > 0$) producing the characteristic hyperbolic functions. The important simplification is, of course, that N, or Λ^2, is a constant,[9] independent of the temperature or pressure variations, thus making Equation [12d] a linear equation.

For the case of uniform pressure, $g(\eta) = 1$, the solution for the tension range ($\Lambda^2 > 0$) can be written

$$\bar{w}(\eta) = -\frac{8}{\Lambda^2}\frac{h}{b}\Pi\eta^2 - \frac{k_2}{\Lambda^2}\eta + k_3 + k_4 \cosh \Lambda\eta + k_5 \sinh \Lambda\eta \quad \ldots\ldots [27]$$

which contains five unknowns k_2, k_3, k_4, k_5, and Λ. The sixth unknown is introduced after substituting Equation [27] into [11a] and integrating for $\bar{v}(\eta)$. In any given case three boundary conditions will be specified at each edge, $\eta = \pm 1$; two on the deflection w, and one on the displacement v. Solutions for the compression range are obtained by formally replacing Λ by $i\Lambda$. All the pertinent functions of the argument $i\Lambda$ are real, however.

Specific Edge Conditions

As a matter of calculation convenience as well as to simplify presentation of the results, the work is carried out in terms of the membrane quantities Π, Equation [18], and Θ, Equation [19]. The first is a nondimensional pressure, which, as can be seen from Equation [17b], is the cube of the membrane deflection in the absence of heating. The second is a nondimensional heating parameter, which from Equation [17c] is equal to the square of the membrane deflection due to temperature alone.[10]

[9] H. M. Berger has found this same thing occurring in his approximate treatment of finite aspect-ratio plates under normal pressure. See, "A New Approach to the Analysis of the Large Deflections of Plates," Calif. Inst. of Tech., PhD thesis, 1954.

[10] For qualitative interpretation of the figures, $|\Theta|^{1/2}$ may be thought of as a measure of deflection in plate thicknesses due to heating or cooling. For the membrane, of course, the interpretation is precise by Equation [17c].

For uniform temperature and pressure (see the Discussion for comments relating to possible antisymmetric deflection modes in the compression range)

$$\frac{w(\eta)}{h} = \frac{8\Pi}{\Lambda^2}\left[\gamma_1 - \eta^2 + \gamma_2 \cosh \Lambda\eta\right] \quad \ldots\ldots [28]$$

Equation [28] is next inserted into Equation [11a] to determine the displacement as

$$\bar{v}(\eta) = \frac{4}{3}\left(\frac{h}{b}\right)^2\left[\Theta + \frac{1}{8}\Lambda^2\right]\eta - \left(\frac{8\Pi}{\Lambda^2}\right)^2 \left\{\frac{4}{3}\eta^3 - \frac{4}{\Lambda}\gamma_2[\Lambda\eta \cosh \Lambda\eta - \sinh \Lambda\eta] + \frac{\Lambda\gamma_2^2}{4}[\sinh 2\Lambda\eta - 2\Lambda\eta]\right\} \quad \ldots\ldots [29]$$

Requiring $v(\pm 1) = 0$ leads to the following transcendental equation for determining Λ when the pressure, temperature, and geometry of the plate are prescribed

$$\Theta + \frac{1}{8}\Lambda^2 = \frac{64\Pi^2}{\Lambda^4}F^2(\Lambda) \quad \ldots\ldots [30]$$

The quantities pertaining to the two boundary conditions selected for analysis are given in Table 1.

The calculations for the membrane stress and central deflection are most conveniently carried out by the following steps:

1 Compute $F^2(\Lambda)$ versus Λ from Table 1.
2 Compute Π for given Λ and Θ from Equation [30].
3 Plot Λ^2 versus Π with parameter Θ.
4 Compute $w(0)$ from Table 1 using the previous step 3.

The calculations are quite sensitive to Λ and involve careful limiting processes especially for Λ in the neighborhood of 0, ∞, and zeros of the trigonometric functions. $F^2(\Lambda)$ and $F^2(i\Lambda)$ are given in Tables 2 and 3 and Fig. 2 for the two boundary conditions.

The membrane stress and central deflection for various combinations of temperature and pressure are given in Figs. 3 to 6.

Combined Stress

For any case but the membrane, the bending and middle-plane

TABLE 2 CLAMPED EDGES

Λ	$F^2(\Lambda)$	Λ	$F^2(i\Lambda)$
0.5	0.00037787	1.0	0.007806
1.0	0.0052493	1.5	0.053602
1.5	0.021447	2.0	0.28444
2.0	0.052011	2.5	1.83252
2.5	0.094615	2.6	2.88004
3.0	0.14427	2.7	4.86376
3.5	0.19535	2.8	9.08103
4.0	0.24724	2.9	20.19523
4.5	0.29532	3.0	63.12526
5.0	0.33965	π	∞
5.5	0.38004	3.2	464.67028
6.0	0.41663	3.3	69.26236
		3.4	28.45890
		3.5	16.13379
		3.7	7.99366
		4.0	4.21558
		4.5	2.48911
		5.0	2.12504
		5.5	2.99313
		5.7	4.56483
		6.0	17.46910
		2π	∞

NOTE: The foregoing values are based on the tabulation by Shaw, Pohle, and Perrone.[2]

TABLE 3 SIMPLY SUPPORTED EDGES

Δ	$F^2(\Lambda)$	Λ	$F^2(i\Lambda)$
0.5	0.00859	0.50	0.01259
1.0	0.08196	0.75	0.08600
1.5	0.22428	1.00	0.45781
2.0	0.37726	1.25	2.93815
2.5	0.50719	1.50	105.66492
3.0	0.60809	$\pi/2$	∞
3.5	0.68436	1.75	26.10120
4.0	0.74085	2.00	6.71386
4.5	0.78594	2.25	3.75349
5.0	0.81999	2.50	2.69251
5.5	0.84673	3.00	1.87632
6.0	0.86805	3.50	1.56387
		4.00	1.45875
		4.50	2.58145
		4.70	448.61348
		$3\pi/2$	∞
		4.8	10.53154
		5.0	2.18959
		5.5	1.34194
		6.0	1.21322
		6.5	1.17326
		7.0	1.15726
		7.5	1.18807
		7.7	1.98296
		$5\pi/2$	∞

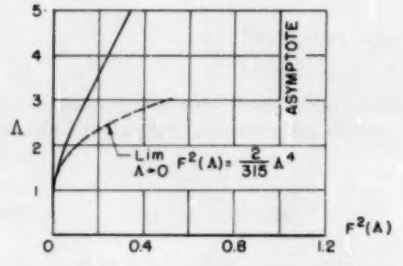

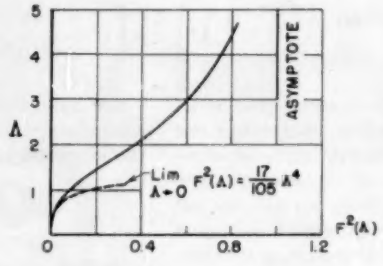

FIG. 2(a) (*left*) CLAMPED CASE

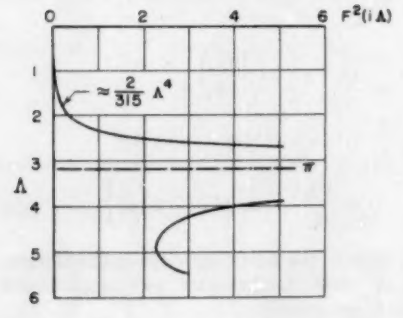

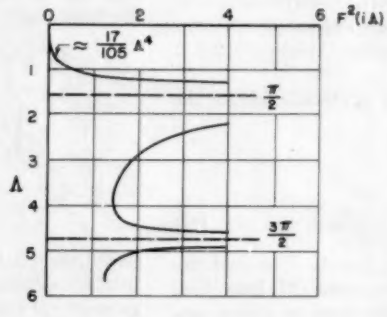

FIG. 2(b) (*right*) SIMPLY SUPPORTED CASE

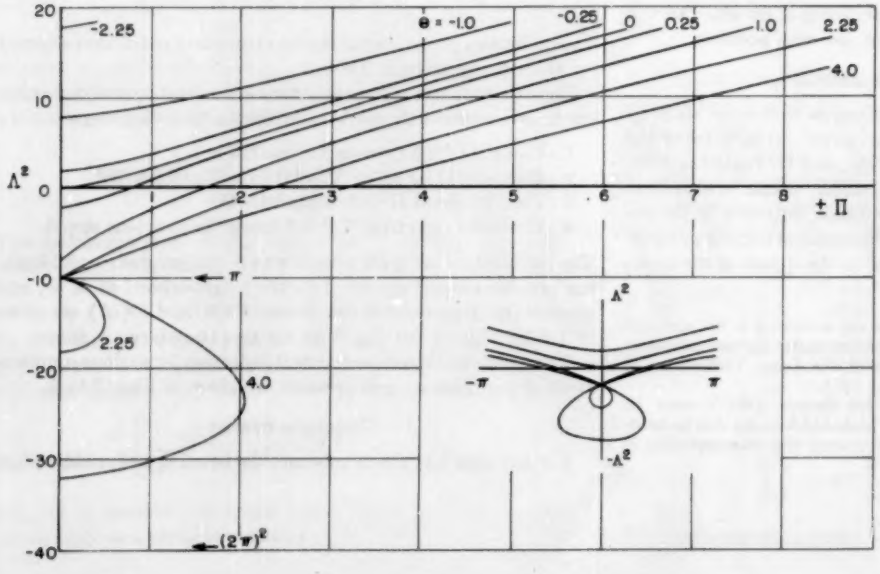

FIG. 3 MEMBRANE STRESS, CLAMPED EDGES

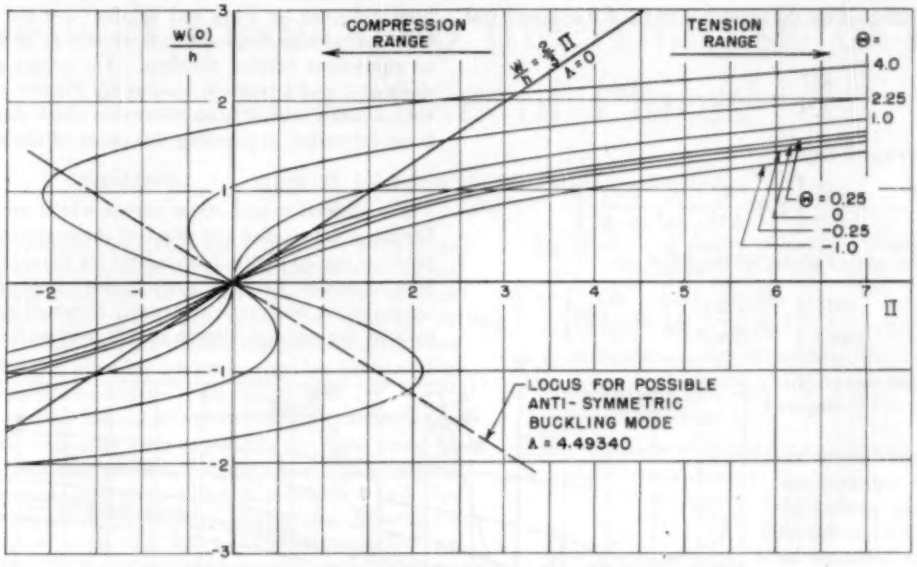

FIG. 4 CENTRAL DEFLECTION, CLAMPED EDGES

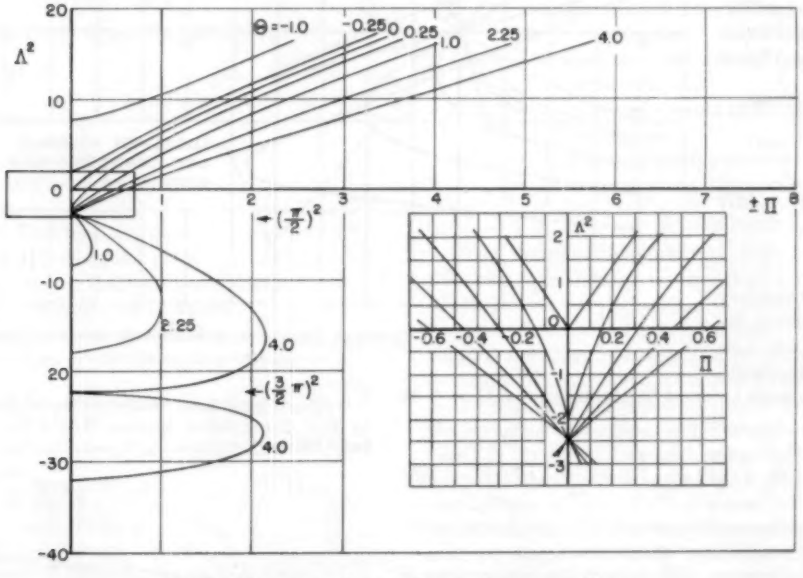

FIG. 5 MEMBRANE STRESS, SIMPLY SUPPORTED EDGES

stresses must be combined to obtain the total surface stresses from the usual relations

$$\left.\begin{aligned}\sigma_b \pm \sigma_m &= 6M_y/h^2 \pm N/h \\ &= -\frac{6D}{h^2}\frac{4}{b}\,\bar{w}'' \pm \frac{4D}{b^2h}\Lambda^2 \\ &= \frac{4D}{b^2h}\left\{\frac{48\Pi}{\Lambda^2}\left[2 - \gamma_2\Lambda^2\cosh\Lambda\eta\right] \pm \Lambda^2\right\}\end{aligned}\right\} \quad . . [31]$$

and can be easily computed for either of the two cases shown in the figures.

DISCUSSION OF THE RESULTS

It should be observed in Figs. 4 and 6 that the deflection is multivalued with each position representing an equilibrium position for the plate. As these points lie in the compression range they are not all necessarily stable. Indeed, there is also the possibility of antisymmetric buckling modes. That is, to say, in the compression range (when Λ is replaced by $i\Lambda$), Equation [27] admits of solutions for which k_2 and k_3 are not necessarily zero, providing Λ is an (antisymmetric) eigenvalue of

clamped edges

$$\Lambda \cot \Lambda = 1 \quad \ldots\ldots [32]$$

simply supported edges

$$\sin \Lambda = 0 \quad \ldots\ldots [33]$$

In these cases then the eigenvalue, say Λ^*, may be calculated and application of the boundary conditions at the edges leads to the following expressions for the deflection: It should be observed that the value of the central deflection, Equation [27] evaluated

at $y = 0$, is not affected by the existence of the antisymmetrical mode and is still

$$\frac{w(0)}{h} = -\frac{8\Pi}{\Lambda^{*2}}\left[\gamma_1(i\Lambda^*) + \gamma_2(i\Lambda^*)\right] \quad [34]$$

Specifically for clamped edges

$$\frac{w(0)}{h} = -\frac{8\Pi}{\Lambda^{*2}}\left[1 + \frac{2}{\Lambda^{*2}} - \frac{2}{\Lambda^* \sin \Lambda^*}\right] \quad [35]$$

and for simply supported edges, where $\Lambda^* = n\pi$

$$\frac{w(0)}{h} = -\frac{8\Pi}{(n\pi)^2}\left\{1 + \frac{2}{(n\pi)^2}\left[1 - (-1)^n\right]\right\} \quad [36]$$

These two loci are shown graphically in Figs. 4 and 6, respectively.

Inasmuch as the distinguishing features of the antisymmetrical modes do not show up in these figures, it is convenient to illustrate its behavior by using the case when the edges are simply supported. The lowest antisymmetric deflection mode in the compression range, valid when $\Lambda = \Lambda^* = \pi$

$$\begin{aligned} \bar{w}(\eta)_{\text{odd}} &= \bar{w}(\eta) - \bar{w}(\eta)_{\text{even}} \\ &= \bar{w}(\eta) + \frac{8\Pi}{\pi^2}\left[1 - \eta^2 + \frac{2(1 + \cos \pi\eta)}{\pi}\right] \quad [37] \\ &= k_3 \sin \pi\eta \end{aligned}$$

after evaluating the boundary conditions on the lateral deflection. The amplitude constant k_3 which is a maximum one fourth across the span is found by requiring $v(\pm 1) = 0$ in the usual manner

$$k_3 = \pm \frac{h}{b}\left\{\frac{8}{3\pi^2}\left[\Theta - \frac{\pi^2}{8} - \frac{64}{\pi^4}\left(1 + \frac{15}{2\pi^2}\right)\Pi^2\right]\right\}^{1/2} \quad [38]$$

This antisymmetric maximum deflection $\bar{w}(1/2)_{\text{odd}} = k_3$ is shown in Fig. 7 as a function of temperature and pressure.

It is evident from Equation [38] that if the temperature is fixed, the antisymmetric contribution to the complete deflection $\bar{w}(\eta)$ vanishes for pressures greater than a critical value of Π. It may be recognized, however, that Equation [38] is no more than Equation [30] evaluated at $i\Lambda^*$, meaning, of course, that $k_3 = 0$ at the precise value of Π corresponding to the even or symmetrical deflection mode at the prescribed value of the temperature Θ. The odd solution thus degenerates into the even solution at the intersection of the locus line of Fig. 6 at the selected temperature.

Stated in an alternative manner, there is a bifurcation point as the pressure is reduced to negative values maintaining the temperature constant; a bifurcation point is approached where at $\Lambda = \Lambda^*$ the plate may reach zero central deflection by going into an antisymmetrical mode at constant stress Λ^* or remaining in a symmetrical mode as the stress increases. These two possibilities are also illustrated in Fig. 7.

The matter of which path is taken is a stability question rather than one of equilibrium and will not be discussed here. In this latter connection, however, a very similar stability problem has been discussed by Fung and Kaplan[11] for the case of a buckled arch having edge displacements which can be treated in terms of an equivalent heating problem. The report analyzes mainly a sinusoidal and a uniform loading by Fourier series solution and also contains several basic references which should be of value to those interested in pursuing this phase of the problem further.

Conclusion

The deflection and stress curves which are presented should furnish a measure of the effect of thermal heating or cooling on pressure loaded plates, particularly for those of high aspect ratio. The extension to finite aspect-ratio plates is not particularly amenable to analytical treatment although as a temporary expedient the usual minimum energy approach can be applied.

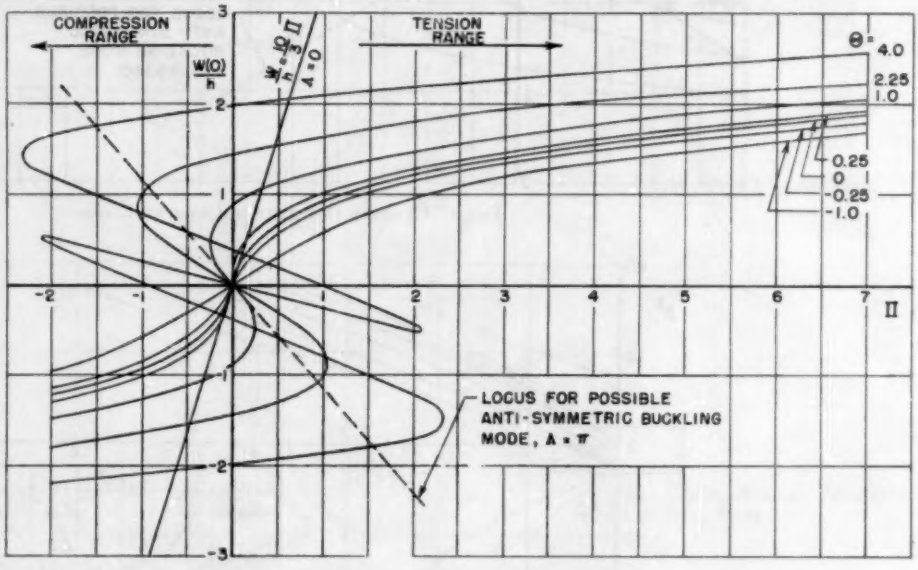

Fig. 6 Central Deflection, Simply Supported Edges

[11] "Buckling of Low Arches or Curved Beams of Small Curvature," by Y. C. Fung and A. Kaplan, NACA Technical Note 2840, November, 1952.

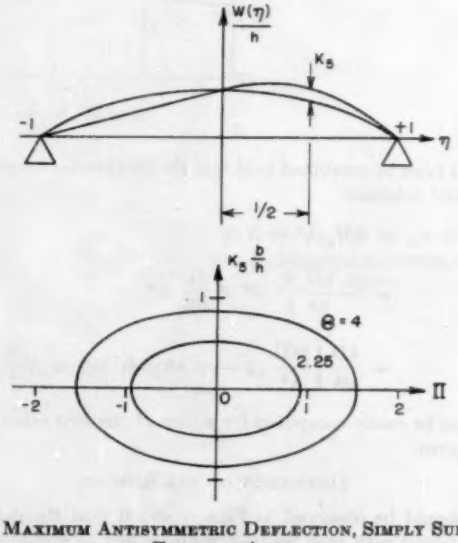

Fig. 7 Maximum Antisymmetric Deflection, Simply Supported Ends and $\Lambda = \pi$

A New Approach to the Analysis of Large Deflections of Plates[1]

By H. M. BERGER,[2] WASHINGTON, D. C.

Simplified nonlinear equations for a flat plate with large deflections are derived by assuming that the strain energy due to the second invariant of the middle-surface strains can be neglected. Computations using the solution of these simplified equations are carried out for the deflection of uniformly loaded circular and rectangular plates with various boundary conditions. Comparisons are made with available numerical solutions of the exact equations. The deflections found by this approach are then used to obtain the stresses for the circular plate and the resulting stresses are compared with existing solutions. In all the cases where comparisons could be made, the deflections and stresses agree with the exact solutions within the accuracy required for engineering purposes.

Nomenclature

The following nomenclature is used in the paper:

D = bending rigidity $= \dfrac{Eh^3}{12(1-\nu^2)}$

E = modulus of elasticity

R = radius of circular plate

U = strain energy

a = half-width of rectangular plate

b = half-length of rectangular plate

e = first invariant of middle-surface strains $= \epsilon_x + \epsilon_y$ in rectangular co-ordinates $= \epsilon_r + \epsilon_\theta$ in cylindrical co-ordinates

e_2 = second invariant of middle-surface strains $= \epsilon_x\epsilon_y - \dfrac{1}{4}\gamma_{xy}^2$ in rectangular co-ordinates $= \epsilon_r\epsilon_\theta$ in cylindrical co-ordinates when there is circular symmetry

h = thickness of plate

q = intensity of uniform load

r, θ, z = cylindrical co-ordinates

u, v = displacements in plane of plate (extensions)

w = deflection of plate in z-direction

x, y, z = rectangular co-ordinates

γ_{xy} = shearing strains of middle surface in rectangular co-ordinates $= \dfrac{\partial u}{\partial y} + \dfrac{\partial v}{\partial x} + \dfrac{\partial w}{\partial x}\dfrac{\partial w}{\partial y}$

ϵ_x, ϵ_y = unit elongation of middle surface in x and y-directions $\epsilon_x = \dfrac{\partial u}{\partial x} + \dfrac{1}{2}\left(\dfrac{\partial w}{\partial x}\right)^2$; $\epsilon_y = \dfrac{\partial v}{\partial y} + \dfrac{1}{2}\left(\dfrac{\partial w}{\partial y}\right)^2$

$\epsilon_r, \epsilon_\theta$ = radial and tangential unit elongations of middle surface $\epsilon_r = \dfrac{du}{dr} + \dfrac{1}{2}\left(\dfrac{dw}{dr}\right)^2$; $\epsilon_\theta = \dfrac{u}{r}$

ν = Poisson's ratio

σ_x, σ_y = normal components of membrane stresses in rectangular co-ordinates

σ_x', σ_y' = normal components of bending stresses in rectangular co-ordinates

σ_r, σ_θ = normal components of membrane stresses in cylindrical co-ordinates

$\sigma_r', \sigma_\theta'$ = normal components of bending stresses in cylindrical co-ordinates

τ_{xy} = membrane shearing stress in rectangular co-ordinates

τ_{xy}' = bending shearing stress in rectangular co-ordinates

Introduction

If the deflection of a plate is of the order of magnitude of its thickness, the differential equations for the deflection and the displacements can be written in terms of one fourth-order and two second-order nonlinear equations. These three equations are coupled together, and solutions of them are difficult to obtain. Several techniques have been used to solve them. For example, S. Levy (1, 2, 3)[3] substituted a double Fourier series solution into the equations for rectangular plates and evaluated the coefficients. Chi-Teh Wang (4, 5) wrote the equations for rectangular plates in a finite-difference form and solved them by the method of successive approximations. S. Way solved the circular-plate equations by substituting a power series into the differential equations (6) and the rectangular-plate equations by substituting a finite-power-series solution into the energy expression, determining the coefficients by setting the first variation of the strain energy equal to the first variation of the potential energy due to the external loading for any variation of each of the coefficients (7).

The purpose of the present investigation is to develop a simple and yet sufficiently accurate method for determining the deflections of plates when that deflection is of the order of magnitude of the thickness. The approach used in the following analysis is to investigate the effect of neglecting the strain energy due to the second invariant of the strains in the middle surface of the plate when deriving the differential equations by energy methods. The resulting differential equations are still nonlinear, but they can be decoupled in such a manner that they may be solved readily. These equations hereafter will be referred to as the approximate equations.

To solve the problem of large deflections of plates completely,

[1] The results presented in this paper are taken from a thesis of the same title submitted in May, 1954, in partial fulfillment of the requirements for the degree of Doctor of Philosophy from the California Institute of Technology, Pasadena, Calif.

[2] Mechanics Branch, Office of Naval Research; formerly, U. S. Naval Ordnance Test Station, Pasadena, Calif.

Presented at the West Coast Conference of the Applied Mechanics Division, Monterey, Calif., September 12–13, 1955, of The American Society of Mechanical Engineers.

Discussion of this paper should be addressed to the Secretary, ASME, 29 West 39th Street, New York, N. Y., and will be accepted until January, 10, 1956, for publication at a later date. Discussion received after the closing date will be returned.

Note: Statements and opinions advanced in papers are to be understood as individual expressions of their authors and not those of the Society. Manuscript received by West Coast Committee of the ASME Applied Mechanics Division, March 7, 1955. Paper No. 55—APM-36.

[3] Numbers in parentheses refer to the Bibliography at the end of the paper.

an estimate of the membrane stresses must be made. This can be done by assuming that the deflection is equal to that given by the solution to the approximate equations and substituting this deflection into the strain-energy integral. The strain energy is then a function of the displacements only and, by the principle of virtual displacements, differential equations can be derived for these displacements. These differential equations are linear, however, and can be solved readily. Knowing these displacements as well as the deflection enables one to approximate the membrane stresses.

The first part of this paper is devoted to the derivation of the approximate differential equations that are used to find the deflection, while the second part of this paper outlines the technique for determining stresses once the deflection is given.

The first part of the Appendix gives solutions for circular plates with uniform loading. The deflections for these cases are compared with available solutions of the exact equations. In the second part of the Appendix, deflections are found for rectangular plates with all edges simply supported and with two edges simply supported and two edges clamped. Aspect ratios of 1, 1.5, 2, and infinity are considered. The agreement with results obtained by considering the complete equations is studied. In the third part of the Appendix, stress calculations are carried out for the clamped circular plate.

The comparison of the results with available exact solutions shows good agreement for all cases where comparisons were possible. The amount of computational effort necessary to find deflections and stresses is considerably less than that required by other methods that have been used in the past.

Derivation of Equations

The standard energy expression for plates with large deflections written in terms of the deflection and the strain of the middle surface is (8)

$$U = \frac{D}{2}\int\int\left\{\left[(\nabla^2 w)^2 + \frac{12}{h^2}e^2\right] - 2(1-\nu)\left[\frac{12}{h^2}e_2 + \frac{\partial^2 w}{\partial x^2}\frac{\partial^2 w}{\partial y^2} - \left(\frac{\partial^2 w}{\partial x \partial y}\right)^2\right]\right\} dx\,dy \quad [1]$$

It is the intent of this investigation to develop a simplified analysis for finding the deflection of plates when that deflection is large enough so that the strain of the middle surface cannot be neglected. To do this we would like to neglect terms in the differential equations that will be derived from Equation [1] which do not affect appreciably the solution for the deflection with the hope that neglecting these terms will materially simplify the ensuing analysis.

Examination of some available exact solutions for the deflection of uniformly loaded plates, such as S. Way's solution for the clamped circular plate (6), leads us to surmise that the terms in the differential equations arising from the second strain invariant of the middle-surface strains e_2 in Equation[1] do not influence appreciably the solution for the deflection. Consequently, as a working hypothesis, the first variation of e_2 is neglected when deriving the differential equations. At the present time there appears to be no completely satisfactory simple physical justification for this approximation, so its justification must be based on comparisons of the resulting approximate solutions with available exact solutions for the deflection.

A feeling for the nature of the approximation can be obtained by noting that the variation with Poisson's ratio ν in the resulting differential equations is confined to the bending rigidity D. Thus the approximation can be interpreted as neglecting part of the variation of the deflection caused by a change in ν. However, any variation with ν arising from the bending rigidity and the boundary conditions will still be present in the proposed solution for the deflection. This will be demonstrated later when studying simply supported circular plates.

Using the afore-mentioned assumption, the strain energy written in terms of the displacements and the deflection is obtained from Equation [1] as

$$U = \frac{D}{2}\int\int\left\{(\nabla^2 w)^2 + \frac{12}{h^2}\left[\frac{\partial u}{\partial x} + \frac{\partial v}{\partial y} + \frac{1}{2}\left(\frac{\partial w}{\partial x}\right)^2 + \frac{1}{2}\left(\frac{\partial w}{\partial y}\right)^2\right]^2 - 2(1-\nu)\left[\frac{\partial^2 w}{\partial x^2}\frac{\partial^2 w}{\partial y^2} - \left(\frac{\partial^2 w}{\partial x \partial y}\right)^2\right]\right\} dx\,dy \quad [2]$$

An application of the principle of virtual work then gives the following equations

$$\frac{\partial e}{\partial x} = 0;\ \frac{\partial e}{\partial y} = 0 \quad [3]$$

$$\nabla^4 w - \frac{12}{h^2}\left[\frac{\partial}{\partial x}\left(e\frac{\partial w}{\partial x}\right) + \frac{\partial}{\partial y}\left(e\frac{\partial w}{\partial y}\right)\right] = \frac{q}{D} \quad [4]$$

from which integration of Equation [3] gives the interesting result that the first (two-dimensional) strain invariant is a constant[4]

$$e \equiv \frac{\partial u}{\partial x} + \frac{\partial v}{\partial y} + \frac{1}{2}\left(\frac{\partial w}{\partial x}\right)^2 + \frac{1}{2}\left(\frac{\partial w}{\partial y}\right)^2 = \frac{\alpha^2 h^2}{12} \quad [5]$$

where α is a normalized constant of integration. Substituting Equation [5] into [4] gives

$$\nabla^4 w - \alpha^2 \nabla^2 w = \frac{q}{D} \quad [6]$$

Equations [5] and [6] are the approximate equations that will be used to determine the deflection of the rectangular plate.

Owing to the constant of integration α the equations retain their essential nonlinearity, but they have been decoupled so that it is possible to solve Equation [6] for w since it is linear in w, and then use this solution in Equation [5] which is linear in u and v to determine α.

In the case where there is circular symmetry, the transformation of the invariants into polar co-ordinates leads immediately to

$$e \equiv \frac{du}{dr} + \frac{u}{r} + \frac{1}{2}\left(\frac{dw}{dr}\right)^2 = \frac{\alpha^2 h^2}{12} \quad [7]$$

$$\left(\frac{d^2}{dr^2} + \frac{1}{r}\frac{d}{dr}\right)\left(\frac{d^2 w}{dr^2} + \frac{1}{r}\frac{dw}{dr} - \alpha^2 w\right) = \frac{q}{D} \quad [8]$$

The foregoing equations contain all the essential features of those for the rectangular plates, but since they are ordinary differential equations, they can be studied more easily.

Determination of Stresses

The deflection as found from Equation [6] or [8] can be used to determine the bending stresses at the surface of the plate which, for the rectangular plate, are given by

$$\sigma_x' = -\frac{6D}{h^2}\left(\frac{\partial^2 w}{\partial x^2} + \nu\frac{\partial^2 w}{\partial y^2}\right) \quad [9]$$

$$\sigma_y' = -\frac{6D}{h^2}\left(\frac{\partial^2 w}{\partial y^2} + \nu\frac{\partial^2 w}{\partial x^2}\right) \quad [10]$$

$$\tau_{xy}' = -\frac{6D}{h^2}(1-\nu)\frac{\partial^2 w}{\partial x \partial y} \quad [11]$$

[4] It should be observed that this fact is consistent with the results for the exact solution for the infinite strip as obtained in (11) and (17).

and, for the circular plate, are given by

$$\sigma_r' = -\frac{6D}{h^2}\left(\frac{d^2w}{dr^2} + \frac{\nu}{r}\frac{dw}{dr}\right) \quad [12]$$

$$\sigma_\theta' = -\frac{6D}{h^2}\left(\nu\frac{d^2w}{dr^2} + \frac{1}{r}\frac{dw}{dr}\right) \quad [13]$$

For the circular plate, for example, it is possible to determine the displacement of the middle surface from Equation [7] once the deflection is known; but one should expect the membrane stresses computed from this displacement to be very inaccurate because the deflection and displacement do not satisfy the equilibrium equations. The error resulting from not satisfying equilibrium had little effect on the deflection, but we should expect it to have a large effect on the membrane stresses. In the case of the rectangular plate it is not even possible to determine the displacements in the plane of the plate uniquely, so it is immediately apparent that the technique used to find the deflection cannot be used to find the membrane stresses.

It is possible, however, to obtain a good approximation to the membrane stresses by using the approximate solution for the deflection. If it is assumed that the deflection is a known function (determined from the approximate equations), one can substitute that deflection into the strain-energy expression given in Equation [1]. Then the principle of virtual work, which holds for any variations of the displacements u and v, can be used to derive the appropriate differential equations for the displacements.

In the case of the rectangular plate the equations obtained in this manner are

$$\frac{\partial^2 u}{\partial x^2} + \frac{1-\nu}{2}\frac{\partial^2 u}{\partial y^2} + \frac{1+\nu}{2}\frac{\partial^2 v}{\partial x \partial y} = -\frac{\partial w}{\partial x}\left(\frac{\partial^2 w}{\partial x^2} + \frac{1-\nu}{2}\frac{\partial^2 w}{\partial y^2}\right) - \frac{1+\nu}{2}\frac{\partial w}{\partial y}\frac{\partial^2 w}{\partial x \partial y} \quad [14]$$

$$\frac{\partial^2 v}{\partial y^2} + \frac{1-\nu}{2}\frac{\partial^2 v}{\partial x^2} + \frac{1+\nu}{2}\frac{\partial^2 u}{\partial x \partial y} = -\frac{\partial w}{\partial y}\left(\frac{\partial^2 w}{\partial y^2} + \frac{1-\nu}{2}\frac{\partial^2 w}{\partial x^2}\right) - \frac{1+\nu}{2}\frac{\partial w}{\partial x}\frac{\partial^2 w}{\partial x \partial y} \quad [15]$$

where the right-hand side in each case is a known function of x and y. The equations, therefore, are linear equations in u and v and can be solved in a straightforward manner.

For the circular plate, the corresponding equation for the displacement u is

$$\frac{d^2u}{dr^2} + \frac{1}{r}\frac{du}{dr} - \frac{u}{r^2} = -\frac{1-\nu}{2r}\left(\frac{dw}{dr}\right)^2 - \frac{1}{2}\frac{d}{dr}\left[\left(\frac{dw}{dr}\right)^2\right] \quad [16]$$

where the right-hand side is a known function of r.

It can be noted that the foregoing three equations are the usual equilibrium equations in the middle plane of the plate. Consequently, the procedure that has been followed in this paper can be interpreted as finding a solution for the deflection that satisfies approximate equations of equilibrium in the plane of the plate and normal to the plane of the plate, and then using this deflection in the equilibrium equations for the plane of the plate to determine the displacements. With this procedure the potential energy is minimized under the assumption that the deflection is given by the approximate result.

Equations for stresses for both uniformly loaded circular plates and rectangular plates have been derived. However, the equations for rectangular plates were so cumbersome that they are not presented in this paper. If one is interested in them, they can be found in the thesis where this approach was initially presented. The proposed procedure for finding the stresses is amply illustrated by studying uniformly loaded circular plates as is done in the Appendix.

Discussion of Results

The approximation based on neglecting the second strain invariant in the strain-energy integral when deriving the differential equations is investigated in the Appendix for uniformly loaded circular and rectangular plates. Maximum deflections are computed for clamped and simply supported circular plates and simply supported and semiclamped rectangular plates. Membrane and bending stresses are computed for clamped circular plates. In all cases where comparisons were possible, good agreement with exact solutions was obtained. The amount of calculation necessary to determine the deflection or the stresses for any given problem is considerably less than that needed when the complete equations are solved. Consequently, this approximation enables one to carry out a simple analysis for plates where the combination of size and loading lies between those simple limit cases that can be analyzed by linear plate theory or membrane theory.

It was possible to check most of the computations carried out in the Appendix with available exact solutions. In the case of uniformly loaded clamped circular plates, it was possible to check the deflections for values of αR from zero to approximately 3.5 and for very large values of αR. For simply supported circular plates it was possible to check the deflection only for very small and very large values of αR. The deflections for uniformly loaded clamped rectangular plates were checked for values of αa from zero to approximately 5.5 and for very large values of αa. For semiclamped rectangular plates the deflections were checked only for very small and very large values of αa. In all these cases agreement was very good. For values of αR or αa other than those specified, no checks were possible. Consequently, the curves that are plotted in this paper for these unchecked values can be considered only as tentative solutions until checks are available to verify their accuracy or until a satisfactory physical interpretation of the approximation used in this paper is obtained.

It appears that no completely satisfactory simple physical interpretation can be given at this time to the approximation resulting from neglecting the second strain invariant. This problem is under investigation, but the results are not ready for presentation. Until some physical interpretation can be found for the approximation used in this paper, the real test of whether or not the proposed analysis will give a good approximation to the solution of any particular problem must be based on whether the deflection and stresses determined in this manner are a good approximation to their true values.

Acknowledgment

The author would like to express his appreciation to Prof. M. L. Williams for suggesting this problem and for his help and encouragement in carrying it through.

BIBLIOGRAPHY

1 "Bending of Rectangular Plates With Large Deflections," by S. Levy, NACA TR 737, 1942.

2 "Square Plate With Clamped Edges Under Normal Pressure Producing Large Deflections," by S. Levy, NACA TR 740, 1942.

3 "Bending With Large Deflections of a Clamped Rectangular Plate With Length-Width Ratio of 1.5 Under Normal Pressure," by S. Levy and S. Greenman, NACA TN 853, 1942.

4 "Non-Linear Large Deflection Boundary Value Problems of Rectangular Plates," by Chi-Teh Wang, NACA TN 1425, 1948.

5 "Bending of Rectangular Plates With Large Deflections," by Chi-Teh Wang, NACA TN 1462, 1948.
6 "Bending of Circular Plates With Large Deflections," by S. Way, Trans. ASME, vol. 56, 1934, p. 627.
7 "Uniformly Loaded, Clamped, Rectangular Plates With Large Deflections," by S. Way, Proceedings of the Fifth International Congress of Applied Mechanics, Cambridge, Mass., 1938, p. 123.
8 "Theory of Plates and Shells," by S. Timoshenko, McGraw-Hill Book Company, Inc., New York, N. Y., 1940, pp. 95 and 345.
9 Ibid., p. 60.
10 Ibid., p. 62.
11 Ibid., p. 5.
12 Ibid., p. 128.
13 "Tables of Functions," by E. Janke and F. Emde, Dover Publications, New York, N. Y., 1945, p. 145.
14 Ibid., p. 128.
15 Ibid., p. 138.
16 "Über den Spannungszustand in kreisrunden Platten mit verschwindender Biegungssteifigkeit," by H. Hencky, *Zeitschrift für Mathematik und Physik*, vol. 63, 1915, p. 311.
17 "The Non-Linear Deflection of Infinite Strip Plates," by F. S. Shaw, F. Pohle, and N. Perrone, PIBAL Report 255, June, 1953.
18 "Die Berechnung dünner rechtekiger Platten mit verschwindender Biegungssteifigkeit," by H. Hencky, *Zeitschrift für angewandte Mathematik und Mechanik*, vol. 1, 1921, p. 81.

Appendix

Circular Plates With Uniform Loading

Since the majority of exact solutions are for uniformly loaded plates, all approximate solutions are computed for uniformly loaded plates in order that the two may be compared. The solution to Equation [8] is

$$w = AJ_0(i\alpha r) + B - \frac{qr^2}{4D\alpha^2} \quad \ldots\ldots [17]$$

where J_0 is the Bessel function of the first kind of zero-order and A and B are arbitrary constants. The coefficient of the Bessel function of the second kind has been set equal to zero because w must be finite at the origin. Using Equation [17] and standard integrals of Bessel functions (13), Equation [7] can be integrated to get

$$u = \frac{\alpha^2 h^2}{24} r + \frac{A^2\alpha^2}{4} r\,[J_1^2(i\alpha r) - J_0(i\alpha r)J_2(i\alpha r)] - \frac{qAr}{2D\alpha^2} J_2(i\alpha r) - \frac{q^2 r^3}{32D^2\alpha^4} \quad \ldots [18]$$

where the constant of integration has been set equal to zero, so that u will be finite at the origin.

The equations for w and u contain three arbitrary constants, A, B, and α. A and B are determined from the boundary conditions on w, and then α is determined from the boundary condition on u. Thus we see that the approximate differential equations can be solved readily even with arbitrary boundary conditions. It remains to be seen, of course, whether the solutions given in Equations [17] and [18] are sufficiently close to the exact solutions to warrant use of the approximation necessary for their derivation.

In order to investigate the accuracy of the approximate solutions as well as to demonstrate the ease with which these solutions can be obtained, two boundary conditions on w are considered in the following analysis—clamped edges and simply supported edges. In both cases u is set equal to zero on the boundary.

Clamped Edges

Assuming that the edges of the plate are restrained from moving and fixed in such a manner that they cannot rotate, the boundary conditions are

$$\left.\begin{aligned} w(R) &= 0 \\ \left.\frac{dw}{dr}\right|_{r=R} &= 0 \\ u(R) &= 0 \end{aligned}\right\} \quad \ldots\ldots [19]$$

From the boundary conditions on w, one can solve for A and B. Doing this, Equation [17] becomes

$$w = \frac{qR^2}{4D\alpha^2}\left[\frac{2[J_0(i\alpha R) - J_0(i\alpha r)]}{i\alpha R J_1(i\alpha R)} + 1 - \left(\frac{r}{R}\right)^2\right] \quad \ldots [20]$$

and Equation [18] becomes

$$u = \frac{\alpha^2 h^2}{24} r - \frac{q^2 R^3 r}{16 D^2 \alpha^4}\left[\frac{J_1^2(i\alpha r) - J_0(i\alpha r)J_2(i\alpha r)}{J_1^2(i\alpha R)} - \frac{4J_2(i\alpha r)}{i\alpha R J_1(i\alpha R)} + \frac{1}{2}\left(\frac{r}{R}\right)^2\right] \quad \ldots [21]$$

Using the boundary condition on u to determine the constant α, one gets

$$\left(\frac{qR^4}{Dh}\right)^2 = \frac{\frac{1}{3}(\alpha R)^6}{\frac{3}{4} + \frac{4}{(\alpha R)^2} + \frac{J_0(i\alpha R)}{i\alpha R J_1(i\alpha R)} + \frac{1}{2}\frac{J_0^2(i\alpha R)}{J_1^2(i\alpha R)}} \quad \ldots [22]$$

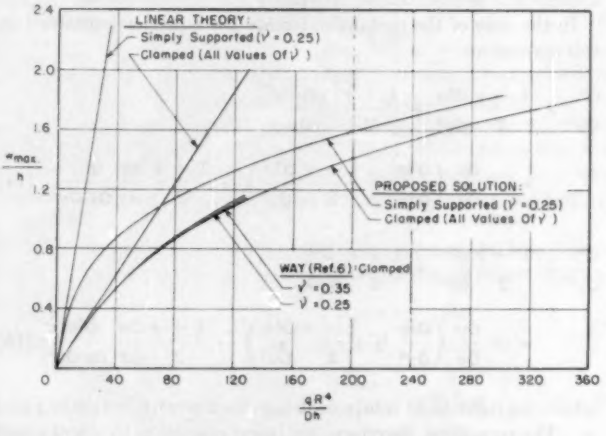

Fig. 1 Center Deflections for Circular Plates

From this equation one finds the proper value of αR to be used in Equations [20] and [21] for the given loading. The resulting solution for the deflection at the center of the plate is plotted in Fig. 1, along with the results of S. Way (6). When the deflection equals the thickness of the plate, a comparison of the two solutions shows an error of less than 2 per cent for $\nu = 0.25$, and less than 1 per cent for $\nu = 0.35$. The deflection at the center of the plate approaches the exact solution as α approaches zero, and the error appears to increase monotonically as α increases.

From examination of Equation [6] we see that the dependence on α disappears as α approaches zero, so we should expect the solution given in Equation [17] to be independent of α as it approaches zero, and therefore the solution should approach the exact linear plate solution as α approaches zero. To show that this is the case, we can take the limit of Equation [20] as α approaches zero. Using the expansions for $J_0(i\alpha R)$ and $J_1(i\alpha R)$ for small α (14), Equation [20] becomes

$$\lim_{\alpha \to 0} \left(\frac{wD}{qR^4} \right) = \frac{1}{64} \left[1 - \left(\frac{r}{R} \right)^2 \right]^2 \quad \ldots\ldots\ldots [23]$$

As was expected, this is the solution for a clamped circular plate with small deflections (9).

The results plotted in Fig. 1 show that the error increases as α increases over the range of values of α for which a comparison could be made. It is of interest, therefore, to investigate the error for very large α. Using the expansions for $J_0(i\alpha R)$ and $J_1(i\alpha R)$ for large α (15) and combining Equations [20] and [22], one gets

$$\lim_{\alpha \to \infty} \left[\frac{w}{\left(\frac{qR^4}{Eh} \right)^{1/3}} \right] = \left(\frac{1 - \nu^2}{4} \right)^{1/3} \left[1 - \left(\frac{r}{R} \right)^2 \right] \ldots [24]$$

For $\nu = 0.3$, the maximum deflection given by Equation [24] is

$$\lim_{\alpha \to \infty} \left[\frac{w_{max}}{\left(\frac{qR^4}{Eh} \right)^{1/3}} \right] = 0.610 \quad \ldots\ldots\ldots [25]$$

Hencky's exact result for the circular membrane is (16)

$$w_{max} = 0.662 \left(\frac{qR^4}{Eh} \right)^{1/3} \quad \ldots\ldots\ldots [26]$$

If the difference between Equations [25] and [26] represents the maximum difference that occurs between the exact solution and the solution given in Equation [20] for all values of α (as is indicated by the trend shown in Fig. 1), the error introduced by the proposed approximation will be less than 8 per cent for uniformly loaded circular plates where the deflection and displacement are zero on the boundary.

Simply Supported Edges

In the case of simply supported edges, it is assumed that the displacement and the deflection of the edge of the plate are zero but that it is free to rotate. The boundary conditions in this case are

$$\left.\begin{aligned} w(R) &= 0 \\ \left. \frac{d^2w}{dr^2} \right|_{r=R} + \frac{\nu}{R} \left. \frac{dw}{dr} \right|_{r=R} &= 0 \\ u(R) &= 0 \end{aligned}\right\} \quad \ldots\ldots\ldots [27]$$

Using the boundary conditions on w to solve for A and B, and substituting these values in Equations [17] and [18], one gets

$$w = \frac{qR^2}{4D\alpha^2} \left\{ 1 - \left(\frac{r}{R} \right)^2 - \frac{2(1+\nu)[J_0(i\alpha R) - J_0(i\alpha r)]}{(\alpha R)^2 J_0(i\alpha R) + (1-\nu) i\alpha R J_1(i\alpha R)} \right\} \ldots [28]$$

and

$$u = \frac{\alpha^2 h^2}{24} r + \frac{q^2 R^2 r}{16 D^2 \alpha^4} \left\{ \frac{(1+\nu)^2 [J_1^2(i\alpha r) - J_0(i\alpha r) J_2(i\alpha r)]}{[\alpha R J_0(i\alpha R) - (1-\nu) i J_1(i\alpha R)]^2} - \frac{4(1+\nu) J_2(i\alpha r)}{\alpha R [\alpha R J_0(i\alpha R) - (1-\nu) i J_1(i\alpha R)]} - \frac{1}{2} \left(\frac{r}{R} \right)^2 \right\} \ldots [29]$$

As in the case of the clamped plate, setting $u(R) = 0$ gives a relation between αR and $\frac{qR^4}{Dh}$.

A plot of the deflection at the center of the plate is given in Fig. 1 for $\nu = 0.25$. Unfortunately, there are no available theoretical results for this case so the deflection cannot be checked, but some information about the results can be obtained by checking the behavior of the solution for small and large values of α.

In the case of the simply supported plate, one finds that the deflection for small values of α is given by

$$\lim_{\alpha \to 0} \left(\frac{wD}{qR^4} \right) = \frac{1}{64} \left[\frac{5 + \nu}{1 + \nu} - \left(\frac{r}{R} \right)^2 \right] \left[1 - \left(\frac{r}{R} \right)^2 \right] \ldots [30]$$

This is the solution for the simply supported circular plate with small deflections (10) so as in the case of the clamped plate, the deflection given in Equation [28] approaches the exact solution as α approaches zero. It should be noted, moreover, that Equation [30] has the proper variation with Poisson's ratio because that variation results from the boundary conditions.

One can show that the deflection for very large values of α is the same as in the case of the clamped plate.

Rectangular Plates With Uniform Loading

The equations that must be solved for the rectangular plate with uniform loading are Equations [5] and [6]. To solve these equations u, v, and w can be expanded in appropriate series. Since the choice of the type of series that is best suited to the problem will depend on the boundary conditions, no general solution for completely arbitrary boundary conditions will be given for the rectangular plate.

As an illustration, consider the solution when two sides, $x = \pm a$, are simply supported, and the two other sides, $y = \pm b$, have arbitrary boundary conditions. To do this we represent w by the Fourier series

$$w = \sum_{n=0}^{\infty} f_n(y) \cos \frac{2n+1}{2a} \pi x \quad \ldots\ldots\ldots [31]$$

This series satisfies, term by term, the boundary conditions for the simply supported edges. By substituting Equation [31] into [6], the differential equation for $f_n(y)$ is obtained. Solving this equation, we get the solution for w

$$w = \frac{q}{D\alpha^4} \left\{ \frac{\cosh \alpha x}{\cosh \alpha a} - 1 + \frac{(\alpha a)^2}{2} \left[1 - \left(\frac{x}{a} \right)^2 \right] \right\} + \sum_{n=0}^{\infty} \cos \beta_n x \{ A_n \cosh \beta_n y + B_n \cosh \delta_n y \} \ldots [32]$$

where the portion of the series that is independent of y has been summed, and the notation

$$\beta_n = \frac{2n+1}{2a} \pi; \quad \delta_n = \left[\left(\frac{2n+1}{2a} \pi \right)^2 + \alpha^2 \right]^{1/2}$$

has been used.

One notes that the first part of Equation [32] is the exact solution for the deflection of a simply supported infinite strip given by Shaw, et al. (17), Timoshenko (11), and others. Since w must be independent of y as b approaches infinity, the second part of Equation [32] should approach zero as b approaches infinity, leaving the solution given in Equation [32] equal to the exact solution. Thus the approximate solution found in this paper approaches the exact solution in the case of rectangular plates as the aspect ratio b/a approaches infinity for any α. By the same argument that was used in the case of circular plates, it can be shown that the solution approaches the exact solution as α approaches zero.

In order to find α, let

$$u = \sum_{k=1}^{\infty} g_k(y) \sin \frac{k\pi x}{a} \quad \ldots\ldots\ldots [33]$$

and

$$v = \sum_{k=0}^{\infty} l_k(y) \cos \frac{k\pi x}{a} \quad \ldots\ldots\ldots\ldots\ldots\ldots [34]$$

where the form has been chosen because we know that u is an odd function of x and v is an even function of x. Expanding $(\partial w/\partial x)^2$ and $(\partial w/\partial y)^2$ in Fourier series, substituting Equations [33] and [34] into [5], and equating zero-order coefficients, a differential equation for $l_0(y)$ is obtained. Integrating this equation gives

$$l_0(y) = \frac{\alpha^2 h^2}{12} y - \frac{1}{4} \sum_{n=0}^{\infty} \left\{ \left[\frac{2q}{aD\beta_n^2\delta_n^2} \right]^2 y - \frac{\alpha^2\beta_n^2}{2} y \right.$$

$$+ \beta_n A_n^2 \sinh \beta_n y \cosh \beta_n y + \frac{\beta_n^2 + \delta_n^2}{2\delta_n} B_n^2 \sinh \delta_n y \cosh \delta_n y$$

$$+ 2\beta_n A_n B_n \sinh \beta_n y \cosh \delta_n y$$

$$\left. + \frac{4q(-)^n}{aD\beta_n^2\delta_n^2} \left[A_n \sinh \beta_n y + \frac{\beta_n}{\delta_n} B_n \sinh \delta_n y \right] \right\} \ldots [35]$$

When the boundary conditions at $y = \pm b$ are given, this equation determines the proper relation between α and the loading.

It is not possible to solve for $g_k(y)$ and $l_k(y)$ independently. It is possible, nevertheless, to find the deflection w. Also, we note that it is not necessary to specify the boundary condition on the displacement parallel to the edge in order to find the deflection. It appears, therefore, that a part of the error introduced by the simplification made herein must lie in the fact that the deflection determined by this analysis does not vary with the boundary condition on the displacement parallel to the edge.

In the following sections the simply supported and clamped boundary conditions at $y = \pm b$ will be considered, and computations of deflections will be carried out for various aspect ratios.

All Edges Simply Supported

Using the boundary conditions on w at $y = \pm b$ when all edges are simply supported to solve for the coefficients A_n and B_n, we can write Equation [32] as

$$w = \frac{q}{D\alpha^4} \left\{ \frac{\cosh \alpha x}{\cosh \alpha a} - 1 + \frac{(\alpha a)^2}{2} \left[1 - \left(\frac{x}{a} \right)^2 \right] \right\}$$

$$+ \sum_{n=0}^{\infty} \cos \beta_n x \left\{ \frac{2q(-)^n}{aD\alpha^2\beta_n^2\delta_n^2} \left[\beta_n^2 \frac{\cosh \delta_n y}{\cosh \delta_n b} - \delta_n^2 \frac{\cosh \beta_n y}{\cosh \beta_n b} \right] \right\} . [36]$$

It can easily be shown that $l_0(b) = 0$ if the shear is zero along the edges $y = \pm b$ or if the plate is restrained from moving parallel to its edge. This boundary condition on $l_0(y)$ when substituted into Equation [35] gives

$$\frac{(\alpha a)^6}{12} = \left(\frac{qa^4}{Dh} \right)^2 \left\{ \frac{1}{(\alpha a)^3} \left[\frac{5}{4} \tanh \alpha a - \frac{\alpha a}{4} \operatorname{sech}^2 \alpha a - \alpha a \right. \right.$$

$$\left. + \frac{1}{6} (\alpha a)^3 \right] - \sum_{n=0}^{\infty} \frac{1}{a^4\beta_n^4\delta_n^4} \left[\frac{\alpha^2\beta_n^2}{2} \operatorname{sech}^2 \delta_n b \right.$$

$$\left. \left. + \frac{\delta_n^4}{\beta_n b} \tanh \beta_n b - \frac{\beta_n^2 \left(\beta_n^2 + \frac{5}{2} \alpha^2 \right)}{\delta_n b} \tanh \delta_n b \right] \right\} \ldots [37]$$

where a portion of the series has been summed. From this equation one finds the proper value of αa to be used in Equation [36] for the desired loading.

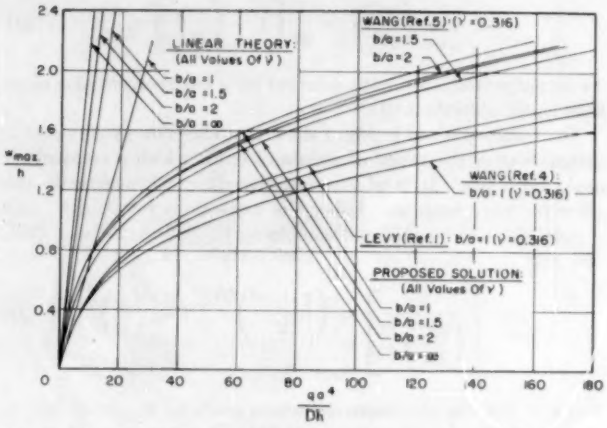

Fig. 2 Center Deflections for Rectangular Plates With All Edges Simply Supported

A plot of the deflection at the center of the plate is given in Fig. 2 for aspect ratios of 1, 1.5, 2, and ∞. The results of Levy (1) and Wang (4), (5) also are plotted in Fig. 2. It should be noted that the series of Equations [36] and [37] converge so rapidly that the use of the first term alone in the calculations would have yielded sufficient accuracy.

Levy assumed that there was no restraint to displacement parallel to the edges of the plate, while Wang assumed that the displacement parallel to the edge was zero. We note that for an aspect ratio of 1, the solution given in this paper lies between the solutions of Levy and Wang. Thus this solution probably can be interpreted as representing the deflection for a plate where the displacement parallel to the edge lies somewhere between zero and the value when there is no restraint against such a displacement.

As in the case of the circular plate, the deflection given in Equation [36], for any aspect ratio, approaches the exact solution (12) as α approaches zero. To investigate the error as the plate approaches the membrane we take the limit of Equation [36] for very large α. In this case, after combining Equations [36] and [37], we get

$$\lim_{\alpha \to \infty} \left[\left(\frac{w}{h} \right) \Big/ \left(\frac{qa^4}{Dh} \right)^{1/3} \right]$$

$$= \frac{\frac{1}{2} \left[1 - \left(\frac{x}{a} \right)^2 \right] - \sum_{n=0}^{\infty} \frac{2(-)^n}{(\beta_n a)^3} \frac{\cosh \beta_n x}{\cosh \beta_n b} \cos \beta_n x}{\left[2 - 12 \frac{a}{b} \sum_{n=0}^{\infty} \frac{1}{(\beta_n a)^5} \tanh \beta_n b \right]^{1/3}} \quad \ldots [38]$$

For $\nu = 0.3$ and $b/a = 1$, the maximum deflection for large α is given by

$$\lim_{\alpha \to \infty} \left[\frac{w_{\max}}{\left(\frac{qa^4}{Eh} \right)^{1/3}} \right] = 0.692 \quad \ldots\ldots\ldots\ldots [39]$$

Hencky's exact result for the square membrane where both u and v are zero at the edges (18) is

$$w_{\max} = 0.665 \left(\frac{qa^4}{Eh} \right)^{1/3} \quad \ldots\ldots\ldots\ldots [40]$$

Thus the error introduced by the assumption used in this paper is 4 per cent for uniformly loaded square membranes with zero displacements and deflection on the boundary.

Two Edges Simply Supported and Two Edges Clamped

Using the boundary conditions for the case when the two edges $x = \pm a$ are simply supported and the two edges $y = \pm b$ are clamped to solve for A_n and B_n, we can write Equation [32] as

$$w = \frac{q}{D\alpha^4}\left\{\frac{\cosh \alpha x}{\cosh \alpha a} - 1 + \frac{(\alpha a)^2}{2}\left[1 - \left(\frac{x}{a}\right)^2\right]\right\} - \frac{2q}{aD}\sum_{n=0}^{\infty} \cos \beta_n x \left\{\frac{(-)^n}{\beta_n^3 \delta_n^2}\left[\frac{\beta_n \cosh \delta_n y}{\sinh \delta_n b} - \frac{\delta_n \cosh \beta_n y}{\sinh \beta_n b}\right]\right\} \quad [41]$$

The boundary conditions on u and v at $y = \pm b$ are the same as those for the simply supported plate. Using the boundary condition $l_6(b) = 0$, Equation [35] becomes

$$\frac{(\alpha a)^2}{12} = \left(\frac{qa^4}{Dh}\right)^2 \left\{\frac{1}{(\alpha a)^7}\left[\frac{5}{4}\tanh \alpha a - \frac{\alpha a}{4}\operatorname{sech}^2 \alpha a - \alpha a + \frac{1}{6}(\alpha a)^3\right] - \sum_{n=0}^{\infty} \frac{\frac{\alpha^2 \beta_n^2}{2}\operatorname{csch}^2 \delta_n b - \frac{\beta_n(\beta_n^2 - \alpha^2)}{\delta_n}\coth \beta_n b + \frac{\beta_n^2\left(\beta_n^2 - \frac{1}{2}\alpha^2\right)}{\delta_n b}\coth \delta_n b}{a^8 \beta_n^8 \delta_n^4 [\delta_n \coth \beta_n b - \beta_n \coth \delta_n b]^2}\right\} \quad [42]$$

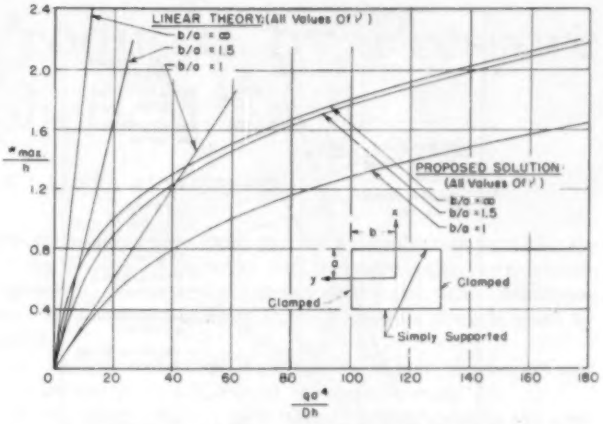

FIG. 3 CENTER DEFLECTIONS FOR RECTANGULAR PLATES WITH TWO EDGES SIMPLY SUPPORTED AND TWO EDGES CLAMPED

A plot of the deflection at the center of the plate is given in Fig. 3 for aspect ratios of 1, 1.5, and ∞. For the square plate the deflection lies between that of the fully clamped plate (2, 7) and that of the simply supported plate. As the load increases or as the aspect ratio approaches infinity, the solution for the semi-clamped plate approaches that for the simply supported one. Also, the limit of the deflection given in Equation [41] approaches the solution for the simply supported plate as α approaches infinity. As α approaches zero, the deflection approaches the exact solution.

Stresses in Circular Plates With Uniform Loading

Integrating Equation [16], using the necessary integral relations of the Bessel functions (13), the displacement is found to be

$$u = -\frac{q^2R^7}{D^2}\left\{\frac{AD}{qR^4}\frac{(1+\nu)}{2(\alpha R)^3}\left[\frac{r}{R} iJ_1(i\alpha R) - iJ_1(i\alpha r)\right] + \frac{AD}{qR^4}\frac{1}{2(\alpha R)^2}\frac{r}{R}[J_0(i\alpha R) - J_0(i\alpha r)] - \frac{3-\nu}{64(\alpha R)^4}\frac{r}{R}\left[1 - \left(\frac{r}{R}\right)^2\right] + \frac{A^2D^2}{q^2R^6}\frac{\nu}{4}(\alpha R)^2\frac{r}{R}\left[J_0^2(i\alpha R) + J_1^2(i\alpha R) - J_0^2(i\alpha r) - J_1^2(i\alpha r)\right] + \frac{A^2D^2}{q^2R^6}\frac{1+\nu}{4} i\alpha R\left[\frac{r}{R} J_0(i\alpha R)J_1(i\alpha R) - J_0(i\alpha r)J_1(i\alpha r)\right]\right\} \quad [43]$$

where the constant of integration has been chosen so that u will be zero on the boundary.

The membrane stresses are given by

$$\sigma_r = \frac{E}{1-\nu^2}\left[\frac{du}{dr} + \frac{1}{2}\left(\frac{dw}{dr}\right)^2 + \nu\frac{u}{r}\right] \quad [44]$$

$$\sigma_\theta = \frac{E}{1-\nu^2}\left[\frac{u}{r} + \nu\frac{du}{dr} + \frac{\nu}{2}\left(\frac{dw}{dr}\right)^2\right] \quad [45]$$

Using the value of u given in Equation [43] the membrane stresses at the center of the plate are found to be

$$(\sigma_r)_{r=0} = (\sigma_\theta)_{r=0} = -\frac{q^2R^6E}{(1-\nu)D^2}\left\{\frac{AD}{qR^4}\frac{1+\nu}{2(\alpha R)^3}\left[iJ_1(i\alpha R) + \frac{\alpha R}{2}\right] + \frac{AD}{qR^4}\frac{[J_0(i\alpha R) - 1]}{2(\alpha R)^2} - \frac{3-\nu}{64(\alpha R)^4} + \frac{A^2D^2}{q^2R^6}\frac{\nu}{4}(\alpha R)^2[J_0^2(i\alpha R) + J_1^2(i\alpha R) - 1] + \frac{A^2D^2}{q^2R^6}\frac{1+\nu}{4}\left[i\alpha R J_0(i\alpha R)J_1(i\alpha R) + \frac{(\alpha R)^2}{2}\right]\right\} \quad [46]$$

The membrane stresses at the edge of the plate are

$$(\sigma_r)_{r=R} = \frac{1}{\nu}(\sigma_\theta)_{r=R} = -\frac{q^2R^6E}{(1-\nu)D^2}\left\{\frac{AD}{qR^4(\alpha R)^3}\left[\frac{1}{2}J_0(i\alpha R) + \frac{i}{\alpha R}J_1(i\alpha R)\right] - \frac{1}{32(\alpha R)^4} + \frac{A^2D^2}{q^2R^6}\frac{(\alpha R)^2}{4}\left[J_0^2(i\alpha R) + J_1^2(i\alpha R) + \frac{2}{\alpha R} iJ_0(i\alpha R)J_1(i\alpha R)\right]\right\} \quad [47]$$

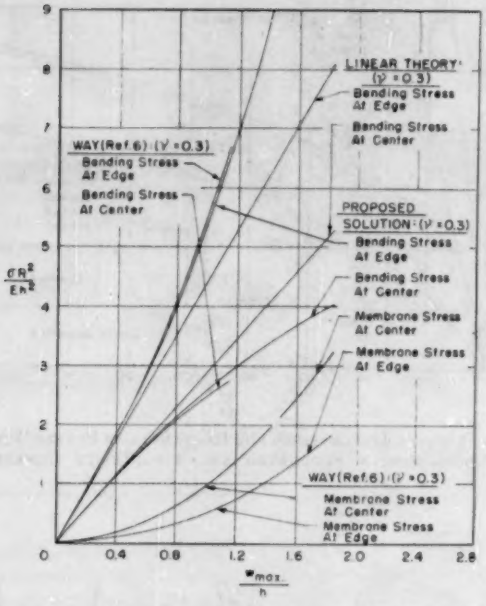

FIG. 4 CENTER AND EDGE STRESSES FOR CLAMPED CIRCULAR PLATES

Substituting Equation [17] in [12] and [13], we find the bending stresses at the center to be

$$(\sigma_r')_{r=0} = (\sigma_\theta')_{r=0} = -\frac{6D(1+\nu)}{h^2}\left[\frac{\alpha^2 A}{2} - \frac{9}{2D\alpha^2}\right] \quad [48]$$

and the bending stresses at the edge to be

$$(\sigma_r')_{r=R} = -\frac{6D}{h^2}\left[\frac{\alpha}{R}A(1-\nu)iJ_1(i\alpha R) + \alpha^2 A J_0(i\alpha R) - \frac{q(1+\nu)}{2D\alpha^2}\right]$$

$$(\sigma_\theta')_{r=R} = -\frac{6D}{h^2}\left[-\frac{\alpha}{R}A(1-\nu)iJ_1(i\alpha R) + \nu\alpha^2 A J_0(i\alpha R) - \frac{q(1+\nu)}{2D\alpha^2}\right] \quad [49]$$

Substitution of the values of A for the clamped and simply supported edges into the foregoing equations determines the membrane and bending stresses for those boundary conditions. In what follows, we shall examine the case of the clamped plate in detail and compare the results with available solutions to the exact equations.

For the clamped plate, Equation [46] becomes

$$(\sigma_r)_{r=0} = (\sigma_\theta)_{r=0} = \frac{q^2R^6E}{(1-\nu)D^3}\frac{1}{16(\alpha R)^4}\left\{\frac{\nu J_0^2(i\alpha R) + \frac{1-\nu}{2}}{J_1^2(i\alpha R)} + \frac{(3-\nu)J_0(i\alpha R) - 2(1-\nu)}{i\alpha R J_1(i\alpha R)} + \frac{3}{4}(1+\nu) + \frac{4}{(\alpha R)^2}(1+\nu)\right\} \quad [50]$$

and Equation [47] becomes

$$(\sigma_r)_{r=R} = \frac{1}{\nu}(\sigma_\theta)_{r=R} = \frac{q^2R^6E}{(1-\nu)D^3}\frac{1}{16(\alpha R)^4}\left\{\frac{J_0^2(i\alpha R)}{J_1^2(i\alpha R)} + \frac{2J_0(i\alpha R)}{i\alpha R J_1(i\alpha R)} + \frac{3}{2} + \frac{8}{(\alpha R)^2}\right\} = \frac{Eh^2\alpha^2}{24(1-\nu)} \quad [51]$$

The bending stresses are given by

$$(\sigma_r')_{r=0} = (\sigma_\theta')_{r=0} = \frac{qR^2}{h^2}\frac{3(1+\nu)}{(\alpha R)^2}\left[1 + \frac{\alpha R}{2iJ_1(i\alpha R)}\right] \quad [52]$$

$$(\sigma_r')_{r=R} = \frac{1}{\nu}(\sigma_\theta')_{r=R} = \frac{qR^2}{h^2}\frac{6}{(\alpha R)^2}\left[1 + \frac{\alpha R J_0(i\alpha R)}{2iJ_1(i\alpha R)}\right] \quad [53]$$

The membrane and bending stresses given in Equations [50] through [53] are plotted in Fig. 4, along with the results of S. Way (6). A comparison of the two solutions over the range that was computed by Way shows a maximum error in the bending stresses of less than 6 per cent. The curves of Way for the membrane stresses could not be distinguished from the curves for the proposed solution over the range that was computed by Way.

The maximum error in the stresses is likely to occur when the error in the deflection is a maximum which appears to be the case for very large α. The membrane stress at the center given by Equation [50] for very large α is

$$\lim_{\alpha\to\infty}\left[\frac{(\sigma_r)_{r=0}}{\left(\frac{q^2R^2E}{h^2}\right)^{1/3}}\right] = \frac{[16(1-\nu^2)]^{2/3}(3-\nu)}{64(1-\nu)} \quad [54]$$

For very large α the stress at the edge given by Equation [51] is

$$\lim_{\alpha\to\infty}\left[\frac{(\sigma_r)_{r=R}}{(\sigma_r)_{r=0}}\right] = \frac{2}{3-\nu} \quad [55]$$

For $\nu = 0.3$, the stresses given by Equations [54] and [55] are

$$\lim_{\alpha\to\infty}\left[\frac{(\sigma_r)_{r=0}}{\left(\frac{q^2R^2E}{h^2}\right)^{1/3}}\right] = 0.359 \quad \text{or} \quad \lim_{\alpha\to\infty}\left[\frac{(\sigma_r)_{r=0}}{\frac{E}{R^2}w_{max}^2}\right] = 0.965 \quad [56]$$

$$\lim_{\alpha\to\infty}\left[\frac{(\sigma_r)_{r=R}}{\left(\frac{q^2R^2E}{h^2}\right)^{1/3}}\right] = 0.266 \quad \text{or} \quad \lim_{\alpha\to\infty}\left[\frac{(\sigma_r)_{r=R}}{\frac{E}{R^2}w_{max}^2}\right] = 0.715 \quad [57]$$

Hencky's exact result for the circular membrane is (16)

$$(\sigma_r)_{r=0} = 0.423\left[\frac{q^2R^2E}{h^2}\right]^{1/3} = 0.965\frac{E}{R^2}w_{max}^2 \quad [58]$$

$$(\sigma_r)_{r=R} = 0.328\left[\frac{q^2R^2E}{h^2}\right]^{1/3} = 0.748\frac{E}{R^2}w_{max}^2 \quad [59]$$

The stress at the center given in Equation [56] is 15 per cent lower than that given in Equation [58] when the stress is written as a function of the loading. However, when it is written as a function of the deflection, the two results are the same. The stress at the edge given in Equation [57] is 19 per cent lower than that given in Equation [59] when it is written as a function of the loading, but it is less than 5 per cent lower when written as a function of the deflection.

Elastic-Stress Waves Produced by Pressure Loads on a Spherical Shell

By J. H. HUTH[1] and J. D. COLE,[2] SANTA MONICA, CALIF.

The paper treats the problem of stresses in a spherical elastic shell subjected to a plane pressure wave traveling across it with constant speed, a case of technical interest when considering the effect of blast waves on the structure of a missile in flight.

Introduction

A PROBLEM of technical interest, which recently has been studied, is the effect of blast waves on the structure of a missile in flight. One such problem is considered here, namely, the calculation of elastic stresses in a thin spherical shell structure resulting from the pressure loading of a blast wave.

The problem is studied with several idealizing assumptions. The blast wave is idealized as a plane wave carrying a pressure jump which moves across the sphere at a constant velocity U. In this respect the motion of the sphere is neglected, as well as the effect of the sphere on the wave. The prediction of the actual pressure distribution is a very complex problem and is put aside for the present.

For analyzing the structure the conventional methods of momentless thin-shell elasticity are adopted.

With these simplifying assumptions the problem can be set up and various methods of solution studied. In spite of the idealizations the equations remain complicated owing to the complex nature of the elastic waves and the geometry. For this reason both analytical and numerical methods have been employed to give an over-all picture of the waves and an estimate of the stresses produced.

Assumptions in Detail

The analysis is subject to the following principal assumptions:

1 The effect of the sphere on the wave is neglected [see references (1)[3] and (2) for attempts to include this effect, in the case of an acoustic wave, for cylindrical and spherical shells].

2 Momentless thin-shell theory is assumed to apply. By Jellett's theorem (3), the vibrational stresses in a closed spherical shell are essentially extensional. Consequently, according to Vlasov, the present analysis should be a good approximation for shells with a ratio of thickness to radius of less than 1/30 (4).

Within the framework of these assumptions, one may draw the following conclusions based on the analysis:

1 As the velocity of the pressure wave increases without limit, the stresses approach those that would result from suddenly applying the pressure uniformly over the entire shell. For this limiting case the peak stress will be twice the static stress in compression, and no tensile stresses arise. The static stress is given by p_0R/h.

2 At lower velocities, larger stresses of both signs result and may become at least four times the static stresses.

3 Maximum shell stress is directly proportional to the pressure behind the shock and the ratio of shell radius to thickness and in addition depends on Poisson's ratio and the ratio of pressure-wave speed to the speed of elastic waves in the shell. Therefore the results given in this paper apply to all thin steel shells.

4 Stresses in the precursor elastic wave are significant but not usually predominant.

5 A "mode" type of solution is useful only for relatively rapid envelopments. For slower envelopments the resulting motion is too rich in harmonics to be described by a few modes.

6 Results of this paper can be combined with information about blast-wave speeds and pressures and missile speeds to estimate the stresses produced. (For an actual blast wave the pressure and velocity will of course be related. Since shell stresses are directly proportional to the pressure in the wave, the results contained herein can be adapted to such a relationship.)

Basic Equations and Their Character

If the shell is considered initially at rest any unsymmetrical load will produce an acceleration of its center of gravity, given by

$$\vec{a} = \frac{\vec{F}}{M} \qquad [1][4]$$

where

$\vec{a}$ = acceleration vector of center of gravity
$\vec{F}$ = net external force vector
M = total mass of shell and contents (pay load)

Usually the equations of motion for a shell are written in a coordinate system whose origin is fixed in the center of gravity of the structure. Therefore a D'Alembert force due to $\vec{a}$ should appear in the equations of motion, although it can be shown that in the linear theory the inclusion of this term has no effect on the shell stresses. Consequently it will be omitted.

Considering only axially symmetric loadings the independent variables are

ϕ = polar angle measured from the axis of symmetry, and taken equal to zero at the pole facing the oncoming wave
t = time

Also the following notation will be used:

ρ = mass density of shell material
R = sphere radius
h = shell thickness

---

[1] Missiles Division, The Rand Corporation. Mem. ASME.

[2] Consultant, The Rand Corporation; Assistant Professor of Aeronautics, California Institute of Technology, Pasadena, Calif.

[3] Numbers in parentheses refer to the Bibliography at the end of the paper.

Presented at the West Coast Conference of the Applied Mechanics Division, Monterey, Calif., September 12–13, 1955, of The American Society of Mechanical Engineers.

Discussion of this paper should be addressed to the Secretary, ASME, 29 West 39th Street, New York, N. Y., and will be accepted until January 10, 1956, for publication at a later date. Discussion received after the closing date will be returned.

Note: Statements and opinions advanced in papers are to be understood as individual expressions of their authors and not those of the Society. Manuscript received by ASME Applied Mechanics Division, January 20, 1955. Paper No. 55—APM-31.

[4] Actually, a nonlinearity exists since the loading depends on the motion of the sphere.

E = modulus of elasticity
ν = Poisson's ratio
W = radial displacement, positive inward
V = tangential displacement, positive in the direction of increasing ϕ
N_ϕ = polar-membrane stress component, positive in tension (force per unit length)
N_θ = hoop-membrane stress component, positive in tension (force per unit length)
$\sigma_{\theta,\phi} = N_{\theta,\phi}/h$ = actual shell stresses (assumed uniform across shell thickness)
$p(\phi, t)$ = given external pressure

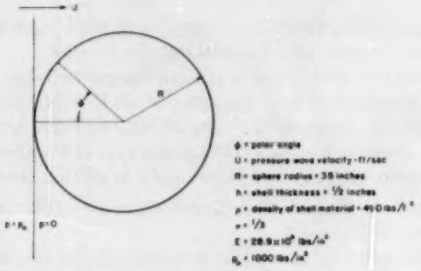
φ = polar angle
U = pressure wave velocity - ft/sec
R = sphere radius = 36 inches
h = shell thickness = 1/2 inches
ρ = density of shell material = 490 lbs/ft³
ν = 1/3
E = 28.9 x 10⁶ lbs/in²
σ_y = 1000 lbs/in²
p = p₀
p = 0

FIG. 1 DETAILS OF SHELL ENVELOPMENT

The resulting dynamic equations are (5)

$$\left.\begin{aligned} &\frac{\partial}{\partial\phi}(\sin\phi\, N_\phi) - \cos\phi N_\theta = \rho h R \sin\phi \frac{\partial^2 V}{\partial t^2} \\ &N_\phi + N_\theta + pR = \rho h R \frac{\partial^2 w}{\partial t^2} \end{aligned}\right\} \quad \ldots [2]$$

Also, from reference (5) one has the following relationships between membrane stresses and displacements

$$\left.\begin{aligned} N_\theta &= \frac{Eh}{R(1-\nu^2)}\left[V\cot\phi + \nu\frac{dV}{d\phi} - (1+\nu)W\right] \\ N_\phi &= \frac{Eh}{R(1-\nu^2)}\left[\frac{dV}{d\phi} + \nu V\cot\phi - (1+\nu)W\right] \end{aligned}\right\} \quad \ldots [3]$$

Equations [2] and [3] form the complete system of differential equations to be studied here, with the initial conditions

$$V = \frac{\partial V}{\partial t} = W = \frac{\partial W}{\partial t} = 0$$

and the boundary conditions

$$V, W \text{ bounded at the poles } \phi = 0, \pi$$

If the expressions for the stresses are introduced into Equations [2], the equations of motion become

$$\left.\begin{aligned} &\frac{Eh}{R(1-\nu^2)}\left[\frac{\partial^2 V}{\partial\phi^2} + \cot\phi\frac{\partial V}{\partial\phi} - (\nu + \cot^2\phi)V\right] \\ &\qquad - \frac{Eh}{R(1-\nu)}\frac{\partial W}{\partial\phi} = \rho h R\frac{\partial^2 V}{\partial t^2} \\ &\frac{Eh}{R(1-\nu)}\left(\frac{\partial V}{\partial\phi} + V\cot\phi - 2W\right) + pR = \rho h R\frac{\partial^2 W}{\partial t^2} \end{aligned}\right\} \quad \ldots [4]$$

The mathematical structure of this system of equations is of interest. If W is regarded as known, then the first of Equations [4] appears as a wave equation for the tangential displacement V with a speed of propagation along the shell surface (constant angular velocity)

$$C_L = \sqrt{\frac{E}{\rho(1-\nu^2)}}$$

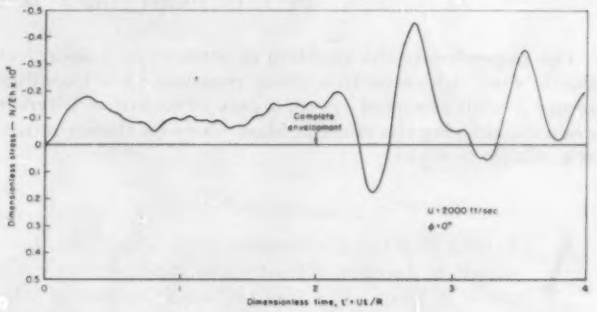

FIG. 1(a) STRESS IN A THIN SPHERICAL SHELL RESULTING FROM ENVELOPMENT BY A PLANE PRESSURE WAVE

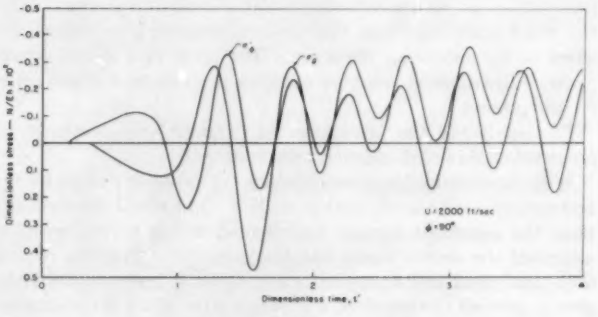

FIG. 1(b)

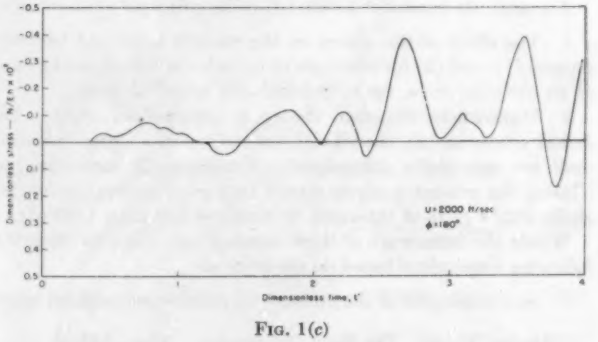

FIG. 1(c)

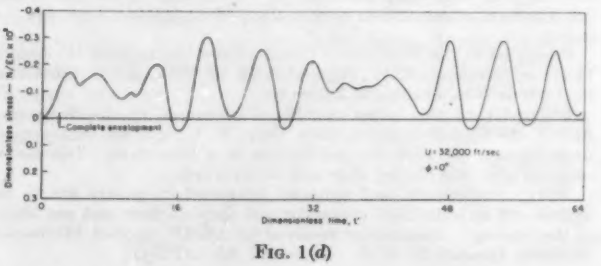

FIG. 1(d)

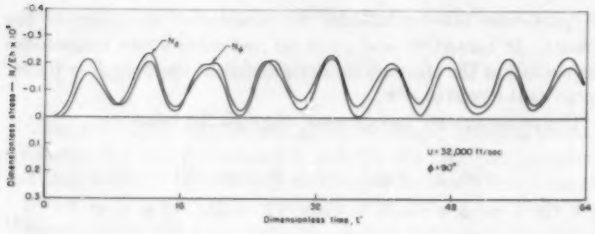

FIG. 1(e)

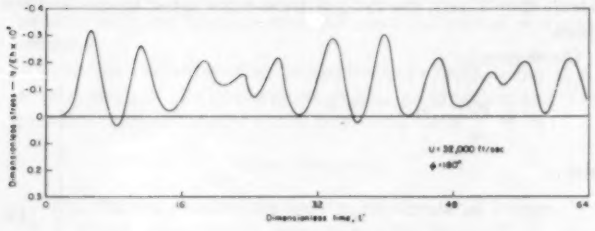

FIG. 1(f)

This speed is very close to the exact speed of longitudinal elastic waves and shows how the stress waves propagate themselves over the surface of the sphere.

On the other hand, if V is regarded as known, then the second of Equations [4] does not have the structure of a wave equation but looks instead like an ordinary differential equation for undamped vibrations with a natural frequency

$$\omega_R = \sqrt{\frac{2E}{\rho R^2(1-\nu)}} = \sqrt{2(1+\nu)}\,\frac{C_L}{R}$$

In fact, if the loading is uniform so that $V = a = 0$, $p = p(t)$, then Equations [4] reduce to

$$\frac{d^2W}{dt^2} + \omega_R{}^2 W = \frac{p(t)}{\rho h} \quad \ldots\ldots\ldots\ldots\ldots\ldots [5]$$

The solution of Equation [5], for p representing a suddenly applied uniform pressure p_0, is

$$W = \frac{p_0}{\rho h \omega_R{}^2}(1 - \cos \omega_R t)$$

and the resulting membrane stresses are

$$N_\phi = N_\theta = -\frac{p_0 R}{2}(1 - \cos \omega_R t) \quad \ldots\ldots\ldots\ldots [6][5]$$

It is clear from Equation [6] that the peak stress is just double the static stress, but that no tensile stresses ever occur. This result for a suddenly applied uniform pressure obviously represents the limiting condition as the blast-wave velocity U approaches infinity.

One of the principal aims of the following sections will be to determine how these results are modified by choosing finite values of U.

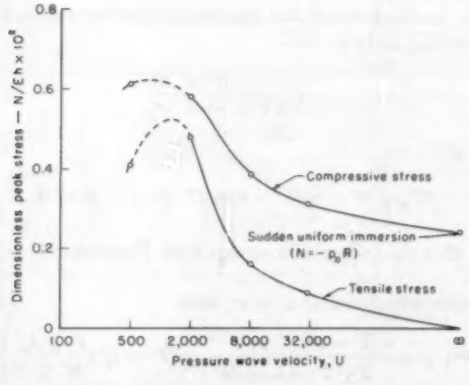

FIG. 2 PEAK STRESSES IN SHELL AS A FUNCTION OF WAVE VELOCITY

THEORETICAL ANALYSIS

Dimensionless Variables. For the analytical work it is convenient to introduce the following dimensionless variables

$$t' = \frac{tC_L}{R} = \text{dimensionless time}$$

$$V' = \frac{V}{R} = \text{dimensionless tangential displacement}$$

$$W' = \frac{W}{R} = \text{dimensionless radial displacement}$$

$$h' = \frac{h}{R} = \text{thickness ratio}$$

$$p' = \frac{pR}{E}\frac{(1-\nu^2)}{h} = \text{dimensionless pressure}$$

$$a' = \frac{R}{C_L{}^2}a = \text{dimensionless acceleration}$$

$$N'_{\phi,\theta} = \frac{N_{\phi,\theta}}{Eh}(1-\nu^2) = \text{dimensionless membrane stresses}$$

This notation will be used throughout the section.

TRAVELING-WAVE SOLUTION

The solution of Equations [4] can be developed in either of two ways; in an infinite series mode solution derived from an expansion of the loading in Legendre polynomials, or in a form derived from a Green's function and leading to a "traveling-wave" solution.

The former approach is generally useful only after several reflections of the elastic wave, and only then if the harmonic content is not so rich as to require a large number of modes for an adequate representation. Near the initial wave front (where the higher modes become quite important) only the latter approach is useful, so that in a sense the two methods are complementary.

Therefore both will be presented beginning with the development based on the Green's function.

First, $\overline{W'}$ can be eliminated from the Laplace transforms of Equation [4], leaving the following differential equation for $\overline{V}'$

$$\frac{d^2\overline{V}'}{d\phi^2} + \cot\phi\,\frac{d\overline{V}'}{d\phi} + \left[\alpha(\alpha+1) - \frac{1}{\sin^2\phi}\right]\overline{V}' = \frac{(1+\nu)}{(1-\nu^2)+s^2}\frac{dp'}{d\phi} \quad [7]$$

where

$$\alpha(\alpha+1) = \frac{2(1-\nu^2) - (1+3\nu)s^2 - s^4}{(1-\nu^2)+s^2}$$

[5] The actual shell stresses σ are directly proportional to p_0R/h, and this feature is preserved in all transient cases.

Equation [7] can be made self-adjoint by multiplying through by $\sin\phi$ and then may be written as

$$L_\phi(\bar{V}') = \frac{d}{d\phi}\left(\sin\phi\,\frac{d\bar{V}'}{d\phi}\right) + \left[\alpha(\alpha+1)\sin\phi - \frac{1}{\sin\phi}\right]\bar{V}' = \frac{(1+\nu)\sin\phi}{(1-\nu^2)+s^2}\frac{d\bar{p}'}{d\phi} \quad [8]$$

$$= F(\phi, s)$$

The solution of Equation [8] can be written down formally in terms of the (as yet to be determined) Green's function as (6)

$$\bar{V}'(\phi, s) = \int_0^\pi G(\phi, \phi';\ s)\ \ F(\phi',\ s)d\phi' \quad [9]$$

The Green's function itself satisfies the equation

$$L_\phi(G) = \delta(\phi - \phi') \quad [10]$$

where $\delta(\phi - \phi')$ is a delta function.
(Note that $G(\phi, \phi') = G(\phi', \phi)$ due to the self-adjoint properties of Equation [8].)

Integration of Equation [10] across the delta function leads to the "jump" condition

$$\left[\frac{dG}{d\phi}\right]_{\phi=\phi'} = \frac{1}{\sin\phi'} \quad [11]$$

Also, G must be continuous at $\phi = \phi'$, and finite at $\phi = 0$ and π.

The independent solutions of $L_\phi(\bar{V}') = 0$ are (7)

$$P_\alpha^1(\cos\phi),\ Q_\alpha^1(\cos\phi)$$

the modified Legendre functions.

The linear combination of these functions satisfying the conditions of the Green's function is

$$G(\phi, \phi';\ s) = -\frac{\pi}{8}\frac{\alpha(\alpha+1)}{\sin\pi\alpha}\begin{cases} f_1(\phi)f_2(\phi') & 0 \le \phi < \phi' \\ f_1(\phi')f_2(\phi) & \phi' < \phi \le \pi \end{cases} \quad [12]$$

with the notation

$$f_1(\phi) = -\frac{2}{\alpha(\alpha+1)}P_\alpha^1(\cos\phi) = \sin\phi F\left(1-\alpha;\ 2+\alpha;\ 2;\ \frac{1-\cos\phi}{2}\right)$$

$$f_2(\phi) = -f_1(\pi - \phi)$$

It should be noted that as $\phi \to 0$

$$f_1(\phi) \to \phi \text{ and } f_2(\phi) \to \frac{-4}{\pi\phi}\frac{\sin\pi\alpha}{\alpha(\alpha+1)}$$

Equations [12] and [9] give an integral representation of the solution for $\bar{V}'$. V' follows from the inversion formula

$$V'(\phi, t') = \frac{1}{2\pi i}\int_{-i\infty}^{i\infty} e^{st'}\,\bar{V}'(\phi, s)ds \quad [13]$$

where the contour lies to the right of all the singularities of V. The wave front is located by those values of t' and ϕ for which the contour integral of Equation [13] can be closed to the right. The behavior of the integrand for large values of s determine when this can be done. (This is related to the fact that the highest powers of s come from the highest time derivatives in the equation and are thus related to its characteristics.)

The procedure now will be to express the stresses in closed form, and then approximate the result for large values of s (small time).

Of particular interest will be the stresses at the poles of the sphere. It cannot be said *ab initio* just what stress magnitudes may result as the elastic waves originated at the pole $\phi = 0$ converge at the pole $\phi = \pi$.

The pressure may be expressed through the relations

$$t' < \frac{2}{M}\begin{cases} p'(\phi, t') = p_0' & 0 \le \phi < \cos^{-1}(1 - Mt') \\ p'(\phi, t') = 0 & \cos^{-1}(1 - Mt') < \phi \le \pi \\ p'(\phi, t') = p_0' & t' > \frac{2}{M} \end{cases} \quad [14]$$

where $M = U/C_L$, the ratio of blast-wave speed to elastic-wave speed.

Consequently

$$\left.\begin{aligned} \bar{p}' &= \frac{p_0'}{s}e^{-\frac{s}{M}(1-\cos\phi)} \\ \text{and} \\ \frac{d\bar{p}'}{d\phi} &= \frac{p_0'\sin\phi}{M}e^{-\frac{s}{M}(1-\cos\phi)} \\ \text{and} \\ F(\phi, s) &= \frac{1+\nu}{(1-\nu^2)+s^2}\frac{p_0'}{M}\sin^2\phi e^{-\frac{s}{M}(1-\cos\phi)} \end{aligned}\right\} \quad [15]$$

From Equation [9], near $\phi = 0$

$$\bar{V}'(\phi, s) = -\frac{\pi}{8}\frac{\alpha(\alpha+1)}{\sin\pi\alpha}\phi\int_0^\pi f_2(\phi', s)d\phi' + 0(\phi^2)$$

and with the aid of Equations [3]

$$\bar{N}_\phi = \bar{N}_\theta = \left[\frac{2(1-\nu^2)+(1+\nu)s^2}{2(1+\nu)+s^2}\right]\times \left[-\frac{\pi}{8}\frac{\alpha(\alpha+1)}{\sin\pi\alpha}\int_0^\pi f_2(\phi')F(\phi', s)d\phi'\right] - \frac{(1+\nu)p'(\phi, s)}{[2(1+\nu)+s^2]} \quad [16]$$

By utilizing the asymtotic expansions (as $s \to \infty$) for f_2 and F

$$F(\phi', s) \cong \frac{p_0'}{M}\frac{(1+\nu)}{s^2}\sin^2\phi' e^{\frac{s}{M}(1-\cos\phi')}$$

$$f_2(\phi', s) \cong \frac{-e^{s(\pi-\phi')}}{\sqrt{\pi\sin\phi'}}\frac{1}{s^{3/2}}$$

it can be shown that the first expression on the right side of Equation [16] will lead to a term proportional to t'^3, while the second to a term proportional to t'^2.

Hence, for small times, the membrane stresses at $\phi = 0$ follow from inverting just the term

$$-\frac{(1+\nu)p'(\phi, s)}{[2(1+\nu)+s^2]}$$

and are given by

$$N'_{\phi,\theta} = -\frac{1}{2}(1+\nu)p_0't'^2 + \ldots \quad \phi = 0 \quad [17]$$

Note that this expression agrees with Equation [6] for small times.

A similar calculation at $\phi = \pi$ yields

$$N'_{\phi,\theta} = \frac{\pi(1+\nu^2)}{2\sqrt{2}}\frac{p_0M^{3/2}}{(1-M^2)^{1/4}}(t' - t_a')^{t' \ge t_a'}_{M \le .7} \quad [18]$$

$$N'_{\phi,\theta} = 0 \qquad t' \le t_a' \qquad \phi = \pi$$

where t_a' represents the arrival time of the first elastic wave

$$t_a' = \pi - \sin^{-1}M + \frac{1-\sqrt{1-M^2}}{M} \quad M \leq .7 \quad \ldots [19]$$

Equation [19] can be explained in simple physical terms as follows: For any wave speed $U > 0$, the effective angular velocity of the pressure wave initially will be greater than that of the elastic waves (C_L/R). But, providing $M \leq 1$, at some angle ϕ the two velocities will become equal. It is at this point that the first elastic wave to reach the far pole $\phi = \pi$ is originated. Hence Equation [19] can be derived just from the geometry of the problem. If $M > .7$, it follows from Hyggens' principle that the pressure and first elastic waves will reach the pole $\phi = \pi$ simultaneously.

Equation [18] shows that no sudden large jump occurs at $\phi = \pi$ as a result of the convergence of the stress waves and hence provides more confidence in the numerical work.

Mode Solution

The foregoing analysis produced a solution in an integral form, from which approximate solutions were obtained in closed form. These approximations show how the stresses develop near the poles during the first few instants of time.

An alternative procedure which has considerable merit when the vibrations are not overly rich in harmonics is an expansion in modes. Such solutions are usually valid after several reflections of the elastic waves from the poles of the sphere.

The 0th mode (purely radial vibrations) can be obtained by applying the average pressure on the sphere as a generalized exciting force, that is

$$\frac{d^2q_0}{dt^2} + \omega_R{}^2 q_0 = \left\{ \begin{array}{ll} \dfrac{p_0 U t}{2R\rho h} & 0 \leq t \leq \dfrac{2R}{U} \\ \dfrac{p_0}{\rho h} & \dfrac{2R}{U} \leq t \end{array} \right\} \quad \ldots [20]$$

where q_0 represents the "generalized" displacement associated with the 0th mode.

From Equations [20] and [3] it follows that the stresses in this mode are

$$\left. \begin{array}{l} N_{\phi,\theta} = -\dfrac{p_0 U}{4}\left(t - \dfrac{1}{\omega_R}\sin\omega_R t\right) \qquad 0 \leq t \leq \dfrac{2R}{U} \\ N_{\phi,\theta} = \dfrac{p_0 U}{4}\left(\dfrac{2R}{U} - \dfrac{\sin\omega_R t}{\omega_R} + \dfrac{\sin\omega_R\left(t - \dfrac{2R}{U}\right)}{\omega_R}\right) \\ \omega_R{}^2 = \dfrac{2E}{(1-\nu)\rho R^2} \qquad \dfrac{2R}{U} \leq t \end{array} \right\} \quad [21]$$

It can be easily verified that Equations [21] approach Equations [6] as $U \to \infty$.

Other modes can be treated in a similar fashion, the appropriate frequencies and displacements having been given by Rayleigh (8).

In fact, for the next mode (ω_1 = frequency of mode)

$$\omega_1{}^2 = \frac{3E}{(1-\nu)\rho R^2} \quad \ldots [22]$$

$$N_{\phi,\theta} = \frac{-3Ep_0U\cos\phi}{4(1-\nu)\rho R^2}\left[\left(\frac{t}{\omega_1{}^2} - \frac{Ut^2}{2R\omega_1{}^2} - \frac{\sin\omega t}{\omega_1{}^3} - \frac{U}{R}\frac{\cos\omega_1 t}{\omega_1{}^4}\right) + \left(\frac{\left(t-\dfrac{2R}{U}\right)}{\omega_1{}^2} - \frac{\sin\omega\left(t-\dfrac{2R}{U}\right)}{\omega_1{}^3} + \frac{U}{2R\omega_1{}^2}\left(t-\frac{2R}{U}\right)^2 + \frac{U}{R}\frac{\cos\omega_1\left(t-\dfrac{2R}{U}\right)}{\omega_1{}^4}\right)H\left(t-\frac{2R}{U}\right)\right]$$

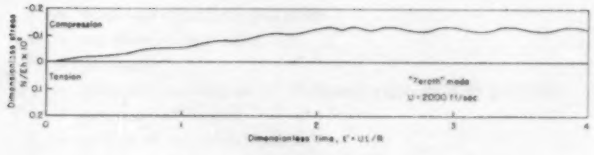

Fig. 3(*a*) Mode Solutions

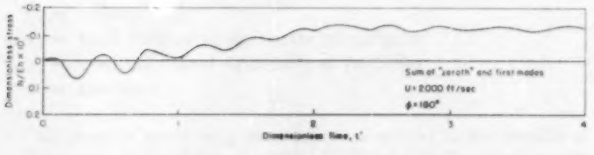

Fig. 3(*c*)

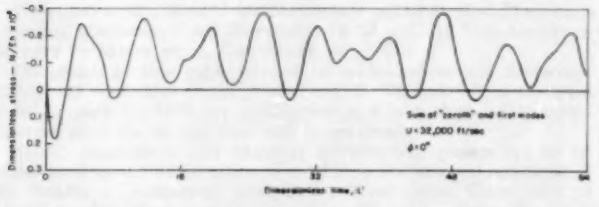

Fig. 3(*e*)

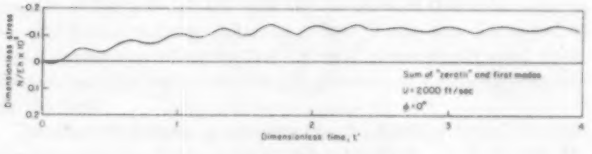

Fig. 3(*b*)

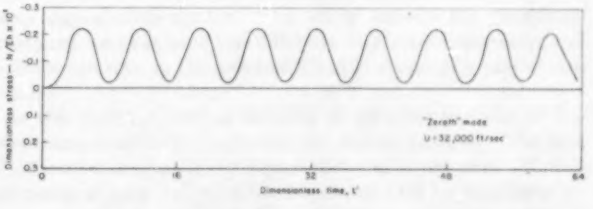

Fig. 3(*d*)

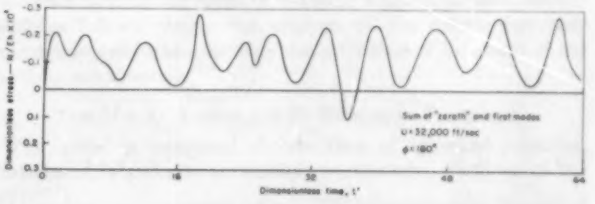

Fig. 3(*f*)

in Rayleigh's notation this would be the first species of the second class of vibrations; the radial motion is in at the poles and out at the equator while the tangential motion is toward the front pole.

For the higher modes N_ϕ and N_θ will no longer be equal.

Numerical Integration

The foregoing analytical results are of considerable interest of themselves, but do not provide an over-all picture of the shell reaction. For this purpose Equations [4] were integrated numerically with the aid of IBM equipment.

Only a few comments are necessary. First, for the numerical work the following dimensionless parameters were found to be somewhat more convenient than the ones used in the analytical work

$$t' = \frac{Ut}{R} \qquad N'_{\theta,\phi} = \frac{N_{\theta,\phi}}{Eh}$$

$$h' = \frac{h}{R}$$

$$W' = \frac{W}{R} \qquad F = \frac{E}{p_0}$$

$$V' = \frac{V}{R} \qquad \delta = \frac{phU^2}{p_0 R}$$

Then, in setting up the approximate difference equations corresponding to the actual differential Equations [4], the Courant-Friedrichs-Lewy condition (9) must be observed to insure convergence. In the case at hand the angular step was taken to be 9 deg, and time step to be approximately 0.04 millisec.

Conclusions

The results are summarized in the accompanying curves. It can be seen that the mode solution represents the stresses very well at a wave speed of 32,000 fps, and less well as the speed decreases.

For each mode there is an optimum speed as regards maximizing the stresses in that mode. The task of finding the speed that yields an over-all maximum does not appear to be tractable mathematically, but that such a speed exists is clearly indicated in the results.

As the velocity U increases, the maximum stresses occur at later times, and move from the equator toward the poles of the sphere.

Strictly speaking, Fig. 2 applies only to maximums occurring during the computed interval of about 6 millisec. This follows from the fact that the excited modes are not integer multiples of each other, and hence the resulting phenomena is "almost periodic." However, since damping actually will become more important later on, one is practically only interested in maxima that occur soon after envelopment.

BIBLIOGRAPHY

1 "The Interaction of an Acoustic Wave and an Elastic Spherical Shell," by P. Mann, Office of Naval Research, Contract N7ONR-35810, Technical Report No. 11, February, 1953.

2 "Response of an Elastic Cylindrical Shell to a Transverse, Step Shock Wave," by R. D. Mindlin and H. H. Bleich, Journal of Applied Mechanics, Trans. ASME, vol. 75, 1953, pp. 189–195.

3 "On the Properties of Extensible Surfaces," by J. H. Jellett, *Royal Irish Academy Transactions*, vol. 22, part 5, 1855, p. 343.

4 "Basic Differential Equations in General Theory of Elastic Shells," by V. S. Vlasov, NACA TM 1241, February, 1951, p. 27.

5 "Theory of Plates and Shells," by S. P. Timoshenko, McGraw-Hill Book Company, Inc., New York, N. Y., 1940, chapter 12.

6 "Methoden der Mathematischen Physik," by R. Courant and D. Hilbert, Interscience Publishers, Inc., New York, N. Y., vol. 1, 1943, p. 265.

7 "Formeln und Satze fur die Speziellen Funktionen der Mathematischen Physik," by W. Magnus and F. Oberhettinger, Julius Springer, Berlin, Germany, 1948, p. 73.

8 "The Theory of Sound," by Lord Rayleigh, Dover Publications, New York, N. Y., vol. 1, 1945, p. 419.

9 "Über die partiellen Differenzengleichungen der Mathematischen Physik," by R. Courant, K. Friedrichs, and H. Lewy, *Mathematische Annalen*, vol. 100, 1928, pp. 32–74.

A Study of the Speed of Sound in Porous Granular Media[1]

By H. BRANDT,[2] LA HABRA, CALIF.

A theory is developed to explain the influence of pressure, porosity, and liquid saturation on the speed of sound through a porous granular medium. An aggregate of randomly stacked spherical particles of four different sizes is used as a model for the porous medium. The volume-pressure relationship of the aggregate is determined by means of the Hertz theory for the deformation of elastic and isotropic spheres in contact. This relationship is extended to embrace the case of liquid saturation of the aggregate. The bulk modulus is derived from the volume-pressure relationship and the speed of sound is determined from the bulk modulus. It is shown how the theory can be extended to apply to the speed of sound through an aggregate comprised of nonspherical granules and finally, in an approximate form, through a consolidated granular medium. As an example of the application of the latter the speed of sound through sandstone under various conditions of pressure and saturation is predicted, and agreement is noted between the predicted results and those derived experimentally.

Nomenclature

The following nomenclature is used in the paper:

- B = bulk modulus
- C_φ = porosity factor for aggregate of spherical particles
- $C_{\varphi L}$ = porosity factor for liquid saturated aggregate of spherical particles
- E = modulus of elasticity of particles
- F = force on spherical particles
- N = number of particles
- P = pressure
- P_e = pressure on outside of enclosed aggregate of particles
- P_L = pressure of liquid
- R = radius of spherical particles
- S = speed of sound
- U = dimensionless diameter ratio of spherical particles; $U = R_{\epsilon-1}/R_\epsilon$
- V = volume
- V_{bulk} = bulk volume of aggregate of particles
- V_{void} = void volume of aggregate of particles
- c = constant
- d = density of particles
- d_L = density of liquid
- $\bar{d}$ = density of aggregate of particles or density of medium under consideration
- g = acceleration of gravity
- k = constant to be obtained from experiment
- r = radius of contact between two deformed particles
- x = variable of integration
- α = void volume in a unit volume of uniformly sized, randomly stacked particles. For spherical particles $\alpha = 0.392$
- Δ = deflection of spherical particles in contact
- ϵ = number of particle sizes in aggregate
- ρ = specific gravity of particles
- ρ_L = specific gravity of liquid
- σ = Poisson's ratio of particles
- $\bar{\sigma}$ = Poisson's ratio of aggregate of particles or Poisson's ratio of medium under consideration
- $\bar{\sigma}_L$ = Poisson's ratio of liquid-saturated aggregate of particles
- φ = porosity, i.e., fraction of void volume per unit volume of porous material

Introduction

The speed of sound through porous media is dependent on the nature and composition of those media. Rocks, for example, are characterized not only by their mineral composition, but by the shape and arrangement of their fundamental particles. The speed of sound through the rock is a function of these characteristics and hence varies in different rocks. Then, too, the speed of sound varies according to the external pressure imposed upon the rock and the bulk modulus and pressure of the liquid saturating the rock.

The effect of mineral composition on the speed of sound through porous media has been investigated extensively (1, 8, 12, 19, 45, 47).[3] Other factors, like the effects of pressure, porosity, and liquid saturation, have been investigated experimentally, and to a lesser degree theoretically. This study extends the theoretical treatment and explains the influence of pressure, porosity, and liquid saturation on the speed of sound in a porous granular material.

In this study, a random stacking of spherical particles of different sizes is used as a model for the porous material. The idea of a model to represent the porous material is not new. Models composed of spherical particles have been used by numerous investigators (20, 42, 48) in studies with porous materials as well as in studies of the speed of sound in porous materials (16, 18, 31, 43). The derivation of the speed of sound in a model of nonspherical particles follows closely the analysis of the spherical-particle model provided certain average characteristics of the shape of the particles are known.

The Model Aggregate of Spherical Particles

The model is composed of four sizes of spherical particles. Particles of largest size are stacked at random. Particles of the

[1] This paper is based on a dissertation presented to the faculty of the University of California in partial fulfillment of the requirements for the degree of Doctor of Philosophy in June, 1954.

[2] Research Engineer, California Research Corporation, a subsidiary of Standard Oil Company of California.

Presented at the West Coast Conference of the Applied Mechanics Division, Monterey, Calif., September 12–13, 1955, of The American Society of Mechanical Engineers.

Discussion of this paper should be addressed to the Secretary, ASME, 29 West 39th Street, New York, N. Y., and will be accepted until January 10, 1956, for publication at a later date. Discussion received after the closing date will be returned.

Note: Statements and opinions advanced in papers are to be understood as individual expressions of their authors and not those of the Society. Manuscript received by West Coast Committee of ASME Applied Mechanics Division, May 19, 1955. Paper No. 55—APM-37.

[3] Numbers in parentheses refer to the Bibliography at the end of the paper.

next smaller size are stacked at random in the interstices of the larger ones without disturbing their arrangement. The smaller these smaller particles are, the more closely will they pack, and the more will be needed. The interstices thus created are occupied in the same way by a random arrangement of still smaller particles until there are four distinct sizes of particles in the model aggregate. The volume remaining void after the process of particle stacking can be calculated as a special case of the more general studies of stackings of particles of arbitrary shape made by Furnas (13, 14) the relevant details of which will be discussed.

Let α be the fraction of voids in a unit volume of uniformly sized, randomly stacked spherical particles; the volume V_1 of solid matter in this unit volume is then $(1 - \alpha)$. Consider the ideal case in which infinitely small particles are stacked randomly in the voids of the larger ones. If the fraction of voids in a unit volume of uniformly, randomly stacked particles of small size is also α, the volume V_2 of smaller particles will be $\alpha(1 - \alpha)$. This reasoning can now be extended to a mixture of four components and one can write for the volumes of the four groups of spherical particles

$$V_1 : V_2 : V_3 : V_4 = 1 : \alpha : \alpha^2 : \alpha^3 \quad \ldots\ldots [1]$$

Theoretically, this proportionality is true only if the diameter ratios (larger size to next smaller size) of particles in the groups are infinite. However, Furnas has shown experimentally that this volume relationship is approximately true in a mixture of particles with diameter ratios as low as five. In addition to the requirement that the aggregate of particles satisfies Equation [1], it is essential that particles occupying the interstices of larger ones form a random-stacking arrangement. This requirement limits the diameter ratio of particles more severely than the diameter ratio of five required for the proportionalities of the volumes.

The void volume of an aggregate of randomly stacked, sized, spherical particles has been determined experimentally by Westman and Hugill (48). These investigators agitated stackings of sized particles so that the bulk volume decreased and the minimum obtainable volume could be observed. The experiments showed that the void fraction per unit volume of randomly stacked spherical particles is 0.392.

Finally, the number of contacts between randomly stacked spherical particles of uniform size must be known. This number has been determined experimentally by Smith, Foote, and Busang (42) who found that the average number of contacts per particle is 8.84.

Bulk and Void Volumes of Randomly Stacked Spherical Particles of Uniform Size

Consider an enclosure with randomly stacked, uniform, spherical particles. The dimensions of this enclosure are assumed to be sufficiently large that the effects of the walls of the enclosure on the particle stacking can be neglected. Let there be N particles of radius R in the enclosure. The volume of the enclosure can then be expressed as

$$V = \frac{4\pi N R^3}{3(1 - \alpha)} \quad \ldots\ldots [2]$$

When the enclosure volume is decreased, the particles inside the enclosure are deformed. This deformation occurs at the points of contact between adjacent particles and causes the center distances between particles in contact to decrease. If the average decrease of the particle radii is Δ, the bulk volume of the enclosure of deformed particles is

$$V_{bulk} = \frac{4\pi N (R - \Delta)^3}{3(1 - \alpha)} \quad \ldots\ldots [3]$$

The particle deformation will be determined according to Hertz's theory for the deformation of isotropic spheres in contact. This theory is true only for small deflections of spherical particles. More specifically, Hertz (44) neglects the term Δ^2. Hence, to introduce values of the deformation expressed by Hertz into Equation [3], it is necessary, for the sake of consistency, to neglect terms of the order of Δ^2 and Δ^3. The bulk volume reduces then to

$$V_{bulk} = \frac{4\pi N R^3}{3(1 - \alpha)} - \frac{4\pi N R^2 \Delta}{(1 - \alpha)} \quad \ldots\ldots [4]$$

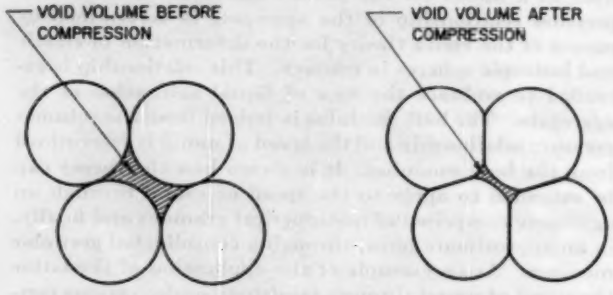

Fig. 1 Stacking of Spherical Particles

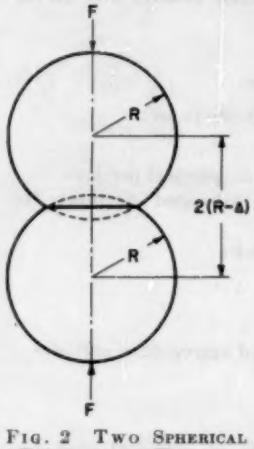

Fig. 2 Two Spherical Particles in Contact

Two volume changes, shown schematically in Fig. 1, occur when the bulk volume decreases: (*a*) The void volume decreases because the centers of the particles approach each other and (*b*) the particles themselves change in volume. The void volume of the aggregate can be calculated by subtracting the volume of the deformed particles from the bulk volume. However, the change in particle volume at the contact point is of the order of Δ^2 which must be neglected to be consistent with the assumption of Hertz's theory which is applied subsequently. Thus changes in particle volume are neglected. A change in bulk volume of the aggregate is then entirely due to a change in the void volume. The void volume of the aggregate can now be obtained by subtracting the volume of the undeformed particles from the bulk volume.
Thus

$$V_{void} = \frac{4\pi\alpha N R^3}{3(1 - \alpha)} - \frac{4\pi N R^2 \Delta}{1 - \alpha} \quad \ldots\ldots [5]$$

The value of Δ as a function of the force between the particles can be obtained from the theory of Hertz (44). With two homogeneous and isotropic spherical particles of equal radii, shown in Fig. 2, the radius of one of the spherical particles at the point of contact decreases by an amount

$$\Delta = \left(\frac{3(1 - \sigma^2)F}{4ER^{1/2}} \right)^{2/3} \quad \ldots\ldots [6]$$

The bulk volume of an aggregate of N_1 particles with radii R_1 reduces to

$$V_{bulk} = \frac{4\pi N_1 R_1^3}{3(1-\alpha)} - \frac{4\pi N_1 R_1^2}{1-\alpha}\left(\frac{3(1-\sigma^2)F_1}{4ER_1^{1/2}}\right)^{2/3} \quad [7]$$

It is assumed in this derivation that all particles have the same material properties and that there exists an average value Δ for the particle deformations. The theory can be expanded readily to include the case of particles of different materials. Instead of an average deformation Δ, a distribution of particle deformations may be used.

Deformation of Particles in Model Aggregate

Consider a mixture of two sizes of particles, in which the smaller occupies the interstices of the larger. Any change in the interstitial volume of the larger particles must now produce an equal change in the bulk volume of the smaller. If Δ_1 is the decrease in radius R_1 of the larger particles and similarly Δ_2 is the decrease in radius R_2 of the smaller particles, the change in interstitial volume of the larger particles can be equated to the change in bulk volume of the smaller particles. Thus, if $U = R_1/R_2$, then

$$\frac{\Delta_2}{\Delta_1} = \frac{1}{\alpha U} \quad [8]$$

This procedure can now be followed for other particles, all of which are stacked in the voids of the next larger ones. The deformations of particles of ϵ sizes in the aggregate can then be written in terms of the deformation of particles of the largest size. Thus, if the subscript 1 refers to the largest particles and ϵ refers to the smaller particles, there is obtained

$$\frac{\Delta_\epsilon}{\Delta_1} = \frac{1}{\alpha_1^{\epsilon-1}U^{\epsilon-1}} \quad [9]$$

The Bulk Volume–Pressure Relationship of a Liquid-Saturated Aggregate of Spherical Particles of Different Sizes

Consider an aggregate of particles in an enclosure with flexible walls which transmit an external pressure P_o to the aggregate of

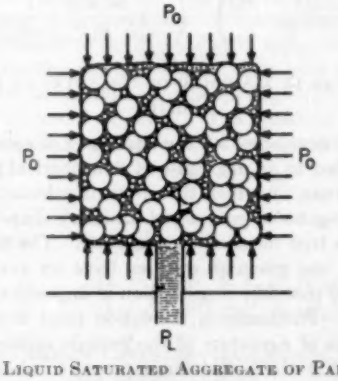

Fig. 3 Liquid Saturated Aggregate of Particles

particles as shown in Fig. 3. A tube passes through one of the flexible walls and a liquid is added to the aggregate through the tube. The use of the flexible enclosure makes the theory conform to experimental techniques (3, 4, 5, 21, 22, 23, 24) of the sound-speed measurement in porous materials. In these experiments the porous material is either enclosed by a jacket and pressurized, or the material is exposed to a liquid under pressure. Both of these possibilities are included in the arrangement of Fig. 3.

An energy balance can now be written which comprises the energy required to compress the aggregate, the energy stored in the deformed particles, and the energy required to compress the liquid. If a pressure P_o is exerted on the aggregate of particles of different sizes, the bulk-volume decrease is equal to the bulk-volume decrease of the largest particles. The energy required to decrease the bulk volume of the aggregate is then

$$\frac{4\pi N_1 R_1^2}{1-\alpha}\int_0^{\Delta_1} P_o\,dx$$

where x is a variable of integration. Since each group of particles of uniform size is assumed to form a random-stacking arrangement, and since there is an average of 8.84 points of contact on each particle in a random stacking, the energy stored in the deformed particles is

$$8.84\sum_{\epsilon=1,2,3,4} N_\epsilon \int_0^{\Delta_\epsilon} F_\epsilon\,dx = 8.84\sum_{\epsilon=1,2,3,4} N_1 U^{2(\epsilon-1)}\int_0^{\Delta_1} F_\epsilon\,dx$$

Since all particles in the aggregate are assumed to have the same material properties, the theory of Hertz gives with Equation [9]

$$\frac{F_\epsilon}{F_1} = \left(\frac{\Delta_\epsilon}{\Delta_1}\right)^{3/2} U^{-\frac{1}{2}(\epsilon-1)} \quad [10]$$

so that

$$8.84N_1\sum_{\epsilon=1,2,3,4}\alpha^{-\frac{3}{2}(\epsilon-1)}\int_0^{\Delta_1} F_1 dx = 8.84N_1 C_{\varphi\epsilon}\int_0^{\Delta_1} F_1 dx \quad [11]$$

where $C_{\varphi\epsilon}$ is a porosity factor

$$C_{\varphi\epsilon} = \sum_{\epsilon=1,2,3,4}\alpha^{-\frac{3}{2}(\epsilon-1)} \quad [12]$$

The energy in the compressed liquid in the voids of the aggregate is

$$\int_0^{\Delta_\epsilon}\left[P_L - B\ln\left(1-\frac{3x}{\alpha R_\epsilon}\right)\right]\frac{4\pi N_\epsilon R_\epsilon^2}{1-\alpha}\,dx = \frac{4\pi N_1 R_1^2}{1-\alpha}\int_0^{\Delta_1}\left[P_L - B\ln\left(1-\frac{3x}{\alpha^\epsilon R_1}\right)\right]dx \quad [13]$$

By equating the energy to decrease the bulk volume of the saturated aggregate to the energy stored in the deformed particles and the energy in the compressed liquid, there results

$$\int_0^{\Delta_1}\left[\frac{4\pi N_1 R_1^2}{1-\alpha}(P_o - P_L) - 8.84N_1 C_{\varphi\epsilon}F_1 + \frac{4\pi N_1 R_1^3 B}{1-\alpha}\ln\left(1-\frac{3x}{\alpha^\epsilon R_1}\right)\right]dx = 0 \quad [14]$$

Equation [14] must be true for any arbitrary, small value of the deformation Δ_1 so that

$$\frac{4\pi N_1 R_1^2}{1-\alpha}(P_o - P_L) - 8.84N_1 C_{\varphi\epsilon}F_1 + \frac{4\pi N_1 R_1^3 B}{1-\alpha}\ln\left(1-\frac{3\Delta_1}{\alpha^\epsilon R_1}\right) = 0 \quad [15]$$

If the logarithmic term is expanded and terms of order Δ_1^2 and higher are neglected to be consistent with the theory of Hertz, there is obtained

$$\frac{4\pi R_1^2(P_o - P_L)}{1-\alpha} - 8.84C_{\varphi\epsilon}F_1 - \frac{12\pi B}{\alpha^\epsilon(1-\alpha)}\left(\frac{3(1-\sigma^2)R_1F_1}{4E}\right)^{2/3} = 0 \quad [16]$$

This equation is solved by successive approximation. As a first approximation of the solution of Equation [16], the term with $C_{\varphi\epsilon}$ can be neglected. As a second approximation there is obtained

$$F_1 = \frac{2.34R_1^2(P_o - P_L)}{C_{\varphi\epsilon} + \frac{9.11B^{3/2}(1-\sigma^2)}{\alpha^{3/2}E(P_o - P_L)^{1/2}}} \quad \ldots\ldots [17]$$

which is adequate.

Since the factor $C_{\varphi\epsilon}$ is a function of α and the porosity is a function of α, the factor $C_{\varphi\epsilon}$ can be expressed in terms of porosity. Table 1 lists numerical values of the term $C_{\varphi\epsilon}^{1/2}\varphi_\epsilon^{1/2}$ for various particle aggregates. The term will be considered equal to

$$C_\varphi^{1/2}\varphi^{1/2} = \frac{2}{3} \quad \ldots\ldots [18]$$

in which the subscript ϵ has been omitted because the relation is now independent of the number of groups of particles in the model aggregate. Substitution of Equation [18] into Equation [17] gives

$$F_1 = \frac{2.34R_1^2(P_o - P_L)}{C_\varphi\left[1 + \frac{30.75B^{2/3}(1-\sigma^2)}{E(P_o - P_L)^{1/3}}\right]} \quad \ldots\ldots [19]$$

Let $C_{\varphi L}$ be the symbol for the porosity factor of the saturated aggregate of particles, then

$$C_{\varphi L} = C_\varphi\left[1 + \frac{30.75B^{2/3}(1-\sigma^2)}{E(P_o - P_L)^{1/3}}\right] \quad \ldots\ldots [20]$$

The bulk volume of the aggregate of particles can now be determined by substituting Equations [19] and [20] into Equation [7]. Thus

$$V_{\text{bulk}} = \frac{4\pi N_1 R_1^3}{3(1-\alpha)} - \frac{4\pi N_1 R_1^3}{1-\alpha}\left(\frac{1.75\,(1-\sigma^2)(P_o - P_L)}{EC_{\varphi L}}\right)^{2/3} \quad \ldots [21]$$

Speed of Sound in the Aggregate of Spherical Particles

The speed of a longitudinal wave (dilatational or sound wave) in an isotropic medium of infinite extent is

$$S = \left[\frac{3g}{\bar{d}}\left(-V\frac{dP}{dV}\right)\left(\frac{1-\bar{\vartheta}}{1+\bar{\vartheta}}\right)\right]^{1/2} \quad \ldots\ldots [22]$$

The bulk modulus of the aggregate of particles can be calculated from the relation between the bulk volume and the pressure. Thus

$$-V\frac{dP_o}{dV} = \frac{C_\varphi^{2/3}(P_o - P_L)^{1/3}\left(1 + \frac{30.75B^{2/3}(1-\sigma^2)}{E(P_o - P_L)^{1/3}}\right)^{2/3}}{2\left(\frac{1.75(1-\sigma^2)}{E}\right)^{2/3}\left(1 + \frac{46.13B^{2/3}(1-\sigma^2)}{E(P_o - P_L)^{1/3}}\right)} - 1.5(P_o - P_L)\frac{\left(1 + \frac{30.75B^{2/3}(1-\sigma^2)}{E(P_o - P_L)^{1/3}}\right)^{2/3}}{\left(1 + \frac{46.13B^{2/3}(1-\sigma^2)}{E(P_o - P_L)^{1/3}}\right)} \quad \ldots [23]$$

If the density of the liquid is d_L and the density of the particles is d, the density of the saturated aggregate of particles is

$$\bar{d} = d - \varphi(d - d_L) \quad \ldots\ldots [24]$$

The speed of sound in the saturated aggregate of spherical particles can now be obtained by substituting Equations [18], [23], and [24] into Equation [22]. Thus

$$S = \left\{\frac{2g}{3\varphi[d - \varphi(d - d_L)]}\left(\frac{1-\bar{\vartheta}_L}{1+\bar{\vartheta}_L}\right)\right. \left[\frac{(P_o - P_L)^{1/3}\left(1 + \frac{30.75B^{2/3}(1-\sigma^2)}{E(P_o - P_L)^{1/3}}\right)^{2/3}}{\left(\frac{1.75\,(1-\sigma^2)}{E}\right)^{2/3}\left(1 + \frac{46.13B^{2/3}(1-\sigma^2)}{E(P_o - P_L)^{1/3}}\right)} - 6.75\varphi(P_o - P_L)\frac{\left(1 + \frac{30.75B^{2/3}(1-\sigma^2)}{E(P_o - P_L)^{1/3}}\right)^{2/3}}{\left(1 + \frac{46.13B^{2/3}(1-\sigma^2)}{E(P_o - P_L)^{1/3}}\right)}\right]^{1/2} \quad \ldots [25]$$

For low pressure the last term in Equation [25] is small compared with the first term. If the former is neglected, the speed of sound reduces to

$$S = \left\{\frac{2g}{3\varphi[d - \varphi(d - d_L)]}\left(\frac{1-\bar{\vartheta}_L}{1+\bar{\vartheta}_L}\right)\right\}^{1/2} \frac{(P_o - P_L)^{1/6}\left(1 + \frac{30.75B^{2/3}(1-\sigma^2)}{E(P_o - P_L)^{1/3}}\right)^{1/3}}{\left(\frac{1.75(1-\sigma^2)}{E}\right)^{1/3}\left(1 + \frac{46.13B^{2/3}(1-\sigma^2)}{E(P_o - P_L)^{1/3}}\right)^{1/2}} \quad \ldots [26]$$

TABLE 1 VALUES OF POROSITY AND VALUES OF $C_{\varphi\epsilon}^{1/2}\varphi_\epsilon^{1/2}$

Values of porosity	Values of $C_{\varphi\epsilon}^{1/2}\varphi_\epsilon^{1/2}$	
$\varphi_1 = \alpha = 0.392$	$\alpha^{1/2}$	$= 0.626$
$\varphi_2 = \alpha^2 = 0.154$	$\alpha^{1/2}(1 + \alpha^{3/2})^{1/2}$	$= 0.674$
$\varphi_3 = \alpha^3 = 0.060$	$\alpha^{1/2}(1 + \alpha^{3/2} + \alpha^3)^{1/2}$	$= 0.684$
$\varphi_4 = \alpha^4 = 0.024$	$\alpha^{1/2}(1 + \alpha^{3/2} + \alpha^3 + \alpha^{9/2})^{1/2}$	$= 0.687$

Speed of Sound in a Medium of Granules of Nonspherical Shape

The theory developed for the aggregate of spherical particles can be extended to an aggregate of nonspherical granules. The studies of Furnas, on which the previous calculations are based, apply to aggregates of granules of arbitrary shape. Thus Equation [1] holds true for such an aggregate. The theory of Hertz requires that the granular surfaces have an average radius of curvature and therefore a restriction is imposed on the shape of the granules. Furthermore, a relation must exist between the average radius of curvature of the granule surfaces and granule volumes so that the bulk-volume-pressure relationship can be written. In the derivation of the formulas for the aggregate of spherical particles, the changes in particle volumes due to pressure was neglected. If this approach is followed, equations similar to Equations [5] and [7] can be written.

Finally, a knowledge of the average number of contacts between sized granules permits an energy balance to be made of the work done in compressing the aggregate and the energy stored in the deformed granules. The speed of sound in the aggregate of nonspherical granules is then dependent on the number of contacts between granules, the void volume of the aggregate, and the relation between the average radius of curvature and the volume of the granules. These factors are all related to the shape of the granules. The presence of these shape-dependent factors in

the formula for the sound speed is not objectionable because the formula includes other constants like the elasticity and Poisson's ratio of the granules. These constants are often unknown and they may be more conveniently written as a single constant. Thus the formula for the speed of sound in the aggregate of spherical particles applies, except for a numerical constant, to an aggregate of granules of the more general shape described.

A single determination of the sound speed provides sufficient information to predict the variation of the sound speed with pressure, or liquid saturation, or porosity. Data obtained by Westman and Hugill (48) show that the void volume in a unit bed of sized nonspherical granules varies little from the value for the spherical particles. If this value is retained, the formula for the speed of sound, as given in Equation [26], can be modified for a dry aggregate to

$$S = \left\{\frac{2g}{3d\varphi(1-\varphi)}\left(\frac{1-\bar{\sigma}}{1+\bar{\sigma}}\right)\right\}^{1/3}\frac{P_o^{1/6}}{k^{1/3}} \quad \ldots\ldots [27]$$

where k is a constant. Data reported on Poisson's ratio by Birch (8) and Zisman (49) show that Poisson's ratio varies from 0.12 to 0.28 for sandstones. Furthermore, Oliphant (40) showed that the variation in Poisson's ratio is small when a dry porous material is saturated with liquid. If Poisson's ratio is taken as 0.20, the speed of sound (fps) in the dry sandstone can be written as a function of pressure (psi), porosity, specific gravity, and a material constant $k(\text{psi})^{-1}$

$$S = \frac{5.75P_o^{1/6}}{\rho^{1/2}\varphi^{1/2}(1-\varphi)^{1/2}k^{1/2}} \quad \ldots\ldots [28]$$

In an aggregate of spherical particles, the liquid pressure is subtracted directly from the outside pressure because the entire particle surfaces are exposed to the liquid. In a consolidated sandstone, the surfaces of the particles are not entirely accessible to the liquid on account of the binding material present between particles.

A net force exerted on the particles located in the outer surface of the core results in a compression of the standstone core. Instead of the pressure term $(P_o - P_L)$ in Equation [26] for the aggregate of spherical particles, the pressure term for the liquid-saturated sandstone should be written as $(P_o - cP_L)$ where c is a parameter of the order of unity. The speed of sound in the saturated porous sandstone can now be written as being approximately equal to

$$S = \frac{5.75(P_o - cP_L)^{1/6}}{\varphi^{1/2}[\rho - \varphi(\rho - \rho_L)]^{1/2}k^{1/2}} \frac{[1 + 17.5B^{2/3}k(P_o - cP_L)^{-1/3}]^{5/6}}{[1 + 26.3B^{2/3}k(P_o - cP_L)^{-1/3}]^{1/2}} \quad [29]$$

Prediction of Certain Experimental Results by Means of the Model Theory

Several experimental results can be predicted by means of the model theory. The theory indicates that the speed of sound is proportional to the $^1/_6$ power of the pressure. This pressure variation is inherent in all model theories in which the elasticity is determined from Hertz's theory. To compare the theoretical pressure variation with experiments, the results of experiments by Nasu (35) are presented on logarithmic co-ordinates in Fig. 4. For comparison, a line with a slope of $^1/_6$ was plotted. The slopes of the experimental curves range from $^1/_2$ to $^1/_7$. The speed of sound is then proportional to the pressure raised to a power which ranges from $^1/_2$ to $^1/_7$. The theoretical value of the exponent of $^1/_6$ is within this range of experimental values reported.

A second application pertains to the formation compaction which is the change in pore volume per unit pore volume per unit pressure. The formation compaction can be calculated from

$$\frac{\text{Change in } V_{\text{void}}}{V_{\text{void}}} = -\frac{3k^{2/3}P_o^{2/3}}{\varphi C_\varphi^{2/3}} \quad \ldots\ldots [30]$$

where k is a material constant. The formation compaction is inversely proportional to $\varphi C_\varphi^{2/3}$ which reduces to a constant, see Table 1.

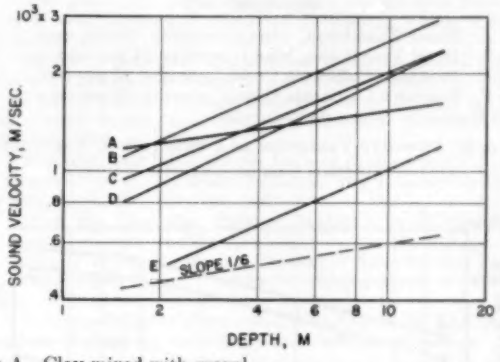

Curve A Clay mixed with gravel
Curve B Vegetation soil changing to clay
Curve C Soil changing gradually to clay
Curve D Soil changing gradually to clay
Curve E Vegetation soil at the surface. Soil changes gradually to clay below surface

Fig. 4 Sound Velocity as a Function of Soil Depth
(Data from reference 35.)

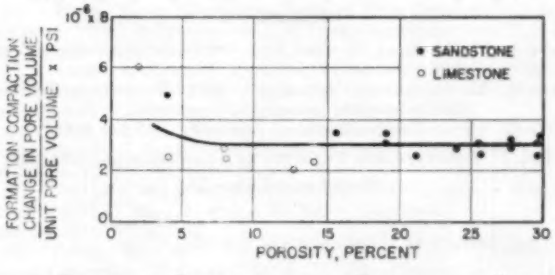

Fig. 5 Formation Compaction as a Function of Porosity
(Data from reference 17.)

According to the model theory, the theoretical formation compaction is independent of porosity. Experimental data reported by Hall (17) on the formation compaction are presented in Fig. 5. It is observed from this figure that theory and experiment agree.

The porosity variation due to pressure will be compared with results obtained by Fatt (11). Fatt investigated the ratio of the porosity at high pressure to the porosity at zero pressure of four reservoir rocks. This ratio can be calculated from

$$\frac{(\text{Porosity at pressure } P_o)}{(\text{Porosity at zero pressure})} = \frac{1}{\varphi}\left(\frac{\text{void volume}}{\text{bulk volume}}\right)_{\text{Pressure } Po} = \frac{\dfrac{4\pi NR^3\varphi}{3(1-\alpha)} - \dfrac{4\pi NR^3}{1-\alpha}\left[\dfrac{1.75(1-\sigma^2)P_o}{EC_\varphi}\right]^{2/3}}{\varphi\left[\dfrac{4\pi NR^3}{3(1-\alpha)} - \dfrac{4\pi NR^3}{1-\alpha}\left(\dfrac{1.75(1-\sigma^2)P_o}{EC_\varphi}\right)^{2/3}\right]} \quad [31]$$

So that the order of magnitude of this ratio might be estimated, the modulus of elasticity of the particles is assumed to be equal to 7×10^6 psi and Poisson's ratio for the particles equal to 0.25.

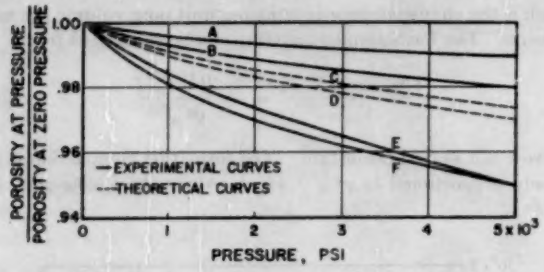

Curve A Basal Tuscaloosa, Miss.; porosity 15 per cent
Curve B Basal Tuscaloosa, Miss.; porosity 24 per cent
Curve E Southern California Coast; porosity 25 per cent
Curve F Southern California Coast; porosity 22 per cent
Curves C and D Theoretical curves

FIG. 6 POROSITY VARIATION AS A FUNCTION OF PRESSURE
(Data from reference 11.)

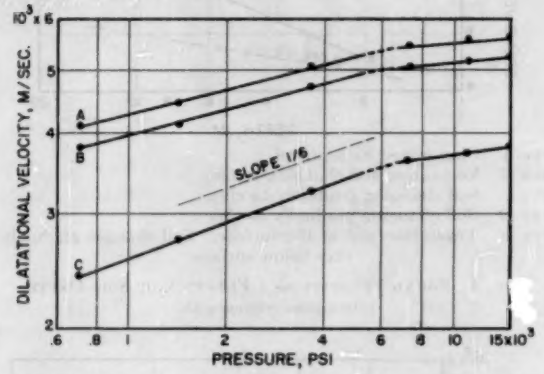

Curve A McKee Sand, Simpson Fm—Ordovician; porosity 8.5 per cent
Curve B Medium-grained light gray to white Tensleep sandstone—Pennsylvanian; porosity 13.7 per cent
Curve C Steven Sand—Miocene; porosity 21.9 per cent

FIG. 7 DILATATIONAL VELOCITY AS A FUNCTION OF PRESSURE
(Data from reference 24.)

The substitution of these values in the ratio gives

$$\frac{(\text{Porosity at pressure } P_e)}{(\text{Porosity at zero pressure})} = \frac{1 - 1.2 \times 10^{-4} P_e^{5/3}}{1 - 1.2 \times 10^{-4} \varphi P_e^{5/3}} \quad [32]$$

This ratio is plotted for various pressures and porosities in Fig. 6. The experimental results by Fatt (11) are included in the figure, and it is noted that theory and experiment are in harmony.

Of the laboratory experiments on the speed of sound in consolidated rocks, those by Hughes, et al. (21, 22, 23, 24) merit special attention. The dilatational velocities as a function of the pressure for three sandstones are presented on logarithmic coordinates in Fig. 7. At low pressures the velocity increases at a rate approximately equal to the pressure raised to the $^1/_6$ power. At high pressures the velocity increases less rapidly. It is probable that the change of slope of the curves in Fig. 7 occurs when the surfaces of contact between deformed particles become large. When the particles are considerably "flattened" at their contact points, subsequent compression becomes increasingly difficult to accomplish. Hertz's theory applies as long as the radius of the surface of contact is small compared to the radius of curvature of the particles. A criterion for establishing whether Hertz's theory applies is to calculate the radius of contact of the spherical particles. If this radius r is expressed as a fraction of the particle radius there results

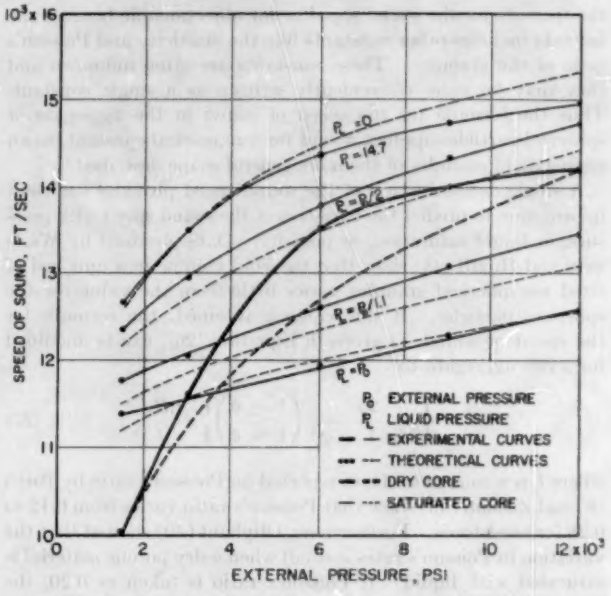

FIG. 8 SPEED OF SOUND AS A FUNCTION OF PRESSURE
(Sandstone description: Specific gravity 2.27; porosity 13 per cent; grain volume 77 per cent; interstitial clay 3 per cent; interstitial silica 1 per cent; interstitial carbonate 6 per cent. Data from unpublished report by D. H. Davis of California Research Corporation.)

$$\frac{r}{R} = \left(\frac{\Delta}{R}\right)^{1/2} = \left(\frac{\alpha}{\varphi}\right)^{1/2} \left(\frac{1.75(1-\sigma^2)P_e}{EC_\varphi}\right)^{1/3} \quad [33]$$

When the pressure is zero the particles are unstressed and the ratio r/R is zero. Because the effect of porosity on the radius of the surface of contact is considered, the ratio r/R is written in the form

$$\frac{r}{R} = 1.5\alpha^{1/2} \left(\frac{1.75(1-\sigma^2)P_e}{E}\right)^{1/3} \quad [34]$$

This ratio is found to be independent of porosity. The remaining factors affecting the radius of the surface of contact are the material properties and the pressure. The three sandstones for which the experimental curves are plotted in Fig. 7 have similar material properties, but different porosities. Thus, since the pressure is the only remaining variable, all curves of the dilatational velocity in Fig. 7 exhibit a change of slope at approximately the same pressure.

As a final correlation between the model theory and experiment, the effect of liquid saturation on the speed of sound will be considered. The experimental data for a dry and a saturated sandstone are plotted in Fig. 8. The theoretical variation of the speed of sound with pressure can be determined from the relation

$$S = \frac{5.75 P_e^{1/6}}{\rho^{1/2} \varphi^{1/2} (1-\varphi)^{1/2} k^{1/3}} \quad [35]$$

in which the constant k is to be calculated from one known value of the speed of sound. If k is calculated for a sound speed of 10,000 fps at 1500 psi, the constant k becomes equal to 37.5×10^{-9} $(\text{psi})^{-1}$. The speed of sound can now be determined for a dry and a saturated core at outside pressures ranging from 1500 to 12,000 psi. The heavy dotted line in the figure is the theoretical speed of sound. This curve deviates less than 10 per cent from the experimental curve. In a saturated sandstone with a liquid under zero pressure, the formula for the speed of sound becomes

$$S = \frac{5.75 P_e^{1/6}}{\varphi^{1/2}[\rho - \varphi(\rho - \rho_L)]^{1/2} k^{1/3}} \frac{(1 + 17.5 B^{2/3} k P_e^{-1/2})^{5/6}}{(1 + 26.3 B^{2/3} k P_e^{-1/2})^{1/2}} \quad [36]$$

The specific gravity and the bulk modulus of the oil with which the sandstone was saturated were taken as 0.864 and 25×10^4 psi, respectively. Substitution of these liquid properties and the value of constant k into Equation [36] determines the speed of sound of the saturated sandstone as a function of pressure. The theoretical curve thus obtained is the dotted curve in Fig. 7, with liquid pressure equal to zero. The experimental curve of the saturated sandstone with a liquid pressure equal to 1 atm is plotted for comparison.

One known value of the speed of sound in the sandstone has thus provided sufficient information to allow the calculation of the speed of sound as a function of pressure in dry and saturated sandstones. When the liquid pressure is not equal to zero the formula for the speed of sound is

$$S = \frac{5.75(P_o - cP_L)^{1/6}}{\varphi^{1/2}[\rho - \varphi(\rho - \rho_L)]^{1/2}k^{1/3}} \cdot \frac{[1 + 17.5B^{3/2}k(P_o - cP_L)^{-1/\eta}]^{3/6}}{[1 + 26.3B^{3/2}k(P_o - cP_L)^{-1/\eta}]^{1/2}} \quad [37]$$

where c is a parameter. If c is calculated from experimental speed-of-sound data under conditions of equal liquid and outside pressures of 3000, 6000, and 9000 psi, the value of c becomes 0.86, 0.87, and 0.88, respectively. The speed of sound in the saturated sandstone has been calculated using an average value of 0.87 for the parameter c. The curves are presented for liquid pressures equal to P_o, $P_o/2$, and zero liquid pressure. The speed of sound is lowest when liquid and outside pressures are equal. At constant outside pressure, but decreasing liquid pressure, the speed of sound increases. The most pronounced increase occurs when the liquid pressure decreases from outside pressure to a value of one half of the outside pressure. If the liquid pressure is less than one half of the outside pressure, the parameter c can be considered equal to unity with sufficient accuracy.

These results have been presented to demonstrate how the model theory might be used to explain certain variations in the speed of sound in porous materials. A model theory, however, oversimplifies the problem and it should not be followed as a theory without limitations. Rather, the model theory should be considered as one of several approaches leading to a better understanding of the problem under investigation.

Acknowledgments

The author is indebted to Profs. P. L. Chambré, L. M. Grossman, J. A. Putnam, W. W. Soroka, and C. J. Vogt of the University of California for their many suggestions, and to Dr. D. H. Davis of California Research Corporation for his interest in this work.

BIBLIOGRAPHY

1 "An Investigation Into the Elastic Constants of Rocks, More Especially With Reference to Cubic Compressibility," by F. D. Adams and E. G. Coker, Carnegie Institution of Washington, Pub. 46, 1906, pp. 1–69.

2 "A Note on the Change of Compressibility With Pressure," by L. H. Adams, *Journal Washington Academy of Sciences*, vol. 17, no. 21, 1927, pp. 529–533.

3 "The Compressibility of Minerals and Rocks at High Pressures," by L. H. Adams and E. D. Williamson, *Journal Franklin Institute*, vol. 195, 1923, pp. 475–592.

4 "Elasticity of Igneous Rocks at High Temperatures and Pressures," by F. Birch, *Bulletin Geological Society of America*, vol. 54, 1943, pp. 263–285.

5 "The Effect of Pressure on the Rigidity of Rocks," by F. Birch and D. Bancroft, Parts I, II, *Journal of Geology*, vol. 46, nos. 1 and 2, 1938, pp. 59–87, 113–141.

6 "Elasticity and Internal Friction in a Long Column of Granite," by F. Birch and D. Bancroft, *Bulletin Seismological Society of America*, vol. 28, no. 4, 1938, pp. 243–254.

7 "New Measurements of the Rigidity of Rocks at High Pressure," by F. Birch and D. Bancroft, *Journal of Geology*, vol. 48, no. 7, 1940, pp. 752–766.

8 "Handbook of Physical Constants," by F. Birch, J. F. Schairer, and H. C. Spicer, Geological Society of America, Special Papers no. 36, 1942.

9 "Effect of Moisture Upon Velocity of Elastic Waves in Amherst Sandstone," by W. T. Born and J. E. Owen, *Bulletin American Association Petroleum Geologists*, vol. 19, no. 1, 1935, pp. 9–18.

10 "The Speed of a Plane Compression Wave in a Soil," by P. L. Chambré, Office of Naval Research Tech. Rep 3, no. 340 040, 1953, pp. 1–11.

11 "The Effect of Overburden Pressure on Relative Permeability," by I. Fatt, *Journal of Petroleum Technology*, Tech. Note 194, 1953, pp. 15–16.

12 "Seismic Velocity as a Function of Depth and Geological Time," by L. Y. Faust, *Geophysics*, vol. 16, no. 2, 1951, pp. 192–206.

13 "Flow of Gases Through Beds of Broken Solids," by C. C. Furnas, United States Department of Commerce, Bureau of Mines Bulletin 307, 1929, pp. 74–83.

14 "Mathematical Relations for Beds of Broken Solids of Maximum Density," by C. C. Furnas, *Industrial and Engineering Chemistry*, vol. 23, no. 9, 1931, pp. 1052–1058.

15 "Über die Elastizität Porōser Medien," by F. Gassmann, Mitteilungen aus dem Institut für Geophysik, no. 17, 1951, pp. 1–23.

16 "Elastic Waves Through a Packing of Spheres," by F. Gassmann, Mitteilungen aus dem Institut für Geophysik, no. 21, 1952, pp. 673–685.

17 "Compressibility of Reservoir Rocks," by H. N. Hall, *Journal of Petroleum Technology*, Tech. Note 149, 1953, pp. 17–19.

18 "Theorie der akustischen Schwingungsausbreitung in gekörnten Substanzen und experimentelle Untersuchungen an Kohlepulver," by G. Hara, *Elektrische Nachrichten-Technik*, vol. 12, no. 7, 1935, pp. 191–200.

19 "The Relation Between Depth, Lithology, and Seismic Wave Velocity in Tertiary Sandstones and Shales," by N. A. Haskell, *Geophysics*, vol. 6, no. 4, 1941, pp. 318–326.

20 "Density and Packing in an Aggregate of Mixed Spheres," by D. R. Hudson, *Journal of Applied Physics*, vol. 20, 1949, pp. 154–162.

21 "Elastic Wave Velocities in Rocks at High Pressures and Temperatures," by D. S. Hughes and J. H. Cross, *Geophysics*, vol. 16, no. 4, 1951, pp. 577–593.

22 "Variation of Elastic Moduli of Igneous Rocks With Pressure and Temperature," by D. S. Hughes and H. J. Jones, *Bulletin Geological Society of America*, vol. 61, no. 8, 1950, pp. 843–856.

23 "Elastic Wave Velocities in Sedimentary Rocks," by D. S. Hughes and H. J. Jones, Transactions American Geophysical Union, vol. 32, no. 2, 1951, pp. 173–178.

24 "Variation of Elastic Wave Velocity With Saturation in Sandstone," by D. S. Hughes and J. L. Kelly, *Geophysics*, vol. 17, no. 4, 1952, pp. 739–752.

25 "Comparison of Statically and Dynamically Determined Young's Modulus of Rocks," by J. M. Ide, Proceedings National Academy of Sciences, vol. 22, no. 2, 1936, pp. 81–92.

26 "The Elastic Properties of Rocks: a Correlation of Theory and Experiment," by J. M. Ide, Proceedings National Academy of Sciences, vol. 22, no. 8, 1936, pp. 482–496.

27 "The Velocity of Sound in Rocks and Glasses as a Function of Temperature," by J. M. Ide, *Journal of Geology*, vol. 45, no. 7, 1937, pp. 689–716.

28 "The Velocity of Elastic Waves in Sand," by K. Iida, *Bulletin Earthquake Research Institute*, Tokyo Imperial University, vol. 16, 1938, pp. 131–144.

29 "Elastic and Viscous Properties of a Certain Kind of Rock," by K. Iida, *Bulletin Earthquake Research Institute*, Tokyo Imperial University, vol. 17, 1939, pp. 59–78.

30 "Determining Young's Modulus and the Solid Viscosity Coefficients of Rocks by the Vibration Method," by K. Iida, *Bulletin Earthquake Research Institute*, Tokyo Imperial University, vol. 17, 1939, pp. 79–92.

31 "Velocity of Elastic Waves in a Granular Substance," by K. Iida, *Bulletin Earthquake Research Institute*, Tokyo Imperial University, vol. 17, 1939, pp. 783–808.

32 "Determination of Fluid Saturation in Porous Media by Ultrasonic Transmission," by E. G. Keller, O. J. Smith, and J. A. Putnam, A.P.I. Project 47, Technical Report no. 3, 1949, pp. 1–32.

33 "Longitudinal Velocities in Some Weathered and Unweathered Carboniferous Rocks," by L. D. Leet, *Bulletin Seismological Society of America*, vol. 28, no. 3, 1938, pp. 163–168.

34 "Velocity of Elastic Waves in Granite," by L. D. Leet and W. M. Ewing, *Physics*, vol. 2, 1932, pp. 160–173.

35 "Studies on the Propagation of an Artificial Earthquake Wave Through Superficial Soil or Sand Layers, and the Elasticity of Soil and Sand," by N. Nasu, *Bulletin Earthquake Research Institute* (in Japanese), Tokyo Imperial University, vol. 18, 1940, pp. 289–304.

36 "Field Determination of the Elastic Property of Soil Layers," by N. Nasu, *Bulletin Earthquake Research Institute*, Tokyo Imperial University, vol. 27, 1949, pp. 101–106.

37 "Some Mechanical Properties of Moist Granular Solids," by P. G. Nutting, *Journal Washington Academy of Sciences*, vol. 17, no. 8, 1927, pp. 185–191.

38 "The Deformation of Granular Solids," by P. G. Nutting, *Journal Washington Academy of Sciences*, vol. 18, no. 5, 1928, pp. 123–126.

39 "Standardized Tests for Determining the Physical Properties of Mine Rocks," by L. Obert, S. L. Windes, and I. W. Duvall, U. S. Bureau of Mines, Report of Investigations 3891, 1946, pp. 1–67.

40 "Comparison of Field and Laboratory Measurements of Seismic Velocities in Sedimentary Rock," by C. W. Oliphant, *Bulletin Geological Society of America*, vol. 61, no. 7, 1950, pp. 759–788.

41 "Anisotropy in the Elastic Behaviour of Rocks," by G. H. S. V. Prasada Rao, Proceedings Indian Academy of Science, vol. 25, no. 3, 1947, pp. 238–246.

42 "Packing of Homogeneous Spheres," by W. O. Smith, P. D. Foote, and P. F. Busang, *Physical Review*, series 2, vol. 34, 1929, pp. 1271–1274.

43 "On the Theory of Elastic Waves in Granular Substance," by T. Takahashi and Y. Satô, *Bulletin Earthquake Research Institute*, Tokyo Imperial University, vol. 27, 1949, pp. 11–16.

44 "Theory of Elasticity," by S. Timoshenko and J. N. Goodier, McGraw-Hill Book Co., Inc., New York, N. Y., 1951, pp. 372–377.

45 "Granite and Limestone Velocity Determinations in Arbuckle Mountains, Oklahoma," by B. B. Weatherby, W. T. Born, and R. L Harding, *Bulletin American Association of Petroleum Geologists*, vol. 18 no. 1, 1934, pp. 106–118.

46 "Influence of Geological Factors on Longitudinal Seismic Velocities," by B. B. Weatherby and L. Y. Faust, *Bulletin American Association of Petroleum Geologists*, vol. 19, no. 1, 1935, pp. 1–8.

47 "Dependence of Seismic Wave Velocity Upon Depth and Lithology," by S. S. West, *Geophysics*, vol. 15, no. 4, 1950, pp. 653–662.

48 "The Packing of Particles," by A. E. R. Westman and H. R. Hugill, *Journal American Ceramic Society*, vol. 13, no. 10, 1930, pp. 767–779.

49 "Young's Modulus and Poisson's Ratio With Reference to Geophysical Applications," by W. A. Zisman, Proceedings National Academy of Sciences, vol. 19, no. 7, 1933, pp. 653–665.

50 "Compressibility and Anisotropy of Rocks at and Near the Earth's Surface," by W. A. Zisman, Proceedings National Academy of Sciences, vol. 19, no. 7, 1933, pp. 666–679.

51 "Comparison of the Statically and Seismologically Determined Elastic Constants of Rocks," by W. A. Zisman, Proceedings National Academy of Sciences, vol. 19, no. 7, 1933, pp. 680–686.

Steady-State Behavior of Systems Provided With Nonlinear Dynamic Vibration Absorbers

By F. R. ARNOLD,[1] STANFORD, CALIF.

The response of vibrating systems subjected to sinusoidal excitations and to the action of nonlinear dynamic vibration absorbers is determined by means of a simple procedure. Extensive information including that from more complicated methods of analysis is obtainable. System behavior is described by means of "response diagrams," and certain peculiarities are discussed.

Introduction

THIS paper stems from investigations of the behavior of nonlinear dynamical systems conducted at Stanford University. The earlier portions of these investigations dealt with the fundamentals of the Ritz averaging method and its application to dynamical systems, of a single degree of freedom, having various types of nonlinearities (1, 2, 3).[2] Later portions extended the method to multi-degree-of-freedom systems and specifically treated systems having two degrees of freedom (4). The nonlinear dynamic vibration absorber is included in the systems studied, and since the behavior has been described by means of dimensionless response diagrams, the author would like to add some of these data and the method of arriving at them to recent published articles discussing this interesting device.

The System and the Problem

The nonlinear dynamic vibration absorber actually treated is included in the more general system illustrated in Fig. 1 where a two-mass two-spring assembly is shown subjected to a harmonic disturbance. The mass of each spring is considered to be negligible. The left-hand spring will be referred to as the "main" spring, and the left-hand mass as the main mass. The right-hand spring is the "coupling" spring, and the right-hand mass is the "auxiliary" or "absorber" mass. The right-hand spring and mass together constitute the auxiliary system, whereas the main mass and spring are the main system. No damping is assumed.

Attention will be concentrated on the special case in which the main spring is linear and the coupling spring is nonlinear such that the restoring force as a function of spring extension is of the form $R(q) = c(q \pm \mu^2 q^3)$. The upper sign before the constant μ_i^2 indicates a "hardening" nonlinearity in the spring characteristic, and the lower is used to denote a "softening" one. For

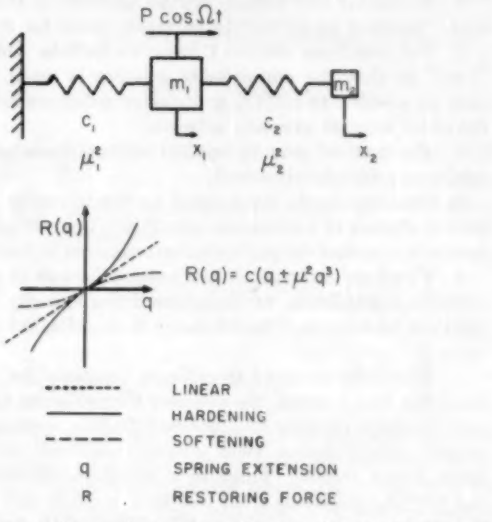

Fig. 1 General Model System and Typical Spring Restoring Force Versus Spring Extension Curve

the linear main spring, the value "zero" is assigned the coefficient μ_1^2 appearing in Fig. 1.

Imagine the model system in a configuration away from its equilibrium position. We know that the differential equations of motion of this system are derivable from Hamilton's principle, but briefly, by inspection, we apply Newton's second law and equate the product of the respective masses and their accelerations to the forces acting on them, then transpose all terms to one side to obtain

$$\left.\begin{aligned} E_1[x_1, x_2] &\equiv m_1\ddot{x}_1 + c_1x_1 - c_2 \\ &\quad [(x_2 - x_1) \pm \mu_2^2(x_2 - x_1)^3] - P\cos\Omega t = 0 \\ E_2[x_1, x_2] &\equiv m_2\ddot{x}_2 + c_2[(x_2 - x_1) \pm \mu_2^2(x_2 - x_1)^3] = 0 \end{aligned}\right\} \ldots [1]$$

Equations [1] constitute the system of ordinary second-order differential equations, nonlinear by virtue of the cubic terms appearing, the solutions of which would yield the displacements x_1 and x_2 as functions of time t.

Method of Solution

Previous investigations of this system have been made to establish, on a theoretical basis, the possibility of improving the action of the dynamic vibration absorber of Frahm. R. E. Roberson (5) has adapted Duffing's method (6) to the absorber problem. He also has extended J. E. Brock's (7) iterative method, for nonlinear single-degree-of-freedom systems, to the two-degree-of-freedom system. Louis A. Pipes (8) also applied a Duffing method to treat a vibration absorber having a coupling spring with a hyperbolic-sine nonlinearity.

The Ritz method (second Ritz method, Ritz averaging method, Ritz-Galerkin method) will be used in the following analysis. It

[1] Assistant Professor of Mechanical Engineering, Stanford University.

[2] Numbers in parentheses refer to the Bibliography at the end of the paper.

Presented at the West Coast Conference of the Applied Mechanics Division, Monterey, Calif., September 12–13, 1955, of The American Society of Mechanical Engineers.

Discussion of this paper should be addressed to the Secretary, ASME, 29 West 39th Street, New York, N. Y., and will be accepted until January 10, 1956, for publication at a later date. Discussion received after the closing date will be returned.

Note: Statements and opinions advanced in papers are to be understood as individual expressions of their authors and not those of the Society. Manuscript received by ASME Applied Mechanics Division, March 1, 1955. Paper No. 55—APM-30.

requires only that we be able to determine, by any means whatever, the differential equation of motion of the system, and that we choose an appropriate function or series of functions of such form that they would be suitable for the expansion of the unknown co-ordinates of the solution in a manner to preserve their essential features. They may be selected as to form and number on the basis of experience, if any.

Several important features of the Ritz method recommend its use:

1 It may be applied to determine steady-state solutions to nonautonomous as well as to autonomous systems.

2 It is easily and quickly applied to arrive at the basic algebraic "starting equations" to be manipulated for the solutions.

3 The solutions obtained have coefficients which are the "best" in that the approximate solution is made to come as close as possible to satisfying the same minimum principle that the exact solution precisely satisfies.

4 The method may be applied without knowledge of what minimum principle is involved.

5 One may apply the method to obtain results even in the known absence of a minimum principle. The suitability of such results is a matter for particular investigation in each case.

6 There are no vague initial assumptions as to smallness of oscillation amplitude or departure from linearity. There is, however, an important initial choice of co-ordinate function to be made.

7 When the assumed co-ordinate functions are sines or cosines, the Ritz method, the so-called Fourier-series approach (6), and the more cumbersome modified Duffing method (5) to the second approximation yield identical algebraic starting equations, hence results. There is a negligible difference between the starting equations from the Ritz method and those from the much more complicated modified Brock method (5); hence the solutions also should be in close agreement.

The Ritz Prescription for Multi-Degree-of-Freedom Systems (9)

Let us imagine an oscillatory system of n degrees of freedom requiring the n co-ordinates $x_1, x_2, \ldots x_k, \ldots x_n$ as functions of time to describe completely its configuration. We wish to describe the behavior under the action of a periodic disturbing force. Assume that we know the n differential equations of type

$$E_k[x_1, x_2, \ldots x_n] = 0; k = 1, 2, \ldots n \quad [2]$$

the solution of which would yield the desired co-ordinates as functions of time. In the absence of a procedure yielding an exact solution, one may obtain an approximate steady-state solution by means of the following:

1 Replace each of the co-ordinates of type $x_k(t)$ by a corresponding approximating function of form

$$\mathfrak{x}_k(t) = \sum_{i=1}^{N} a_{ki}\psi_i(t); k = 1, 2, \ldots n \quad [3]$$

where the coefficients a_{ki} constitute a set of nN unknown constants, whereas the functions $\psi_i(t)$ are selected functions of time which we may choose as to form and number as being suitable for the expansion of the unknown co-ordinates in a manner to preserve their essential features.

2 Introduce the $\mathfrak{x}_k(t)$ into the differential expressions $E_k[x_1, x_2, \ldots x_n]$ of Equations [2] so that we have a set of functions of time

$$E_k[\mathfrak{x}_1(t), \mathfrak{x}_2(t), \ldots \mathfrak{x}_n(t)]; k = 1, 2, \ldots n \quad [4]$$

none of which will, in general, be exactly equal to zero.

3 Perform all of the integrations of type

$$\int_{t_0}^{t_1} E_k[\mathfrak{x}_1(t), \mathfrak{x}_2(t), \ldots \mathfrak{x}_n(t)]\psi_i(t)dt = 0 \quad [5]$$

$$k = 1, 2, \ldots n$$
$$i = 1, 2, \ldots N$$

and the interval t_0 to t_1 is a period of the motion. Equations [5] will constitute a set of nN algebraic equations in the nN unknown coefficients of type a_{ki} and are the Ritz conditions to be satisfied.

4 Solve the algebraic equations of [5] for the coefficients a_{ki} and insert them in the Series [3] to obtain the approximate solution sought.

Ritz Conditions for Dynamic Vibration Absorber System

We shall undertake the determination of those approximate solutions for which we consider a single-term co-ordinate function, $\psi(t)$, to be an adequate representation. Therefore, in place of the unknown functions $x_1(t)$ and $x_2(t)$, we assume the approximating functions

$$\left.\begin{aligned}\mathfrak{x}_1(t) &= Q_1\psi(t)\\ \mathfrak{x}_2(t) &= Q_2\psi(t)\end{aligned}\right\} \quad [6]$$

where Q_1 and Q_2 are undetermined coefficients of the function $\psi(t)$ which still remains to be selected.

The Ritz conditions then take the form

$$\left.\begin{aligned}\int_{t_0}^{t_1} E_1[\mathfrak{x}_1(t), \mathfrak{x}_2(t)]\psi(t)dt = 0\\ \int_{t_0}^{t_1} E_2[\mathfrak{x}_1(t), \mathfrak{x}_2(t)]\psi(t)dt = 0\end{aligned}\right\} \quad [7]$$

where the interval t_0 to t_1 is a period of the motion.

We are interested in a system acted upon by a harmonic disturbance; hence a disturbing term of sine or cosine character will appear in one of the integrands of Equations [7]. We intuitively feel that a single-function representation of the motion also should be a sine or cosine. Having in mind the orthogonality relations between such functions by which integrals, over a period, of the product of two unlike functions, or of two like functions of different harmonics, vanish, we know that unless $\psi(t)$ is precisely the same function as the disturbance, the integrations as performed will contain no contribution from the disturbance term. The algebraic equations which result from Equations [7] will correspond to free, and not forced, vibrations. Thus we are convinced that $\psi(t)$ must be given the same trigonometric character and frequency as the disturbance function.

Still with the orthogonality relations in mind, we may now see that the formal integrations of Equations [7] are avoidable and the same effect obtained, except for a constant multiplier, π, of no interest, if we introduce the $\mathfrak{x}_1(t)$ and $\mathfrak{x}_2(t)$ into the differential equations, replace higher powers of the trigonometric functions by terms of multiple arguments, and retain only those terms which have the same frequency as $\psi(t)$; e.g., $\cos^3 \Omega t$ must be replaced by $^3/_4 \cos \Omega t + {}^1/_4 \cos 3\Omega t$ and the second term rejected if $\psi(t) = \cos \Omega t$.

A comment should be added on what appears, at first, to be a serious limitation of the Ritz method if one were confined to looking for single-term solutions which have the same frequency as the disturbance. The limitation is only an apparent one. If one wishes to find single-term subharmonic solutions, one first assumes a two-term approximation consisting of a subharmonic component and a component of the "fundamental" frequency of the disturbance. After the algebraic equations involving all four unknown amplitudes are obtained, and not before, one arbitrarily may set the amplitude of the fundamental frequency terms

to zero, and the resulting equations may be used to find the subharmonic component coefficients and equations expressing the restrictive relations associated with them. Such approximate solutions are to be regarded as corresponding to those exact solutions which are predominantly subharmonic in character but which in reality may contain small components of all of the sub and superharmonics.

Solutions by Ritz Method

Since the disturbance function of the system of Fig. 1 is $P \cos \Omega t$, the approximating single-term displacement functions assumed are

$$\left.\begin{aligned} x_1(t) &= Q_1 \cos \Omega t \\ x_2(t) &= Q_2 \cos \Omega t \end{aligned}\right\} \quad \ldots\ldots [8]$$

In accordance with the procedure of the preceding section, the functions of Equations [8] and their appropriate derivatives are introduced into the differential Equations [1] to obtain, after deletion of multiple-frequency terms, the following algebraic starting equations to be solved for the unknown amplitudes Q_1 and Q_2 as functions of the system parameters

$$\left.\begin{aligned} -m_1\Omega^2 Q_1 + c_1 Q_1 - c_2(Q_2 - Q_1) \mp {}^3/_4\, c_2\mu_2^2(Q_2 - Q_1)^3 \\ - P = 0 \\ -m_2\Omega^2 Q_2 + c_2(Q_2 - Q_1) \pm {}^3/_4\, c_2\mu_2^2(Q_2 - Q_1)^3 = 0 \end{aligned}\right\} \quad \ldots\ldots [9]$$

For purposes of displaying the solutions of Equations [9], it is convenient to dedimensionalize the equations before solving. Two procedures may be used. Each has certain advantages peculiar to it. One method will be designated the $\bar{Q}$-method yielding $\bar{Q}$-plots (response diagrams) in which forced vibrations are best compared with free. The other, or $\bar{R}$-method, yields $\bar{R}$-plots (response diagrams) which permit comparison of the effects of altering the nonlinearity coefficient μ_2^2 while the disturbance amplitude is kept fixed. The latter method also yields equations better adapted to the synthesis of systems to achieve desired behavior, and is basically similar to the procedure followed by Roberson in treating his equations of the vibration absorber.

The dimensionless equations of the $\bar{Q}$-method are

$$\left.\begin{aligned} (1 - \eta^2)\bar{Q}_1 - \bar{\kappa}^2\bar{m}(\bar{Q}_2 - \bar{Q}_1) \mp \bar{\kappa}^2\bar{m}(\bar{Q}_2 - \bar{Q}_1)^3 = \bar{s} \\ -\eta^2\bar{Q}_2 + \bar{\kappa}^2(\bar{Q}_2 - \bar{Q}_1) \pm \bar{\kappa}^2(\bar{Q}_2 - \bar{Q}_1)^3 = 0 \end{aligned}\right\} \quad \ldots\ldots [10]$$

where

$$\left.\begin{aligned} \bar{m} &= \frac{m_2}{m_1}, \quad \bar{\kappa}^2 = \frac{c_2/m_2}{c_1/m_1}, \quad \eta^2 = \frac{\Omega^2}{c_1/m_1} \\ \bar{s} &= \sqrt{\frac{3}{4}}\,\mu_2 \frac{P}{c_1}, \quad \bar{Q}_i = \sqrt{\frac{3}{4}}\,\mu_2 Q_i \end{aligned}\right\} \quad \ldots\ldots [11]$$

The equations of the $\bar{R}$-method are

$$\left.\begin{aligned} (1 - \eta^2)\bar{R}_1 - \bar{\kappa}^2\bar{m}(\bar{R}_2 - \bar{R}_1) \mp \bar{\kappa}^2\bar{m}\bar{s}^2(\bar{R}_2 - \bar{R}_1)^3 = 1 \\ -\eta^2\bar{R}_2 + \bar{\kappa}^2(\bar{R}_2 - \bar{R}_1) \pm \bar{\kappa}^2\bar{s}^2(\bar{R}_2 - \bar{R}_1)^3 = 0 \end{aligned}\right\} \quad \ldots [12]$$

where

$$\bar{R}_i = \frac{Q_i}{s} = \frac{\bar{Q}_i}{\bar{s}}, \; s = \frac{P}{c_1} \quad \ldots\ldots [13]$$

If all parameters of a system are known and it is wished to determine the system response to various disturbance amplitudes and frequencies, it is convenient to work with Equations [10] to display the behavior of both free and forced oscillations. Because of the simple relations between the $\bar{Q}$ and $\bar{R}$ co-ordinates, one may easily make transformations from one system to the other if desired. In this paper, operations will be confined to the $\bar{Q}$ equations. To obtain data for the response diagrams, $\bar{\kappa}$ and m are considered fixed for a particular system, and we seek to obtain solutions for $\bar{Q}_1$ and $\bar{Q}_2$ as functions of η^2 and $\bar{s}$ (i.e., dimensionless displacements as functions of dimensionless frequency squared and dimensionless disturbance amplitude).

Equations [10] may be transformed into a single equation of type $f(\eta^2, \bar{Q}_2 - \bar{Q}_1) = 0$ by multiplying the first of Equations [10] by $-\eta^2$, the second by $-(1 - \eta^2)$, and adding the results. One thereby obtains

$$\begin{aligned} (\bar{Q}_2 - \bar{Q}_1)\eta^4 - \{\bar{s} + [1 + \bar{\kappa}^2(1 + \bar{m})] \\ (\bar{Q}_2 - \bar{Q}_1) \pm \bar{\kappa}^2(1 + \bar{m})\,(\bar{Q}_2 - \bar{Q}_1)^3\}\eta^2 \\ + \bar{\kappa}^2[(\bar{Q}_2 - \bar{Q}_1) \pm (\bar{Q}_2 - \bar{Q}_1)^3] = 0 \end{aligned} \quad \ldots\ldots [14]$$

Assuming $\bar{Q}_2 - \bar{Q}_1 \neq 0$, we may divide through by it to find

$$\begin{aligned} \eta^4 - \Bigg[1 + \bar{\kappa}^2(1 + \bar{m}) \pm \bar{\kappa}^2(1 + \bar{m})\,(\bar{Q}_2 - \bar{Q}_1)^2 \\ + \frac{\bar{s}}{\bar{Q}_2 - \bar{Q}_1}\Bigg]\eta^2 + \bar{\kappa}^2\,[1 \pm (\bar{Q}_2 - \bar{Q}_1)^2] = 0 \end{aligned} \quad \ldots\ldots [15]$$

which holds for all conditions except that for $Q_2 - Q_1 = 0$. From Equations [10] we have also

$$\left.\begin{aligned} \bar{Q}_1 &= \frac{\bar{\kappa}^2\bar{m}}{1 - \eta^2}\left[(\bar{Q}_2 - \bar{Q}_1) \pm (\bar{Q}_2 - \bar{Q}_1)^3 + \frac{\bar{s}}{\bar{\kappa}^2\bar{m}}\right] \\ \text{and} \\ \bar{Q}_2 &= \frac{\bar{\kappa}^2}{\eta^2}\,[(\bar{Q}_2 - \bar{Q}_1) \pm (\bar{Q}_2 - \bar{Q}_1)^3] \end{aligned}\right\} \quad \ldots [16]$$

Equations [15] and [16] are sufficient to plot the complete response diagrams ($\bar{Q}$-plots) point by point by assuming values for $(\bar{Q}_2 - \bar{Q}_1)$. Only the condition where $(\bar{Q}_2 - \bar{Q}_1) = 0$ requires special treatment. This situation is of interest and is easily identified.

If we put $\bar{Q}_2 - \bar{Q}_1 = 0$ into Equations [16], the second of them tells us that η^2 must be zero if $\bar{Q}_2$ is not to be. Further introduction of $\eta^2 = 0$ in the first of Equations [16] then yields $\bar{Q}_1 = \bar{s}$. Thus we have the static deflection configuration $\bar{Q}_1 = \bar{Q}_2 = \bar{s}$ if $\eta^2 = 0$ and we use only the upper signs corresponding to the hardening coupling spring. However, the lower signs, corresponding to a softening coupling spring, yield two additional static configurations resulting in

$$\begin{aligned} &(a)\ \bar{Q}_1 = \bar{s},\ \bar{Q}_2 = \bar{s} \\ &(b)\ \bar{Q}_1 = \bar{s},\ \bar{Q}_2 = \bar{s} + 1 \\ &(c)\ \bar{Q}_1 = \bar{s},\ \bar{Q}_2 = \bar{s} - 1 \end{aligned}$$

The configurations of (b) and (c) are beyond the bounds we shall specify for a softening coupling spring; that is, we do not permit a softening spring to be stretched or compressed to the point at which it ceases to "restore."

To continue with the determination of the complete response characteristics, free-vibration behavior is found by the introduction of $\bar{s} = 0$ into the starting Equations [10] and the elimination of $(\bar{Q}_2 - \bar{Q}_1)$ terms which yield

$$\bar{Q}_2 = \frac{1 - \eta^2}{\bar{m}\,\eta^2}\,\bar{Q}_1 \quad \ldots\ldots [17]$$

Substituting the right side of Equation [17] for $\bar{Q}_2$ in the second of Equations [10] and solving for $\bar{Q}_1^2$, we find

$$\pm \bar{Q}_1^2 = \frac{\bar{m}^2\eta^4\{\eta^4 - [1 + \bar{\kappa}^2(1 + \bar{m})]\eta^2 + \bar{\kappa}^2\}}{\bar{\kappa}^2\,[\eta^2(1 + \bar{m}) - 1]} \quad \ldots [18]$$

by means of which the $\bar{Q}_i$ versus η^2 curves for the free vibrations of the system may be plotted. They constitute the "backbone" curves for the complete response diagrams.

Inspection of the numerator and the denominator of Equation [18] will show that the backbone curves cross the η^2-axis at two values indicated

$$\eta_{I,II}^2 = \frac{1 + \bar{\kappa}^2(1 + \bar{m}) \pm \sqrt{[1 + \bar{\kappa}^2(1 + \bar{m})]^2 - 4\bar{\kappa}^2}}{2} \quad \ldots [19]$$

and that an asymptote exists at

$$\eta_\infty^2 = \frac{1}{1 + m} \quad \ldots [20]$$

As one might expect, the two values of frequency ratio indicated in Equation [19] coincide with the natural frequencies of the purely linear system.

The procedure used to obtain data for the remaining curves of the response diagrams of Figs. 2 through 4 consisted of the following steps:

1 Into Equation [15], having numerical values for $\bar{\kappa}$, $\bar{m}$, and $\bar{s}$, a selected value Δ, for $(\bar{Q}_2 - \bar{Q}_1)$, was introduced, and the resulting quadratic equation solved for values of η^2.

2 The value of Δ used in step 1, and the values of η^2 determined therefrom, were then introduced into the second of Equations [16] to evaluate the corresponding $\bar{Q}_2$. $\bar{Q}_1$ then follows from $\bar{Q}_1 = \bar{Q}_2 - \Delta$.

3 Steps 1 and 2 were repeated for additional values of Δ and a graph made of $\bar{Q}_i$ versus n^2 which constitutes the response curve of the system for the particular value of dimensionless forcing-function amplitude $\bar{s}$ used.

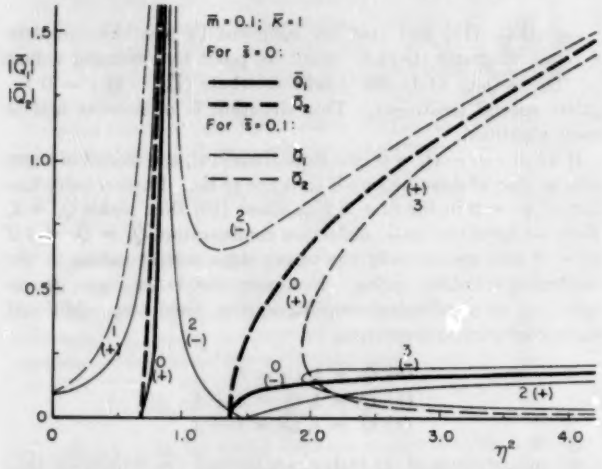

FIG. 2 RESPONSE DIAGRAM ($\bar{Q}$-PLOT) FOR SYSTEM WITH HARDENING COUPLING SPRING; $\bar{s}$ = 0 AND 0.10; $\bar{m}$ = 0.1; $\bar{\kappa}$ = 1.0

Fig. 2 shows the system response in the case of a hardening coupling spring. Figs. 3 and 4 show the system response characteristics for a softening coupling spring. Fig. 4 shows the response of a system for which the softening coupling spring has been chosen to produce optimum suppression of main mass amplitude. This latter figure, then, describes the behavior of a system coinciding with Roberson's optimum system-parameter recommendations. In the case of a softening coupling spring, to avoid stretching or compressing the spring beyond the point at which its restoring force is on the verge of becoming negative, one should "operate" within regions for which

$$|(\bar{Q}_2 - \bar{Q}_1)| \leq \sqrt{3/4}$$

For comparison purposes, Fig. 5 is an $\bar{R}$-plot showing the effects of variation in the nonlinearity coefficient μ_2 since

$$\bar{R}_i = Q_i/s, \; \bar{s} = \sqrt{3/4}\,\mu_2 s$$

and we let the variation in $\bar{s}$ occur through the varying of μ_2 while considering s a constant system parameter. Curves are numbered to show correspondence of branches and given + or − signs to indicate in-phase or out-of-phase motion, respectively, relative to the disturbance.

SOME SYSTEM PECULIARITIES

Since the examination of response diagrams does not give quantitative data on limiting values of amplitude, though suspicions might be aroused in certain directions, we may complete

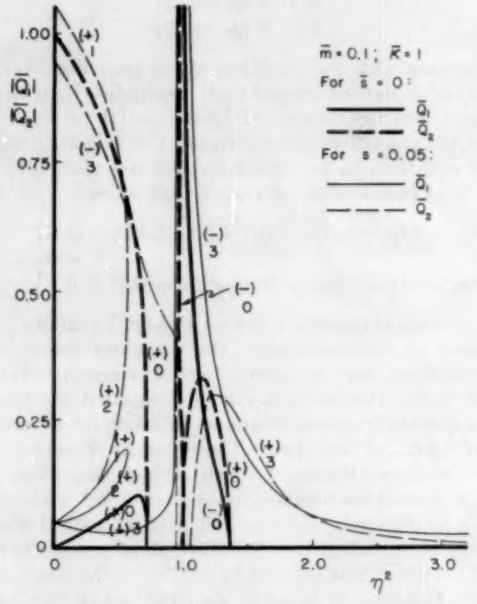

FIG. 3 RESPONSE DIAGRAM ($\bar{Q}$-PLOT) FOR SYSTEMS WITH SOFTENING COUPLING SPRING; $\bar{s}$ = 0 AND 0.05; $\bar{m}$ = 0.1; $\bar{\kappa}$ = 1.0

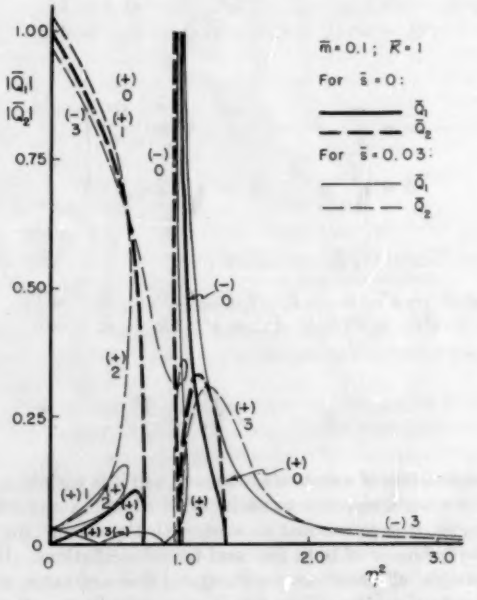

FIG. 4 RESPONSE DIAGRAM ($\bar{Q}$-PLOT) FOR SYSTEM WITH "IDEAL" SOFTENING COUPLING SPRING; $\bar{s}$ = 0 AND 0.03; $\bar{m}$ = 0.1; $\bar{\kappa}$ = 1.0

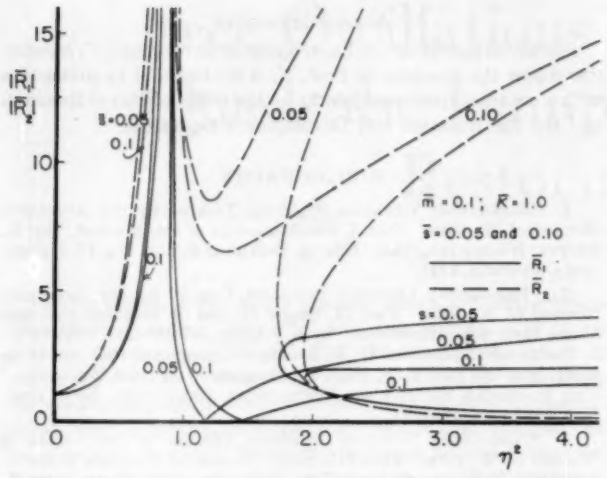

FIG. 5 COMPOSITE RESPONSE DIAGRAM ($\bar{R}$-PLOT) FOR SYSTEMS WITH HARDENING COUPLING SPRING; $\bar{s}$ = 0.05 AND 0.10; $\bar{m}$ = 0.1; $\bar{\kappa}$ = 1.0

the picture of system behavior by a critical examination of the nature of the equations leading to the curves presented. We ask the following questions:

(*a*) What are the conditions for which $\bar{Q}_1 = 0$?
(*b*) Are there any resonance conditions?
(*c*) What are the ranges of values for $\bar{Q}_1$ and $\bar{Q}_2$?

In seeking a condition for which $\bar{Q}_1 = 0$, it should be pointed out that this condition does not mean that the main mass will be exactly at rest as it could be for a completely linear system or for one in which the nonlinearity is in the main spring only. For these latter systems, such an "at-rest" condition corresponds to an exact solution of the differential equations concerned. For the system treated here, the nonlinearity in the coupling spring prevents such an exact solution. While we shall find conditions which make $\bar{Q}_1 = 0$, we must appreciate that this is an "average" value in the "Ritz averaging" sense, which takes into consideration the effects of all sub and superharmonic components which the real motion contains, in attempting to satisfy the "minimum principle" of the system.

To determine the value of η^2 at which $\bar{Q}_1 = 0$, and which we designate by the symbol η_0^2, we introduce $\bar{Q}_1 = 0$ into the Equations [10]. The results are

$$\left.\begin{aligned} \pm\bar{Q}_2^3 + \bar{Q}_2 &= \frac{-\bar{s}}{\bar{\kappa}^2\bar{m}} \\ \eta^2\bar{Q}_2 &= \bar{\kappa}^3[\pm\bar{Q}_2^3 + \bar{Q}_2] \end{aligned}\right\} \quad \ldots\ldots\ldots\ldots [21]$$

For a selected value of $\bar{s}$, the first of Equations [21] is a cubic equation in Q_2 for which we may find the roots $(\bar{Q}_2)_{01}$, $(\bar{Q}_2)_{02}$, and $(\bar{Q}_2)_{03}$. For the system with hardening coupling spring, there will be just one real and negative root. For the system with softening coupling spring, there will be one real positive root, and not more than two real negative roots depending on the magnitude of the $-\bar{s}/\bar{\kappa}^2\bar{m}$ term.

Now, the second of Equations [21] may be written

$$\eta^2\bar{Q}_2 = -\frac{\bar{s}}{\bar{m}} \quad \ldots\ldots\ldots\ldots\ldots\ldots [22]$$

by the substitution of $-\bar{s}/\bar{\kappa}^2\bar{m}$ for the $(\pm\bar{Q}_2^3 + \bar{Q}_2)$ term appearing in it. If we introduce the quantities of type $(\bar{Q}_2)_{0i}$ one at a time into Equation [22] and solve for η^2, we find several values for the frequency ratio $(\eta_0^2)_i$, at which $\bar{Q}_1 = 0$, to be

$$(\eta_0^2)_i = -\frac{\bar{s}}{\bar{m}(\bar{Q}_2)_{0i}} \quad \ldots\ldots\ldots\ldots\ldots\ldots [23]$$

where i equals 2 at most since only negative values of the $(\bar{Q}_2)_{0i}$ lead to positive values of $(\eta_0^2)_i$. We therefore find always only one such frequency ratio for the hardening-coupling spring system, and at most two of them for the softening-coupling-spring system. These particular frequency ratios are called "crossing points" because they are the values at which the response curve related to $\bar{Q}_1$ touches or crosses the η^2-axis.

The fact that the backbone has infinite amplitudes at $\eta_\infty^2 = 1/(1 + \bar{m})$ leads us to examine the behavior of the forced-vibration equations in that region. This may best be done through Equations [14] and [16] where we rewrite Equation [14] by grouping coefficients of like powers of $(\bar{Q}_2 - \bar{Q}_1)$ to obtain

$$\pm\bar{\kappa}^3[\eta^2(1 + \bar{m}) - 1](\bar{Q}_2 - \bar{Q}_1)^3 + \{\eta^2(1 - \eta^2) + \bar{\kappa}^3[\eta^2(1 + \bar{m}) - 1]\}(\bar{Q}_2 - \bar{Q}_1) + \eta^2\bar{s} = 0 \quad \ldots\ldots [24]$$

For any assigned value of η^2, Equation [24] becomes a function of $(\bar{Q}_2 - \bar{Q}_1)$ for which the roots, together with Equations [16], yield solutions to our dynamical problem. Therefore, if we may determine how the roots behave with changes in η^2, that behavior, plus Equations [16], will show the corresponding behavior of $\bar{Q}_1$ and $\bar{Q}_2$.

Choosing $\eta^2 = 1/(1 + \bar{m})$, we insert it in Equation [24] and imagine what the graph of the resulting function of $(\bar{Q}_2 - \bar{Q}_1)$ would be. The result would be a straight line in view of the vanishing of the coefficient of the cubic term. The graph of the function corresponding to any other fixed value of η^2 will be a definite cubic curve. Notice for the hardening coupling spring system, however, if we approach the special value of η_∞^2 from above, we have a curve, corresponding to each value of η^2 assumed, which is of such shape that there is but one real and negative root for the function of $(\bar{Q}_2 - \bar{Q}_1)$. The closer we get to η_∞^2, the closer the root gets to the finite value corresponding to the linear function resulting from $\eta^2 = \eta_\infty^2$. Now, if we imagine we approach the special value of η_∞^2 from below, we find curves of such shape that there is a negative root near that of the linear-function case, but also there is a very large positive as well as a very large negative root. The closer η^2 approaches η_∞^2, the farther out toward positive and negative infinity are the large roots found. Thus, as we approach η_∞^2 from below, we have the root values of $(\bar{Q}_2 - \bar{Q}_1)$ approaching positive and negative infinity as well as a finite value. From Equations [16] we see that both $\bar{Q}_1$ and $\bar{Q}_2$ similarly approach positive and negative infinite values as well as a finite value each. We are thus able to say that $\eta_\infty^2 = 1/(1 + \bar{m})$ is the resonance frequency for the hardening-coupling-spring system.

A similar investigation for the softening-coupling-spring system, using the lower signs in Equation [24], shows that its resonance frequency is the same as that of the hardening.

We are also interested in what happens to the amplitudes as η^2 approaches infinity. Again, we refer to Equations [16] and [24]. For the hardening system, we observe that for very large η^2, and increasing, the difference $(\bar{Q}_2 - \bar{Q}_1)$ does three things in satisfying Equation [24]. It goes toward infinity in the positive and negative directions, as well as toward zero positively. From Equations [16] we see that $\bar{Q}_1$ goes toward zero negatively while $\bar{Q}_2$ does so positively. Also $\bar{Q}_1$ goes to plus and minus infinity while $\bar{Q}_2$ does so with opposite sign.

For the softening system, $(\bar{Q}_2 - \bar{Q}_1)$ goes only toward zero in satisfying Equation [24] as η^2 increases without limit. Thus, from Equations [16], $\bar{Q}_1$ goes toward zero negatively while $\bar{Q}_2$ does so positively.

Thus we now know toward what limits the response curves are tending in Figs. 2 through 5.

Conclusions

One of the most striking characteristics of system response is the apparent existence of up to three modes of oscillation for a single value of disturbance frequency. In spite of the absence of a stability criterion for multi-degree-of-freedom systems, we may look with suspicion on the stability of those modes corresponding to branches of the response curves lying closest to and under the backbone curves. What is known about the stability of nonlinear single-degree-of-freedom systems (10) leads one to judge these modes to be unstable.

Points of vertical tangency in the curves, the locus of which may be determined analytically, indicate the occurrence of "jump" phenomena if any part of the branch leading into the reversion point corresponds to a stable motion.

Unlike the purely linear undamped system, there is only one resonance frequency

$$\Omega = \sqrt{c_1/(m_1 + m_2)}$$

However, at this frequency, again unlike the linear system, there is the possibility of a mode of vibration for which the main mass is substantially at rest. From the response diagrams, one sees that, depending upon whether the resonance value of η^2 is approached from the high side or the low side, the amplitude of the main mass, $\bar{Q}_1$, approaches zero or positive infinity accordingly. The branch of the $\bar{Q}_1$ curve leading to negative infinity is probably unstable, but the existence of a vertical tangency in this curve indicates that mode of vibration could not be approached with certainty via gradual change in disturbance frequency from either direction.

Cyril Atkinson of the University of California at Berkeley has investigated several types of nonlinear two-degree-of-freedom systems using the analog computer at Stanford University to verify, experimentally, suspected stability; it is hoped his results will be generally available before long.

Certainly, it appears that the nonlinear vibration absorber has the possibilities suggested by Roberson, with the softening coupling spring having a decided advantage if the higher-amplitude modes characteristic of this system at low frequencies are unstable or can be avoided.

Acknowledgment

The investigation of nonlinear systems at Stanford University was under the direction of Prof. Karl Klotter and in connection with a contract sponsored jointly by the Office of Naval Research and the Air Research and Development Command.

BIBLIOGRAPHY

1 "Non-Linear Vibration Problems Treated by the Averaging Method of W. Ritz: Part I, Fundamentals of the Method," by K. Klotter, N6-onr-251, Task Order 2, Technical Report No. 17/I, Stanford University, 1951.

2 "Non-Linear Vibration Problems Treated by the Averaging Method of W. Ritz: Part II, Single Degree of Freedom Systems; Single Term Approximations," by K. Klotter, N6-onr-251, Task Order 2, Technical Report No. 17/II, Stanford University, 1951; or "Proceedings of the First U. S. National Congress of Applied Mechanics," The American Society of Mechanical Engineers, New York, N. Y., 1952, pp. 125–131.

3 "Non-Linear Vibration Problems Treated by the Averaging Method of W. Ritz: Part III, Single Degree of Freedom Systems: Non-Odd Restoring Forces; Two Term Approximations," by K. Klotter and James A. Plough, N6-onr-251, Task Order 2, Technical Report 17/III, Stanford University, 1952.

4 "Steady-state Oscillations in Nonlinear Systems of Two Degrees of Freedom," by F. R. Arnold, N6-onr-251, Task Order 2, Technical Report No. 24, Stanford University, 1953.

5 "Synthesis of a Nonlinear Dynamic Vibration Absorber," by R. E. Roberson, *Journal of The Franklin Institute*, vol. 254, no. 3, 1952, pp. 205–220.

6 "Nonlinear Vibrations in Mechanical and Electrical Systems," by J. J. Stoker, Interscience Publishers, Inc., New York, N. Y., first edition, 1950, pp. 83–90, 92.

7 "An Iterative Numerical Method for Nonlinear Vibrations," by J. E. Brock, Journal of Applied Mechanics, Trans. ASME, vol. 73, 1951, pp. 1–11.

8 "Analysis of a Nonlinear Dynamic Vibration Absorber," by L. A. Pipes, Journal of Applied Mechanics, Trans. ASME, vol. 75, 1953, pp. 515–518.

9 "Steady-state Oscillations in Nonlinear Systems of Two Degrees of Freedom," by F. R. Arnold, PhD thesis, Stanford University, 1953, pp. 160–175.

10 "A Comprehensive Stability Criterion for Forced Vibrations in Nonlinear Systems," by K. Klotter and E. Pinney, Journal of Applied Mechanics, Trans. ASME, vol. 75, 1953, pp. 9–12.

Free Oscillations of Systems Having Quadratic Damping and Arbitrary Restoring Forces

By KARL KLOTTER,[1] STANFORD, CALIF.

In this paper, systems are treated which are subjected to quadratic damping forces (of any magnitude) and to restoring forces of any type. The differential equations of motion for such systems can be transformed into linear differential equations of first order for the velocity squared, whatever the restoring forces may be. A first integral can be obtained readily. From it the exact relationships between any two consecutive maximum displacements ("amplitudes") are derived. These relationships are discussed in detail for various types of restoring forces. Examples are worked out numerically and illustrated by graphs.

The System and Its Differential Equation

The differential equation of motion for a mechanical system of one degree of freedom (or of the phenomenon occurring in a one-loop electrical circuit) is a differential equation of second order, $E(\ddot{q}, \dot{q}, q, t) = 0$, or more specifically

$$\ddot{q} + \kappa^2 h(\dot{q}, q, t) = 0 \quad \ldots\ldots [1]$$

with time t as the independent variable and some appropriately chosen quantity q (displacement, current, voltage . . . .) as the dependent variable. In Equation [1] the constants and functions are selected in such a way as to make κ have dimension of a reciprocal of time, hence h to have the dimension of q.

If, in particular, the independent variable t does not appear explicitly in the argument of h in Equation [1]

$$\ddot{q} + \kappa^2 h(\dot{q}, q) = 0 \quad \ldots\ldots [2]$$

the system is called autonomous. And it is well known that in this case by use of the identity

$$\ddot{q} = \frac{1}{2}\frac{dV}{dq}$$

with V denoting $\dot{q}^2$, Equation [2] may be transformed into

$$\frac{dV}{dq} + 2\kappa^2 h_1(V, q) = 0 \quad \ldots\ldots [3]$$

which is a differential equation of first order for V as a function of q.

There are many types of first-order differential equations which allow integration. Among them the linear equations play a prominent role. The linear subcase of differential Equation [3] is related to some important types of original differential Equations [2], as will be shown now.

The linear differential equation of the type of Equation [3] reads

$$\frac{dV}{dq} + \varphi(q)V + \psi(q) = 0 \quad \ldots\ldots [4]$$

The original differential equations of the form of Equation [2] which lead to a linear differential equation of the form of Equation [4] therefore read

$$\ddot{q} + \frac{1}{2}\varphi(q)(\dot{q})^2 + \frac{1}{2}\psi(q) = 0 \quad \ldots\ldots [5]$$

We consider three examples.

Example A

$$\ddot{q} + \frac{\delta}{2}\dot{q}^2(\operatorname{sgn}\dot{q}) + \kappa^2 f(q) = 0 \quad \ldots\ldots [6]$$

where

$$\varphi = (\operatorname{sgn}\dot{q})\delta \quad \text{and} \quad \psi(q) = 2\kappa^2 f(q)$$

Equation [6] describes the free oscillations of a system having quadratic damping and arbitrary restoring forces. Each swing between rest points (points of return) (where $\dot{q}$ changes sign) of this system is described by one linear differential equation of the type of Equation [6]. This example *A* will be treated in detail in the subsequent parts of the present paper. Before we confine our attention to this case, however, we point to two more examples which are special cases of Equation [5].

Example B

$$\ddot{q} - (\operatorname{sgn}\dot{q})(\epsilon/2)\dot{q}^2(1 - \alpha^2 q^2) + \kappa^2 f(q) = 0 \quad \ldots\ldots [7]$$

where

$$\varphi(q) = -(\operatorname{sgn}\dot{q})\epsilon(1 - \alpha^2 q^2) \quad \text{and} \quad \psi(q) = 2\kappa^2 f(q)$$

Example C

$$\ddot{q} - (\kappa^2 s)(\operatorname{sgn}\dot{q})(1 - \beta^2\dot{q}^2) + \kappa^2 f(q) = 0 \quad \ldots\ldots [8]$$

where

$$\varphi = +2\kappa^2 s\beta^2(\operatorname{sgn}\dot{q})$$

and

$$\psi(q) = 2\kappa^2[f(q) - s(\operatorname{sgn}\dot{q})]$$

The differential equations for both examples, *B* and *C*, may be called "modified v. d. Pol differential equations." They provide a mechanism for feeding energy into the system for small values q or $\dot{q}$ and for extracting energy from the system for large values q or $\dot{q}$; thus they will lead to self-sustained vibrations, as v.d. Pol's differential equation

[1] Professor of Engineering Mechanics, Timoshenko Laboratory, Stanford University. Mem. ASME.

Presented at the West Coast Conference of the Applied Mechanics Division, Monterey, Calif., September 12–13, 1955, of The American Society of Mechanical Engineers.

Discussion of this paper should be addressed to the Secretary, ASME, 29 West 39th Street, New York, N. Y., and will be accepted until January 10, 1956, for publication at a later date. Discussion received after the closing date will be returned.

Note: Statements and opinions advanced in papers are to be understood as individual expressions of their authors and not those of the Society. Manuscript received by the West Coast Committee of the ASME Applied Mechanics Division, March 26, 1955. Paper No. 55—APM-34.

$$\ddot{q} - \delta\dot{q}(1 - \alpha^2 q^2) + \kappa^2 q = 0 \quad [9]$$

does. The actual and detailed treatment, however, of these modified v. d. Pol differential equations [7] and [8] will be left to a separate paper.

The First Integral

As was pointed out in the foregoing, we are going to treat here Equation [6], which is equivalent to

$$\frac{dV}{dq} + (\text{sgn } \dot{q})\delta V + 2\kappa^2 f(q) = 0 \quad [10]$$

First, we confine our attention to motions starting from rest at a positive displacement $q = Q_1$, therefore having negative velocity $\dot{q}$. Hence sgn $\dot{q} = -1$, and the differential Equation [10] becomes

$$\frac{dV}{dq} - \delta V = -2\kappa^2 f(q) \quad [11]$$

This differential equation, being linear, admits of a solution in terms of quadratures. Fitting the solution to the initial conditions specified, we obtain

$$V(q) = 2\kappa^2 e^{\delta q} \int_q^{Q_1} e^{-\delta\sigma} f(\sigma) d\sigma \quad [12]$$

Making use of the abbreviation

$$N(q) = \int_0^q e^{-\delta\sigma} f(\sigma) d\sigma \quad [13]$$

we obtain for Equation [12] the expression

$$V(q) = 2\kappa^2 e^{\delta q}[N(Q_1) - N(q)] \quad [14]$$

Equation [14] describes the motion as long as differential Equation [11] holds; that is, as long as a negative velocity exists, which means, until the next "point of return" or "maximum displacement" Q_2 is reached. This second maximum displacement Q_2 is determined by the subsequent zero of Equation [14], hence by

$$N(Q_1) = N(Q_2) \quad [15]$$

Equation [15] gives the (transcendental) relationship between a maximum displacement Q_1 on the positive side and the subsequent maximum displacement Q_2 on the negative side. Both arguments, Q_1 and Q_2, render the same value to the function $N(q)$, explained by Equation [13]. To simplify the nomenclature we will refer to Equation [15] as the amplitude relationship—taking the liberty of using the term amplitude as synonymous with maximum displacement.

Next, we should consider the motion from the negative to the positive side, when $\dot{q}$ is positive. In case the function $f(q)$ in the term for the restoring force is an odd function, $f(-q) = -f(q)$, by reversing the direction of the co-ordinate q we create for the second swing exactly the same conditions as they existed for the first one; hence the same equations and relations apply as they have been used for the first swing. In case, however, the function $f(q)$ is not odd, but composed of odd and even terms, $f = f_o + f_e$ with $f_o(-q) = -f_o(+q)$ and $f_e(-q) = f_e(+q)$, as we reverse the direction of q we have to replace the function $f_o(q) + f_e(q)$ by $f_o(q) - f_e(q)$. By doing so we again create for the second swing the same conditions as existed for the first swing and the diagram may be used for either swing.

Subsequently we will evaluate the amplitude Relationship [15] for a number of cases, differing in regard to the function $f(q)$. In the next section we consider odd functions $f(q)$ of type $f(q) = \mu^{n-1}q^n$; then we proceed in the following section to other odd functions $f(q)$ (polynomials in q, and sin q); after those we consider nonodd functions $f(q)$.

Amplitude Relationships for Odd Restoring Forces Proportional to Pure Powers of Displacement

For

$$f(q) = \mu^{n-1}q^n \quad [16]$$

the function $N(q)$, defined by Equation [13], becomes

$$N(q) = \frac{\mu^{n-1}}{\delta^{n+1}}\{n! - e^{-\delta q}[(\delta q)^n + n(\delta q)^{n-1} + n(n-1)(\delta q)^{n-2} + \ldots + n!]\} \quad [17]$$

Two successive amplitudes Q_1 and Q_2 are two arguments q which render the same value to the function $N(q)$. The functional value N itself is irrelevant. Therefore, instead of using the function $N(q)$, we may work with any other function derived from it. We will demonstrate this procedure by way of examples.

First, we consider the subcase $n = 1$, that is, $f(q) = q$. Here

$$N(q) = \frac{1}{\delta^2}[1 - e^{-\delta q}(\delta q + 1)] \quad [18]$$

Instead of using this function $N(q)$ as it stands, we deal with the function $y = -\ln[-(\delta^2 N - 1)]$. Writing x for δq, we obtain

$$y = x - \ln(x + 1) \quad [19]$$

Two successive amplitudes Q_1 and Q_2 are such values for which the arguments $x_1 = \delta Q_1$ and $x_2 = \delta Q_2$ render the same value to the function y. Figs. 1(*a*) and 1(*b*) show the plot of $y(x)$ given by Equation [19] and exhibit a pair of abscissas x_1 and x_2, belonging to one swing.

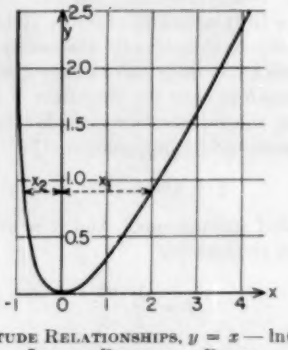

Fig. 1(*a*) Amplitude Relationships, $y = x - \ln(x + 1)$ for $x \leqq 4$; Linear Restoring Force

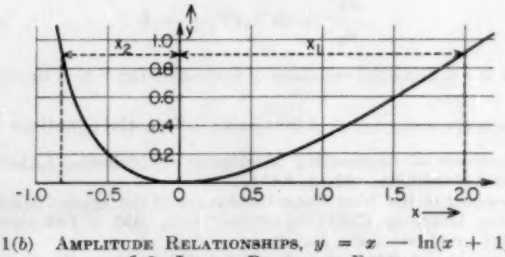

Fig. 1(*b*) Amplitude Relationships, $y = x - \ln(x + 1)$ for $x \leqq 2$; Linear Restoring Force

An important feature may be especially noted: The presence of an asymptote to the diagram at $x = -1$ means that the absolute value of the second amplitude Q_2, because of $|x_2| < 1$, never exceeds $1/\delta$, however large the starting amplitude Q_1 may have been. This fact is in strict contrast to the behavior of a linearly damped

system, where any amplitude has a fixed ratio to the preceding one, $|Q_2|/|Q_1| = \exp(\vartheta/2)$ with ϑ denoting the logarithmic decrement of the system.

The linear subcase, which we just described, was treated by R. v. Mises (1)[2] in 1914. In the publication quoted a diagram corresponding to Fig. 1(*a*) is reproduced and its implications are discussed. However, it seems that up to the present time it was never realized that the procedure is not restricted to linear functions $f(q)$. The linearity of the differential Equation [11] is in no way impaired, if $f(q)$ is a nonlinear function, because in that equation q plays the role of the independent variable rather than that of the dependent one.

We proceed to the second subcase, $n = 3$, that is, $f(q) = \mu^2 q^3$. From Equation [17], by writing again $x = \delta Q$, we find

$$N(x) = (\mu^2/\delta^4)\left\{6 - e^{-x}[x^3 + 3x^2 + 6x + 6]\right\}$$

Here we replace N by

$$y = -\ln\left\{-[(\delta^4/\mu^2)N - 6]\right\} + \ln 6$$

and obtain

$$y = x - \ln\left(\frac{x^3}{6} + \frac{x^2}{2} + x + 1\right) \quad \ldots\ldots\ldots [20]$$

Figs. 2(*a*), 2(*b*), and 2(*c*) show plots for the Function [20]. Here the same general features appear as in the former case. In particular, an asymptote exists which puts an upper bound to any second amplitude; the abscissa of the asymptote is found to be $x_a = -1.596$.

Briefly we indicate the results for the third case, $f(q) = \mu^4 q^5$. Here a pair of amplitudes is determined by a pair of abscissas x rendering the same value to the function

$$y = x - \ln\left(\frac{x^5}{120} + \frac{x^4}{24} + \frac{x^3}{6} + \frac{x^2}{2} + x + 1\right) \quad [21]$$

A plot of Equation [21] is shown in Fig. 3. The asymptote is found at $x_a = -2.180$.

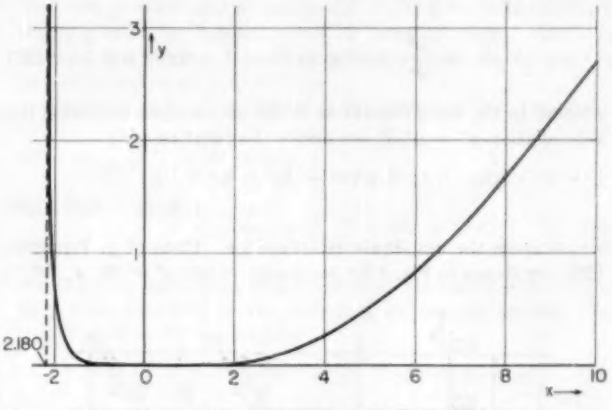

FIG. 3 AMPLITUDE RELATIONSHIPS EQUATION [21] FOR SYSTEM HAVING $f = \mu^4 q^5$

In the general case, with n not specified, from the Expression [17] for the function $N(q)$ by the same procedures as applied for the particular cases treated, we find the expression for y to be

$$y = x - \ln\left(1 + x + \frac{x^2}{2!} + \frac{x^3}{3!} + \ldots + \frac{x^n}{n!}\right) \quad [22]$$

The abscissa x_a of the asymptote to the plot is given by the first negative zero of the polynomial in the argument of the logarithm.

It may be well to note that for use in the vicinity of the origin the amplitude relationships given by Equations [19 to 21] or [22] will be replaced profitably by their respective power-series expansions. By way of example, we treat here the cases of $n = 1$ and $n = 3$.

In the first case, $n = 1$, if we expand the Function [19] (retaining terms up to third power in x) we find

$$y = \frac{x^2}{2}\left(1 - \frac{2}{3}x\right)$$

from this the relationship between x_1 and $X_2 = |x_2| = -x_2$ follows as

$$X_2^2\left(1 + \frac{2}{3}X_2\right) = x_1^2\left(1 - \frac{2}{3}x_1\right) \quad \ldots\ldots [23]$$

Equation [23] is a cubic equation for X_2. It may be solved as such. An approximate solution is obtained by putting $X_2 = x_1(1 - \epsilon)$ and retaining first powers in ϵ alone. Thus one finds

$$X_2 = x_1\left(1 - \frac{2}{3}x_1\right) \quad \ldots\ldots\ldots\ldots [24]$$

In the second case, $n = 3$, a corresponding procedure (retaining terms up to x^6) leads to

$$X_2^4\left[1 + \frac{4}{5}X_2\right] = x_1^4\left[1 - \frac{4}{5}x_1\right] \quad \ldots\ldots [25]$$

[2] Numbers in parentheses refer to the Bibliography at the end of the paper.

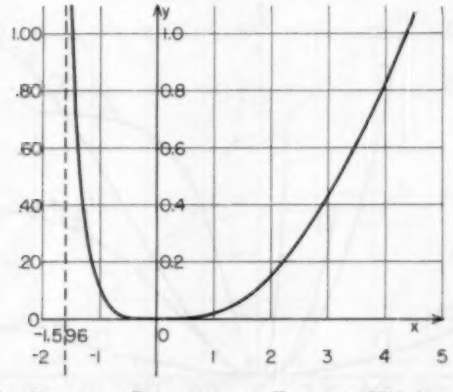

FIG. 2(*a*) AMPLITUDE RELATIONSHIPS EQUATION [20] FOR $x \leqq 4.50$ PURELY CUBIC RESTORING FORCE

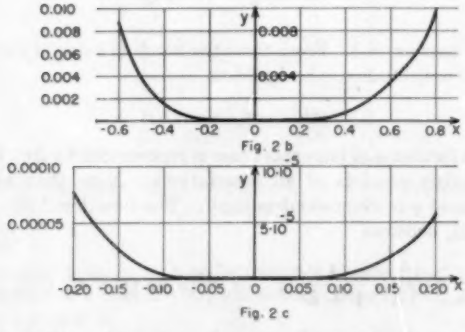

FIG. 2(*b*) (*above*) AMPLITUDE RELATIONSHIPS EQUATION [20] FOR $x \leqq 0.8$; PURELY CUBIC RESTORING FORCE

FIG. 2(*c*) (*below*) AMPLITUDE RELATIONSHIPS EQUATION [20] FOR $x \leqq 0.2$; PURELY CUBIC RESTORING FORCE

and

$$X_2 = x_1\left(1 - \frac{2}{5}\,x_1\right) \quad \ldots\ldots\ldots\ldots\ldots [26]$$

AMPLITUDE RELATIONSHIPS FOR OTHER ODD RESTORING FORCES

(*a*) As a first case we consider $f(q) = q + \mu^2 q^3$, corresponding to a "hardening" spring. Here the function $N(q)$ according to Equation [17] becomes

$$N(q) = \frac{1}{\delta^2}\,[1 - e^{-x}(x+1)] + \frac{\mu^2}{\delta^4}\,[6 - e^{-x}(x^3 + 3x^2 + 6x + 6)] \quad \ldots\ldots [27]$$

whence, in the same manner as in the earlier cases and using the abbreviation $p^2 = \mu^2/\delta^3$, we derive the function $y(x)$

$$y = x - \ln[(x+1) + p^2(x^3 + 3x^2 + 6x + 6)] + \ln[1 + 6p^2] \quad [28]$$

which gives the amplitude relationships. Plots of y, Equation [28], are shown in Fig. 4 for parameter values $p^2 = 10;\ 1;\ 10^{-1};$

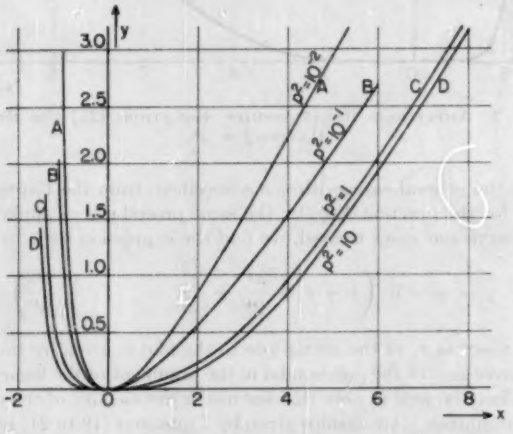

FIG. 4 AMPLITUDE RELATIONSHIPS EQUATION [28] FOR SYSTEM HAVING $f = q + \mu^2 q^3$

10^{-2}. The plot for $p^2 = 10$ for all practical purposes coincides already with that for $p^2 = \infty$ shown in Fig. 2; hence this plot applies for all parameter values $p^2 \geqq 10$. For parameter values $p^2 \ll 1$, practically $p^2 \leqq 10^{-2}$, the plot for $p = 0$ shown in Fig. 1 applies. Each one of the curves in Fig. 4 has a vertical asymptote on the left side. The abscissas x_a of these asymptotes, denoting the value of the first negative (dimensionless) amplitude x_2 which follows a very large positive one, $x_1 \gg 1$, are given in Table 1.

TABLE 1 ABSCISSAS OF ASYMPTOTES

p^2	x_a
$\gg 1$	−1.596
10^2	−1.595
10^1	−1.582
10^0	−1.473
10^{-1}	−1.154
10^{-2}	−1.019
$\ll 1$	−1.000

(*b*) Next, we consider the case of a "softening spring," described by $f(q) = q - \mu^2 q^3$. Here some caution has to be exerted, because displacements q whose absolute values transcend the value $1/\mu$ do not cause the system to return but to go off indefinitely. Hence such displacements are not admissible if oscillations are considered.

Furthermore, another peculiar difficulty arises, which, however, is one of representation rather than an intrinsic one: If we would proceed just as we did before in the case of a hardening spring, because of the minus sign now appearing in front of μ^2, we would have to change the sign in front of p^2 in Equation [28], which gives the amplitude relationships. But then negative arguments in the logarithms may appear. Hence the procedure using logarithms is an inappropriate one in this case and it is better to stay with the relationship

$$Y = 1 - e^{-x}(1+x) - 6p^2\left[1 - e^{-x}\left(1 + x + \frac{x^2}{2} + \frac{x^3}{6}\right)\right] \quad [29]$$

which follows from Equation [27] by putting $Y = \delta^3 N$ and changing the sign in front of p^2. Plots are shown in Fig. 5. As abscissas the values px are used instead of x. And because of $|q| < (1/\mu)$ the abscissas $px = \mu q$ have to stay smaller than 1. The values of Y corresponding to $xp = 1$, denoted by Y_{max} for the four curves of Fig. 5 are listed in Table 2.

TABLE 2 SPECIAL VALUES FOR CURVES IN FIG. 5

Curve	p^2	Y_{max}	$-px_2$
A	10^{-2}	0.9405	0.09612
B	10^{-1}	0.5894	0.2630
C	1.0	0.1503	0.4960
D	10	0.0213	0.7242

The last column of Table 2 shows the absolute values of the negative abscissas $-px_2$ which lead to the same functional values

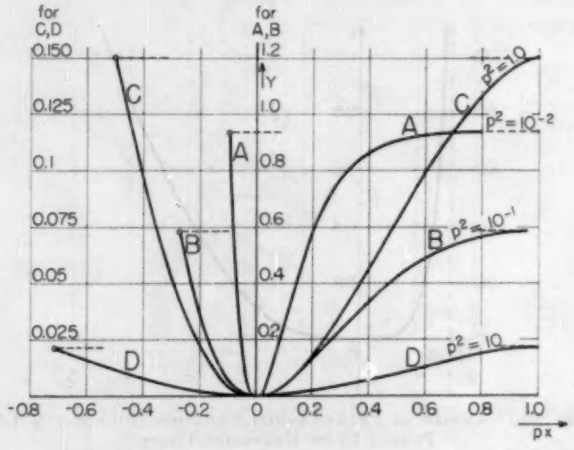

FIG. 5 AMPLITUDE RELATIONSHIPS EQUATION [29] FOR SYSTEM HAVING $f = q - \mu^2 q^3$

Y_{max} as does $px = 1$. From them the absolute value of the largest negative amplitude can be found as

$$|Q_2|_{max} = (-px_2)/\mu$$

(*c*) A further and important case is represented by $f(q) = \sin q$; it comprises pendula of all descriptions. Note that here the co-ordinate q is dimensionless itself. The function $N(Q)$, Equation [13], becomes

$$N(Q) = \frac{1}{1+\delta^2}\,[1 - e^{-\delta Q}(\delta \sin Q + \cos Q)] \quad \ldots\ldots [30]$$

In its stead the derived function, $Y = 1 - (1+\delta^2)N$, that is

$$Y = e^{-\delta Q}(\delta \sin Q + \cos Q) \quad \ldots\ldots\ldots\ldots [31]$$

may be used for determining a pair of amplitudes Q_1, Q_2 according

to Equation [15]. A plot of Equation [31] with the dimensionless quantity δ serving as a parameter of the family of curves is shown in Fig. 6. From this plot the relationship between Q_1 and Q_2 may be derived (again with δ serving as a parameter). In Fig. 7 such

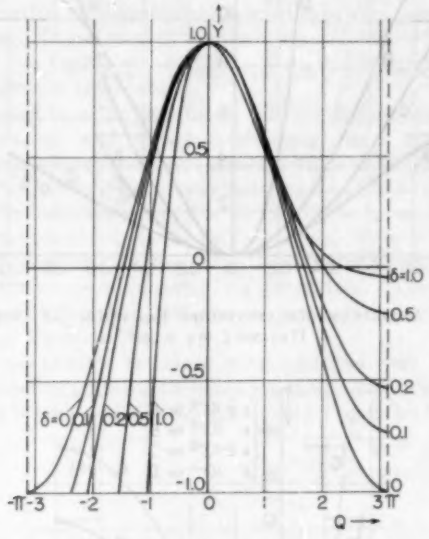

FIG. 6 AMPLITUDE RELATIONSHIPS EQUATION [31] FOR SYSTEM HAVING $f = \sin q$

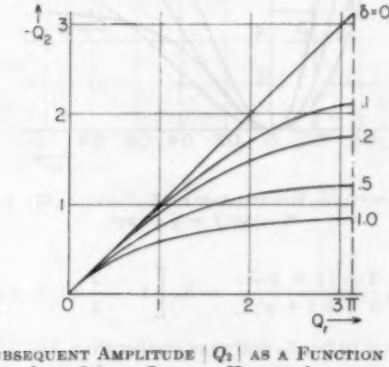

FIG. 7 SUBSEQUENT AMPLITUDE $|Q_2|$ AS A FUNCTION OF PREVIOUS ONE, Q_1, FOR SYSTEMS HAVING $f = \sin q$

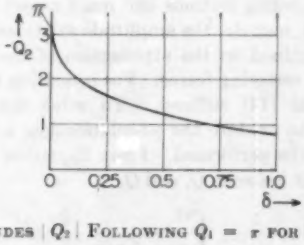

FIG. 8 AMPLITUDES $|Q_2|$ FOLLOWING $Q_1 = \pi$ FOR SYSTEMS HAVING $f = \sin q$

curves, giving $|Q_2| = -Q_2$ as functions of Q_1, are shown. Finally, in Fig. 8 those values of $-Q_2$ which result from $Q_1 = \pi$ are shown as a function of δ.

AMPLITUDE RELATIONSHIPS FOR NONODD RESTORING FORCES

The procedure to be adopted if the function $f(q)$, representing the restoring force, is not purely odd but composed of odd and even parts, was spoken of already toward the end of the second section. If for the swing with negative velocity the function f is represented by $f = f_0 + f_e$, then for the swing in the opposite direction we have to use $f = f_0 - f_e$ in order to compensate for the reversal of the direction of the co-ordinates.

We content ourselves with a detailed discussion of one single case. For this we choose

$$f(q) = q + \mu q^2 \quad \ldots\ldots\ldots\ldots\ldots\ldots [32]$$

as represented by curve (a) in Fig. 9. That curve may be interpreted as exhibiting a "hardening" effect for positive displacements q and a "softening" effect for negative ones. From the diagram it is obvious that the negative displacements q must be limited to the range $|-q| < (1/\mu)$.

The function $N(q)$, as defined in the second section, becomes

$$N(q) = \frac{1}{\delta^2}\left[1 - e^{-\delta q}(1 + \delta q)\right] + \frac{\mu}{\delta^2}\left\{2 - e^{-\delta q}\left[2 + 2\delta q + (\delta q^2)\right]\right\} \quad \ldots\ldots [33]$$

Avoiding the use of logarithmic functions for the same reasons as they were described in the preceding section, we replace $N(q)$ simply by $Y = \delta^2 N$ and obtain

$$Y = (1 + 2p) - e^{-x}[(1 + x) + p(2 + 2x + x^2)] \ldots [34]$$

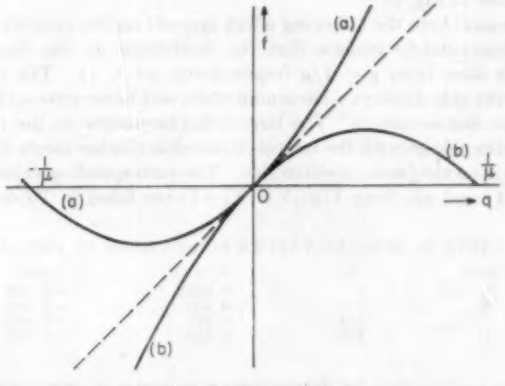

FIG. 9 FUNCTIONS
(a) $f = q + \mu q^2$
(b) $f = q - \mu q^2$

where x denotes δq and p stands for μ/δ. Plots of Equation [34] with $xp = \mu q$ as abscissas are shown in Fig. 10 for the parametric values $p = 2$, 1, 1/2, and 1/4. We will discuss a few features.

We realize that because of $|-q| < 1/\mu$ the abscissas on the negative side are limited to the range $|-xp| < 1$. The values which the function Y adopts at the argument $xp = -1$ (for the three curves A, B, C) are 0.0539; 0.2817; and 2.0000, respectively.

The function Y for large positive values of x tends toward $Y_{max} = 1 + 2p$. The numerical values of this quantity Y_{max} for the four curves A, B, C, D, respectively, are 5, 3, 2, 3/2.

Hence we realize (and this fact can be proved quite generally) that for parameter values $p > 1/2$ the functional value Y at $xp = -1$ is smaller than the asymptotic value Y_{max} for large arguments. This means that for $p > 1/2$ the amplitudes on the positive side have to be restricted so as not to allow the system to shoot beyond $q = -1/\mu$ on the negative side. The maximum values which are permissible on the positive side are determined

by $Y(px) = Y(-1)$. For $p = 2(A)$ and $p = 1(B)$ the respective values are

$$(A)\ px = 0.6114 \qquad (B)\ px = 0.7933$$

For the parameter value $p = 1/2$ we see that $Y(-1) = Y_{max}$ (the common value being $Y = 2$). A very large starting value, hence, leads exactly to

$$|Q_2| = 1/\mu$$

For parametric values $p < 1/2$, on the other hand, we find

$$Y_{max} < Y(-1)$$

Hence there is no restriction on the positive starting amplitude. Here, then, the largest amplitude x_2 on the negative side is determined by $Y(px_2) = Y_{max}$ as is the case for hardening springs. Curve (D) with $p = 1/4$ gives an example. There we find $Y_{max} = 3/2$ and $px_2 = -0.3170$.

All of the discussion in this section so far pertains to a swing from right to left (with $\dot{q} < 0$). For the subsequent swing from left to right we agreed on reversing the direction of q, which is equivalent to replacing $f = q + \mu q^2$ by $f = q - \mu q^2$, see curve (b) in Fig. 9. The function Y which applies here is Equation [34] with the sign in front of p being changed, hence

$$Y = (1 - 2p) - e^{-x}[(1 + x) - p(2 + 2x + x^2)] \quad [35]$$

Plots are found in Fig. 11 for the same parameter values as used for those in Fig. 10.

Because here the softening effect appears on the positive side, one immediately realizes that the limitations on the displacements stem from $q < 1/\mu$ (equivalently $px < 1$). The (now) negative side displays a hardening effect and hence puts no limits on the displacements. The largest displacements on the (now) negative side go with the largest permissible displacements $1/\mu$ or $xp = 1$ on the (now) positive side. The corresponding values for $Y(+1)$ and px_2 from $Y(px_2) = Y(+1)$ are listed in Table 3.

TABLE 3 SPECIAL VALUES FOR CURVES IN FIG. 11

Curve	p	$Y(+1)$	x_1p
A	2	0.0325	−0.420
B	1	0.104	−0.361
C	1/2	0.271	−0.279
D	1/4	0.528	−0.187

One realizes that for determining a sequence of amplitudes (of System [32], e.g.) one has to use Equations [34] and [35] alternately—corresponding to an alternate use of diagrams, Figs. 10 and 11.

Of course, in the same manner as before, in the vicinity of the origin, the functions Y may be replaced by their power-series expansions. Thus from Equation [34] by retaining terms up to x^3 we find the cubic equation for $X_2 = -x_2$

$$X_2^2[3 + 2(1 - p)X_2] = x_1^2[3 - 2(1 - p)x_1]$$

and, replacing X_2 by $x_1(1 - \epsilon)$, retaining first powers in ϵ alone, we obtain

$$X_2 = x_1 \frac{3 + x_1(1 - p)}{3 + 3x_1(1 - p)} \approx x_1\left[1 - \frac{2}{3}(1 - p)x_1\right] \quad [36]$$

Equation [36] tells that in the vicinity of the origin there is

$$X_2 \gtrless x_1 \quad \text{if} \quad p \gtrless 1$$

The curve for $p = 1$ is practically symmetrical in the vicinity of 0.

For the "return journey" from left to right, because p is to be replaced by $-p$, we find simply

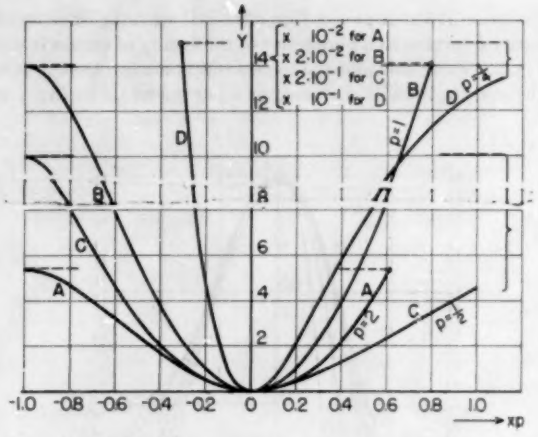

FIG. 10 AMPLITUDE RELATIONSHIPS EQUATION [34] FOR SYSTEM HAVING $f = q + \mu q^2$

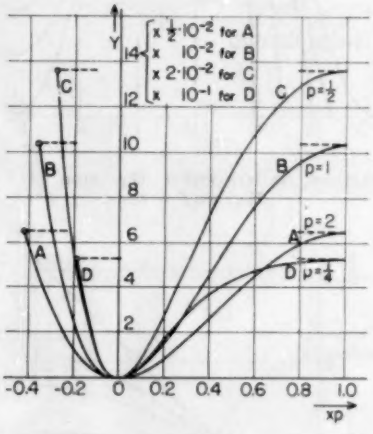

FIG. 11 AMPLITUDE RELATIONSHIPS EQUATION [35] FOR SYSTEM HAVING $f = q - \mu q^2$

$$X_3 = X_2 \frac{3 + (1 + p)X_2}{3 + 3(1 + p)X_2} \approx X_2\left[1 - \frac{2}{3}(1 + p)X_2\right] \quad [37]$$

As we expect it to be, X_3 is always smaller than X_2.

CONCLUSION

1 In the preceding sections one main aspect of our problem has been treated, namely, the amplitude relationships. Thus information was gained on the attenuation of the oscillations for various kinds of restoring forces. For procuring this information the first integral [14] sufficed. To solve the problem completely, that is, to produce the q-t-relationship, a further integration will have to be performed. From Equation [14] we find for the time T_s spent between Q_1 and Q_2

$$T_s = \frac{1}{\kappa\sqrt{2}} \int_{Q_2}^{Q_1} \frac{du}{\sqrt{e^{\beta u}[N(Q_1) - N(u)]}} \quad [38]$$

The nature of the integrand in Equation [38] is such that no closed-form solutions can be hoped for. Hence the integral will have to be solved in some numerical way. Estimates, even good estimates, for the expression [38] may be achieved by replacing the functions in the integrand by simpler ones. In this way upper and lower limits for the true values of Equation [38] may be established. This program, however, will require some special consideration and hence will merit a separate treatment. Nu-

merical evaluation, however, will suffice in most instances, and this is where we have to leave the problem at present.

2 Recently, two papers (2, 3) dealt extensively with the attenuation of free oscillations under the action of various types of damping forces, including the quadratic damping. Comprehensive as the earlier treatments are in regard to the types of damping forces admissible, the magnitudes of those forces were restricted to small values. In our present treatment no such restriction is introduced; the results obtained here are valid for (quadratic) damping forces of any amount.

3 In regard to earlier literature it will be sufficient to say that when oscillations with quadratic damping forces have been treated the restoring forces were assumed linear in all cases. To the author's knowledge, nonlinear restoring forces have not been considered in this connection. For the case of the linear restoring forces the treatment in (1) is the only exact one. Prior to (1) and also later, a number of approximate formulas for the amplitude relationship have been suggested, e.g. (4) and (5). They essentially agree with Equation [23], derived here by the power-series expansion of Equation [19].

4 Whereas hitherto the linear damping forces were thought of as the easiest to treat and therefore were preferred to the extent of replacing other types of damping forces by "equivalent linear" ones, we now realize that, particularly if the restoring forces are not linear, one need not shy away from approximating a damping force-velocity relationship by a quadratic expression. In fact, in conjunction with nonlinear restoring forces the quadratic damping forces (but not the linear ones) allow exact procedures (in all autonomous cases), as we have shown. One, therefore, may even be inclined in certain instances to replace other types of damping forces by "equivalent quadratic" ones.

BIBLIOGRAPHY

1 "Elemente der Techn. Hydrodynamik, 1," by R. v. Mises, Leipzig and Berlin, Germany, 1914, p. 188; reproduced in Techn. Schwingungslehre by K. Klotter, Springer-Verlag, Berlin-Göttingen-Heidelberg, Germany, second edition, 1951, p. 130.

2 "The Attenuation of Damped Free Vibrations and the Derivation of the Damping Law From Recorded Data," by K. Klotter, Second National Congress of Applied Mechanics, Ann Arbor, Mich., 1954, p. 85.

3 "Zur Analyse der Dämpfung freier Schwingungen," by H. Kauderer, *Ingenieur-Archiv*, vol. 22, 1954, p. 251.

4 "Über Schwingungen nach dem quadratischen Widerstandsgesetz," by R. Grammel, *Physikalische Zeitschrift*, vol. 14, 1913, p. 20.

5 "Zur Frage der Schwingungen nach dem quadratischen Widerstandskraftgesetz," by Th. Pöschl, *Physikalische Zeitschrift*, vol. 29, 1928, p. 938.

Perturbation Methods Applied to Nonlinear Dynamics

By RICHARD BELLMAN,[1] SANTA MONICA, CALIF.

We wish to present a simple technique which will in many cases increase the range of effectiveness of perturbation and power-series methods in situations in which the equations treated contain parameters which assume only positive values.

Introduction

THE simplest equations to consider, from the mathematical point of view, are linear equations with constant coefficients such as

$$\ddot{u} + a\dot{u} + bu = 0 \quad [1]$$

which occurs in circuit theory, or

$$u_{xx} = u_t \quad [2]$$

which occurs in the theory of heat conduction.

However, these equations are only approximations to the actual equations governing the physical systems under consideration. For certain ranges of frequency, voltage, current, or temperature, they serve admirably, and for certain other ranges, they fail notably. Consequently, in place of the simple linear Equation [1], in the theory of the multivibrator, we encounter the equation

$$\ddot{u} + \lambda(u^2 - 1)\dot{u} + u = 0 \quad [3]$$

the famed equation of Van der Pol (1, 2),[2] and in problems involving radiation we meet the equation

$$u_{xx} = u_t + au^3 \quad [4]$$

of reference (3).

These are nonlinear equations which means that the superposition method which consists of forming a complete solution as a sum of partial solutions breaks down completely. In place of this, it is customary to fall back upon the technique of solution in terms of a series expansion in the form of a power series, a Fourier series, or series involving some other orthogonal set, or alternatively in terms of various parameters appearing in the equation.

This is particularly the case when we are dealing with slightly nonlinear equations, as, for example, Equation [3] for small λ or Equation [4] for small a.

It frequently happens that these parameters do not take both positive and negative values, but are restricted to be either of one sign or the other because of their physical significance. Thus λ in Equation [3] is always positive. It is easy to think of many other parameters occurring in applied mathematics such as coupling coefficients, strength of shocks, and so on, which are intrinsically positive.

This positivity does not seem to have been utilized to full advantage. In this paper we wish to discuss a simple technique which in many cases will increase the range of effectiveness of perturbation and power-series methods in situations in which we treat equations containing parameters which assume only positive values.

The Traditional Perturbation Technique

Let us suppose that we have a linear equation which we write in the form

$$L(u) = 0 \quad [5]$$

and a nonlinear equation which has the form

$$L(u) + \epsilon N(u) = 0 \quad [6]$$

where $N(u)$ is a nonlinear term and ϵ is a small parameter. In general, $N(u)$ will be a power series in u lacking constant and linear terms.

Let u_0 be a solution of the linear equation. We then attempt a solution of the nonlinear equation having the form

$$u = u_0 + \epsilon u_1 + \epsilon^2 u_2 + \ldots \quad [7]$$

Assuming that $N(u)$ has derivatives of all orders in the neighborhood of $u = u_0$, we obtain a system of linear inhomogeneous equations

$$\left.\begin{aligned} L(u_1) + N(u_0) &= 0 \\ L(u_2) + u_1 N'(u_0) &= 0 \\ &\cdot \\ &\cdot \\ &\cdot \end{aligned}\right\} \quad [8]$$

which we solve recursively.

In many cases, in order to use this technique most effectively, we must introduce some preliminary transformations to take account of the fact that nonlinear equations have movable singularities. This is the basis of the Lindstedt technique in the theory of periodic solutions of nonlinear differential equations, which we shall discuss briefly, and the Lighthill technique in the study of the behavior of nonlinear differential equations in the neighborhood of a singularity (4).

Returning to the perturbation expansion obtained from the system of Equations [8], there are now two cases to consider. Either the expansion converges for ϵ restricted to some nonzero neighborhood of $\epsilon = 0$, or it diverges for all nonzero ϵ and represents a divergent series. We shall consider only the first case where the solution of the nonlinear equation is an analytic function of ϵ for $|\epsilon| < r$, where $r > 0$.

There is a corresponding discussion for the case of asymptotic series, but it is more complicated and we shall not discuss it here.

Power Series and Singularities

As we know, the radius of convergence of a power series

---

[1] The Rand Corporation.

[2] Numbers in parentheses refer to the Bibliography at the end of the paper.

Presented at the West Coast Conference of the Applied Mechanics Division, Monterey, Calif., September 12–13, 1955, of The American Society of Mechanical Engineers.

Discussion of this paper should be addressed to the Secretary, ASME, 29 West 39th Street, New York, N. Y., and will be accepted until January 10, 1956, for publication at a later date. Discussion received after the closing date will be returned.

Note: Statements and opinions advanced in papers are to be understood as individual expressions of their authors and not those of the Society. Manuscript received by West Coast Committee of the ASME Applied Mechanics Division, March 26, 1955. Paper No. 55—APM-33.

$$f(z) = \sum_{n=0}^{\infty} c_n z^n \quad [9]$$

representing an analytic function around the origin is determined by the distance from the origin to the nearest singularity of $f(z)$. Consequently, in considering the power-series expansion of a function such as $\sqrt{1+z}$, even if we are interested only in positive values of z, we are restricted in our use of the series by the behavior of the function for negative values of z, in this case $z = -1$.

In problems in which we are interested in the behavior of a function $f(z)$ within a circular region, it follows that power series are an ideal tool. On the other hand, in a large class of problems encountered in applied mathematics, where we are concerned with the behavior of a function along the positive real axis, power series are not the ideal tool.

There is, however, no other analytic instrument which possesses the simplicity of power series in relation to the basic operations of algebra and calculus, operations such as multiplication and differentiation.

Consequently, we must compromise and modify the power series which occur so as to make their convergence selective in so far as direction is concerned. We shall discuss this in the next sections.

A Modified Perturbation Technique

Before treating more complicated cases, let us consider a simple example. Suppose that we consider the power series for $\sqrt{1+z}$

$$\sqrt{1+z} = 1 + \frac{1}{2}z - \frac{1}{8}z^2 + \ldots \quad [10]$$

Since there is a branch point of $z = -1$, we know that the series converges for $|z| < 1$, and diverges for $|z| > 1$.

To take advantage of the positivity of z, let us make the change of variable

$$w = z/(1+z), \quad \text{or} \quad z = w/(1-w) \quad [11]$$

Then

$$\left.\begin{aligned}\sqrt{1+z} &= \sqrt{1/(1-w)} = 1 + \frac{1}{2}w + \frac{3}{8}w^2 + \ldots \\ &= 1 + \frac{1}{2}\left(\frac{z}{1+z}\right) + \frac{3}{8}\left(\frac{z}{1+z}\right)^2 + \ldots\end{aligned}\right\} \quad [12]$$

The series in w converges for $|w| < 1$, which means that the series for $\sqrt{1+z}$ in terms of $z/(1+z)$ converges for $|z/(1+z)| < 1$. This region in the z-plane includes all positive z! Consequently, we have a series expansion for $\sqrt{1+z}$ which converges for all $z \geq 0$.

What we have performed is an analytic continuation of $\sqrt{1+z}$ into the region of greatest interest to us, or equivalently we have performed a conformal mapping which distorts the z-plane in such a way as to make the convergence selective.[3] These are well-known techniques as far as the independent variable occurring in the equation is concerned. They do not, however, seem to have been utilized in connection with the analytic dependence of the solution upon the parameters in the equation.

Some Further Examples

In reference (5) some further examples of this general idea were considered. The first concerned the expansion of the positive solution of the equation

$$x + x^2 = z \quad [13]$$

for $z > 0$, or, more generally, that of

$$x + x^k = z \quad [14]$$

The second was the expansion of the solution of

$$x + \lambda A x = c \quad [15]$$

in terms of λ, where x and c are vectors and A is a positive definite matrix. In this case, if we are interested only in positive values of λ, it is possible to obtain a power-series expansion in terms of $\lambda/(\lambda + a)$ (where the choice of a depends upon the matrix A) which converges for all positive λ.

An analogous problem arises from the integral equation

$$f(t) + \lambda \int_0^T K(s,t) f(s)\,ds = g(t) \quad [16]$$

where $K(s,t)$ is positive definite.

An effective method of solving integral equations by means of power series is particularly important since the Fredholm solution is computationally of little worth; refer to (6) for related results.

In passing, we note that precisely an equation of the foregoing form arises from the problem of determining the minimum over f of the quadratic functional

$$\int_0^T \left[g(s) - \int_0^T H(s,t) f(t)\,dt\right]^2 ds + \lambda \int_0^T f^2(s)\,ds \quad [17]$$

where $H(s,t)$ is not necessarily symmetric, and $\lambda > 0$. Questions of this type arise in engineering and economic-control problems (7, 8).

A rigorous theoretical discussion of the foregoing problems is not difficult because the linearity of the operators permits us to determine the location of the singularities of the solutions as functions of the parameters, and thus to make the appropriate transformations.

In the next section we shall discuss a nonlinear problem where there is as yet no theoretical justification for the success of the method.

The Van der Pol Equation

Let us now consider the Van der Pol equation

$$\ddot{x} + \lambda(x^2 - 1)\dot{x} + x = 0 \quad [18]$$

where $\lambda > 0$.

As pointed out previously, the equation must be transformed suitably before a perturbation method can be applied successfully to the problem of determining the periodic solution. The key to the transformation is the observation, based upon experimental evidence, that the frequency as well as the amplitude of a periodic solution depends upon λ.

We thus make a change of variable

$$t = s/[1 + a_1\lambda + a_2\lambda^2 + \ldots] = s/f(\lambda) \quad [19]$$

where $f(\lambda)$ is as yet undetermined. The new equation takes the form

$$f^2(\lambda)\frac{d^2x}{ds^2} + f(\lambda)\lambda(x^2 - 1)\frac{dx}{ds} + x = 0 \quad [20]$$

The point of this transformation is to obtain a new equation whose period is 2π, as in the case when $\lambda = 0$.

We now set

$$x = \cos s + \lambda u_1(s) + \ldots \quad [21]$$

where the coefficient functions $u_1(s)$, $u_2(s)$, and so on, are to be periodic functions of s of period 2π. This condition turns out

[3] The equivalence between analytic continuation and summability techniques on one hand and conformal mapping on the other is believed to have been pointed out first by Gronwall.

to be sufficient to determine the unknown coefficients in $f(\lambda)$, reference (2). This is the Lindstedt technique.

Observe that we are using power series in λ, although we are only interested in positive values of λ. Let us now, following Shohat (9), show how we may obtain an expansion in terms of a new parameter, $r = \lambda/(1 + \lambda)$.

Since it is known that $f(\lambda) \sim 1/\lambda$ as $\lambda \to \infty$, we begin by writing Equation [20] in the form

$$[\lambda f(\lambda)]^2 \frac{d^2x}{ds^2} + [\lambda f(\lambda)]\lambda^2(x^2 - 1)\frac{dx}{ds} + \lambda^2 x = 0 \ldots [22]$$

Now set

$$\left.\begin{aligned} \lambda &= r/(1 - r) = r + r^2 + \ldots \\ \lambda f(\lambda) &= r + c_2 r^2 + c_3 r^3 + \ldots \\ x &= \cos s + r u_1(s) + r^2 u_2(s) + \ldots \end{aligned}\right\} \ldots [23]$$

The Lindstedt technique described previously may be employed and furnishes the values

$$c_2 = 1, \quad c_3 = 15/16, \quad c_4 = 13/16 \ldots [24]^4$$

TABLE 1 COMPARISON OF NUMERICAL VALUES

λ	$f(\lambda)$ computed using Equation [24]	$f(\lambda)$ computed by Van der Pol
0.33	0.98	0.99
1.0	0.93	0.90
2.0	0.77	0.78
8.0	0.35	0.39
10.0	0.30	0.31

From Table 1, comparing numerical values obtained from the foregoing series with those obtained by Van der Pol using a different computational procedure, it seems quite reasonable to conjecture that the series for $f(\lambda)$ in terms of $r = \lambda/(1 + \lambda)$ converges for all $\lambda > 0$. A theoretical justification of this would be of the utmost importance.

It may be conjectured that a similar technique will be successful in treating the inhomogeneous equation

$$\ddot{x} + \lambda(x^2 - 1)\dot{x} + x = a \cos wt \ldots [25]$$

and in treating coupled circuits. In this last case, the parameter would be the coefficient of coupling.

[4] Note that we are merely regrouping the terms of the power series in λ when we obtain the power series in r. Consequently, if the perturbation technique has already been applied in the conventional manner, the new series may be obtained by purely arithmetic operations.

BIBLIOGRAPHY

1 "Lectures on Differential Equations," by S. Lefschetz, Princeton University Press, 1946.

2 "Nonlinear Vibrations in Mechanical and Electrical Systems," by J. Stoker, Interscience Publishers, New York, N. Y., 1950.

3 "On the Existence and Boundedness of Solutions of Nonlinear Partial Differential Equations of Parabolic Type," by R. Bellman, Trans. of the American Mathematical Society, vol. 64, 1948, pp. 21–44.

4 "A Technique for Rendering Approximate Solutions to Physical Problems Uniformly Valid," by S. Lighthill, *Philosophical Magazine*, vol. 40, 1949, pp. 1179–1201.

5 "On Perturbation Methods Involving Expansions in Terms of a Small Parameter," by R. Bellman, *Quarterly of Applied Mathematics* (to appear).

6 "On the Summability of Solutions of Linear Integral Equations," by R. Bellman, *Duke Mathematical Journal*, vol. 17, 1950, pp. 53–55.

7 "On Some Variational Problems Occurring in the Theory of Dynamic Programming," by R. Bellman, I. Glicksberg, and O. Gross, Proceedings of the National Academy of Science, vol. 39, 1953, pp. 298–301.

8 "On Some Variational Problems Occurring in the Theory of Dynamic Programming," by R. Bellman, I. Glicksberg, and O. Gross, Rendiconti del Palermo (to appear).

9 "On Van der Pol's and Related Nonlinear Differential Equations," by J. Shohat, *Journal of Applied Physics*, vol. 15, 1944, pp. 568–574.

Aerodynamic Interference of Cascade Blades in Synchronized Oscillation[1]

By CHIEH-CHIEN CHANG[2] and WEN-HWA CHU[3]

The failure of a compressor is sometimes due to flutter of the blades. Essentially, this problem is equivalent to a cascade in oscillation. The present analysis is to find the aerodynamic load on cascade in synchronized harmonic oscillations, pitching, and flapping. Conformal mapping is used. Two characteristic parameters are involved in the force and moment. One is μ which is related to the gap-chord ratio. The other is k which is known as reduced frequency. The main results are expressed in terms of these two parameters. Most can be reduced to closed form. The rest are given in graphs. The wake interference involves one new function $C(\mu,k)$ which is related to a ratio of two hypergeometric functions and which reduces to Theodorsen's function $C(k)$ in the limit of infinite gap. In a certain range of frequency and gap-chord ratio, the analysis shows quantitatively that single-oscillation airfoil theory may lead to inaccurate estimation of interference effect between blades.

Introduction

SOME preliminary contributions of the authors (1)[4] on the cascade problem were distributed and presented in 1952. Since then, there have been a number of interesting papers (2, 3) available on cascade interference. Those results are, however, predicted from the classical theory (4, 5) of a single oscillating airfoil with some modification. The interference effect of adjacent blades of cascade on aerodynamic loading is considered somehow qualitative rather than quantitative. Apparently there is a need for more accurate theory to give quantitative estimation of the mutual interference. It is expected that the present treatment may serve such purpose.

The cascade at small angle of attack is assumed in a uniform stream of perfect incompressible fluid and is under quasi-steady harmonic oscillation. Two modes are considered, namely, pitching and flapping. The effects of camber, thickness, and stagger of oscillating airfoils of the cascade are all neglected.

All the airfoils of the cascade are assumed to oscillate in synchronization. Consequently, conformal-mapping technique is adopted.

The mathematical treatment is rather involved. The essential part of the results is reduced to closed form. The rest is given in graphs. The wake interference effect involves one new function $C(\mu, k)$, which reduces to the well-known Theodorsen function (4) as the gap between the adjacent cascade airfoils goes to infinity. In that limiting case, both normal force and pitching moment agree with the known results of a single oscillating airfoil as expected. When gap-chord ratio is much smaller than unity, the result must be applied with caution as the effect of airfoil thickness is no longer negligible.

Another interesting case of cascade with adjacent blades oscillating in opposite phase reached the authors in an unpublished report (6).

Differential Equation

In a two-dimensional, irrotational, and unsteady flow of inviscid incompressible fluid, it is well known that velocity potential ϕ satisfies the Laplace equation, i.e.

$$\nabla^2\phi = 0 \qquad [1]$$

where ϕ is related to the velocity components u and v by

$$u = \frac{\partial\phi}{\partial x}, \quad v = \frac{\partial\phi}{\partial y} \qquad [2]$$

Here the time derivative $\partial\phi/\partial t$ does not enter into Equation [1]. Actually, time dependence of ϕ comes from the moving boundary condition as specified later.

Mapping Function

Conformal-mapping technique is employed in the analysis. One strip region including a typical airfoil[5] of the cascade in the z-plane is mapped onto the entire exterior region of a unit circle in the ζ-plane as shown in Fig. 1. The reciprocal relations between z and ζ are

$$z = \frac{1}{\mu}\left\{\ln\left(\zeta^2 + 2\zeta\coth\mu + 1\right) - \ln\left(2\zeta\,\mathrm{csch}\,\mu\right)\right\} \qquad [3a]$$

$$\zeta = \mathrm{csch}\,\mu\left\{\nu^{-z} + \left(\nu^{-z} - \nu^{-1}\right)^{1/2}\left(\nu^{-z} - \nu\right)^{1/2} - \cosh\mu\right\} \qquad [3b]$$

where

$$z = x + iy \qquad [4a]$$

$$\zeta = \xi + i\eta \qquad [4b]$$

$$\mu = \frac{\pi c}{G} \qquad [4c]$$

(Here c is airfoil chord length and G is gap.)
and

$$\nu = \exp(-\mu) \qquad [4d]$$

Boundary Conditions

When the cascade is oscillated in pitching and flapping of very small displacement, the effect of displacement may be neglected

[1] This paper is done under Contract AF 18(600)428 of the United States Air Force, monitored by the Office of Scientific Research, Air Research and Development Command.

[2] Professor, Department of Aeronautical Engineering, University of Minnesota, Minneapolis, Minn. Formerly, Research Professor, Institute for Fluid Dynamics and Applied Mathematics, University of Maryland, College Park, Md.

[3] Research Assistant, Institute for Fluid Dynamics and Applied Mathematics, University of Maryland, College Park, Md.

[4] Numbers in parentheses refer to the Bibliography at the end of the paper.

Presented at the National Conference of the Applied Mechanics Division, Troy, N. Y., June 16–18, 1955, of The American Society of Mechanical Engineers.

Discussion of this paper should be addressed to the Secretary, ASME, 29 West 39th Street, New York, N. Y., and will be accepted until January 10, 1956, for publication at a later date. Discussion received after the closing date will be returned.

Note: Statements and opinions advanced in papers are to be understood as individual expressions of their authors and not those of the Society. Manuscript received by ASME Applied Mechanics Division, August 11, 1954. Paper No. 55—APM-16.

[5] It is clear that cascade consists of infinite number of such typical strips. Both the continuity of the flow and the multiplicity of transformation are correctly represented by the logarithm terms as shown in Equation [3a].

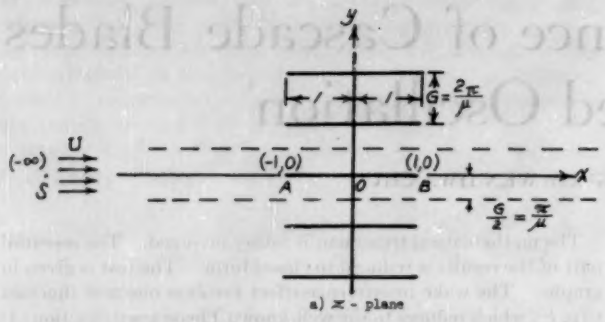

FIG. 1(*a*) GEOMETRY OF CASCADE IN PHYSICAL PLANE
(Here chord $c = 2$ is chosen.)

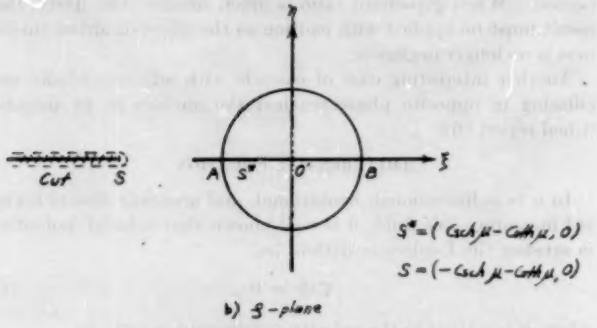

FIG. 1(*b*) CIRCLE PLANE

in the boundary within the accuracy of thin airfoil theory and only the oscillating velocity and angle of attack will be considered. The velocity component normal to the principal airfoil is approximately

$$\left(\frac{\partial\phi}{\partial n}\right)_{\pm} = \pm\{U\bar{\alpha}_{\pm} + U\alpha + (x-a)\dot{\alpha} - \dot{h}\} \quad [5]$$

where

n = outward normal away from the fluid
$\bar{\alpha} = \bar{\alpha}(x)$ = time-mean angle of attack
$\alpha = \alpha(t)$ = transient angle of attack measured from $\bar{\alpha}$
$\dot{\alpha} = \dfrac{d\alpha}{dt}$
$\dot{h} = \dfrac{dh}{dt}$ = flapping velocity (positive flapping displacement corresponds upward)
U = chordwise velocity component of main flow; and the subscripts + and — are used to indicate, respectively, upper and lower surfaces

It is well known in conformal-mapping technique that the corresponding velocity component $\partial\phi(\zeta)/\partial n$ normal to the unit circle ($\zeta = e^{i\theta}$) can be obtained from the corresponding velocity components $\partial\phi(z)/\partial n$ in Equation [5] and a scale factor $|(dz)/(d\zeta)|$ as follows

$$\frac{\partial\phi(\zeta)}{\partial n} = \frac{\partial\phi(z)}{\partial n}\left|\frac{dz}{d\zeta}\right| \quad [6]$$

Here, the scale factor can be shown to be

$$\left|\frac{dz}{d\zeta}\right| = \frac{1}{\mu}\left|\frac{\sin\theta}{\coth\mu + \cos\theta}\right| \quad [7]$$

Another boundary condition is that upstream undisturbed velocity is $U + iV$, a constant, which, in effect, is the condition of irrotationality.

However, the flow through the cascade is in an infinitely connected region and undetermined to an infinite number of degrees. This indeterminateness of the flow can be removed by imposing Kutta-Joukowski's condition to the trailing edge of every airfoil of the cascade at all instants. Consequently, on the unit circle, the corresponding point ($r = 1$, $\theta = 0$) must have vanishing velocity, i.e.

$$\frac{\partial\phi}{\partial\theta} = 0 \quad [8a]$$

and

$$\frac{\partial\phi}{\partial r} = 0 \quad [8b]$$

This hypothesis seems consistent with experimental observation.

DECOMPOSITION OF VELOCITY POTENTIAL

The potential is conveniently decomposed into three parts as

$$\phi = \bar{\phi} + \phi_1' + \phi_2' \quad [9]$$

where $\bar{\phi}$ is the well-known potential corresponding to $\bar{\alpha}$ or to steady flow (7) and will not be reconsidered here. Term ϕ_1' represents noncirculatory oscillating flow to be determined directly by the oscillating motion of the cascade. It is equivalent to the potential of a doublet sheet which replaces each oscillating airfoil. The term ϕ_2' represents the circulatory oscillating flow which corresponds to the wake-vortex sheet and bounded vortex or circulation of each airfoil. The strength of such vorticity can be determined from Kutta-Joukowski's condition in Equation [8].

According to the boundary condition Equation [6], ϕ_1' and ϕ_2' can be decomposed further and specified, respectively, as

$\phi_{1\alpha}'$ and $\phi_{2\alpha}'$ corresponding to $\alpha(t)$

$\phi_{1\dot{\alpha}}'$ and $\phi_{2\dot{\alpha}}'$ corresponding to $\dot{\alpha}(t)$

and

$\phi_{1\dot{h}}'$ and $\phi_{2\dot{h}}'$ corresponding to $\dot{h}(t)$

In other words

$$\phi_1' = \phi_{1\alpha}' + \phi_{1\dot{\alpha}}' + \phi_{1\dot{h}}' \quad [10a]$$

$$\phi_2' = \phi_{2\alpha}' + \phi_{2\dot{\alpha}}' + \phi_{2\dot{h}}' \quad [10b]$$

(*a*) *Noncirculating Oscillating Flow.* For the pitching (α, $\dot{\alpha}$) and flapping ($\dot{h}$) motion of the oscillating cascade, the normal velocity on both sides of the typical plate airfoil is the same in magnitude and direction with reference to the stationary coordinates. Consequently, each airfoil acts as a sheet of doublet with time-dependent strength. With such a simplified picture, it is still rather complicated to determine the mutual aerodynamic interference in the physical plane directly. However, in the circle plane, such oscillating flow corresponds to a source sheet in the upper half circumference and sink sheet on the lower half circumference of the unit circle during upward motion. The reverse is true during the downward motion. The strength of the foregoing source-sink system varies with time and position and is directly related to the normal velocity $\partial\phi'/\partial n$ on the circle which is connected with normal velocity on the airfoil in Equation [6] and the scale factor $|(dz)/(d\zeta)|$. Details are given in

Table 1 where the value of $|(dz)/(d\zeta)|$ is obtained from Equation [7], and θ_1 represents the argument of a point $(e^{i\theta_1})$ on the unit circle.

TABLE 1 DECOMPOSITION OF BOUNDARY CONDITIONS

$$\frac{\partial \phi_1'}{\partial y} \qquad \frac{\partial \phi_1'}{\partial n}(\zeta) = \mp \frac{\partial \phi_1'}{\partial y}\left|\frac{dz}{d\zeta}\right|$$

$-$ = upper surface
$+$ = lower surface

α:	$-U\alpha$	,	$U\alpha\mu^{-1}\sin\theta_1(\cos\theta_1+\coth\mu)^{-1}$
$\dot{\alpha}$:	$-(x-a)\dot{\alpha}$,		$(x-a)\,\dot{\alpha}\,\mu^{-1}\sin\theta_1(\cos\theta_1+\coth\mu)^{-1}$
$\dot{h}$:	$\dot{h}$	,	$-\dot{h}\mu^{-1}\sin\theta_1(\cos\theta_1+\coth\mu)^{-1}$

Since ϕ_1' is an odd function of θ_1, the potential of the system can be determined conveniently from Green's third identity (8) in the circle plane, i.e.

$$\phi_1'(r,\theta) = -\frac{1}{\pi}\oint \frac{\partial \phi_1'(\zeta)}{\partial n}\ln R\, ds \qquad [11]$$

where for the present case the contour of integration is the unit circle

$ds = d\theta_1$ and $R = [(r\cos\theta - \cos\theta_1)^2 + (r\sin\theta - \sin\theta_1)^2]^{1/2}$ [12]

is the distance between a point $\zeta = re^{i\theta}$ and the source element on the circle at $e^{i\theta_1}$.

$$\frac{\partial \phi'(\zeta)}{\partial n}$$

represents the source strength as given in Table 1 and $\ln R$ is the potential of unit source. In particular, the point of interest lies on the unit circle where $\zeta = e^{i\theta}$. After some calculation, $\phi_1'(\theta)$ the potential on the circle is expressed according to the component boundary conditions α, $\dot{\alpha}$, and $\dot{h}$, respectively, as follows

$$\phi_{1\alpha}'(\theta) = \frac{-U\alpha}{2\pi\mu}\int_0^{\pi}\frac{\sin\theta_1}{\cos\theta_1+\coth\mu}\ln\frac{1-\cos(\theta-\theta_1)}{1-\cos(\theta+\theta_1)}\,d\theta_1 = \frac{U\alpha}{\mu}\left[\theta - 2\tan^{-1}\left(\nu\tan\frac{\theta}{2}\right)\right] \qquad [13a]$$

$$\phi_{1\dot{\alpha}}'(\theta) = -\frac{\dot{\alpha}}{2\pi\mu}\int_0^{\pi}\left[\frac{1}{\mu}\ln(\cosh\mu+\sinh\mu\cos\theta_1) - a\right]\frac{\sin\theta_1}{\cos\theta_1+\coth\mu}\ln\frac{1-\cos(\theta-\theta_1)}{1-\cos(\theta+\theta_1)}\,d\theta_1$$

$$= \frac{\dot{\alpha}}{\mu^2}\left\{\left[\ln\frac{1+\cosh\mu}{2} - \mu a\right]\theta + 2\tan^{-1}\left(\nu\tan\frac{\theta}{2}\right)\left[\ln\frac{1+\cosh\mu}{2} + \mu a\right] - \ln(1+\tanh\mu\cos\theta)\left[\cos^{-1}\frac{\cos\theta+\tanh\mu}{1+\tanh\mu\cos\theta} - \theta\right] + \int_0^{\theta}\frac{\ln(1+\tanh\mu\cos\theta)}{\cosh\mu+\sinh\mu\cos\theta}\,d\theta - \int_0^{\theta}\ln(1+\tanh\mu\cos\theta)\,d\theta\right\} \qquad [13b]$$

and

$$\phi_{1\dot{h}}'(\theta) = -\frac{\dot{h}}{U\alpha}\phi_{1\alpha}'(\theta) \qquad [13c]$$

when $\theta = 0 \pm \pi$, it is easy to show that $\phi_{1\alpha}' = \phi_{1\dot{\alpha}}' = \phi_{1\dot{h}}' = 0$ as required in odd functions. The two integrals in Equation [13b] are not so easy to express in closed form. In the sense of von Karman and Sears (5), ϕ_1' may be called the potential due to apparent mass. Equation [13] is valid for any motion of arbitrary dependence on time, and may be transformed to the physical plane. However, this is rather unnecessary as shown later.

Now, the Kutta-Joukowski condition, Equation [8a], is applied to find ϕ_2', i.e.

$$\frac{\partial \phi_1'}{\partial \theta} + \frac{\partial \phi_2'}{\partial \theta} = 0 \qquad [14]$$

at $B(r = 1, \theta = 0)$. For later convenience, a quantity $Q(\mu, t)$ is introduced as follows

$$Q(\mu,t) = \frac{2}{Uc}\frac{\partial \phi_1'}{\partial \theta} = \frac{2}{Uc}\left(\frac{\partial \phi_{1\alpha}'}{\partial \theta} + \frac{\partial \phi_{1\dot{\alpha}}'}{\partial \theta} + \frac{\partial \phi_{1\dot{h}}'}{\partial \theta}\right) \qquad [15a]$$

at $\theta = 0$, $r = 1$. With Equation [13], it is easy to show that

$$Q(\mu,t) = \frac{1-\nu}{\mu}\left[\left(\alpha - \frac{\dot{h}}{U}\right) + \frac{c}{2}\frac{\dot{\alpha}}{U}\left(\coth\frac{\mu}{2}\ln\frac{1+\cosh\mu}{2} - a\right)\right] \qquad [15b]$$

where $c/2$ the half-chord length is hereafter introduced to replace unity for dimensional consideration.

(*b*) *Circulatory Oscillating Flow.* The circulatory oscillating flow is attributed to the circulation about each airfoil and the vorticities shed in its wake owing to small oscillations. In fact, the circulation about each airfoil changes with time and a vortex sheet is shed behind the trailing edge of each airfoil. Thus, in the whole cascade, wake-vortex sheets are infinite in number. At any time t, the length of the vortex sheet is equal to $U(t - t_0)$, where t_0 is the starting time of vortex shedding, because the vortex travels practically with the velocity U. Since no viscous dissipation is considered, the strength of each vortex element remains unaltered after its generation. The strength of the vortex sheet is therefore a function of

$$t - \frac{xc}{U2}$$

In case of quasi steady oscillation, the length of the vortex sheet, then, is semi-infinitely long, and the vortex intensity becomes periodic with time. Thus we assume

$$\gamma(x,t) = \gamma_0\exp\left[i\omega\left(t - \frac{xc}{2U}\right) + i\varphi_0\right] \qquad [16]$$

where $\omega/(2\pi)$ is the frequency of oscillation; γ_0, a positive constant, is the amplitude of vortex intensity to be determined; and φ_0 is the unknown phase lag between the vortex intensity $\gamma(x,t)$ and the harmonic oscillations of the airfoil such as

$$\alpha(t) = \alpha_0 e^{i\omega t} \qquad [17a]$$

and

$$\dot{h}(t) = \dot{h}_0 e^{i(\omega t + \nu_0)} \qquad [17b]$$

Here α_0 and $\dot{h}_0$ are given positive constants, being amplitudes of α and $\dot{h}$, respectively. ν_0 is a given phase lag between α and $\dot{h}$. On account of geometrical complexity and mutual interference in the physical plane, it is rather difficult to find $\gamma_0 e^{i\varphi_0}$ directly. Fortunately, in the circle plane, there is only one vortex sheet on

the real axis attached to the unit circle at $B(\theta = 0)$. For an element of the vortex sheet (say, $d\Gamma = \bar{\gamma}(\xi)d\xi$), the potential on the circle ($e^{i\theta}$), which satisfies the condition

$$\left(\frac{\partial\phi}{\partial r}\right)_{r=1} = 0$$

can be shown by image method

$$d\phi_2'(\xi,\eta) = \frac{\bar{\gamma}(\xi')d\xi'}{2\pi}\tan^{-1}\frac{\eta\left(\xi' - \frac{1}{\xi'}\right)}{1 + \xi^2 + \eta^2 - \left(\xi' + \frac{1}{\xi'}\right)\xi} \quad [18a]$$

Owing to the nonconstant scale factor $|(dz)/(d\zeta)|$, $\bar{\gamma}(\xi')$ is not periodic as expected in the physical plane, Equation [16], and is difficult to evaluate in the circle plane. Transformation of Equation [18a] to the physical plane is necessary and possible because of the conservation of circulation about the corresponding vortex elements in both planes, i.e.

$$d\Gamma = \bar{\gamma}(\xi')d\xi' = \gamma(x')dx' \quad [18b]$$

For any point on the airfoil of the cascade, the contribution to the potential due to vortex element $\gamma(x')dx'$ is obtained from Equation [18a]

$$d\phi_2'(x, 0^+) = \frac{\gamma(x')dx'}{2\pi}$$

$$\tan^{-1}\frac{[1 - \xi^2(x)]^{1/2}[(\nu^{x'}\operatorname{csch}\mu - \coth\mu)^2 - 1]^{1/2}}{1 - \xi(x)[\nu^{x'}\operatorname{csch}\mu - \coth\mu]} \quad [18c]$$

where

$$\eta^2(x) + \xi^2(x) = 1$$

has been applied, and

$$\xi(x) = \nu^x \operatorname{csch}\mu - \coth\mu$$

Thus summing up all the vortex wakes from $x = 1$ to $x = \infty$

$$\phi_2'(x, 0^+) = \frac{1}{2\pi}\int_1^\infty \tan^{-1}$$

$$\frac{[1 - \xi^2(x)]^{1/2}[(\nu^{x'}\operatorname{csch}\mu - \coth\mu)^2 - 1]^{1/2}}{1 - \xi(x)[\nu^{x'}\operatorname{csch}\mu - \coth\mu]}\gamma(x')dx' \quad [19a]$$

Now, we can express ϕ_2' on the circle, i.e.

$$\phi_2'(\theta) = \frac{1}{2\pi}\int_1^\infty \tan^{-1}\frac{\sin\theta[(\nu^{x'}\operatorname{csch}\mu - \coth\mu)^2 - 1]^{1/2}}{1 - \cos\theta\,[\nu^{x'}\operatorname{csch}\mu - \coth\mu]}\gamma(x')dx' \quad [19b]$$

Without resorting to integral equation, the present conformal-mapping technique gives an elegant construction of the integral in Equation [19]. The difficulty in obtaining this integral is the core of the problem and had puzzled some early investigators as learned from private communication.

Differentiating Equation [19b] with respect to θ and then substituting into Equation [14] when $\theta = 0$ and finally making use of Equations [15a] and [16], we have the identity

$$Q(\mu, l) = \lim_{\epsilon\to 0^+}\frac{1}{2\pi U}(\gamma_0 e^{i\varphi_0})e^{i\omega t}\int_1^\infty e^{-(ik+\epsilon)x}\left[\frac{1 - \nu^{x+1}}{1 - \nu^{x-1}}\right]^{1/2}dx$$

where $k = \dfrac{\omega c}{2U}$ and a damping factor $e^{-\epsilon x}$ with limit $\epsilon \to 0^+$ is introduced to insure convergence of the integral (9). Then

$$\gamma_0 e^{i\varphi_0} = \frac{2\pi U e^{-i\omega t}\,Q(\mu, l)}{\lim_{\epsilon\to 0^+}\int_1^\infty e^{-(ik+\epsilon)x}\left[\frac{1 - \nu^{x+1}}{1 - \nu^{x-1}}\right]^{1/2}dx} \quad [20]$$

With the relations of Equations [15a] and [17a] we can introduce $\bar{Q}(\mu,k)$ as

$$\bar{Q}(\mu, k) = e^{-i\omega t}\,Q(\mu, l) = \frac{1 - \nu}{\mu}\left[\left(\alpha_0 - \frac{h_0 e^{i\nu_0}}{U}\right) + ik\alpha_0\left(\frac{\coth\frac{\mu}{2}}{\mu}\ln\frac{1 + \cosh\mu}{2} - a\right)\right] \quad [21]$$

With the substitution of $y = \nu^{(x-1)}$, the denominator of Equation [20] can be shown to be

$$\frac{1}{\mu e^{ik}}\lim_{\epsilon\to 0^+}\int_0^1 y^{\frac{ik+\epsilon}{\mu}-1}(1 - y)^{-1/2}(1 - \nu^2 y)^{1/2}\,dy$$

which is related to hypergeometrical function (10).
Thus Equation [20] can be rewritten as

$$\gamma_0 e^{i\varphi_0} = \frac{2\pi U\bar{Q}(\mu,k)\mu e^{ik}\,\Gamma\left(\frac{1}{2} + \frac{ik}{\mu}\right)}{\Gamma\left(\frac{1}{2}\right)\Gamma\left(\frac{ik}{\mu}\right)F\left(-\frac{1}{2}, \frac{ik}{\mu}; \frac{1}{2} + \frac{ik}{\mu}; \nu^2\right)} \quad [22a]$$

where $\Gamma(\,)$ and $F(\,)$ represent gamma function and hypergeometric function, respectively. For a single airfoil, i.e., when $\mu \to 0$, it checks the well-known result

$$\gamma_0 e^{i\varphi_0} = -4U\bar{Q}(0, k)[H_1^{(2)}(k) + iH_0^{(2)}(k)]^{-1} \quad [22b]$$

where $H_n^{(2)}(\,)$ is the Hankel function of order n of the second kind.

The phase lag φ_0 is of basic importance in oscillating cascade and airfoil. So far, very little attention has been paid to its significance to approximate oscillating wing theory. Further development on φ_0 will be given in a separate note. Now with Equation [22a], we can rewrite [19]

$$\phi_2'(\theta, l) = \lim_{\epsilon\to 0^+}\frac{2\pi UQ(\mu, l)\mu e^{ik}\,\Gamma\left(\frac{ik}{\mu} + \frac{1}{2}\right)}{\Gamma\left(\frac{1}{2}\right)\Gamma\left(\frac{ik}{\mu}\right)F\left(-\frac{1}{2}, \frac{ik}{\mu}; \frac{1}{2} + \frac{ik}{\mu}; \nu^2\right)}$$

$$\int_1^\infty e^{-(ik+\epsilon)x}\tan^{-1}\frac{\sin\theta[(\nu^x\operatorname{csch}\mu - \coth\mu)^2 - 1]^{1/2}}{1 - \cos\theta\,(\nu^x\operatorname{csch}\mu - \coth\mu)}dx \quad [23]$$

Thus $\phi_2'(\theta,l)$ is completely determined.

Aerodynamic Forces and Moment

It is well known that the pressure increment is

$$\Delta p = p_\infty - p = \rho\left(\frac{\partial\phi}{\partial t} + U\frac{\partial\phi}{\partial x}\right) \quad [24]$$

With $\phi_1'(\theta)$ in Equation [13] and $\phi_2'(\theta)$ in Equation [23], we can evaluate the normal force Y' and the moment M' about elastic axis $x = a$ which are defined as

$$Y' = \int_{-1}[(\Delta p)_+ - (\Delta p)_-]\,dx \quad [25a]$$

$$M' = \int_{-1}^{1} [-(\Delta p)_+ + (\Delta p)_-](x - a)\, dx \quad [25b]$$

After some long computations, the final results can be expressed as follows

$$(a) \quad \underline{Y' = Y_1' + Y_2'} \quad [26a]$$

$$Y_1' = \frac{c}{2}\rho U^2 \left\{ [ik\nu_1 + k^2(\nu_1 a + \nu_1\nu_2 - F_1)]\alpha - \frac{ik\nu_1 h}{U} \right\} \quad [26b]$$

$$Y_2' = \frac{c}{2}\rho U^2 \left\{ [1 + ik(\nu_6 - a)]\nu_2\alpha - \frac{\nu_2 h}{U} \right\} C(\mu, k) \quad [26c]$$

$$(b) \quad \underline{M' = M_1' + M_2'} \quad [27a]$$

$$M_1' = \frac{c^2}{4}\rho U^2 \left\{ [2(F_1 - \nu_1\nu_2)ik + \nu_1 + k^2(F_2 + \nu_2 F_1 - \nu_1\nu_2^2 + \nu_1 a^2)]\alpha - [(\nu_1 a + F_1 - \nu_1\nu_2)ik + \nu_1] \frac{h}{U} \right\} \quad [27b]$$

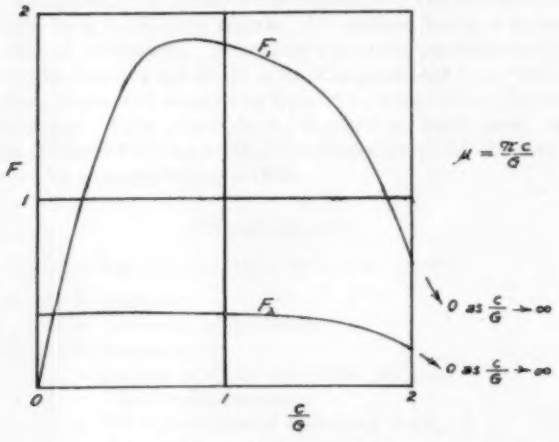

FIG. 2 THE FUNCTIONS F_1 AND F_2

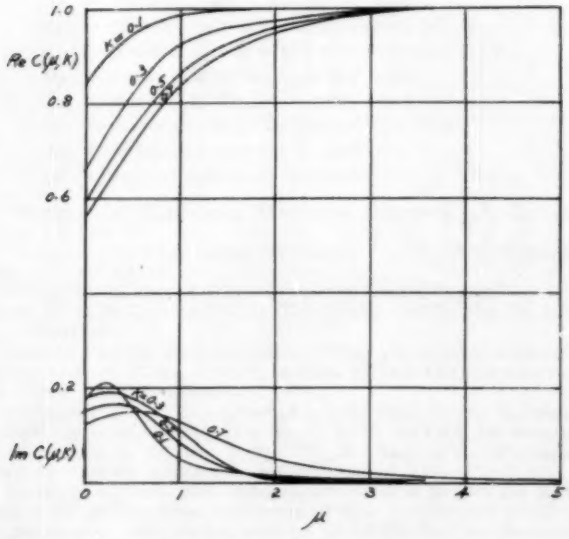

FIG. 3 THE FUNCTIONS $C(\mu, k)$

$$M_2' = \frac{c^2}{4}\rho U^2 \left\{ [1 + (\nu_6 - a)ik][(\nu_5 + a\nu_3)C(\mu,k) - \nu_1]\alpha - [(\nu_5 + a\nu_3)C(\mu,k) - \nu_1] \frac{h}{U} \right\} \quad [27c]$$

where Y_1', M_1' and Y_2', M_2' are attributed to ϕ_1' and ϕ_2', respectively

$$F_1 = F_1(\mu) = \frac{1}{\mu^3}\int_0^\pi \ln^2(1 + \tanh\mu\cos\theta)\,[\operatorname{sech}\mu\,(1 + \tanh\mu\cos\theta)^{-1} - 1]\, d\theta \quad [28a]^6$$

$$F_2 = F_2(\mu) = \frac{1}{\mu^4}\ln\frac{1 + \cosh\mu}{2}\int_0^\pi \ln^2(1 + \tanh\mu\cos\theta)\,[\operatorname{sech}\mu\,(1 + \tanh\mu\cos\theta)^{-1} + 1]d\theta - \frac{1}{3\mu^4}\int_0^\pi \ln^3(1 + \tanh\mu\cos\theta)[1 - \operatorname{sech}\mu\,(1 + \tanh\mu\cos\theta)^{-1}]\, d\theta \quad [28b]$$

$$\nu_1 = \nu_1(\mu) = 4\pi\,\mu^{-2}\ln\left[\frac{1}{2}(1 + \cosh\mu)\right] \quad [29a]$$

$$\nu_2 = \nu_2(\mu) = \mu^{-1}\ln\cosh\mu \quad [29b]$$

$$\nu_3 = \nu_3(\mu) = 2\pi\,\mu^{-1}(1 - \nu) \quad [29c]$$

$$\nu_4 = \nu_4(\mu) = \frac{1}{2}(1 + \nu) \quad [29d]$$

$$\nu_5 = \nu_5(\mu) = \nu_1\nu_4 \quad [29e]$$

$$\nu_6 = \nu_1\nu_4/\nu_3 \quad [29f]$$

and $C(\mu, k) = \lim_{\epsilon \to 0^+}$

$$\frac{\int_1^\infty \exp[-(ik + \epsilon)x](1 - \nu^x)[1 - \nu^{x+1}]^{-1/2}[1 - \nu^{x-1}]^{-1/2}\, dx}{\int_1^\infty \exp[-(ik + \epsilon)x](1 - \nu^{x+1})^{-1/2}(1 - \nu^{x-1})^{-1/2}\, dx}$$

$$= 1 - \nu(1 - \nu)\frac{\left(\frac{ik}{\mu}\right)F\left(\frac{1}{2}, 1 + \frac{ik}{\mu}; \frac{3}{2} + \frac{ik}{\mu}; \nu^2\right)}{\left(\frac{ik}{\mu} + \frac{1}{2}\right)F\left(-\frac{1}{2}, \frac{ik}{\mu}; \frac{1}{2} + \frac{ik}{\mu}; \nu^2\right)} \quad [30]$$

Here $F_1(\mu)$ and $F_2(\mu)$ are shown in Fig. 2 as functions of c/G and $C(\mu,k)$ is given in Fig. 3 versus μ at various values of k. $C(\mu,k)$ is of basic importance to our problem. In the limit of infinite gap ($\mu \to 0$), the foregoing results check with those of the single oscillating airfoil theory. In particular, Equation [30] becomes

$$\lim_{\mu \to 0} C(\mu, k) = C(k) = \frac{H_1^{(2)}(k)}{H_1^{(2)}(k) + iH_0^{(2)}(k)}$$

which is the well-known Theodorsen function.

BIBLIOGRAPHY

1 "Aerodynamic Characteristics of an Oscillating Cascade," by Chieh-Chien Chang and Wen-Hwa Chu, paper presented to the 8th International Congress on Theoretical and Applied Mechanics, Istanbul, Turkey, August 20–28, 1952; summary soon to be published in the Proceedings. Paper was distributed by the Office of Scientific Research, Air Research and Development Command, United States Air Force, September, 1952.

2 "Aerodynamic Interference Between Moving Blade Rows," by N. H. Kemp and W. R. Sears, *Journal of the Aeronautical Sciences*, vol. 20, 1953, pp. 585–604.

[6] The identity $F_1 - \nu_1\nu_2 = 0$ has been pointed out by Dr. Nelson H. Kemp in his discussion at the Troy meeting. A direct analytic proof will be given in the authors' closure.

3 "On Asymmetric Flow in an Axial-Flow Compressor Stage," by W. R. Sears, JOURNAL OF APPLIED MECHANICS, Trans. ASME, vol. 75, 1953, pp. 57–62.

4 "General Theory of Aerodynamic Instability and Mechanism of Flutter," by Th. Theodorsen, NACA TR 496, 1934.

5 "Airfoil Theory for Non-Uniform Motion," by Th. von Karman and W. R. Sears, *Journal of the Aeronautical Sciences*, vol. 5, 1938, pp. 379–390.

6 "An Investigation of the Flexure-Torsion Flutter Characteristics of Airfoils in Cascade," by G. M. Lilley, The College of Aeronautics, Cranfield, England, Report No. 60, May, 1952.

7 "General Aerodynamic Theory-Perfect Fluids," by Th. von Karman and J. M. Burgers, vol. 2, 1935, p. 95, of "Aerodynamic Theory," edited by W. F. Durand, Julius Springer, Berlin, Germany.

8 "Partial Differential Equations in Physics," by A. Sommerfield, Academic Press, Inc., New York, N. Y., 1949, p. 48.

9 "On Theodorsen Function in Incompressible Flow and C-Function in Supersonic Flow," by Chieh-Chien Chang, *Journal of the Aeronautical Sciences*, vol. 19, 1932, pp. 717–718.

10 "A Course of Modern Analysis," by E. T. Whittaker and G. N. Watson, The Macmillan Company, New York, N. Y., 1948, p. 293.

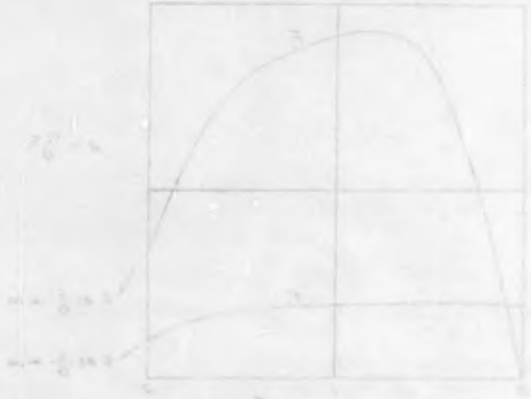

A Study of the Stability of Plane Fluid Sheets

By W. W. HAGERTY[1] AND J. F. SHEA,[2] ANN ARBOR, MICH.

In studying the performance of a system for producing sprays of any kind it would be desirable to arrive at an expression which would relate the drop-size distribution and the spatial distribution of the drops in terms of the variables of the system including pressure, density, surface tension, and geometry. In an earlier study of the performance of hollow-cone swirl-type nozzles,[3] photographs were taken of the region where the fluid sheet breaks up into drops. These photographs showed that before the break-up occurred, waves or ripples appeared on the surface of the liquid sheet. It was believed that the waves were responsible for the break-up and that frequency and wave length of the ripples might be related to the size range of drops produced. Difficulties were encountered in an analytical treatment of the stability of the surface produced by a swirl-type nozzle, the surface being a hyperboloid of revolution. Therefore a system was selected for study in which a flat sheet of fluid is produced by a slender orifice, and which may be subjected to waves of any desired frequency. This plane sheet, exposed on both sides, appears to have the essential characteristics of the sheet produced by a conventional nozzle.

Nomenclature

The following nomenclature is used in the paper:

A, A_1, A_2 = constants
a = half-width of fluid sheet
B, B_1, B_2 = constants
f = frequency, cycles per second (cps)
f_c = lowest stable frequency
H = initial amplitude of disturbing wave
h_1 = disturbance on surface $y = a$
h_2 = disturbance on surface $y = -a$
n = wave number of disturbing wave
p_{A1} = pressure in surrounding medium, $y > a$
p_{A2} = pressure in surrounding medium, $y < -a$
p_W = pressure in the fluid at any point
q = velocity of the fluid at any point
R_1 = radius of curvature on surface $y = a$
R_2 = radius of curvature on surface $y = -a$
T = surface tension of the fluid
t = time
u = velocity in x-direction
V = mean velocity of fluid sheet
V' = mean velocity of surrounding medium
v = velocity in y-direction
$\mathbf{W}$ = Weber's number, dimensionless parameter
x = direction along sheet in direction of motion
y = distance perpendicular to sheet measured from center line
β_D = growth rate of unstable dilational wave
β_S = growth rate of unstable sinuous wave
γ = density ratio
Δ_D = logarithmic decrement for dilational wave
Δ_S = logarithmic decrement for sinuous wave
λ = wave length of disturbing wave
ρ_A = density of surrounding medium
ρ_W = density of fluid medium
Φ_{A1} = velocity potential in surrounding medium, $y > a$
Φ_{A2} = velocity potential in surrounding medium, $y < -a$
Φ_W = velocity potential in fluid region
ϕ = phase angle between disturbances on upper and lower surfaces
Ω = frequency ratio, f/f_c
ω = frequency of disturbing wave
ω_0 = real circular frequency

The Theoretical Problem

The problem of the growth of waves upon a flat sheet of fluid has been treated by Rayleigh.[4] The present analysis develops expressions for the growth rate of the waves in terms of surface tension, frequency, sheet thickness, and velocity, based on Rayleigh's analysis of the one-sided sheet. The method of introducing the boundary conditions in the present treatment also differs somewhat from the original.

The idealized system to be treated here is shown in Fig. 1. The width of the sheet is $2a$, the density of the fluid, ρ_W. It is moving vertically with velocity V through another fluid of density ρ_A and velocity V'. The following assumptions will be made:

1 The velocity of the sheet is great enough so that the effect of gravity will be ignored.

2 Both fluids are inviscid.

3 A surface tension T exists between the two fluids.

4 The surfaces at $y = \pm a$ are disturbed by small waves of amplitude H and frequency ω but of arbitrary phase with respect to one another.

5 Steady-state conditions have been reached.

Potential Flow Equations

By virtue of assumption (2), Laplace's equation must be satisfied in all three fluid regions. In order to treat both symmetrical

---

[1] Professor of Engineering Mechanics, University of Michigan. Mem. ASME.

[2] Instructor in Engineering Mechanics, University of Michigan. Assoc. Mem. ASME.

[3] "The Mechanism of Disintegration of Liquid Sheets," by J. L. York, H. E. Stubbs, and M. R. Tek, Trans. ASME, vol. 75, 1953, pp. 1279–1286.

Presented at the National Conference of the Applied Mechanics Division, Troy, N. Y., June 16–18, 1955, of The American Society of Mechanical Engineers.

Discussion of this paper should be addressed to the Secretary, ASME, 29 West 39th St., New York, N. Y., and will be accepted until January 10, 1956, for publication at a later date. Discussion received after the closing date will be returned.

Note: Statements and opinions advanced in papers are to be understood as individual expressions of their authors and not those of the Society. Manuscript received by ASME Applied Mechanics Division, August 23, 1954. Paper No. 55—APM-21.

[4] "Theory of Sound," by Lord Rayleigh (J. W. Strutt), The Macmillan Company, Ltd., London, England, second edition, 1894; two volumes reprinted by Dover Publications, New York, N. Y., vol. 2, 1954, pp. 376–381.

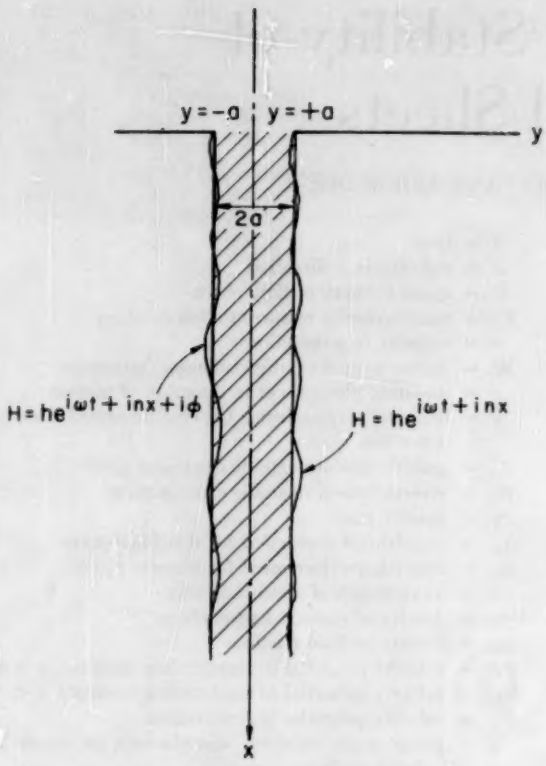

FIG. 1 IDEALIZED FLUID-SHEET SYSTEM

and antisymmetrical waves at the same time, the equations of the disturbed surface are assumed to be

$$h_1 = He^{i\omega t + inx}, \quad y = a \qquad [1a]$$

and

$$h_2 = He^{i\omega t + inx + i\phi}, \quad y = -a \qquad [1b]$$

The boundary conditions are as follows:

1 The velocity of the fluid normal to the boundary vanishes, i.e.

$$\frac{D}{Dt}[h_1 - y] = 0, \quad y = a \qquad [2a]$$

and

$$\frac{D}{Dt}[h_2 - y] = 0, \quad y = -a \qquad [2b]$$

2 The velocities approach that of the undisturbed streams at points remote from the common boundary.

The velocity potentials which satisfy these conditions are as follows:

$a \leq y \leq -a$

$$\Phi_W = (A \cosh ny + B \sinh ny)e^{i\omega t + inx} + Vx \qquad [3a]$$

where

$$A = \frac{i\left(\frac{\omega}{n} + V\right)(1 - e^{i\phi})}{2 \sinh na} H \qquad [3b]$$

and

$$B = \frac{i\left(\frac{\omega}{n} + V\right)(1 + e^{i\phi})}{2 \cosh na} H \qquad [3c]$$

$y > a$

$$\Phi_{A1} = B_1 e^{-ny + inx + i\omega t} + V'x \qquad [4a]$$

where

$$B_1 = iH\left(V' + \frac{\omega}{n}\right)e^{na} \qquad [4b]$$

$y < -a$

$$\Phi_{A2} = A_2 e^{-ny + inx + i\omega t} + V'x \qquad [5a]$$

where

$$A_2 = iH\left(V' + \frac{\omega}{n}\right)e^{na + i\phi} \qquad [5b]$$

PRESSURE AND SURFACE-TENSION FORCES

The stability of the sheet depends on the relationship between the surface tension and pressure forces acting at the surface of the sheet. The excess pressure on either side of the interface can be found from Bernoulli's equation, written in the form

$$\frac{V^2}{2} = \frac{\partial \Phi}{\partial t} + \frac{q^2}{2} + \frac{\Delta p}{\rho} \qquad [6]$$

Solving for the excess pressure in each region by substituting Equations [3], [4], and [5] into [6] yields

$$\Delta p_W = in\rho_W \left\{\frac{\omega}{n} + V\right\} \{A \cosh ny + B \sinh ny\} e^{i\omega t + inx} \qquad [7]$$

$$\Delta p_{A1} = in\rho_A \left\{\frac{\omega}{n} + V'\right\} B_1 e^{-ny + i\omega t + inx} \qquad [8]$$

and

$$\Delta p_{A2} = -in\rho_A \left\{\frac{\omega}{n} + V'\right\} A_2 e^{-ny + i\omega t + inx} \qquad [9]$$

Consider an element cut from the sheet as shown in Fig. 2. The equilibrium of the upper surface requires

$$\Delta p_W - \Delta p_{A1} = -\frac{T}{R_1} = -T\frac{\partial^2 h_1}{\partial x^2}, \quad y = a \qquad [10]$$

The equilibrium of the lower surface requires

$$\Delta p_W - \Delta p_{A2} = -\frac{T}{R_2} = T\frac{\partial^2 h_2}{\partial x_2}, \quad y = -a \qquad [11]$$

Substituting Equations [1a], [3], [4], [7], [8] into [10] yields

$$\frac{n\rho_W}{2}\left(\frac{\omega}{n} + V\right)^2 \{(1 - e^{i\phi}) \coth na + (1 + e^{i\phi}) \tanh na\} + n\rho_A\left(\frac{\omega}{n} + V'\right)^2 = n^2 T \qquad [12]$$

Similarly, substituting Equations [1b], [3], [5], [7], [9] into [11] yields

$$\frac{n\rho_W}{2}\left(\frac{\omega}{n} + V\right)^2 \{(1 - e^{i\phi}) \coth na - (1 + e^{i\phi}) \tanh na\} - n\rho_A\left(\frac{\omega}{n} + V'\right)^2 e^{i\phi} = -n^2 T e^{i\phi} \qquad [13]$$

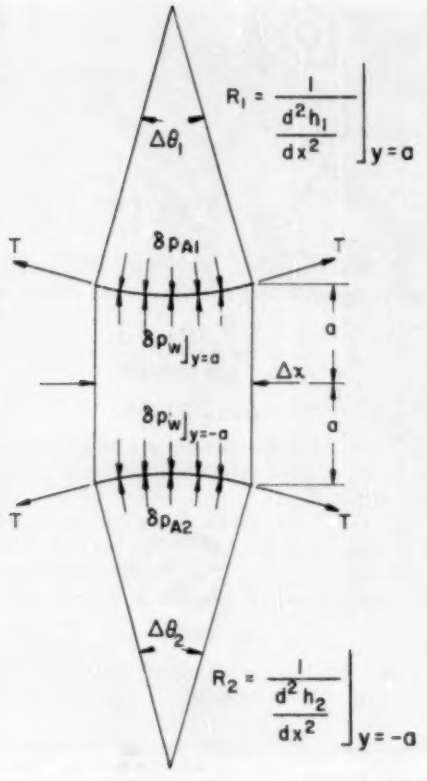

FIG. 2 ELEMENT OF DISTURBED FLUID SHEET

Summing Equations [12] and [13] yields

$$n\rho_W\left(\frac{\omega}{n}+V\right)^2\coth na(1-e^{i\phi}) + n\rho_A\left(\frac{\omega}{n}+V'\right)^2(1-e^{i\phi}) = n^2T(1-e^{i\phi}) \quad [14]$$

and subtracting Equations [13] from [12] yields

$$n\rho_W\left(\frac{\omega}{n}+V\right)^2\tanh na(1+e^{i\phi}) + n\rho_A\left(\frac{\omega}{n}+V'\right)^2(1+e^{i\phi}) = n^2T(1+e^{i\phi}) \quad [15]$$

From Equation [14], either

$$(1-e^{i\phi}) = 0 \quad [16]$$

or

$$n\rho_W\left(\frac{\omega}{n}+V\right)^2\coth na + n\rho_A\left(\frac{\omega}{n}+V'\right)^2 = n^2T \quad [17]$$

Similarly, from Equation [15], either

$$(1+e^{i\phi}) = 0 \quad [18]$$

or

$$n\rho_W\left(\frac{\omega}{n}+V\right)^2\tanh na + n\rho_A\left(\frac{\omega}{n}+V'\right)^2 = n^2T \quad [19]$$

Since Equations [17] and [19] cannot be satisfied simultaneously, either Equation [16] or [18] must be satisfied. Equation [16] implies $\phi = 0$; Equation [18] implies $\phi = \pi$. The case of $\phi = 0$ corresponds to a symmetrical or sinuous wave as shown by Fig. 3(*a*), and $\phi = \pi$ corresponds to an unsymmetrical or dilational wave as in Fig. 3(*b*). The relationship between frequency ω and wave number n for the sinuous wave is given by Equation [19], for the dilational wave by Equation [17].

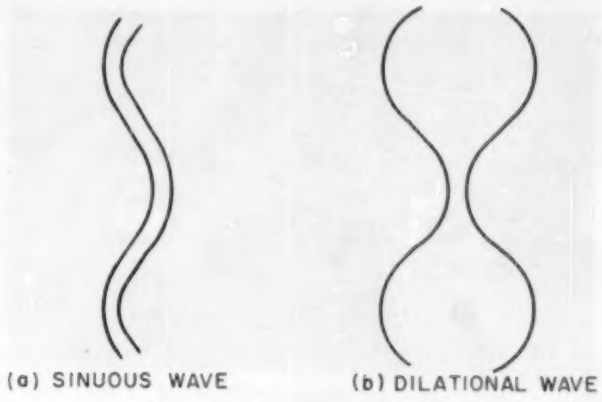

FIG. 3 BASIC WAVE FORMS

The stability is determined by the nature of ω. Since a time dependence of the form $e^{i\omega t}$ has been assumed, if ω becomes complex, say, $w_0 \pm i\beta$, the exponential term becomes $e^{i\omega_0 t \pm \beta t}$. One component corresponds to a wave which grows exponentially with time. Therefore the unstable waves are those for which ω becomes complex.

ANALYSIS OF THE SINUOUS WAVE

For the sinuous wave ($\phi = 0$), with $V' = 0$, the frequency Equation [19] reduces to

$$\omega^2(\tanh na + \gamma) + 2\omega nV\tanh na + n^2V^2\tanh na - \frac{n^2T}{\rho_W} = 0 \quad [20]$$

Solving Equation [20] for ω yields

$$\omega = -\frac{nV\tanh na}{(\tanh na+\gamma)} \pm \frac{\sqrt{\frac{n^2T}{\rho_W}(\tanh na+\gamma) - n^2V^2\gamma\tanh na}}{(\tanh na+\gamma)} \quad [21]$$

For the particular case of interest, that of a fluid being sprayed into a gas, the ratio γ is quite small and can be neglected in comparison with tanh na over most of the unstable region.

In this case Equation [21] reduces to

$$\omega = -nV \pm \sqrt{\frac{\frac{n^2T}{\rho_W} - n^2V^2\gamma}{\tanh na}} \quad [22]$$

The unstable region consists of those wave numbers (n) which render the term under the radical negative. The sheet is unstable if

$$n < \frac{\rho_A V^2}{T} \quad [23]$$

From Equation [22] the real circular frequency is $\omega_o = nV$. The upper bound of the unstable frequencies is therefore

$$f_c = \frac{\omega_o}{2\pi} = \frac{\rho_A V^2}{2\pi T} \quad [24]$$

For frequencies below f_c the growth rate (β_S) is

$$\beta_S = \sqrt{\frac{n^2V^2\gamma - \frac{n^3T}{\rho_W}}{\tanh na}} \quad [25]$$

Analysis of the Dilational Wave

For the dilational wave ($\phi = \pi$), with $V' = 0$, the frequency Equation [17] reduces to

$$\omega^2(\coth na + \gamma) + 2nV\omega \coth na + n^2V^2 \coth na - \frac{n^3T}{\rho_W} = 0 \quad [26]$$

Assuming $\gamma \ll \coth na$, Equation [26] can be solved for ω yielding

$$\omega = -nV \pm \sqrt{\frac{\frac{n^3T}{\rho_W} - n^2V^2\gamma}{\coth na}} \quad [27]$$

The unstable region consists of those wave numbers (n) which render the second term imaginary. The relationship is the same as in Equation [23].

As in the case of the sinuous wave, the upper bound of the unstable frequencies is given by Equation [24].

For frequencies below f_c, the growth rate (β_D) is

$$\beta_D = \sqrt{\frac{n^2V^2\gamma - \frac{n^3T}{\rho_W}}{\coth na}} \quad [28]$$

It is interesting to note that the dilational wave is that wave experienced in a uniform channel of depth a. In this case the bottom of the channel corresponds to the axis of symmetry of the fluid region.

Representation of Equations

The dominant wave in the unstable region has the form

$$y = He^{\beta t + i\omega t + inx} \quad [29]$$

During one complete cycle, t increases by $2\pi/\omega$, and x increases by $2\pi/n$. The ratio of the amplitude at the end of the cycle y_2, to the amplitude at the beginning of the cycle y_1, is

$$\frac{y_2}{y_1} = e^{\frac{2\pi}{\omega}\beta} = e^{\beta/f} \quad [30]$$

The logarithmic decrement Δ is defined as the natural logarithm of the ratio of the amplitudes in successive cycles. Therefore

$$\Delta = \ln \frac{y_2}{y_1} = \beta/f \quad [31]$$

For the sinuous wave, using Equations [24] and [25] and defining the dimensionless parameters

$$\Omega = f/f_c \quad [32]$$

and

$$\mathbf{W} = \frac{V^2\rho_A a}{T} \quad [33]$$

Equation [31] reduces to

$$\Delta_S = 2\pi \sqrt{\frac{\gamma(1-\Omega)}{\tanh \Omega\mathbf{W}}} \quad [34]$$

$\mathbf{W}$ is Weber's number.

Similarly, using Equations [24], [28], [32], and [33], the logarithmic decrement for the dilational wave reduces to

$$\Delta_D = 2\pi \sqrt{\frac{\gamma(1-\Omega)}{\coth \Omega\mathbf{W}}} \quad [35]$$

Theoretical Curves

The growth rate β has been plotted as a function of frequency f for several different sheet velocities for both sinuous and dilational waves in Fig. 4.

Fig. 5 is a plot of Δ_S for various Weber's number in the range of interest. The Δ_D are so small that they have not been plotted. Frequency ratios below 0.1 have been omitted because such waves were not found on the sheet during experiments.

Experimental Study

The apparatus used in the experimental study of the problem is shown in Fig. 6. Means are provided to pass a controlled quan-

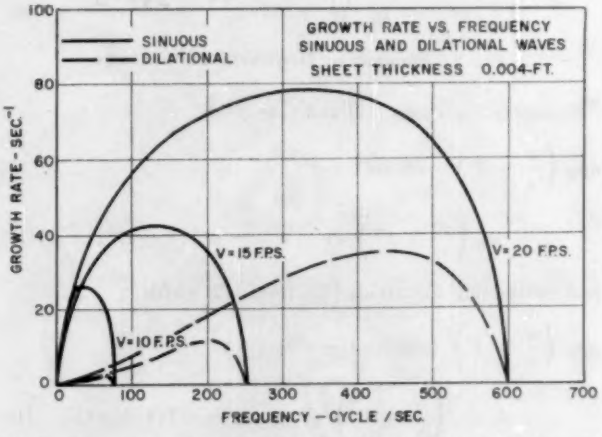

Fig. 4 Growth Rate Versus Frequency Sinuous and Dilational Waves; Sheet Thickness 0.004 Ft

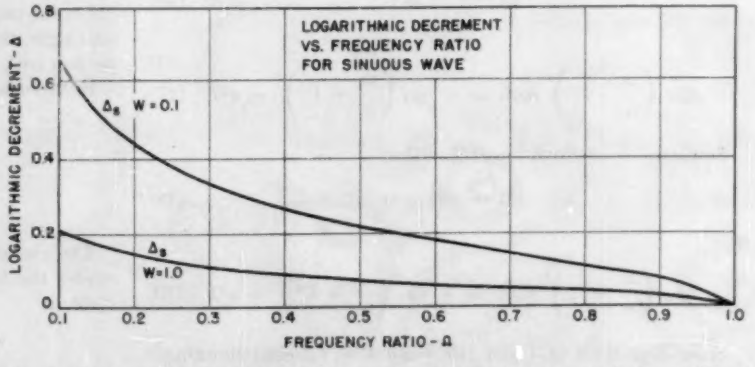

Fig. 5 Logarithmic Decrement Versus Frequency Ratio for Sinuous Wave

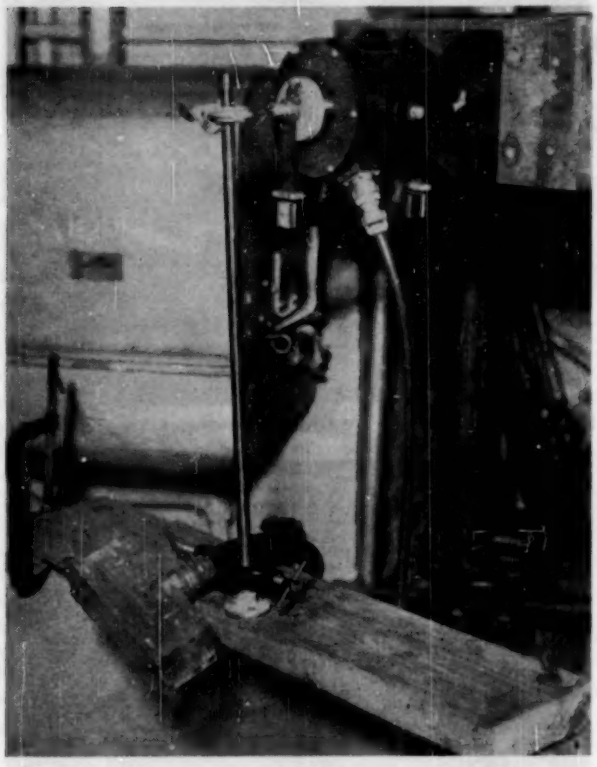

FIG. 6 EXPERIMENTAL SETUP FOR FLAT-SHEET STUDY

FIG. 7 NOZZLE AND SHEET

tity of water or other fluid through the nozzle of Fig. 7, producing the type of sheet shown.

The plane sheet produced is initially 6 in. wide and about $^1/_{16}$ in. thick. The velocity can be varied continuously up to 25 fps. The width of the sheet decreases as a result of surface tension as shown in Fig. 7. However, sufficient area remains between the edges of the sheet to permit study of the behavior of the surface.

Figs. 8, 9, and 10 illustrate the growth of waves on a sheet moving at 15 fps. Figs. 8 and 9 show waves of 75 cps and 200 cps, respectively. The data from these figures and others not shown are plotted in Fig. 12 and compare reasonably well with the theory.

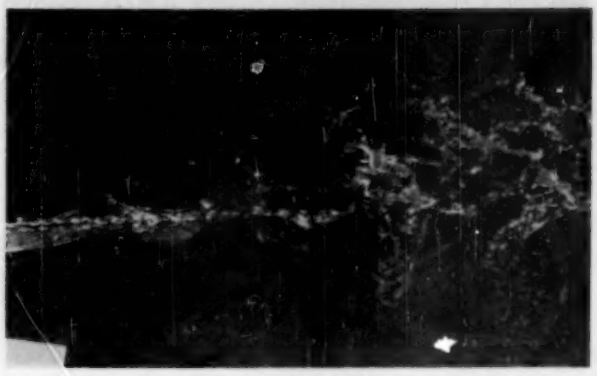

FIG. 8 75-CPS WAVE; SHEET VELOCITY 15 FPS

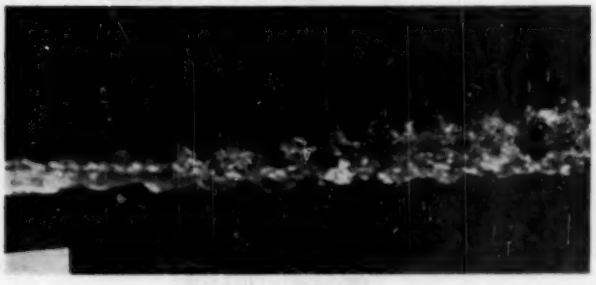

FIG. 9 200-CPS WAVE; SHEET VELOCITY 15 FPS

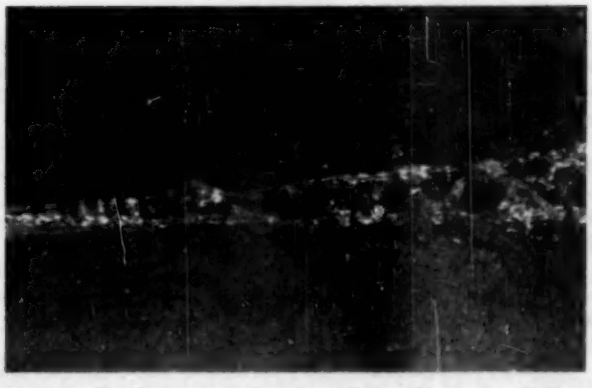

FIG. 10 NO FREQUENCY IMPOSED; SHEET VELOCITY 15 FPS

Fig. 10 shows the growth of waves on the sheet when no frequency is introduced at the nozzle. The view shows that a high-frequency wave is superimposed on the sheet. The frequency of this wave is very nearly the frequency of the dilational wave of maximum growth rate, about 120 cps for the 15-fps sheet.

When low-frequency waves (20 to 30 cps) were introduced onto the sheet, higher frequency waves were superimposed on the base wave. The growth rates of the base wave were quite small and the secondary waves again were close to the frequency of maximum growth rate.

The cause of these waves is not completely clear. There may be a mechanical element in the system which has a resonant frequency near 120 cps. It is also possible that the base wave is not purely sinusoidal, but contains a profusion of higher harmonics. The component of the wave which grows is then the one with the highest growth rate.

FIG. 11 20-CPS WAVE; SHEET VELOCITY 10 FPS

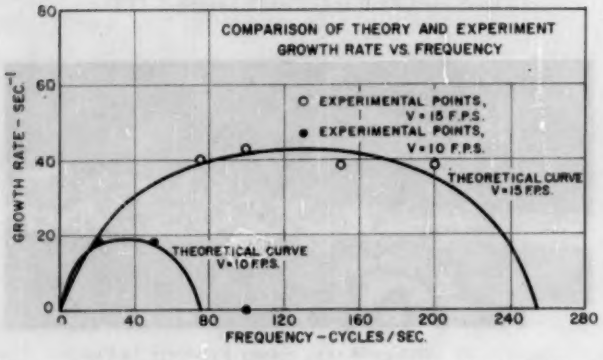

FIG. 12 COMPARISON OF THEORY AND EXPERIMENT GROWTH RATE VERSUS FREQUENCY

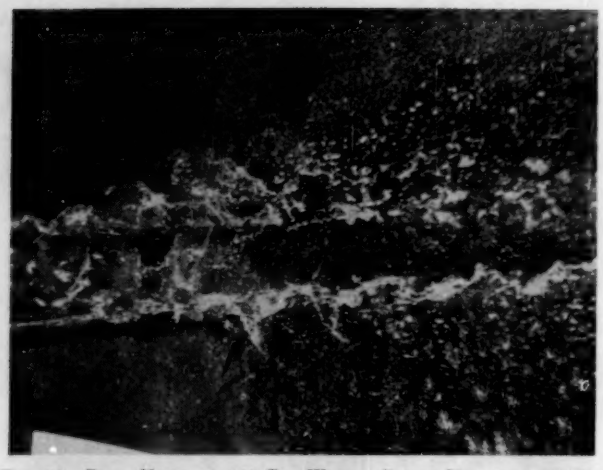

FIG. 13 PLAN VIEW OF 100-CPS WAVE; SHEET VELOCITY 15 FPS

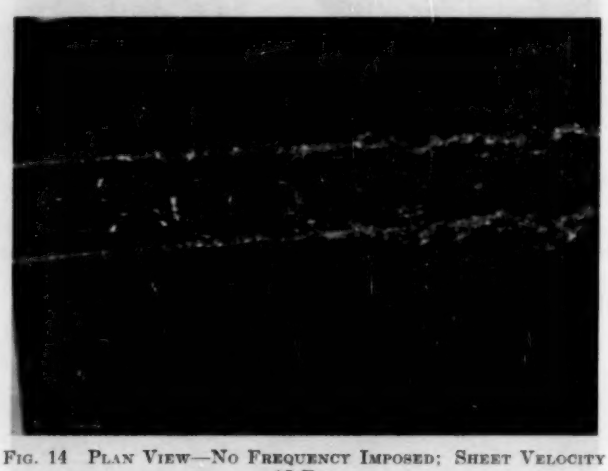

FIG. 14 PLAN VIEW—NO FREQUENCY IMPOSED; SHEET VELOCITY 15 FPS

The latter explanation is the more likely because the secondary waves are not present when the base frequency is high, even though the growth rates are quite small, as is the case for the 200 cps wave, Fig. 9.

Fig. 11 shows a 20-cps wave on a sheet with 10 fps velocity. Theory predicts the cutoff frequency is about 77 cps. The 20-cps wave has a growth rate which agrees quite well with the theory, Fig. 12. The maximum growth rate is quite close to that of the 20-cps wave and no large secondary waves are noticeable.

Figs. 13 and 14 show the surface of the sheet for a wave of 100 cps and the natural sheet at a sheet velocity of 15 fps. As can be seen, the sheet begins to break up from the action of the waves, and the distribution of the spray is affected by the waves.

Although the figures show only the sinuous wave, this does not imply the absence of a dilational wave on the sheet. From Equations [25] and [28] it can be seen that the growth rate for the sinuous waves (β_S) is always larger than the growth rate for the dilational wave (β_D)

$$\beta_S = \beta_D \coth na \quad [36]$$

Components of both types of waves are imposed on the sheet at the nozzle. The sinuous wave grows faster, however, and masks the dilational wave. There is experimental evidence, based on the mechanism by which the sheet breaks up, to show that the dilational wave also grows.

CONCLUSIONS

As a result of the theoretical and experimental work described in this paper, the following conclusions may be drawn:

1 Only two types of waves are possible at any given frequency. Either the two surfaces of the sheet oscillate in phase to produce sinuous waves or they oscillate out of phase as in the dilational wave. The latter wave corresponds to the wave existing in a channel whose depth is half the thickness of the fluid sheet.

2 For a given fluid sheet, both types of waves are unstable over the same range of frequencies, the lowest stable frequency being

$$f_c = \frac{\rho_A V^2}{2\pi T} \quad [24]$$

This frequency is thus independent of the thickness and also of the density of the liquid in the sheet.

3 The growth rate β_S for the sinuous wave is always greater than the growth rate β_D for the dilational wave of the same frequency. This is expressed by

$$\beta_S/\beta_D = \coth na \quad [36]$$

If a disturbance is applied to the sheet at a given frequency, in general, it will contain some components of each type of wave. Since the sinuous wave grows faster all disturbances measured experimentally were of sinuous waves.

4 Frequency, velocity, and wave length are related in the same way for both types of waves. This relation is useful in determining the velocity of the sheet and is expressed as

$$f = V/\lambda \quad [37]$$

ACKNOWLEDGMENT

The authors wish to acknowledge the financial support and encouragement for this work which was done under contract with the Power Plant Lab. of the Wright Air Development Center and which has agreed to the publication of this paper.

Integral Methods in Natural-Convection Flow

By SALOMON LEVY,[1] SCHENECTADY, N. Y.

This paper presents an evaluation of the range of application, accuracy, and usefulness of integral methods in natural-convection flow. The study reveals (*a*) that integral methods may be utilized to obtain approximate answers to free-convection problems whenever exact analytical solutions become too involved. Specific-flow examples considered here (natural convection from inclined plate, horizontal cylinder, arbitrary body, or within enclosed channels) confirm their adaptability to complicated configurations. (*b*) Over-all accuracy of the solutions is good. For inclined plates the derived equations reduce at high Grashof numbers to the correlation proposed and verified by Rich (1)[2] while in the case of horizontal cylinders the results compare satisfactorily with the theoretical values of Hermann (2) and the accepted experimental relations (12). (*c*) The integral method of solution may be extended to apply to low Prandtl number fluids, laminar or turbulent flow, variable wall temperature, and convection within confined spaces.

Introduction

EXACT theoretical investigations of natural-convection flow have been presented for vertical plates (3), cylinders (2), and channels (4). Unfortunately, natural-convection problems in turbine blades or atomic reactors usually involve more complex configurations, and a calculation method capable of supplementing exact solutions must be available at all times. Von Kármán's integral method of solution which has played such a role in the boundary-layer field is the logical choice in natural-convection theory.

Von Kármán's integral equations were used previously by Squire (5) to determine the heat transfer by free convection from a vertical plate. More recently they have been utilized to deal with low Prandtl number fluids (6), enclosed tubes (7), and constant heat generation (8). The purpose of this report is to ascertain their application to complex-flow systems and to evaluate their accuracy by means of specific-flow examples.

Basic Equations

First, consider a body of arbitrary shape and large curvature, maintained at temperature T_w, and heated or cooled by free convection from a surrounding medium at constant temperature T_1. For two-dimensional laminar flow the momentum, energy, and continuity equations are

$$u\frac{\partial u}{\partial x} + v\frac{\partial u}{\partial y} = \beta g(T - T_1)\sin\phi + \nu\nabla^2 u - \frac{1}{\rho}\frac{\partial p}{\partial x} \quad [1]$$

$$u\frac{\partial v}{\partial x} + v\frac{\partial v}{\partial y} = -\beta g(T - T_1)\cos\phi + \nu\nabla^2 v - \frac{1}{\rho}\frac{\partial p}{\partial y} \quad [2]$$

$$u\frac{\partial(T - T_1)}{\partial x} + v\frac{\partial(T - T_1)}{\partial y} = \alpha\nabla^2(T - T_1) \quad [3]$$

$$\frac{\partial u}{\partial x} + \frac{\partial v}{\partial y} = 0 \quad [4]$$

where

$$\nabla^2 = \frac{\partial^2}{\partial x^2} + \frac{\partial^2}{\partial y^2}$$

The co-ordinates x and y are measured along and perpendicular to the body surface as shown in Fig. 1. The angle ϕ contained

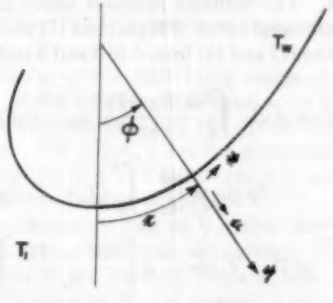

Fig. 1 System of Co-Ordinates

between the perpendicular to the surface and the vertical is a known given function of x. The terms u and v represent velocities in x and y-directions while T and p correspond to temperature and pressure. Note that the kinematic viscosity ν and thermal diffusivity α are assumed constant in Equations [1] and [2] and that the variation in the density ρ is accounted for in the buoyant term only, which is defined in terms of the coefficient of expansion β and the gravitational constant g.

At the outer edge of the free-convection field where the velocities u and v and their derivatives equal zero, Equations [1] and [2] give

$$y \to \infty \qquad \frac{\partial p}{\partial x} = \frac{\partial p}{\partial y} = 0$$

and the term p represents the difference between the local pressure and the pressure at the edge of the free-convection field.

Introduction of the stream function ψ so that

$$u = \frac{\partial \psi}{\partial y} \qquad v = -\frac{\partial \psi}{\partial x}$$

---

[1] Engineer, Heat Transfer Equipment Unit, Atomic Power Equipment Engineering, General Electric Company.

[2] Numbers in parentheses refer to the Bibliography at the end of the paper.

Presented at the National Conference of the Applied Mechanics Division, Troy, N. Y., June 16–18, 1955, of The American Society of Mechanical Engineers.

Discussion of this paper should be addressed to the Secretary, ASME, 29 West 39th Street, New York, N. Y., and will be accepted until January 10, 1956, for publication at a later date. Discussion received after the closing date will be returned.

Note: Statements and opinions advanced in papers are to be understood as individual expressions of their authors and not those of the Society. Manuscript received by ASME Applied Mechanics Division, August 16, 1954. Paper No. 55—APM-22.

satisfies the continuity equation, and Equations [1], [2], and [3] become, after elimination of the pressure

$$\frac{\partial\psi}{\partial y}\frac{\partial}{\partial x}(\nabla^2\psi) - \frac{\partial\psi}{\partial x}\frac{\partial}{\partial y}(\nabla^2\psi) = \nu\nabla^4\psi + \beta g\sin\phi\frac{\partial(T-T_1)}{\partial y} - \beta g\left[\cos\phi\frac{\partial(T-T_1)}{\partial x} - (T-T_1)\sin\phi\frac{d\phi}{dx}\right] \quad [5]$$

$$\frac{\partial\psi}{\partial y}\frac{\partial(T-T_1)}{\partial x} - \frac{\partial\psi}{\partial x}\frac{\partial(T-T_1)}{\partial y} = \alpha\nabla^2(T-T_1) \quad [6]$$

Further simplification is obtained if the temperature and velocity changes are assumed confined to a small boundary layer next to the body surface. According to accepted boundary-layer approximations it becomes possible to write

$$\frac{\partial^2}{\partial x^2} \ll \frac{\partial^2}{\partial y^2}$$

and Equations [5] and [6] become

$$\frac{\partial\psi}{\partial y}\frac{\partial^3\psi}{\partial x\partial y^2} - \frac{\partial\psi}{\partial x}\frac{\partial^3\psi}{\partial y^3} = \nu\frac{\partial^4\psi}{\partial y^4} + \beta g\left[\sin\phi\frac{\partial(T-T_1)}{\partial y} + \frac{\partial}{\partial x}\{(T-T_1)\cos\phi\}\right] \quad [7]$$

$$\frac{\partial\psi}{\partial y}\frac{\partial(T-T_1)}{\partial x} - \frac{\partial\psi}{\partial x}\frac{\partial(T-T_1)}{\partial y} = \alpha\frac{\partial^2(T-T_1)}{\partial y^2} \quad [8]$$

A complete solution of these two partial differential equations is a difficult task. The solutions proposed herein are obtained instead from the integral forms of Equations [7] and [8]. Integration of Equations [7] and [8] from 0 to δ and 0 to δ_T yields

$$\left[\nu\frac{\partial^2 u}{\partial y^2}\right]_0^\delta + (\cos\phi)\beta g\int_0^\delta\frac{\partial(T-T_1)}{\partial x}dy - \beta g(T_w-T_1)\sin\phi - \beta g\sin\phi\frac{d\phi}{dx}\int_0^\delta(T-T_1)dy = 0 \quad [9]$$

$$\frac{\partial}{\partial x}\int_0^{\delta_T}u(T-T_1)dy - \alpha\left[\frac{\partial(T-T_1)}{\partial y}\right]_0^{\delta_T} = 0 \quad [10]$$

The thickness of velocity and temperature profile are taken equal ($\delta = \delta_T$) because Bonilla (9) has found that the assumption leads to very small errors. The method of solution of Equations [9] and [10] consists of assuming velocity and temperature profiles which in term are substituted in the integral equations. The velocity and temperature distributions are chosen so that the following boundary conditions are satisfied

$$y = 0 \quad u = 0 \quad T = T_w$$

$$y = \delta \quad u = 0 \quad T = T_1 \quad \frac{\partial u}{\partial y} = \frac{\partial(T-T_1)}{\partial y} = 0$$

and are taken identical to those proposed by Eckert (6)

$$u = u_1\frac{y}{\delta}\left(1-\frac{y}{\delta}\right)^2 \quad [11]$$

$$\frac{T-T_1}{T_w-T_1} = \left(1-\frac{y}{\delta}\right)^2 \quad [12]$$

Substitution of Equations [11] and [12] into Equations [9] and [10] leads to

$$\frac{6\nu u_1}{\delta^2} = \beta g(T_w-T_1)\left[\left(1+\frac{1}{3}\delta\frac{d\phi}{dx}\right)\sin\phi\right] - \frac{1}{3}\left[\cos\phi\frac{d}{dx}\{\delta(T_w-T_1)\}\right]\beta g \quad [13]$$

$$\frac{1}{30}\frac{d}{dx}[u_1\delta(T_w-T_1)] = \frac{2\alpha}{\delta}(T_w-T_1) \quad [14]$$

Equations [13] and [14] are two first-order differential equations which determine u_1 and δ in terms of x for the specified boundary conditions at $x = 0$. The point $x = 0$ is taken at the lowest point of the body and there the angle ϕ is equal to zero (continuous body) or exhibits a finite discontinuity (wedge, inclined plate). The character of the flow there is similar to a stagnation point flow and u_1 equals zero. The corresponding value of δ is determined from Equation [13]. If the angle ϕ equals zero, Equation [13] gives $u_1 = 0$, if $d\delta/dx = 0$. If, on the other hand, ϕ is discontinuous at $x = 0$, Equation [13] reveals that $\delta = 0$ at the origin if $u_1 = 0$.

In nondimensional form Equations [13] and [14] are

$$\frac{6\dfrac{u_1 D}{\alpha}}{(\delta/D)^2} = N_{Pr}N_{Gr}\left[\left(1+\frac{1}{3}\frac{\delta}{D}\frac{d\phi}{dx/D}\right)\sin\phi\right] - \frac{1}{3}\cos\phi\left[\frac{d}{dx/D}\left\{\frac{\delta}{D}N_{Gr}\right\}\right]N_{Pr} \quad [15]$$

$$\frac{1}{30}\frac{d}{dx/D}\left\{\frac{u_1 D}{\alpha}\frac{\delta}{D}N_{Gr}\right\} = 2\frac{N_{Gr}}{\delta/D} \quad [16]$$

where the Grashof number is defined in terms of an arbitrary dimension D

$$N_{Gr} = \frac{\beta g(T_w-T_1)D^3}{\nu^2}$$

and the Prandtl number is equal to

$$N_{Pr} = \frac{\nu}{\alpha}$$

The boundary-layer thickness δ/D and the term $u_1 D/\alpha$ are computed from Equations [15] and [16]. Once δ/D is determined as a function of x/D the heat-transfer coefficient is obtained from

$$h = \frac{q}{T_w-T_1} = -\frac{k}{T_w-T_1}\left[\frac{\partial(T-T_1)}{\partial y}\right]_{y=0} = 2\frac{k}{\delta}$$

and the local Nusselt number is

$$N_{Nu} = \frac{hD}{k} = \frac{2}{\delta/D} \quad [17]$$

The heat-transfer coefficient may be computed, therefore, if solutions of Equations [15] and [16] are available. Such solutions will be presented in a later section. Note that for constant wall temperature Equation [16] can be integrated for both sets of boundary conditions at $x = 0$ and yields

$$\frac{u_1 D}{\alpha} = \frac{60}{\delta/D}\int_0^{x/D}\frac{1}{\delta/D}dx/D \quad [18]$$

Equation [15] becomes

$$\int_0^{x/D} \frac{1}{\delta/D}\, dx/D = \left(\frac{\delta}{D}\right)^3 \frac{N_{Gr} N_{Pr}}{360}\left[\sin\phi - \frac{1}{3}\frac{d}{dx/D}\left(\frac{\delta}{D}\cos\phi\right)\right] \quad [19]$$

Equation [19] is an integral equation for δ/D and its solution, when substituted in Equation [17], leads to the Nusselt number which can be obtained now from the solution of a single equation instead of the two Equations [15] and [16].

When the flow mechanism is turbulent Equations [9] and [10] are valid if the terms

$$\left[\nu \frac{\partial^2 u}{\partial y^2}\right]_0^\delta \quad \text{and} \quad \left[\alpha \frac{\partial T}{\partial y}\right]_0^\delta$$

are replaced, respectively, by

$$\left[\frac{1}{\rho}\frac{\partial \tau}{\partial y}\right]_0^\delta \quad \text{and} \quad \left[\frac{1}{\rho c_p} q\right]_0^{\delta_T}$$

where τ, q, c_p correspond to shear stress, heat rate, and specific heat. Because the shear stress and heat-rate-transfer distribution within a turbulent boundary layer are not known, the upper limits are replaced by y and δ in Equation [9] which in turn is integrated from 0 to δ. There results

$$\frac{\partial}{\partial x}\int_0^\delta u^2 dy = -\frac{\tau_w}{\rho} + \beta g(T_w - T_1)\sin\phi \int_0^\delta \frac{T - T_1}{T_w - T_1}\, dy + \beta g \frac{d}{dx}\left[\cos\phi (T_w - T_1)\int_0^\delta dy \int_y^\delta \frac{T - T_1}{T_w - T_1}\, dy\right] \quad [20]$$

$$\rho c_p \frac{\partial}{\partial x}\int_0^\delta u\,(T - T_1) dy = q_w \quad [21]$$

where the subscript w represents conditions at the wall.

The method of solution follows the technique of Eckert and Jackson (10) and assumes

$$\frac{u}{u_1} = \left(\frac{y}{\delta}\right)^{1/7}\left(1 - \frac{y}{\delta}\right)^4 \quad [22]$$

$$\frac{T - T_1}{T_w - T_1} = 1 - \left(\frac{y}{\delta}\right)^{1/7} \quad [23]$$

$$\tau_w = 0.0225\,\rho u_1^2 \left(\frac{u_1\delta}{\nu}\right)^{-1/4} \quad [24]$$

$$q_w = 0.0225\,\rho c_p\, u_1 (T_w - T_1)\left(\frac{u_1\delta}{\nu}\right)^{-1/4} N_{Pr}^{-3/4} \quad [25]$$

Equations [20] and [21] become

$$0.0523\frac{d}{dx/D}\left[\left(\frac{u_1 D}{\alpha}\right)^2 \frac{\delta}{D}\right] = 0.125\, N_{Gr} N_{Pr}^2 \frac{\delta}{D}\sin\phi - 0.0225\left(\frac{u_1 D}{\alpha}\right)^{7/} N_{Pr}^{1/4}\left(\frac{\delta}{D}\right)^{-1/4} + 0.0917\, N_{Pr}^2 \frac{d}{dx/D}\left\{\left(\frac{\delta}{D}\right)^2 N_{Gr}\cos\phi\right\} \quad [26]$$

$$0.0366\frac{d}{dx/D}\left[\left(\frac{u_1 D}{\alpha}\right)\frac{\delta}{D} N_{Gr}\right] = 0.0225\left(\frac{u_1 D}{\alpha}\right)^{3/4}\left(\frac{\delta}{D}\right)^{-1/4} N_{Pr}^{-3/10} N_{Gr} \quad [27]$$

The boundary conditions are

$$\frac{u_1 D}{\alpha} = \left(\frac{u_1 D}{\alpha}\right)_t \quad \text{and} \quad \frac{\delta}{D} = \left(\frac{\delta}{D}\right)_t$$

which correspond to the values calculated from Equations [15] and [16] at the transition point. Transition is assumed to take place when the local Grashof number defined in terms of x equals 10^9.

Next, consider free-convection within a heated vertical tube closed at the bottom and opening into a reservoir of cold fluid at the top. Lighthill (7) has considered such a system and a similar solution is given here. The flow in the vertical tube is shown in Fig. 2. It consists of a layer of thickness δ flowing upward, the remainder of the tube being occupied by cold fluid flowing down. If the tube length is equal to or less than l_1 the stagnant region does not exist and the upflow convective layer increases with x. For $x > l_1$, δ reaches a constant value d and such a flow occurs for $l_1 < x < l_2$. When $x > l_2$ a stagnant region exists at the closed section of the tube.

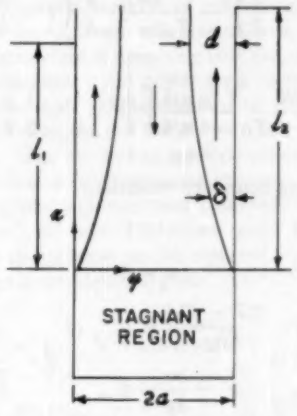

FIG. 2 NATURAL CONVECTION IN ENCLOSED TUBE

All the present equations deal with laminar flow within a rectangular section at constant wall temperature T_w and of large vertical dimension in the direction perpendicular to the x and y-co-ordinates. Extension of the present method to variable wall temperature, turbulent flow, inclined tubes or tubes of arbitrary section is performed easily. The governing equations are Equations [7] and [8], the buoyant term being defined in terms of the constant hydrostatic temperature T_s (4) (T_s equals T_1 in the previous sections). The term p now represents the difference between the local pressure and the hydrostatic pressure evaluated at T_s. The corresponding integral equations are for ν not equal to zero at $y = \delta$

$$\left[\nu\frac{\partial^2 u}{\partial y^2}\right]_0^\delta - \beta g(T_w - T_1) = -\left(\frac{\partial u}{\partial y}\right)_\delta \frac{d}{dx}\int_0^\delta u\, dy \quad [28]$$

$$\left[\nu\frac{\partial^2 u}{\partial y^2}\right]_\delta^a - \beta g(T_1 - T_s) = \frac{d}{dx}\left\{\left(\frac{u^2}{2}\right)_{y=a}\right\} + \left(\frac{\partial u}{\partial y}\right)_\delta \frac{d}{dx}\int_\delta^a u\, dy \quad [29]$$

$$\frac{d}{dx}\int_0^\delta u\,(T - T_s)\, dy = \alpha\left[\frac{\partial}{\partial y}(T - T_s)\right]_0^\delta + (T_1 - T_s)\frac{d}{dx}\int_0^\delta u\, dy \quad [30]$$

$$\frac{d}{dx}\int_\delta^a u(T-T_s)dy = \alpha\left[\frac{\partial}{\partial y}(T-T_s)\right]_\delta^a + (T_1-T_s)\frac{d}{dx}\int_\delta^a u\,dy \quad \ldots\ldots [31]$$

The velocity and temperature profiles are taken as

$$\frac{u}{u_1} = \frac{y}{\delta}\left(1-\frac{y}{\delta}\right)^2 - \frac{K\delta}{u_1}\left(\frac{y}{\delta}\right)^2\left(1-\frac{y}{\delta}\right) \quad 0 \leqq y \leqq \delta \quad \ldots [32]$$

$$\frac{u}{u_1} = \frac{K\delta}{u_1}\,\frac{1-y/\delta}{1-a/\delta}\left[\frac{a}{\delta}-\frac{1}{2}-\frac{1}{2}\,\frac{y}{\delta}\right] \quad \delta \leqq y \leqq a \quad \ldots [33]$$

$$\frac{T-T_1}{T_w-T_1} = \left(1-\frac{y}{\delta}\right)^2 - \frac{G\delta}{T_w-T_1}\,\frac{y}{\delta}\left(1-\frac{y}{\delta}\right) \quad 0 \leqq y \leqq \delta \quad \ldots\ldots [34]$$

$$\frac{T-T_1}{T_w-T_1} = \frac{G\delta}{T_w-T_1}\,\frac{1-y/\delta}{1-a/\delta}\left[\frac{a}{\delta}-\frac{1}{2}-\frac{1}{2}\,\frac{y}{\delta}\right] \quad \delta \leqq y \leqq a \quad \ldots\ldots [35]$$

with the following boundary conditions

$y = 0$	$u = 0$	$T = T_w$
$y = \delta$	$u = 0$	$\dfrac{\partial u}{\partial y} = K$
$T = T_1$	$\dfrac{\partial(T-T_1)}{\partial y} = G$	
$y = a$	$\dfrac{\partial u}{\partial y} = 0$	$\dfrac{\partial(T-T_1)}{\partial y} = 0$

The profiles were chosen so that they reduce to those of Equations [11] and [12] when $a/\delta \to \infty$. Further, parabolic equations typical of laminar flow in a tube were used for $\delta \leqq y \leqq a$. Velocity and temperature and their gradients were assumed continuous at the point $y = \delta$. The value of $K\delta/u_1$ is obtained from a mass balance across the tube or

$$\int_0^a u\,dy = 0 \quad \ldots\ldots [36]$$

and

$$\frac{K\delta}{u_1} = \frac{1}{1-4\left(\frac{a}{\delta}-1\right)^2} \quad \ldots\ldots [37]$$

With T_s vanishing from the equations, the integral equations become

$$\nu\frac{Gu_1}{\delta^2}\left[1+\frac{K\delta}{u_1}\right] - \beta g(T_w-T_1) = -\frac{u_1}{\delta}\,\frac{K\delta}{u_1} \frac{d}{dx}\left\{\frac{u_1\delta}{12}\left[1-\frac{K\delta}{u_1}\right]\right\} \quad \ldots\ldots [38]$$

$$\frac{1}{2}\beta g G\delta\left[\frac{a}{\delta}-1\right] = \frac{1}{8}\frac{d}{dx}\left\{u_1^2\left(\frac{K\delta}{u_1}\right)^2\left(\frac{a}{\delta}-1\right)^2\right\} - \frac{u_1}{\delta}\,\frac{K\delta}{u_1}\,\frac{d}{dx}\left\{\frac{u_1\delta}{12}\left[1-\frac{K\delta}{u_1}\right]\right\} \quad \ldots\ldots [39]$$

$$\frac{1}{60}\frac{d}{dx}\left\{u_1\delta(T_w-T_1)\left(2-\frac{K\delta}{u_1}-\frac{G\delta}{T_w-T_1}+\frac{K\delta}{u_1}\,\frac{G\delta}{T_w-T_1}\right)\right\} + \frac{u_1\delta}{12}\left(1-\frac{K\delta}{u_1}\right)\frac{d}{dx}(T_w-T_1) = \alpha\,\frac{T_w-T_1}{\delta}\left(2+\frac{2\delta G}{T_w-T_1}\right) \quad \ldots\ldots [40]$$

$$\frac{d}{dx}\left[u_1\delta(T_w-T_1)\,\frac{K\delta}{u_1}\,\frac{G\delta}{T_w-T_1}\,\frac{2}{15}\left(\frac{a}{\delta}-1\right)^2\right] - \frac{u_1\delta}{12}\left(1-\frac{K\delta}{u_1}\right)\frac{d}{dx}(T_w-T_1) + \alpha G = 0 \quad \ldots\ldots [41]$$

Equations [38] to [41] are four differential equations for the four variables u_1, δ/a, G, $T_w - T_1$. The boundary conditions are

$$x = 0 \qquad u_1 = 0 \qquad \delta = 0 \qquad G = 0 \qquad T_1 = B$$

where B represents the fluid temperature at $x = 0$.

The method of solution first consists of obtaining the length l_2. The value of B is equal to 0 or $T_w - T_1 = 0$ and the integration process may be carried forward through Equations [38] to [41] until $(d\delta)/(dx) = 0$. When this value is reached the length l_1 is obtained, and for larger values of x the integration is continued with the value $\delta = d$ (corresponding to $d\delta/dx = 0$) maintained constant. When the temperature T at the center line ($y = a$) reaches the temperature T_0 of the cold fluid reservoir the length l_2 is determined. If the tube length L is greater than l_2 the region of negative x of length $L - l_2$ is a stagnant region containing fluid at the temperature T_w. If the tube length is smaller than l_2 the calculation method proceeds as before, various values of B being assumed until the center-line fluid exit temperature is found equal to T_0 at $x = L$. If the tube is open at the bottom and closed at the top, the method of solution proceeds in a similar manner while a combination of two such solutions may be used to solve the case of free convection between parallel plates (7). Note again that the plates may be insulated or may have prescribed wall-temperature variations. When compared to Lighthill's method (7) the present calculation technique yields the complete solution, accounts for a larger number of boundary conditions and configurations, and reduces to the vertical-plate method if a/δ is very large. On the other hand, Lighthill's solutions are computed more readily and their use is recommended for the case of circular tube at constant wall temperature.

Discussion of Basic Equations

The basic differential Equations [7] and [8] differ from those used by Hermann (2) who neglected the term

$$\frac{\partial}{\partial x}[(T-T_1)\cos\phi]$$

Previous solutions assumed that

$$\frac{v}{u} \approx \epsilon$$

$$\frac{y}{x} \approx \epsilon$$

where ϵ is a small quantity, and terms of order

$$\epsilon\left(-1/\rho\,\frac{\partial p}{\partial x}\right)$$

with respect to terms of order 1 $[u(\partial u)/(\partial x)]$ were neglected. Equations [7] and [8] are obtained from the assumptions

$$\frac{\partial^2\psi}{\partial x^2} << \frac{\partial^2\psi}{\partial y^2} \qquad \frac{\partial^2 T}{\partial x^2} << \frac{\partial^2 T}{\partial y^2}$$

and only terms of order ϵ^2 are left out of the equations. A nondimensional analysis of Equation [7] reveals that

$$N_{Gr}\sin\phi \approx 1/\epsilon^2 \qquad N_{Gr}\cos\phi \approx 1/\epsilon^2$$

as compared to Hermann's result

$$N_{Gr} \sin \phi \approx 1/\epsilon^4 \qquad N_{Gr} \cos \phi \approx 1/\epsilon^4$$

To the same order of approximation (10 per cent for $\epsilon = 0.1$) the present solutions apply for $N_{Gr} \sin \phi = 10^3$ as compared to $N_{Gr} \sin \phi = 10^4$ for Hermann's equations. Smaller values of Grashof number and angles ϕ approaching zero may be accounted for.

This improvement is not obtained, however, without some new approximations in the solutions. Examination of Equation [9] reveals that the kinetic-energy terms do not appear in the integral form of the momentum equation. Under those conditions all results will be expressed in terms of the combined grouping $N_{Gr}N_{Pr}$ which leads to satisfactory correlation for all fluids with the possible exception of liquid metals (9). Because the kinetic-energy terms must be retained in the momentum equation for liquid metals, Equation [7] must be integrated twice with respect to y from y to δ and from 0 to δ and the corresponding result is

$$\frac{1}{105}\frac{d}{dx/D}\left\{\frac{\delta}{D}\left(\frac{u_1 D}{\alpha}\right)^2\right\}\left\{\frac{1}{N_{Pr}} = -\frac{u \cdot D/\alpha}{\delta/D} + \frac{1}{3} N_{Gr} \sin \phi \frac{\delta}{D} + \frac{1}{12}\frac{d}{dx/D}\left\{\left(\frac{\delta}{D}\right)^3 \cos \phi\, N_{Gr}\right\}\right. \quad [42]$$

Equation [42] is more complicated than Equation [15] and its use should be limited to low Prandtl number fluids.

Method of Solution and Typical Solutions

Closed-form solutions of Equations [15] and [16] can be derived for simple configurations and will be discussed first.

Vertical Plate. In the case of a vertical plate ($\phi = \pi/2$) maintained at constant temperature, Equations [17] and [18] can be solved directly to give

$$\frac{x}{D} N_{Nu} = \frac{2}{\sqrt[4]{480}} \sqrt[4]{N_{Gr} N_{Pr} \left(\frac{x}{D}\right)^3} \quad [43]$$

For air with a Prandtl number of 0.714 Equation [48] becomes

$$N_{Nu} = 0.393\, N_{Gr}^{1/4} \left(\frac{x}{D}\right)^{-1/4} \quad [44]$$

as compared to the numerical constant of 0.378 obtained by Eckert (6) or 0.360 derived by Schmidt and Beckmann (3). The discrepancy in the numerical constant can be explained in terms of the assumed velocity profile. Equation [11] gives

$$\left.\frac{\partial^2 u}{\partial y^2}\right|_{y=\delta} \neq 0$$

which is not correct for a free surface. A polynomial of the third order with $y = \delta$, $u = 0$, $(\partial^2 u)/(\partial y^2) = 0$ reduces the numerical constant to 0.387 while a quartic also satisfying $(\partial u)/(\partial y) = 0$ brings the numerical constant down to 0.354 or within 2 per cent of the exact solution (3). For low Prandtl numbers Equation [42] reduces to Eckert's equation

$$N_{Nu} = 0.508\, N_{Pr}^{1/2} (0.952 + N_{Pr})^{-1/4} N_{Gr}^{1/4} \left(\frac{x}{D}\right)^{-1/4} \quad [45]$$

Horizontal Plate. Consider next the case of a horizontal plate facing upward ($\phi = \pi$). Direct integration of Equations [15] and [16] is possible once again and for constant wall temperature

$$N_{Nu} = \frac{2}{\sqrt[5]{4500}} [N_{Gr} N_{Pr}]^{1/5} \left(\frac{x}{D}\right)^{-1/5} \quad [46]$$

For low Prandtl numbers Equation [42] gives

$$N_{Nu} = \frac{2}{\sqrt[5]{4500}} (N_{Gr} N_{Pr}^2)^{1/5} \frac{1}{\left[\frac{16}{21} + N_{Pr}\right]^{1/5}} \left(\frac{x}{D}\right)^{-1/5} \quad [47]$$

Analytical solutions for a horizontal plate are not available and experimental results have been obtained only by Weise (11). His results cannot be used because of the rapid collision at the mid-point of the plate of the two thermal boundary layers generated at each edge. Equations [46] and [47] reveal that when the term $\partial[(T - T_1) \cos \phi]/\partial x$ predominates the $1/4$-power law is replaced by a $1/5$-power law. For inclined plates the exponent of the Grashof number will vary, therefore, from $1/4$ to $1/5$. A successive approximation method of solution may be used to demonstrate that the $1/4$ power will predominate.

The accepted procedure of assuming that the coefficient u_1 and boundary-layer thickness δ are power-type variation of the distance x is not essential. Differentiation of Equation [19] reveals that δ must follow the law Cx^r if $\delta = 0$ at $x = 0$.

Inclined Plate. The method of solution consists of first solving Equations [15] and [16] neglecting the term $\cos \phi\, (d\delta)/(dx)$ and of evaluating the neglected term from this first approximation. Equations [15] and [16] then yield the second approximation and the process can be repeated as many times as desired. The first approximation gives

$$\frac{u_1 D}{\alpha} = \sqrt{\frac{40}{3}} \sqrt{N_{Gr} N_{Pr} \sin \phi} \left(\frac{x}{D}\right)^{1/2} \quad [48]$$

$$\frac{\delta}{D} = \sqrt[4]{480} \sqrt[4]{\frac{1}{N_{Gr} N_{Pr} \sin \phi}} \left(\frac{x}{D}\right)^{1/4} \quad [49]$$

and the second approximation becomes

$$N_{Nu} = \frac{2}{\sqrt[4]{480}} [N_{Gr} N_{Pr} \sin \phi]^{1/4} \left(\frac{x}{D}\right)^{-1/4} \frac{1 - \frac{1}{3}(\cot \phi) \sqrt[4]{\frac{480\, D^3}{N_{Gr} N_{Pr} x^3}}}{\left\{1 - \frac{1}{6}(\cot \phi) \sqrt[4]{\frac{480\, D^3}{N_{Gr} N_{Pr} x^3}}\right\}^{1/3}} \quad [50]$$

The ratio of inclined to vertical heat-transfer coefficient is

$$\frac{(N_{Nu})_\phi}{(N_{Nu})_{\phi = \frac{\pi}{2}}} = [\sin \phi]^{1/4} \frac{1 - \frac{1}{3}(\cot \phi) \sqrt[4]{\frac{480\, D^3}{N_{Gr} N_{Pr} x^3}}}{\left\{1 - \frac{1}{6}(\cot \phi) \sqrt[4]{\frac{480\, D^3}{N_{Gr} N_{Pr} x^3}}\right\}^{1/3}} \quad [51]$$

Further approximations become too complicated and are not necessary unless the angle ϕ approaches zero or π or $N_{Gr} N_{Pr}$ is small. Experimental data for inclined plates have been obtained by Rich (1). For the range of Grashof numbers and angles considered by Rich, Equation [51] simplifies to

$$(N_{Nu})_\phi = (N_{Nu})_{\phi = \pi/2} [\sin \phi]^{1/4} \quad [52]$$

which agrees with the experimental results.

Horizontal Circular Cylinder at Constant Temperature. Further confirmation of the method of solution is obtained from the case of a horizontal cylinder. The method of successive approximations is utilized once again. For $\phi = 2x/D$ Equations [15] and [16] become

$$\frac{d}{dx/D}\left(\frac{\delta}{D}\right)^4 + \frac{8}{3}\left(\cot\frac{2x}{D}\right)\left(\frac{\delta}{D}\right)^4 - \frac{4}{3}\frac{360}{N_{Gr}N_{Pr}}\frac{1}{\sin\frac{2x}{D}} = 0 \quad \text{.....[53]}$$

which is a first-order differential equation. The solution is for

$$\left.\frac{d\,\delta/D}{dx/D}\right|_{x=0} = 0$$

$$\left(\frac{\delta}{D}\right)^4 = \frac{240}{N_{Gr}N_{Pr}}\frac{1}{\left(\sin\frac{2x}{D}\right)^{4/3}}\int_0^{2x/D}(\sin\phi)^{1/3}\,d\phi \quad \text{..[54]}$$

and the local heat transfer is

$$N_{Nu} = \frac{2}{\sqrt[4]{240}}(N_{Gr}N_{Pr})^{1/4}\left(\sin\frac{2x}{D}\right)^{1/3}\left\{\int_0^{2x/D}(\sin\phi)^{1/3}\,d\phi\right\}^{-1/3} \quad \text{.....[55]}$$

For $N_{Gr}\cos\phi > 10^4$ no further approximations are necessary. Hermann's results (2) are valid for the same range, and comparison of Equation [55] with the values derived by Hermann yields an evaluation of the accuracy of the present method. For purposes of comparison Equation [55] is written

$$\frac{(N_{Nu})_\phi}{(N_{Nu})_{\phi=\pi/2}} = \frac{\int_0^{\pi/2}(\sin\phi)^{1/3}\,d\phi}{\int_0^{\phi}(\sin\phi)^{1/3}\,d\phi}(\sin\phi)^{1/3} \quad \text{.....[56]}$$

Table 1 shows Hermann's results and the values computed from Equation [56]. The comparison is very satisfactory.

TABLE 1 LOCAL HEAT-TRANSFER COEFFICIENT AROUND HORIZONTAL CYLINDER. VALUES OF $(N_{Nu})_\phi/(N_{Nu})_{\phi=\pi/2}$

ϕ	0	30	60	90	120	150	165	180
Present.....	1.14	1.13	1.08	1.00	0.88	0.69	0.54	0
Hermann....	1.14	1.13	1.08	1.00	0.88	0.69	0.54	0

The average heat-transfer coefficient is computed from Equation [55]

$$(N_{Nu})_{avg} = 0.44\,[N_{Gr}N_{Pr}]^{1/4} \quad \text{.....[57]}$$

which is 10 per cent higher than Hermann's and about 10 per cent lower than the accepted experimental correlation for horizontal cylinders (12). The order of discrepancy between the present result and Hermann's is the same as for the vertical-plate case and one suspects that a velocity profile with

$$\left.\frac{\partial^2 u}{\partial y^2}\right|_{y=\delta} = 0$$

will give an answer closer to Hermann's.

When $N_{Gr}\cos\phi < 10^4$ a second approximation is necessary. Equations [15] and [16] can be written

$$\frac{d}{d\,x/D}\left(\frac{\delta}{D}\right)^4 + \frac{8}{3}\left(\cot\frac{2x}{D}\right)\left(\frac{\delta}{D}\right)^4 - \frac{4}{3}\frac{360}{N_{Gr}N_{Pr}}\frac{1}{\sin\frac{2x}{D}} = \frac{4}{9}\frac{\left(\frac{\delta}{D}\right)^4}{\sin\frac{2x}{D}}\frac{d^3}{d(x/D)^3}\left(\frac{\delta}{D}\cos\frac{2x}{D}\right) \quad \text{.....[58]}$$

The term on the right-hand side of Equation [58] is evaluated from Equation [54] and the second approximation to $(\delta/D)^4$ is obtained from the addition to Equation [54] of the particular integral

$$\frac{8}{9}\left[\frac{240}{N_{Gr}N_{Pr}}\right]^{1/4}\frac{1}{\left(\sin\frac{2x}{D}\right)^{4/3}}\int_0^{2x/D}K(\sin\phi)^{4/3}\frac{d^3}{d\phi^3}(K^{1/3}\cos\phi)d\phi \quad \text{.....[59]}$$

where

$$K = \frac{1}{\left(\sin\frac{2x}{D}\right)^{4/3}}\int_0^{2x/D}(\sin\phi)^{1/3}\,d\phi \quad \text{.....[60]}$$

The second approximation to $(\delta/D)^4$ becomes

$$\left(\frac{\delta}{D}\right)^4 = \frac{240}{N_{Gr}N_{Pr}}\frac{1}{\left[\sin\frac{2x}{D}\right]^{4/3}}\left\{\int_0^{2x/D}(\sin\phi)^{1/3}\,d\phi + \frac{8}{9}\left[\frac{240}{N_{Gr}N_{Pr}}\right]^{1/3}\int_0^{2x/D}K(\sin\phi)^{4/3}\frac{d^3}{d\phi^3}(K^{1/3}\cos\phi)d\phi\right\} \quad \text{.....[61]}$$

and as the product $N_{Gr}N_{Pr}$ becomes large, Equation [61] reduces to Equation [54].

Numerical evaluation of the expression in Equation [59] shows that it is negative and therefore the heat-transfer coefficient exceeds the values predicted by Equation [57]. This increase is larger as the product $N_{Gr}N_{Pr}$ decreases and thus follows the experimental trend. Values of Nusselt modulus, N_{Nu}, obtained from Equations [61] and [57], are shown in Fig. 3 for various values of $N_{Gr}N_{Pr}$. The results are plotted in terms of

$$\frac{N_{Nu}}{[N_{Gr}N_{Pr}]^{1/4}}\sqrt[4]{240}$$

The average Nusselt number $(N_{Nu})_{avg}$ is shown in Fig. 4 where the correlation proposed by McAdams (12) is plotted. Correspondence between theory and tests is satisfactory and the second approximation leads to corrections in the right direction. Similar results for low Prandtl number fluids were computed by a method of finite difference and are shown in Figs. 5 and 6. The experimental data of Hyman, Bonilla, and Ehrlich (14) are reproduced in Fig. 6 and compare satisfactorily with the analytical prediction.

Arbitrary Body. Previous solutions show that integral methods give accurate answers and can be applied to the more general case of an arbitrary body. For a given function $\phi = \phi(x)$ Equations [15] and [16] may be solved by means of a finite-difference method. If $N_{Gr}\cos\phi$ is larger than 10^4 the term

$$\frac{\partial}{\partial x}[(T - T_1)\cos\phi]$$

is negligible and the initial value of δ/D is obtained from a limiting process. For constant wall temperature there results

$$\left(\frac{\delta}{D}\right)_{x=0}^4 = \frac{360}{N_{Gr}N_{Pr}}\frac{1}{[d\phi/d(x_D)]_{x=0}}$$

For smaller value of N_{Gr} the successive-approximations method is recommended.

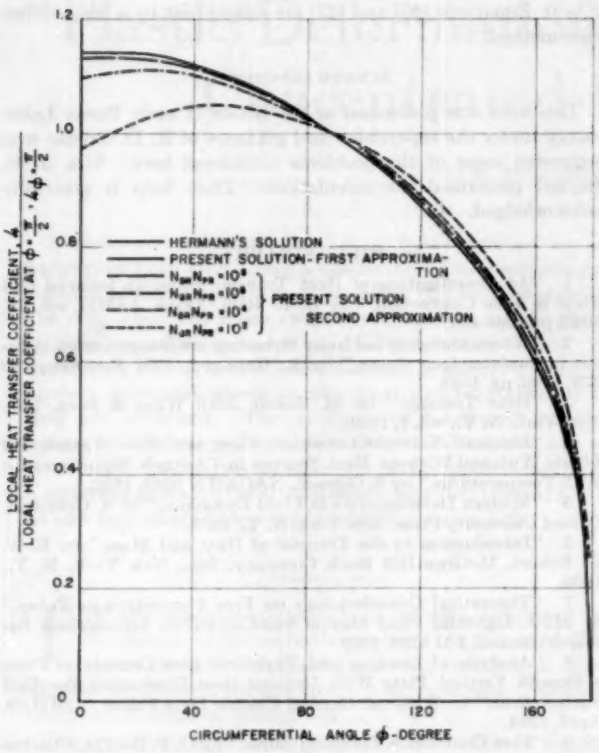

FIG. 3 LOCAL HEAT-TRANSFER COEFFICIENT FOR NATURAL CONVECTION AROUND CIRCULAR HORIZONTAL CYLINDER

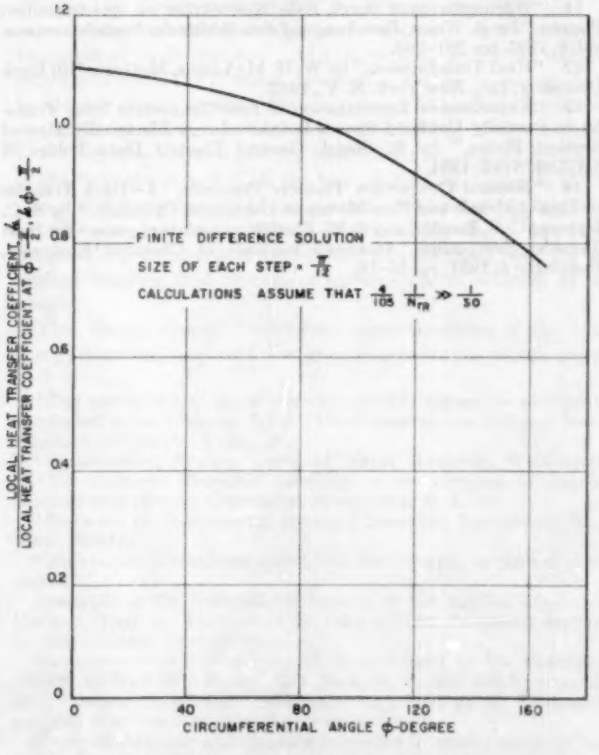
FINITE DIFFERENCE SOLUTION
SIZE OF EACH STEP = π/12
CALCULATIONS ASSUME THAT 4/105 1/N_PR ≫ 1/50
CIRCUMFERENTIAL ANGLE φ-DEGREE

FIG. 5 LOCAL HEAT-TRANSFER COEFFICIENT FOR NATURAL CONVECTION AROUND CIRCULAR HORIZONTAL CYLINDER FOR LOW PRANDTL NUMBER FLUID

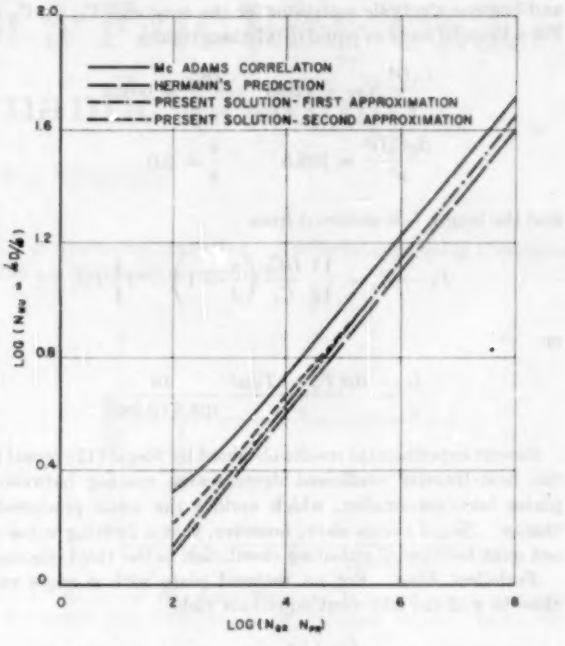

FIG. 4 AVERAGE HEAT-TRANSFER COEFFICIENT FOR NATURAL CONVECTION AROUND CIRCULAR HORIZONTAL CYLINDER

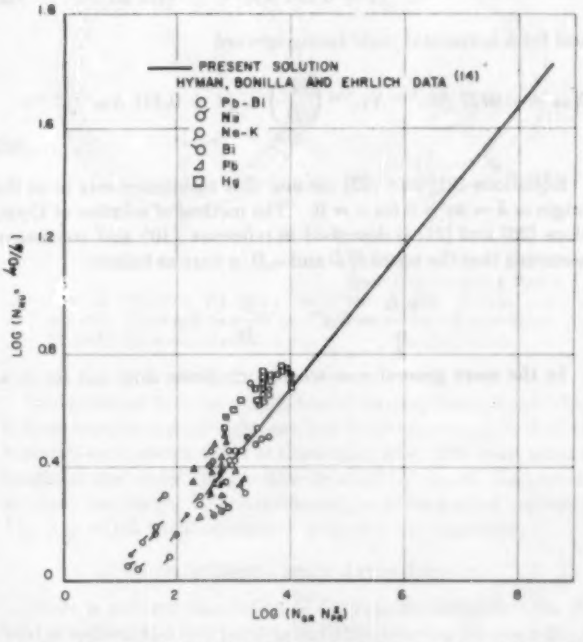

FIG. 6 AVERAGE HEAT-TRANSFER COEFFICIENT FOR NATURAL CONVECTION AROUND CIRCULAR HORIZONTAL CYLINDER FOR LOW PRANDTL NUMBER FLUID

Enclosed Channels. No complete solution will be presented here. Only a conservative estimate of the length l_3 will be obtained. If one assumes $\delta = d =$ const at all x, Equations [38] to [41] admit solutions of the form

$$u_1 = C_1 x$$
$$T_w - T_1 = C_2 x$$
$$G = C_3 x$$

and become algebraic equations for the constants C_1, C_2, C_3, d/a. For a Prandtl number equal to 0.7 there results

$$\frac{C_1 D^2}{\nu} N_{Pr} = 12.95 \qquad \frac{DC_3}{C_2} = 0.033$$

$$\frac{\beta g C_2 D^4}{\nu^2} = 105.5 \qquad \frac{a}{d} = 2.0$$

and the length l_2 is obtained from

$$T_0 - T_w = \left\{ \frac{1}{2} \frac{DC_3}{C_2} \left(\frac{a}{d} - 1 \right) - 1 \right\} C_2 l_2$$

or

$$\frac{l_2}{a} = \frac{\beta g (T_w - T_0) a^2}{\nu^2} \frac{16}{105.5\ (0.983)}$$

Recent experimental results obtained by Siegel (13) reveal that the heat-transfer coefficient decreases as spacing between the plates becomes smaller, which verifies the trend predicted by theory. Siegel's tests show, however, that a limiting value may not exist because of pulsating circulation in the third dimension.

Turbulent Flow. For an inclined plate with ϕ angle values close to $\pi/2$ the turbulent equations yield

$$N_{Nu} = 0.0295\, N_{Gr}^{2/5} \left(\frac{x}{D} \right)^{1/5} N_{Pr}^{2/15} [1 + 0.494\, N_{Pr}^{2/3}]^{-2/5} (\sin \phi)^{2/5} \quad \ldots\ldots [62]$$

and for a horizontal plate facing upward

$$N_{Nu} = 0.0727\, N_{Gr}^{4/11} N_{Pr}^{5/11} \left(\frac{x}{D} \right)^{1/11} [1 + 0.441\, N_{Pr}^{2/3}]^{-4/11} \quad \ldots\ldots [63]$$

Equations [61] and [62] assume that turbulence sets in at the origin or $\delta = u_1 = 0$ for $x = 0$. The method of solution of Equations [26] and [27] is described in reference (10) and consists of assuming that the terms δ/D and $u_1 D/\alpha$ vary as follows

$$\frac{u_1 D}{\alpha} = C_1 x^m \qquad \frac{\delta}{D} = C_2 x^n$$

In the more general case where turbulence does not set in at $x = 0$, Equations [26] and [27] are solved best by a finite-difference method.

Acknowledgments

This work was performed at the Knolls Atomic Power Laboratory under the supervision and guidance of R. D. Brooks who suggested some of the problems considered here. Mrs. J. E. Biglieri performed the calculations. Their help is gratefully acknowledged.

Bibliography

1 "An Investigation of Heat Transfer From an Inclined Flat Plate in Free Convection," by B. R. Rich, Trans. ASME, vol. 75, 1953, pp. 489–499.

2 "Wärmeübergang bei freier Stromung am waagerechten zylinder in zweiatomigen Gasen," by R. Hermann, *VDI Forschungsheft* 379, 1926, pp. 1–24.

3 "Heat Transfer," by M. Jakob, John Wiley & Sons, Inc., New York, N. Y., vol. 1, 1949.

4 "Laminar Natural-Convection Flow and Heat Transfer of Fluids With and Without Heat Sources in Channels With Constant Wall Temperatures," by S. Ostrach, NACA TN 2863, 1952.

5 "Modern Developments in Fluid Dynamics," by S. Goldstein, Oxford University Press, New York, N. Y., 1938.

6 "Introduction to the Transfer of Heat and Mass," by E. R. G. Eckert, McGraw-Hill Book Company, Inc., New York, N. Y., 1950.

7 "Theoretical Considerations on Free Convection in Tubes," by M. J. Lighthill, Fluid Motion Sub-Committee Aeronautical Research Council, FM 1758, 1952.

8 "Analysis of Laminar and Turbulent Free Convection From a Smooth Vertical Plate With Uniform Heat Dissipation Per Unit Surface Area," by R. Siegel, General Electric Data Folder R 54GL89, April, 1954.

9 "Free Convection Transfer Course," by C. F. Bonilla, Charleston Section of the American Institute of Chemical Engineers, 1952.

10 "Analysis of Turbulent Free-Convection Boundary Layer on Flat Plate," by E. R. G. Eckert and T. W. Jackson, NACA Report 1015, 1951.

11 "Wärmeübergang durch freie Konvektion an quadratischen Platten," by R. Weise, *Forschung auf dem Gebiete des Ingenieurwesens*, vol. 6, 1935, pp. 281–292.

12 "Heat Transmission," by W. H. McAdams, McGraw-Hill Book Company, Inc., New York, N. Y., 1942.

13 "Experimental Investigation of Free-Convection Heat Transfer in Partially Confined Spaces Between Large Electrically Heated Vertical Plates," by R. Siegel, General Electric Data Folder R 54GL98, April, 1954.

14 "Natural Convection Transfer Processes. I—Heat Transfer to Liquid Metals and Non-Metals at Horizontal Cylinders," by S. C. Hyman, C. F. Bonilla, and S. W. Ehrlich, preprints of papers for Heat Transfer Symposium, American Institute of Chemical Engineers, December 5, 1951, pp. 55–76.

Plastic Deformations of a Free Ring Under Concentrated Dynamic Loading[1]

By R. H. OWENS[2] and P. S. SYMONDS[3]

A concentrated time-dependent force acts on an unsupported thin ring along a diameter. The problem considered in this paper is to determine the deformations of the ring when the force magnitudes are such that plastic strains large compared with elastic strains occur. By neglecting elastic strains and assuming ideally plastic behavior, approximations to the final deformations of the ring are obtained. The analysis is developed for force pulses of arbitrary shape, but numerical results are obtained only in the special case of a rectangular force pulse. A criterion is stated for conditions when this type of analysis can be expected to provide satisfactory results.

Introduction

THIS analysis is an extension to an unsupported ring of ductile material of the methods employed in (1, 3, 4).[4] These references dealt with large plastic deformations of beams subjected to dynamic loading, under conditions such that elastic deformations could be disregarded.

The hypothesis that a satisfactory approximation to the final deformation in the ring subjected to a concentrated, dynamic load, Fig. 2, can be obtained by ignoring elastic strains (and hence elastic vibrations) leads to a "plastic-rigid" type of theory. Briefly, this theory assumes that the ring remains rigid until the moment developed in the ring at some section attains a value M_0, the yield or limit moment. At this section, unlimited bending may occur while the moment equals M_0; that is, the tangents on either side of this section ultimately may make a finite angle with one another. Such a material is described by Fig. 1. As discussed in (1), M_0 may be computed by the formula $M_0 = \sigma_y Z_p$, where σ_y is the yield stress and Z_p is the sum of the first moments of the upper and lower halves of the section area under consideration about its neutral axis. When a section of the ring sustains the moment M_0, a "plastic hinge" is said to exist there, and the unlimited bending that transpires corresponds to rotation at the hinge.

This theory should yield useful approximations if the total energy absorbed in plastic flow greatly exceeds the elastic energy that can be stored in the ring. A criterion expressing this state of affairs is developed subsequently.

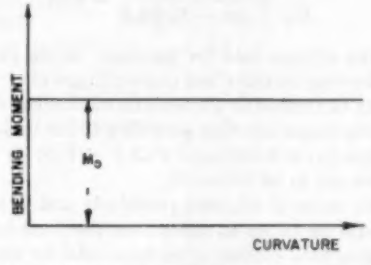

Fig. 1 Relation Between Bending Moment and Curvature According to Hypothesis of "Plastic-Rigid" Behavior

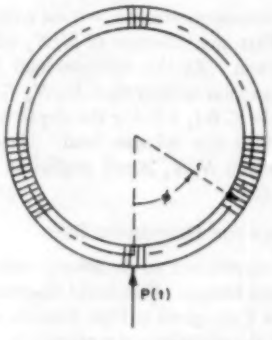

Fig. 2 Shaded Regions Indicate Regions in Which Plastic Deformation Occurs

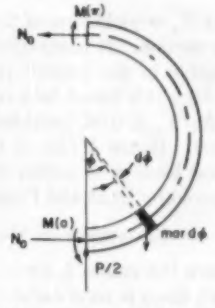

Fig. 3 Free-Body Diagram of Half-Ring in First Phase of Motion—Rigid-Body Translation

It is assumed that the middle line of the ring has radius r which is large enough to permit the analysis to be carried out as if all the material were concentrated at the middle line. The mass per unit length of the middle line will be denoted by m and the time-dependent load by $P(t)$. The configuration to be studied appears in Fig. 2 in which small changes in geometry are neglected.

Motion Immediately After Impact

There is uniform translation of the ring immediately after the load is applied and this persists until the bending moment due to inertia forces attains the value M_0 at certain sections of the ring.

Let it be assumed that these plastic regions first occur at $\varphi = 0, \pi$. By symmetry, the shear force $V = 0$ at $\varphi = \pi$ and $V = P/2$ at $\varphi = 0$. Equilibrium equations written for the free-body diagram shown in Fig. 3 yield the results

$$P = 2\pi rma \quad [1]$$

$$N_0 = \frac{1}{2r}\int_0^{\pi} (r \sin \varphi) mar d\varphi = rma \quad [2]$$

The moment $M(\varphi)$ at any section can then be obtained as

---

[1] The results in this paper were obtained in the course of research conducted under Contract N7onr-35810 between the Office of Naval Research and Brown University.

[2] Mathematics Branch, Office of Naval Research, Washington, D. C.; formerly Research Associate in the Division of Applied Mathematics, Brown University, Providence, R. I.

[3] Professor of Engineering, Brown University, Providence, R. I. Mem. ASME.

[4] Numbers in parentheses refer to the Bibliography at the end of the paper.

Presented at the National Conference of the Applied Mechanics Division, Troy, N. Y., June 16–18, 1955, of The American Society of Mechanical Engineers.

Discussion of this paper should be addressed to the Secretary, ASME, 29 West 39th Street, New York, N. Y., and will be accepted until January 10, 1956, for publication at a later date. Discussion received after the closing date will be returned.

Note: Statements and opinions advanced in papers are to be understood as individual expressions of their authors and not those of the Society. Manuscript received by ASME Applied Mechanics Division, February 21, 1955. Paper No. 55—APM-27.

$$M(\varphi) = M_0\left[1 - \frac{Pr}{2M_0}\sin\varphi + \frac{Pr}{2M_0}\frac{\varphi}{\pi}\sin\varphi\right] \ldots [3]$$

If additional plastic regions occur, they will be located at stationary points of $M(\varphi)$. Setting $dM/d\varphi = 0$ gives

$$\sin\varphi = (\pi - \varphi)\cos\varphi \ldots [4]$$

The solution of interest is $\varphi = \xi = 1.11$ radians or about 64 deg, where $d^2M/d\varphi^2 > 0$ implying $M(\varphi)$ is a minimum. Let the load P be increased until this minimum attains the value $-M_0$ so that Equation [3] gives the result

$$\frac{Pr}{M_0} = \frac{2\pi}{(\pi - \xi)\sin\xi} = 6.88 \ldots [5]$$

where P is the collapse load for the ring. When Pr/M_0 exceeds this value, the ring contains four plastic hinges at $\varphi = 0, \xi, \pi, 2\pi - \xi$, and may be treated as a kinematic mechanism since the segments between hinges are rigid according to the basic hypothesis. As in reference (1) it is assumed that $\xi = \xi(t)$; in special cases $\xi(t)$ may turn out to be constant.

Strictly the value of M_0 used previously and in the following analysis should be taken to depend on the local value of axial force, according to a relation of the type valid for small N

$$\frac{M}{M_0} + k\left(\frac{N}{N_y}\right)^2 = 1$$

where N_y = yield force of the cross section and $k = 1$ for a rectangular section. It is expected that the influence of N/N_y will be negligible in the present problem. At the collapse load $P = 6.88\,M_0/r$ it is found for a rectangular section that $N_0/N_y \leq 0.03$ and $N_\xi/N_y \leq 0.08$, provided $h/r \leq 0.1$, h being the depth of the section. Hence $M/M_0 \geq 0.99$ at the collapse load. Cases of statical loading on arches in which N/N_y is not negligible were discussed by Onat and Prager (5).

Equations of Motion for Deforming Ring

Since the points ξ, $2\pi - \xi$ correspond to stationary values of $M(\varphi)$, there is no shear at these hinges. Free-body diagrams of the two segments joined at $\varphi = \xi$ are given in Figs. 4 and 5, along with the notation to be used in the equations of motion.

Although the mass of each segment changes because of the motion of the hinge at $\varphi = \xi$, Newton's equations may be used in the form "summation of forces equals product of mass and acceleration of center of mass," and "summation of torques about center of mass equals product of moment of inertia about center of mass and angular acceleration," since the rate of transfer of momentum from one segment to the other across the hinge due to the changing mass is zero and hence no impulsive forces are applied at the hinge point.

The analysis is based on the six equations of motion for the two segments hinged instantaneously at ξ, together with two equations which express continuity of velocity at the hinge point ξ. It is shown in the Appendix that continuity of velocity insures continuity of displacement; the acceleration is discontinuous, in general, at a moving hinge. Thus eight equations are available for the determination of eight unknowns y_0, y_π, θ_0, θ_π, ξ, N_0, N_π, N_ξ. Here y_0, y_π are linear displacements at $\varphi = 0$, $\varphi = \pi$, respectively; θ_0, θ_π are rotations of elements of the ring at $\varphi = 0$, $\varphi = \pi$; ξ is the angle of the interior hinge; and N_0, N_ξ, N_π are axial forces acting at $\varphi = 0$, ξ, and π, respectively. Sign conventions are shown in Figs. 4 to 6. All these quantities are functions of time, and dots will be used to denote time derivatives.

The equations of motion and continuity equations at the hinge are derived in the Appendix making use of Figs. 4 and 5. The six equations of motion can be reduced to three by eliminating N_0, N_π, N_ξ. These, together with the two continuity equations, form a system of five simultaneous equations which can be written as

$$a_{i1}\dot{v}_0 + a_{i2}\dot{v}_\pi + a_{i3}\dot{\omega}_0 + a_{i4}\dot{\omega}_\pi + a_{i5}(\xi, \dot{\xi}, \omega_0, \omega_\pi) = 0 \ldots [6.i]$$

where $i = 1, 2 \ldots 5$, and the symbols v_0, v_π, ω_0, ω_π are defined as follows

$$v_0 \equiv \frac{mr^2}{M_0}\dot{y}_0; \quad v_\pi = \frac{mr^2}{M_0}\dot{y}_\pi; \omega_0 = \frac{-mr^2}{M_0}\dot{\theta}_0; \quad \omega_\pi = \frac{mr^2}{M_0}\dot{\theta}_\pi$$

These all have dimensions of time, so that their derivatives and the coefficients a_{ij} are dimensionless. It is convenient also to define the following symbols

$$\frac{Pr}{M_0} \equiv \mu; \quad \frac{mr^2}{M_0}(\dot{\theta}_\pi + \dot{\theta}_0) \equiv \omega = \omega_\pi - \omega_0 \ldots [7]$$

The coefficients a_{ij} are shown in matrix form in Table 1.

In order to express the accelerations $\dot{v}_0$, $\dot{v}_\pi$, $\dot{\omega}_0$, $\dot{\omega}_\pi$ explicitly in terms of ξ and μ let the Equations [6] be considered as a system of five algebraic linear equations in the four unknowns $\dot{v}_0$, $\dot{v}_\pi$, $\dot{\omega}_0$, $\dot{\omega}_\pi$. These algebraic equations will be compatible and have a solution only if the determinant of the matrix a_{ij} vanishes. This determinant may be split into three determinants by breaking up the last column. The result is the equation

$$D_1(\xi) - \frac{\mu}{2}\bar{D}_1(\xi) - \omega\dot{\xi}D_2(\xi) = 0 \ldots [8]$$

where D_1, $\bar{D}_1$, D_2 may be reduced to third-order determinants by Chio's method (2), in which form they were used in the numerical

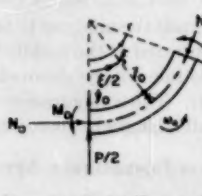

Fig. 4 Free-Body Diagram of Lower Segment, in Second Phase of Motion—Plastic Hinges at $\varphi = 0, \pi, \pm\xi$

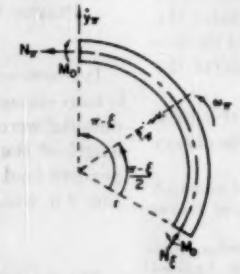

Fig. 5 Free-Body Diagram of Upper Segment in Second Phase of Motion

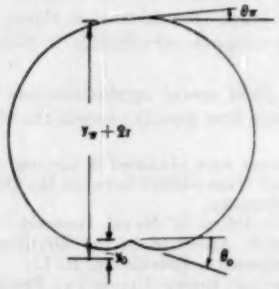

Fig. 6 Symbols Defining Main Final Deformations

TABLE 1 COEFFICIENTS OF a_{ij} IN MATRIX FORM

	j = 1	2	3	4	5
1	$(1-\cos\xi)(\xi-\sin\xi)$	0	$(1-\cos\xi)^2$ $-2\sin\xi(\xi-\sin\xi)$	0	$2\sin\xi$ $-\frac{1}{2}\mu(1-\cos\xi)$
2	0	$(1+\cos\xi)(\pi-\xi-\sin\xi)$	0	$(1+\cos\xi)^2$ $-2\sin\xi(\pi-\xi$ $-\sin\xi)$	$-2\sin\xi$
3	ξ	$\pi-\xi$	$1-\cos\xi$	$1+\cos\xi$	$-\frac{1}{2}\mu$
4	1	-1	$\sin\xi$	$-\sin\xi$	$-\dot{\omega}\xi\cos$
5	0	0	$1-\cos\xi$	$1+\cos\xi$	$-\dot{\omega}\xi\sin\xi$

TABLE 2 ELEMENTS OF b_{ij} AND c_i

	j = 1	2	3	4	c_i
1	$(1-\cos\xi)(\xi-\sin\xi)$	0	$(1-\cos\xi)^2$ $-2(\xi-\sin\xi)\sin\xi$	0	$-2\sin\xi$ $+\frac{1}{2}\mu(1-\cos\xi)$
2	0	$(1+\cos\xi)(\pi-\xi-\sin\xi)$	0	$(1+\cos\xi)^2$ $-2(\pi-\xi-\sin\xi)\sin\xi$	$2\sin\xi$
3	ξ	$\pi-\xi$	$1-\cos\xi$	$1+\cos\xi$	$\frac{1}{2}\mu$
4	$\sin\xi$	$-\sin\xi$	$1-\cos\xi$	$-(1+\cos\xi)$	0

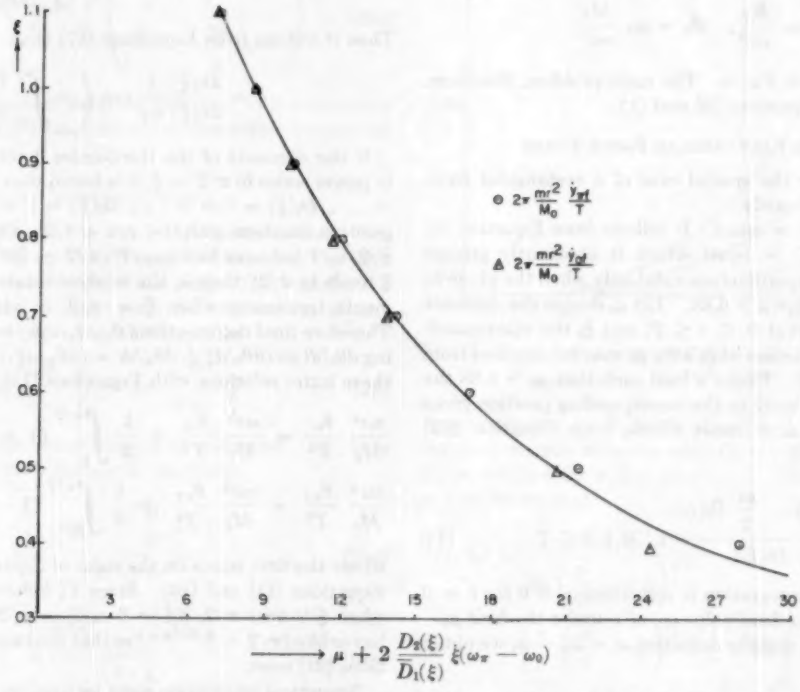

FIG. 7 PLOT OF ξ VERSUS $\mu + 2\dot{\xi}(\omega_\pi - \omega_1)D_2(\xi)/\overline{D}_1(\xi)$. THIS IS ξ_0 VERSUS μ_0 FOR RECTANGULAR FORCE PULSE

computations. The quantity $\mu + 2D_2/\overline{D}_1\dot{\xi}\omega \equiv 2D_1/\overline{D}_1$ is plotted against ξ in Fig. 7. For the sake of brevity we omit here, and subsequently, explicit definitions of the determinants, which are derived from the tables by standard methods. The significance of Equation [8] is that the system [6] then has a unique algebraic solution in $\dot{v}_0$, $\dot{v}_\pi$, $\dot{\omega}_0$, and $\dot{\omega}_\pi$, which may be obtained by eliminating the $\ddot{\xi}$ terms from the last two of Equations [6]and using the resulting equation with the first three. We thus obtain a system of equations of the following form

$$b_{i1}\dot{v}_0 + b_{i2}\dot{v}_\pi + b_{i3}\dot{\omega}_0 + b_{i4}\dot{\omega}_\pi = c_i \quad \ldots\ldots [9.i]$$

where $i = 1, 2, 3, 4$, and the elements b_{ij} and c_i are shown in Table 2. Solutions are

$$\dot{v}_0 = \frac{\Delta_1(\mu,\xi)}{\Delta(\xi)},\ \dot{v}_\pi = \frac{\Delta_2(\mu,\xi)}{\Delta(\xi)},\ \dot{\omega}_0 = \frac{\Delta_3(\mu,\xi)}{\Delta(\xi)},$$

$$\dot{\omega}_\pi = \frac{\Delta_4(\mu,\xi)}{\Delta(\xi)} \quad \ldots\ldots [10]$$

where $\Delta(\xi) = |b_{ij}|$ and $\Delta_j(\mu, \xi)$ is the determinant obtained by replacing the jth column of the b_{ij} matrix by c_i.

In particular

$$\dot{\omega} \equiv \dot{\omega}_\pi - \dot{\omega}_0 = \frac{\Delta_4(\mu,\xi) - \Delta_3(\mu,\xi)}{\Delta(\xi)}$$

and since Δ_4 and Δ_3 differ in only one column, they may be combined, giving

$$\dot{\omega}\Delta(\xi) = |c_{ij}| \quad \ldots\ldots [11]$$

where the elements c_{ij} are shown in Table 3.

If the last column of the c_{ij} matrix is broken up so that two determinants are formed, Equation [11] can be written in the form

$$\dot{\omega}D_2(\xi) = D_4(\xi) - \frac{\mu}{2}\overline{D}_3(\xi) \quad \ldots\ldots [12]$$

where D_3, $\overline{D}_3$ may be reduced by Chio's method to third-order

TABLE 3 ELEMENTS OF c_{ij}

	j = 1	2	3	4
1	$(1-\cos\xi)(\xi-\sin\xi)$	0	$(1-\cos\xi)^2 - 2(\xi-\sin\xi)\sin\xi$	$-2\sin\xi + \frac{1}{2}\mu(1-\cos\xi)$
2	0	$(1+\cos\xi)(\pi-\xi-\sin\xi)$	$(1+\cos\xi)^2 - 2(\pi-\xi-\sin\xi)\sin\xi$	$2\sin\xi$
3	ξ	$\pi-\xi$	2	$\frac{1}{2}\mu$
4	$\sin\xi$	$-\sin\xi$	$-2\cos\xi$	0

determinants. $D_2(\xi)$ can be shown to be identical with $\Delta(\xi)$.

The derivation of the equations expressing continuity across the hinge in the Appendix shows that

$$(1-\cos\xi)\omega_0 + (1+\cos\xi)\omega_\pi = 0 \quad [13]$$

Consequently, if ω is known, ω_0 and ω_π follow from Equations [7] and [13]. Then the major deformations may be obtained by integrating

$$\dot\theta_0 = -\omega_0 \frac{M_0}{mr^2}, \quad \dot\theta_\pi = \omega_\pi \frac{M_0}{mr^2}$$

giving θ_0, θ_π as defined in Fig. 6. The main problem, therefore, is to solve the pair of Equations [8] and [12].

Solution for Rectangular Force Pulse

Numerical results for the special case of a rectangular force pulse are obtained most easily.

Let $\dot\xi = 0$ so that $\xi = \text{const}$. It follows from Equation [8] that $\mu/2 = D_1(\xi)/\bar D_1(\xi) = \text{const}$ which is necessarily greater than 3.44, since all the equations are valid only when the hinge at $\varphi = \xi$ is present, i.e., when $\mu > 6.88$. Let μ_0 denote the constant value of μ in the interval $0 \le t \le T$, and ξ_0 the corresponding value of ξ. The variation of ξ_0 with μ_0 may be obtained from Fig. 7 on putting $\dot\xi = 0$. Under a load such that $\mu_0 > 6.88$ the hinge moves instantaneously to the corresponding position given by Fig. 7. Then also $\dot\omega = \text{const}$ which, from Equation [12] gives

$$\omega = \frac{D_3(\xi_0) - \frac{\mu_0}{2}\bar D_3(\xi_0)}{D_2(\xi_0)}\, t, \quad 0 < t \le T \quad [14]$$

where the constant of integration is zero since $\omega = 0$ for $t = 0$. Putting T for t gives the final value ω_T of ω under the load μ_0.

From Equations [13] and the definition $\omega = \omega_\pi - \omega_0$ we obtain

$$\frac{mr^2}{M_0}\frac{d\theta_0}{dt} = \frac{1}{2}(1+\cos\xi_0)\omega \quad [15a]$$

$$\frac{mr^2}{M_0}\frac{d\theta_\pi}{dt} = \frac{1}{2}(1-\cos\xi_0)\omega \quad [15b]$$

Introducing Equation [14] into [15], performing the integration, and replacing t by T gives the angular deformations θ_{0T}, $\theta_{\pi T}$ at the end of the loading interval

$$\frac{mr^2}{M_0}\frac{\theta_{0T}}{T^2} = \frac{1}{4}(1+\cos\xi_0)\frac{\omega_T}{T} \quad [16a]$$

$$\frac{mr^2}{M_0}\frac{\theta_{\pi T}}{T^2} = \frac{1}{4}(1-\cos\xi_0)\frac{\omega_T}{T} \quad [16b]$$

When $T < t$, $\mu \equiv 0$ and Equations [8], [12] reduce to

$$D_1(\xi) = \omega\dot\xi D_2(\xi); \quad \dot\omega D_3(\xi) = D_3(\xi) \quad [17]$$

Writing $\dot\omega = \dot\xi\frac{d\omega}{d\xi}$, and combining Equations [17], we obtain the differential equation

$$\frac{d\omega}{\omega} = \frac{D_3(\xi)}{D_1(\xi)}\,d\xi \quad [18]$$

This may be integrated, using the initial condition $\xi = \xi_0, \omega = \omega_T$, with the result

$$\omega(\xi,\xi_0) = \omega_T \exp\int_{\xi_0}^{\xi}\frac{D_3(\xi)}{D_1(\xi)}\,d\xi \quad [19]$$

Then it follows from Equations [17] that

$$\dot\xi = \frac{D_1(\xi)}{D_2(\xi)}\frac{1}{\omega_T}\exp\left(-\int_{\xi_0}^{\xi}\frac{D_3(\xi)}{D_1(\xi)}\,d\xi\right) \quad [20]$$

If the elements of the third-order determinants are expanded in power series in $\pi/2 - \xi$, it is found that $D_1(\xi) = -a(\pi/2-\xi) + \ldots$, $D_2(\xi) = -b + \ldots$, $D_3(\xi) = c + \ldots$, where a, b, c are positive numbers with $0 < c/a < 1/2$. Consequently, for ξ near $\pi/2$, ω/T behaves like $(\omega_T/T)(\pi/2-\xi)^{c/a}$ and tends to zero as ξ tends to $\pi/2$; that is, the relative rotation of the two ring segments terminates when $\xi = \pi/2$, in view of Equations [15]. Therefore final deformations θ_{0f}, $\theta_{\pi f}$ may be obtained by integrating $d\theta_0/dt \equiv (d\theta_0/d\xi)\dot\xi$, $d\theta_\pi/dt = (d\theta_\pi/d\xi)\dot\xi$ up to $\xi = \pi/2$. Using these latter relations with Equations [15] we obtain the results

$$\frac{mr^2}{M_0}\frac{\theta_{0f}}{T^2} = \frac{mr^2}{M_0}\frac{\theta_{0T}}{T^2} + \frac{1}{2}\int_{\xi_0}^{\pi/2}(1+\cos\xi)\frac{\omega}{T^2\dot\xi}\,d\xi \quad [21a]$$

$$\frac{mr^2}{M_0}\frac{\theta_{\pi f}}{T^2} = \frac{mr^2}{M_0}\frac{\theta_{\pi T}}{T^2} + \frac{1}{2}\int_{\xi_0}^{\pi/2}(1-\cos\xi)\frac{\omega}{T^2\dot\xi}\,d\xi \quad [21b]$$

where the first terms on the right of Equations [21] are given by Equations [14] and [16]. Since $T\dot\xi$ behaves like $(\pi/2-\xi)^{1-c/a}$ when ξ is near $\pi/2$, $T\dot\xi \to 0$ as $\xi \to \pi/2$. However, $\omega/T^2\dot\xi$ behaves like $(\pi/2-\xi)^{2c/a-1}$ so that the improper integrals in Equations [21] exist.

Numerical integration must be used on the foregoing formulas. Since all the integrands have infinite singularities at $\pi/2$, numerical methods will be used up to $\xi = 1.5$ from which point the integrands are approximated to by the terms in their power series up to $(\pi/2-\xi)$. For this reason Equations [21] will be modified. Put

$$\Phi(\xi,\xi_0) = (1+\cos\xi)\frac{\omega}{T^2\dot\xi} \quad [22a]$$

$$\Psi(\xi,\xi_0) = (1-\cos\xi)\frac{\omega}{T^2\dot\xi} \quad [22b]$$

From the expansions previously given for D_1, D_2, D_3 it can be shown that for $1.5 \le \xi \le \pi/2$

$$\Phi(\xi,\xi_0) \cong \left(1+\frac{\pi}{2}-\xi\right)\left[\frac{\omega(1.5,\xi_0)}{T}\right]^2 \frac{b}{a}\frac{(\pi/2-\xi)^{2c/a-1}}{(\pi/2-1.5)^{2c/a}} \quad [23a]$$

$$\Psi(\xi, \xi_0) \cong \left[1 - \left(\frac{\pi}{2} - \xi\right)\right]\left[\frac{\omega(1.5, \xi_0)}{T}\right]^2 \frac{b}{a}\frac{(\pi/2 - \xi)^{2c/a-1}}{(\pi/2 - 1.5)^{2c/a}} \quad \ldots\ldots [23b]$$

Then Equations [21] become

$$\frac{mr^2}{M_0}\frac{\theta_{0f}}{T^2} = \frac{mr^2}{M_0}\frac{\theta_{0T}}{T^2} + \frac{1}{2}\int_{\xi_0}^{1.5}\Phi(\xi, \xi_0)d\xi + \frac{1}{2}\frac{b}{a}\left[\frac{\omega(1.5, \xi_0)}{T}\right]^2\left(\frac{a}{2c} + \frac{\frac{\pi}{2} - 1.5}{\frac{2c}{a} + 1}\right) \quad \ldots. [24a]$$

$$\frac{mr^2}{M_0}\frac{\theta_{\pi f}}{T^2} = \frac{mr^2}{M_0}\frac{\theta_{\pi T}}{T^2} + \frac{1}{2}\int_{\xi_0}^{1.5}\Psi(\xi, \xi_0)d\xi + \frac{1}{2}\frac{b}{a}\left[\frac{\omega(1.5, \xi_0)}{T}\right]^2\left(\frac{a}{2c} - \frac{\frac{\pi}{2} - 1.5}{\frac{2c}{a} + 1}\right) \quad \ldots. [24b]$$

which are the expressions for deformations used in the computations. The resulting (nondimensional) deformations are plotted against μ in Fig. 8.

Check on Numerical Results

When relative rotation of the two ring segments ceases, the velocities $\dot{y}_0$, $\dot{y}_\pi$ must be equal. Then either one may be used to compute the linear momentum of the ring. The impulse PT (for the rectangular load pulse) equals the momentum at any time $t \geq T$, and hence we can write the formulas

$$\mu_0 = 2\pi\frac{mr^2}{M_0}\frac{\dot{y}_0}{T} = 2\pi\frac{mr^2}{M_0}\frac{\dot{y}_\pi}{T} \quad \ldots\ldots [25]$$

From considerations like those leading to Equation [12], it is evident that we can write solutions in the form

$$\frac{mr^2}{M_0}\ddot{y}_0 = \frac{D_0(\xi) - \frac{\mu}{2}\bar{D}_0(\xi)}{D_2(\xi)} \quad \ldots\ldots [26a]$$

$$\frac{mr^2}{M_0}\ddot{y}_\pi = \frac{D_\pi(\xi) - \frac{\mu}{2}\bar{D}_\pi(\xi)}{D_2(\xi)} \quad \ldots\ldots [26b]$$

where D_0, $\bar{D}_0$ are derivable from $\Delta_1(\mu, \xi)$, and D_π, $\bar{D}_\pi$ from $\Delta_2(\mu, \xi)$ of Equations [10]. Integration is first performed while μ is constant, the results at $t = T$ being

$$\frac{mr^2}{M_0}\frac{\dot{y}_{0T}}{T} = \frac{D_0(\xi_0) - \frac{\mu_0}{2}\bar{D}_2(\xi_0)}{D_2(\xi_0)} \quad \ldots\ldots [27a]$$

$$\frac{mr^2}{M_0}\frac{\dot{y}_{\pi T}}{T} = \frac{D_\pi(\xi_0) - \frac{\mu_0}{2}\bar{D}_\pi(\xi_0)}{D_2(\xi_0)} \quad \ldots\ldots [27b]$$

For $T < t$, $\mu = 0$ and Equations [26] become

$$\frac{mr^2}{TM_0}\frac{d\dot{y}_0}{d\xi} = \frac{D_0(\xi)}{T\xi D_2(\xi)} \equiv -A(\xi, \xi_0) \quad \ldots\ldots [28a]$$

$$\frac{mr^2}{TM_0}\frac{d\dot{y}_\pi}{d\xi} = \frac{D_\pi(\xi)}{T\xi D_2(\xi)} \equiv B(\xi, \xi_0) \quad \ldots\ldots [28b]$$

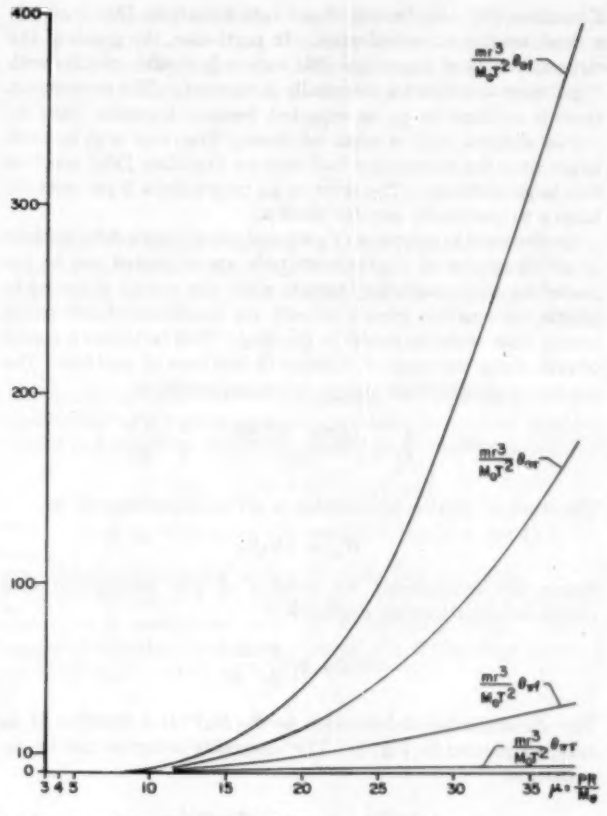

Fig. 8 Final Deformations Versus $\mu = Pr/M_0$ for Rectangular Force Pulse

Approximations for A and B when $1.5 \leq \xi \leq \pi/2$ are obtained in the same manner as before with $D_0 = c/2 + 2\pi(\pi/2 - \xi) + \ldots$, $D_\pi = -c/2 + 2\pi(\pi/2 - \xi) + \ldots$. Then for $1.5 \leq \xi \leq \pi/2$ it can be shown that

$$A(\xi, \xi_0) \cong \frac{\omega(1.5, \xi_0)}{Ta\left(\frac{\pi}{2} - 1.5\right)^{c/a}}\left\{\frac{c}{2}\left(\frac{\pi}{2} - \xi\right)^{c/a-1} + 2\pi\left(\frac{\pi}{2} - \xi\right)^{c/a}\right\} \quad \ldots. [29a]$$

$$B(\xi, \xi_0) \cong \frac{\omega(1.5, \xi_0)}{Ta\left(\frac{\pi}{2} - 1.5\right)^{c/a}}\left\{\frac{2}{c}\left(\frac{2}{\pi} - \xi\right)^{c/a-1} - 2\pi\left(\frac{\pi}{2} - \xi\right)^{c/a}\right\} \quad \ldots. [29b]$$

Using these approximations, integration of Equations [28] up to $\xi = \pi/2$ gives

$$\frac{mr^2}{M_0}\frac{\dot{y}_0}{T} = \frac{mr^2}{M_0}\frac{\dot{y}_{0T}}{T} - \int_{\xi_0}^{1.5}A(\xi, \xi_0)d\xi - \frac{\omega(1.5, \xi_0)}{T}\left[\frac{1}{2} + \frac{2\pi}{a + c}\left(\frac{\pi}{2} - 1.5\right)\right] \quad \ldots. [30a]$$

$$\frac{mr^2}{M_0}\frac{\dot{y}_\pi}{T} = \frac{mr^2}{M_0}\frac{\dot{y}_{\pi T}}{T} + \int_{\xi_0}^{1.5}B(\xi, \xi_0)d\xi + \frac{\omega(1.5, \xi_0)}{T}\left[\frac{1}{2} - \frac{2\pi}{a + c}\left(\frac{\pi}{2} - 1.5\right)\right] \quad \ldots. [30b]$$

Equations [30] may be introduced into Equations [25] to obtain a check on the numerical work. In particular, the graph of the right members of Equations [25] versus ξ_0 should coincide with Fig. 7 since this figure is essentially μ_0 versus ξ_0. The error shown there is smallest for $\dot{y}_\pi$, as expected, because Equation [30b] involves addition only of small numbers. The error in $\dot{y}_0$ is much larger since the subtraction indicated by Equation [30a] involves two large numbers. The error in $\dot{y}_\pi$ ranges from 9 per cent for large μ to practically zero for small μ.

As discussed in reference (1), an analysis of plastic deformations in which strains of elastic magnitude are neglected can be expected to give satisfactory results when the energy absorbed in plastic deformation greatly exceeds the maximum elastic strain energy that could be stored in the ring. This furnishes a means of estimating the range of validity of this type of analysis. The maximum elastic strain energy can be estimated as

$$W_e = \int_0^{2\pi} \frac{M_0^2 \cos^2 \varphi \, r \, d\phi}{2EI} = \frac{\pi}{2} \frac{M_0^2 r}{EI}$$

The work of plastic deformation is given approximately by

$$W_p = 2M_0\theta_{0f}$$

Hence the requirement for validity of the assumption that elastic deformations are negligible is

$$2M_0\theta_{0f} \gg \frac{\pi}{2} \frac{M_0^2 r}{EI}$$

The dimensionless deformation $mr^2\theta_{0f}/M_0T^2$ is a function of μ_0 only, as plotted in Fig. 8. The inequality criterion can be rewritten as

$$\frac{mr^2\theta_{0f}}{M_0T^2} = f(\mu_0) \gg \frac{\pi}{4} \frac{mr^4}{EIT^2}$$

The period τ of the lowest flexural mode of free vibration of the ring is given by

$$\tau = 2\pi \frac{\sqrt{5}}{6} \sqrt{\frac{mr^4}{EI}}$$

Hence the foregoing inequality can be expressed as

$$\frac{mr^2\theta_{0f}}{M_0T^2} = f(\mu_0) \gg \frac{9}{20\pi} \frac{\tau^2}{T^2} = 0.14 \frac{\tau^2}{T^2}$$

This inequality, in conjunction with Fig. 8, provides a convenient means for estimating the value of the load μ_0, for a given period ratio τ/T, above which the neglect of elastic deformations in the present analysis can be expected to be justified. Conversely, for a given load magnitude μ_0, the foregoing inequality can be used to estimate the upper limit of the ratio τ/T above which the present results should be valid.

Conclusion

The present results for a rectangular force pulse can probably be used to obtain fair estimates of the deformations which force pulses of quite different shapes will produce. Solutions of other problems (3), (4) have been carried out for a variety of force pulse shapes, e.g., a half-sine pulse, a triangular, or an exponential pulse, as well as for a rectangular pulse. Comparison of the results of these solutions shows that the curves of dimensionless deformation (analogous to that plotted in Fig. 8) for the rectangular pulse of duration T, and maximum dimensionless load μ_0 give reasonably good values of the same dimensionless parameter for other force pulse shapes, provided in all cases μ_0 stands for the peak load and T stands for the time such that $\mu_0 T$ is the total impulse $\int_0^\infty \mu \, dt$. Hence the dimensionless deformations plotted in Fig. 8 can be used tentatively to estimate the corresponding quantity for force pulses of general shape, by interpreting μ_0 as the peak (dimensionless) load and T as the total impulse divided by peak load.

It should also be re-emphasized that the present analysis assumes geometry changes can be neglected in the equations of motion, so that the results cannot be expected to hold when the distortions are very large. It would be desirable to investigate these and other neglected effects experimentally as well as analytically.

Bibliography

1 "Large Plastic Deformation of Beams Under Transverse Impact," by E. H. Lee and P. S. Symonds, Journal of Applied Mechanics, Trans. ASME, vol. 74, 1952, pp. 308–314.

2 "The Calculus of Observations," by E. T. Whittaker and G. Robinson, Blackie & Son, Ltd., London, England, fourth edition, 1944, p. 71.

3 "Dynamic Load Characteristics in Plastic Bending of Beams," by P. S. Symonds, Journal of Applied Mechanics, Trans. ASME, vol. 75, 1953, pp. 475–481.

4 "Large Plastic Deformations of Beams Under Blast Type Loading," by P. S. Symonds, Technical Report All-99 of Brown University to Office of Naval Research; Proceedings of Second U. S. National Congress of Applied Mechanics, Ann Arbor, Mich., June, 1954.

5 "The Limit Design of Arches," by E. T. Onat and W. Prager, *Journal of Mechanics and Physics of Solids*, vol. 1, 1953, pp. 77–89.

Appendix

Figs. 4 and 5 show free-body diagrams of the two ring segments of arc ξ, $\pi - \xi$, respectively. The radii $\bar{r}_0$, $\bar{r}$ of the centers of mass of the segments, and their centroidal moments of inertia I_0, I_π are given by the following expressions

$$\left.\begin{aligned} \bar{r}_0 &= \frac{2r}{\xi} \sin \frac{\xi}{2}; \quad \bar{r}_\pi = \frac{2r}{\pi - \xi} \cos \frac{\xi}{2} \\ I_0 &= \frac{mr^2}{\xi} [\xi^2 - 2(1 - \cos \xi)]; \\ I_\pi &= \frac{mr^2}{\pi - \xi} [(\pi - \xi)^2 - 2(1 + \cos \xi)] \end{aligned}\right\} \quad \ldots [31]$$

The equations of motion for the lower segment may be obtained from Fig. 4. These are

$$\frac{P}{2} - N_\xi \sin \xi = mr\xi \left(\ddot{y}_0 + \bar{r}_0 \sin \frac{\xi}{2} \dot{\omega}_0 \right) \ldots\ldots [32]$$

$$N_0 - N_\xi \cos \xi = -mr\xi \left(r - \bar{r}_0 \cos \frac{\xi}{2} \right) \dot{\omega}_0 \ldots\ldots [33]$$

$$2M_0 + N_0 \left(r - \bar{r}_0 \cos \frac{\xi}{2} \right) - N_\xi \left(r - \bar{r}_0 \cos \frac{\xi}{2} \right) - P \frac{\bar{r}_0}{2} \sin \frac{\xi}{2} = I_\xi \dot{\omega}_0 \ldots [34]$$

After introducing into Equations [32] and [33] the values for $\bar{r}_0$, I_0 from Equations [31], the following equations are obtained

$$N_0 \sin \xi = \frac{P}{2} \cos \xi - mr\xi \cos \xi \ddot{y}_0 + mr^2(1 - \cos \xi - \xi \sin \xi)\dot{\omega}_0 \ldots [35]$$

$$N_\xi \sin \xi = \frac{P}{2} - mr\xi \ddot{y}_0 - mr^2(1 - \cos \xi)\dot{\omega}_0 \ldots\ldots [36]$$

Equation [6.1] results from combining Equations [34], [35], and [36], and introducing the notation defined in the text.

Similarly, the equations for the upper segment are obtained from Fig. 5. We obtain

$$N_\xi \sin \xi = mr(\pi - \xi)\left[\ddot{y}_\pi + \ddot{r}_\pi \sin \frac{\pi - \xi}{2}\dot{\omega}_\pi\right] \ldots [37]$$

$$N_\xi \cos \xi - N_\pi = mr(\pi - \xi)\left(r - \ddot{r}_\pi \cos \frac{\pi - \xi}{2}\right)\dot{\omega}_\pi \ldots [38]$$

$$-2M_b + (N_\pi + N_\xi)\left(r - \ddot{r}_\pi \cos \frac{\pi - \xi}{2}\right) = I_\pi \dot{\omega}_\pi \ldots [39]$$

Combining Equations [37] and [38], after introducing $\ddot{r}_\pi$, I_π from Equations [31], yields the result

$$N_\pi \sin \xi = mr(\pi - \xi)(\cos \xi)\ddot{y}_\pi + mr^2[1 + \cos \xi - (\pi - \xi) \sin \xi]\dot{\omega}_\pi \ldots [40]$$

and substituting this equation and [37] into [39] gives Equation [6.2].

Finally, elimination of N_ξ between Equations [32], [37] leads to the third independent equation of equilibrium, Equation [6.3].

The remaining two equations relating the five unknowns ($\dot{v}_0$, $\ddot{r}_\pi$, $\dot{\omega}_0$, $\dot{\omega}_\pi$, ξ) are equations of kinematic conditions. They follow from the fact that the vector displacement is continuous across the hinge section. This can be shown to imply that the vector velocity is continuous across the hinge, but the vector acceleration is, in general, discontinuous, the jump being proportional to the product $\dot{\xi}(\omega_\pi - \omega_0)$. The appropriate equations can be derived in a manner very similar to that used in (1). Equations for the two components of displacement are the starting point

$$\left.\begin{aligned} y - y_0 &= r\int_0^\varphi \theta \cos \varphi \, d\varphi \\ x - x_0 &= -r\int_0^\varphi \theta \sin \varphi \, d\varphi \end{aligned}\right\} \ldots\ldots\ldots [41]$$

Here $\theta(\varphi, t)$ stands for the small rotation (positive counterclockwise) of an infinitesimal segment $r\,d\varphi$ at a point specified by φ. For a point with $\varphi > \xi$, each integral must be written in the form

$$\int_0^\xi + \int_\xi^\varphi$$

Differentiation with respect to time, as in (1), then leads to equations relating velocities and accelerations to angular displacements and velocities and to $\dot{\xi}$. In this way it can be shown that

$$\dot{y}_0 - \dot{y}_\pi = r(\omega_\pi - \omega_0) \sin \xi$$

$$\dot{x}_0 - \dot{x}_\pi = 0 = r\omega_0(1 - \cos \xi) + r\omega_\pi(1 + \cos \xi)$$

and that Equations [6.4] and [6.5] of the text are valid.

In the derivation it is assumed, as in (1), that the angular deformation is continuous except at a stationary hinge. The increase of curvature at a point through which the hinge passes is given by $(\omega_\pi - \omega_0)/r\dot{\xi}$, as in (1).

Torsion of Circular Shafts of Variable Diameter

By M. M. ABBASSI,[1] ALEXANDRIA, EGYPT

By using spherical polar co-ordinates, the stress function for circular shafts of variable diameter is expressed in terms of the Legendre associated functions of the second order. It is obtained for various curves forming the generating surface of the shaft.

Introduction

THE general theory of the problem of torsion of circular shafts of variable diameter was given by Michell (1)[2] and Love (2). The stress functions are already obtained for some shapes of curves forming the generating surface of the shaft.

Consider a shaft in the form of a body of revolution twisted by couples M_t applied at the ends. The axis of the shaft is taken as the z-axis.

Using cylindrical polar co-ordinates (r, θ, z), where r and θ define the position of a point in the plane of a cross section, the only nonvanishing stresses are $\widehat{r\theta}$ and $\widehat{\theta z}$ and these are given by

$$\widehat{r\theta} = -\frac{1}{r^2}\frac{\partial \psi}{\partial z}, \quad \widehat{\theta z} = \frac{1}{r^2}\frac{\partial \psi}{\partial r} \ldots\ldots\ldots\ldots [1]$$

where ψ is a stress function satisfying the equation

$$\frac{\partial^2 \psi}{\partial r^2} - \frac{3}{r}\frac{\partial \psi}{\partial r} + \frac{\partial^2 \psi}{\partial z^2} = 0 \ldots\ldots\ldots\ldots [2]$$

(reference 3). Different solutions of Equation [2] were given by Poritsky (4) and Wilhoit (5).

The condition that the surface is free from traction is given by

$$\psi = \text{const on entire surface} \ldots\ldots\ldots\ldots [3]$$

The magnitude of the torque M_t at any cross section of radius a is given by

$$M_t = \int_0^{2\pi}\int_0^a \widehat{\theta z}\, r^2\, dr\, d\theta = 2\pi \int_0^a r^2\, \widehat{\theta z}\, dr = 2\pi \int_0^a \frac{\partial \psi}{\partial r}\, dr$$

or

$$M_t = 2\pi[\psi(a, z) - \psi(0, z)] \ldots\ldots\ldots\ldots [4]$$

Solution in Spherical Co-Ordinates

Putting $\psi = r^2 F$ where F is a function of r and z, Equation [2] becomes

$$\frac{\partial^2 F}{\partial r^2} + \frac{1}{r}\frac{\partial F}{\partial r} + \frac{\partial^2 F}{\partial z^2} - \frac{4F}{r^2} = 0 \ldots\ldots\ldots [5]$$

To find the solution in the spherical co-ordinates (R,ϕ,θ) we put

$$z = R\cos\phi,\ r = R\sin\phi,\ \theta = \theta$$

and noting that

$$\frac{\partial}{\partial z} = \cos\phi\frac{\partial}{\partial R} - \frac{\sin\phi}{R}\frac{\partial}{\partial \phi}$$

$$\frac{\partial}{\partial r} = \sin\phi\frac{\partial}{\partial R} + \frac{\cos\phi}{R}\frac{\partial}{\partial \phi}$$

Equation [5] becomes

$$\frac{\partial^2 F}{\partial R^2} + \frac{2}{R}\frac{\partial F}{\partial R} + \frac{1}{R^2}\frac{\partial^2 F}{\partial \phi^2} + \frac{\cot\phi}{R^2}\frac{\partial F}{\partial \phi} - \frac{4F}{R^2\sin^2\phi} = 0 \ldots [6]$$

The substitution $F = wR^n$ or $F = w/R^{n+1}$ in Equation [6] where w is a function of ϕ only gives (6)

$$\frac{d^2 w}{d\phi^2} + \cot\phi\frac{dw}{d\phi} + \left[n(n+1) - \frac{4}{\sin^2\phi}\right]w = 0 \ldots [7]$$

Denoting $\cos\phi = z/R$ by x, Equation [7] reduces to

$$(1-x^2)\frac{d^2 w}{dx^2} - 2x\frac{dw}{dx} + \left[n(n+1) - \frac{4}{1-x^2}\right]w = 0 \ldots [8]$$

Equation [8] is the Legendre associated equation and is satisfied by $P_n^2(x)$ and $Q_n^2(x)$ which are the Legendre associated functions of degree n and order 2, of the first and second kind, respectively (7, 8).

Its general solution is given by

$$w = AP_n^2(x) + BQ_n^2(x)$$

where A,B are constants. It follows that the general solution for the stress function ψ is given by

$$\frac{\psi}{r^2} = \sum_{n=0}^{\infty}\left(A_n R^n + \frac{B_n}{R^{n+1}}\right)P_n^2(x) + \left(C_n R^n + \frac{D_n}{R^{n+1}}\right)Q_n^2(x) \ldots [9]$$

It is known that both $P_0^2(x)$ and $P_1^2(x)$ are equal to zero and, therefore, there must be two special solutions for Equation [8] when $n = 0$ and $n = 1$. Putting $n = 0$, Equation [8] becomes

$$(1-x^2)\frac{d^2 w}{dx^2} - 2x\frac{dw}{dx} - \frac{4}{1-x^2}w = 0 \ldots\ldots [10]$$

Since $Q_0^2(x)$ is a solution of Equation [10] and noting that

$$Q_0^2(x) = \frac{2x}{1-x^2}$$

it can be easily found that

$$w = (1-x)/(1+x)$$

---

[1] Assistant Professor of Mathematics, Alexandria University.

[2] Numbers in parentheses refer to the Bibliography at the end of the paper.

Presented at the National Conference of the Applied Mechanics Division, Troy, N. Y., June 16–18, 1955, of The American Society of Mechanical Engineers.

Discussion of this paper should be addressed to the Secretary, ASME, 29 West 39th Street, New York, N. Y., and will be accepted until January 10, 1956, for publication at a later date. Discussion received after the closing date will be returned.

Note: Statements and opinions advanced in papers are to be understood as individual expressions of their authors and not those of the Society. Manuscript received by ASME Applied Mechanics Division, September 14, 1954. Paper No. 55—APM-19.

is also a solution of Equation [10]. Hence the missing solution of Equation [8] when $n = 0$ and which is not given by the general solution, Equation [9], leads to a stress function ψ where

$$\frac{\psi}{r^2} = \left(A_0 + \frac{B_0}{R}\right)\frac{1-x}{1+x} \quad \ldots\ldots\ldots\ldots [11]$$

Similarly, putting $n = 1$, Equation [8] becomes

$$(1-x^2)\frac{d^2w}{dx^2} - 2x\frac{dw}{dx} - 2\frac{1+x^2}{1-x^2}w = 0 \ldots\ldots [12]$$

Since

$$Q_1^2(x) = \frac{2}{1-x^2}$$

is a solution of Equation [12], it can be easily shown that

$$w = \frac{(1-x)(2+x)}{(1+x)}$$

is also a solution of Equation [12]. Hence the missing solution of Equation [8] when $n = 1$ and which is not given by the general solution, Equation [9], leads to a stress function ψ where

$$\frac{\psi}{r^2} = \left(A_1 R + \frac{B_1}{R^2}\right)\frac{(1-x)(2+x)}{1+x} \quad \ldots\ldots\ldots [13]$$

The solutions given by $Q_n^2(x)$ are in most cases not of practical importance and do not make the right-hand side of Equation [4] constant but depend on z which is impossible since M_t is constant. Putting $C_n = D_n = 0$ in Equation [9], and adding to the general solution, Equation [9], those given by Equations [11] and [13] we get

$$\frac{\psi}{r^2} = \left(A_0 + \frac{B_0}{R}\right)\frac{1-x}{1+x} + \left(A_1 R + \frac{B_1}{R^2}\right)\frac{(1-x)(2+x)}{1+x} + \sum_{n=2}^{\infty}\left(A_n R^n + \frac{B_n}{R^{n+1}}\right)P_n^2(x) \ldots [14]$$

Putting $x = \cos\phi$ and $r = R\sin\phi$, we obtain the following solution for the stress function ψ

$$\psi = (A_0 R^2 + B_0 R)(1-\cos\phi)^2 + (A_1 R^3 + B_1)(1-\cos\phi)^2(2+\cos\phi) + \sum_{n=2}^{\infty}\left(A_n R^{n+2} + \frac{B_n}{R^{n-1}}\right)\sin^2\phi P_n^2(\cos\phi) \ldots [15]$$

$P_n^2(\cos\phi)$ can be obtained for different values of n by using the following recurrence relation

$$(n-1)P_{n+1}^2(\cos\phi) - (2n+1)\cos\phi\, P_n^2(\cos\phi) + (n+2)P_{n-1}^2(\cos\phi) = 0 \ldots\ldots [16]$$

(reference 9).

Knowing that

$$P_0^2(\cos\phi) = P_1^2(\cos\phi) = 0 \text{ and } P_2^2(\cos\phi) = 3\sin^2\phi$$

we obtain the following values of $P_n^2(\cos\phi)$

$$P_2^2(\cos\phi) = 3\sin^2\phi$$

$$P_3^2(\cos\phi) = 15\cos\phi\sin^2\phi$$

$$P_4^2(\cos\phi) = \frac{15}{2}\sin^2\phi(7\cos^2\phi - 1)$$

$$P_5^2(\cos\phi) = \frac{105}{2}\sin^2\phi\cos\phi(3\cos^2\phi - 1)$$

and so on.

Possible Shapes of Circular Shafts of Variable Diameter

The solution given by Equation [15] leads to possible shapes of circular shafts of variable diameter. We shall now consider some simple curves forming the generating surface of the shaft.

1 Consider a solution of Equation [15] obtained by putting all constants saving A_3 equal to zero. We have

$$\psi = A_3 R^5 \sin^3\phi\, P_3^2(\cos\phi)$$
$$= 15\, A_3 R^5 \sin^4\phi\cos\phi$$
$$= 15\, A_3 r^4 Z$$

or

$$\psi = cr^4 Z$$

The shaft whose generating curve is given by $r^4 Z = k$, where k is a constant, has $\psi = cr^4 Z$ as a stress function. Equation [4] gives

$$C = \frac{M_t}{2\pi k}$$

The shape of the shaft is shown in Fig. 1.

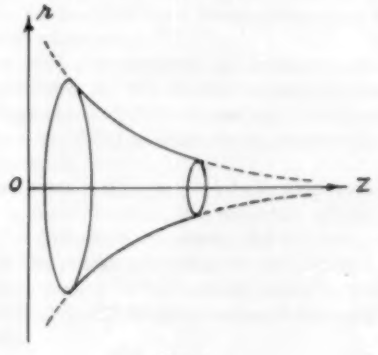

FIG. 1

2 Consider a solution of Equation [15] obtained by putting all constants saving A_4 equal to zero. We have

$$\psi = A_4 R^6 \sin^2\phi\, P_4^2(\cos\phi)$$
$$= \frac{15}{2}A_4 R^6 \sin^4\phi(7\cos^2\phi - 1)$$
$$= \frac{15}{2}A_4 r^4(6Z^2 - r^2)$$

or

$$\psi = cr^4(r^2 - 6Z^2)$$

The shaft whose generating curve is given by

$$r^6 - 6r^4 Z^2 = k$$

where k is a constant has

$$\psi = cr^4(r^2 - 6Z^2)$$

as a stress function.

Equation [4] gives

$$C = \frac{M_t}{2\pi k}$$

The shape of the shaft is shown in Fig. 2.

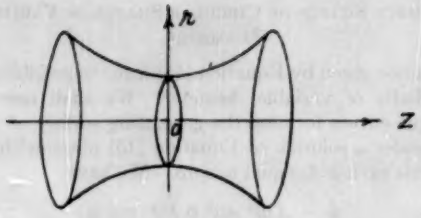

FIG. 2

Other solutions of Equation [15] can be similarly obtained.

It should be mentioned that the stress functions for long shafts of constant diameter, conical and paraboloid shafts also can be obtained from Equation [15] by putting all constants zero except A_3, B_1, and A_0 in the first, second, and third case, respectively.

The author recommends reference (10) for further literature on the subject.

BIBLIOGRAPHY

1 "The Uniform Torsion and Flexure of Incomplete Tores, With Application to Helical Springs," by J. H. Michell, Proceedings of the London Mathematical Society, London, England, vol. 31, 1900, p. 141.

2 "A Treatise on the Mathematical Theory of Elasticity," by A. E. H. Love, Cambridge University Press, Cambridge, England, fourth edition, 1927.

3 "Theory of Elasticity," by S. Timoshenko, McGraw-Hill Book Company, Inc., New York, N. Y., 1934.

4 "Stress Fields of Axially Symmetric Shafts in Torsion and Related Fields," by H. Poritsky, Proceedings of Symposia on Applied Mathematics, vol. 3, 1950, p. 163.

5 "An Addition to Poritsky's Solutions of a Differential Equation of Torsion," by J. C. Wilhoit, Jr., *Quarterly of Applied Mathematics*, vol. 11, January, 1954, p. 499.

6 "Torsion of a Circular Cylinder Having a Spherical Cavity," by C. B. Ling, *Quarterly of Applied Mathematics*, vol. 10, July, 1952, p. 149.

7 "Spherical Harmonics," by T. M. MacRobert, Dover Publications, New York, N. Y., second revised edition, 1948.

8 "Applied Mathematics for Engineers and Physicists," by L. A. Pipes, McGraw-Hill Book Company, Inc., New York, N. Y., 1946.

9 "Partial Differential Equations in Physics," by A. Sommerfeld, Lectures on Theoretical Physics, Academic Press, New York, N. Y., vol. 6, 1949, p. 132.

10 "Kerbspannungslehre, Grundlagen für genaue Spannungsrechnung," by H. Neuber, Julius Springer, Berlin, Germany, 1937; English translation by David Taylor Model Basin, Navy Department, Washington, D. C., 1945.

Large Plastic Deformations of Circular Membranes

By N. A. WEIL[1] and N. M. NEWMARK[2]

An investigation is presented for the plastic behavior of clamped circular membranes subjected to hydrostatic pressure, based on the Hencky-Mises theory. New strain-displacement relations, valid for finite deformations in the plastic domain, are introduced. The solution is presented in terms of two simultaneous implicit integral equations, which can be solved by numerical methods. The solution also permits the formulation of the instability condition. Experimental work consisted of bulge tests carried out on annealed copper plates of two thicknesses, whose τ-γ curve was previously determined from uniaxial tests. A good correlation is obtained between theoretical predictions and experimental results.

Nomenclature

The following nomenclature is used in the paper:

N = force per unit width, lb/in.
a = radius of undeflected diaphragm, in.
h = thickness of membrane, in.
σ = N/h = true stress, psi
ϵ = natural strain
τ = octahedral shear stress, psi
γ = octahedral shear strain
P = hydrostatic pressure, psi
p = $Pa/\bar{h}$ = relative pressure, psi
η = $h/\bar{h}$ = dimensionless thinning
r = radial distance from pole, in.
ρ = r/a = dimensionless radial distance
w = vertical deflection, in.
ω = w/a = dimensionless deflection
u = horizontal displacement, in.
v = u/a = dimensionless horizontal displacement
R = radial radius of curvature, in.

Subscripts r, θ, z denote quantities acting in meridional, circumferential, and normal (i.e., principal) directions. Subscript o refers to variables at pole (crown). Overbars represent quantities in the undeformed flat plate.

Introduction

The plastic behavior of thin, clamped diaphragms subjected to lateral pressure has been the subject of numerous investigations. Experimental studies employing the "bulge test" aimed at the evaluation of the bursting pressure of frangible disks (1, 2, 3)[3] or at the affirmation of plasticity laws in metals (4, 5, 6, 7). Hydraulic bulging of thin metal plates is particularly suitable for the latter aspect, since bulging yields instability strains in the neighborhood of 0.7 to 1.1 (6), and has a consistency superior to that of the uniaxial tensile test (8). Studies also were made to attempt a formulation of the instability condition for hydraulically formed bulges (7, 9).

A detailed treatment of the hydraulically formed bulge was presented by Gleyzal (10). Agreement between his analysis and experimental values is outstanding at low loads; in the vicinity of the instability pressure, the deviation of theory from experiments is of the order of 15 to 20 per cent. An approximate solution of this problem was evolved by Hill (11) for materials whose plastic properties can be described by a linear stress-strain relationship with reasonable accuracy.

The current work is an extension of Gleyzal's analysis. An improved law governing the relationship between strains and deformations for large plastic deflections has been introduced,[4] and the end results were simplified to allow for an easier evaluation of the governing quantities.

The analysis assumes that the τ-γ relationship (universal stress-strain curve) is known for the given material. Elastic strains are neglected in the derivation; similarly, the τ-γ curve is supposed to reflect only the plastic properties of the material. A dimensionless notation is used throughout the paper to provide for an easy adaptation of results to various sizes of diaphragms made of different metals.

Plasticity Laws

The derivation is based on Hencky's "deformation"-theory

$$\left.\begin{aligned} \epsilon_i &= \gamma[\sigma_i - (\sigma_j + \sigma_k)/2]/3\tau \\ i, j, k &= 1, 2, 3 \text{ and } i \neq j \neq k \end{aligned}\right\} \quad \ldots\ldots\ldots [1]$$

and the Mises flow conditions

$$\left.\begin{aligned} \tau &= [(\sigma_1 - \sigma_2)^2 + (\sigma_2 - \sigma_3)^2 + (\sigma_3 - \sigma_1)^2]^{1/2}/3 \\ \dot{\gamma} &= 2[(\epsilon_1 - \epsilon_2)^2 + (\epsilon_2 - \epsilon_3)^2 + (\epsilon_3 - \epsilon_1)^2]^{1/2}/3 \end{aligned}\right\} \quad \ldots [2]$$

It is further assumed that materials are incompressible in the plastic range, that is

$$\sum_{i=1}^{3} \epsilon_i = 0 \quad \ldots\ldots\ldots\ldots\ldots\ldots [3]$$

In a thin diaphragm the principal stresses and strains lie in the radial, circumferential, and normal directions of the membrane, as shown in Fig. 1(*a*); also the average normal stress is negligible as compared to the other two principal stresses, so that it is admissible to set $\sigma_3 = \sigma_z = 0$. Therefore Equations [1] and [2] can be reduced to

---

[1] Development Engineer, The M. W. Kellogg Company, New York, N. Y.

[2] Research Professor, Structural Engineering, University of Illinois, Urbana, Ill. Mem. ASME.

Presented at the National Conference of the Applied Mechanics Division, Troy, N. Y., June 16–18, 1955, of The American Society of Mechanical Engineers.

Discussion of this paper should be addressed to the Secretary, ASME, 29 West 39th Street, New York, N. Y., and will be accepted until January 10, 1956, for publication at a later date. Discussion received after the closing date will be returned.

Note: Statements and opinions advanced in papers are to be understood as individual expressions of their authors and not those of the Society. Manuscript received by ASME Applied Mechanics Division, September 10, 1954. Paper No. 55—APM-20.

[3] Numbers in parentheses refer to the Bibliography at the end of the paper.

[4] These strain-displacement laws are similar to the ones developed by McGregor, Coffin, and Fisher (12) for the analysis of large deflections of thick-walled cylinders in the plastic region.

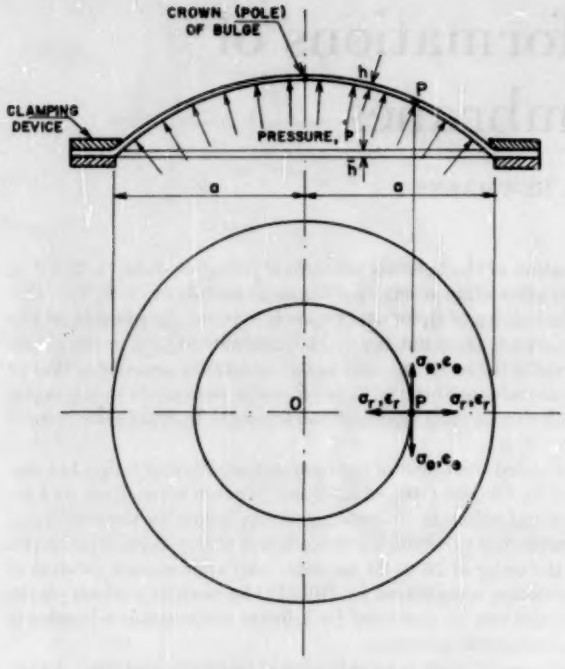

FIG. 1(a) PRINCIPAL STRESSES AND STRAINS

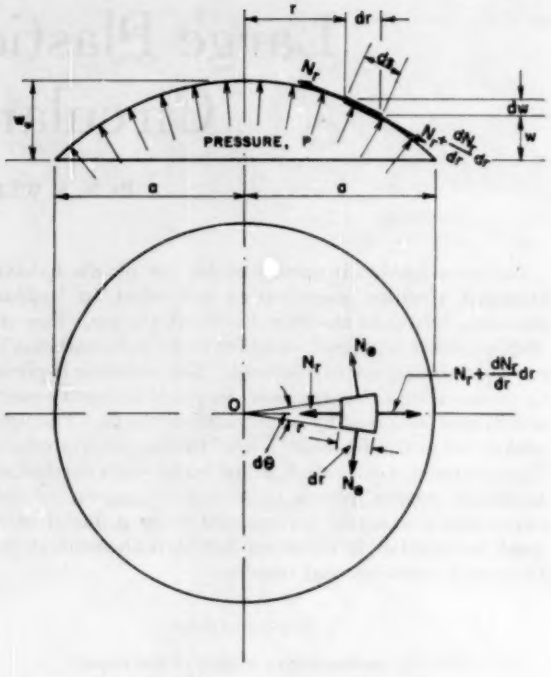

FIG. 1(b) FORCES ACTING ON A SMALL ELEMENT

$$\left.\begin{aligned}\sigma_r &= 2\tau(2\epsilon_r + \epsilon_\theta)/\gamma \\ \sigma_\theta &= 2\tau(2\epsilon_\theta + \epsilon_r)/\gamma\end{aligned}\right\} \quad \ldots\ldots [4]$$

$$\left.\begin{aligned}\tau &= \sqrt{2}(\sigma_r^2 - \sigma_r\sigma_\theta + \sigma_\theta^2)^{1/2}/3 \\ \gamma &= 2\sqrt{2}(\epsilon_r^2 + \epsilon_r\epsilon_\theta + \epsilon_\theta^2)^{1/2}/\sqrt{3}\end{aligned}\right\} \quad \ldots\ldots [5]$$

STRAIN-DISPLACEMENT RELATIONSHIPS

The initial and "stretched" infinitesimal lengths on the bulged diaphragm, as shown in Fig. 2(*a*), can be given by

$$\left.\begin{aligned}d\bar{s}^2 &= d\bar{r}^2 + \bar{r}^2 d\bar{\theta}^2 \\ ds^2 &= dr^2 + r^2 d\theta^2 + dw^2\end{aligned}\right\} \quad \ldots\ldots [6]$$

The radial displacements can be expressed as

$$u = r - \bar{r} \quad \ldots\ldots [7]$$

The natural surface strain in any direction will be derived from the basic formula

$$\epsilon_i = \ln\left(\frac{ds}{d\bar{s}}\right)_i \quad \ldots\ldots [8]$$

where the subscript indicates the orientation of strain.

In the radial direction $d\theta = d\bar{\theta} = 0$; using this condition and Equations [6] and [7] one obtains

$$\left(\frac{ds}{d\bar{s}}\right)_r = \left[1 + \left(\frac{dw}{dr}\right)^2\right]^{1/2}\left(1 - \frac{du}{dr}\right)^{-1}$$

Expanding this expression, ignoring all terms past the second power of infinitesimals, and inserting the resulting expression into Equation [8] yields the dimensionless form

$$\epsilon_r = \ln\left[1 + v' + \frac{1}{2}(\omega')^2\right] \quad \ldots\ldots [9]$$

where primes denote differentiation with respect to ρ.

In the circumferential direction $d\bar{r} = 0$, $d\theta = d\bar{\theta}$ and, from Equation [7], $dr = du$. Therefore

$$\left(\frac{ds}{d\bar{s}}\right)_\theta = \frac{1}{\bar{r}}\left[\left(\frac{du}{d\theta}\right)^2 + r^2 + \left(\frac{dw}{d\theta}\right)^2\right]^{1/2}$$

Since $df/d\theta = 0$ by radial symmetry, the dimensionless form of the circumferential strain becomes

$$\epsilon_\theta = \ln\frac{\rho}{\rho - v} \quad \ldots\ldots [10]$$

Lastly, the normal (through thickness) strain can be simply given by

$$\epsilon_z = \ln\frac{h}{\bar{h}}$$

which, by the law of volume constancy, modifies to (in dimensionless form)

$$\eta = \exp\epsilon_z = \exp(-\epsilon_r - \epsilon_\theta) \quad \ldots\ldots [11]$$

EQUATIONS OF STATIC EQUILIBRIUM

The forces acting on a cap of radius r cut from the center of the deflected diaphragm are shown in Fig. 2(*b*). Equilibrium of the vertical force components demands that

$$\pi r^2 P = 2\pi r N_r \frac{dw}{(dw^2 + dr^2)^{1/2}}$$

Introduction of dimensionless quantities modifies this equation to

$$\sigma_r = \rho p[1 + (\omega')^2]^{1/2}/2\eta \quad \ldots\ldots [12]$$

A second equation of statics is obtained by considering the equilibrium of forces on an infinitesimally small element, as shown in Fig. 1(*b*). Projection of forces in the meridional tangent direction yields

$$N_\theta\, ds\, d\theta\frac{dr}{ds} - (r + dr)d\theta(N_r + dN_r) + r\, d\theta\, N_r = 0$$

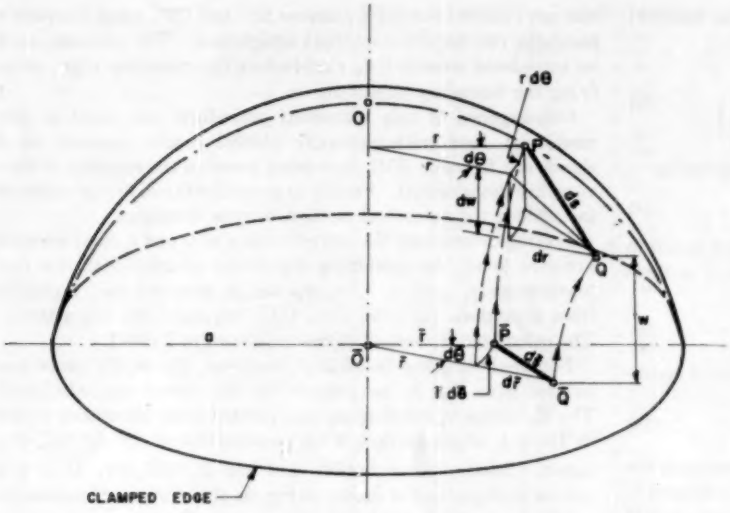

FIG. 2(a) VARIATION OF LENGTH ELEMENT WITH DEFORMATION OF BULGE

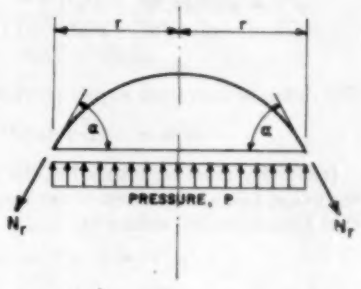

FIG. 2(b) FORCES ACTING ON A CENTRAL CAP OF BULGE

After simplification and rearrangement, one obtains

$$\sigma_\theta = (1 + \eta'\rho/\eta)\sigma_r + \rho\sigma_r' \quad \ldots\ldots [13]$$

Equations [12] and [13] will be recognized as the membrane equations for shells or revolution (13), with the ramification that the stresses considered here are true stresses.[5]

SOLUTION OF THE EQUATIONS

Equations [4], [9], [10], [11], [12], [13], and the second of Equations [5] provide eight equations in eight unknowns. One can eliminate v by expressing it from Equation [10] and inserting the resulting expression into Equation [9] to obtain

$$\epsilon_r = \ln [2 + (\rho\epsilon_\theta - 1)\exp(-\epsilon_\theta) + (\omega')^2/2] \quad \ldots\ldots [14]$$

In addition, ω' can be expressed from Equation [12] as

$$\omega' = -\rho p[4\sigma_r^2\eta^2 - \rho^2 p^2]^{-1/2} \quad \ldots\ldots [15]$$

Insertion of Equation [15] into [14] further eliminates ω, leading to

$$\exp \epsilon_r = 2 + (\rho\epsilon_\theta' - 1)\exp(-\epsilon_\theta) + \rho^2 p^2(8\sigma_r^2\eta^2 - 2\rho^2 p^2)^{-1}$$

or

$$\epsilon_\theta' = [\exp(\epsilon_r + \epsilon_\theta) - 2\exp\epsilon_\theta + 1]\rho^{-1} - \rho p^2(8\sigma_r^2\eta^2 - 2\rho^2 p^2)^{-1}\exp\epsilon_\theta \quad \ldots\ldots [16]$$

From Equations [4]

$$\sigma_r(2\epsilon_\theta + \epsilon_r) = \sigma_\theta(2\epsilon_r + \epsilon_\theta) \quad \ldots\ldots [17]$$

which, combined with Equation [13], yields

$$d\sigma_r/\sigma_r = (\epsilon_\theta - \epsilon_r)(2\epsilon_r + \epsilon_\theta)^{-1}\, d\rho/\rho - d\eta/\eta$$

or, after performing the integration

$$\sigma_r = \sigma_o \exp\left[\int_0^\rho (\epsilon_\theta - \epsilon_r)(2\epsilon_r + \epsilon_\theta)^{-1}\rho^{-1} d\rho + \epsilon_r + \epsilon_\theta - 2\epsilon_o\right] \quad \ldots\ldots [18]$$

At the pole ($\rho = 0$) Equation [5] simplifies to

$$\left.\begin{aligned} \tau_o &= \sqrt{2}\,\sigma_o/3 \\ \gamma_o &= 2\sqrt{2}\,\epsilon_o \end{aligned}\right\} \quad \ldots\ldots [19]$$

so that Equation [18] can be rewritten as

$$\sigma_r = \frac{3}{\sqrt{2}}\tau_o \exp\left[\int_0^\rho \frac{\epsilon_\theta - \epsilon_r}{\rho(2\epsilon_r + \epsilon_\theta)} d\rho + \epsilon_r + \epsilon_\theta - 2\epsilon_o\right] \quad [20]$$

Combining this result with the first of Equations [4] and the second of Equations [5], and expressing ϵ_r yields

$$\epsilon_r = \frac{\sqrt{3}\,\tau_o}{2\tau}(\epsilon_r^2 + \epsilon_r\epsilon_\theta + \epsilon_\theta^2)^{1/2} \exp\left[\int_0^\rho \frac{\epsilon_\theta - \epsilon_r}{\rho(2\epsilon_r + \epsilon_\theta)} d\rho + \epsilon_r + \epsilon_\theta - 2\epsilon_o\right] - \frac{\epsilon_\theta}{2} \quad \ldots\ldots [21]$$

A similar expression can be derived for ϵ_θ by integrating Equation [16] after substitution of Equations [20] and [11]

$$\epsilon_\theta = \epsilon_o - \int_0^\rho \left\{ p^2\rho \exp\epsilon_\theta \left[36\tau_o^2 \exp\left(2\int_0^\rho \frac{\epsilon_\theta - \epsilon_r}{\rho(2\epsilon_r + \epsilon_\theta)} d\rho - 4\epsilon_o\right) - 2\rho^2 p^2\right]^{-1} - \frac{1}{\rho}[\exp(\epsilon_r + \epsilon_\theta) - 2\exp\epsilon_\theta + 1]\right\} d\rho \quad \ldots\ldots [22]$$

Equations [21] and [22] represent implicit integral equations containing the two unknowns ϵ_θ and ϵ_r as functions of the independent variable ρ. These equations are solvable numerically for any pressure p if the correct value of the parameter ϵ_o is known. Note that ϵ_r, ϵ_θ, and ϵ_o fully determine τ and τ_o by means of the τ-γ function and Equations [5] and [19], respectively.

THE INSTABILITY CONDITION

Hydraulic bulging of diaphragms is one of a family of problems which exhibits the so-called instability phenomenon. In this application "instability" designates the point beyond which further straining leads to a reduction of the load (pressure) supported by the structure. If the pressure medium is connected with a sufficiently large reservoir (so that the volume increase of the bulge does not appreciably lower the applied pressure), a violent blowout takes place when the diaphragm reaches instability

[5] For linear elasticity $\eta' = 0$.

This condition may be investigated in the following manner: From Equation [15]

$$\left.\begin{aligned}(\omega')^2 &= \rho^2 p^3[4\sigma_r{}^2\eta^2 - \rho^2 p^2]^{-1} \\ \omega'' &= -p[4\sigma_r{}^2\eta^2 - \rho^2 p^2]^{-1/2}\{1 + \rho(4\sigma_r{}^2\eta^2 \\ &\quad - \rho^2 p^2)^{-1}[\rho p^2 - 4\sigma_r\eta(\sigma_r\eta)']\}\end{aligned}\right\} \quad \ldots [23]$$

The radius of curvature at any point of the bulge is given by

$$R/a = -[1 + (\omega')^2]^{3/2}(\omega'')^{-1} \quad \ldots [24]$$

Instability must be initiated at the point of greatest strain in the bulge, i.e., at the crown of the diaphragm. Here $\rho = 0$, so that Equations [23] reduce to

$$(\omega_o')^2 = 0; \quad \omega_o'' = -p/2\sigma_o\eta_o$$

which, by Equation [24], stipulates that the polar radius of curvature be

$$R_o/a = 2\sigma_o\eta_o/p \quad \ldots [25]$$

The last equation is easily recognized as the membrane equation ($\sigma = PR_o/2h_o$) for a spherical shell of radius R_o and thickness h_o subjected to a pressure P. By combination with Equations [11] and [19] it can be transformed into

$$dp = p\left(\frac{d\tau_o}{\tau_o} - \frac{d\gamma_o}{\sqrt{2}} - \frac{dR_o}{R_o}\right) \quad \ldots [26]$$

Instability is characterized by $dp = 0$. From Equation [26] then, the following condition must be satisfied at the maximum pressure

$$\frac{d\tau_o}{\tau_o d\gamma_o} - \frac{dR_o}{R_o d\gamma_o} = \frac{1}{\sqrt{2}} \quad \ldots [27]$$

The instability criterion incorporated in Equation [27] has been postulated previously by Brown and Sachs (7) in a slightly modified form. Equation [27] permits a prediction of the bursting strain or pressure from the material properties (τ-γ curve) alone, provided that an independent explicit relation between R_o and γ_o can be secured. Such an expression could not be obtained from this derivation, so that the instability pressure had to be determined from numerical calculations.

Numerical Work

The τ-γ curve, Fig. 3, was secured from experiments to be described later. To effect a comparison between theory and experiment, $a = 5.75$ in. was used, which corresponds with the dimensions of the plates tested. The radial distance was subdivided into 6 intervals. Initial values for the ϵ_r and ϵ_θ distributions were derived from an approximate solution (14). The iteration process was next carried out on Equations [21] and [22], using Simpson's parabolic rule for the numerical integration. The solution could be considered correct if ϵ_θ vanished at the clamping edge, satisfying the boundary condition.

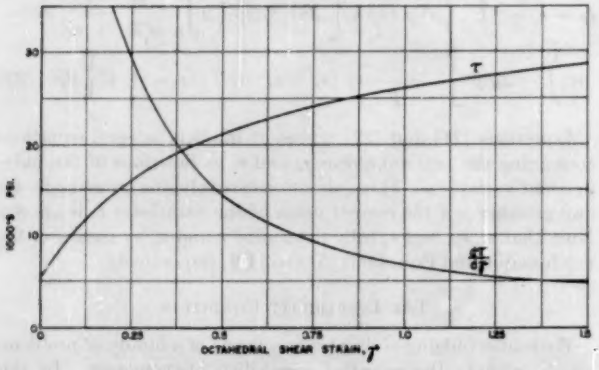

Fig. 3 The τ-γ Curve and Its Derivative

Convergence of this numerical procedure was rapid at low pressures; four trials generally yielded results accurate to 3 significant figures. With increasing pressure the rapidity of convergence deteriorated. Finally at $p = 53{,}800$ psi, in the region of instability, the numerical method became divergent.

Having determined the correct values of ϵ_θ and ϵ_r for a selected pressure level, the remaining significant quantities in the test plate, namely, ϵ_z, w, u, h, σ_r, σ_θ, and R_o were obtained explicitly from Equations [3], [15], [10], [11], [4], and [25], respectively The calculated numerical values are shown in Table 1.

For predicting the instability condition, the $d\tau/d\gamma$ curve was secured from Fig. 3; next the $\tau^{-1}\, d\tau/d\gamma$ curve[6] was calculated. The R_o versus γ_o relationship was plotted from the results shown in Table 1, which permitted the construction of the $R_o{}^{-1}dR_o/d\gamma_o$ curve. Lastly, the $\tau^{-1}d\tau/d\gamma$ and the $R_o{}^{-1}dR_o/d\gamma_o + 1/\sqrt{2}$ curves were plotted as shown in Fig. 4; their intersection denotes the instability shear strain (octahedral), according to Equation [27]. The instability stress and strain may be obtained from Equations [19]; the polar radius of curvature can be determined from the $R_o - \gamma_o$ curve by extrapolation.[7] Equation [25] finally yields the ultimate pressure that the diaphragm can support. The theoretical values obtained by this sequence of calculation are shown in Table 2.

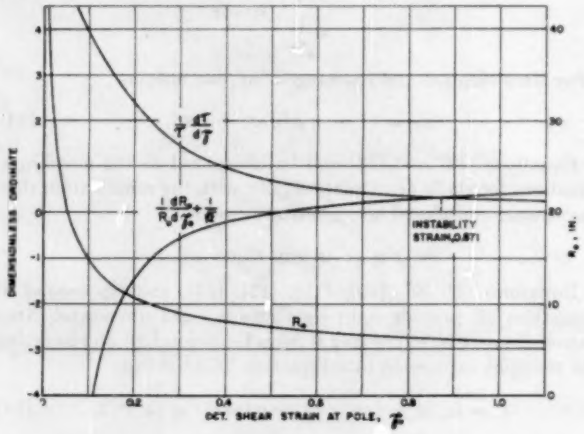

Fig. 4 Construction for Instability

Experimental Program

The experimental program included tests on annealed and cold-rolled copper sheets of two thicknesses. Results are presented here only for the annealed copper specimens, since calculations were restricted to diaphragms made of this material. The τ-γ curve was derived from uniaxial tests. The biaxial tests were conducted in the apparatus shown in Fig. 5. During the tests, measurements of vertical deflection and horizontal displacement were taken by means of a carefully calibrated bridge. Strains were measured both by a set of specially constructed clip strain-gages (shown in Fig. 5), and also by a 20 lines-to-the-inch

[6] Due to the "universality" of the τ-γ relation, the o subscript, as postulated in Equation [27], need not be observed in the construction of this curve.

[7] This method is permissible, since the $R_o - \gamma_o$ relation is asymptotic to $R_o = a$ at high strains.

TABLE 1 RESULTS OF THEORETICAL CALCULATIONS

Relative pressure p, psi	Radial dist, r, in.	Radial strain, ϵ_r, %	Circ strain, ϵ_θ, %	Vert defl, w, in.	Horiz displ, u, in.	Radial stress, σ_r, psi	Circ stress, σ_θ, psi	Polar curvature R_0, in.
2760	0	0.30	0.30	0.342	0	12060	12060	49.95
	1	0.29	0.29	0.334	0.0029	12040	12030	
	2	0.28	0.27	0.302	0.0053	11990	11810	
	3	0.25	0.22	0.251	0.0068	11890	11490	
	4	0.22	0.17	0.180	0.0068	11720	10790	
	5	0.14	0.08	0.088	0.0042	11430	9780	
	5.75	0.08	0	0	0	10910	5460	
5510	0	0.90	0.90	0.582	0	14350	14350	29.42
	1	0.88	0.88	0.569	0.0088	14340	14310	
	2	0.86	0.81	0.514	0.0162	14270	13930	
	3	0.78	0.68	0.428	0.0204	14130	13480	
	4	0.68	0.50	0.306	0.0199	13890	12500	
	5	0.47	0.25	0.148	0.0124	13500	10990	
	5.75	0.30	0	0	0	12780	6390	
11020	0	2.20	2.20	0.954	0	18650	18650	18.62
	1	2.19	2.16	0.933	0.0179	18600	18520	
	2	2.15	2.02	0.846	0.0408	18430	18060	
	3	2.05	1.75	0.708	0.0530	18100	17170	
	4	1.87	1.34	0.510	0.0538	17610	15770	
	5	1.54	0.69	0.249	0.0348	16860	13070	
	5.75	1.21	0	0	0	15910	7950	
22040	0	4.98	4.98	1.484	0	26180	26180	12.36
	1	4.96	4.95	1.452	0.0507	26140	26120	
	2	4.91	4.75	1.321	0.0973	26000	25710	
	3	4.76	4.08	1.113	0.1250	25540	24270	
	4	4.52	3.15	0.810	0.1279	24720	21940	
	5	4.20	1.59	0.402	0.0802	23380	17270	
	5.75	3.92	0	0	0	21860	10930	
35820	0	9.63	9.63	2.056	0	35370	35370	9.3
	1	9.60	9.58	2.013	0.1106	35330	35300	
	2	9.49	9.24	1.839	0.1935	35080	34770	
	3	9.18	8.32	1.562	0.2603	34410	33300	
	4	8.50	6.55	1.157	0.2707	33050	30320	
	5	7.76	3.52	0.584	0.1792	30930	24040	
	5.75	7.41	0	0	0	28450	14220	
51800	0	21.51	21.51	3.052	0	48280	48280	6.97
	1	21.05	21.06	2.994	0.2348	47860	47860	
	2	20.31	20.50	2.759	0.4550	47320	47460	
	3	18.73	18.94	2.375	0.6256	45940	46110	
	4	16.16	15.67	1.795	0.6787	43390	42960	
	5	13.55	9.18	0.960	0.4808	39340	34600	
	5.75	11.50	0	0	0	34070	17040	

TABLE 2 SIGNIFICANT VALUES AT INSTABILITY

	Polar stress, σ_θ, psi	Polar strain, ϵ_θ	Radius of curve, R_0, in.	Bursting pressure, p, psi
Theory	53500	0.308	6.13	54200
Experiment (avg of 2 tests)	...	...	..	55800

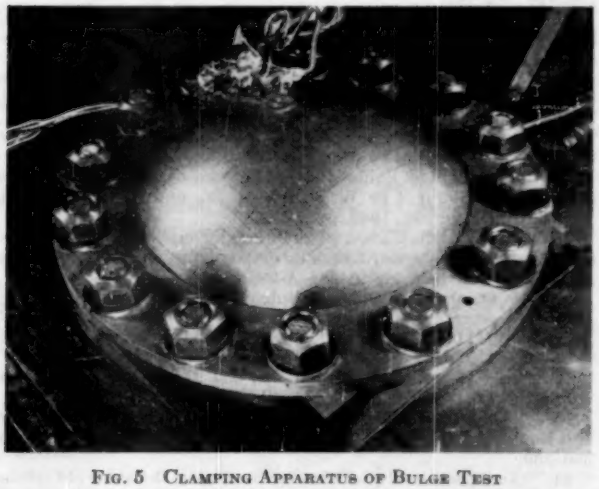

FIG. 5 CLAMPING APPARATUS OF BULGE TEST

photogrid using a microscope of about ×9 magnification (not shown).

The pressure was released before measurements were taken. This retained only the plastic component of strain, in line with the assumptions made in the analysis. For sake of safety of the operating personnel, no strain or deflection measurements were taken at instability; only the maximum pressure was observed. This accounts for the lack of experimental stress and strain data at instability in Table 2. All tests were continued to bursting.

Two "thin" plates and one "thick" plate were tested, having thicknesses of 0.02087, 0.02020, and 0.1303 in., respectively. The test results are shown in Figs. 6 to 8, inclusive. Experimental values referring to the thin plates were averaged in the figures.

The theoretical values of Table 1 are also plotted in Figs. 6 to 8. The agreement between theory and experiment is quite good. While it is not shown here, the agreement was similarly adequate for the radial distribution of stresses, strains, and vertical deflections. Less favorable agreement was found for the horizontal displacement values, Fig. 9. This was ascribed to a tendency of the plate to "draw into the bulge," which could not be prevented completely by the clamping mechanism. The result of this "drawing in" would be to reduce the measured values of horizontal displacements, as portrayed by Fig. 9.

Regarding the mode of failure of the specimens, one thin plate fractured prematurely; the pressure was still on the increase when a pin-point leak developed under a gage mark. The observed fracture strain (in the plane of the sheet) was 0.227. The thick plate went through instability and ruptured at a fracture strain of 0.430. These values bracket the theoretical instability value of $\epsilon_\theta = 0.308$, as given in Table 2. The second thin plate, which failed as the pressure reached a plateau, exhibited a fracture strain of 0.323. In place of more direct measurements, these comments are offered in substantiation of the theoretically calculated values for the instability strain.

ACKNOWLEDGMENTS

The investigation described in this paper formed part of a research study resulting from a co-operative agreement between the University of Illinois and the Copper and Brass Research Associa-

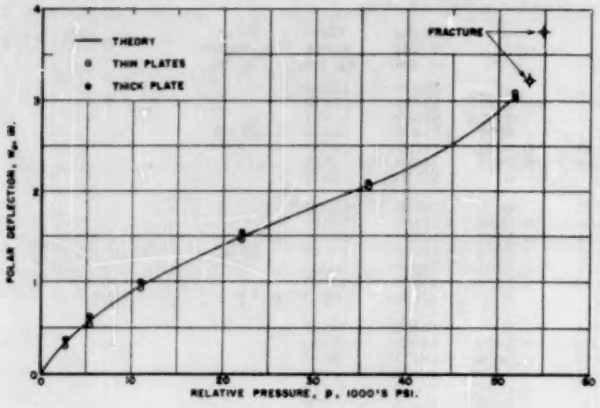

FIG. 6 POLAR DEFLECTION AS FUNCTION OF PRESSURE

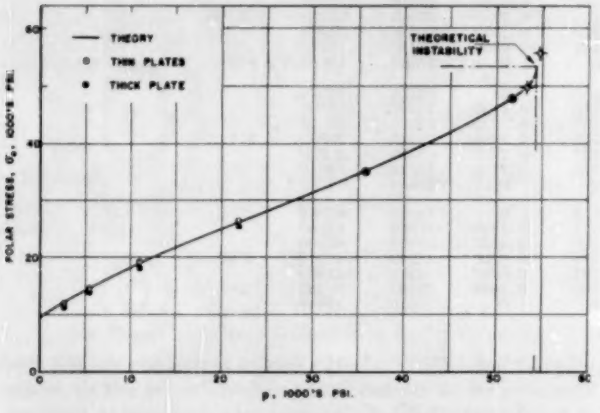

FIG. 8 POLAR STRESS AS FUNCTION OF PRESSURE

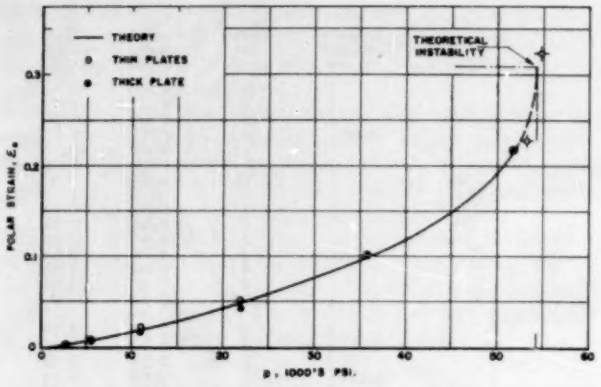

FIG. 7 POLAR STRAIN AS FUNCTION OF PRESSURE

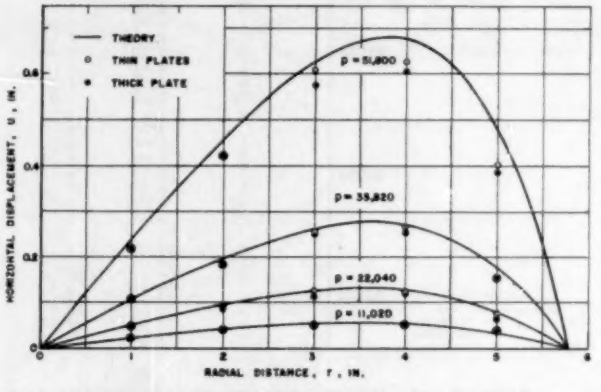

FIG. 9 HORIZONTAL DISPLACEMENTS AT SELECTED PRESSURES

ciation. All tests described herein were conducted in the Structural Research Laboratory of the Department of Civil Engineering at the University of Illinios. The analytical and experimental results formed part of the thesis of N. A. Weil submitted in partial fulfillment of the requirements for the PhD degree at the University of Illinois.

The authors wish to acknowledge their indebtedness to W. H. Munse, Research Associate Professor of Civil Engineering, for his valuable contributions in the organization of the experimental work.

BIBLIOGRAPHY

1 "Frangible Disks as Protection for Pressure Vessels," by M. E. Bonyun, Trans. AICE, vol. 31, 1935, pp. 256–277.

2 "Design and Manufacture of Bursting Disks," by C. F. Lake and N. P. Inglis, Proceedings of The Institution of Mechanical Engineers, vol. 142, 1940, pp. 365–378.

3 "Rupture Diaphragms; Characteristics, Uses and Size Calculations," by T. S. Murphy, Jr., *Chemical and Metallurgical Engineering*, vol. 51, November, 1944, pp. 103–112; December, 1944, pp. 99–103.

4 "Circular Bulging of Aluminum Alloy Sheets at Room and Elevated Temperatures," by G. Sachs, G. Espey, and G. B. Kasik, Trans. ASME, vol. 68, 1946, pp. 161–173.

5 "Some Problems in Unstable Plastic Flow Under Biaxial Tension," by W. T. Lankford and E. Saibel, Trans. AIME, vol. 171, 1947, pp. 562–573.

6 "The Plastic Flow of Aluminum Alloy Sheet Under Combined Loads," by W. T. Lankford, J. R. Low, Jr., and M. Gensamer, Trans. AIME, vol. 171, 1947, pp. 574–604.

7 "Strength and Failure Characteristics of Thin Circular Membranes," by W. F. Brown, Jr. and G. Sachs, Trans. ASME, vol. 70, 1948, pp. 241–251.

8 "Bulge Testing of Sheet Metal," by H. Thielsch, *Metal Progress*, vol. 56, July, 1949, pp. 86–88.

9 "Strength and Failure Characteristics of Metal Membranes in Circular Building," by W. F. Brown, Jr., and F. C. Thompson, Trans. ASME, vol. 71, 1949, pp. 575–586.

10 "Plastic Deformation of a Circular Diaphragm Under Pressure," by A. N. Gleyzal, JOURNAL OF APPLIED MECHANICS, Trans. ASME, vol. 70, 1948, pp. A-288–A-296.

11 "A Theory of the Plastic Bulging of a Metal Diaphragm by Lateral Pressure," by R. Hill, *Philosophical Magazine*, 7th series, vol. 41, 1950, pp. 1133–1142.

12 "The Plastic Flow of Thick-Walled Tubes With Large Strains," by C. W. McGregor, L. F. Coffin, Jr., and J. C. Fisher, *Journal of Applied Physics*, vol. 19, 1948, pp. 291–297.

13 "Theory of Plates and Shells," by S. Timoshenko, McGraw-Hill Book Company, Inc., New York, N. Y., 1940, paragraph 73, pp. 356–359.

14 "An Approximate Solution for the Plastic Behavior of Circular Membranes," by N. A. Weil, submitted to ASCE for publication.

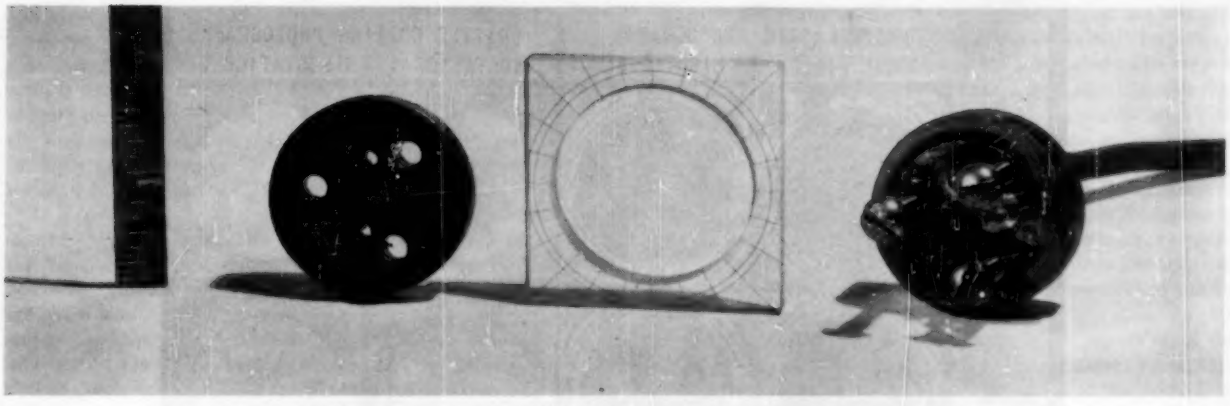

FIG. 1 LOADING JIG USED TO APPLY HYDROSTATIC PRESSURE TO INTERIOR BOUNDARY OF SQUARE PLATE

Stress Distribution in Square Plates With Hydrostatically Loaded Central Circular Holes

BY A. J. DURELLI[1] AND J. BARRIAGE,[2] CHICAGO, ILL.

The stress distribution in square plates with hydrostatically loaded central circular holes was determined using photoelasticity and brittle coatings. Photoelasticity was used to determine the maximum shear lines (isochromatics) and a brittle coating was used to determine the directions of the principal stresses (isostatics). The investigation was conducted for plates with holes producing seven ratios of the diameter to the square side (D/a). Curves are presented which show the distribution of the maximum shear stress along the axis and along the diagonal of the square plate, as a function of D/a, Figs. 3 and 4. The maximum principal stress along the exterior and interior boundaries as a function of D/a, Figs. 5 and 6, has also been given. A comparison is made of the stress ratios (σ_1/P) at a point on the axis of the square at the interior boundary with that calculated for a thick-wall cylinder using Lamé's equation, Fig. 1. Stress ratios (σ_1/P) also are determined for a point on the diagonal of the square plate at the interior boundary, Fig. 8. A diffused-light polariscope was used. The loading jig consisted of rubber tubing in a grooved block. The photoelastic material (CR39) was calibrated automatically. No new methods are developed in the paper but it is felt that the use of the presently available methods has been simplified appreciably.

INTRODUCTION

THE distribution of stresses in square plates with central circular holes hydrostatically loaded is difficult to solve by use of the mathematical theory of elasticity. No records were found in the literature of experimental determinations with the exception of a qualitative analysis conducted by Coker and Filon.[3] The recent development of a jig[4] enabling the easy application of uniform loading to boundaries of complicated shapes suggested the use of photoelasticity as a relatively fast way of solving this problem.

The results published in this paper are new but the techniques used have been described previously in papers,[4,5] by members of the Armour Research Foundation staff. The authors would like to emphasize the ease with which this relatively complicated determination was conducted using these techniques.

DESCRIPTION OF THE TEST

The loading jig is a plug made of two steel circular plates with an insert, of approximately the thickness of the model, around which rubber tubing is placed, see Fig. 1. Thus the rubber tubing is confined in a rectangular channel one side of which is formed by the model. Nitrogen gas under pressure is applied to the tube and

[1] Supervisor of Stress Analysis Section, Armour Research Foundation. Assoc. Mem. ASME.

[2] Assistant Engineer, Stress Analysis Section, Armour Research Foundation.

Presented at the National Conference of the Applied Mechanics Division, Troy, N. Y., June 16–18, 1955, of THE AMERICAN SOCIETY OF MECHANICAL ENGINEERS.

Discussion of this paper should be addressed to the Secretary, ASME, 29 West 39th Street, New York, N. Y., and will be accepted until January 10, 1956, for publication at a later date. Discussion received after the closing date will be returned.

NOTE: Statements and opinions advanced in papers are to be understood as individual expressions of their authors and not those of the Society. Manuscript received by ASME Applied Mechanics Division, September 3, 1954. Paper No. 55—APM-12.

[3] "A Treatise on Photoelasticity," by E. G. Coker and L. N. Filon, Cambridge University Press, Cambridge, England, 1931, p. 318.

[4] "Some Unorthodox Procedures in Photoelasticity," by A. J. Durelli and R. L. Lake, Proceedings of the Society for Experimental Stress Analysis, vol. 9, 1951, pp. 97–122.

[5] "Device for Applying Uniform Loading to Boundaries of Complicated shape," by A. J. Durelli, R. L. Lake, and C. H. Tsao, Proceedings of the Society for Experimental Stress Analysis, vol. 11, 1953, pp. 55–61.

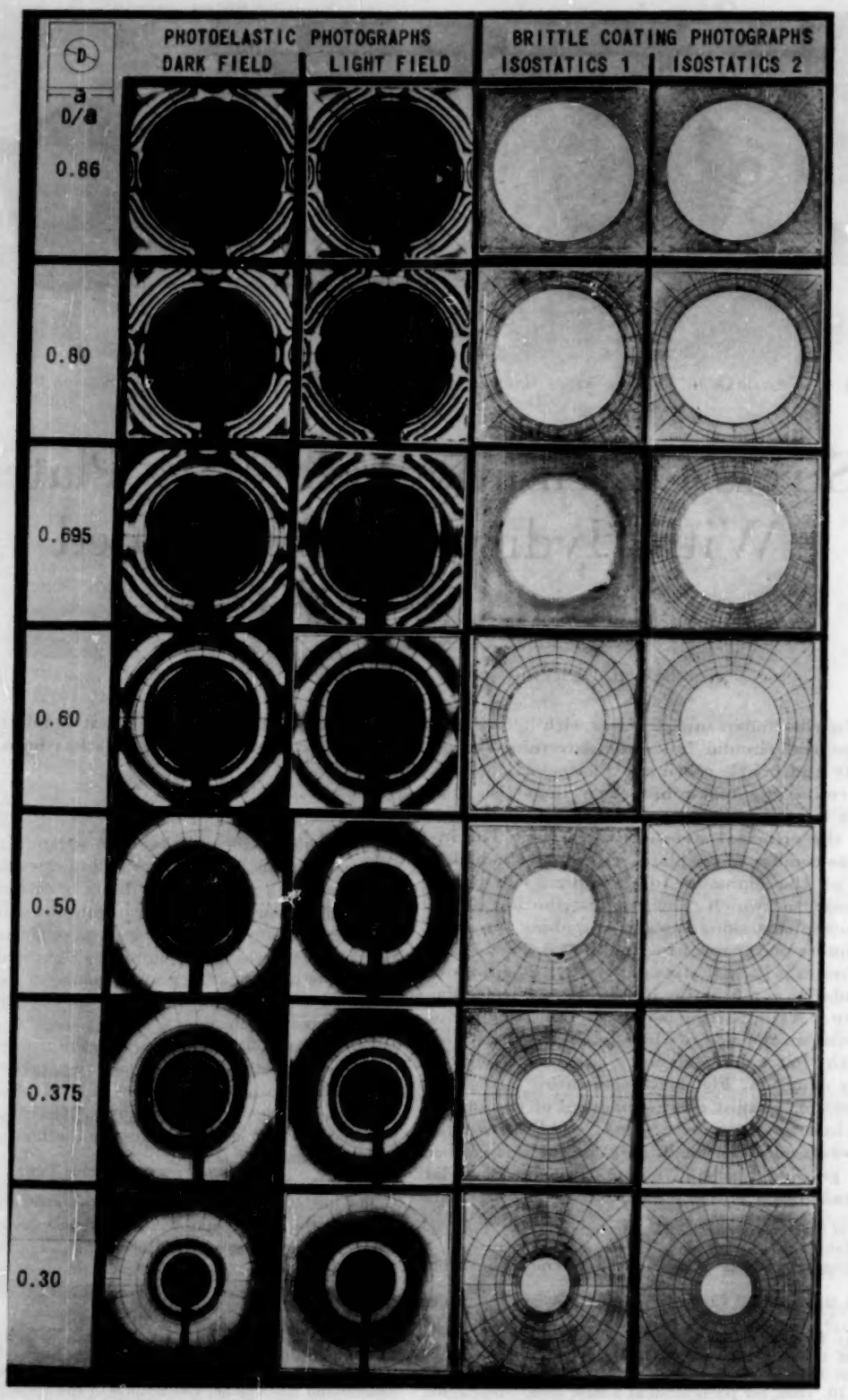

FIG. 2 STRESS DISTRIBUTION IN SQUARE PLATES WITH HYDROSTATICALLY LOADED CENTRAL CIRCULAR HOLES

the expansion of the tube inside the rectangular shaped groove produces the hydrostatic loading of the specimen. The hole diameter of the plate was made a few thousandths of an inch smaller than the diameter of the jig to avoid extrusion and failure of the tube under the pressure. Since the plastic deforms under the loading, the final diameter of the hole is very close to the diameter of the plug and the observation of the stresses can be made up to the actual boundary of the hole.

As a result of the action of friction between the tube and the groove walls, and because of the effect of the rubber tube thickness on the pressure distribution, the calibration of the material was made using a calibration fixture which reproduced very closely the same loading conditions as on the model. The calibration fixture has been described in detail.[4] It consists essentially of a rubber tube placed in a rectangular groove, the top of which consists of a rectangular piece of the photoelastic material taken from the same sheet as the model. When the rubber tubing is submitted to pressure it transmits a force to the rectangular insert which in turn transmits this force to a steel base. A calibration disk of the photoelastic material placed on edge between the steel base and the frame of the fixture is loaded in diametral compression as the pressure is increased. Since at the time of the test both the calibration fixture and the model loading jig are operating under the same conditions, i.e., the rectangular insert (in this case CR39) is of the same thickness as the model, the rubber tubing the same as in the loading jig; therefore the effective pressure is the same in both cases.

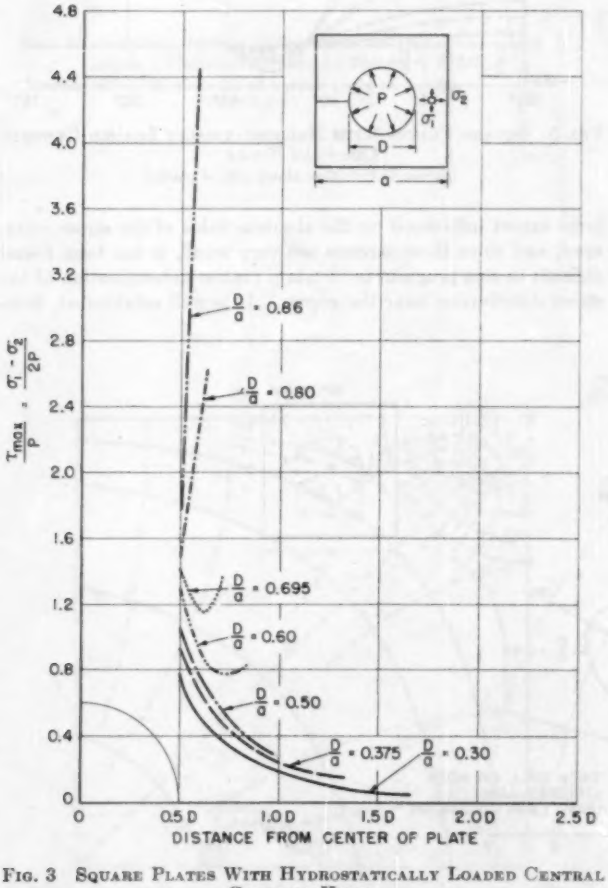

FIG. 3 SQUARE PLATES WITH HYDROSTATICALLY LOADED CENTRAL CIRCULAR HOLES
(Distribution of maximum shear stress along a line from center to mid-point of one side.)

The models were machined from the same sheet of Columbia resin (CR39) whose nominal thickness was 0.260 in. The internal diameter of the models was turned on a lathe and the outside boundaries were finished with a router or, in the case of the smaller models, the outside boundaries were hand-filed. All the models were scribed to enable compensation readings to be made at the same positions.

Following the photoelastic tests the models were sprayed with a brittle coating (Stresscoat), permitted to dry, then loaded as in the photoelastic tests. This load produced strains large enough to cause the brittle coating to crack perpendicular to the principal stress σ_1. Since the principal stresses are orthogonal these cracks formed the isostatics corresponding to the principal stress σ_2. By employing the relaxation-loading technique, i.e., spraying of the model with brittle coating, application of loading conditions, drying of the coating, and then relieving of the load, it was possible to crack the coating perpendicular to the compressive principal stress σ_2. These cracks formed the isostatics corresponding to the principal stress σ_1. (An enlargement of the isostatics formed by the brittle coating is given in Fig. 11.)

RESULTS AND CONCLUSIONS

The light and dark-field photoelastic photographs and the brittle-coating photographs obtained from the tests are shown in Fig. 2.

Evaluatior of the data results in curves of the maximum shear-stress distribution along the axis and diagonal (Figs. 3 and 4) and in curves of the stress ratio σ_1/p along the exterior and interior boundaries (Figs. 5 and 6) of the square plates. The values of stresses are referred to the internal pressure P.

In Fig. 3 where the maximum shear stress is plotted as a function of position along the axis of the plate it may be observed that the position of maximum shear stress moves from the interior

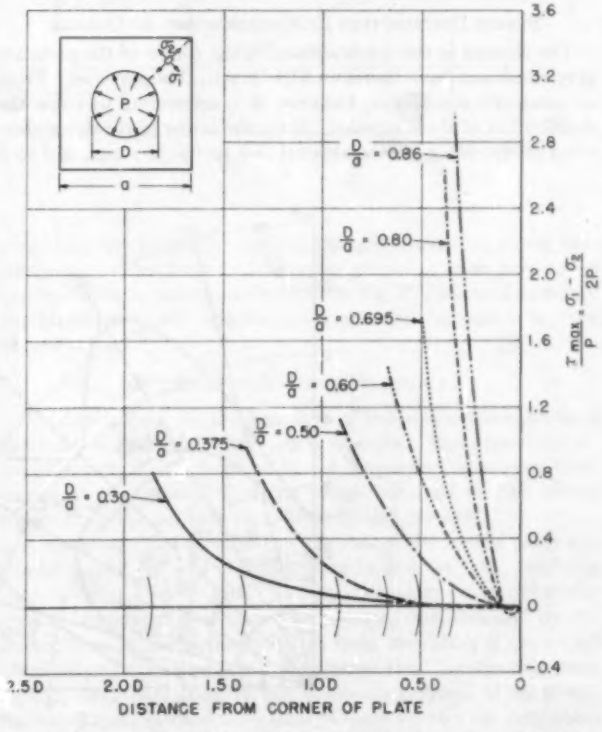

FIG. 4 SQUARE PLATES WITH HYDROSTATICALLY LOADED CENTRAL CIRCULAR HOLES
(Distribution of maximum shear stress along diagonal.)

boundary for the lower D/a ratios ($D/a = 0.3$) to the exterior boundary for the higher D/a ratios ($D/a = 0.86$).

In Fig. 4 the shear stress is plotted for the various D/a ratios as a function of the position along the diagonal of the square. The curves are plotted with the position of exterior boundary (or corner) common to all plates. As can be seen in the photoelastic photographs, Fig. 2, and as further explained in the discussion of the stress distribution in the neighborhood of the corner, the curves must drop below zero over a short distance between zero points on the diagonal. For $D/a = 0.86$ a value of somewhat less than one-half fringe exists just beyond the inner zero point, but since for all curves this was not determined accurately the latter portions are dashed indicating the approximate solution.

The stress distribution along the side of the plate is shown in Fig. 5. Here again, between the two singular points (in this case points of zero stress) and because of the reversal in the sign of the stress, the curves drop somewhat below zero for a short distance.

Fig. 6 shows the stress distribution on the interior boundary. As the square plate becomes large with respect to the hole, the stress distribution approaches that of a thick-wall cylinder except near the corners of the plate.

In Fig. 7 the stress ratio (σ_1/P) is plotted for a point on the axis of the plate at the interior boundary for the seven D/a ratios. Also shown is the corresponding value obtained from Lamé's solution for thick-wall cylinders. As the D/a ratio approaches zero, the effect of the corners on the stress at the point considered becomes small; therefore the experimental curve has been extrapolated to the value of $\sigma_1/P = 1$.

Fig. 8 shows the stress ratio σ_1/P as a function of the D/a ratios for a point on the diagonal at the interior boundary.

With the stress distribution completely defined along the boundaries and for the two cross sections (the axis and diagonal), Laplace's equation may be used to separate the stresses inside the field using, for instance, the conducting-paper analogy.

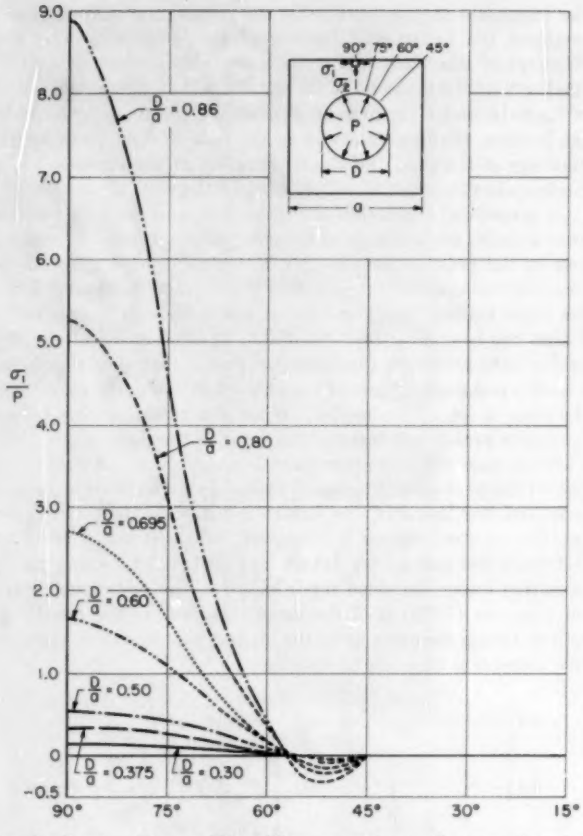

FIG. 5 SQUARE PLATES WITH HYDROSTATICALLY LOADED CENTRAL CIRCULAR HOLES
(Stress distribution along side of plate.)

STRESS DISTRIBUTION IN NEIGHBORHOOD OF CORNER

The stresses in the neighborhood of the corner of the plate are very small and have therefore little practical importance. From an academic standpoint, however, it is interesting to know the distribution of these stresses. Since the errors of the determinations made, using photoelasticity and brittle coatings, are to a large extent influenced by the absolute value of the stress measured, and since these stresses are very small, it has been found difficult in this program to obtain a precise determination of the stress distribution near the corner. It is well established, how-

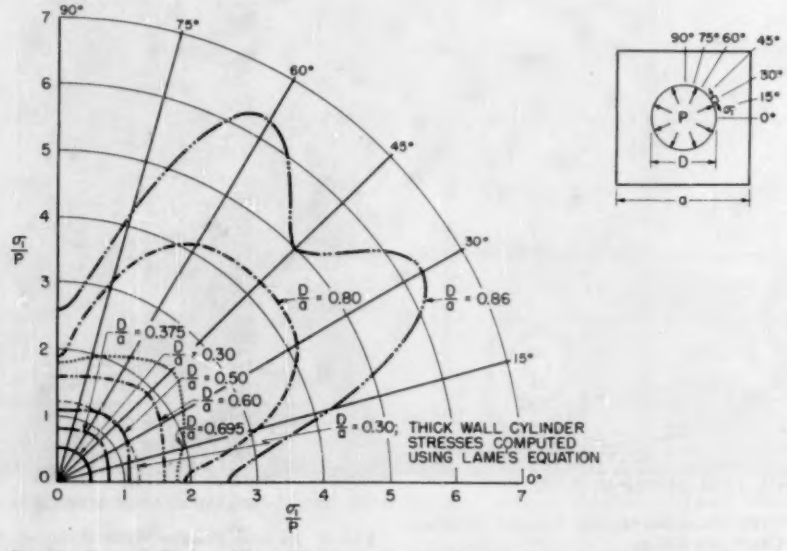

FIG. 6 SQUARE PLATES WITH HYDROSTATICALLY LOADED CENTRAL CIRCULAR HOLES
(Stress distribution along interior boundary.)

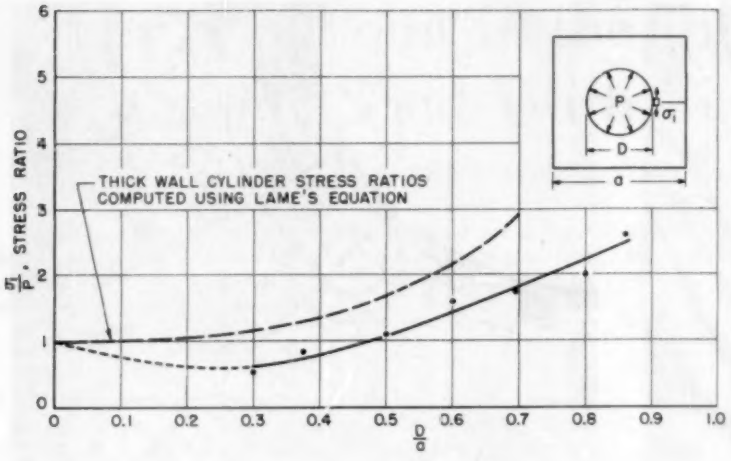

FIG. 7 SQUARE PLATES WITH HYDROSTATICALLY LOADED CENTRAL CIRCULAR HOLES
(Stress ratios on axis of square at interior boundary.)

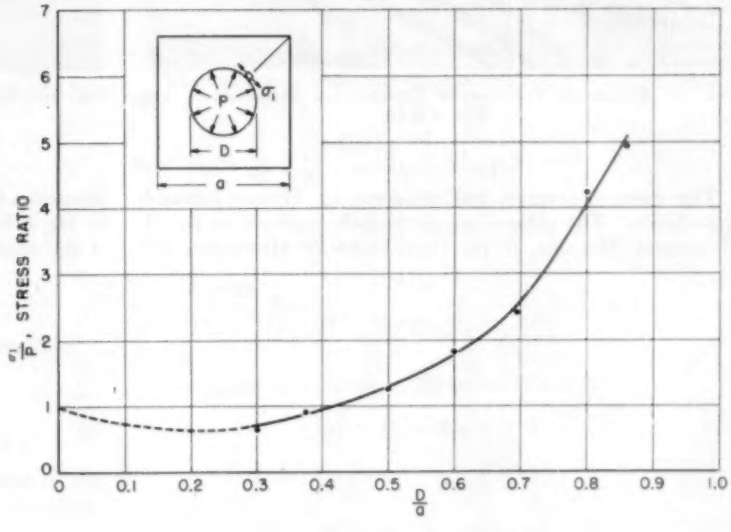

FIG. 8 SQUARE PLATES WITH HYDROSTATICALLY LOADED CENTRAL CIRCULAR HOLES
(Stress ratios on diagonal of square plate at interior boundary.)

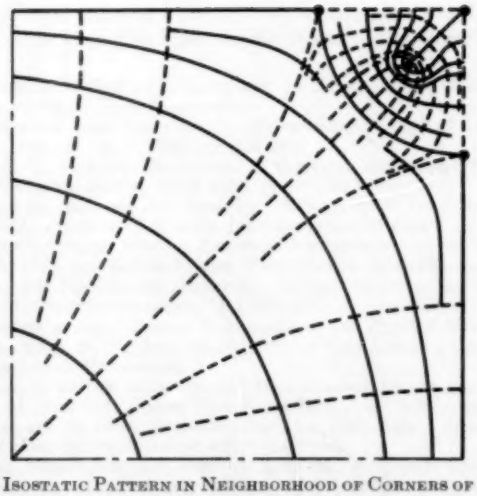

FIG. 9 ISOSTATIC PATTERN IN NEIGHBORHOOD OF CORNERS OF PLATES
(It seems likely that four singular points are present. Isostatic family parallel to σ_1 is represented solid, and isostatic family parallel to σ_2 is represented dashed.)

ever, that the boundary stresses change sign and it seems very likely that there exist four singular points in each corner. A typical isostatic pattern is depicted in Fig. 9. Enlarged details of the photoelastic and brittle-coating patterns are shown in Figs. 10 and 11.

ACCURACY OF DETERMINATIONS

No direct check on the accuracy of the stress determinations has been conducted for this series of tests. From previous experience with similar tests conducted, employing these same techniques, it is estimated that the values obtained for the curves shown in this paper may be in error by ±3 per cent.

A static-equilibrium check on the axis of the square plate was conducted for the test corresponding to $D/a = 0.86$, assuming that σ_2 varies linearly from the inside boundary ($\sigma_2 = P$) to the outside boundary ($\sigma_2 = 0$). The stress σ_1 was obtained by deducing this linear distribution of σ_2 from the values of $(\sigma_1 - \sigma_2)$ obtained photoelastically. It is believed that for this thin cross section, the assumption of the linear distribution of σ_2 is sufficiently accurate, since the values of these stresses are very small compared to the values of σ_1. The total normal force across the axis of the square plate checked to within ±2.5 per cent of the product of the internal pressure and the diameter of the hole.

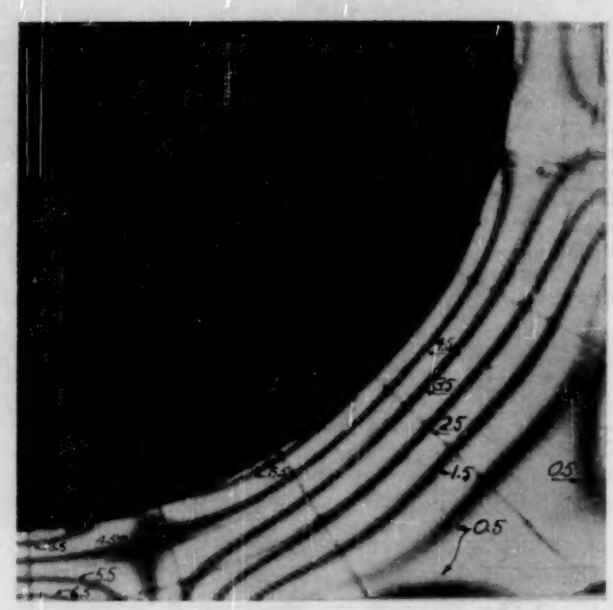

FIG. 10 ENLARGED PORTION OF LIGHT-FIELD PHOTOGRAPH FOR $D/a = 0.86$

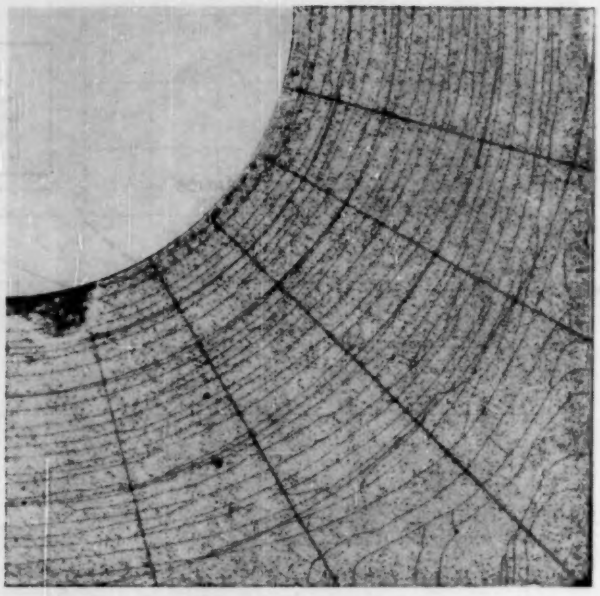

FIG. 11 ENLARGED PORTION OF BRITTLE-COATING PHOTOGRAPH SHOWING ISOSTATIC 1
(Relaxation test with refrigeration.)

ACKNOWLEDGMENT

This research program was sponsored by Armour Research Foundation. The authors are particularly indebted to Dr. G. Nothmann, Manager of the Department of Mechanism and Dynamics Research, for his support. The manuscript was read by Mr. J. W. Dally who made many valuable suggestions. Some of the brittle-coating tests were conducted by Mr. S. Okubo.

Force at Point in the Interior of a Semi-Infinite Solid With Fixed Boundary

By LEIF RONGVED,[1] STATE COLLEGE, PA.

The Papkovitch functions are determined for a force acting at a point in the interior of a semi-infinite isotropic solid with a fixed plane boundary. The normal traction on the boundary is then calculated.

Introduction

THE problem of a force at a point in the interior of a semi-infinite solid with free boundary has been solved by Mindlin.[2,3] In the first of these papers[2] Mindlin, starting with Kelvin's solution for a force in an infinite body, guessed the nuclei of strain to be added outside the region to satisfy the boundary conditions. In the second paper[3] Mindlin showed how the solution may be obtained directly by an ingenious analysis applying potential theory. The same analysis is applied in this paper to solve the same problem, except that the boundary is assumed to be fixed.

Papkovitch Functions

The displacement $\mathbf{u}$ in terms of the Papkovitch[4] functions $\mathbf{B}$ and β is given by

$$\mathbf{u} = \mathbf{B} - \frac{1}{4(1-\nu)} \nabla [\mathbf{r} \cdot \mathbf{B} + \beta] \quad \ldots [1]$$

where the functions $\mathbf{B}$ and β satisfy the differential equations

$$\mu \nabla^2 \mathbf{B} = -\mathbf{F} \quad \ldots [2]$$

$$\mu \nabla^2 \beta = \mathbf{r} \cdot \mathbf{F} \quad \ldots [3]$$

where $\mathbf{F}$ is the body force. The proof of completeness of the Papkovitch functions including body forces was given by Mindlin.[3]

Force at a Point

Kelvin's definition of a force, $\mathbf{P}$, at a point, 0, is as follows. Let the body force $\mathbf{F}$ be zero everywhere except in a closed region T. Let T diminish indefinitely, always enclosing the point 0, but such that

$$\lim_{T \to 0} \int_T \mathbf{F} d\tau = \mathbf{P} \quad \ldots [4]$$

Force Normal to Fixed Plane Boundary

Let $z = 0$ be the fixed plane boundary, and let the force P_z act at the point $(0,0,c)$. Let $F_x = F_y = 0$ for $z \geqslant 0$, and in accordance with Equation [4] let

$$P_z = \lim_{T \to 0} \int_T F_z d\tau \quad \ldots [5]$$

where the region T encloses the point $(0,0,c)$.

The condition of vanishing displacement on $z = 0$ is by Equation [1]

$$\left.\begin{aligned} u_x &= B_x - \frac{1}{4(1-\nu)} \frac{\partial}{\partial x} (xB_x + yB_y + \beta) = 0 \\ u_y &= B_y - \frac{1}{4(1-\nu)} \frac{\partial}{\partial y} (xB_x + yB_y + \beta) = 0 \\ u_z &= \frac{3-4\nu}{4(1-\nu)} B_z - \frac{1}{4(1-\nu)} \frac{\partial}{\partial z} (xB_x + yB_y + \beta) = 0 \end{aligned}\right\} \quad \ldots [6]$$

on $z = 0$.

The Condition [6] is satisfied if we let

$$B_x = B_y = 0 \text{ in } z \geqslant 0 \quad \ldots [7]$$

$$\beta = 0 \quad \text{on } z = 0 \quad \ldots [8]$$

$$(3-4\nu)B_z - \frac{\partial \beta}{\partial z} = 0 \quad \text{on } z = 0 \quad \ldots [9]$$

Equation [7] satisfies also two of the three scalar equations contained in Equation [2]. The Laplacian of β is zero for $z \geqslant 0$ except in the region T enclosing $(0,0,c)$, where its value is given by Equation [3]. Then in virtue of Equation [8] we have, using Green's analysis

$$\beta = -\lim_{T \to 0} \frac{1}{4\pi\mu} \int_T G\zeta F_z d\tau \quad \ldots [10]$$

where G, the Green's function, is

$$G = \frac{1}{r_1} - \frac{1}{r_2}$$

where

$$r_1 = [(x-\xi)^2 + (y-\eta)^2 + (z-\zeta)^2]^{1/2}$$

and

$$r_2 = [(x-\xi)^2 + (y-\eta)^2 + (z+\zeta)^2]^{1/2}$$

where

(x, y, z) is any point in $z \geqslant 0$ and (ξ, η, ζ) is a source point in T Apparently Equation [10] then becomes

---

[1] Assistant Professor, Department of Engineering Mechanics, The Pennsylvania State University.

[2] "Force at a Point in the Interior of a Semi-Infinite Solid," by R. D. Mindlin, *Physics*, vol. 7, 1936, pp. 195–202.

[3] By R. D. Mindlin, Proceedings of the First Midwestern Conference on Solid Mechanics, April, 1953, pp. 56–59.

[4] "Solution générale des équations différentielles fundamentales d'élasticité, exprimée par trios function harmoniques," by P. F. Papkovitch, *Comptes Rèndus*, Academie des Sciencies, Paris, France, vol. 195, 1922, pp. 513–515; also, "Expressions génerales des composantes des tensions ne renferment comme functions arbritrares que des functions harmoniques," pp. 754–756.

Presented at the National Conference of the Applied Mechanics Division, Troy, N. Y., June 16–18, 1955, of The American Society of Mechanical Engineers.

Discussion of this paper should be addressed to the Secretary, ASME, 29 West 39th Street, New York, N. Y., and will be accepted until January 10, 1956, for publication at a later date. Discussion received after the closing date will be returned.

Note: Statements and opinions advanced in papers are to be understood as individual expressions of their authors and not those of the Society. Manuscript received by ASME Applied Mechanics Division, August 2, 1954. Paper No. 55—APM-14.

$$\beta = -\frac{cP_z}{4\pi\mu}\left(\frac{1}{R_1}-\frac{1}{R_2}\right) \quad [11]$$

where

$$R_1 = [x^2 + y^2 + (z-c)^2]^{1/2}$$

and

$$R_2 = [x^2 + y^2 + (z+c)^2]^{1/2}$$

The Laplacian of Equation [9] is zero for $z \geqslant 0$ except in the region T enclosing $(0,0,c)$, where its value is given by Equations [2] and [3].

Hence

$$(3-4\nu)B_z - \frac{\partial\beta}{\partial z} = \frac{3-4\nu}{4\pi\mu}\lim_{T\to 0}\int_T GF_z\,d\tau + \frac{1}{4\pi\mu}\lim_{T\to 0}\int_T G\frac{\partial(\zeta F_z)}{\partial\zeta}\,d\tau$$

Integrating the last term by parts and noting that $F_z = 0$ on the boundary we get

$$(3-4\nu)B_z - \frac{\partial\beta}{\partial z} = \frac{(3-4\nu)P_z}{4\pi\mu}\left(\frac{1}{R_1}-\frac{1}{R_2}\right) + \frac{cP_z}{4\pi\mu}\frac{\partial}{\partial z}\left(\frac{1}{R_1}+\frac{1}{R_2}\right)$$

by Equation [11] then

$$B_z = \frac{P_z}{4\pi\mu}\left(\frac{1}{R_1}-\frac{1}{R_2}\right) + \frac{cP_z}{2\pi(3-4\nu)\mu}\frac{\partial}{\partial z}\left(\frac{1}{R_2}\right) \quad [12]$$

Equations [7], [11], and [12] constitute the solution for the case of a force normal to the fixed-plane boundary. These equations inserted in Equation [1] yield the displacement, and then

$$\sigma = \lambda(\nabla\cdot\mathbf{u})\mathbf{I} + \mu(\nabla\mathbf{u} + \mathbf{u}\nabla) \quad [13]$$

gives the stress.

One finds without difficulty that the normal traction on $z = 0$ is

$$\sigma_{zz} = \frac{cP_z}{\pi(3-4\nu)}\left(\frac{1-2\nu}{R_2^3} + \frac{3}{2}\frac{c^2}{R_2^5}\right) \quad [14]$$

The maximum value of the normal traction on the boundary occurs at $x = y = 0$ and equals

$$\sigma_{zz} = \frac{(5-4\nu)P_z}{2\pi(3-4\nu)c^2} \quad [15]$$

Force Parallel to Fixed Plane Boundary

Let $z = 0$ be the fixed plane boundary, and let the force P_x be parallel to the x-axis, acting at the point $(0,0,c)$. Let $F_y = F_z = 0$ for $z \geqslant 0$ and let in accordance with Equation [4]

$$P_x = \lim_{T\to 0}\int_T F_x\,d\tau \quad [16]$$

where the region T encloses the point $(0,0,c)$. The Condition [6] is satisfied if we set

$$B_x = 0 \quad \text{in } z \geqslant 0 \quad [17]$$

$$B_z = 0 \quad \text{on } z = 0 \quad [18]$$

$$\beta = 0 \quad \text{on } z = 0 \quad [19]$$

$$B_z - \frac{1}{3-4\nu}\left(x\frac{\partial B_z}{\partial z} + \frac{\partial\beta}{\partial z}\right) = 0 \quad \text{on } z = 0 \quad [20]$$

By Equations [3] and [19] and again using Green's analysis we get

$$\beta = -\frac{1}{4\pi\mu}\lim_{T\to 0}\int_T G\xi F_x\,d\tau$$

Now as $T \to 0$, $\xi \to 0$, hence the right side of this equation vanishes and

$$\beta = 0 \quad \text{in } z \geqslant 0 \quad [21]$$

In virtue of Equations [2] and [18]

$$B_x = \frac{1}{4\pi\mu}\lim_{T\to 0}\int_T GF_x\,dx$$

or

$$B_x = \frac{P_x}{4\pi\mu}\left(\frac{1}{R_1}-\frac{1}{R_2}\right) \quad [22]$$

By Equations [20] and [21] we get

$$B_z = \frac{1}{3-4\nu}x\frac{\partial B_x}{\partial z} \quad \text{on } z = 0$$

Then by Equation [22]

$$B_z = \frac{x}{3-4\nu}\frac{P_x}{4\pi\mu}\frac{\partial}{\partial z}\left(\frac{1}{R_1}-\frac{1}{R_2}\right) \quad \text{on } z = 0$$

which may be written

$$B_z = -\frac{cP_x}{2\pi(3-4\nu)\mu}\frac{\partial}{\partial x}\left(\frac{1}{R_2}\right) \quad \text{on } z = 0 \quad [23]$$

One notes that if we let

$$B_z = -\frac{cP_x}{2\pi(3-4\nu)\mu}\frac{\partial}{\partial x}\left(\frac{1}{R_2}\right) \quad \text{in } z \geqslant 0 \quad [24]$$

B_z is harmonic, and satisfies Equations [2] and [20].

Equations [17], [21], [22], and [24] constitute the solution for the case of a force parallel to the fixed plane boundary. These equations inserted in Equations [1] and [13] give the displacement and the stress.

One finds without difficulty that the normal traction on $z = 0$ is

$$\sigma_{zz} = -\frac{3c^3P_x}{2\pi(3-4\nu)}\frac{x}{R_2^5} \quad [25]$$

The maximum value of the normal traction on the boundary occurs at $y = 0$, $x = \pm c/2$ and equals

$$\sigma_{zz} = \pm\frac{24}{25\sqrt{5}}\frac{P_x}{\pi c^2(3-4\nu)} \quad [26]$$

Free Vibrations of Thin Cylindrical Shells Having Finite Lengths With Freely Supported and Clamped Edges

By YI-YUAN YU,[1] SYRACUSE, N. Y.

Free vibrations of thin cylindrical shells having finite lengths are investigated on the basis of a set of three differential equations which are derived in a similar manner as Donnell obtained his equations for the bending and buckling problems. The equations can be solved readily after a simplifying assumption is introduced. In this manner the frequency equations are obtained for cylindrical shells with both edges freely supported, with both edges clamped, and with one edge freely supported and the other edge clamped. It is found that the lowest frequency given by the frequency equation is the smallest in the first case, larger in the third, and the largest in the second. The other two frequencies yielded by the frequency equation are approximately the same in all cases. As a result of the approximations, the characteristic equations for the three cases are found to be similar to the frequency equations for the lateral vibration of beams with similar end conditions. For the case of freely supported edges the normal functions obtained are identical in form with those assumed by Flügge and by Arnold and Warburton. For the same case, natural frequencies of one numerical example are computed by means of the present method, and the results are in good agreement with those obtained by these previous authors.

Introduction

Lord Rayleigh (1)[2] considered two types of vibrations in the theory of thin shells, the extensional mode and the inextensional mode. He investigated in detail the extensional vibrations of an infinitely long cylindrical shell. The frequency equation was obtained for the general case, and particular cases were discussed. He also advanced the theory of inextensional vibration of thin shells and calculated the frequencies of the inextensional modes of a cylindrical shell of an arbitrary length. Lamb and later Love (2) established the inexactness of the inextensional theory; however, they concluded that the correction is limited to regions near the edges and therefore has small effect on the frequencies.

Love also formulated the general equations of vibration for thin cylindrical shells and described the method of attack, but he did not actually solve the general case. Instead, only the extensional modes of cylindrical shells having finite lengths were discussed by first reducing the general equations. Another form of the general equations of vibration was given by Flügge (3), who also presented a method of approach to the general problem but considered it as too complicated to be actually used. He solved only the problem of a shell with freely supported edges by first assuming displacement components in the form of trigonometric functions. A numerical example was given, and he concluded that there are no purely extensional or inextensional vibrations of the shell. The general methods of both these authors will be described later as would be applied to the equations of vibration to be obtained.

Instead of formulating the differential equations on the basis of an infinitesimal shell element, displacement components consistent with boundary conditions may be assumed first and the strain and kinetic energies of the entire shell expressed in terms of the displacements. Lagrange equations may then be written to give relations connecting the displacements and their derivatives. Arnold and Warburton (4, 5) used this method in solving the general problem of cylindrical-shell vibrations. Numerical results were obtained for shells having both edges either freely supported or clamped. A similar approach was used recently by Baron and Bleich (6) to compute the natural frequencies and modes of infinitely long cylindrical shells; corrections were made to Rayleigh's extensional modes.

In the present paper the general problem of free vibrations of thin cylindrical shells is to be investigated on the basis of a set of differential equations which are derived in a similar manner as Donnell (7) obtained his equations for the bending and buckling of cylindrical shells. Similar to the latter ones, the three equations of vibration are also in a more desirable form than the usual ones. A single dependent variable w appears in the first of these equations and the dependent variables are u and w in the second and v and w in the third; u, v, and w are the displacement components of the shell in the longitudinal, circumferential, and radial directions, respectively. To solve these equations, of which the first is of the eighth order, a simplifying assumption is introduced so that the eighth-degree auxiliary equation is replaced by another of the fourth degree, which can then be solved readily. Three cases of cylindrical shells having finite lengths with freely supported and clamped edges are investigated.

Derivation of Equations of Vibration

If the rotatory inertia effect is neglected, the equations of motion for an element of a cylindrical shell can be written as

$$\left.\begin{aligned} &\frac{\partial N_x}{\partial x} + \frac{1}{a}\frac{\partial N_{\varphi x}}{\partial \varphi} = \rho h \frac{\partial^2 u}{\partial t^2} \\ &\frac{1}{a}\frac{\partial N_\varphi}{\partial \varphi} + \frac{\partial N_{x\varphi}}{\partial x} - \frac{Q_\varphi}{a} = \rho h \frac{\partial^2 v}{\partial t^2} \end{aligned}\right| \quad \ldots\ldots\ldots [1]$$

---

[1] Associate Professor of Mechanical Engineering, L. C. Smith College of Engineering, Syracuse University. Assoc. Mem. ASME.

[2] Numbers in parentheses refer to the Bibliography at the end of the paper.

Presented at the National Conference of the Applied Mechanics Division, Troy, N. Y., June 16–18, 1955, of The American Society of Mechanical Engineers.

Discussion of this paper should be addressed to the Secretary, ASME, 29 West 39th Street, New York N. Y., and will be accepted until January 10, 1956, for publication at a later date. Discussion received after the closing date will be returned.

Note: Statements and opinions advanced in papers are to be understood as individual expressions of their authors and not those of the Society. Manuscript received by ASME Applied Mechanics Division, April 19, 1954. Paper No. 55—APM-13.

$$\left.\begin{aligned}
&\frac{\partial Q_x}{\partial x}+\frac{1}{a}\frac{\partial Q_\varphi}{\partial \varphi}+\frac{N_\varphi}{a}=\rho h\frac{\partial^2 w}{\partial t^2}\\
&\frac{\partial M_{x\varphi}}{\partial x}-\frac{1}{a}\frac{\partial M_\varphi}{\partial \varphi}+Q_\varphi=0\\
&\frac{1}{a}\frac{\partial M_{\varphi x}}{\partial \varphi}+\frac{\partial M_x}{\partial x}-Q_x=0\\
&N_{x\varphi}-N_{\varphi x}=0
\end{aligned}\right\}\quad\ldots\ldots[1]$$

(*continued*)

which are obtained by substituting the translatory inertia forces for the static forces in the equilibrium equations for the element. One form of these equilibrium equations involving only the static force in the radial direction is given by Timoshenko (8), whose notations also have been used in these equations. In addition, ρ indicates the density of the material and t the time. By following the same procedure as given in reference (8), Equations [1] lead to the following equations which involve only displacement components as the dependent variables

$$\left.\begin{aligned}
&\frac{\partial^2 u}{\partial x^2}+\frac{1-\mu}{2}\frac{\partial^2 u}{\partial s^2}+\frac{1+\mu}{2}\frac{\partial^2 v}{\partial x\partial s}-\frac{\mu}{a}\frac{\partial w}{\partial x}=\frac{1-\mu^2}{E}\rho\frac{\partial^2 u}{\partial t^2}\\
&\frac{1+\mu}{2}\frac{\partial^2 u}{\partial x\partial s}+\frac{1-\mu}{2}\frac{\partial^2 v}{\partial x^2}+\frac{\partial^2 v}{\partial s^2}-\frac{1}{a}\frac{\partial w}{\partial s}+\frac{h^2}{12a}\left[\frac{1-\mu}{a}\frac{\partial^2 v}{\partial x^2}+\frac{1}{a}\frac{\partial^2 v}{\partial s^2}+\frac{\partial^4 w}{\partial x^2\partial s}+\frac{\partial^4 w}{\partial s^3}\right]=\frac{1-\mu^2}{E}\rho\frac{\partial^2 v}{\partial t^2}\\
&\frac{1}{a}\left(\mu\frac{\partial u}{\partial x}+\frac{\partial v}{\partial s}-\frac{w}{a}\right)-\frac{h^2}{12}\nabla^4 w-\frac{h^2}{12}\left[\frac{2-\mu}{a}\frac{\partial^3 v}{\partial x^2\partial s}+\frac{1}{a}\frac{\partial^3 v}{\partial s^3}\right]=\frac{1-\mu^2}{E}\rho\frac{\partial^2 w}{\partial t^2}
\end{aligned}\right\}\quad\ldots[2]$$

in which

$$s=a\varphi$$

and

$$\nabla^4=\nabla^2\nabla^2=\left(\frac{\partial^2}{\partial x^2}+\frac{\partial^2}{\partial s^2}\right)\left(\frac{\partial^2}{\partial x^2}+\frac{\partial^2}{\partial s^2}\right)$$

As advanced by Donnell, we shall consider the components u and v to be of the order of magnitude of $w\sqrt{h/a}$; then the terms in connection with the square brackets in Equations [2] are of a higher order than the others and may be neglected. These equations are therefore reduced to the following simpler form

$$\frac{\partial^2 u}{\partial x^2}+\frac{1-\mu}{2}\frac{\partial^2 u}{\partial s^2}+\frac{1+\mu}{2}\frac{\partial^2 v}{\partial x\partial s}-\frac{\mu}{a}\frac{\partial w}{\partial x}=\frac{1-\mu^2}{E}\rho\frac{\partial^2 u}{\partial t^2}\quad\ldots[3]$$

$$\frac{1+\mu}{2}\frac{\partial^2 u}{\partial x\partial s}+\frac{1-\mu}{2}\frac{\partial^2 v}{\partial x^2}+\frac{\partial^2 v}{\partial s^2}-\frac{1}{a}\frac{\partial w}{\partial s}=\frac{1-\mu^2}{E}\rho\frac{\partial^2 v}{\partial t^2}\quad\ldots[4]$$

$$\frac{\mu}{a}\frac{\partial u}{\partial x}+\frac{1}{a}\frac{\partial v}{\partial s}-\frac{w}{a^2}-\frac{h^2}{12}\nabla^4 w=\frac{1-\mu^2}{E}\rho\frac{\partial^2 w}{\partial t^2}\quad\ldots\ldots[5]$$

It may be seen that neglecting the terms in connection with the brackets in Equations [2] is equivalent to neglecting the term Q_φ/a in the second of Equations [1] and the terms

$$\frac{1}{a}\frac{\partial v}{\partial s}\quad\text{and}\quad\frac{1}{a}\frac{\partial v}{\partial x}$$

in the expressions for the change of curvature and twist of the middle surface of the shell.[3]

We proceed to rearrange Equations [3], [4], and [5] in a similar manner as indicated by Donnell. Applying $\partial^2/\partial x^2$, $\partial^2/\partial s^2$, and $\partial^2/\partial t^2$ to Equation [3], solving in each case for the term involving v, and substituting these expressions in the equation obtained by applying $\partial^2/(\partial x\partial s)$ to Equation [4], we find

$$\nabla^4 u-\frac{\mu}{a}\frac{\partial^3 w}{\partial x^3}+\frac{1}{a}\frac{\partial^3 w}{\partial x\partial s^2}=-\frac{2(1+\mu)}{E}\rho\frac{\partial^2}{\partial t^2}\left(\frac{1-\mu^2}{E}\rho\frac{\partial^2 u}{\partial t^2}-\frac{3-\mu}{2}\nabla^2 u+\frac{\mu}{a}\frac{\partial w}{\partial x}\right)\quad\ldots\ldots[6]$$

in which v has been eliminated. Similarly, applying $\partial^2/\partial x^2$, $\partial^2/\partial s^2$, and $\partial^2/\partial t^2$ to Equation [4], solving in each case for the term involving u, and substituting these in Equation [3], after applying $\partial^2/(\partial x\partial s)$ to it, we obtain

$$\nabla^4 v-\frac{2+\mu}{a}\frac{\partial^3 w}{\partial x^2\partial s}-\frac{1}{a}\frac{\partial^3 w}{\partial s^3}=-\frac{2(1+\mu)}{E}\rho\frac{\partial^2}{\partial t^2}\left(\frac{1-\mu^2}{E}\rho\frac{\partial^2 v}{\partial t^2}-\frac{3-\mu}{2}\nabla^2 v+\frac{1}{a}\frac{\partial w}{\partial s}\right)\quad\ldots\ldots[7]$$

in which u has been eliminated. To derive a third equation in which w will be the only dependent variable, we first apply

$$\frac{\mu}{a}\frac{\partial}{\partial x}\quad\text{and}\quad\frac{1}{a}\frac{\partial}{\partial s}$$

to Equations [6] and [7], respectively, and add the results, thus

$$\nabla^4\left(\frac{\mu}{a}\frac{\partial u}{\partial x}+\frac{1}{a}\frac{\partial v}{\partial s}\right)-\frac{\mu^2}{a^2}\frac{\partial^4 w}{\partial x^4}-\frac{2}{a^2}\frac{\partial^4 w}{\partial x^2\partial s^2}-\frac{1}{a^2}\frac{\partial^4 w}{\partial s^4}=-\frac{2(1+\mu)}{E}\rho\frac{\partial^2}{\partial t^2}\left[\frac{1-\mu^2}{E}\rho\frac{\partial^2}{\partial t^2}\left(\frac{\mu}{a}\frac{\partial u}{\partial x}+\frac{1}{a}\frac{\partial v}{\partial s}\right)-\frac{3-\mu}{2}\nabla^2\left(\frac{\mu}{a}\frac{\partial u}{\partial x}+\frac{1}{a}\frac{\partial v}{\partial s}\right)+\frac{\mu^2}{a^2}\frac{\partial^2 w}{\partial x^2}+\frac{1}{a^2}\frac{\partial^2 w}{\partial s^2}\right]\quad..[8]$$

It is seen that in this equation u and v always appear together in the form of the expression

$$\frac{\mu}{a}\frac{\partial u}{\partial x}+\frac{1}{a}\frac{\partial v}{\partial s}$$

Solving for this expression from Equation [5] in terms of w and its derivatives, substituting the result into Equation [8] and simplifying we find finally

$$\frac{h^2}{12}\nabla^8 w+\frac{1-\mu^2}{a^2}\frac{\partial^4 w}{\partial x^4}=-\frac{2(1+\mu)}{E}\rho\frac{\partial^2}{\partial t^2}\left[\left(\frac{1-\mu^2}{E}\rho\frac{\partial^2}{\partial t^2}-\frac{3-\mu}{2}\nabla^2\right)\left(\frac{1-\mu^2}{E}\rho\frac{\partial^2 w}{\partial t^2}+\frac{w}{a^2}+\frac{h^2}{12}\nabla^4 w\right)+\frac{1-\mu}{2}\nabla^4 w+\frac{\mu^2}{a^2}\frac{\partial^2 w}{\partial x^2}+\frac{1}{a^2}\frac{\partial^2 w}{\partial s^2}\right]\quad\ldots[9]$$

Equations [6], [7], and [9] will be the basis for our further in-

[3] The simplified equations should preferably be looked upon as being derived according to this second viewpoint of neglecting all except the most important terms due to shell action in Equations [1] and the curvature and twist expressions. At the Conference, the author had the opportunity of consulting Prof. L. H. Donnell, who is also of the opinion that the order-of-magnitude analysis is not to be taken seriously.

vestigation.[4] By putting the right-hand sides of these equations equal to zero and inserting terms due to static loadings, Donnell's equations may be obtained.

The General Problem

We assume the shell to vibrate in a normal mode with a natural circular frequency ω and the displacement components u, v, and w to be proportional to a simple harmonic function of ωt. Since the displacement must further be periodic in φ with period 2π, its components will also be proportional to the sine or cosine of multiples of φ. It remains to determine the components as functions of x. Without losing generality their general form may be taken as

$$\left.\begin{aligned} u &= \sum_i A_i e^{\lambda_i \frac{x}{l}} \cos m\varphi \sin \omega t \\ v &= \sum_i B_i e^{\lambda_i \frac{x}{l}} \sin m\varphi \sin \omega t \\ w &= \sum_i C_i e^{\lambda_i \frac{x}{l}} \cos m\varphi \sin \omega t \end{aligned}\right\} \quad (i = 1, 2, \ldots, 8) \ldots [10]$$

in which l is the given length of the shell, m an arbitrarily chosen positive integer equal to the number of circumferential waves, A_i, B_i, C_i are constant coefficients, and λ_i is to be solved from the auxiliary equations derived from the vibration equations. In the present case one of these equations, Equation [9], will be sufficient for the determination of λ_i. Since this equation is of the eighth order, its auxiliary equation will be of the eighth degree and have eight roots; consequently, each of the foregoing summations contains eight terms. As in all problems of small vibrations, while the ratios between one another of the coefficients A_i, B_i, C_i can be found, their absolute values are indeterminate.

For a shell of given dimensions and an arbitrarily chosen value of m, the problem is to find the frequency equation as well as to determine the displacement components as functions of x.

The method of solution according to Love (2) would be as follows: The displacement components must satisfy the system of vibration Equations [6], [7], and [9]. Substitution of Equation [10] in these yields

$$A_i\left[\frac{2}{1-\mu}\Omega^2 - \frac{3-\mu}{1-\mu}\Omega m^2\left(1 - \frac{\lambda_i^2 a^2}{m^2 l^2}\right) + m^4\left(1 - \frac{\lambda_i^2 a^2}{m^2 l^2}\right)^2\right] = C_i \lambda_i \frac{a}{l}\left[\frac{2\mu}{1-\mu}\Omega + m^2\left(1 + \mu\frac{\lambda_i^2 a^2}{m^2 l^2}\right)\right] \quad (i = 1, 2, \ldots, 8) \ldots [11]$$

$$B_i\left[\frac{2}{1-\mu}\Omega^2 - \frac{3-\mu}{1-\mu}\Omega m^2\left(1 - \frac{\lambda_i^2 a^2}{m^2 l^2}\right) + m^4\left(1 - \frac{\lambda_i^2 a^2}{m^2 l^2}\right)^2\right] = C_i m\left[-\frac{2}{1-\mu}\Omega + m^2\left\{1 - (2+\mu)\frac{\lambda_i^2 a^2}{m^2 l^2}\right\}\right] \quad (i = 1, 2, \ldots, 8) \ldots [12]$$

$$(1-\mu)(1-\mu^2)\left(\frac{\lambda_i a}{l}\right)^4 = 2\Omega^2 - \Omega^2\left[2 + (3-\mu)m^2\left(1 - \frac{\lambda_i^2 a^2}{m^2 l^2}\right) + 2km^4\left(1 - \frac{\lambda_i^2 a^2}{m^2 l^2}\right)^2\right] + \Omega\left[(3-\mu)m^2\left(1 - \frac{\lambda_i^2 a^2}{m^2 l^2}\right) - 2m^2\left(1 - \mu^2\frac{\lambda_i^2 a^2}{m^2 l^2}\right) + (1-\mu)m^4\left(1 - \frac{\lambda_i^2 a^2}{m^2 l^2}\right)^2 + (3-\mu)km^6\left(1 - \frac{\lambda_i^2 a^2}{m^2 l^2}\right)^3\right] - (1-\mu)km^8\left(1 - \frac{\lambda_i^2 a^2}{m^2 l^2}\right)^4 \quad (i = 1, 2, \ldots, 8) \ldots [13]$$

in which the following dimensionless quantities have been introduced

$$\Omega = \frac{1-\mu^2}{E}\rho a^2\omega^2, \quad k = \frac{h^2}{12a^2}$$

The displacement components also must satisfy the boundary conditions, which are eight in number, four for each of the two edges $x = 0$ and $x = l$. These conditions relating u, v, w, and their derivatives lead to equations that are linear and homogeneous in A_i, B_i, and C_i. By means of Equations [11] and [12] we can eliminate A_i and B_i and obtain eight linear homogeneous equations connecting the eight values of C_i. For C_i to be nonvanishing the determinant of their coefficients in these equations, which are functions of the unknowns Ω and λ_i, must be set equal to zero. Theoretically, λ_i may be solved in terms of Ω from Equation [13] and thus eliminated from this final relationship, which then consists of Ω as the only unknown and constitutes the frequency equation. The equation is cubic in Ω, and its three roots determine the three natural frequencies of the shell. As it is rather difficult to solve Equation [13] for λ_i explicitly, this method is not practical.

Flügge (3) gave another procedure for solving the vibration problem. The length l of the cylinder instead of the frequency is taken as the unknown, and the displacement components are taken as functions of the radius a instead of the length, i.e., l being replaced by a in Equations [10]. Equations [11], [12], and [13] similarly may be obtained, with the exception that the ratio a/l is now replaced by unity in all equations. From Equation [13] λ_i may be solved in terms of m, Ω, and the given dimensions of the shell a and h. The boundary conditions may then be expressed exclusively in terms of C_i, through elimination of A_i and B_i by means of Equations [11] and [12]. When the determinant of the coefficients C_i is set equal to zero, an equation is obtained which consists of l as the only unknown. The equation will be transcendent in l, and the lowest value of l satisfying this equation represents the length of the shell that will oscillate with a frequency corresponding to Ω, with m circumferential waves or $2m$ nodal lines parallel to the element of the shell, and without any nodal circles. The higher values of l satisfying the equation correspond to modes with successively increasing number of nodal circles. This procedure is thus essentially one of trial and error so far as determining the frequency is concerned. Although Flügge himself did not actually use this procedure because of its complexity, it appears to be the most promising one to give more precise results.

To solve the general problem on the basis of Equations [6], [7], and [9] is therefore still rather involved, though these equations are of a simpler form than the usual ones. For the remaining part of our present study, we shall make the following assumption

$$\frac{|\lambda_i^2|\, a^2}{m^2 l^2} \ll 1 \ldots [14]$$

in which the absolute sign is necessary because of the fact that λ_i may be imaginary. The assumption will therefore restrict the application of the following method as well as the results to be ob-

[4] The recent work of Naghdi and Berry (9) came to the author's attention after these equations had been obtained. These authors started with three equations which are essentially the same as Equations [2] except that a different coefficient in front of the term $\partial^2 v/\partial x^2 \partial s$ was used and external loading included. They used a similar procedure and obtained three equations which are analogous to but much lengthier than Equations [6], [7], and [9]. No attempt was made by these authors to solve the vibration problem.

tained to comparatively long shells with a fairly small number of longitudinal waves[5] and large number of circumferential waves.

By virtue of the assumption just introduced, Equations [11], [12], and [13] are now reduced to the following much simplified form

$$A_i = C_i\lambda_i M\frac{a}{l}\ (i = 1, 2, 3, 4) \quad \ldots\ldots [15]$$

$$B_i = C_i N\ (i = 1, 2, 3, 4) \quad \ldots\ldots [16]$$

$$(1-\mu)(1-\mu^2)\left(\frac{\lambda_i a}{l}\right)^4 = F\ (i = 1, 2, 3, 4) \quad \ldots\ldots [17]$$

in which
$$M = \frac{2\mu\Omega + (1-\mu)m^2}{2\Omega^2 - (3-\mu)m^2\Omega + (1-\mu)m^4}$$

$$N = \frac{-2m\Omega + (1-\mu)m^3}{2\Omega^2 - (3-\mu)m^2\Omega + (1-\mu)m^4}$$

$$F = 2\Omega^3 - \Omega^2[2 + (3-\mu)m^2 + 2km^4] + \Omega[(1-\mu)m^2(m^2+1) + (3-\mu)km^6] - (1-\mu)km^8$$

Since Equation [17] is now of the fourth degree, there will be only four roots of λ_i and four sets of values of A_i, B_i, and C_i. Obviously the roots of λ_i are of the form

$$\lambda_1 = K, \quad \lambda_2 = -K, \quad \lambda_3 = iK, \quad \lambda_4 = -iK \quad \ldots [18]$$

where K is a real number.

We proceed to investigate three particular cases.

Shells With Both Edges Freely Supported

The boundary conditions for this case are

$$u = v = w = M_x = 0 \qquad \text{at } x = 0 \text{ and } x = l$$

The last condition of zero moment is equivalent to, by neglecting the term

$$\frac{1}{a}\frac{\partial v}{\partial s}$$

in the expression for the change of curvature in the φ-direction in accordance with the foregoing derivation of the vibration equations

$$\frac{\partial^2 w}{\partial x^2} + \mu\frac{\partial^2 w}{\partial s^2} = 0 \quad \text{at} \quad x = 0 \quad \text{and} \quad x = l$$

Substituting Equation [10] into these conditions and making use of Equations [15] and [16] we find

$$u = 0: \sum_i C_i\lambda_i = 0, \quad \sum_i C_i\lambda_i e^{\lambda_i} = 0 \quad (i = 1, 2, 3, 4)$$

$$\left.\begin{aligned} w = v = 0: &\sum_i C_i = 0, \quad \sum_i C_i e^{\lambda_i} = 0 \quad (i = 1, 2, 3, 4) \\ M_x = 0: &\sum_i C_i\lambda_i^2 = 0, \quad \sum_i C_i\lambda_i^2 e^{\lambda_i} = 0 \quad (i = 1, 2, 3, 4) \end{aligned}\right\} [19]$$

Only four of these equations can be satisfied by the four sets of values of C_i and λ_i. We shall neglect the requirement $u = 0$, which is the least essential one. Physically, this means that the shell at the freely supported edge is restricted to remain circular but may move freely in the longitudinal direction. Substituting Equations [18] in [19] and equating the determinant of the coefficients of C_i equal to zero in order to have nonvanishing solutions of C_i, we obtain

$$\begin{vmatrix} 1 & 1 & 1 & 1 \\ e^K & e^{-K} & e^{iK} & e^{-iK} \\ K^2 & K^2 & -K^2 & -K^2 \\ K^2e^K & K^2e^{-K} & -K^2e^{iK} & -K^2e^{-iK} \end{vmatrix} = 0$$

which leads to

$$16iK^4 \sinh K \sin K = 0 \quad \ldots\ldots [20]$$

The characteristic values of K are therefore given by

$$K = n\pi \quad (n = 1, 2, 3, \ldots)$$

The first characteristic value $K = 0$ corresponds to the trivial case of zero displacement and is therefore excluded. The roots of λ_i are now

$$\lambda_1 = n\pi, \quad \lambda_2 = -n\pi, \quad \lambda_3 = in\pi, \quad \lambda_4 = -in\pi$$

and the frequency equation is, by substituting λ_i in Equation [17]

$$2\Omega^3 - \Omega^2[2 + (3-\mu)m^2 + 2km^4] + \Omega[(1-\mu)m^2(m^2+1) + (3-\mu)km^6] - (1-\mu)km^8 - (1-\mu)(1-\mu^2)\left(\frac{n\pi a}{l}\right)^4 = 0 \quad \ldots\ldots [21]$$

Any three of the coefficients C_i may be put in terms of the fourth one by substituting the values of λ_i just obtained into any three of Equations [19] and solving; thus

$$C_1 = C_2 = 0, \quad C_3 = -C_4$$

By further making use of Equations [15] and [16] the displacement components in Equations [10] become finally for the present case

$$\left.\begin{aligned} u &= MC\frac{n\pi a}{l}\cos\frac{n\pi x}{l}\cos m\varphi \sin\omega t \\ v &= NC\sin\frac{n\pi x}{l}\sin m\varphi \sin\omega t \\ w &= C\sin\frac{n\pi x}{l}\cos m\varphi \sin\omega t \end{aligned}\right\} \quad \ldots\ldots [22]$$

in which $C = 2iC_3$.

With the conclusion that the method of indeterminate shell length is rather complicated, Flügge used a different approach to solve the problem of a shell with freely supported edges. He assumed the displacements in a form satisfying the boundary conditions, and these displacements may immediately be identified with the ones obtained here in Equations [22]. The frequency equation was then obtained by substituting the displacements into the vibration equations; his result is, in our notations

$$\begin{aligned} 2\Omega^3 - \Omega^2[2 + (3-\mu)(p^2+m^2) + 2k(p^2+m^2)^2] \\ + \Omega[2(1-\mu^2)p^2 + (1-\mu)(p^2+m^2)(p^2+m^2+1) \\ + (3-\mu)k(p^2+m^2)^3] - (1-\mu)(1-\mu^2)p^4 \\ - (1-\mu)k(p^2+m^2)^4 \\ + (1-\mu)k[2\{\mu p^6 + 3p^4m^2 + (4-\mu)p^2m^4 + m^6\} \\ - 2(2-\mu)p^2m^2 - m^4] = 0 \end{aligned} \quad \ldots [23]$$

in which
$$p = \frac{n\pi a}{l}$$

Subjected to the same assumption as before, namely, since $|\lambda_i^2| = n^2\pi^2$

[5] The reason for this is that $|\lambda_i^2|$ should be relatively small. According to the results to be obtained for the various cases, this requires that n, n', or n'' be small, which correspond to small number of longitudinal waves. In the freely supported case the values of n are integers representing exactly the number of longitudinal half-waves.

$$p^2 = \frac{|\lambda_i^2|a^2}{l^2} << m^2$$

Equation [23] would be reduced to

$$2\Omega^3 - \Omega^2[2 + (3 - \mu)m^2 + 2km^4] + \Omega[(1 - \mu)m^2(m^2 + 1) + (3 - \mu)km^6] - (1 - \mu)(1 - \mu^2)\left(\frac{n\pi a}{l}\right)^4 - (1 - \mu)km^8 + (1 - \mu)k(2m^6 - m^4) = 0 \quad [24]$$

With the exception of the additional last term on the left-hand side, this equation is the same as Equation [21]. The minor difference is attributed to the use of different equations of vibration.

Consider now Flügge's numerical example. The given data are

$a = 8.50$ meters	$l = 42.30$ meters
$h = 9.3$ cm	$\rho g = 2.4$ tons/cu meter
$E = 210{,}000$ kg/cm^2	$\mu = 1/6$
$m = 4$	$n = 1$

from which

$$\Omega = 8.20 \times 10^{-6}\omega^2, \qquad k = 10^{-5}$$

The value $(n\pi a/ml)^2 = 0.0249$ is seen to be small compared with unity, though not quite negligible. Substitution of these numerical quantities in Equations [21], [23], and [24] yield, respectively[6]

$$\Omega^3 - 23.7\Omega^2 + 113.4\Omega - 0.337 = 0$$
$$\Omega^3 - 24.2\Omega^2 + 119.3\Omega - 0.329 = 0 \quad [25]$$
$$\Omega^3 - 23.7\Omega^2 + 113.4\Omega - 0.304 = 0$$

from which the frequencies are found to be, respectively

$\omega_1 = 19.05$ sec^{-1},	$\omega_2 = 901$ sec^{-1},	$\omega_3 = 1443$ sec^{-1}
$\omega_1 = 18.36$ sec^{-1},	$\omega_2 = 918$ sec^{-1},	$\omega_3 = 1452$ sec^{-1}
$\omega_1 = 18.09$ sec^{-1},	$\omega_2 = 901$ sec^{-1},	$\omega_3 = 1443$ sec^{-1}

The difference is in no case greater than 6 per cent, and the lowest frequency obtained by the present method is only 3.76 per cent higher than Flügge's result.

To solve for the natural frequency of a shell with freely supported edges, Arnold and Warburton (4) also assumed the displacement components in the form given in Equations [22]. By means of the strain relations of Timoshenko, they expressed the strain and kinetic energies in terms of these displacements and wrote three Lagrange equations. The frequency equation was obtained in the usual way of setting a determinant of coefficients equal to zero. Numerical results for the lowest frequency were presented in the form of graphs. Experiments also were carried out. For the foregoing numerical example, their frequency equation yields

$$\omega_1 = 18.1 \text{ sec}^{-1}$$

which is lower than Flügge's result but almost exactly equal to the result obtained from the simplified Flügge's equation.

Shells With Both Edges Clamped

In this case the boundary conditions are

$$u = v = w = \frac{\partial w}{\partial x} = 0, \quad \text{at } x = 0 \text{ and } x = l$$

Making use of Equations [10], [15], and [16] as before, we find

$$\left.\begin{aligned} w = v = 0 &: \sum_i C_i = 0, \qquad \sum_i C_i e^{\lambda_i} = 0 \\ \frac{\partial w}{\partial x} = u = 0 &: \sum_i C_i\lambda_i = 0, \qquad \sum_i C_i\lambda_i e^{\lambda_i} = 0 \end{aligned}\right\} \quad (i = 1, 2, 3, 4) \quad [26]$$

All four conditions can be satisfied without difficulty. Substituting the four values of λ_i from Equation [18] in these and equating the determinant of the coefficients of C_i equal to zero, we have

$$\begin{vmatrix} 1 & 1 & 1 & 1 \\ e^K & e^{-K} & e^{iK} & e^{-iK} \\ K & -K & iK & -iK \\ Ke^K & -Ke^{-K} & iKe^{iK} & -iKe^{-iK} \end{vmatrix} = 8iK^2(\cos K \cosh K - 1) = 0 \quad [27]$$

The first root of K satisfying this condition is evidently zero, which, as in the case of freely supported edges, is also related to the trivial case of zero displacement. Higher characteristic values of K may be computed to any desired degree of accuracy by the trial-and-error method. We shall write these values as

$$K = n'\pi$$

and the successive values of n' are

$$1.506, \qquad 2.500, \qquad 3.500, \qquad 4.500, \qquad \ldots$$

The four roots of λ_i are therefore

$$\lambda_1 = n'\pi, \qquad \lambda_2 = -n'\pi, \qquad \lambda_3 = in'\pi, \qquad \lambda_4 = -in'\pi$$

The frequency equation is

$$2\Omega^3 - \Omega^2[2 + (3 - \mu)m^2 + 2km^4] + \Omega[(1 - \mu)m^2(m^2 + 1) + (3 - \mu)km^6] - (1 - \mu)km^8 - (1 - \mu)(1 - \mu^2)\left(\frac{n'\pi a}{l}\right)^4 = 0 \quad [28]$$

To find the displacement we solve for any three of C_i in terms of the fourth by means of any three of Equations [26]. Substitution of the result in Equation [10] yields

$$\left.\begin{aligned} w &= 2C_1[(\sinh n'\pi - \sin n'\pi) - (\cosh n'\pi - \cos n'\pi)]^{-1}\left[(\sinh n'\pi - \sin n'\pi)\left(\cosh\frac{n'\pi x}{l} - \cos\frac{n'\pi x}{l}\right) - (\cosh n'\pi - \cos n'\pi)\left(\sinh\frac{n'\pi x}{l} - \sin\frac{n'\pi x}{l}\right)\right]\cos m\varphi \sin\omega t \\ u &= Ma\frac{\partial w}{\partial x} \\ v &= -\frac{Na}{m}\frac{\partial w}{\partial s} \end{aligned}\right\} \quad [29]$$

The first three terms in Equations [21] and [28] are identical. As can be seen from the foregoing numerical example, the two higher frequencies may be computed approximately from the equation obtained by putting these terms equal to zero. The conclusion is therefore arrived at that these higher frequencies are practically the same for both freely supported and clamped edges. The lowest frequency, on the other hand, may be computed approximately from the equation formulated by putting equal to zero the Ω-term and the constant terms in Equations [21] or [28]. This third frequency is therefore always lower for freely supported

[6] A numerical error exists in Flügge's original computation. His results show that a wrong value 0.329/2 was used in the place of 0.329 in Equation [25].

than for clamped edges. As the ratio a/l becomes smaller, the difference between the two cases also diminishes, which obviously must be true.

The present case of clamped edges also was considered by Arnold and Warburton (5) using the same method described before.

Shells With One Edge Freely Supported and Other Edge Clamped

Making the same adjustment for the boundary condition of a freely supported edge as before, namely, assuming that u may be nonvanishing, we may write the boundary conditions for the present case as

$$w = v = M_x = 0 \qquad \text{at } x = 0$$

$$u = v = w = \frac{\partial w}{\partial x} = 0 \qquad \text{at } x = l$$

which lead to

$$\left.\begin{aligned} \sum_i C_i = 0, \qquad & \sum_i C_i\lambda_i^2 = 0 \\ \sum_i C_i e^{\lambda_i} = 0, \qquad & \sum_i C_i\lambda_i e^{\lambda_i} = 0 \end{aligned}\right\} (i = 1, 2, 3, 4)$$

Equating the determinant of the coefficients of C_i equal to zero yields

$$\tan K - \tanh K = 0 \qquad \text{.....[30]}$$

the roots of which are

$$K = n''\pi$$

with the consecutive values of n'' equal to

$$1.250, \quad 2.250, \quad 3.250, \quad 4.250, \quad \ldots\ldots$$

The four roots of λ_i are therefore

$$\lambda_1 = n''\pi, \quad \lambda_2 = -n''\pi, \quad \lambda_3 = in''\pi, \quad \lambda_4 = -in''\pi$$

It is evident that the consecutive lowest frequencies for this case lie between the corresponding ones for the two former cases and that the two higher frequencies are approximately equal to those for the former cases.

Discussion

It will be interesting to compare the vibration of cylindrical shells with the lateral vibration of beams. The frequency equations for beams with both ends freely supported, with both ends clamped, and with one end freely supported and the other end clamped are, respectively, according to Timoshenko (10)

$$\left.\begin{aligned} &\sin kl = 0 \\ &\cos kl \cosh kl - 1 = 0 \\ &\tan kl - \tanh kl = 0 \end{aligned}\right\} \qquad \text{.....[31]}$$

in which l is the length of the beam and k is the characteristic number related to the circular frequency p by the definition

$$k^4 = p^2/a^2$$

a^2 being a factor determined by the cross-sectional dimensions and the properties of the material of the beam. It is now clear that the three Equations [31] are entirely similar to Equations [20], [27], and [30], respectively, for cylindrical shells with similar edge conditions. There are two reasons for this similarity: (*a*) Equation [17] after simplification is of the same fourth degree and of the same simplest form as the auxiliary equation derived from the differential equation governing the normal function in the beam problems. (*b*) The simplified boundary conditions for the shell also may be seen to be similar to those for a beam. As a result, the problem of the vibration of cylindrical shells becomes closely related to that of the lateral vibration of beams.

As was pointed out earlier, the simplifying assumption introduced in Equation [14] will indeed restrict the application of the foregoing results to comparatively long cylindrical shells with a fairly small number of longitudinal waves and large number of circumferential waves. For short shells with a large number of longitudinal waves or small number of circumferential waves, some other method for solving Equations [6], [7], and [9] will have to be used, and Galerkin's method seems applicable. The range of validity of the present approximation depends not only upon the inaccuracy resulted from the assumption in Equation [14], but also upon the accuracy of the three equations of motion [6], [7], and [9]. While the accuracy of Donnell's original static equations have been discussed recently by Hoff (11), that of the corresponding dynamic equations remains to be investigated. Using Flügge's result as a basis for comparison we have seen that in the numerical example the discrepancy was less than 4 per cent when $|\lambda_i^2|\, a^2/(m^2l^2)$ was equal to about 1/40. Although a quantitative analysis of the exact range of validity is still lacking, the present method nevertheless represents one that may be applied in a simple manner to cylindrical shells having any arbitrary lengths with any combination of the freely supported and clamped-edge conditions.

BIBLIOGRAPHY

1 "Theory of Sound," by Lord Rayleigh, The Macmillan Company, New York, N. Y., second edition, vol. 1, chapter XA, 1894.

2 "Mathematical Theory of Elasticity," by A. E. H. Love, Dover Publications, Inc., New York, N. Y., fourth edition, 1944, pp. 543–549.

3 "Statik und Dynamik der Schalen," by W. Flügge, Julius Springer, Berlin, Germany, 1934, pp. 227–232.

4 "Flexural Vibrations of the Walls of Thin Cylindrical Shells Having Free Supported Ends," by R. N. Arnold and G. B. Warburton, Proceedings of the Royal Society of London, England, series A, vol. 197, 1949, pp. 238–256.

5 "The Flexural Vibrations of Thin Cylinders," by R. N. Arnold and G. B. Warburton, Proceedings of the Institution of Mechanical Engineers, vol. 167, 1953, pp. 62–74.

6 "Tables for Frequencies and Modes of Free Vibration of Infinitely Long Thin Cylindrical Shells," by M. L. Baron and H. H. Bleich, Journal of Applied Mechanics, Trans. ASME, vol. 76, 1954, pp. 178–184.

7 "Stability of Thin-Walled Tubes under Torsion," by L. H. Donnell, Washington, D. C., NACA Technical Report No. 479, 1933.

8 "Theory of Plates and Shells," by S. Timoshenko, McGraw-Hill Book Company, Inc., New York, N. Y., 1940, p. 440.

9 "On the Equations of Motion of Cylindrical Shells," by P. M. Naghdi and J. G. Berry, Journal of Applied Mechanics, Trans. ASME, vol. 76, 1954, pp. 160–166.

10 "Vibration Problems in Engineering," by S. Timoshenko, D. Van Nostrand Company, Inc., New York, N. Y., second edition, 1934, pp. 338–345.

11 "The Accuracy of Donnell's Equations," by N. J. Hoff, Journal of Applied Mechanics, Trans. ASME, vol. 77, 1955, pp. 329–334.

Buckling of Laminated Columns

By L. G. CLARK,[1] BRYAN, OHIO

A theory is developed to determine the buckling of laminated columns composed of two or more laminations and riveted or fixed together at certain points along the column. The laminations can be of different size and material but must be long in comparison to the cross-sectional dimensions. The final result is presented in a form suitable for easy application. It is shown that for two laminations joined at an infinite number of points the problem reduces to that of a simple column. Two pinned-end columns were tested and the results are in satisfactory agreement with the theory.

Introduction

THE theory of buckling of a solid column or beam with longitudinal loads is well known and has been investigated for many diverse cases. Also much work has been done concerning the buckling of built-up columns, sandwich plates, and so on. However, to the author's knowledge, there is very little known about the buckling of laminated columns where the laminations are joined at a discrete number of points. The theory of the deflection of a beam of this construction has been carried out by the author,[2] which involves the use of a special integrated boundary condition. This same type of boundary condition will be used to develop a theory for the determination of the buckling load of a laminated column. Only elastic buckling is considered.

"n" Laminations Joined at Arbitrary Points

Figs. 1 and 2 will be used to define the problem and some of the nomenclature.

Fig. 1 is a typical laminated column where it is desired to find the critical value of P. It will be found necessary to deal with the problem by regions. A region is defined as that length L, Fig. 1, of a column between any two adjacent joining points.

Fig. 2 is a detailed drawing of part of an arbitrary region where the column is composed of n laminations. At x equal to zero the heavy line represents a point where the laminations are rigidly attached together by some means such as a rivet or spot weld. It is assumed that there is no relative movement between laminations at this point; that is, there is no shear strain in the rivet or weld. The upper part of the figure is a section of the column taken between the joining points of the region. The usual assumption is made that plane sections in the lamination remain plane. We denote by F_k the compressive force in lamination k acting at the neutral axis of the lamination and by m_k the couple at the upper end of lamination k; y_k is the deflection from the zero load position; y_0 is the deflection of lamination 1 at x equal to zero. The conditions of load at x equal to zero can always be represented by the force P and a couple M. Terms a_k and b_k are assumed constant for each lamination.

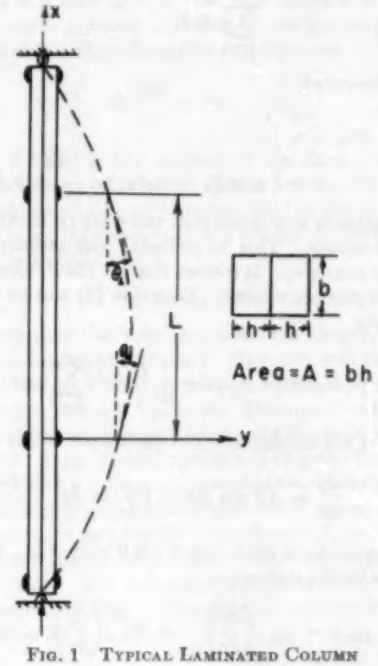

Fig. 1 Typical Laminated Column

Equilibrium Equations

From equilibrium of the free body of Fig. 2

$$P = F_1 + F_2 + \ldots + F_k + \ldots + F_n \ldots\ldots [1]$$

Moments about point A, assuming small displacements, result in

$$m_1 + m_2 + \ldots + m_n + F_1a_1 + F_2(a_1 + a_2 + b_1) + F_3(a_1 + a_2 + a_3 + b_1 + b_2) + \ldots + F_n(a_1 + a_2 + \ldots + a_n + b_1 + \ldots + b_{n-1}) + P(y_1 - y_0) - M = 0 \ldots [2]$$

The necessary assumptions are not only that the displacements are small but that any separation of the laminations is negligible.

Thus $$y_1 = y_2 = y_3 = \ldots = y_k = \ldots = y_n = y \ldots\ldots [3]$$

From elementary beam theory

$$E_kI_k\frac{d^2y_k}{dx^2} = m_k \ldots\ldots [4]$$

where E_k and I_k are the elastic modulus and the area moment of inertia, respectively, of lamination k.

Equation [2] can then be written as

$$(E_1I_1 + E_2I_2 + \ldots E_nI_n)\frac{d^2y}{dx^2} + Py = Py_0 + M - F_1a_1 - F_2(a_1 + a_2 + b_1) \ldots [5]$$

Defining the following terms

[1] Formerly, Assistant Professor of Engineering Mechanics, University of Michigan; now Consulting Engineer, Aro Equipment Corporation. Assoc. Mem. ASME.

[2] "Deflection of Laminated Beams," by L. G. Clark. Trans. ASCE, vol. 119, 1954, p. 721.

Presented at the National Conference of the Applied Mechanics Division, Troy, N. Y., June 16–18, 1955, of The American Society of Mechanical Engineers.

Discussion of this paper should be addressed to the Secretary, ASME, 29 West 39th Street, New York, N. Y., and will be accepted until January 10, 1956, for publication at a later date. Discussion received after closing date will be returned.

Note: Statements and opinions advanced in papers are to be understood as individual expressions of their authors and not those of the Society. Manuscript received by ASME Applied Mechanics Division, September 9, 1954. Paper No. 55—APM-18.

$$\left.\begin{aligned} \frac{P}{\sum_{k=1}^{n} E_k I_k} &= \beta^2, \quad \frac{M}{\sum_{k=1}^{n} E_k I_k} = \gamma, \quad \frac{a_1}{\sum_{k=1}^{n} E_k I_k} = \alpha_1 \ldots \\ \frac{a_1 + \ldots + a_j + b_1 + \ldots + b_{j-1}}{\sum_{k=1}^{n} E_k I_k} &= \alpha_j \end{aligned}\right\} \ldots [6]$$

Equation [5] becomes

$$\frac{d^2y}{dx^2} + \beta^2 y = \beta^2 y_0 + \gamma - (+ \alpha_1 F_1 + \alpha_2 F_2 + \ldots + \alpha_n F_n) \ldots [7]$$

The assumption is now made that there are no frictional forces between laminations. This is probably not strictly true but should be very nearly so. It follows that all the F_k forces are constant in the region considered. Equation [7] can be integrated directly to yield

$$y = A \sin \beta x + B \cos \beta x + y_0 + \frac{1}{\beta^2}\left(\gamma - \sum_{k=1}^{n} \alpha_k F_k\right) \ldots [8]$$

where A and B are constants. The derivative of y is

$$\frac{dy}{dx} = A\beta \cos \beta x - B\beta \sin \beta x \ldots [9]$$

In the region considered the range of x is $0 < x < L$. The boundary conditions for the region are

$$y_{x=0} = y_0, \; y_{x=L} = y_L, \; \left(\frac{dy}{dx}\right)_{x=0} = \theta_0, \; \left(\frac{dy}{dx}\right)_{x=L} = \theta_L \ldots [10]$$

Using the boundary conditions on the slope, Equation [9] gives

$$\left.\begin{aligned} A &= \theta_0/\beta \\ B &= \frac{\theta_0 \cos \beta L - \theta_L}{\beta \sin \beta L} \end{aligned}\right\} \ldots [11]$$

Equation [8] is now written as

$$y = \frac{\theta_0}{\beta} \sin \beta x + \frac{\theta_0 \cos \beta L - \theta_L}{\beta \sin \beta L} \cos \beta x + y_0 + \frac{1}{\beta^2}\left(\gamma - \sum_{k=1}^{n} \alpha_k F_k\right) \ldots [12]$$

Using the remaining boundary conditions of Equations [10] the following two equations are obtained

$$0 = \frac{\theta_0 \cos \beta L - \theta_L}{\beta \sin \beta L} + \frac{1}{\beta^2}\left(\gamma - \sum_{k=1}^{n} \alpha_k F_k\right) \ldots [13]$$

$$y_L - y_0 = \frac{\theta_0}{\beta} \sin \beta L + \frac{\theta_0 \cos \beta L - \theta_L}{\beta \sin \beta L} \cos \beta L + \frac{1}{\beta^2}\left(\gamma - \sum_{k=1}^{n} \alpha_k F_k\right) \ldots [14]$$

It can be shown that if the values of all the F_k's are known then by use of Equations [12], [13], and [14] certain buckling and deflection problems can be solved. The use of these equations will be demonstrated after it is shown how the F_k's are obtained.

Form of F_k

It has been assumed that there is no relative displacement between any two laminations at the points where they are joined together. This being the case, at the contact plane of two adjacent laminations the elongation between the joining points of a region for one lamination is equal to the elongation of the adjacent lamination for the region.

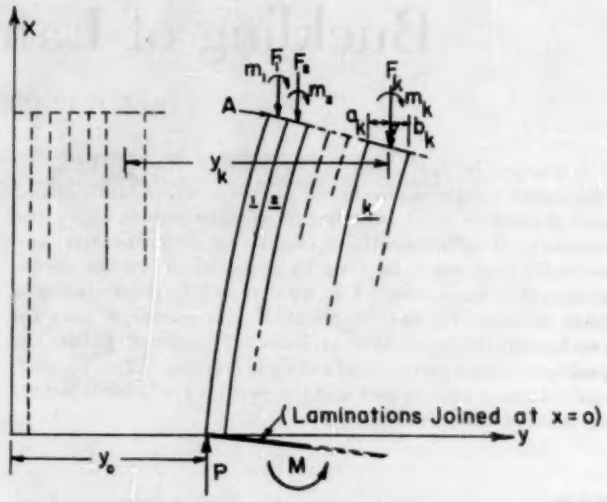

Fig. 2 Section of Column

Referring to Fig. 2 consider the two laminations k and $k + 1$. From ordinary beam theory, the strain γ_k of a longitudinal fiber at the contact plane of lamination k is

$$\gamma_k = -\frac{m_k b_k}{E_k I_k} - \frac{F_k}{A_k E_k} \ldots [15]$$

and for lamination $k + 1$

$$\gamma_{k+1} = \frac{m_{k+1} a_{k+1}}{E_{k+1} I_{k+1}} - \frac{F_{k+1}}{A_{k+1} E_{k+1}} \ldots [16]$$

where A_k and A_{k+1} are the cross-sectional areas of lamination k and $k + 1$, respectively.

In order that the elongation of the two laminations at the contact plane be equal, the following relationship must exist

$$\int_0^L \left(\frac{m_k b_k}{E_k I_k} + \frac{F_k}{A_k E_k}\right) dx = \int_0^L \left(-\frac{m_{k+1} a_{k+1}}{E_{k+1} I_{k+1}} + \frac{F_{k+1}}{A_{k+1} E_{k+1}}\right) dx \ldots [17]$$

by noting that the F_k and F_{k+1} forces are constant and that $m_k = E_k I_k \frac{d^2y}{dx^2}$ Equation [17] can be written as

$$(b_k + a_{k+1}) \int_0^L \frac{d^2y}{dx^2} dx = \left(\frac{F_{k+1}}{A_{k+1} I_{k+1}} - \frac{F_k}{A_k E_k}\right) L \ldots [18]$$

or

$$\frac{b_k + a_{k+1}}{L} (\theta_L - \theta_0) = \frac{F_{k+1}}{A_{k+1} I_{k+1}} - \frac{F_k}{A_k E_k} \ldots [19]$$

There are $n - 1$ equations of the type of Equation [19]. All of the $n - 1$ equations like [19] and the equilibrium equation $P = \sum_{k=1}^{n} F_k$ will allow for each F_k to be obtained in terms of P and $(\theta_L - \theta_0)$. Using this form of the F_k in Equations [13] and [14] one obtains the desired form of the equations where θ_0, θ_L, y_L, y_0, P, and M are the terms of importance.

Limit Proof of Theory

The proof of the equations is valid only to the extent that in the limit the usual differential equation of bending is obtained. That is, as $L \to dx$, which is equivalent to allowing the number of joining points to approach infinity, the equations should reduce to those of a solid column or beam. It will be shown that this is the case. For simplicity consider n laminations all of the same material and the same rectangular cross section, as

$$\left.\begin{aligned} L &\to dx \\ \theta_L &\to \theta_0 + d\theta_0 \\ y_L &\to y_0 + dy_0 \\ \cos \beta L &\to 1 \\ \sin \beta L &\to \beta dx \end{aligned}\right\} \quad \ldots\ldots\ldots\ldots\ldots [20]$$

Equations [13] and [14] become

$$0 = -\frac{1}{\beta^2}\frac{d\theta_0}{dx} + \frac{1}{\beta^2}\left(\gamma - \sum_{k=1}^{n} \alpha_k F_k\right) \ldots\ldots [21]$$

$$dy_0 = \theta_0 dx - \frac{1}{\beta^2}\frac{d\theta_0}{dx} + \frac{1}{\beta^2}\left(\gamma - \sum_{k=1}^{n} \alpha_k F_k\right) \ldots [22]$$

Subtracting Equation [21] from [22] and rearranging terms gives $\theta_0 = (dy_0/dx)$ which is to be expected. Adding Equations [21] and [22] results in

$$dy_0 = \theta_0 dx - \frac{2}{\beta^2}\frac{d^2y}{dx^2} + \frac{2}{\beta^2}\left(\gamma - \sum_{k=1}^{n} \alpha_k F_k\right) \ldots [23]$$

Using $\theta_0 = (dy_0/dx)$ and factoring out $2/\beta^2$ gives

$$\frac{d^2y_0}{dx^2} = \gamma - \sum_{k=1}^{n} \alpha_k F_k \ldots\ldots\ldots\ldots [24]$$

By adding the first $(k-1)$ equations of [19] it is seen that

$$F_k = (k-1)AEh\frac{d\theta_0}{dx} + F_1 \ldots\ldots\ldots\ldots [25]$$

where A is the area and h is the thickness of one lamination. But

$$P = \sum_{k=1}^{n} F_k = \sum_{k=1}^{n} (k-1)AEh\frac{d\theta_0}{dx} + nF_1 \ldots [26]$$

or

$$F_1 = \frac{P}{n} - AEh\frac{d\theta_0}{dx}\frac{n-1}{2} \ldots\ldots\ldots\ldots [27]$$

Equation [25] becomes

$$F_k = AEh\frac{d\theta_0}{dx}\left(k - \frac{n+1}{2}\right) + \frac{P}{n} \ldots\ldots [28]$$

Multiplying Equation [28] by α_k, Equations [6], and adding all $\alpha_k F_k$, Equation [24] is written as

$$\frac{d^2y_0}{dx^2}\left[1 + \frac{Ah^2}{12I}(n^2-1)\right] = \gamma - \frac{Ph}{2EI} \ldots\ldots [29]$$

Although not obvious, Equation [29] is the form for the differential equation of bending of a beam composed of n laminations where all laminations are alike and rigidly joined at all points of contact, that is, a solid column. To verify Equation [29] the case of two identical laminations will be treated. Fig. 1 is considered the schematic drawing where the dimension h is in the plane of bending and is the thickness of one lamination. The laminations are joined at an infinite number of points. For the two laminations Equation [29] becomes

$$\frac{d^2y_0}{dx^2}\left\{1 + \frac{h^2A}{4I}\right\} = \frac{M}{2EI} - \frac{Ph}{2EI} \ldots\ldots\ldots [30]$$

From Fig. 1 it is seen that $Ah^2 = 12\,I$ where it is remembered that I is the area moment of inertia of one lamination about its own neutral axis. Thus Equation [30] becomes

$$EI\frac{d^2y}{dx^2} = M - Ph \ldots\ldots\ldots\ldots [31]$$

where $I = 8\,I$ and is the moment of inertia of the entire cross section with respect to the neutral axis. From Fig. 2 it is seen that the right-hand side of Equation [31] is the moment about the neutral axis. Equation [31] is the usual differential equation of bending for a solid beam.

Example

To demonstrate the application of the theory, two special cases of buckling will be treated. The first will be to find the critical buckling load of a pinned-end column composed of two laminations and joined at the ends. The second case will be the buckling of the same column except with the ends and the third points joined. Experimental results will be given for verification.

Case I is that of a column composed of two rectangular laminations, each of which has an elastic modulus E, a moment of inertia I with respect to its own neutral axis, a length L, and an area $A = bh$ (b and h are the cross-sectional dimensions where h is in the plane of buckling). The problem is represented by the center portion of the column in Fig. 1. There is one region only. It is seen from Equations [6] that

$$\alpha_1 = \frac{h}{4EI}, \quad \alpha_2 = \frac{3h}{4EI} \ldots\ldots\ldots\ldots [32]$$

and from symmetry $\theta_L = -\theta_0$. Also

$$P = F_1 + F_2 \ldots\ldots\ldots\ldots [33]$$

and from Equation [19]

$$-\frac{2hAE}{L}\theta_0 = F_2 - F_1 \ldots\ldots\ldots\ldots [34]$$

Equations [33] and [34] combine to give

$$\left.\begin{aligned} F_1 &= \frac{P}{2} + \frac{hAE}{L}\theta_0 \\ F_2 &= \frac{P}{2} - \frac{hAE}{L}\theta_0 \end{aligned}\right\} \ldots\ldots\ldots\ldots [35]$$

Again from symmetry only one of the two Equations [13] and [14] is needed. Using Equation [13] and substituting the foregoing values of F_1, F_2, and $\gamma = 0$, the following form is obtained

$$\theta_0\left[\frac{\cos \beta L + 1}{\sin \beta L} + \frac{Ah^2}{2IL\beta}\right] = \frac{Ph}{2\beta EI} \ldots\ldots\ldots [36]$$

The condition for buckling is that θ_0 go to infinity. The right-hand side of Equation [36] is to remain finite so the bracketed term must go to zero. Noting that $Ah^2 = 12\,I$ then

$$\beta L(\cos \beta L + 1) = -6 \sin \beta L \ldots\ldots\ldots [37]$$

is the characteristic equation to determine βL or P where

$$\beta^2 = \frac{P}{2EI}$$

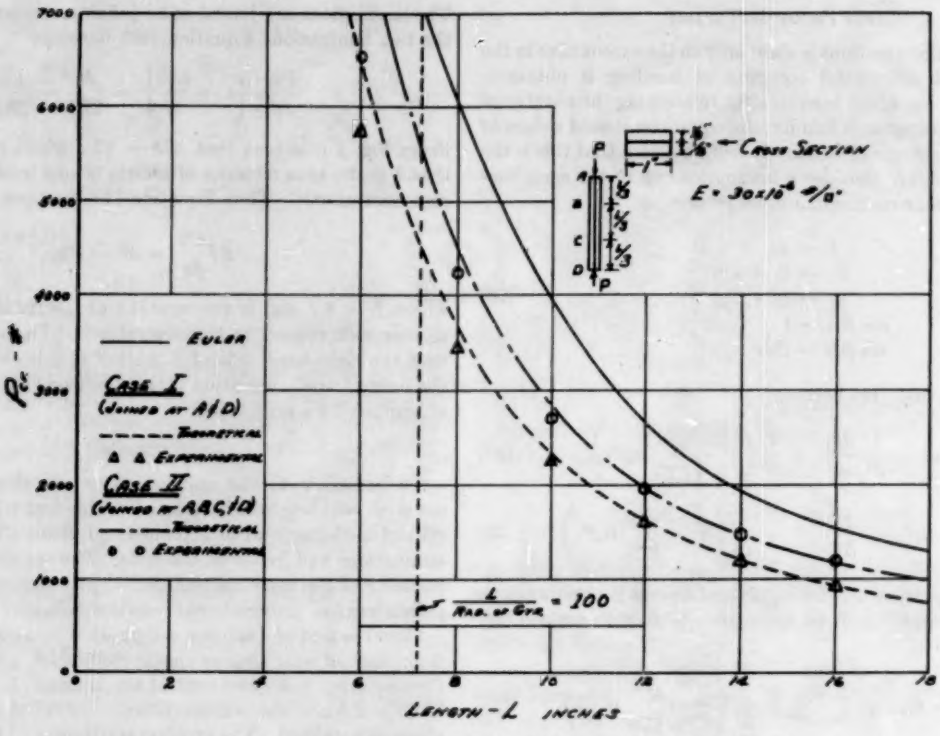

FIG. 3 EXPERIMENTAL VERIFICATION OF LAMINATED-COLUMN THEORY

Upon carrying out this calculation it is found that

$$\beta L = 1.56\pi \quad \text{or} \quad P_{cr} = \frac{2(1.56)^2\pi^2 EI}{L^2} \qquad [38]$$

If the beam were solid then

$$\beta L = 2\pi \quad \text{or} \quad P_{cr} = \frac{8\pi^2 EI}{L^2} \qquad [39]$$

where it is remembered that $8I = \bar{I}$ if $\bar{I}$ is the moment of inertia of the entire cross section. The critical buckling load for the laminated column is only 0.608 times as large as for the solid column of the same cross section.

Case II is represented by the column shown in Fig. 1, where the laminations are joined at the third points. It is seen that there are three regions that need be treated to get the critical values of P. The algebraic manipulation will not be shown. It is seen that Equations [13] and [14] can be written for the three regions and the slopes and deflections at the intermediate joining points eliminated. The resulting characteristic equation, using the same dimensions as Case I, is

$$\varphi^2 = 2\varphi^2 \cos^2 \varphi + 15\varphi \cos \varphi \sin \varphi + \varphi^2 \cos \varphi - 3\varphi \sin \varphi + 16 \sin^2 \varphi \qquad [40]$$

where

$$\varphi = \frac{\beta L}{3} \text{ and } \beta^2 = \frac{P}{2EI}$$

The minimum value of φ for this equation is

$$\varphi = \frac{\beta L}{3} = 0.576\pi$$

or

$$P_{cr} = \frac{2(1.728)^2\pi^2 EI}{L^2} \qquad [41]$$

P_{cr} as determined for the laminated column is 74.6 per cent of the critical load for the solid column.

EXPERIMENTAL VERIFICATION

The final means of verifying the theory will be by experiment. Fig. 3 is a plot of the data for Cases I and II as compared to the theory. Euler's buckling curve is included for comparison. Spot welds are used as a means of joining the laminations.

Fig. 3 shows that the agreement of theory and experiment are very good except for short columns. This is expected in the light of other work that has been done concerning the buckling of columns. It is also seen from Fig. 3 that the critical slenderness ratio L/r (r is the radius of gyration for the total section) for the laminated columns is lower than for the solid column. Taking (L/r) equal to approximately 100 (mild steel) for the solid column then for Cases I and II the values of (L/r) are 78 and 86.4, respectively.

CONCLUSIONS

The theory, as presented, seems to be applicable to long laminated columns in so far as the columns do not lie near the transition point. Near the transition point, Fig. 3, it is shown that the predicted buckling loads are too high in the same manner that the Euler formula gives high critical loads for a solid column.

A point of interest is the application of the integrated boundary conditions to obtain needed equations. It is suggested that a similar approach may be used in the deflection and buckling of laminated plates. It is expected that in the case of plates the problem would be cumbersome.

Thin Circular Conical Shells Under Arbitrary Loads[1]

By N. J. HOFF,[2] BROOKLYN, N. Y.

Equations defining the displacements of the median surface of a conical shell under arbitrary loads are developed. In their derivation only the essential parts of the strain energy are considered and three simultaneous partial differential equations are obtained through the use of the variational calculus. When the minimum radius of curvature of the median surface of the cone is made to approach a constant value, the cone goes over into a cylinder. At the same time the equations here developed for the cone are transformed into the Donnell equations of the theory of cylindrical shells. It is shown how eigenfunctions of the homogeneous equations can be constructed and how particular solutions can be found for any arbitrary loading.

Introduction

EVEN though the general theory of thin circular conical shells is discussed in some detail in Love's "Elasticity" (1),[3] the rigorous equations governing the deformations of the median surface of the shell, as presented by Pflüger (2) and Nollau (3), have never been solved exactly for a constant wall thickness and arbitrary loading. It is the purpose of this paper to present equations which are easier to solve while accurate enough for practical purposes in a wide range of the parameters involved. The equations are derived by calculating the strain energy stored in the shell on the basis of simplified expressions for the strain quantities and by minimizing the total potential energy of the system. This procedure was recently followed by Kempner (4) when he rederived Donnell's equations (5) of the circular cylindrical shell.

When the cone angle approaches zero, the present equations go over into the Donnell equations. It is reasonable to expect therefore that for small cone angles the limitations in accuracy of the present equations will be the same as those of the Donnell equations. This means that the equations should be accurate enough for engineering purposes in most cases; this was shown to be true for the Donnell equations (6). The theory should be applied only to truncated cones because near the apex the fundamental requirement of thin-shell theory, namely, that the wall thickness should be small as compared to the diameter, is violated. It is suggested that the equations be used only when the cone angle α is not greater than 30 deg.

Membrane Stresses

Fig. 1 shows the notation and the sign convention adopted in this analysis. The x-co-ordinate is measured along the generators, and not along the axis of the cone; nevertheless it will be designated as the axial co-ordinate for lack of a better expression. The direction of the axial displacement u is the same as that of x. The circumferential co-ordinate φ is measured in planes perpendicular to the axis of the cone and circumferential displacements v take place along the circles which are the lines of intersection of the median surface of the cone with planes perpendicular to the axis of the cone. Finally the radial displacement w is directed inward along the normal to the median surface.

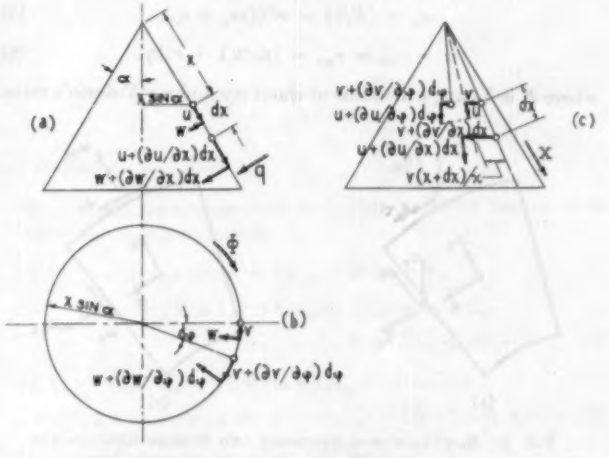

FIG. 1 NOTATION FOR CO-ORDINATES, DISPLACEMENTS, AND SURFACE LOADS

It can be seen from Fig. 1(*a*) that the axial membrane strain ϵ_x is given by

$$\epsilon_x = \partial u/\partial x = u_{,x} \quad \ldots\ldots\ldots\ldots\ldots\ldots [1]$$

The circumferential membrane strain ϵ_φ is influenced by the axial displacement u and by the radial displacement w in addition to the variation in the circumferential displacement; in accordance with Fig. 1(*b*)

$$\epsilon_\varphi = (1/x \sin \alpha)[(dv/d\varphi) + u \sin \alpha - w \cos \alpha]$$
$$= (1/x \sin \alpha)[v_{,\varphi} + u \sin \alpha - w \cos \alpha] \quad \ldots\ldots\ldots\ldots [2]$$

Experience with the analysis of cylindrical shells has shown that u is generally much smaller than v and w. Moreover, the derivative $v_{,\varphi}$ is larger than v itself when the wave length of the deformations is small. Finally in Equation [2], u is multiplied by $\sin \alpha$ which is a small quantity when the cone angle is small. The analysis will therefore be carried out on the assumption that the

---

[1] This work was performed under a consulting contract with the Knolls Atomic Power Laboratory, Schenectady, N. Y., operated by the General Electric Company for the United States Atomic Energy Commission.

[2] Professor, Head of the Department of Aeronautical Engineering and Applied Mechanics, Polytechnic Institute of Brooklyn. Mem. ASME.

[3] Numbers in parentheses refer to the Bibliography at the end of the paper.

Presented at the National Conference of the Applied Mechanics Division, Troy, N. Y., June 16–18, 1955, of THE AMERICAN SOCIETY OF MECHANICAL ENGINEERS.

Discussion of this paper should be addressed to the Secretary, ASME, 29 West 39th Street, New York, N. Y., and will be accepted until January 10, 1956, for publication at a later date. Discussion received after the closing date will be returned.

NOTE: Statements and opinions advanced in papers are to be understood as individual expressions of their authors and not those of the Society. Manuscript received by ASME Applied Mechanics Division, September 10, 1954. Paper No. 55—APM-29.

circumferential strain is defined accurately enough by the equation

$$\epsilon_\varphi = (1/x \sin \alpha)(v_{,\varphi} - w \cos \alpha) \quad [2a]$$

The increment $(\partial v/\partial x)dx$ divided by dx does not constitute one component of the angle of shear γ because at a distance dx from the point of reference, the displacement v must be magnified by a factor $(x + dx)/x$ in order to maintain the original right angle between the axial and circumferential lines. The other component, however, is $(\partial u/\partial \varphi)d\varphi$ divided by $x \sin \alpha \, d\varphi$. Consequently

$$\begin{aligned}\gamma &= (\partial v/dx) - (1/x \sin \alpha)[v \sin \alpha - (\partial u/\partial \varphi)] \\ &= v_{,x} - (1/x \sin \alpha)[v \sin \alpha - u_{,\varphi}] \quad [3]\end{aligned}$$

In this equation the term $v \sin \alpha$ will be disregarded. The order of magnitude of v is about the same as that of $u_{,\varphi}$ but it is multiplied by the small number $\sin \alpha$. The calculations will therefore be made on the basis of the definition

$$\gamma = v_{,x} + (1/x \sin \alpha)u_{,\varphi} \quad [3a]$$

This definition introduces inaccuracies in the analysis when α is large.

In thin-shell theory it is customary to disregard the remaining three strain components. On this basis the membrane stresses can be written as

$$\sigma_x = [E/(1 - \nu^2)](\epsilon_x + \nu\epsilon_\varphi) \quad [4]$$

$$\sigma_\varphi = [E/(1 - \nu^2)](\nu\epsilon_x + \epsilon_\varphi) \quad [5]$$

$$\tau = \tau_{x\varphi} = \tau_{\varphi x} = [E/2(1 + \nu)]\gamma \quad [6]$$

where E is Young's modulus of elasticity and ν is Poisson's ratio.

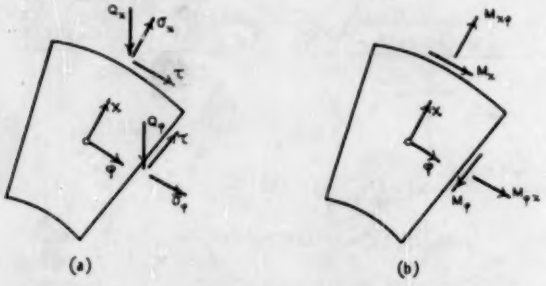

FIG. 2 NOTATION FOR STRESSES AND STRESS RESULTANTS

Substitutions from Equations [1], [2a], [3a] yield

$$\sigma_x = [E/(1 - \nu^2)][u_{,x} + (\nu/x \sin \alpha)(v_{,\varphi} - w \cos \alpha)] \quad [4a]$$

$$\sigma_\varphi = [E/(1 - \nu^2)][\nu u_{,x} + (1/x \sin \alpha)(v_{,\varphi} - w \cos \alpha)] \quad [5a]$$

$$\tau = [E/2(1 + \nu)][v_{,x} + (1/x \sin \alpha)u_{,\varphi}] \quad [6a]$$

BENDING AND TORSION

In the calculation of the stresses and strains caused by the bending and the twisting of the elements of the shell the effect of the initial curvature of the shell is entirely disregarded. The expressions for the bending moments and the torques are written in the same way as for a flat plate with the exception that the length of the element in the circumferential direction is $x \sin\alpha \, d\varphi$ instead of dy. The curvatures in the x and φ-directions and the twist are

$$\kappa_x = \partial^2 w/\partial x^2 = w_{,xx} \quad [7]$$

$$\kappa_\varphi = (1/x^2 \sin^2 \alpha)\partial^2 w/\partial \varphi^2) = (1/x^2 \sin^2 \alpha)w_{,\varphi\varphi} \quad [8]$$

$$\kappa_{x\varphi} = \kappa_{\varphi x} = (1/x \sin \alpha)(\partial^2 w/\partial x \partial \varphi) = (1/x \sin \alpha)w_{,x\varphi} \quad [9]$$

These expressions are considerably simpler than the ones given by Langhaar (7), but they are inaccurate when the angle α is large. The bending moments and the torque are

$$M_x = -D(\kappa_x + \nu\kappa_\varphi) \quad [10]$$

$$M_\varphi = -D(\nu\kappa_x + \kappa_\varphi) \quad [11]$$

$$M_{x\varphi} = -M_{\varphi x} = D(1 - \nu)\kappa_{x\varphi} \quad [12]$$

where the bending rigidity D is defined as

$$D = Eh^3/[12(1 - \nu^2)] \quad [13]$$

and h is the thickness of the shell. Substitutions yield

$$M_x = -D[w_{,xx} + (\nu/x^2 \sin^2 \alpha)w_{,\varphi\varphi}] \quad [14]$$

$$M_\varphi = -D[\nu w_{,xx} + (1/x^2 \sin^2 \alpha)w_{,\varphi\varphi}] \quad [15]$$

$$M_{x\varphi} = -M_{\varphi x} = D[(1 - \nu)/x \sin \alpha]w_{,x\varphi} \quad [16]$$

STRAIN ENERGY

The conditions of equilibrium will be established with the aid of the principle that the actual displacements u, v, w make the total potential energy of the system a minimum. The strain energy U_m stored in the shell in consequence of the membrane stresses is

$$\begin{aligned}U_m &= (h/2E)\int_S [(\sigma_x + \sigma_\varphi)^2 - 2(1 + \nu)(\sigma_x\sigma_\varphi - \tau_{x\varphi}^2)]dS \\ &= [hE/2(1 - \nu^2)]\int_S \{(\epsilon_x + \epsilon_\varphi)^2 - 2(1 - \nu)[\epsilon_x\epsilon_\varphi \\ &\qquad - (1/4)\gamma_{x\varphi}^2]\}dS \quad [17]\end{aligned}$$

where the symbol S below the integral sign indicates that the integration must be extended over the entire area of the median surface of the shell.

The strain energy U_b stored in the shell in consequence of bending and torsion is

$$U_b = (D/2)\int_S [\kappa_x + \kappa_\varphi)^2 - 2(1 - \nu)(\kappa_x\kappa_\varphi - \kappa_{x\varphi}^2)] \, dS \quad [18]$$

The change δU_m in the membrane strain energy caused by variations δu, δv, and δw in the displacements can be written as

$$\begin{aligned}\delta U_m = h\int_S [&\sigma_x\delta u_{,x} + (\sigma_\varphi/x \sin \alpha)\delta v_{,\varphi} - (\sigma_\varphi/x \sin \alpha) \cos\alpha \, \delta w \\ &+ \tau_{x\varphi}\delta v_{,x} + (\tau_{x\varphi}/x \sin \alpha)\delta u_{,\varphi}]dS \quad [19]\end{aligned}$$

The derivatives of the variations can be eliminated through integration by parts. If the shell segment is limited by the lines

$$x = a, \quad x = b, \quad \varphi = \xi, \quad \text{and} \quad \varphi = \zeta$$

one obtains

$$\begin{aligned}\delta U_m = {} & hb \sin \alpha \int_\xi^\zeta (\sigma_x\delta u + \tau\delta v)_{x=b} \, d\varphi - ha \sin \alpha \int_\xi^\zeta (\sigma_x\delta u + \tau\delta v)_{x=a} \, d\varphi \\ & + h\int_a^b (\sigma_\varphi\delta v + \tau\delta u)_{\varphi=\zeta} \, dx - h\int_a^b (\sigma_\varphi\delta v + \tau\delta u)_{\varphi=\xi} \, dx \\ & - h\int_a^b \int_\xi^\zeta \{[(x \sin\alpha \, \sigma_x)_{,x} + \tau_{,\varphi}]\delta u + [\sigma_{\varphi,\varphi} + (x \sin\alpha \, \tau)_{,x}] \, \delta v \\ & + \sigma_\varphi \cos\alpha \, \delta w\}d\varphi \, dx \quad [20]\end{aligned}$$

The change δU_b in the strain energy of bending and torsion caused by variations δu, δv, and δw in the displacements is

$$\delta U_b = D\int_S \{[w_{,xx} + (\nu/x^2\sin^2\alpha)w_{,\varphi\varphi}]\,\delta w_{,xx} + [(1/x^2\sin^2\alpha)w_{,\varphi\varphi} + \nu w_{,xx}](1/x^2\sin^2\alpha)\delta w_{,\varphi\varphi} + [2(1-\nu)/x^2\sin^2\alpha]w_{,x\varphi}\delta w_{,x\varphi}\}dS \ldots [21]$$

Integrations by parts result in

$$(1/D)\delta U_b = \int_\xi^\zeta \{[x\sin\alpha\, w_{,xx} + (\nu/x\sin\alpha)w_{,\varphi\varphi}]\,\delta w_{,x}\}_{x=b}\,d\varphi - \int_\xi^\zeta \{[x\sin\alpha\, w_{,xx} + (\nu/x\sin\alpha)w_{,\varphi\varphi}]\delta w_{,x}\}_{x=a}\,d\varphi$$

$$- \int_\xi^\zeta \left[\{(x\sin\alpha\, w_{,xx})_{,x} + [(\nu/x\sin\alpha)w_{,\varphi\varphi}]_{,x} + 2(1-\nu)(1/x\sin\alpha)w_{,x\varphi\varphi}\}\,\delta w\right]_{x=b} d\varphi$$

$$+ \int_\xi^\zeta \left[\{(x\sin\alpha\, w_{,xx})_{,x} + [(\nu/x\sin\alpha)w_{,\varphi\varphi}]_{,x} + 2(1-\nu)(1/x\sin\alpha)w_{,x\varphi\varphi}\}\delta w\right]_{x=a} d\varphi$$

$$+ \int_a^b \{[(1/x^2\sin^3\alpha)w_{,\varphi\varphi} + (\nu/x\sin\alpha)w_{,xx}]\delta w_{,\varphi}\}_{\varphi=\zeta}\,dx - \int_a^b \{[(1/x^2\sin^3\alpha)w_{,\varphi\varphi} + (\nu/x\sin\alpha)w_{,xx}]\delta w_{,\varphi}\}_{\varphi=\xi}\,dx$$

$$+ 2(1-\nu)\int_a^b \{(1/x\sin\alpha)w_{,x\varphi}\,\delta w_{,x}\}_{\varphi=\zeta}\,dx - 2(1-\nu)\int_a^b \{(1/x\sin\alpha)w_{,x\varphi}\delta w_{,x}\}_{\varphi=\xi}\,dx$$

$$- \int_a^b \{[(1/x^2\sin^3\alpha)w_{,\varphi\varphi\varphi} + (\nu/x\sin\alpha)w_{,xx\varphi}]\delta w\}_{\varphi=\zeta}\,dx + \int_a^b \{[(1/x^2\sin^3\alpha)w_{,\varphi\varphi\varphi} + (\nu/x\sin\alpha)w_{,xx\varphi}]\delta w\}_{\varphi=\xi}\,dx$$

$$+ \int_\xi^\zeta\int_a^b \{(x\sin\alpha\, w_{,xx})_{,xx} + (1/x\sin\alpha)w_{,xx\varphi\varphi} + [(1/x\sin\alpha)w_{,\varphi\varphi}]_{,xx} + (1/x^2\sin^3\alpha)w_{,\varphi\varphi\varphi\varphi} - [2(1-\nu)/x^2\sin\alpha]w_{,\varphi\varphi}\}\,\delta w\,dx\,d\varphi \ldots [22]$$

Potential of the Loads

If X, Φ, and q designate the surface loads per unit area acting in the axial, circumferential, and radial directions, as shown in Fig. 1, the change δV_L in the potential of these loads during a virtual displacement is

$$\delta V_L = -\int_a^b\int_\xi^\zeta (X\delta u + \Phi\delta v + q\delta w)x\sin\alpha\,d\varphi\,dx \ldots [23]$$

Similarly, the change δV_m in the potential of the edge stresses σ_x^*, σ_φ^*, and τ^* can be written as

$$\delta V_m = -h\int_\xi^\zeta \{b[\sigma_x^*\delta u + \tau^*\delta v]_{x=b} - a[\sigma_x^*\delta u + \tau^*\delta v]_{x=a}\}\sin\alpha\,d\varphi - h\int_a^b \{[\sigma_\varphi^*\delta v + \tau^*\delta u]_{\varphi=\zeta} - [\sigma_\varphi^*\delta v + \tau^*\delta u]_{\varphi=\xi}\}\,dx \ldots [24]$$

If, in addition, bending moments M_x^* and M_φ^*, torques $M_{x\varphi}^*$ and $M_{\varphi x}^*$, and shear forces Q_x^* and Q_φ^*, all of which refer to a unit length of the boundary, are applied as external loads to the edges of the conical shell, the change δV_b in their potential during the virtual displacements is

$$\left.\begin{aligned}\delta V_b = &-\int_\xi^\zeta \{b[-M_x^*\delta w_{,x} + (1/b\sin\alpha)M_{x\varphi}^*\delta w_{,\varphi} + Q_x^*\delta w]_{x=b} - a[-M_x^*\delta w_{,x} + (1/a\sin\alpha)M_{x\varphi}^*\delta w_{,\varphi} + Q_x^*\delta w]_{x=a}\}\sin\alpha\,d\varphi \\ &- \int_a^b \{[-(1/x\sin\alpha)M_\varphi^*\delta w_{,\varphi} - M_{\varphi x}^*\delta w_{,x} + Q_\varphi^*\delta w]_{\varphi=\zeta} - [-(1/x\sin\alpha)M_\varphi^*\delta w_{,\varphi} - M_{\varphi x}^*\delta w_{,x} + Q_\varphi^*\delta w]_{\varphi=\xi}\}\,dx\end{aligned}\right\} \ldots [25]$$

Equilibrium in Axial and Circumferential Directions

When the system is in equilibrium, the changes in the total potential energy of the system vanish for any arbitrary virtual displacement. One condition of equilibrium is therefore that the sum of those terms in the surface integral which are multiplied by δu vanish

$$(x\sin\alpha\,\sigma_x)_{,x} + \tau_{,\varphi} + x\sin\alpha\,(X/h) = 0 \ldots [26]$$

A second condition can be stated in a similar manner with respect to δv

$$\sigma_{\varphi,\varphi} + (x\sin\alpha\,\tau)_{,x} + x\sin\alpha\,(\Phi/h) = 0 \ldots [27]$$

Substitution from Equations [4a], [5a], and [6a] results in the two simultaneous equations

$$[E/(1-\nu^2)][u_{,x}x\sin\alpha + \nu(v_{,\varphi} - w\cos\alpha)]_{,x} + [E/2(1+\nu)][v_{,x} + (u_{,\varphi}/x\sin\alpha)]_{,\varphi} + (X/h)x\sin\alpha = 0 \ldots [28]$$

$$[E/(1-\nu^2)][\nu u_{,x} + (1/x\sin\alpha)(v_{,\varphi} - w\cos\alpha)]_{,\varphi} + [E/2(1+\nu)][v_{,x}x\sin\alpha + u_{,\varphi}]_{,x} + (\Phi/h)x\sin\alpha = 0 \ldots [29]$$

It is possible to solve Equation [29] for $u_{,x\varphi}$

$$u_{,x\varphi} = -[2/(1+\nu)](1/x\sin\alpha)w_{,\varphi\varphi} - [(1-\nu)/(1+\nu)] \times (v_{,x}x\sin\alpha)_{,x} + [2/(1+\nu)](\cos\alpha/x\sin\alpha)w_{,\varphi} - (2/E)(1-\nu)(\Phi/h)x\sin\alpha \ldots [30]$$

If Equation [28] is differentiated with respect to φ, multiplied by $x\sin\alpha$, and subsequently differentiated with respect to x, one obtains

$$[x\sin\alpha(x\sin\alpha\,u_{,x\varphi})_{,x}]_{,x} + (1/2)(1+\nu)(x\sin\alpha\,v_{,\varphi\varphi x})_{,x} - \nu\cos\alpha\,(x\sin\alpha\,w_{,\varphi x})_{,x} + (1/2)(1-\nu)u_{,x\varphi\varphi\varphi} + (1/Eh)(1-\nu^2)(x^2\sin^2\alpha\,X_{,\varphi})_{,x} = 0 \ldots [31]$$

Substitution of $u_{,x\varphi}$ from Equation [30] into Equation [31] and rearrangements result in the equation

$$H_1(v) = \cos\alpha[(2+\nu)x\sin\alpha\,(x\sin\alpha\,w_{,x\varphi})_{,x} + w_{,\varphi\varphi\varphi}] - [(1-\nu^2)/Eh]\{[2/(1-\nu)]x\sin\alpha[x\sin\alpha\,(x^2\sin^2\alpha\,\Phi)_{,x}]_{,x} + x^2\sin^3\alpha\,\Phi_{,\varphi\varphi} - [(1+\nu)/(1-\nu)]x\sin\alpha\,(x^2\sin^2\alpha\,X_{,\varphi})_{,x}\} \ldots [32]$$

where the differential operator H_1 is defined as

$$H_1(z) = x \sin\alpha\{x \sin\alpha\,[x \sin\alpha(x \sin\alpha\, z_{,x})_{,x}]_{,x}\}_{,x} + 2x \sin\alpha\,(x \sin\alpha\, z_{,\varphi\varphi x})_{,x} + z_{,\varphi\varphi\varphi\varphi} \ldots [33]$$

Equation [28] is next solved for $v_{,\varphi}$

$$v_{,\varphi} = -[2/(1+\nu)](x \sin\alpha\, u_{,x})_{,x} + [2\nu/(1+\nu)] \cos\alpha\, w_{,x} - [(1-\nu)/(1+\nu)](u_{,\varphi\varphi}/x \sin\alpha) - (2/Eh)(1-\nu)Xx \sin\alpha \ldots [34]$$

Differentiation of Equation [29] with respect to φ, multiplication by $x \sin\alpha$, and subsequent differentiation with respect to x lead to

$$(1/2)(1+\nu)(x \sin\alpha\, u_{,\varphi\varphi x})_{,x} - \cos\alpha\, w_{,x\varphi\varphi} + (1/Eh)(1-\nu^2)(x^2 \sin^2\alpha\, \Phi_{,\varphi})_{,x} + v_{,\varphi\varphi\varphi x} + (1/2)(1-\nu)[x \sin\alpha\,(x \sin\alpha\, v_{,\varphi x})_{,x}]_{,x} = 0 \ldots [35]$$

Substitution of $v_{,x\varphi}$ from Equation [34] and rearrangements yield the differential equation

$$H_1(u) = \cos\alpha\{\nu x \sin\alpha\,[x \sin\alpha\,(x \sin\alpha\, w_{,x})_{,x}]_{,x} - x \sin\alpha\, w_{,\varphi\varphi x}\} - (1/Eh)(1-\nu^2)\{x \sin\alpha[x \sin\alpha\,(x^2 \sin^2\alpha\, X)_{,x}]_{,x} + [2/(1-\nu)]x^2 \sin^2\alpha\, X_{,\varphi\varphi} - [(1+\nu)/(1-\nu)]x \sin\alpha\,(x^2 \sin^2\alpha\, \Phi_{,\varphi})_{,x}\} \ldots [36]$$

where the differential operator H_1 has the same meaning as in Equation [33].

Equilibrium in Radial Direction

When the sum of those terms in the surface integrals which are multiplied by δw is set equal to zero, one obtains

$$(x \sin\alpha\, w_{,xx})_{,xx} + \frac{w_{,xx\varphi\varphi}}{x \sin\alpha} + \left[\frac{w_{,\varphi\varphi}}{x \sin\alpha}\right]_{,xx} + \frac{w_{,\varphi\varphi\varphi\varphi}}{x^3 \sin^3\alpha} - 2(1-\nu)\frac{w_{,\varphi\varphi}}{x^3 \sin\alpha} - (h/D)\cos\alpha\,\sigma_\varphi - (q/D)x \sin\alpha = 0 \ldots [37]$$

After this equation is multiplied by $x \sin\alpha$, it is convenient to introduce a second differential operator

$$H_2(z) = x \sin\alpha\,(x \sin\alpha\, z_{,xx})_{,xx} + z_{,xx\varphi\varphi} + x \sin\alpha\left[\frac{z_{,\varphi\varphi}}{x \sin\alpha}\right]_{,xx} + \frac{z_{,\varphi\varphi\varphi\varphi}}{x^2 \sin^2\alpha} - 2(1-\nu)\frac{z_{,\varphi\varphi}}{x^2} \ldots [38]$$

Equation [37] can then be written in the shorthand notation

$$H_2(w) - (h/D)\cos\alpha\, x \sin\alpha\,\sigma_\varphi - (q/D)x^2 \sin^2\alpha = 0 \ldots [39]$$

Now the operator H_1 is applied to each term of this equation, σ_φ is replaced by the expression given for it in Equation [5a], and use is made of Equations [32] and [36] to express u and v in terms of w. After manipulations the following partial differential equation is obtained in w alone

$$H_1[H_2(w)] + (Eh/D)\cos^2\alpha\, x \sin\alpha\{x \sin\alpha[x \sin\alpha(x \sin\alpha\, w_{,x})_{,x}]_{,x}\}_{,x} + (\cos\alpha/D)\Big[\nu x \sin\alpha\{x \sin\alpha[x \sin\alpha(x^2 \sin^2\alpha\, X)_{,x}]_{,x}\}_{,x} - x \sin\alpha(x^2 \sin^2\alpha\, X_{,\varphi\varphi})_{,x} + (2+\nu)x \sin\alpha[x \sin\alpha(x^2 \sin^2\alpha\, \Phi_{,\varphi})_{,x}]_{,x} + x^2 \sin^2\alpha\, \Phi_{,\varphi\varphi\varphi}\Big] - (1/D)H_1(qx^2 \sin^2\alpha) = 0 \ldots [40]$$

When the loads and the boundary conditions are prescribed, Equation [40] can be solved for w. The expression obtained for w can then be substituted in Equations [32] and [36] and they in turn can be solved for u and v.

Boundary Conditions

The requirement that the changes in the total potential energy of the system represented by the line integrals vanish furnishes the boundary conditions. One obtains the following:

1 Along the circles $x = a$ and $x = b$

$$\{[E/(1-\nu^2)][u_{,x} + (\nu/x \sin\alpha)(v_{,\varphi} - w \cos\alpha)] - \sigma_x^*\}\delta u = 0 \ldots [41]$$

$$\{[E/2(1+\nu)][v_{,x} + (1/x \sin\alpha)u_{,\varphi}] - \tau^*\}\delta v = 0 \ldots [42]$$

$$\{(x \sin\alpha\, w_{,xx})_{,x} + [(\nu/x \sin\alpha)w_{,\varphi\varphi}]_{,x} + 2(1-\nu)(1/x \sin\alpha)w_{,x\varphi\varphi} + x \sin\alpha(Q_x^*/D) - (M_{x\varphi,\varphi}^*/D)\}\delta w = 0 \ldots [43]$$

$$[x \sin\alpha\, w_{,xx} + (\nu/x \sin\alpha)w_{,\varphi\varphi} + (x \sin\alpha/D)M_x^*]\delta w_{,x} = 0 \ldots [44]$$

2 Along the generators $\varphi = \xi$ and $\varphi = \zeta$

$$\{[E/2(1+\nu)][v_{,x} + (1/x \sin\alpha)u_{,\varphi}] - \tau^*\}\delta u = 0 \ldots [45]$$

$$\{[E/(1-\nu^2)][\nu u_{,x} + (1/x \sin\alpha)(v_{,\varphi} - w \cos\alpha)] - \sigma_\varphi^*\}\delta v = 0 \ldots [46]$$

$$\{(1/x^3 \sin^3\alpha)w_{,\varphi\varphi\varphi} + (\nu/x \sin\alpha)w_{,xx\varphi} + 2(1-\nu)(1/x \sin\alpha)w_{,x\varphi}]_{,x} + (Q_\varphi^*/D) + (1/D)M_{\varphi x,x}^*\}\delta w = 0 \ldots [47]$$

$$[(1/x^2 \sin^2\alpha)w_{,\varphi\varphi} + (\nu/x \sin\alpha)w_{,xx} + (1/x \sin\alpha)(M_\varphi^*/D)]\delta w_{,\varphi} = 0 \ldots [48]$$

3 At the corners

$$\{[2(1-\nu)/x \sin\alpha]w_{,x\varphi} - (M_{x\varphi}^*/D) + (M_{\varphi x}^*/D)\}\delta w = 0 \ldots [49]$$

The conditions of equilibrium as listed are satisfied if either the expressions multiplying the virtual displacements vanish, or the displacements cannot take place because they are incompatible with the geometric conditions.

Solution of Differential Equations

A complete investigation of the solutions of the differential equations of the cone is beyond the scope of this paper. However, it will be indicated that solutions can be obtained to them. If z designates the function

$$z = x^n \sin p\varphi \ldots [50]$$

application of the operator H_1 to it results in

$$H_1(z) = M_n z \ldots [51]$$

where M_n is not an operator but the polynomial

$$M_n = (p^2 - n^2 \sin^2\alpha)^2 \ldots [52]$$

Similarly, application of the operator H_2 to z yields

$$H_2(z) = N_n z/x^2 \ldots [53]$$

where N_n represents the polynomial

$$N_n = n(n-1)^2(n-2)\sin^2\alpha - 2[(n-1)^2 - 1 + \nu]p^2 + (p^4/\sin^2\alpha) \ldots [54]$$

If first H_2 and subsequently H_1 are applied to z one obtains

$$H_1[H_2(z)] = M_{n-2}N_n(z/x^2) \ldots [55]$$

where M_{n-2} can easily be derived from the definition of M_n given in Equation [52]

$$M_{n-2} = [p^2 - (n-2)^2 \sin^2\alpha]^2$$

Finally, the operator H_3 can be defined as

$$H_3(z) = x \sin \alpha\{x \sin \alpha[x \sin \alpha(x \sin\alpha\, z_{,x})_{,x}]_{,x}\}_{,x} \ldots [56]$$

If this is applied to z, the result is

$$H_3(z) = n^4(\sin^4 \alpha)z \ldots [57]$$

Eigenfunctions of the Differential Equation

With the aid of these relationships it is easy to show that an eigenfunction of Equation [40]—a solution of the homogeneous equation obtained from Equation [40] when the load terms are absent—that is, when

$$X = \Phi = q = 0 \ldots [58]$$

is represented by the following infinite series

$$w = \sin p\varphi \sum_{n=0,1,2,\ldots}^{\infty} a_{2n}x^{m+2n} \ldots [59]$$

The coefficient a_{2n+2} can be calculated from the coefficient a_{2n} if it is recognized that the homogeneous version of the left-hand member of Equation [40] can vanish only if

$$(M_{2n}N_{2n+2})a_{2n+2} = -4K^4(m+2n)^4 \sin^4\alpha\, a_{2n} \ldots [60]$$

where

$$4K^4 = (Eh/D)\cos^2\alpha \ldots [61]$$

The series converges absolutely if, in the limit as n increases beyond all bounds, the absolute value of the ratio r of the $(2n+2)$th term to the $(2n)$th term is less than unity. If p and m are kept constant while n is permitted to increase without bounds, the following expression, valid for very large values of n, is obtained for the ratio

$$r = -(1/4)(K/n)^4(x^2/\sin^2\alpha) \ldots [62]$$

The absolute value of this ratio is obviously smaller than unity when n is sufficiently large and thus the series defined in Equation [59] converges absolutely. However, the value of n is large beyond which the terms decrease in absolute value.

The first coefficient a is of course arbitrary. But the value of m must be determined from the condition that

$$M_{m-2}N_m = 0$$

The product vanishes if either factor is zero. When

$$M_{m-2} = 0 \ldots [63]$$

one obtains the double real roots

$$m_1 = m_2 = (p/\sin\alpha) + 2 \ldots [64]$$

$$m_3 = m_4 = -(p/\sin\alpha) + 2 \ldots [65]$$

Because of the double roots the function of x in the solution can be $x^{m_1}\log x$ and $x^{m_3}\log x$ in addition to x^{m_1} and x^{m_3}. The series based on the logarithmic solutions are a little more troublesome to calculate than the ones containing only powers of x. In order to cancel the logarithmic term in the expression obtained from an application of the operator H_3 to $x^n \log x \sin p\varphi$, the operation $H_1[H_2(w)]$ must be performed on the function $\alpha x^{n+2}\log x \sin p\varphi$. The number α can be so chosen that the sum of the two logarithmic terms vanishes. But $H_1[H_2(w)]$ contributes a term containing $x^n \sin p\varphi$ which does not add up to zero with the like term obtained when the operator H_3 was applied to $x^n \log x \sin p\varphi$. Hence a term $\beta x^{n+2}\sin p\varphi$ must be introduced with the factor β so chosen to cancel out the sum of the terms $x^n \sin p\varphi$.

When the second factor vanishes

$$N_m = 0 \ldots [66]$$

it is convenient to introduce the number s defined as

$$s = m - 1 \ldots [67]$$

Equation [66] can then be written as

$$s^2(s^2-1)\sin^2\alpha - 2(s^2 - 1 + \nu)p^2 + (p^4/\sin^2\alpha) = 0 \ldots [68]$$

Solution of this biquadratic for s^2 yields

$$s^2 = (1/2)[1 + 2(p/\sin\alpha)^2] \pm (1/2)[1 - 4(1-2\nu)(p/\sin\alpha)^2]^{1/2} \ldots [69]$$

When the shell is closed in the φ-direction, p usually represents all the positive integers. As ν is generally taken to be 0.3 and since $\sin\alpha$ cannot be greater than unity, the expression under the root is negative. Hence s^2 is a complex number. The absolute value of s is

$$|s| = 2^{-1/2}[2 + 8\nu(p/\sin\alpha)^2 + 4(p/\sin\alpha)^4]^{1/4} \ldots [70]$$

and the principal value of the angle ψ subtended by s with the real axis in the complex plane is

$$\psi = (1/2) \times \tan^{-1}\{[-1 + 4(1-2\nu)(p/\sin\alpha)^2]^{1/2}/[1 + 2(p/\sin\alpha)^2]\} \ldots [71]$$

when the positive sign is selected in the expression for s^2. A second value is $\psi + \pi$.

It is worth noting that ψ approaches zero when p is increased beyond all limits; as a matter of fact, the imaginary part of s is quite small when the value of p is moderately large provided $\sin\alpha$ is small. For large values of p and small values of $\sin\alpha$ the absolute value of the number s differs little from the real quantity

$$|s| \simeq (p/\sin\alpha) \ldots [72]$$

If both ψ and $\psi + \pi$ and both signs in the expression for s^2 are considered, the following four roots can be calculated

$$m_5 = \beta_1 + i\vartheta_1 \qquad m_6 = \beta_1 - i\vartheta_1 \ldots [73]$$

$$m_7 = \beta_2 + i\vartheta_2 \qquad m_8 = \beta_2 - i\vartheta_2 \ldots [74]$$

where

$$\left.\begin{aligned} \beta_1 &= 1 + |s|\cos\psi \\ \beta_2 &= 1 + |s|\cos(\psi+\pi) \\ \vartheta_1 &= |s|\sin\psi \\ \vartheta_2 &= |s|\sin(\psi+\pi) \end{aligned}\right\} \ldots [75]$$

β_1 is positive while β_2 is generally negative.

The terms in the infinite series representing the displacement w can be brought into a real form if it is observed that

$$x^{\beta+i\vartheta} = e^{(\beta+i\vartheta)\log x} \ldots [76]$$

and

$$x^{\beta-i\vartheta} = e^{(\beta-i\vartheta)\log x} \ldots [77]$$

Combination of these two solutions each of which may be multiplied by an arbitrary constant of integration leads to solutions of the types

$$e^{\beta\log x}\cos(\vartheta\log x)$$

and

$$e^{\beta\log x}\sin(\vartheta\log x)$$

Hence the radial displacement w contains oscillatory functions as well as monotonically varying functions of x.

Particular Integrals

If the assumption

$$w = x^n \sin p\varphi \quad [78]$$

is made, where p and n are arbitrary integers, the first two terms in the left-hand member of Equation [40] become

$$M_{n-2}N_n(w/x^2) + 4K^4n^4 \sin^4\alpha\, w$$

The assumption can be used to obtain particular solutions of the inhomogeneous differential equations if the loads are represented by the series

$$X = \sum_{p=1,2,3,\ldots}^{\infty} T_{X(p)} \sin p\varphi \quad [79]$$

$$\Phi = \sum_{p=1,2,3,\ldots}^{\infty} T_{\Phi(p)} \cos p\varphi \quad [80]$$

$$q = \sum_{p=1,2,3,\ldots}^{\infty} T_{q(p)} \sin p\varphi \quad [81]$$

where $T_{X(p)}$, $T_{\Phi(p)}$, and $T_{q(p)}$ represent Taylor series in x. One possible procedure of solution consists therefore of expanding the given loads into Fourier series in φ with coefficients which are Taylor series in x. The operations indicated in Equation [40] for the load terms are next performed. The result again contains terms which are products of powers of x by trigonometric functions of φ. The terms can now be rearranged in pairs in such a manner that the ratio of the coefficient of x^n to that of x^{n-1} in any one pair is

$$4K^4n^4 \sin^4\alpha / M_{n-2}N_n$$

The assumption of Equation [78] is the solution for such a pair of load terms.

Acknowledgments

The author is indebted to the General Electric Company, to the Atomic Energy Commission, and to Dr. John Zickel, the project supervisor, for their permission to publish this paper. He also wishes to express his gratitude to Profs. Joseph Kempner and Frederick V. Pohle of the Polytechnic Institute of Brooklyn, Brooklyn, N. Y., who checked the calculations.

BIBLIOGRAPHY

1 "A Treatise on the Mathematical Theory of Elasticity," by A. E. H. Love, Cambridge University Press, fourth edition, 1927; reprinted by Dover Publications, New York, N. Y., 1944, p. 601.

2 "Stabilität dünner Kegelschalen," by A. Pflüger, *Ingenieur-Archiv*, vol. 8, no. 3, June, 1937, p. 151.

3 "Der Spannungszustand der biegungssteifen Kegelschale mit linear veränderlicher Wandstärke unter beliebiger Belastung," by H. Nollau, *Zeitschrift für Angewandte Mathematik und Mechanik*, vol. 24, 1944, p. 10.

4 "Derivation of Generalized Donnell-Type Equations for Circular Cylindrical Shells With Application to Shells With Line Loads Along Generatrices; Part VI of "Deformations and Stresses Caused in Circular Cylindrical Shells by Pipe Attachment," by Joseph Kempner, Knolls Atomic Power Laboratory, Schenectady, N. Y., Report No. KAPL-926, June, 1953.

"Remarks on Donnell's Equations," by Joseph Kempner, Journal of Applied Mechanics, Trans. ASME, vol. 77, 1955, pp. 117 and 118.

5 "Stability of Thin-Walled Tubes Under Torsion," by L. H. Donnell, NACA Technical Report No. 479, Washington, D. C., 1933.

"A Discussion of Thin Shell Theory," by L. H. Donnell, Proceedings of the Fifth International Congress for Applied Mechanics, John Wiley & Sons, Inc., New York, N. Y., 1939, p. 66.

6 "The Accuracy of Donnell's Equations," by N. J. Hoff, Journal of Applied Mechanics, Trans. ASME, vol. 77, 1955, pp. 329–334.

7 "A Strain-Energy Expression for Thin Elastic Shells," by H. L. Langhaar, Journal of Applied Mechanics, Trans. ASME, vol. 71, 1949, p. 183.

On the Nonlinear Oscillations of Viscoelastic Plates[1]

By A. CEMAL ERINGEN,[2] LAFAYETTE, IND.

Equations of motion of the three-dimensional finite oscillation theory are integrated across the plate thickness to obtain a second-order theory of oscillations for plates. For this purpose, components of the displacement vector are assumed to have power-series expansions in the transverse co-ordinate, and a systematic perturbation procedure in a nondimensional thickness parameter is used. Stress-strain relations include the hereditary damping.

Introduction

THERE is a large *static* deflection theory for plates due to Föppl, von Karman, and Timoshenko (1)[3] which proved to be very useful in dealing with second-order deflections. Recent general theories concerning shells (2, 3, 4), on the other hand, are written in tensor notation or in intrinsic co-ordinates which seem to be complicated for the application.

In classical theory of small flexural oscillations it is known that the theory breaks down when the wave length is comparable with the thickness. Thus the corrections due to rotary inertia and *shear deformations* were made by Timoshenko (5), Uflyand (6), and Mindlin (7). For impact problems where the transient stage is important the internal damping effect must be taken into account.

This paper is concerned with the formulation of a second-order oscillation theory. It thus takes into account (*a*) finite transverse deflection, (*b*) shear deformation, (*c*) rotary inertia, (*d*) internal damping, (*e*) body force and moments. Consequently, the present theory is the generalization of Föppl-Karman-Timoshenko theory of large static deflection on the one hand, and Uflyand-Mindlin theory of small oscillation on the other hand.

Equations of motion of the three-dimensional finite-oscillation theory is integrated across the plate thickness. To this end the following assumptions are made: (*a*) Power series expansion in transverse co-ordinate; (*b*) Hooke's law. These assumptions are usual. By use of a systematic perturbation procedure in a nondimensional thickness parameter a priori assumptions concerning order of magnitudes of various quantities are avoided.

Components of Strain Tensor

Let x_α be the right-handed rectangular co-ordinates of a point of the plate before deformation. We select the (x_1, x_2)-plane as the median plane. The planes $x_3 = \pm h/2$ are taken as the upper and lower faces. Components of the deformation vector $\mathbf{u}$ referred to x_α are u_α. Hence a rectangular parallelepiped with diagonal vector $d\mathbf{r} = \mathbf{i}_\alpha dx_\alpha$ (unit vectors $\mathbf{i}_\alpha$ directed along the edges of lengths dx_α) after deformation becomes a parallelepiped, in general not rectangular, with corresponding diagonal $d\mathbf{r} + d\mathbf{u}$, the edge vectors $\mathbf{g}_\alpha$ and unit base vectors $\mathbf{e}_\alpha = \mathbf{g}_\alpha/|\mathbf{g}_\alpha|$ (α not to be summed)

$$\left.\begin{aligned} d\mathbf{r} + d\mathbf{u} &= \frac{\partial(\mathbf{r} + \mathbf{u})}{\partial x_\alpha}\, dx_\alpha = \mathbf{g}_\alpha dx_\alpha \\ \mathbf{g}_\alpha &= \left(\delta_{\alpha\beta} + \frac{\partial u_\beta}{\partial x_\alpha}\right)\mathbf{i}_\beta \\ \mathbf{e}_\alpha &= \mathbf{g}_\alpha/|\mathbf{g}_\alpha| = e_{\alpha\beta}\mathbf{i}_\beta \end{aligned}\right\} \quad \ldots\ldots [1]$$

Here $\delta_{\alpha\beta}$ is the Kronecker delta which is 1 when $\alpha = \beta$ and zero when $\alpha \neq \beta$.

Throughout the paper we use the usual summation convention. Thus repeated small Greek indexes are summed over the range 1, 2, 3, and repeated small Latin indexes are summed over 1, 2. In the expressions where the summation sign Σ appears or subscripts inside parentheses appear, this convention does not apply.

The square of the line element ds^2 of the deformed body and the components of the strain tensor $\epsilon_{\alpha\beta}$ are given by

$$\left.\begin{aligned} ds^2 = \mathbf{g}_\alpha \cdot \mathbf{g}_\beta\, dx_\alpha dx_\beta &= g_{\alpha\beta} dx_\alpha dx_\beta = (\delta_{\alpha\beta} + 2\epsilon_{\alpha\beta}) dx_\alpha dx_\beta \\ 2\epsilon_{\alpha\beta} &= \frac{\partial u_\alpha}{\partial x_\beta} + \frac{\partial u_\beta}{\partial x_\alpha} + \frac{\partial u_\gamma}{\partial x_\alpha}\frac{\partial u_\gamma}{\partial x_\beta} \end{aligned}\right\} \quad \ldots [2]$$

We assume that $u_\alpha(x_1, x_2, x_3, t)$ can be expanded into power series of x_3/h

$$\left.\begin{aligned} u_i/ae^2 &= u_i^0(y_1, y_2, t) + y_3 u_i^1(y_1, y_2, t) \\ &\qquad + (ey_3)^2 u_i^2(y_1, y_2, t) + \ldots \\ u_3/ae &= u_3^0(y_1, y_2, t) + (ey_3)^2 u_3^2(y_1, y_2, t) \\ &\qquad + (ey_3)^2 u_3^4(y_1, y_2, t) + \ldots \end{aligned}\right\} \quad \ldots [3]$$

where y_α are nondimensional co-ordinates, t is the time, a is a typical length, and e is a small parameter

$$y_i = x_i/a, \quad y_3 = x_3/ae, \quad e = h/a, \quad e \ll 1 \ldots\ldots [4]$$

We note that in Equations [3] superscripts on u_i^2, u_3^2, etc., are not powers but identifying indexes; on $(ey_3)^2, \ldots$ however, they represent powers.

The explicit forms of the strain components are obtained by substituting Equations [3] into [2]; hence

$$\left.\begin{aligned} 2\epsilon_{ij}/e^2 &= u_{i,j}^0 + u_{j,i}^0 + u_{3,i}^0 u_{3,j}^0 \\ &\qquad + y_3(u_{i,j}^1 + u_{j,i}^1) + 0(e^2) \\ 2\epsilon_{33}/e^2 &= u_i^1 u_i^1 + 4y_3 u_3^2 + 0(e^2) \\ 2\epsilon_{3i}/e &= u_i^1 + u_{3,i}^0 + 0(e^2) \end{aligned}\right\} \quad \ldots [5]$$

where indexes after a comma represent differentiation; i.e., $u_{i,j}^0 = \partial u_i^0/\partial y_j$, etc. In Equations [5] the second-order terms represent

---

[1] Research contained here was sponsored by the Office of Naval Research.

[2] Associate Professor of Engineering Sciences, Purdue University.

[3] Numbers in parentheses refer to the Bibliography at the end of the paper.

Presented at the National Conference of the Applied Mechanics Division, Troy, N. Y., June 16–18, 1955, of The American Society of Mechanical Engineers.

Discussion of this paper should be addressed to the Secretary, ASME, 29 West 39th Street, New York, N. Y., and will be accepted until January 10, 1956, for publication at a later date. Discussion received after the closing date will be returned.

Note: Statements and opinions advanced in papers are to be understood as individual expressions of their authors and not those of the Society. Manuscript received by ASME Applied Mechanics Division, July 2, 1954. Paper No. 55—APM-15.

the effect of large deformations which would be encountered in a second-order theory. The second-order terms occurring in the expressions of ϵ_{ij} are identical to those of Föppl-Karman-Timoshenko theory of large static deflection. The classical plate theory assumes $u_i^1 = -u_{3,i}^0$, hence $\epsilon_{3i} = 0(e^3)$. Consequently, the transverse shear strains ϵ_{3i} as well as ϵ_{33} are taken as zero. The present theory will not ignore these strain components.

Stress-Strain Relations for an Elastic Medium With Internal Damping

Generalizing Alfrey's (8, 9) stress-strain relations to homogeneous, isotropic compressible materials we write

$$\left.\begin{aligned} P_1\sigma_{\alpha\beta} &= P_2\theta\delta_{\alpha\beta} + 2P_3\epsilon_{\alpha\beta}, \quad \theta = \epsilon_{\alpha\alpha} \\ P_\alpha &= \sum_{i=0}^{m_\alpha} a_{\alpha i}\,\partial^i/\partial t^i \end{aligned}\right\} \ldots\ldots [6]$$

Here $a_{\alpha i}$ are constants.

Applying the Laplace transform with respect to t and setting $\epsilon_{\alpha\beta}(x_1, x_2, x_3, 0)$, $\sigma_{\alpha\beta}(x_1, x_2, x_3, 0)$ and their derivatives w.r. to time at $t = 0$, zero, from Equations [6] we solve for $\bar{\sigma}_{\alpha\beta}$ and invert it

$$\left.\begin{aligned} \sigma_{\alpha\beta} &= \lambda_*\theta\delta_{\alpha\beta} + 2\mu_*\epsilon_{\alpha\beta} \\ \lambda_*\phi(t) &= \lambda\phi(t) + \int_0^t l(t-\tau)\phi(\tau)d\tau \\ \mu_*\phi(t) &= \mu\phi(t) + \int_0^t m(t-\tau)\phi(\tau)d\tau \\ \bar{l}(s) &= \bar{l}_2(s) - \lambda, \ \bar{m}(s) = \bar{l}_3(s) - \mu \end{aligned}\right\} \ldots\ldots [7]$$

where l_2 and l_3 are inverse transforms of

$$\bar{l}_\alpha(s) = \left(\sum_{i=0}^{m_\alpha} a_{\alpha i}\, s^i\right)\Big/\left(\sum_{i=0}^{m_1} a_{1i}\, s^i\right) \ldots\ldots\ldots [8]$$

Here s is the argument of the transform; λ, μ are Lamé constants.

We notice that the general internal damping stated by Equations [6] is identical to hereditary damping, Equations [7], of V. Volterra (10) which is usually treated as a different and rather more general phenomenon. In practice $l(t)$ and $m(t)$ are found from experiment and are usually expressed in the form (11)

$$\sum_i A_i \exp(-a_i t)$$

This, of course, is a special case of Equation [8]. It is of interest also to note that if we take $l(t) = \lambda'\partial\delta(t)/\partial t$ and $m(t) = \mu'\partial\delta(t)/\partial t$, where $\delta(t)$ is the Dirac delta function,[4] in Equation [7] we obtain Voigt-Sezawa (12, 13) type of stress-strain relations, namely

$$\sigma_{\alpha\beta} = (\lambda + \lambda'\partial/\partial t)\theta\delta_{\alpha\beta} + 2(\mu + \mu'\partial/\partial t)\epsilon_{\alpha\beta} \ldots\ldots [9]$$

Stress Resultants and Stress Couples

We now introduce stress resultants $N_{\alpha\beta}$, stress couples M_{ij}, plate body-force and moment components F_α and G_α

$$\left.\begin{aligned} N_{\alpha\beta}/h &= \int_{-1/2}^{1/2} \sigma_{\alpha\beta}\, dy_3, \quad M_{ij}/h^2 = \int_{-1/2}^{1/2} \sigma_{ij} y_3 dy_3 \\ heF_\alpha &= \int_{-1/2}^{1/2} f_\alpha dy_3, \quad heG_\alpha/12 = \int_{-1/2}^{1/2} f_\alpha y_3 dy_3 \end{aligned}\right\} \ldots [10]$$

Here f_α are the body-force components per unit mass. $N_{\alpha\beta}$ and M_{ij} would become usual physical stress resultants and couples used in engineering if we make the convention $N_{12} = -N_{21}$ and $M_{12} = -M_{21}$.

[4] This, of course, is valid in the sense of a distribution function. See Schwartz (18).

Combining Equations [5], [7], and [10], we obtain

$$\left.\begin{aligned} \sigma_{ij} &= h^{-1}N_{ij} + 12h^{-2}y_3M_{ij} + 0(e^4) \\ \sigma_{32} &= e^4(q + 2py_3) + 0(e^6), \quad \sigma_{3i} = h^{-1}N_{3i} + 0(e^5) \end{aligned}\right\} \ldots [11]$$

where[5]

$$\left.\begin{aligned} 2e^2p &= [\sigma_{33}(y_1, y_2, {}^1/_2, t) - \sigma_{33}(y_1, y_2, -{}^1/_2, t)]/e^2 \\ &= \lambda_*(u_{i,i}^1 + 2u_3^2) + 4\mu_*u_3^2 \\ 2e^2q &= [\sigma_{33}(y_1, y_2, {}^1/_2, t) + \sigma_{33}(y_1, y_2, -{}^1/_2, t)]/e^2 \\ &= 2\lambda_*\left(u_{i,i}^0 + \frac{1}{2}u_{2,i}^0u_{3,i}^0 + \frac{1}{2}u_i^1u_i^1\right) + 2\mu_*(u_i^1u_i^1) \end{aligned}\right\} \ldots [12]$$

We now eliminate u_3^2 and ${}^1/_2(u_i^1u_i^1)$ from Equations [10]. To do this, we apply the Laplace transform with respect to time to Equations [12] and to Equations [10] after the integrations are carried out. We then eliminate u_3^2 and ${}^1/_2(u_i^1u_i^1)$ among the resulting equations and take the inverse transform. This leads to

$$\left.\begin{aligned} N_{ij}/he^2 &= H_*\left(u_{k,k}^0 + \frac{1}{2}u_{3,k}^0u_{3,k}^0\right)\delta_{ij} \\ &\quad + G_*(u_{i,j}^0 + u_{j,i}^0 + u_{2,i}^0u_{3,j}^0) \\ N_{33}/he^2 &= e^2q, \quad N_{3i}/he^2 = \kappa eG'_*(u_i^1 + u_{3,i}^0) \end{aligned}\right\} \ldots [13]$$

$$12M_{ij}/h^2e^2 = H_*u_{k,k}^1\delta_{ij} + G_*(u_{i,j}^1 + u_{j,i}^1) \ldots\ldots [14]$$

Here H_*, etc., operators are defined similarly to Equations [7] and are related to $\bar{l}_2(s)$ and $\bar{l}_3(s)$ by

$$\bar{H} = 2\bar{l}_3\bar{l}_2/(\bar{l}_2 + 2\bar{l}_3), \quad G_* = \mu_* \ldots\ldots [15]$$

where bar above the letters represents Laplace transforms. Hence, for example, $H(t)$ is the inverse transform of $\bar{H}(s)$, etc. These functions depend on the "hereditary characteristics" of the medium, and must be determined from the experiment. Further we define

$$E_*\phi(t) = (1-\nu^2)(H_* + 2G_*)\phi(t) = E\phi(t) + \int_0^t \epsilon(t-\tau)\phi(\tau)d\tau \ldots [16]$$

It is of interest to note that for zero internal damping

$$H_* \to \nu E/(1-\nu^2), \ G_* \to G, \ E_* \to E \ldots\ldots [17]$$

where E, G, ν are Young's modulus, shear modulus, and Poisson's ratio, respectively. For the case of zero internal damping Equations [13] and [14] reduce to classical plate stress-strain relations if we drop the nonlinear terms and set $u_i^1 = -u_{3,i}^0$, leading to zero transverse shear resultant. The factor $\kappa e^2G'$ replaces G in the transverse direction. This is done in order to take into account the nonuniform distribution of σ_{3i} across the thickness and to account for the transverse shear deformability of the media (16). Thus the effect of transverse shear deformation can readily be recognized by the terms containing G' in the following. Constant κ has the same meaning as those used by Timoshenko (5), Mindlin (7), and Reissner (14).

[5] Order of magnitudes of p and q may be seen to be consistent by starting with the stress-strain relations for an orthotropic media (16). This, however, makes the effect of transverse normal stress deformation disappear from the final equations. This effect is unimportant. However, it is taken into account in (16).

Equations of Motion

Let $\mathfrak{d}_\alpha$ be the force per unit deformed area acting on the surface whose normal before deformation was x_α. We define physical $\sigma_{\alpha\beta}$ components of stress tensor by

$$\mathfrak{d}_\alpha = \sigma_{\alpha\beta}\mathbf{e}_\beta \quad \ldots\ldots [18]$$

The total force acting on the deformed area $dA_{(\alpha)}$ is given by

$$\left.\begin{aligned} \mathfrak{d}_\alpha dA_{(\alpha)} &= \sigma_{\alpha\beta}\mathbf{e}_\beta dA_{(\alpha)}, \quad dA_{(\alpha)} = h_\alpha dS_{(\alpha)} \\ h_1 = |\mathfrak{g}_2 \times \mathfrak{g}_3|, &\quad h_2 = |\mathfrak{g}_3 \times \mathfrak{g}_1|, \quad h_3 = |\mathfrak{g}_1 \times \mathfrak{g}_2| \\ dS_{(1)} = dx_2 dx_3, &\quad dS_{(2)} = dx_3 dx_1, \quad dS_{(3)} = dx_1 dx_2 \end{aligned}\right\} \ldots [19]$$

The total force $\mathfrak{s}_\alpha$ per unit of undeformed area is obtained by dividing $\mathfrak{d}_\alpha dA_{(\alpha)}$ by $dS_{(\alpha)}$

$$\mathfrak{s}_\alpha = h_\alpha e_{\beta\gamma}\sigma_{\alpha\beta}\mathbf{i}_\gamma \ (\alpha \text{ not summed}) \quad \ldots\ldots [20]$$

Equations of force equilibrium $(\partial\mathfrak{s}_\alpha/\partial x_\alpha) + \rho\mathbf{P} = 0$ gives

$$\frac{\partial}{\partial x_1}(h_1 e_{\beta\gamma}\sigma_{1\beta}) + \frac{\partial}{\partial x_2}(h_2 e_{\beta\gamma}\sigma_{2\beta}) + \frac{\partial}{\partial x_3}(h_3 e_{\beta\gamma}\sigma_{3\beta}) + \rho P_\gamma = 0 \quad \ldots\ldots [21]$$

where $\mathbf{P} = P_\gamma \mathbf{i}_\gamma$ is the body force per unit mass and ρ is the mass density of the undeformed volume. Equations of motion are obtained by invoking d'Alembert's principle, i.e.

$$P_\gamma = f_\gamma - \partial^2 u_\gamma/\partial t^2 \quad \ldots\ldots [22]$$

Equations of moment equilibrium lead to $\sigma_{\alpha\beta} = \sigma_{\beta\alpha}$.[6] Equations [21] are exact and contain no restriction in respect to magnitudes of strain and rotations. We note that when strains are small as compared to unity $|\mathfrak{g}_\beta| \leqq 1$ and area ratios $h_i \leqq 1$; hence Equation [21] leads to Trefftz theory (17); for Trefftz's pseudo stress components $k_{\alpha\beta}$ are related to $\sigma_{\alpha\beta}$ by $k_{\alpha\beta} = h_\alpha\sigma_{\alpha\beta}/\sqrt{\mathfrak{g}_{\alpha\alpha}}$ (α not summed).

Integrating Equation [21] across the thickness once directly and once after multiplying by y_3 and keeping only the lowest order terms and putting surface shear $\sigma_{3i} = 0$ at the upper and lower surfaces we obtain macroscopic plate equations

$$\left.\begin{aligned} a^{-1}N_{ij,i} + 0(\epsilon^5) &= \rho a^2\epsilon^3\left(\frac{\partial^2 u_j^0}{\partial t^2} - F_j\right) + 0(\epsilon^5) \\ a^{-1}N_{33,i} + 2\epsilon^4 p + \epsilon a^{-1}(N_{ji}u_{3,i}^0)_{,j} &\\ + 0(\epsilon^6) &= \rho a^2\epsilon^2\frac{\partial^2 u_3^0}{\partial t^2} + 0(\epsilon^4) \\ (ah)^{-1}M_{ij,i} - h^{-1}N_{j3} + 0(\epsilon^5) &\\ = \frac{1}{12}\rho a^2\epsilon^3\left(\frac{\partial^2 u_j^1}{\partial t^2} - G_j\right) &+ 0(\epsilon^5) \end{aligned}\right\} \ldots [23]$$

and another equation in which the lowest order term is $0(\epsilon^5)$, hence is neglected. The second equation of Equations [23] and [13] are combined to

$$\left.\begin{aligned} \kappa\epsilon^2 G'_* u_{i,i}^1 &= -\kappa\epsilon^2 G'_*\Delta u_3^0 + \rho a^2\frac{\partial^2 u_3^0}{\partial t^2} - 2\epsilon^2 p - \epsilon^2 N, \\ \epsilon^2 hN &= (N_{ji}u_{3,i}^0)_{,j}, \quad \Delta = \frac{\partial^2}{\partial y_1^2} + \frac{\partial^2}{\partial y_2^2} \end{aligned}\right\} \ldots [24]$$

With the use of Equations [13], [14], and [24], the remaining Equations of [23] are transformed to

$$\Delta_{G^*}\Delta_{E^*}u_i^0 = (1-\nu^2)A_i(u_3^0, F) \quad \ldots\ldots [25]$$

$$\kappa\epsilon^2 G'_*(\Delta_{G^*}u_i^1 - 12\kappa G'_* u_i^1) = B_i(u_3^0, p, N) \quad \ldots\ldots [26]$$

where

$$\left.\begin{aligned} A_i(u_3^0, F) = -\Delta_G{}^*\Big[&\frac{1}{2}H_*(u_{3,j}^0 u_{3,j}^0)_{,i} + G_*(u_{3,i}^0 u_{3,j}^0)_{,j} \\ &+ \rho a^2 F_i\Big] + (H_* + G_*)G_*(u_{3,j}^0\Delta u_{3,i}^0 - u_{3,i}^0\Delta u_{3,j}^0)_{,j} \\ &+ \rho a^2(H_* + G_*)(F_{j,i} - F_{i,j})_{,j} \\ &- \rho a^2[f + g, (u_{i,j}^0 - u_{j,i}^0)_{,j}], \\ B_i(u_3^0, p, N) = \kappa\epsilon^2 G'_*(12\kappa G'_* u_{3,i}^0 &- \rho a^2 G_i) \\ &+ (H_* + G_*)\left(\kappa\epsilon^2 G'^* \Delta u_{3,i}^0 - \rho a^2\frac{\partial^2 u_{3,i}^0}{\partial t^2}\right. \\ &\left. + \epsilon^2 N_{,i} + 2\epsilon^2 p_i\right), \\ \Delta_E{}^* = E_*\Delta - (1-\nu^2)\rho a^2\partial^2/\partial t^2, &\quad \Delta_G{}^* = G^*\Delta - \rho a^2\partial^2/\partial t^2 \end{aligned}\right\} \ldots [27]$$

In obtaining these equations, the following properties of star operators E_*, H_*, G'_*, etc., are used, which can be proved easily from the defining equations

$$\left.\begin{aligned} E_* G'_* &= G'_* E_*, \quad [E_*\phi(y_1, y_2, t)]_{,i} = E_*\phi_{,i}, \\ \frac{\partial}{\partial t}(E_*\phi) - E_*\frac{\partial\phi}{\partial t} &= \epsilon(t)\phi(y_1, y_2, 0), \\ \frac{\partial^2}{\partial t^2}(E_*\phi) - E_*\frac{\partial^2\phi}{\partial t^2} &= [\epsilon, \phi] \\ = \frac{\partial\epsilon(t)}{\partial t}\phi(y_1, y_2, 0) &+ \epsilon(t)\frac{\partial\phi}{\partial t}(y_1, y_2, 0) \end{aligned}\right\} \ldots [28]$$

Elimination of u_i^1 between Equations [24] and [26] yields

$$\begin{aligned} -\kappa\epsilon^2 G'_* D_*\Delta^2 u_3^0 + \rho a^2\left(D_* + \frac{h^2}{12}\kappa\epsilon^2 G'_*\right)\Delta(\partial^2 u_i^0/\partial t^2) \\ - \rho h a^4\kappa\epsilon^2 G'_*(\partial^2 u_3^0/\partial t^2) - \frac{1}{12}\rho^2 h^3 a^4(\partial^4 u_i^0/\partial t^4) \\ - 2\epsilon^2 D_*\Delta p + 2h^3\kappa\epsilon^2 G'_* p + \frac{1}{6}\rho h^3\epsilon^2 a^2(\partial^2 p/\partial t^2) - \epsilon^2 D_*\Delta N \\ + h^3\kappa\epsilon^2 G'_* N + \frac{1}{12}\rho h^5(\partial^2 N/\partial t^2) + \frac{1}{12}\rho h^3 a^2\kappa\epsilon^2 G'_* G_{i,i} \\ + \frac{1}{12}\rho a^2 h^3\,[\kappa\epsilon^2 g', \Delta u_3^0 + u_{i,i}^1] = 0 \quad \ldots [29] \end{aligned}$$

where

$$D_* = \frac{h^3}{12(1-\nu^2)}E_* \quad \ldots\ldots [30]$$

Here the operator D_* takes the place of the bending rigidity of the classical plate theory. $[\kappa\epsilon^2 g', \ldots]$ is known when the initial conditions are given.

Equations [25], [26], and [29] are the equations of motion. It is interesting to note that these equations *are nonlinear in only displacement* component u_3^0. Hence after Equations [25] and [29] are solved simultaneously Equations [26] reduce to linear inhomogeneous differential equations. Observe also that there is no coupling effect among displacement components u_1^0, u_2^0, u_1^1, u_2^1.

[6] Strictly speaking, this is true only when $|\mathfrak{g}_\alpha| = 1$ which is the case for the present approximation.

We now introduce plane dilatation θ_0 and plane rotation ω_0, and notice the following dual relations

$$\left.\begin{aligned} \theta_0 &= u_{i,i}, \quad \omega_0 = u_{1,2} - u_{2,1} \\ \Delta u_1{}^0 &= \theta_{0,1} + \omega_{0,2}, \quad \Delta u_2{}^0 = \theta_{0,2} - \omega_{0,1} \end{aligned}\right\} \ldots\ldots [31]$$

The first of Equations [23] can now be transformed to

$$\left.\begin{aligned} E_*\Delta\theta_0 - \rho a^2(1-\nu^2)\partial^2\theta_0/\partial t^2 = \\ -(1-\nu^2)\left[\frac{1}{2}H_*\Delta(u_{3,i}{}^0 u_{3,i}{}^0)\right. \\ \left. + G_*(u_{3,i}{}^0 u_{3,j}{}^0)_{,ij} + \rho a^2 P_{i,i}\right], \\ G_*\Delta\omega_0 - \rho a^2\partial^2\omega_0/\partial t^2 = G_*(u_{3,2}{}^0\Delta u_{3,1}{}^0 - u_{3,1}{}^0\Delta u_{3,2}{}^0) \\ + \rho a^2(P_{1,2} - P_{2,1}) \end{aligned}\right\} \ldots [32]$$

These equations replace Equation [25] and are the analogs of the plane dilatational and rotational waves of the classical theory. In the classical theory, of course, the nonlinear terms which appear on the right of Equations [32] are missing.

The following observations are useful:

(*a*) In case of zero internal damping terms like $[\epsilon, \phi] = 0$ and all star-indexed quantities G'_*, E_*, D_*, etc., must be replaced by nonstar quantities G', E, D, etc. To this end we use Relations [17].

(*b*) The transverse shear-deformation effect is eliminated by letting $G'_* \to \infty$.

(*c*) The rotary inertia effect is eliminated by letting $\rho h^3/12 \to 0$ while $\rho a^4 h$ remains finite.

(*d*) Small deformation theory is obtained by taking N_{ij} constant in the Expression [24] of N.

Perturbation in Time

In flexural vibrations, the transient state in planar wave propagation is unimportant. For plates with finite boundaries a few milliseconds after the motion begins the planar stress wave will be felt everywhere. Hence, by making perturbation in time and also ignoring body forces and moments, a great deal of simplification can be achieved. Thus let

$$\tau = \epsilon t \ldots\ldots [33]$$

The lowest order terms of the first of Equations [23] are now reduced to

$$N_{ij,i} = 0 \ldots\ldots [34]$$

These equations are satisfied by Airy's stress function

$$N_{11} = \epsilon^2\phi_{,22}, \quad N_{12} = -\epsilon^2\phi_{,12}, \quad N_{22} = \epsilon^2\phi_{,11} \ldots [35]$$

Elimination of $u_i{}^0$ from Expression [13] of N_{ij} now leads to

$$E_*\Delta^2\phi = 4(1-\nu^2)h(H_* + G_*)G_*(u_{3,12}{}^0 u_{3,12}{}^0 - u_{3,11}{}^0 u_{3,22}{}^0) \ldots [36]$$

Equation of transverse vibration is obtained by combining Equations [29] and [35]. The only change in Equation [29] will be in the expression of N

$$hN = \phi_{,22}u_{3,11}{}^0 - 2\phi_{,12}u_{3,12}{}^0 + \phi_{,11}u_{3,22}{}^0 \ldots\ldots [37]$$

Equation [29] with N given by Equation [37] and Equation [36] must be solved simultaneously to determine ϕ and $u_3{}^0$. Once this is done, one can use Equation [13] to determine $u_i{}^0$. Deformation components $u_i{}^1$ can now be solved from Equation [26].

Plates With No Internal Damping

The case of zero internal damping is of great practical interest. In this case, with use of Relations [17], Equations [25], [26], [29], and [36] can be written down immediately. Here we only give the expression corresponding to Equations [29] and [36]

$$\begin{aligned} -D\Delta^2 u_3{}^0 + \left(\rho\frac{h^5}{12} + \frac{\rho a^2 D}{\kappa G'}\right)\Delta(\partial^2 u_3{}^0/\partial\tau^2) \\ - \rho a^2 h^3(\partial^2 u_3{}^0/\partial\tau^2) - (\rho^2 h^5 a^2/12\kappa G')(\partial^4 u_3{}^0/\partial\tau^4) \\ - (2D/\kappa G')\Delta p + 2h^3 p + 2(\rho h^5/12\kappa G')(\partial^2 p/\partial\tau^2) \\ - (D/\kappa G')\Delta N + h^3 N + (\rho h^5/12\kappa G')(\partial^2 N/\partial\tau^2) = 0 \ldots [38] \end{aligned}$$

$$\Delta^2\phi = hE(u_{3,12}{}^0 u_{3,12}{}^0 - u_{3,11}{}^0 u_{3,22}{}^0) \ldots\ldots [39]$$

We note that if in Equation [38] we take $\rho h^3/12 = 0$ and $\partial/\partial\tau = 0$, we obtain static plate equation [70] of Reissner (15). If we also let $G' \to \infty$ we obtain static plate equations of Föppl-Karman-Timoshenko theory. Uflyand-Mindlin theory (6, 7) results by taking $N \equiv 0$ in Equation [38]. (Also Equation [39] is identical to that of Föppl-Karman-Timoshenko theory.)

Other types of approximations may be obtained by using one or several of simplifications explained in the section Equations of Motion.

Boundary and Initial Conditions

The boundary conditions on surface traction $\mathbf{s}_\nu$ consist of prescribing $\mathbf{s}_\nu = s_\alpha \mathbf{i}_\alpha$ acting on a deformed edge surface Σ which had $\boldsymbol{\nu} = \nu_\alpha \mathbf{i}_\alpha$ as its normal before deformation. This follows from the equation of force equilibrium $\mathbf{s}_\nu dS_{(\nu)} = \sum_\alpha \mathbf{s}_\alpha dS_{(\alpha)}$ of an infinitesimal tetrahedron before deformation, with sides perpendicular to $\boldsymbol{\nu}$ and $\mathbf{i}_\alpha$. Hence, with the use of Equation [20], we find

$$s_\alpha = e_{\beta\alpha}(h_1\nu_1\sigma_{1\beta} + h_2\nu_2\sigma_{2\beta} + h_3\nu_3\sigma_{3\beta}) \text{ on } \Sigma \ldots\ldots [40]$$

Stress resultants and stress couples acting at the edge surface are obtained, respectively, by integrating Equation [40] directly and by multiplying by x_3 and integrating across the thickness, and keeping only the lowest order terms

$$\left.\begin{aligned} N_i = N_{ji}\nu_j, \quad N_3 = (N_{j3} + \epsilon N_{ji}u_{3,i}{}^0)\nu_j \\ M_i = M_{ji}\nu_j \end{aligned}\right\} \ldots\ldots [41]$$

where N_α and M_i are the components of edge surface tractions and moments referred to Cartesian co-ordinates of the undeformed medium, and N_j and M_{ji} are stress resultants and couples which are given by Equations [13] and [14]. Stress couples M_{ij} can be expressed in terms deflection $u_3{}^0$ and transverse shear resultants N_{3i} by eliminating $u_i{}^1$ between the equations for N_{3i} of Equations [13] and M_{ij} of Equation [14]. Hence

$$\begin{aligned} 12\kappa G_*{}'M_{ij} = -\kappa\epsilon^2 h^2 G'_*(H_*\Delta u_3{}^0\delta_{ij} + 2G_* u_{3,ij}{}^0) \\ + a[H_* N_{3k,k}\delta_{ij} + G_*(N_{3i,j} + N_{3j,i})] \ldots [42] \end{aligned}$$

In case of zero internal damping this reduces to

$$\begin{aligned} a^2 M_{ij}/h = -D[\nu\Delta u_3{}^0\delta_{ij} + (1-\nu)u_{3,ij}{}^0] + (a/h)^2(D/\kappa G'h) \\ \times\left[\nu N_{3k,k}\delta_{ij} + \frac{1}{2}(1-\nu)(N_{3i,j} + N_{3j,i})\right] \ldots [43] \end{aligned}$$

In these equations the terms containing $u_3{}^0$ are identical to those of the classical plate theory, while the terms containing N_{3i} are due to transverse shear deformation. Equations [43] are analogs of Reissner's equation [10] of (14). Note that like Reissner's theory we have three conditions, Equations [42], in case of zero membrane forces. In the present theory there are altogether five boundary conditions, Equations [41].

Edge-support conditions on displacements consist of specifying $u_\alpha{}^0$, $u_i{}^1$ and/or their derivatives in various directions depending upon the type of support. For example, a built-in end condition in the direction $\boldsymbol{\nu}$ is obtained by taking

$$\partial u_z^0/\partial x_\nu = 0 \text{ or } u_{3,i}{}^0 \nu_i = 0$$

Initial conditions are obtained by prescribing the time-dependent variables and their time derivatives of first order at an initial time.

Finally, reference may be made to (16) for the expression of strain energy, a somewhat different approach to the present problem, and for the form of equations in engineering notation.

BIBLIOGRAPHY

1 "The Mathematical Theory of Elasticity," by A. E. H. Love, Dover Publications, New York, N. Y., 1944, p. 558.

2 "Applied Mechanics," Theodore von Karman anniversary volume, 1941, "The Intrinsic Theory of Elastic Shells and Plates," by J. L. Synge and W. Z. Chien.

3 "The Intrinsic Theory of Thin Shells and Plates," by W. Z. Chien, *Quarterly of Applied Mathematics*, vol. 1, 1943, pp. 297–327; vol. 2, 1944, pp. 43–59, 120–135.

4 "The Equilibrium of Thin Elastic Shells," by A. E. Green and W. Zerna, *The Quarterly Journal of Mechanics and Applied Mathematics*, vol. 3, 1950, pp. 9–22.

5 "Vibration Problems in Engineering," by S. Timoshenko, D. Van Nostrand Company, Inc., New York, N. Y., 1937, pp. 338 and 342.

6 "The Propagation of Waves in Transverse Vibrations of Bars and Plates" (Russian), by Ya. S. Uflyand, Akad. Nauk, USSR, *Prikl. Mat. Meh.*, vol. 12, 1948, pp. 287–300.

7 "Influence of Rotatory Inertia and Shear on Flexural Motions of Isotropic Elastic Plates," by R. D. Mindlin, JOURNAL OF APPLIED MECHANICS, Trans. ASME, vol. 73, 1951, pp. 31–38.

8 "Non-Homogeneous Stresses in Visco-Elastic Media," by T. Alfrey, *Quarterly of Applied Mathematics*, vol. 2, 1944, pp. 113–119.

9 "Methods of Representing of Properties of Visco-Elastic Materials," by T. Alfrey, *Quarterly of Applied Mathematics*, vol. 3, 1945–1946, p. 143.

10 "Theory of Functionals and the Integral and Integro-Differential Equations," by V. Volterra, Blackie and Son, London, England, 1930.

11 "On Elastic Continua With Hereditary Characteristics," by E. Volterra, JOURNAL OF APPLIED MECHANICS, Trans. ASME, vol. 73, 1951, pp. 273–279.

12 "Über innere Reibung fester Körper inbesondere der Metalle," by W. Voigt, *Annalen der Physik*, vol. xlvii, 1892, p. 671.

13 "On the Decay of Waves in Visco-Elastic Solid Bodies," by K. Sezawa, Earthquake Research Inst. Bulletin, Tokyo University, Japan, vol. 43, 1926–1927, pp. 1–3.

14 "On Bending of Elastic Plates," by E. Reissner, *Quarterly of Applied Mathematics*, vol. 5, 1947, pp. 55–58.

15 "Finite Deflection of Sandwich Plates," by E. Reissner, *Journal of the Aeronautical Sciences*, vol. 15, 1948, pp. 435–440.

16 "Nonlinear Oscillations of Visco-Elastic Plates," by A. C. Eringen, Office of Naval Research, Technical Report No. 4, 1952, pp. 14–15.

17 "Über die Ableitung der Stabilitätskriterien des elastischen Gleichgewichts aus der Elastizitätstheorie endlicher Deformationen," by E. Treffts, Proceedings of the Third International Congress of Applied Mechanics, 1931, pp. 44–50.

18 "Theorie des Distributions," by L. Schwartz, Herman and Company, Paris, France, vols. 1 and 2, 1950.

Forced Vibration of a Clamped Rectangular Plate in Fluid Media[1]

By GORDON C. K. YEH[2] and JOHANN MARTINEK,[3] WASHINGTON, D. C.

Forced vibration of a thin rectangular plate clamped in a rigid infinite baffle is analyzed. The plate is assumed to separate two different fluid media and the vibration is excited by a simple plane wave of high frequency (as compared with $c/2\sqrt{\pi ab}$) normally incident from one side of the plate. Using the characteristic shape functions, the Lagrange equations of motion of the plate are set up in generalized co-ordinates. The solutions of the equations render series expressions for the plate deflection and an energy-transmission coefficient. Certain numerical results are given.

Nomenclature

The following nomenclature is used in the paper:

a = plate width
b = plate length
h = plate thickness
c, c_1, c_2 = wave velocity in fluid media
ρ_1, ρ_2 = fluid density
q, q_{mn}, q_{rs} = generalized co-ordinates
p = excess pressure
p_1 = excess pressure of incident wave
p_1' = excess pressure of reflected wave
p_2 = excess pressure of transmitted wave
w = dynamic normal displacement of plate
u = particle displacement of fluid
t = time
T_0 = period
T = kinetic energy of plate
V = potential energy of plate
ω = circular frequency of incident wave
x, y, z = Cartesian co-ordinates
Q_{mn} = generalized force
E = Young's modulus
μ = Poisson's ratio
$D = \dfrac{Eh^3}{12(1-\mu^2)}$ = flexural rigidity of the plate
m, n, r, s = odd integers
γ = specific weight of plate
g = gravitational acceleration
$\overline{m} = \dfrac{\gamma h}{g}$ = area density of plate
λ = wave length
λ_{mn} = coefficients defined by Equation [23]
$\tau = \bar{W}_2^{T_0}/\bar{W}_1^{T_0}$ = transmission coefficient
$\bar{W}_1^{T_0}$ = mean rate of incident energy in first medium arriving at interface 1
$\bar{W}_2^{T_0}$ = mean rate of energy transmitted to second medium at interface 2
$\Re e$ = real part of . . .
$\phi_m(x)$, $\phi_n(y)$ = characteristic functions for normal modes of vibration of a beam clamped at both ends
α_m, α_n, β_m, β_n = parameters in functions $\phi_m(x)$ and $\phi_n(y)$
E_{mr}, E_{ms}, F_{nr}, F_{ns} = definite integrals defined by Equations [17]
C_{mn}^{mn}, C_{mn}^{rn}, C_{mn}^{ms}, C_{mn}^{rs} = coefficients defined by Equations [16]
k_{mn}^{mn}, k_{mn}^{rs} = coefficients defined by Equations [28]
δ_1, δ_2 = coefficients defined by Equations [38]

Dots denote derivatives with respect to time.
Prime marks denote derivatives with respect to $\beta_m x$ or $\beta_n y$.
Other symbols will be defined as they are introduced.

Introduction

In this paper the forced vibration of a rectangular plate is analyzed where the interactions of the surrounding fluid media are taken into account. The plate is clamped in an infinite rigid baffle which separates two different fluid media. A normal incident simple plane wave in the first medium sets the plate in motion and the radiation of the plate produces a reflected wave in the first medium and a transmitted wave in the second medium both of which in turn affect the motion of the plate. The following assumptions are made: (*a*) The fluid media satisfy the conditions for the validity of the simplified (small amplitude) wave equation; (*b*) the incident wave has a high frequency such that

$$\frac{\omega}{c_1} \gg \sqrt{\frac{\pi}{ab}} \text{ and } \frac{\omega}{c_2} \gg \sqrt{\frac{\pi}{ab}}$$

(*c*) the plate is composed of a material which is isotropic, devoid of damping, and which obeys Hooke's law; and (*d*) the deflections and the thickness of the plate are small compared with its other dimensions.

Morse (1)[4] has discussed such a problem for a rectangular membrane in one fluid medium where the motion is excited by a distributed driving force instead of an incident wave. Vogel (2) has solved such a problem for a simply supported plate in one fluid

---

[1] The ideas in this work originated in the course of a project carried out under contract NObs 2937, Task Order No. 2 sponsored by the Bureau of Ships.

[2] Staff Scientist, Research Division, Reed Research, Inc. Assoc. Mem. ASME.

[3] Staff Scientist, Research Division, Reed Research, Inc.

Presented at the National Conference of the Applied Mechanics Division, Troy, N. Y., June 16–18, 1955, of The American Society of Mechanical Engineers.

Discussion of this paper should be addressed to the Secretary, ASME, 29 West 39th Street, New York, N. Y., and will be accepted until January 10, 1956, for publication at a later date. Discussion received after the closing date will be returned.

Note: Statements and opinions advanced in papers are to be understood as individual expressions of their authors and not those of the Society. Manuscript received by ASME Applied Mechanics Division, August 20, 1954. Paper No. 55—APM-24.

[4] Numbers in parentheses refer to the Bibliography at the end of the paper.

medium as applied to acoustics. The present analysis may be considered as an extension of Vogel's solution to a clamped plate in two different fluid media.

Equation of Motion in Cartesian Co-Ordinates

Consider the plane $z = 0$ at the middle surface of the undeflected flat plate. For small deflections of a thin plate the effect of the static deflections upon the dynamic deflections may be neglected. The equation of motion for the dynamic deflections of the plate is

$$\bar{m}\ddot{w} + D\nabla^4 w = p(x, y, 0, t) \quad [1]$$

where the forcing function $p(x, y, 0, t)$ consists of the excess pressures from the incident wave $p_i(x, y, 0, t)$, the reflected wave $p_1'(x, y, 0, t)$ and the transmitted wave $p_2(x, y, 0, t)$ such that

$$p(x, y, 0, t) = p_i(x, y, 0, t) + p_1'(x, y, 0, t) - p_2(x, y, 0, t) \quad [2]$$

For a simple plane wave normally incident on the plate we have

$$p_i(x, y, 0, t) = p_0 \cos \omega t \quad [3]$$

and

$$\dot{u}_i(x, y, 0, t) = p_i(x, y, 0, t)/\rho_1 c_1 \quad [4]$$

Under assumption (b) the reflected wave and the transmitted wave are such that the pressure at any point on the plate is ρc times the local particle velocity at that point (see Conclusions at the end of the paper).

$$p_1'(x, y, 0, t) = \rho_1(-c_1)\dot{u}_1'(x, y, 0, t) \quad [5]$$

$$p_2(x, y, 0, t) = \rho_2 c_2 \dot{w} \quad [6]$$

The condition of continuity requires at the interface of the first medium and the plate

$$\dot{u}_i(x, y, 0, t) + \dot{u}_1'(x, y, 0, t) = \dot{w} \quad [7]$$

Substituting Equations [3 to 7] into Equation [2] we have

$$p(x, y, 0, t) = 2p_0 \cos \omega t - (\rho_1 c_1 + \rho_2 c_2)\dot{w} \quad [8]$$

Hence the equation of motion Equation [1] becomes

$$\bar{m}\ddot{w} + (\rho_1 c_1 + \rho_2 c_2)\dot{w} + D\nabla^4 w = 2p_0 \cos \omega t \quad [9]$$

Lagrange Equations

It is expedient to express and solve the equation of motion in generalized co-ordinates. If the location of the origin of the Cartesian co-ordinates is such that the lines $x = 0$, $x = a$, $y = 0$, and $y = b$ coincide with the edges of the clamped plate the dynamic deflection of the plate can be expressed among others in the form of a double series

$$w = \sum_{m=1}^{\infty}\sum_{n=1}^{\infty} q_{mn}(t)\phi_m(x)\phi_n(y) \quad [10]$$

where $\phi_m(x)$ and $\phi_n(y)$ are characteristic functions representing normal modes of vibration of a clamped-clamped beam (see, for example, reference 3) and are expressed as follows

$$\phi_m(x) = \cosh \beta_m x - \cos \beta_m x - \alpha_m(\sinh \beta_m x - \sin \beta_m x) \quad [11]$$

$$\phi_n(y) = \cosh \beta_n y - \cos \beta_n y - \alpha_n(\sinh \beta_n y - \sin \beta_n y) \quad [12]$$

Owing to symmetry of the plate and the pressures with respect to the lines $x = a/2$ and $y = b/2$ only odd values of m and n will show up in Equation [10]. Terms m and n are assumed to be consecutive odd integers throughout this analysis. In Equation [10] the coefficients $q_{mn}(t)$ are to be determined as solutions of the Lagrange equations

$$\frac{d}{dt}\left(\frac{\partial T}{\partial \dot{q}_{mn}}\right) - \frac{\partial T}{\partial q_{mn}} + \frac{\partial V}{\partial q_{mn}} = Q_{mn} \quad [13]$$

and are generalized co-ordinates. In Equation [13] Q_{mn} are the generalized forces.

The potential energy or the bending-strain energy for a clamped plate[5] is

$$V = \frac{D}{2}\int_0^a \int_0^b \left(\frac{\partial^2 w}{\partial x^2} + \frac{\partial^2 w}{\partial y^2}\right)^2 dx\, dy \quad [14]$$

Substituting Equation [10] into Equation [14] and using the integral formulas in reference (5) we have

$$V = \frac{D}{ab}\sum_{m=1}^{\infty}\sum_{\substack{n=1 \\ (mn \neq rs)}}^{\infty}\sum_{r=1}^{\infty}\sum_{s=1}^{\infty} C_{mn}{}^{rs} q_{mn}(t) q_{rs}(t) + \frac{D}{2ab}\sum_{m=1}^{\infty}\sum_{n=1}^{\infty} C_{mn}{}^{mn} q_{mn}{}^2(t) \quad [15]$$

where

$$\left.\begin{aligned} C_{mn}{}^{mn} &= 2E_{mm}F_{nn} + (\beta_m a)^4\left(\frac{b}{a}\right)^2 + (\beta_n b)^4\left(\frac{a}{b}\right)^2 \\ C_{mn}{}^{rn} &= E_{mr}F_{nn} \quad (m \neq r) \\ C_{mn}{}^{ms} &= E_{mm}F_{ns} \quad (n \neq s) \\ C_{mn}{}^{rs} &= E_{mr}F_{ns} \quad (m \neq r,\ n \neq s) \end{aligned}\right\} \quad [16]$$

In Equations [16] the nondimensional coefficients are in terms of the following nondimensional definite integrals

$$\left.\begin{aligned} E_{mm} &= a\int_0^a \phi_m(x)\frac{d^2\phi_m(x)}{dx^2}\,dx = a\alpha_m\beta_m(2 - \alpha_m\beta_m a) \\ F_{nn} &= b\int_0^b \phi_n(y)\frac{d^2\phi_n(y)}{dy^2}\,dy = b\alpha_n\beta_n(2 - \alpha_n\beta_n b) \\ E_{mr} &= \underset{(r\neq m)}{E_{rm}} = a\int_0^a \phi_m(x)\frac{d^2\phi_r(x)}{dx^2}\,dx = \frac{8a\beta_m{}^2\beta_r{}^2(\alpha_m\beta_m - \alpha_r\beta_r)}{\beta_m{}^4 - \beta_r{}^4} \\ F_{ns} &= \underset{(n\neq s)}{F_{sn}} = b\int_0^b \phi_n(y)\frac{d^2\phi_s(y)}{dy^2}\,dy = \frac{8b\beta_n{}^2\beta_s{}^2(\alpha_n\beta_n - \alpha_s\beta_s)}{\beta_n{}^4 - \beta_s{}^4} \end{aligned}\right\} \quad [17]$$

[5] See, for example, reference (4), p. 288.

TABLE 1 VALUES OF α_m AND $\beta_m L$ FOR CLAMPED-CLAMPED BEAM FUNCTION

m	α_m	$\beta_m L$
1	0.9825022158	4.7300408
3	0.9999664501	10.9956078
5	0.9999999373	17.2787596
$m > 5$	$\alpha_m \doteq 1.0$	$\beta_m L \doteq (2m + 1)\frac{\pi}{2}$

TABLE 2 INTEGRALS E_{mr} AND F_{mr} OF CHARACTERISTIC FUNCTIONS FOR CLAMPED-CLAMPED BEAM

$$E_{mr} = F_{mr} = L\int_0^L \phi_m \frac{d^2\phi_r}{dx^2}\,dx$$

m	1	3	5
1	−12.30262	9.73079	7.61544
3	9.73079	−98.90480	24.34987
5	7.61544	24.34987	−263.99798

Values of α_m and $\beta_m L$ and E_{mr} and F_{mr} have been taken from reference (3), are computed according to Equations [17] and are presented in Tables 1 and 2, respectively.

The kinetic energy T of the vibrating plate is

$$T = \frac{\overline{m}}{2}\int_0^a\int_0^b \dot{w}^2 dxdy \qquad [18]$$

which, when Equation [10] is used, becomes

$$T = \frac{ab\overline{m}}{2}\sum_{m=1}^{\infty}\sum_{n=1}^{\infty}\dot{q}_{mn}^2(t) \qquad [19]$$

The mn-th generalized force may be written as

$$Q_{mn} = \int_0^a\int_0^b p(x, y, 0, t)\phi_m(x)\phi_n(y)dxdy \qquad [20]$$

Substituting Equation [8] into Equation [20] we have

$$Q_{mn} = 2p_0\cos\omega t\int_0^a\int_0^b \phi_m(x)\phi_n(y)dxdy - (\rho_1c_1 + \rho_2c_2)\int_0^a\int_0^b \dot{w}\phi_m(x)\phi_n(y)dxdy \qquad [21]$$

and using the expression Equation [10], we obtain

$$Q_{mn} = ab\lambda_{mn}p_0\cos\omega t - ab(\rho_1c_1 + \rho_2c_2)\dot{q}_{mn}(t) \qquad [22]$$

where

$$\lambda_{mn} = \frac{32\alpha_m\alpha_n}{(\beta_m a)(\beta_n b)} \qquad [23]$$

With the substitution of Equations [15], [19], and [22] into Equations [13], the Lagrange equations become

$$\ddot{q}_{mn}(t) + \frac{\rho_1c_1 + \rho_2c_2}{\overline{m}}\dot{q}_{mn}(t) + \frac{D}{\overline{m}a^2b^2}\sum_{r=1}^{\infty}\sum_{s=1}^{\infty}C_{mn}^{rs}q_{rs}(t) = \frac{\lambda_{mn}}{\overline{m}}p_0\cos\omega t = \frac{\lambda_{mn}}{\overline{m}}p_0\,\mathrm{Re}e^{i\omega t} \qquad [24]$$

Solutions of Lagrange Equations

A particular solution of Equation [24] can be taken in the form

$$q_{mn}(t) = \mathrm{Re}\,\bar{q}_{mn}(t) = \mathrm{Re}|q_{mn}|e^{i(\omega t+\theta_{mn})} \qquad [25]$$

Substituting Equation [25] into Equation [24] we have

$$-\omega^2\bar{q}_{mn}(t) + i\omega\frac{\rho_1c_1 + \rho_2c_2}{\overline{m}}\bar{q}_{mn}(t) + \frac{D}{\overline{m}a^2b^2}\sum_{r=1}^{\infty}\sum_{s=1}^{\infty}C_{mn}^{rs}\bar{q}_{rs}(t) = \frac{\lambda_{mn}}{\overline{m}}p_0e^{i\omega t} \qquad [26]$$

Hence $q_{mn}(t)$ can be obtained by taking the real part of the solution for the following equation

$$\sum_{r=1}^{\infty}\sum_{s=1}^{\infty}k_{mn}^{rs}\bar{q}_{rs}(t) = \frac{\lambda_{mn}}{\overline{m}\omega^2}p_0e^{i\omega t} \qquad [27]$$

where

$$\left.\begin{aligned} k_{mn}^{rs} &= \frac{D}{\overline{m}\omega^2a^2b^2}C_{mn}^{rs} \quad (mn \neq rs) \\ k_{mn}^{mn} &= \left(\frac{D}{\overline{m}\omega^2a^2b^2}C_{mn}^{mn} - 1\right) + i\left(\frac{\rho_1c_1 + \rho_2c_2}{\overline{m}\omega}\right) \end{aligned}\right\} \qquad [28]$$

There will be one equation of the type of Equation [27] for each coefficient $q_{mn}(t)$ taken in the series Equation [10]. Hence Equation [27] represents a system of infinite number of linear algebraic simultaneous equations which can be solved for infinite number of unknowns $q_{mn}(t)$ ($mn = 11$ to $\infty\,\infty$). In practice, it is sufficient to take a finite number of terms in the series, say, up to $m = M$ and $n = N$. Then Equation [27] becomes

$$\sum_{r=1}^{M}\sum_{s=1}^{N}k_{mn}^{rs}\bar{q}_{rs}(t) = \frac{\lambda_{mn}}{\overline{m}\omega^2}p_0e^{i\omega t}\ (m = 1, 3, \ldots M,\ n = 1, 3, \ldots N) \qquad [29]$$

The steady-state solutions thus obtained can always be expressed as follows

$$q_{mn}(t) = |q_{mn}|\cos(\omega t + \theta_{mn}) \qquad [30]$$

When the dynamic deflection is known the bending moments and stresses at any point on the plate and the reaction forces at the plate edges at any instant can be derived immediately from the fundamental formulas in the theory of plates.

Transmission Coefficient τ

We define, after Vogel (2), the transmission coefficient τ as the ratio of mean rate of energy transmitted to the second fluid medium at the interface 2 over mean rate of incident energy in the first fluid medium arriving at the interface 1

$$\tau = \frac{\overline{W}_2T_0}{\overline{W}_1T_0} \qquad [31]$$

For the present analysis we can write

$$\overline{W}_1T_0 = \frac{1}{T_0}\int_0^{T_0}dt\int_0^a\int_0^b\frac{1}{2}p_1(x, y, 0, t)\dot{u}_1(x, y, 0, t)dxdy \qquad [32]$$

and

$$\overline{W}_2T_0 = \frac{1}{T_0}\int_0^{T_0}dt\int_0^a\int_0^b\frac{1}{2}p_2(x, y, 0, t)\dot{w}(x, y, t)dxdy \qquad [33]$$

Using Equations [3] and [4] we reduce Equation [32] to the following form

$$\overline{W}_1T_0 = \frac{abp_0^2}{4\rho_1c_1} \qquad [34]$$

Substituting Equations [6], [10], and [30] into Equation [33] and using the orthogonality relations of the characteristic functions, we have

$$\overline{W}_2T_0 = \frac{ab\rho_2c_2\omega^2}{4}\sum_{m=1}^{\infty}\sum_{n=1}^{\infty}|q_{mn}|^2 \qquad [35]$$

Hence the transmission coefficient can be expressed in terms of the amplitudes of the generalized co-ordinates as follows

$$\tau = \frac{\omega^2}{p_0^2}(\rho_1 c_1)(\rho_2 c_2)\sum_{m=1}^{\infty}\sum_{n=1}^{\infty}|q_{mn}|^2 \quad \ldots\ldots [36]$$

Solutions for a Four-Term Series

Take the first four terms in the series expression of w. Then $M = 3$ and $N = 3$ in Equations [29]. Equations [16] and Tables 1 and 2 give

$$\left.\begin{aligned}
C_{11}^{11} &= 302.71 + 500.56\left[\left(\frac{b}{a}\right)^2 + \left(\frac{a}{b}\right)^2\right] \\
C_{13}^{13} &= 2433.6 + 500.56\left(\frac{b}{a}\right)^2 + 14618\left(\frac{a}{b}\right)^2 \\
C_{31}^{31} &= 2433.6 + 14618\left(\frac{b}{a}\right)^2 + 500.56\left(\frac{a}{b}\right)^2 \\
C_{33}^{33} &= 19564 + 14618\left[\left(\frac{b}{a}\right)^2 + \left(\frac{a}{b}\right)^2\right] \\
C_{11}^{13} &= C_{11}^{31} = C_{13}^{11} = C_{31}^{11} = -119.71 \\
C_{11}^{33} &= C_{13}^{31} = C_{31}^{13} = C_{33}^{11} = 94.688 \\
C_{13}^{33} &= C_{31}^{33} = C_{33}^{13} = C_{33}^{31} = -962.42
\end{aligned}\right\} \ldots [37]$$

Consider a square plate ($a = b$) and use the following notations

$$\left.\begin{aligned}
\delta_1 &= \frac{\bar{m}\omega^2}{D}a^4 \\
\delta_2 &= \frac{\rho_1 c_1 + \rho_2 c_2}{\bar{m}\omega}
\end{aligned}\right\} \ldots\ldots [38]$$

Equations [28] and [37] then give values of k_{mn}^{rs}, Equation [23] and Table 1 give values of λ_{mn}, and Equations [29] the simultaneous equations. It can be seen that for a square plate $q_{13} = q_{31}$ and the system of four equations, Equations [29] can be reduced to one of three equations as follows

$$\left.\begin{aligned}
&[(1303.8 - \delta_1) + \delta_1\delta_2 i]\bar{q}_{11} - 239.43\bar{q}_{13} + 94.688\bar{q}_{33} \\
&\qquad = 1380.7 \times 10^{-3}\frac{\delta_1}{\bar{m}\omega^2}p_0 e^{i\omega t} \\
&-239.43\bar{q}_{11} + [(35293 - 2\delta_1) + 2\delta_1\delta_2 i]\bar{q}_{13} - 1924.8\bar{q}_{33} \\
&\qquad = 1209.0 \times 10^{-3}\frac{\delta_1}{\bar{m}\omega^2}p_0 e^{i\omega t} \\
&94.688\bar{q}_{11} - 1924.8\bar{q}_{13} + [(48800 - \delta_1) - \delta_1\delta_2 i]\bar{q}_{33} \\
&\qquad = 264.66 \times 10^{-3}\frac{\delta_1}{\bar{m}\omega^2}p_0 e^{i\omega t}
\end{aligned}\right\} \ldots [39]$$

Solutions of Equations [39] by Cramer's rule are

$$\left.\begin{aligned}
\bar{q}_{11} &= \frac{\Delta_{11}}{\Delta}\frac{\delta_1}{\bar{m}\omega^2}p_0 e^{i\omega t} \\
\bar{q}_{13} &= \frac{\Delta_{13}}{\Delta}\frac{\delta_1}{\bar{m}\omega^2}p_0 e^{i\omega t} \\
\bar{q}_{33} &= \frac{\Delta_{33}}{\Delta}\frac{\delta_1}{\bar{m}\omega^2}p_0 e^{i\omega t}
\end{aligned}\right\} \ldots\ldots [40]$$

and are finite as long as $\Delta \neq 0$.

In Equations [40] the following symbols are used

$$\left.\begin{aligned}
\Delta &= \{2.2377 \times 10^{12} - 1.8918 \times 10^9\delta_1 + 1.3550 \times 10^5\delta_1^2(1 - \delta_2^2) - 2\delta_1^3(1 - 3\delta_2^2)\} + \delta_1\delta_2 i\{1.8918 \times 10^9 - 2.7100 \times 10^5\delta_1 + 2\delta_1^2(3 - \delta_2^2)\} \\
\Delta_{11} &= \{2.3859 \times 10^9 - 1.8372 \times 10^5\delta_1 + 2.7613\delta_1^2(1 - \delta_2^2)\} + \delta_1\delta_2 i\{1.8372 \times 10^5 - 5.5226\delta_1\} \\
\Delta_{13} &= \{9.3450 \times 10^7 - 6.1414 \times 10^4\delta_1 + 1.2090\delta_1^2(1 - \delta_2^2)\} + \delta_1\delta_2 i\{6.1414 \times 10^4 - 2.4179\delta_1\} \\
\Delta_{33} &= \{1.9148 \times 10^7 - 1.2620 \times 10^4\delta_1 + 0.52931\delta_1^2(1 - \delta_2^2)\} + \delta_1\delta_2 i\{1.2620 \times 10^4 - 1.0586\delta_1\}
\end{aligned}\right\} \ldots [41]$$

Numerical Example

Take an aluminum square plate surrounded by air and suppose the plate, the fluid media, and the incident wave have the following parameter values in cgs units

$$\left.\begin{aligned}
a = b = 100;\ h = 0.1;\ \bar{m} = 0.27 \\
E = 7 \times 10^{11};\quad \mu = 0.3;\quad D = 6.4103 \times 10^7 \\
\rho_1 c_1 = \rho_2 c_2 = 39.69;\quad \omega = 24{,}000
\end{aligned}\right\} \ldots [42]$$

Then we have from Equations [38]

$$\left.\begin{aligned}
\delta_1 &= 2.4261 \times 10^6 \\
\delta_2 &= 1.2250 \times 10^{-2}
\end{aligned}\right\} \ldots\ldots [43]$$

and from Equations [41]

$$\left.\begin{aligned}
\Delta &= (-28.539 + 1.0493i) \times 10^{24} \\
\Delta_{11} &= (162.46 - 3.9815i) \times 10^{15} \\
\Delta_{13} &= (71.135 - 1.7432i) \times 10^{15} \\
\Delta_{33} &= (31.148 - 0.76327i) \times 10^{15}
\end{aligned}\right\} \ldots\ldots [44]$$

From Equations [40], [42], and [25] we obtain the solutions as follows

$$\left.\begin{aligned}
q_{11} &= |q_{11}|\cos(\omega t + \theta_{11}) \\
q_{13} = q_{31} &= |q_{13}|\cos(\omega t + \theta_{13}) \\
q_{33} &= |q_{33}|\cos(\omega t + \theta_{33})
\end{aligned}\right\} \ldots\ldots [45]$$

where

$$\left.\begin{aligned}
|q_{11}| &= 8.8771 \times 10^{-9}p_0; \quad \theta_{11} = \pi + \arctan 1.2250 \times 10^{-2} \\
|q_{13}| = |q_{31}| &= 3.8869 \times 10^{-9}p_0; \quad \theta_{13} = \theta_{31} = \pi + \arctan 1.2251 \times 10^{-2} \\
|q_{33}| &= 1.7019 \times 10^{-9}p_0; \quad \theta_{33} = \pi + \arctan 1.2252 \times 10^{-2}
\end{aligned}\right\} \ldots [46]$$

Substituting these values into Equation [36] we have the transmission coefficient

$$\left.\begin{aligned}
&\tau = 1.0155 \times 10^{-4} \\
\text{or}\quad &10\log_{10}\tau = -39.93 \text{ decibels}
\end{aligned}\right\} \ldots\ldots [47]$$

Vogel has computed and verified by tests the transmission coefficient of this same plate with simply supported edges in the same fluid medium under the same incident wave. He obtained[6]

$$\left.\begin{aligned}
&2 \times 10^{-4} < \tau < 3 \times 10^{-4} \\
\text{or}\quad &-37 < 10\log_{10}\tau < -34 \text{ decibels}
\end{aligned}\right\} \ldots\ldots [48]$$

[6] Reference (2), p. 71.

Hence the transmissivity of a clamped plate is somewhat lower than that for a simply supported plate, as is to be expected.

Results for Additional Cases

Results for the following four cases have been worked out by using the present method. It is interesting to compare them with those obtained in the foregoing numerical example.

1 Take the same plate and incident wave as in the numerical example but two different fluid media, air and water, such that

$$\left.\begin{aligned}\rho_1 c_1 &= 39.69\\ \rho_2 c_2 &= 146{,}000\end{aligned}\right\} \quad [49]$$

We have the transmission coefficient

$$\left.\begin{aligned}\tau &= 7.3407 \times 10^{-4}\\ \text{or}\qquad 10\log_{10}\tau &= -31.34 \text{ decibels}\end{aligned}\right\} \quad [50]$$

Comparing this with Equation [47] we see that the presence of water on one side of the plate increases the transmissivity of the plate.

2 Take the same plate and incident wave as in the numerical example but take water as the fluid medium surrounding the plate such that

$$\rho_1 c_1 = \rho_2 c_2 = 146{,}000 \quad [51]$$

We have the transmission coefficient

$$\left.\begin{aligned}\tau &= 0.67643\\ \text{or}\qquad 10\log_{10}\tau &= -1.698 \text{ decibels}\end{aligned}\right\} \quad [52]$$

Comparing this with Equations [47] and [50] we see that a plate in water-water has a much higher transmissivity than one in air-air or in air-water.

3 Consider the case $\omega = 24{,}000$ and $\rho_1 c_1 = \rho_2 c_2 = 0$ with other parameter values the same as those in Equations [42]. We see from Equation [9] that this is the case of forced vibration of a plate in vacuum under an oscillating distributed force of intensity $2p_0$. For this case we have

$$\left.\begin{aligned}\delta_1 &= 2.4261 \times 10^{8}\\ \delta_2 &= 0\end{aligned}\right\} \quad [53]$$

The amplitude at the center of the plate is found to be

$$\left|w\left(\frac{a}{2},\frac{a}{2}\right)\right| = 4.1984 \times 10^{-9}(2p_0) \quad [54]$$

Comparison of solutions for the generalized co-ordinates of the foregoing cases shows that the presence of fluid media reduces the amplitudes and increases the phase angles of the generalized co-ordinates as to be expected.

4 Consider the case $\omega = 0$ and $\rho_1 c_1 = \rho_2 c_2 = 0$. We see from Equation [9] that this is the case of bending of a plate in vacuum under a static distributed load of intensity $2p_0$. For this case we have

$$\delta_1 = 0;\ \delta_1\delta_2 = 0 \text{ and } \frac{\delta_1}{m\omega^2} = \frac{a^4}{D} \quad [55]$$

The deflection at the center of the plate is found to be

$$w\left(\frac{a}{2},\frac{a}{2}\right) = 1.3758 \times 10^{-3}\left(\frac{2p_0a^4}{Eh^3}\right) \quad [56]$$

for $\mu = 0.3$.

This value checks with the known result[7]

$$0.0138\,(2p_0a^4/Eh^3)$$

so closely that it shows by using characteristic functions four terms are sufficient for evaluating static deflections.

Conclusions

A method of analysis for the forced vibration of a clamped rectangular plate in fluid media has been presented. The analysis applies to that range of physical problems where the pressure of fluid reaction at any point on the plate is directly proportional to the local velocity of the fluid particles (instead of the average velocity over the plate). Such is the case if the wave velocity in the fluid medium is much slower than that in the plate, for the different parts of the medium are relatively slow in letting each other know what motions they are undergoing. This range is also related to the size of the plate in comparison with the ratio of wave velocity and the frequency. For a circular plate of radius $\bar{a}$ the criterion for this range is[8]

$$\omega/c \gg 1/\bar{a}.$$

If we assume that this applies approximately to a rectangular plate of same area, the criterion would be

$$\frac{\omega}{c} \gg \sqrt{\frac{\pi}{ab}} \text{ or } \lambda \ll 2\sqrt{\pi ab}$$

This means the wave lengths in both fluid media should be of small order compared with the edge lengths of the plate.

Contrary to the case of a simply supported plate (2), the use of characteristic functions for a clamped plate does not render normal (or principal) co-ordinates as can be seen from Equation [15] where both the square terms and product terms of the generalized co-ordinates occur. Therefore, the solutions of the generalized co-ordinates rely on a system of simultaneous equations rather than discrete expressions. This makes the solution less neat than that for a simply supported plate.

Formulations and numerical results have been presented based on a four-term series. It already has been seen that four terms are sufficient for static deflections. The convergence for dynamic deflections, however, is somewhat slower, at least for the particular plate and incident wave taken for the numerical example in this paper. This method has the advantage that the solutions can be made as accurate as desirable by taking more terms in the series.

Comparisons of results for a clamped plate and a simply supported plate will render information of practical interest. It is also easy to extend the present analysis to plates with other boundary conditions.

BIBLIOGRAPHY

1 "Vibration and Sound," by P. M. Morse, McGraw-Hill Book Company, Inc., New York, N. Y., second edition, 1948, p. 198.

2 "Sur les Vibrations de Certains Systèmes Élastiques dans un Champ Sonore," by T. Vogel, Publications Scientifiques et Techniques du Ministère de l'Air No. 209, 1948.

3 "Tables of Characteristic Functions Representing Normal Modes of Vibration of a Beam," by D. Young and R. P. Felgar, Jr., The University of Texas Engineering Research Series No. 44, July, 1949.

4 "Applied Elasticity," by C. T. Wang, McGraw-Hill Book Company, Inc., New York, N. Y., 1953.

5 "Formulas for Integrals Containing Characteristic Functions of a Vibrating Beam," by R. P. Felgar, Jr., The University of Texas Bureau of Engineering Research Circular No. 14, 1950.

6 "Theory of Plates and Shells," by S. Timoshenko, McGraw-Hill Book Company, Inc., New York, N. Y., 1940.

[7] See, for example, reference (6), p. 228.

[8] See, for example, reference (1), p. 336.

Nonlinear Dynamic Coupling in a Beam Vibration

By P. H. McDONALD, JR.,[1] RALEIGH, N. C.

This investigation treats the vibration of a uniform beam with hinged ends which are restrained, and which has arbitrary initial conditions of motion. A representative example is discussed in which the beam is subjected to a concentrated lateral force at the mid-point of its span and released from rest at the deflected position. The equations of motion are found to be inherently nonlinear, even for small vibrations, and there is dynamic coupling of the modes. It is found that the frequencies of the various modes are functionally related to the initial conditions, particularly the amplitudes of all the modes.

Introduction

IN THE theory of small linear vibrations of a beam, it is found that the complete motion can be described as the sum of an infinite number of separate, distinct sinusoidal modes. Usually, the modes are statically and dynamically independent of each other. The amplitude and frequency of a given mode are not functionally related, nor are the amplitudes and frequencies of various modes dependent upon each other.

It is of interest to determine whether or not such conditions exist in the vibration of a beam whose equations of motion are essentially nonlinear. It is particularly desirable to know whether or not it is possible to proceed to a solution by an analysis comparable to that of the linear case in which the deflection of the beam is taken to be the sum of sinusoidal modes superposed upon each other.

An opportunity to investigate such questions is provided in the case of a uniform beam whose hinged ends are axially restrained. The nonlinear effect in this example is produced by the axial stretching of the beam. A similar problem is encountered in the theory of plates, where it is shown that the magnitude of the axial force produced depends upon the lateral deflections. A discussion of the problem of the vibration of a uniform beam (or bar) with hinged, axially restrained ends also provides technical information about the amplitudes and frequencies of the natural vibration of such a beam. This information may be of value to machine and structural designers since the analysis shows that significant changes in the frequencies occur if the beam ends are restrained.

The Equations of Motion

Consider the beam illustrated in Fig. 1 whose pin end supports are restrained against both vertical and horizontal displacement.

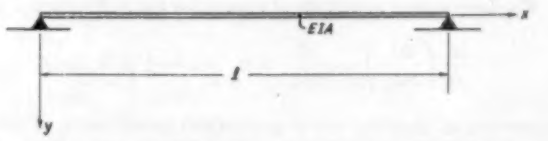

Fig. 1 Beam With Hinged End Supports Axially Restrained

Let the deflection y be represented by the series

$$y = \sum_{n=1}^{\infty} a_n u_n \sin \frac{n\pi x}{l} \quad \ldots\ldots [1]$$

where the u_n are functions of time only and are to be determined. The energies possessed by the beam during vibration are as follows:

Kinetic energy

$$T = \frac{1}{2}\gamma A \int_0^l \left(\frac{\partial y}{\partial t}\right)^2 dx = \frac{\gamma A l}{4} \sum_{n=1}^{\infty} a_n^2 \dot{u}_n^2 \quad \ldots\ldots [2]$$

in which γ is the mass density of the beam, A is the cross-sectional area of the beam, and $\dot{u}_n$ is the time derivative of u_n.

Potential energy of bending

$$V_1 = \frac{1}{2} EI \int_0^l \left(\frac{\partial^2 y}{\partial x^2}\right)^2 dx = \frac{\pi^4 EI}{4l^3} \sum_{n=1}^{\infty} n^4 a_n^2 u_n^2 \quad \ldots\ldots [3]$$

with E the modulus of elasticity of the beam material, I the statical moment of inertia of the cross section about the neutral axis.

Potential Energy of Stretching. If one support were free to move horizontally, the beam would assume the elastic curve shown dotted in Fig. 2. The supports would approach each other by the amount Δ, where

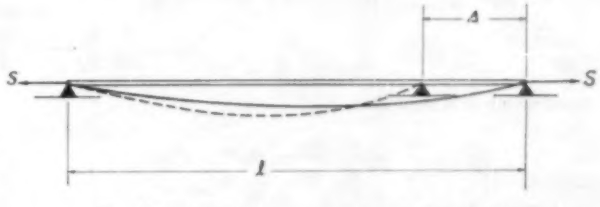

Fig. 2 Beam Stretched by Axial Force S

$$\Delta = \frac{1}{2} \int_0^l \left(\frac{\partial y}{\partial x}\right)^2 dx \quad \ldots\ldots [4]$$

Let the axial force S be applied to stretch the beam back to its fixed distance l between supports. The elastic potential energy of stretching becomes

$$V_2 = \frac{1}{2} S\Delta = \frac{1}{2} \frac{\Delta^2 AE}{l} = \frac{AE}{2l} \left[\frac{1}{2} \int_0^l \left(\frac{\partial y}{\partial x}\right)^2 dx\right]^2$$

$$= \frac{AE\pi^4}{32l^3} \left\{\sum_{n=1}^{\infty} n^2 a_n^2 u_n^2\right\}^2 \quad \ldots\ldots [5]$$

---

[1] Research Associate Professor of Mechanical Engineering, North Carolina State College.

Presented at the National Conference of the Applied Mechanics Division, Troy, N. Y., June 16–18, 1955, of The American Society of Mechanical Engineers.

Discussion of this paper should be addressed to the Secretary, ASME, 29 West 39th Street, New York, N. Y., and will be accepted until January 10, 1956, for publication at a later date. Discussion received after the closing date will be returned.

Note: Statements and opinions advanced in papers are to be understood as individual expressions of their authors and not those of the Society. Manuscript received by ASME Applied Mechanics Division, August 17, 1954. Paper No. 55—APM-23.

The Lagrangian function $L = T - V$, where $V = V_1 + V_2$, may now be formed

$$L = \frac{\gamma A l}{4} \sum_{n=1}^{\infty} a_n^2 \dot{u}_n^2 - \frac{\pi^4 EI}{4l^3} \sum_{n=1}^{\infty} n^4 a_n^2 u_n^2 - \frac{AE\pi^4}{32l^3} \left\{ \sum_{n=1}^{\infty} n^2 a_n^2 u_n^2 \right\}^2 \quad \ldots [6]$$

The Lagrangian equations of motion for the system are

$$\frac{d}{dt}\left(\frac{\partial L}{\partial \dot{u}_n}\right) - \frac{\partial L}{\partial u_n} = 0, \quad (n = 1, 2, 3, \ldots) \quad \ldots [7]$$

where the u_n play the role of generalized co-ordinates. Upon introducing Equation [6], these equations become

$$\ddot{u}_n + \alpha n^4 u_n + \beta n^2 u_n \sum_{m=1}^{\infty} m^2 a_m^2 u_m^2 = 0 \quad \ldots [8]$$

where

$$\alpha = \frac{\pi^4 EI}{\gamma A l^4}, \quad \beta = \frac{\pi^4 E}{4\gamma l^4} \quad \ldots [9]$$

Note that

$$\frac{\alpha}{\beta} = 4\,\frac{I}{A} = 4R^2 \quad \ldots [10]$$

where R is the radius of gyration of the beam cross section.

Separation of the Modes

Equations [8] are for $n = 1, 2, 3 \ldots, r, \ldots, s, \ldots$. They can be solved for

$$\Theta = \sum_{m=1}^{\infty} m^2 a_m^2 u_m^2$$

as follows

$$\Theta = -\frac{1}{\beta n^2}\frac{\ddot{u}_n}{u_n} - n^2\frac{\alpha}{\beta} = -\frac{1}{r^2\beta}\frac{\ddot{u}_r}{u_r} - r^2\frac{\alpha}{\beta} = -\frac{1}{s^2\beta}\frac{\ddot{u}_s}{u_s} - s^2\frac{\alpha}{\beta}$$

from which it is seen that

$$\frac{\ddot{u}_r}{u_r} = \frac{r^2}{s^2}\frac{\ddot{u}_s}{u_s} - r^2(r^2 - s^2)\alpha$$

or, letting r be m

$$\frac{\ddot{u}_m}{u_m} = \frac{m^2}{s^2}\frac{\ddot{u}_s}{u_s} - m^2(m^2 - s^2)\alpha \quad \ldots [11]$$

The form of Equations [8] and [11] suggests the Jacobian elliptic functions as possible solutions. Therefore let

$$u_m = cn(\omega_m t + \lambda_m, k_m) \quad \ldots [12]$$

be a solution of Equations [8] and [11] subject to later revision and proof. ω_m is the "circular" frequency of the elliptic cosine function, k_m is its modulus, and λ_m is a "phase angle" for the function.

From the known properties of the elliptic functions

$$\ddot{u}_m = (2k_m^2 - 1)\omega_m^2 cn(\omega_m t + \lambda_m, k_m) - 2k_m^2\omega_m^2 cn^3(\omega_m t + \lambda_m, k_m) = (2k_m^2 - 1)\omega_m^2 u_m - 2k_m^2\omega_m^2 u_m^3$$

or

$$\frac{\ddot{u}_m}{u_m} = (2k_m^2 - 1)\omega_m^2 - 2k_m^2\omega_m^2 u_m^2$$

$$\frac{\ddot{u}_s}{u_s} = (2k_s^2 - 1)\omega_s^2 - 2k_s^2\omega_s^2 u_s^2$$

Substituting these in Equation [11] and reducing

$$u_m^2 = \frac{m^2 k_s^2 \omega_s^2}{s^2 k_m^2 \omega_m^2} u_s^2 + \left(\frac{2k_m^2 - 1}{2k_m^2}\right) + \frac{m^2(m^2 - s^2)\alpha}{2k_m^2\omega_m^2} - \frac{m^2(2k_s^2 - 1)\omega_s^2}{2s^2 k_m^2 \omega_m^2}$$

The sum $\Theta = \sum_{m=1}^{\infty} m^2 a_m^2 u_m^2$ can now be formulated

$$\Theta = \frac{k_s^2\omega_s^2 B}{s^2} u_s^2 + \left[\frac{C}{2} + \frac{\alpha D}{2} - \frac{\alpha s^2 B}{2} - \frac{\omega_s^2(2k_s^2 - 1)B}{2s^2}\right] \quad \ldots [13]$$

with

$$B = \sum_{m=1}^{\infty} \frac{m^4 a_m^2}{k_m^2\omega_m^2}, \quad C = \sum_{m=1}^{\infty} \frac{m^2 a_m^2}{k_m^2}(2k_m^2 - 1),$$

$$D = \sum_{m=1}^{\infty} \frac{m^6 a_m^2}{k_m^2\omega_m^2} \quad \ldots [14]$$

When Equation [13] is put into [8] one obtains

$$\ddot{u}_s + \xi_s u_s + \zeta_s u_s^3 = 0 \quad \ldots [15]$$

$$\xi_s = \alpha s^4 + \frac{1}{2}\beta s^2 C + \frac{1}{2}\beta s^2 \alpha D - \frac{1}{2}\beta s^4 \alpha B - \frac{1}{2}\beta\omega_s^2(2k_s^2 - 1)B$$

$$\zeta_s = \beta k_s^2 \omega_s^2 B$$

Equation [15] is satisfied by $u_s = cn(\omega_s t + \lambda_s, k_s)$ provided that

$$\left.\begin{aligned} \zeta_s - 2k_s^2\omega_s^2 &= 0 \\ \xi_s + (2k_s^2 - 1)\omega_s^2 &= 0 \end{aligned}\right\} \quad \ldots [16]$$

The u_m functions have thus been separated, and at the same time equations have been found for the constants involved.

Determination of Constants

The simultaneous solution of Equations [16] requires that $B = 2/\beta$ and $C = -\alpha D$, or

$$\sum_{m=1}^{\infty} \frac{m^4 a_m^2}{k_m^2\omega_m^2} = \frac{2}{\beta} \quad \ldots [17]$$

$$\sum_{m=1}^{\infty} \frac{m^2 a_m^2}{k_m^2}(2k_m^2 - 1) = -\alpha \sum_{m=1}^{\infty} \frac{m^6 a_m^2}{k_m^2\omega_m^2} \quad \ldots [18]$$

It remains to find values for ω_m and k_m such that Equations [17] and [18] are fulfilled

$$\omega_m^2 = \frac{\alpha m^4}{1 - 2k_m^2} \quad \text{or} \quad k_m^2 = \frac{1}{2}\left(1 - \frac{\alpha m^4}{\omega_m^2}\right) \quad \ldots [19]$$

satisfies Equation [18], and when this is set into Equation [17]

$$\sum_{m=1}^{\infty} \frac{a_m^2}{k_m^2} = 2\frac{\alpha}{\beta} + \sum_{m=1}^{\infty} a_m^2 = \sum_{m=1}^{\infty} \frac{2a_m^2}{\left(1 - \dfrac{\alpha m^4}{\omega_m^2}\right)} \quad \ldots\ldots [20]$$

The reduction of Equation [20] will be illustrated for the case where the beam is released from rest; that is, the initial velocity will be assumed to be zero. Then, at $t = 0$

$$y = y_0(x) = \sum_{n=1}^{\infty} a_n cn(\lambda_n, k_n) \sin \frac{n\pi x}{l}$$

$$\left(\frac{dy}{dt}\right)_0 = 0 = -\sum_{n=1}^{\infty} a_n \omega_n sn(\lambda_n, k_n)\, dn(\lambda_n, k_n) \sin \frac{n\pi x}{l}$$

Since $a_n \neq 0$, $\omega_n \neq 0$, $\sin n\pi x/l$ is not everywhere zero, therefore

$$\left.\begin{aligned} sn(\lambda_n, k_n) dn(\lambda_n, k_n) &= 0 \\ \text{or} \\ \lambda_n = sn^{-1}(0, k_n) &= 0 \\ dn(\lambda_n, k_n) = dn(0, k_n) &= 1 \end{aligned}\right\} \quad \ldots\ldots [21]$$

$$y_0(x) = \sum_{n=1}^{\infty} a_n cn(0, k_n) \sin \frac{n\pi x}{l} = \sum_{n=1}^{\infty} a_n \sin \frac{n\pi x}{l} \quad \ldots [22]$$

Equation [11] applies for all values of the time. Hence

$$\frac{\ddot{u}_m(0)}{u_m(0)} = \frac{m^2}{s^2} \frac{\ddot{u}_s(0)}{u_s(0)} - m^2(m^2 - s^2)\alpha$$

But

$$\frac{\ddot{u}_m(0)}{u_m(0)} = (2k_m^2 - 1)\omega_m^2 - 2k_m^2\omega_m^2 = -\omega_m^2$$

so that

$$\omega_m^2 = \frac{m^2}{s^2}\omega_s^2 + m^2(m^2 - s^2)\alpha \quad \ldots\ldots [23]$$

If this is inserted into the right two members of Equation [20] and the result factored and reduced, the formula

$$\omega_s^2 = s^2\alpha\left(s^2 + \frac{1}{4R^2}\sum_{m=1}^{\infty} m^2 a_m^2\right) \quad \ldots\ldots [24]$$

is obtained. From the known relation, Equation [19], k_s^2 can now be determined as

$$k_s^2 = \frac{1}{2}\left(1 - \frac{s^2}{s^2 + \dfrac{1}{4R^2}\displaystyle\sum_{m=1}^{\infty} m^2 a_m^2}\right) \quad \ldots\ldots [25]$$

and the dependence of the modulus and frequency upon the initial displacement curve is evident.

A Particular Example

To show explicitly how the foregoing equations are applied, consider the particular beam illustrated in Fig. 3. A load P is applied at the center of the beam and the beam assumes its deflected position under the load. It may be noted that the static deflection of the beam under such a load is nonlinear with respect to P.

Now if the load is suddenly removed, the beam will undergo its natural vibration with the following initial conditions of motion

$$t = 0, \quad y = y_0(x) = \sum_{n=1}^{\infty} a_n \sin \frac{n\pi x}{l}$$

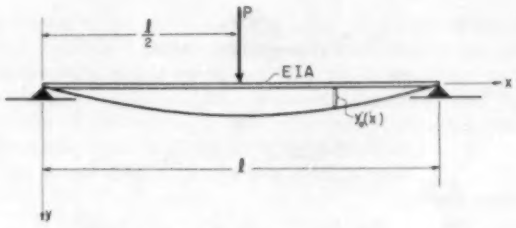

Fig. 3 Beam With Ends Hinged and Load at Mid-Span

$$\frac{dy}{dt} = \left(\frac{dy}{dt}\right)_0 = 0, \quad \text{(for all values of } x\text{)}$$

The a_n are those which would exist in the static case at the instant of release of the load. These are determined by considering the elastic potential energy of the beam as follows:

From Equations [3] and [5] the elastic energy at the initial instant is

$$V(0) = \frac{\pi^4 EI}{4l^3}\sum_{n=1}^{\infty} n^4 a_n^2 + \frac{AE\pi^4}{32l^3}\left\{\sum_{n=1}^{\infty} n^2 a_n^2\right\}^2$$

since $u_n(0) = 1$. For the virtual displacement da_n there is:

1 The work of the force P

$$P \sin \frac{n\pi \dfrac{l}{2}}{l} da_n = P \sin \frac{n\pi}{2} da_n$$

2 The increase of strain energy

$$dV = \frac{\partial V}{\partial a_n} da_n = \left(\frac{n^4\pi^4 EI}{2l^3} a_n + \frac{n^2\pi^4 AE}{8l^3} a_n \sum_{m=1}^{\infty} m^2 a_m^2\right) da_n$$

These must be equal, and hence

$$a_n = \frac{2Pl^3}{n^2\pi^4 EI\left(n^2 + \dfrac{\sigma}{4R^2}\right)} \sin \frac{n\pi}{2} \quad \ldots\ldots [26]$$

where

$$\sigma = \sum_{m=1}^{\infty} m^2 a_m^2 \quad \ldots\ldots [27]$$

Now write

$$a_n = \frac{2Pl^3}{\pi^4 EI} A_n \sin \frac{n\pi}{2} \quad \ldots\ldots [28]$$

so that A_n is a pure number and also so that

$$A_n = \frac{1}{n^2\left(n^2 + \dfrac{\sigma}{4R^2}\right)} \quad \ldots\ldots [29]$$

This can be solved for σ as follows

$$\frac{\sigma}{4R^2} = \frac{1}{n^2 A_n} - n^2 = \frac{1}{r^2 A_r} - r^2 = \frac{1}{s^2 A_s} - s^2$$

so that

$$\frac{1}{A_r} = \frac{r^2}{s^2 A_s} - r^2(s^2 - r^2)$$

or

$$A_r = \frac{s^2 A_s}{r^3 - r^2 s^2 (s^2 - r^2) A_s} \quad [30]$$

Note that ($s = 1$)

$$A_r = \frac{A_1}{r^2[1 + (r^3 - 1)A_1]} \quad [31]$$

Assume that

$$\frac{1}{A_r} = \alpha_r - \beta_r A_r^2, \quad \frac{1}{A_s} = \alpha_s - \beta_s A_s^2 \quad [32]$$

where the α_r, β_r and α_s, β_s are constants to be determined. Using these in Equation [30] one obtains

$$A_r^2 = \frac{r^2}{s^2}\frac{\beta_s}{\beta_r} A_s^2 + \frac{r^2}{\beta_r}(s^2 - r^3) + \frac{\alpha_r}{\beta_r} - \frac{r^2}{s^2}\frac{\alpha_s}{\beta_r}$$

or letting r be m

$$A_m^2 = \frac{r^2}{s^2}\frac{\beta_s}{\beta_m} A_s^2 + \frac{m^2}{\beta_m}(s^2 - m^2) + \frac{\alpha_m}{\beta_m} - \frac{m^2}{s^2}\frac{\alpha_s}{\beta_m} \quad [33]$$

By using Equation [28]

$$\sigma = \left(\frac{2Pl^3}{\pi^4 EI}\right)^2 \sum_{m=1,3,5,\ldots}^{\infty} m^2 A_m^2 \quad [34]$$

and this becomes

$$\sigma = \left(\frac{2Pl^3}{\pi^4 EI}\right)^2 \left[\frac{\beta_s}{s^2}\psi A_s^2 + \left(s^2 - \frac{\alpha_s}{s^2}\right)\psi + \lambda - \chi\right] \quad [35]$$

when the result given by Equation [33] is introduced. In this equation

$$\left.\begin{aligned} \psi &= \sum_{m=1,3,5\ldots}^{\infty} \frac{m^4}{\beta_m} \\ \lambda &= \sum_{m=1,3,5,\ldots}^{\infty} \frac{\alpha_m m^2}{\beta_m}, \quad \chi = \sum_{m=1,3,5,\ldots}^{\infty} \frac{m^6}{\beta_m} \end{aligned}\right\} \quad [36]$$

From Equation [29]

$$s^4 + \frac{s^2\sigma}{4R^2} = \frac{1}{A_s} = \alpha_s - \beta_s A_s^2$$

by using Equation [32]. If Equation [35] is introduced on the left-hand side, it is found that

$$\left[s^4 + \left(\frac{Pl^3}{\pi^4 EIR}\right)^2 (s^2\psi - \alpha_s\psi + s^2\lambda - s^2\chi)\right] + \left(\frac{Pl^3}{\pi^4 EIR}\right)^2 \beta_s \psi A_s^2 = \alpha_s - \beta_s A_s^2$$

This is satisfied and the representation of Equation [32] is verified if

$$\left.\begin{aligned} s^4 + \left(\frac{Pl^3}{\pi^4 EIR}\right)^2 [(s^4 - \alpha_s)\psi + s^2(\lambda - \chi)] &= \alpha_s \\ \left(\frac{Pl^3}{\pi^4 EIR}\right)^2 \beta_s \psi A_s^2 &= -\beta_s A_s^2 \end{aligned}\right\}$$

These are simultaneous equations for the determination of α_s and β_s. The second gives

$$\psi = -\frac{1}{\left(\frac{Pl^3}{\pi^4 EIR}\right)^2} \quad [37]$$

and using this in the first yields

$$s^2(\lambda - \chi)\left(\frac{Pl^3}{\pi^4 EIR}\right)^2 = 0$$

now

$$\left(\frac{Pl^3}{\pi^4 EIR}\right)^2$$

is not zero, and likewise $s^2 = 1, 9, 25, \ldots$ is not zero; therefore $\lambda = \chi$

or

$$\sum_{m=1,3,5,\ldots}^{\infty} \frac{m^6}{\beta_m} = \sum_{m=1,3,5,\ldots}^{\infty} \frac{m^2\alpha_m}{\beta_m}$$

a solution of which is

$$\alpha_m = m^4 \quad [38]$$

If Equation [37] is written in the form

$$\sum_{m=1,3,5,\ldots}^{\infty} \frac{m^4}{\beta_m} = -\frac{1}{\left(\frac{Pl^3}{\pi^4 EIR}\right)^2}$$

it can easily be verified that it is satisfied by

$$\beta_m = -\frac{\pi^6}{960}\left(\frac{Pl^3}{\pi^4 EIR}\right)^2 m^{10} \quad [39]$$

This employs the fact that

$$\sum_{m=1,3,5,\ldots}^{\infty} \frac{1}{m^6} = \frac{\pi^6}{960}$$

By using Equations [38] and [39] in [35], one finds that

$$\sigma = \left(\frac{2Pl^3}{\pi^4 EI}\right)^2 \frac{\pi^6}{960} s^2 A_s^2 \quad (s = 1, 3, 5, \ldots)$$

On putting this into Equation [29], an equation is obtained in which A_s is the only unknown

$$s^4 A_s\left[1 + \frac{\pi^6}{960}\frac{1}{4R^2} s^6 \left(\frac{2Pl^3}{\pi^4 EI}\right)^2 A_s^2\right] = 1 \quad [40]$$

Because this is a cubic equation, it will often be found simpler to solve Equation [40] for A_1 and use Equation [31] to obtain the other A's. Thus for $s = 1$

$$\frac{\pi^6}{960}\frac{1}{4R^2}\left(\frac{2Pl^3}{\pi^4 EI}\right)^2 A_1^3 + A_1 - 1 = 0 = f(A_1) \quad [41]$$

An analysis of Equation [41] reveals that there is one real positive root, and that it is less than unity in value. The general graph of Equation [41] is shown in Fig. 4, from which it is evident that Newton's method may be applied to determine the numerical value of A_1. A point such as A_{10} should be taken as the starting point for the application of the method.

From Equation [29]

$$\sigma = 4R^2\left(\frac{1}{n^2 A_n} - n^2\right)$$

so that Equations [24] and [25] for the "circular" frequency and modulus become

$$\left.\begin{aligned} \omega_n^2 &= \frac{\alpha}{A_n} \\ k_n^2 &= \frac{1}{2}(1 - n^4 A_n) \end{aligned}\right\} \quad \ldots\ldots\ldots\ldots [42]$$

Note that k_n^2 can also be written

$$k_n^2 = \frac{1}{2}\left[\frac{1 - A_1}{1 + (n^2 - 1)A_1}\right]$$

which, since A_1 is less than unity, shows that k_n^2 is less than $^1/_2$ in numerical value.

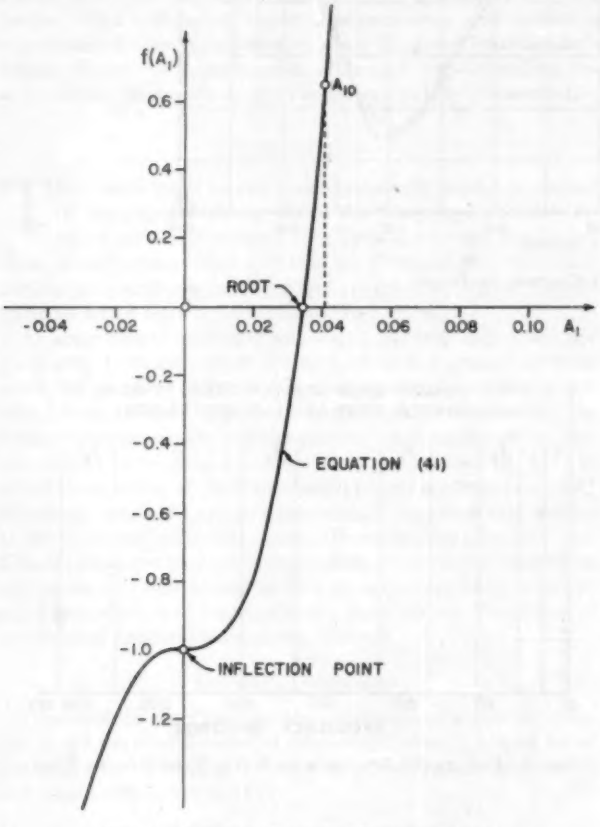

FIG. 4 GENERAL GRAPH OF EQUATION [41]

The complete equation for the deflection of the beam can now be written

$$y(x, t) = \left(\frac{2Pl^3}{\pi^4 EI}\right) \sum_{n=1,3,5,\ldots}^{\infty} (-1)^{\frac{n-1}{2}} A_n \, cn\left[\sqrt{\frac{\alpha}{A_n}}\, t, \sqrt{\frac{1}{2}(1 - n^4 A_n)}\right] \sin\frac{n\pi x}{l} \quad \ldots\ldots [43]$$

It is interesting to compare this with the equation which would be obtained in the linear case where there is no end restraint of the beam. For the conditions given in Fig. 3, the latter is

$$y(x, t) = \left(\frac{2Pl^3}{\pi^4 EI}\right) \sum_{n=1,3,5,\ldots}^{\infty} (-1)^{\frac{n-1}{2}} \frac{1}{n^4} \, cn(n^2\sqrt{\alpha}\, t, 0) \sin\frac{n\pi x}{l} \quad \ldots\ldots [44]$$

since $cn(n^2\sqrt{\alpha}\, t, 0) = \cos(n^2\sqrt{\alpha}\, t)$. The form of the elliptic cosine function does not differ greatly from that of the ordinary trigonometric cosine for values of k which are likely to be encountered in Equation [43]. However, the amplitudes and frequencies of the various modes as given by Equation [43] may vary widely from those found in Equation [44].

The period of the function $cn\ u$ is $4K$, where

$$K = \int_0^{\frac{\pi}{2}} \frac{d\phi}{\sqrt{1 - k^2 \sin^2\phi}} \quad \ldots\ldots [45]$$

is the complete elliptic integral of the first kind to the modulus k. This is a tabulated function and there are also practical methods of obtaining it directly when k is known.

Because each mode of vibration has its own modulus k_n, each will therefore have its own K_n, unlike the linear case where the period of every $\cos u$ function has the value of 2π. The period T_n of each mode is thus seen to be that value of t for which $\omega_n t = 4K_n$. The frequency of the nth mode then becomes

$$f_n = \frac{1}{T_n} = \frac{\omega_n}{4K_n} \text{ cycles/sec} \quad \ldots\ldots [46]$$

Let the beam be a mild steel rod $^1/_2$ in. diam and 10 ft long with the load P equal to 100 lb. Then

$$I = \frac{\pi}{4}\left(\frac{1}{4}\right)^4 \text{ in.}^4, \quad 4R^2 = \frac{1}{16} \text{ sq in.}$$

$$\frac{2Pl^3}{\pi^4 EI} = \frac{2 \times 100 \times (120)^3}{\pi^4 \times 30 \times 10^6 \times \frac{\pi}{4}\left(\frac{1}{4}\right)^4} = 38.548 \text{ in.}$$

$$\frac{\pi^6}{960} \times \frac{1}{4R^2} \times \left(\frac{2Pl^3}{\pi^4 EI}\right)^2 = 1.001442 \times 16 \times (38.548)^2 = 23{,}804.79$$

$$23{,}804.79\, A_1^3 + A_1 - 1 = 0, \quad A_1 = 0.03436$$

$$A_3 = \frac{A_1}{(3)^2[1 - (9 - 1)A_1]} = 0.00299, \quad A_5 = 0.00075$$

$$A_7 = 0.00026, \quad A_9 = 0.00011, \quad A_{11} = 0.00005$$

$$\alpha = \frac{\pi^4 EI}{\gamma A l^4} = \frac{\pi^4 E R^2}{\gamma l^4} = \frac{\pi^4 \times 30 \times 10^6 \times 1728 \times 386}{64 \times 490 \times (120)^4} = 299.74/\text{sec}^2$$

$$\omega_1^2 = \frac{\alpha}{A_1} = \frac{299.74}{0.03436} = 8723.64/\text{sec}^2, \quad \omega_1 = 93.40/\text{sec}$$

$$\omega_3 = 316.38/\text{sec}, \quad \omega_5 = 630.84/\text{sec}, \quad \omega_7 = 1{,}064.14/\text{sec}$$

$$\omega_9 = 1{,}627.56/\text{sec}, \quad \omega_{11} = 2{,}325.49/\text{sec}$$

$$k_1^2 = \frac{1}{2}(1 - A_1) = 0.48282, \quad k_1 = 0.69485$$

$$k_3 = 0.61540, \quad k_5 = 0.51440, \quad k_7 = 0.42690, \quad k_9 = 0.35888$$

$$k_{11} = 0.30700$$

$$K_1 = 1.83729, \quad K_3 = 1.76304, \quad K_5 = 1.69375$$

$$K_7 = 1.65078, \quad K_9 = 1.62540, \quad K_{11} = 1.60991$$

$$f_1 = \frac{\omega_1}{4K_1} = 12.7 \text{ cps}, \quad f_3 = 44.9 \text{ cps}$$

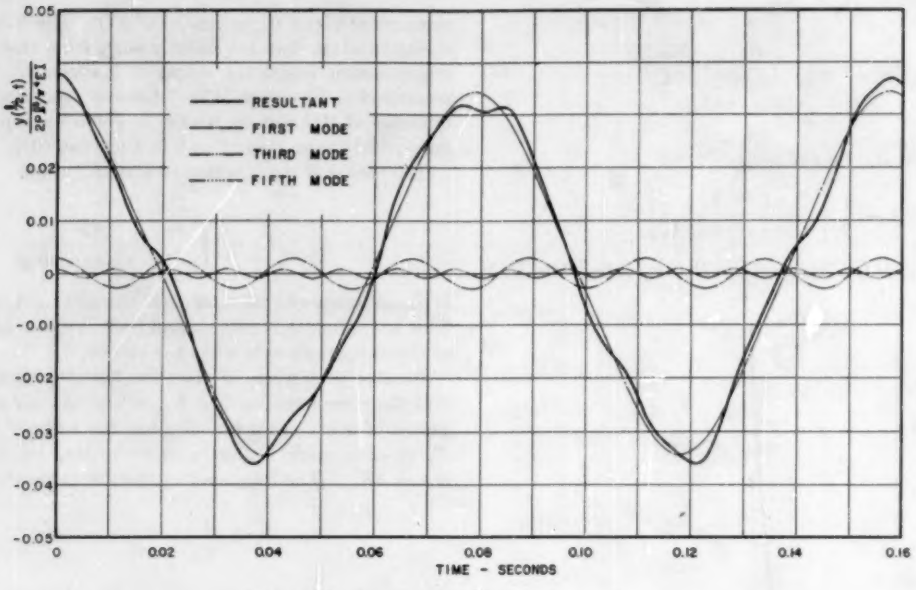

FIG. 6 DISPLACEMENT OF CENTER OF BEAM

$f_5 = 93.1$ cps, $f_7 = 161.1$ cps, $f_9 = 250.3$ cps,

$f_{11} = 361.1$ cps

Fig. 5 shows the frequency spectrum plotted from the foregoing data together with that of the linear case of Equation [44]. Fig. 6 is a graph of the displacement of the center of the beam with time.

REFERENCES

1 "The Effect of an Axial Force on the Vibration of Hinged Bars," by S. Woinowsky-Krieger, JOURNAL OF APPLIED MECHANICS, Trans. ASME, vol. 72, 1950, p. 35.

2 "Free Vibrations of a Pin-Ended Column With Constant Distance Between Pin Ends," by David Burgreen, JOURNAL OF APPLIED MECHANICS, Trans. ASME, vol. 73, 1951, p. 135.

3 "Applied Elasticity," by John Prescott, Longmans, Green and Company, London, England, first edition, 1924, pp. 239–243.

4 "Vibration Problems in Engineering," by S. Timoshenko, D. Van Nostrand Company, Inc., New York, N. Y., first edition, 1928, pp. 253–255.

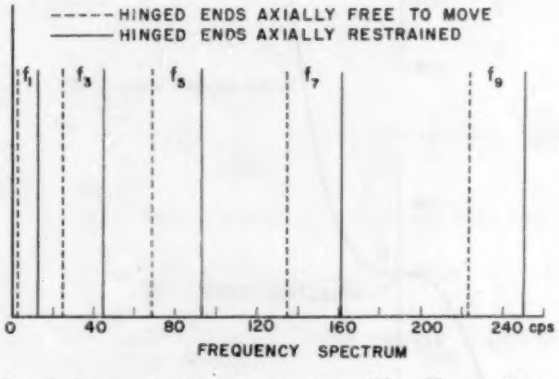

FIG. 5 FREQUENCY SPECTRUM OF BEAM WITH HINGED ENDS

Some Solutions of the Timoshenko Beam Equations[1]

By B. A. BOLEY[2] and C. C. CHAO,[3] NEW YORK, N. Y.

Solutions are obtained by the method of Laplace transformation for four types of loadings applied to a semi-infinite beam. Numerical results are presented for two of these, both for suddenly applied and gradually varying loads. The effects of shear deformations and rotatory inertia are taken into account according to Timoshenko's beam model. A comparison with the corresponding results of the Bernoulli-Euler theory are briefly presented.

Introduction

THE behavior of beams under transverse impact is studied in this paper with the aid of the Timoshenko model (1)[4] which takes into account the effects of rotatory inertia and shear deformations. The solutions are obtained with the aid of the Laplace transform technique and are given in terms of definite integrals which have to be evaluated numerically.

An approximate method of solution of this type of problem had previously been developed (2) as part of the present project; one of the purposes of the investigation described here was to provide a basis for the comparison, carried out in reference (2), between the approximate and the present exact solutions. Attention should be brought to some recent publications (3, 4, 8) in which the solution of the Timoshenko beam equations is also obtained by means of Laplace transforms in a manner very similar to the one described in this paper. However, the boundary conditions considered here are different from those employed in those references, and were chosen so that by combining them with the aid of the principle of superposition a great variety of solutions of problems of practical interest would result.

General Discussion

Timoshenko's equations for the displacement y and the rotation ψ of a beam with constant cross-sectional area A, moment of inertia I, mass density ρ, Young's modulus E, shear modulus G, and shear coefficient k' are (1)

$$\left.\begin{aligned} EI(\partial^2\psi/\partial x^2) + k'AG[(\partial y/\partial x) - \psi] - \rho I(\partial^2\psi/\partial t^2) &= 0 \\ \rho A(\partial^2 y/\partial t^2) - k'AG[(\partial^2 y/\partial x^2) - (\partial\psi/\partial x)] &= 0 \end{aligned}\right\} \quad [1]$$

or in nondimensional form

$$\left.\begin{aligned} \psi'' + (1/\gamma)(y_1' - \psi) - \ddot{\psi} &= 0 \\ \ddot{y}_1 - (1/\gamma)(y_1'' - \psi') &= 0 \end{aligned}\right\} \quad [1a]$$

where dots and primes indicate differentiation with respect to the nondimensional variables $t_1 = (c_1 t/r)$ and $x_1 = (x/r)$, and where $y_1 = (y/r)$. Here $c_1 = (E/\rho)^{1/2}$ is the velocity of propagation of longitudinal waves, r is the radius of gyration of the cross section, x is the distance along the beam measured from the end at which impact occurs, t is time, and $\gamma = (E/k'G)$. The shear force Q and the bending moment M are given by

$$\left.\begin{aligned} [Q/(k'AG)] &= (\partial y/\partial x) - \psi = y_1' - \psi \\ [Mr/(EI)] &= r(\partial\psi/\partial x) = \psi' \end{aligned}\right\} \quad [1b]$$

The Laplace transforms

$$Y = L(y_1) = \int_0^\infty y_1 e^{-pt_1}\,dt_1; \quad \Psi = L(\psi) = \int_0^\infty \psi e^{-pt_1}\,dt_1 \quad [1c]$$

must satisfy the equations

$$\left.\begin{aligned} \Psi'' + (1/\gamma)(Y' - \Psi) - p^2\Psi &= 0 \\ p^2 Y - (1/\gamma)(Y'' - \Psi') &= 0 \end{aligned}\right\} \quad [2]$$

provided that the beam is initially at rest.

The solution of Equations [2] is

$$Y = C_1 e^{-\lambda_1 x_1} + C_2 e^{-\lambda_2 x_1} + C_3 e^{\lambda_1 x_1} + C_4 e^{\lambda_1 x_1}$$

$$\Psi = \frac{\lambda_1^2 - \gamma p^2}{\lambda_1}(C_3 e^{\lambda_1 x_1} - C_1 e^{-\lambda_1 x_1}) + \frac{\lambda_2^2 - \gamma p^2}{\lambda_2}(C_4 e^{\lambda_2 x_1} - C_2 e^{-\lambda_2 x_1}) \quad [2a]$$

where

$$\left.\begin{aligned} \lambda_{1,2} &= Bp^{1/2}[p \pm N(p^2 - a^2)^{1/2}]^{1/2} \\ B &= [(\gamma + 1)/2]^{1/2} \\ a &= 2/(\gamma - 1) \\ N &= (\gamma - 1)/(\gamma + 1) \end{aligned}\right\} \quad [2b]$$

and where the C coefficients are arbitrary functions of p which depend on the boundary conditions. In this paper only beams extending to infinity in the positive x-direction are considered; if the solution is to be finite at infinity it then follows that

$$C_3 = C_4 = 0 \quad [2c]$$

Equations [2a] were solved for four special cases corresponding to the following conditions of sudden loading at $x = 0$:

Problem I: Step velocity and zero bending moment.
Problem II: Step moment and zero displacement.
Problem III: Step angular velocity and zero force.
Problem IV: Step force and zero rotation.

These boundary conditions are expressed in mathematical form in Table 1; the corresponding expressions for Y and Ψ are also listed there. From these quantities the Laplace transforms (denoted by the symbol L) of shear force Q, bending moment M, velocity y', and angular velocity ψ' are easily found with the aid of Equations [1b]; the results are in nondimensional form as follows

[1] The work reported here was sponsored by the Office of Naval Research, U. S. Navy, under Contract Nonr—266 (20), Project NR-064-401.

[2] Associate Professor of Civil Engineering, Institute of Air Flight Structures, Columbia University.

[3] Research Assistant, Department of Civil Engineering, Institute of Air Flight Structures, Columbia University.

[4] Numbers in parentheses refer to the Bibliography at the end of the paper.

Presented at the National Conference of the Applied Mechanics Division, Troy, N. Y., June 16–18, 1955, of The American Society of Mechanical Engineers.

Discussion of this paper should be addressed to the Secretary, ASME, 29 West 39th Street, New York, N. Y., and will be accepted until January 10, 1956, for publication at a later date. Discussion received after the closing date will be returned.

Note: Statements and opinions advanced in papers are to be understood as individual expressions of their authors and not those of the Society. Manuscript received by ASME Applied Mechanics Division, January 10, 1955. Paper No. 55—APM-28.

TABLE 1 DESCRIPTION AND SOLUTIONS OF PROBLEMS I, II, III, IV

	B. C. @ $x_1 = 0$		TRANSFORMED SOLUTIONS			SOLUTIONS				
	ACT.	TRANF.	Y	Ψ	$Y' - \Psi$		$\theta/_{KAG} = y_1' - \psi$	$\dot{\psi}$	$M/EI = \psi'$	$\dot{y}$
PROBLEM I	$y_1 = v_0 t_1$; $\psi' = 0$	$Y = \frac{v_0}{p^2}$; $\Psi' = 0$	$\frac{V_0 a}{2p^3\sqrt{p^2-a^2}}\left\{(\gamma p^2 - \lambda_2^2)e^{-\lambda_1 x_1} - (\gamma p^2 - \lambda_1^2)e^{-\lambda_2 x_1}\right\}$	$\frac{V_0 a}{2p\sqrt{p^2-a^2}}\left\{\frac{e^{-\lambda_1 x_1}}{\lambda_1} - \frac{e^{-\lambda_2 x_1}}{\lambda_2}\right\}$	$\frac{V_0 \gamma a}{2p\sqrt{p^2-a^2}}\left\{-\frac{\gamma p^2 - \lambda_2^2}{\lambda_1}e^{-\lambda_1 x_1} + \frac{\gamma p^2 - \lambda_1^2}{\lambda_2}e^{-\lambda_2 x_1}\right\}$	$t_1 < x_1$	0	0	0	0
						$x_1 < t_1 < \sqrt{\gamma}\, t_1$	$V_0\gamma(I_1 + I_2)$	$-V_0 a(I_3 + I_4)$	$V_0 a(I_5 + I_6)$	$V_0(I_7 + I_8 + \frac{1}{2})$
						$x_1\sqrt{\gamma} < t_1$	$V_0\gamma I_2$	$-V_0 a I_4$	$V_0 a I_6$	$V_0(I_8 + 1)$
PROBLEM II	$y_1 = 0$; $\psi' = M_0$	$Y = 0$; $\Psi = \frac{M_0}{p}$	$\frac{M_0 a}{2p^2\sqrt{p^2-a^2}}\left\{e^{-\lambda_1 x_1} - e^{-\lambda_2 x_1}\right\}$	$\frac{M_0 a}{2p^2\sqrt{p^2-a^2}}\left\{\frac{\gamma p^2 - \lambda_1^2}{\lambda_1}e^{-\lambda_1 x_1} - \frac{\gamma p^2 - \lambda_2^2}{\lambda_2}e^{-\lambda_2 x_1}\right\}$	$\frac{M_0 \gamma a}{2\sqrt{p^2-a^2}}\left\{-\frac{e^{-\lambda_1 x_1}}{\lambda_1} - \frac{e^{-\lambda_2 x_1}}{\lambda_2}\right\}$	$t_1 < x_1$	0	0	0	0
						$x_1 < t_1 < \sqrt{\gamma}\, t_1$	$M_0\gamma a(I_3 + I_4)$	$M_0(I_9 + I_{10})$	$M_0(I_{11} + I_{12} + \frac{1}{2})$	$-M_0 a(I_5 + I_6)$
						$x_1\sqrt{\gamma} < t_1$	$M_0\gamma a I_4$	$M_0 I_{10}$	$M_0(I_{12} + 1)$	$-M_0 a I_6$
PROBLEM III	$y_1' - \psi = 0$; $\dot{\psi} = \omega_0$	$Y' - \Psi = 0$; $\Psi = \frac{\omega_0}{p^2}$	$\frac{\omega_0 a}{2p^3\sqrt{p^2-a^2}}\left(\lambda_1 e^{-\lambda_1 x_1} + \lambda_2 e^{-\lambda_2 x_1}\right)$	$\frac{-\omega_0 a}{2p^3\sqrt{p^2-a^2}}\left\{(\gamma p^2 - \lambda_1^2)e^{-\lambda_1 x_1} - (\gamma p^2 - \lambda_2^2)e^{-\lambda_2 x_1}\right\}$	$\frac{\omega_0 \gamma a}{2p\sqrt{p^2-a^2}}\left(e^{-\lambda_1 x_1} - e^{-\lambda_2 x_1}\right)$	$t_1 < x_1$	0	0	0	0
						$x_1 < t_1 < \sqrt{\gamma}\, t_1$	$-\omega_0\gamma a(I_5 + I_6)$	$\omega(I_{11} + I_{12} + \frac{1}{2})$	$\omega_0(I_{13} + I_{14})$	$\omega_0 a(I_{15} + I_{16})$
						$x_1\sqrt{\gamma} < t_1$	$-\omega_0\gamma a I_6$	$\omega_0(I_{12} + 1)$	$\omega_0(I_{14} + 1)$	$\omega_0 a(I_{16} + \frac{x_1}{a})$
PROBLEM IV	$y' - \psi = F_0$; $\psi = 0$	$Y' - \Psi = \frac{F_0}{p}$; $\Psi = 0$	$\frac{F_0 a}{2\gamma p^4\sqrt{p^2-a^2}}\left\{-\lambda_1(\gamma p^2 - \lambda_2^2)e^{-\lambda_1 x_1} + \lambda_2(\gamma p^2 - \lambda_1^2)e^{-\lambda_2 x_1}\right\}$	$\frac{F_0 a}{2\gamma p^2\sqrt{p^2-a^2}}\left(-e^{-\lambda_1 x_1} + e^{-\lambda_2 x_1}\right)$	$\frac{F_0 a}{2p^2\sqrt{p^2-a^2}}\left\{(\gamma p^2 - \lambda_2^2)e^{-\lambda_1 x_1} - (\gamma p^2 - \lambda_1^2)e^{-\lambda_2 x_1}\right\}$	$t_1 < x_1$	0	0	0	0
						$x_1 < t_1 < \sqrt{\gamma}\, t_1$	$F_0(I_7 + I_8 + \frac{1}{2})$	$\frac{F_0 a}{\gamma}(I_5 + I_6)$	$-\frac{F_0 a}{\gamma}(I_{15} + I_{16})$	$\frac{F_0}{\gamma}(I_{17} + I_{18})$
						$x_1\sqrt{\gamma} < t_1$	$F_0(I_8 + 1)$	$\frac{F_0 a}{\gamma} I_6$	$-\frac{F_0 a}{\gamma}(I_{16} + \frac{x_1}{a})$	$\frac{F_0}{\gamma}(I_{18} + \sqrt{\gamma}\, x_1)$

$$\left.\begin{aligned} L\{Q/(k'AG)\} &= Y' - \Psi \\ L\{Mr/(EI)\} &= \Psi' \\ L\{y'_1\} &= pY \\ L\{\psi'\} &= p\Psi \end{aligned}\right\} \quad \ldots\ldots\ldots\ldots [3]$$

The inverse transformation, required to obtain the quantities listed, was carried out as outlined in the next section; the final expressions are collected in Table 1. Some numerical results, obtained with the aid of these formulas, are presented in Figs. 1 to 8 and are discussed later.

Symbols for Table 1

$$R = (\rho^2 + N^2\phi_1^2)^{1/2}$$

$$\phi_1 = (a^2 - \rho^2)^{1/2} \qquad \phi_2 = [\rho(R + \rho)/2]^{1/2}$$

$$\phi_3 = [\rho(R - \rho)/2]^{1/2} \qquad \phi_4 = \rho^{1/2}[N(a^2 + \rho^2)^{1/2} - \rho]^{1/2}$$

$$I_1 = \frac{1}{B\pi}\int_0^a \frac{1}{R\phi_1\rho}\{(\phi_2\rho + \phi_1\phi_3)\cosh(\rho t_1 - B\phi_2 x_1)\cos B\phi_3 x_1 + (\phi_2\phi_1 - \rho\phi_3)\sinh(\rho t_1 - B\phi_2 x_1)\sin B\phi_3 x_1\}d\rho$$

$$I_2 = \frac{1}{B\pi}\int_0^b \frac{\rho - (a^2 + \rho^2)^{1/2}}{(a^2 + \rho^2)^{1/2}\phi_4}\cos\rho t_1 \cosh B\phi_4 x_1 d\rho$$

$$I_3 = \frac{1}{B\pi}\int_0^a \frac{1}{R\phi_1\rho}\{\phi_2\sinh(\rho t_1 - B\phi_2 x_1)\cos B\phi_3 x_1 - \phi_3\cosh(\rho t_1 - B\phi_2 x_1)\sin B\phi_3 x_1\}d\rho$$

$$I_4 = \frac{1}{B\pi}\int_0^a \frac{\sin\rho t_1 \cosh B\phi_4 x_1}{(a^2 + \rho^2)^{1/2}\phi_4}d\rho$$

$$I_5 = \frac{1}{\pi}\int_0^a \frac{1}{\phi_1\rho}\sinh(\rho t_1 - B\phi_2 x_1)\cos B\phi_3 x_1\, d\rho$$

$$I_6 = \frac{1}{\pi}\int_0^b \frac{\cos\rho t_1 \sinh B\phi_4 x_1}{(a^2 + \rho^2)^{1/2}\rho}d\rho$$

$$I_7 = -\frac{1}{\pi}\int_0^a \left\{\frac{1}{\phi_1}\cosh(\rho t_1 - B\phi_2 x_1)\cos B\phi_3 x_1 + \frac{1}{\rho}\sinh(\rho t_1 - B\phi_2 x)\sin B\phi_3 x_1\right\}d\rho$$

$$I_8 = \frac{1}{\pi}\int_0^b \frac{\rho - (a^2 + \rho^2)^{1/2}}{(a^2 + \rho^2)^{1/2}\rho}\sin\rho t_1 \sinh B\phi_4 x_1\, d\rho$$

$$I_9 = \frac{1}{B\pi}\int_0^a \frac{1}{R\phi_1\rho}\{(\phi_2\rho - \phi_1\phi_3)\cosh(\rho t_1 - B\phi_2 x_1)\cos B\phi_3 x_1 - (\phi_2\phi_1 + \rho\phi_3)\sinh(\rho t_1 - B\phi_2 x_1)\sin B\phi_3 x_1\}d\rho$$

$$I_{10} = \frac{1}{B\pi}\int_0^b \frac{\rho + (a^2 + \rho^2)^{1/2}}{(a^2 + \rho^2)^{1/2}\phi_4}\cos\rho t_1 \cosh B\phi_4 x_1\, d\rho$$

$$I_{11} = -\frac{1}{\pi}\int_0^a \left\{\frac{1}{\phi}\cosh(\rho t_1 - B\phi_2 x_1)\cos B\phi_3 x_1 - \frac{1}{\rho}\sinh(\rho t_1 - B\phi_2 x_1)\sin B\phi_3 x_1\right\}d\rho$$

$$I_{12} = \frac{1}{\pi}\int_0^b \left\{\frac{1}{\rho} + \frac{1}{(a^2 + \rho^2)^{1/2}}\right\}\sin\rho t_1 \sinh B\phi_4 x_1\, d\rho$$

$$I_{13} = \frac{B}{\pi}\int_0^a \frac{1}{\phi_1\rho^2}\{(\phi_2\rho + \phi_1\phi_3)[\cosh(\rho t_1 - B\phi_2 x_1)\cos B\phi_3 x_1 - 1] - (\phi_2\phi_1 + \rho\phi_3)\sinh(\rho t_1 - B\phi_2 x_1)\sin B\phi_3 x_1\}d\rho$$

$$I_{14} = \frac{2B}{\pi}\int_0^b \frac{\phi_4[\rho + (a^2 + \rho^2)^{1/2}]}{\rho^2(a^2 + \rho^2)^{1/2}}\left[\sinh^2\frac{B\phi_4 x_1}{2}\cos\rho t_1 + \sin^2\left(\frac{\rho t_1}{2}\right)\right]d\rho$$

$$I_{15} = \frac{B}{\pi}\int_0^a \frac{1}{\phi_1\rho^2}\{\phi_2\cos B\phi_3 x_1 \sinh(\rho t_1 - B\phi_2 x_1) + \phi_3\sin B\phi_3 x_1\cosh(\rho t_1 - B\phi_2 x_1)\}d\rho$$

$$I_{16} = -\frac{1}{\pi}\int_0^b \frac{\phi_4\sin\rho t_1 \cosh B\phi_4 x_1}{(a^2 + \rho^2)^{1/2}\rho^2}d\rho$$

$$I_{17} = \frac{B}{\pi}\int_0^a \frac{1}{\phi_1\rho^2}\{(\phi_2\rho - \phi_1\phi_3)[\cosh(\rho t_1 - B\phi_2 x_1)\cos B\phi_3 x_1 - 1] + (\phi_2\phi_1 + \rho\phi_3)\sinh(\rho t_1 - B\phi_2 x_1)\sin B\phi_3 x_1\}d\rho$$

$$I_{18} = \frac{2B}{\pi}\int_0^b \frac{\rho - (a^2 + \rho^2)^{1/2}}{(a^2 + \rho^2)^{1/2}\rho^2}\phi_4\left[\sin^2\frac{\rho t_1}{2}\cosh B\phi_4 x_1 - \sinh^2\frac{B\phi_4 x_1}{2}\right]d\rho$$

Inverse Transformations

Inspection of Table 1 and of Equations [3] shows that all quantities whose inverse transforms are desired are of the form

$$F(p, x_1) = L[f(t_1, x_1)] = F_1(p)e^{-\lambda_1 x_1} + F_2(p)e^{-\lambda_2 x_1} \ldots [4]$$

where the functions F_1 and F_2 are easily obtained from the expressions for Y and Ψ listed in Table 1 and have the following properties

(i) $F_1(p) \to 0$ and $F_2(p) \to 0$ as $|p| \to \infty$ . . . . . [4a]

(ii) $\lim_{|p|\to\infty}[\lambda_1/(p\gamma^{1/2})] = 1$ and $\lim_{|p|\to\infty}[\lambda_2/p] = 1$ . . . . [4b]

(iii) F_1 does not contain the quantity λ_2, though it sometimes contains λ_2^2; F_2 contains λ_2.

The function

$$f(t_1, x_1) = [1/(2\pi i)]\int_{c-i\infty}^{c+i\infty} F(p, x_1)e^{pt_1}\,dp = I_1 + I_2 \ldots [5]$$

where

$$I_1 = [1/(2\pi i)]\int_{Br_1} F_1(p)e^{(pt_1 - \lambda_1 x_1)}\,dp \ldots\ldots [5a]$$

$$I_2 = [1/(2\pi i)]\int_{Br_1} F_2(p)e^{(pt_1 - \lambda_2 x_1)}\,dp \ldots\ldots [5b]$$

and where the constant c is chosen so that all singularities of $F(p, x_1)$ in the complex p-plane lie to the left of the line $p = c$ [Br_1 in Figs. 9, 10(a), or 10(b)]. Use of Equation [5] requires integration along a suitable path; the paths chosen in the present problems are indicated in Table 2 and in Figs. 9, 10(a), and 10(b) and are discussed later. These paths are the same as those used in (3, 4, 8). An illustrative example is presented in the Appendix. Three cases may be distinguished, depending on the path used.

TABLE 2 PATHS OF CONTOUR INTEGRATION

Integral	Path of Fig. 9[a]	Path of Fig. 10(a)[b]	Path of Fig. 10(b)
$\int_{Br_1} F_1(p)e^{(pt_1 - \lambda_1 x_1)}\,dp$	$x_1\sqrt{\gamma} > t_1$	$x_1\sqrt{\gamma} < t_1$	....
$\int_{Br_1} F_2(p)e^{(pt_1 - \lambda_2 x_1)}\,dp$	$x_1 > t_1$	....	$x_1 < t_1$

[a] The integrals vanish in this case in the region indicated.
[b] This path is a special case of that of Fig. 10(b); thus, if the latter were used here, no contributions would be obtained from I_4, I_5, I_{14}, I_{15}.

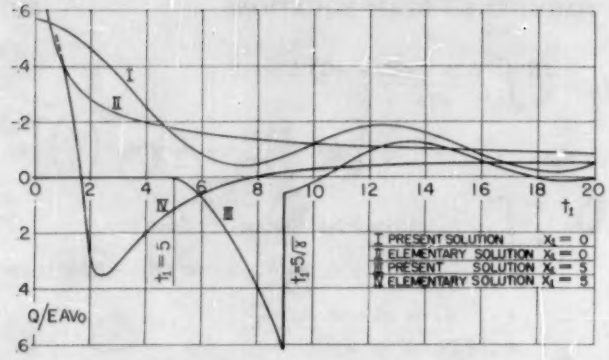
Q/EAVo
I PRESENT SOLUTION $x_1 = 0$
II ELEMENTARY SOLUTION $x_1 = 0$
III PRESENT SOLUTION $x_1 = 5$
IV ELEMENTARY SOLUTION $x_1 = 5$
$t_1 = 5$
$t_1 = 5/8$
t_1

FIG. 1 VARIATION WITH TIME OF THE SHEAR FORCE IN PROBLEM I; $x_1 = 0$ AND $x_1 = 5$

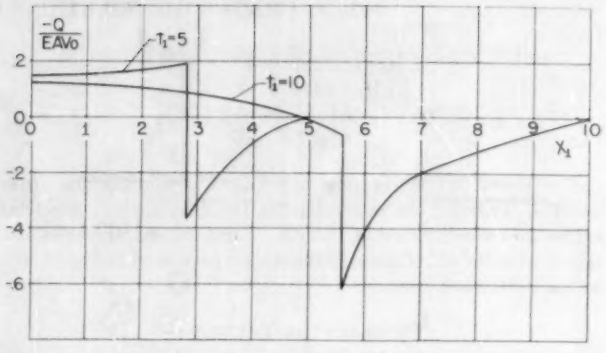

FIG. 2 VARIATION WITH POSITION OF THE SHEAR FORCE IN PROBLEM I; $t_1 = 5$ AND $t_1 = 10$

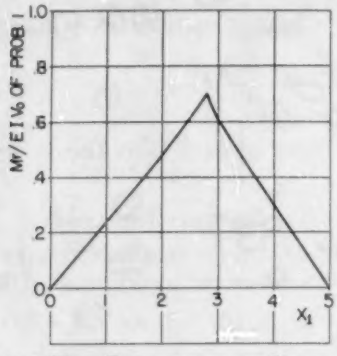

FIG. 3 VARIATION WITH POSITION OF THE BENDING MOMENT OF PROBLEM I, VELOCITY OF PROBLEM II, SHEAR FORCE OF PROBLEM III, AND ROTATIONAL VELOCITY OF PROBLEM IV; $t_1 = 5$

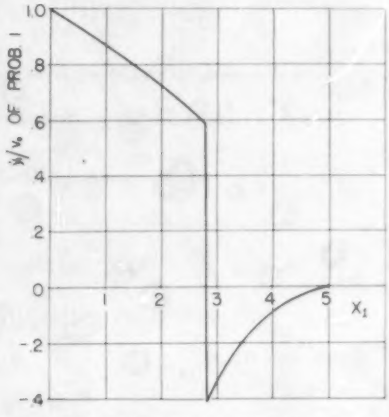

FIG. 4 VARIATION WITH POSITION OF THE VELOCITY OF PROBLEM I, SHEAR FORCE OF PROBLEM IV; $t_1 = 5$

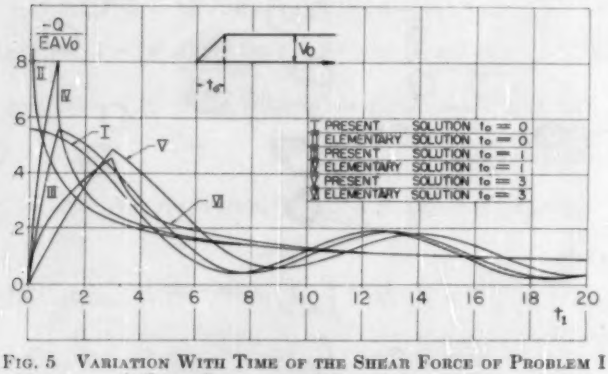
-Q/EAVo
Vo
t_0
I PRESENT SOLUTION $t_0 = 0$
II ELEMENTARY SOLUTION $t_0 = 0$
III PRESENT SOLUTION $t_0 = 1$
IV ELEMENTARY SOLUTION $t_0 = 1$
V PRESENT SOLUTION $t_0 = 3$
VI ELEMENTARY SOLUTION $t_0 = 3$
t_1

FIG. 5 VARIATION WITH TIME OF THE SHEAR FORCE OF PROBLEM I (LOAD GRADUALLY APPLIED); $x_1 = 0$

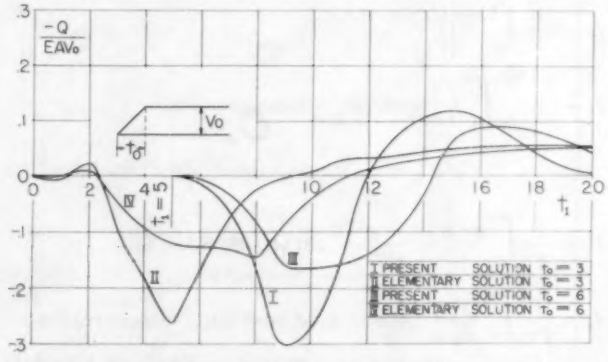

FIG. 6 VARIATION WITH TIME OF THE SHEAR FORCE OF PROBLEM I (LOAD GRADUALLY APPLIED); $x_1 = 5$

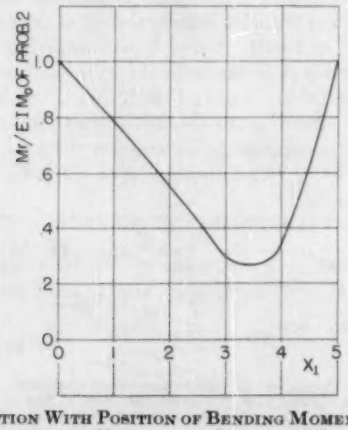

FIG. 7 VARIATION WITH POSITION OF BENDING MOMENT OF PROBLEM II, ROTATIONAL VELOCITY OF PROBLEM III; $t_1 = 5$

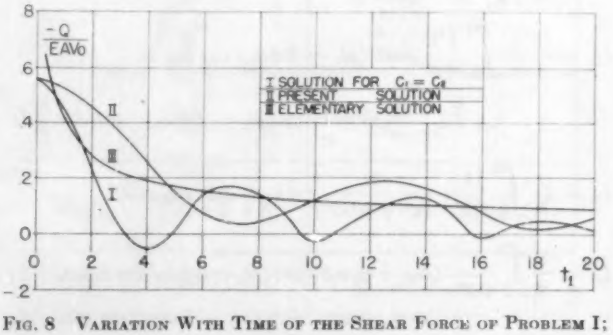

FIG. 8 VARIATION WITH TIME OF THE SHEAR FORCE OF PROBLEM I; $x_1 = 0$, $c_1 = c_2$

Path of Fig. 9. This path is used in the region indicated in Table 2. The integrals along Br_1 are equal to those along Br_2 since no singularities lie between these paths. Then

$$I_1 = \lim_{|p|\to\infty} \int_{Br_2} F_1(p)e^{(t_1 - x_1\gamma^{1/2})p}\,dp \quad [6a]$$

$$I_2 = \lim_{|p|\to\infty} \int_{Br_2} F_2(p)e^{(t_1 - x_1)p}\,dp \quad [6b]$$

with the aid of Equations [4b]. Use of Equations [4a] and of Jordan's lemma (5) shows that

$$I_1 = 0 \text{ for } x_1\gamma^{1/2} > t_1 \quad [6c]$$

$$I_2 = 0 \text{ for } x_1 > t_1 \quad [6d]$$

These equations show that a disturbance is set up by the impact which propagates with two wave fronts, advancing, respectively, with the velocities c_1 and c_2, where

$$c_1 = (E/\rho)^{1/2};\ c_2 = (Gk'/\rho)^{1/2} = c_1/\gamma^{1/2} \quad [7]$$

Consider, however, the behavior of $[p + N(p^2 - a^2)]$ when $p = i/\gamma^{1/2}$, for example; both the quantities p and $(p^2 - a^2)^{1/2}$ have imaginary parts greater than zero, and therefore their sum cannot be zero. Note, incidentally, that this is not true of their difference, appearing in the quantity $[p - N(p^2 - a^2)^{1/2}]$, which will be discussed later in conjunction with the path of Fig. 10(*b*). Similar results hold for $p = -i/\gamma^{1/2}$.

The following conclusions may be easily shown to hold for the contour integration along the path of Fig. 10(*a*):

(*a*) Integration along $AB + B'A'$ as $R \to \infty$ gives a zero result according to Jordan's lemma and Equations [4a] and [4b].

(*b*) Integration along $l_1 + L_1$ gives a zero result.

(*c*) Integration along the two small circles r_1 and r_2 gives a zero result as their radii approach zero.

(*d*) Integration along the small circle r_0 (as its radius approaches zero) gives a zero result provided that the exponent of p in the denominator of $F_1(p)$ is less than 1. With this proviso, the final result is

$$I_1 = [1/(2\pi i)] \int_{L_2+L_3+l_3+l_2} F_1(p)e^{(pt_1 - \lambda_1 x_1)}\,dp;\ x_1\gamma^{1/2} < t_1 \quad [10]$$

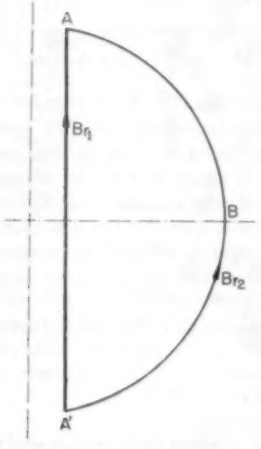

FIG. 9 PATH OF INTEGRATION (See Table 2.)

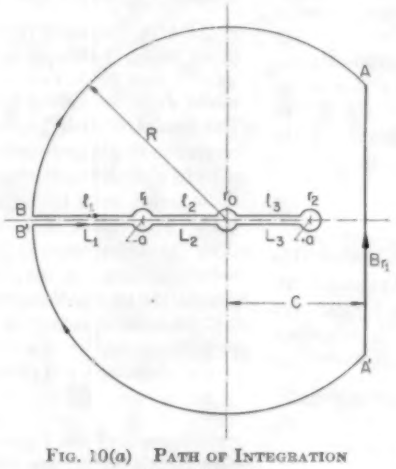

FIG. 10(*a*) PATH OF INTEGRATION (See Table 2.)

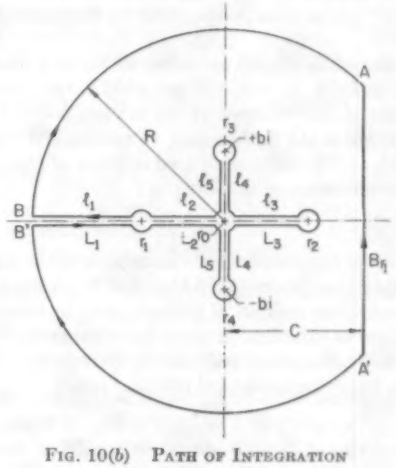

FIG. 10(*b*) PATH OF INTEGRATION (See Table 2.)

Path of Fig. 10(a). This path applies to the calculation of the integral I_1 in the range $x_1\gamma^{1/2} < t_1$. The function $F_1e^{-\lambda_1 x_1}$ appearing in that integral does not contain the quantity $[p - N(p^2 - a^2)^{1/2}]^{1/2}$ which is part of λ_2, but contains the four quantities $p^{1/2}$, $(p-a)^{1/2}$, $(p+a)^{1/2}$, and $[p + N(p^2 - a^2)^{1/2}]^{1/2}$. If these four quantities are made single valued and analytic by a suitable restriction on their arguments and suitable branch cuts, so will the quantity $F_1e^{-\lambda_1 x_1}$ be. The first three are clearly single valued if the argument θ of each of the functions p, $(p-a)$, $(p+a)$ is restricted to the range

$$-\pi < \theta < \pi \quad [8]$$

and will be also analytic if the branch cut of Fig. 10(*a*) is established. The argument of $[p + N(p^2 - a^2)^{1/2}]^{1/2}$ will also be single valued if the argument of $[p + N(p^2 - a^2)^{1/2}]$ is also restricted to the range [8]. Note that this restriction is consistent with the previous choice of signs made implicitly in Equations [2b] and [2c], where positive signs were chosen for the real parts of λ_1 and λ_2 in establishing Equation [2c]. There remains to show that no further branch cuts are required; this will be the case if the quantity $[p + N(p^2 - a^2)^{1/2}]$ is never zero. This quantity could be zero only if $p^2 = N^2(p^2 - a^2)$, i.e., if

$$p = \pm i/\gamma^{1/2} \quad [9]$$

If the exponent of p in the denominator of $F_1(p)$ exceeds unity, branch points of higher order arise; the integrations around the small circle r_0 does not vanish at the limit and therefore the required inverse transformation is very difficult. This difficulty can be circumvented, however, with the use of Table 3, which has been set up in accordance with the reciprocal relations listed later, Equations [13]. In Problem I, for example, the quantities $(y_1' - \psi)$ and ψ' can be obtained directly from the contour integration, as their transforms satisfy the proviso attached to Equation [10]. The remaining quantities, i.e., ψ' and y_1', can then be derived from Equations [1a] as shown at the end of the Appendix. In Problem II, only $(y_1' - \psi)$ can be obtained directly, but y_1' is found immediately (see Table 1) from the previously derived expression for ψ' of Problem I; the remaining quantities are again solved for from Equations [1a]. In Problems III and IV no quantities can be found directly, and use of the reciprocal relations is immediately required.

Path of Fig. 10(b). As indicated previously, the branch cut of Fig. 10(*a*) is no longer adequate for the evaluation of I_2 because of the presence (in λ_2) of the quantity $[p - N(p^2 - a^2)^{1/2}]^{1/2}$. For convenience write

$$p - N(p^2 - a^2)^{1/2} = (1 - N^2)(p + bi)(p - bi)/[p + N(p^2 - a^2)^{1/2}] \quad [11]$$

where

$$b = 1/\gamma^{1/2} \quad [11a]$$

The argument of the denominator is uniquely determined as in the previous discussion; the numerator will be single valued if the argument θ of each of the functions $(p + bi)$ and $(p - bi)$ is restricted to the range (consistent with that implied in Equations [2b] and [2c])

$$-\frac{\pi}{2} < \theta < \frac{3\pi}{2} \quad [11b]$$

and will be analytic if the additional branch cut shown in Fig. 10(b) is introduced. In this manner the quantity $[p - N(p^2 - a^2)^{1/2}]^{1/2}$ also becomes single valued and analytic and the contour integration can be performed. In a similar manner to the foregoing, the final result is

$$I_2 = [1/(2\pi i)] \int_{L_2+L_3+L_4+L_5+l_4+l_5+l_6} F_2(p) e^{(pt_1 - \lambda_2 x_1)}\, dp; \quad x_1 < t_1 \quad [12]$$

with the proviso that the exponent of p in the denominator of $F_2(p)$ is less than unity (refer to discussion following Equation [10]).

Attention should be called to the fact that integration along $L_3 + L_4 + l_4 + l_5$ will not yield a zero result in this case because of the presence of the branch points at $p = \pm bi$. This portion of the path would, of course, give no contribution if the path of Fig. 10(b) were used in place of that of Fig. 10(a) in the determination of the integral I_1.

Discussion of Results

Some numerical results pertaining to the problems described in Table 1 are presented in Figs. 1 to 8. A few general remarks concerning the method of solution and the behavior of Timoshenko beams as exhibited in these figures are collected in the following:

1 Inspection of the transformed solution of Table 1 shows that the following reciprocal relations hold:

$$\left.\begin{aligned} (y_1^*/v_0) \text{ of Prob. I} &= (Q/k'AGF_0) \text{ of Prob. IV} \\ (\psi^*/v_0) \text{ of Prob. I} &= -Q/M_0\gamma k'AG \text{ of Prob. II} \\ (Mr/EIM_0) \text{ of Prob. II} &= \psi^*/\omega_0 \text{ of Prob. III} \\ y^*/\omega_0 \text{ of Prob. III} &= -Mr\gamma/EIF_0 \text{ of Prob. IV} \\ (Mr/EIv_0) \text{ of Prob. I} &= -y^*/M_0 \text{ of Prob. II} \\ &= -Q/\gamma\omega_0 k'AG \text{ of Prob. III} \\ &= \gamma\psi^*/F_0 \text{ of Prob. IV} \end{aligned}\right\} \quad [13]$$

As a consequence of these relations Table 3 (as well as the solutions in Table 1) exhibits symmetry about its principal diagonal.

TABLE 3 PROCEDURE FOR SOLUTION

Problem	$y_1' - \psi$	ψ^*	ψ'	y_1^*
1	CI	CI	Eq. [1a]	Eq. [1a]
2	CI or from ψ' of Prob. I	Eq. [1a]	Eq. [1a]	From ψ' Prob. I
3	From ψ' Prob. I	From ψ' Prob. II	Eq. [1a]	Eq. [1a]
4	From y_1' Prob. I	From y_1' Prob. II	Eq. [1a] or from y_1' Prob. III	Eq. [1a]

Notes:
CI: Inversion by complex contour integration.
Eq. [1a]: Integration with respect to x_1 and t_1 with the aid of Equation [1a].

2 It was previously mentioned that, in general, two wave fronts arise, traveling with velocities c_1 and c_2, respectively, Equations [7]. Figs. 1, 2, 3, 4, and 7, together with the observations listed under item 1, further indicate that discontinuities in shear force and velocity are propagated with constant magnitude and with a speed c_2, and that discontinuities in bending moment and angular velocity are propagated also with constant magnitude but with a speed c_1. Thus, at the wave front traveling with speed c_1, the shear-force and velocity expressions are continuous functions of x and t, though their derivatives with respect to either of these independent variables may be discontinuous and, similarly, for the moment and angular velocity expressions at the wave front traveling with speed c_2. These results are in agreement with those of references (2) and (6).

3 It is of interest to note that in Problem I, for example, the maximum shear force does not occur at the struck end ($x = 0$); larger values of this force occur with opposite signs in Figs. 1 and 2 near the shear discontinuity because of the presence of bending deformations between the two wave fronts. In Problem II, however, the applied moment appears to be equal to the maximum moment of the beam, Fig. 7, in agreement with the discussion of Table 2 of reference (4) contained in that reference.

4 Results were also obtained for the special case of $c_1 = c_2$. This case is physically impossible but is useful in providing a mathematical check on the contour integration since the inverse transformation can be obtained here in terms of tabulated functions (see reference (6) for instance). For example, the shear forces in Problems I and II are, respectively

$$\left.\begin{aligned} [Q/(k'AGv_0)] &= -\cos(t_1/2)J_0[(t_1^2 - x_1^2)^{1/2}/2] \text{ for } t_1 > x_1 \\ [Q/(k'AGM_0)] &= -\sin(t_1/2)J_0[(t_1^2 - x_1^2)^{1/2}/2] \text{ for } t_1 > x_1 \end{aligned}\right\} \quad [14]$$

where J_0 is the Bessel function of the first kind of order zero. The results of Table 1 were checked by substituting $c_1 = c_2$ in the corresponding expressions of that table, then expanding the results in a double-power series in x_1 and t_1, and finally comparing these series, term by term, with similar expansions of Equations [14]. The values of the shear force given by the first of Equations [14] are plotted in Fig. 8, together with the corresponding actual solution; it may be noticed that, as may have been expected, the two curves differ widely.

5 Results obtained on the basis of the elementary Bernoulli-Euler equation

$$EI(\partial^4 y/\partial x^4) + \rho A(\partial^2 y/\partial t^2) = 0 \quad [15]$$

(which results from Equations [1] if shear deformation and rotatory inertia effects are omitted) are plotted in Figs. 1 and 5 for purposes of comparison with the exact results. The agreement between corresponding curves is bad ahead of the slower disturbance front. Fig. 1 shows that behind this front, however, the exact solution oscillates about that of Equation [15] and does not differ too greatly from it. These oscillations represent the response of the lowest thickness-shear mode of vibration of the beam. Some use of the Bernoulli-Euler solutions in obtaining approximate results was made in reference (2).

6 Some results pertaining to gradually applied loads are plotted in Figs. 5 and 6. They were obtained from the curves of Fig. 1 with the aid of Duhamel's superposition rule (7) and numerical integration. The results for $x_1 = 0$, Fig. 5, show that the elementary solution is an adequate approximation if the load is not too rapidly applied ($t_0 > 3$, say). For $x_1 = 5$, Fig. 6, the maximum shear force calculated from Equation [15] is in good agreement with the exact value for $t_0 = 3$. The time history of the shear force, however, is different even for $t_0 = 6$. This is not surprising because no wave fronts traveling with finite speeds arise from the Bernoulli-Euler equation.

7 The solutions are given in Table 1 in terms of definite integrals which must be evaluated numerically. Such integrations were carried out with the aid of either Simpson's or Weddle's rule (9), after suitable modifications (indicated later as an example for the integral I_2) to take into account the improper nature of these integrals.

The integrand of I_2 of Table 1 (denoted here by I_2^*) becomes infinite at both limits. Write however

$$I_2 = \int_0^\beta I_2^* d\rho + \int_\beta^b I_2^* d\rho;\ 0 < \beta < b \quad \ldots\ldots [16]$$

then each of these integrals is improper at one of its limits only. With the change of variable

$$\rho = \xi^2 \quad \ldots\ldots [16a]$$

the first integral is no longer improper and can be evaluated readily; similarly for the second integral with the aid of the change of variable

$$\rho - b = \xi^2 \quad \ldots\ldots [16b]$$

The accuracy of the numerical calculations can be estimated by means of a comparison of the calculated and exact values of the discontinuities occurring at $x = c_1 t$ and $x = c_2 t$. These exact values are known from the discussion given under item 2 of conclusions. The comparison in question is presented for a number of cases in Table 4.

TABLE 4 ACCURACY OF NUMERICAL INTEGRATION

Prob.	Quantity	Discontinuity x_1	Discontinuity t_1	Calculated value	Exact value	Per cent error
I	$-Q/EAV_0$	0	0	0.5590	0.5590	0
	$-Q/EAV_0$	$5/\sqrt{\gamma}$	5	0.5573	0.5590	0.31
	$-Q/EAV_0$	5	$5\sqrt{\gamma}$	0.5543	0.5590	0.84
	$\mathfrak{M}'/V_0$	5	5	−0.0043	0	..
	$\mathfrak{M}'/V_0$	$5/\sqrt{\gamma}$	5	0.9985	1	0.15
	Mr/EIV_0	5	5	0.0037	0	..
	Mr/EIV_0	$5/\sqrt{\gamma}$	5	0.0026	0	..
II	Mr/EIV_0	5	5	0.9922	1	0.78
	Mr/EIV_0	$5/\sqrt{\gamma}$	5	0.00059	0	..

ACKNOWLEDGMENT

The authors wish to express their appreciation to Mr. Patrick O'Leary and to Dr. F. H. T. Liu for their contributions to this work, and to Prof. Jerome H. Weiner for his invaluable assistance in connection with the complex integrations described herein.

BIBLIOGRAPHY

1 "Vibration Problems in Engineering," by S. Timoshenko, D. Van Nostrand Company, Inc., New York, N. Y., 1937.
2 "An Approximate Theory of Lateral Impact on Beams," by B. A. Boley, JOURNAL OF APPLIED MECHANICS, Trans. ASME, vol. 77, 1955, pp. 69–76.
3 "Transverse Impact of Long Beams, Including Rotatory Inertia and Shear Effects," by M. A. Dengler and M. Goland, Proceedings of the First U. S. National Congress of Applied Mechanics, 1952, p. 179.
4 "Flexural Waves in Beams According to the More Exact Theory of Bending," by J. Miklowitz, NAVORD Report 2049, 1953.
5 "Laplace Transformation," by W. T. Thomson, Prentice-Hall, Inc., New York, N. Y., 1950.
6 "On Traveling Waves in Beams," by R. W. Leonard and B. Budiansky, NACA Technical Note 2874, January, 1953.
7 "Mathematical Methods in Engineering," by Th. von Karman and M. A. Biot, McGraw-Hill Book Company, Inc., New York, N. Y., first edition, 1940, p. 403.
8 "The Propagation of Waves in the Transverse Vibration of Bars and Plates," by Ya. S. Uflyand, *Prikladina Matematika i Mekhanika*, vol. 12, May-June, 1948, pp. 287–300.
9 "The Mathematics of Physics and Chemistry," by H. Margenau and G. M. Murphy, D. Van Nostrand Company, Inc., New York, N. Y., 1943.

Appendix

As an illustration of the inverse transformations described earlier in this paper, some details of the solution of Problem I are presented here. The transforms of various quantities pertaining to that problem are given in Table 1. Inspection shows that in the denominator of the quantities $L\{\Psi'\} = p\Psi$ and $L\{Q/(k'AG)\} = Y' - \Psi$ of Equations [3] the power of p is $(1/2)$ and therefore satisfies the proviso listed with Equations [10] and [12]. This is not true of the remaining quantities of Equations [3], which will therefore be considered later in accordance with the discussion following Equation [10].

To illustrate the contour integration, the term of the form $F_2(p)e^{-\lambda_2 x_1}$ (see Equation [4]) of $Y' - \Psi$ will be taken up in detail; from Table 1 and Equations [2b], this term can be written as

$$F_2(p)e^{-\lambda_2 x_1} = \frac{v_0\gamma[p - (p^2 - a^2)^{1/2}]\, e^{-Bp^{1/2}[p - N(p^2-a^2)^{1/2}]^{1/2}x_1}}{2B(p^2 - a^2)^{1/2}p^{1/2}[p - N(p^2 - Q^2)^{1/2}]^{1/2}} \quad \ldots\ldots [A1]$$

According to Table 2, the contour integration must be carried out along the path of Fig. 10(*b*); in particular, only the portions of that path listed in Equation [12] need be considered as indicated in the following.

Along line L_2, for example

$$p = \rho e^{-i\pi};\ p + a = a - \rho;\ p - a = (a + \rho)e^{-i\pi} \quad \ldots [A2]$$

Then

$$p^{1/2} = -i\rho^{1/2};\ (p + a)^{1/2} = (a - \rho)^{1/2}$$
$$(p - a) = -i(a + \rho)^{1/2} \quad \ldots [A2a]$$

Combination of these quantities yields

$$(p^2 - a^2)^{1/2} = e^{-i\pi/2}(a^2 - \rho^2)^{1/2} = \phi_1 e^{-i\pi/2} = -i\phi_1 \quad \ldots [A2b]$$

$$[p + N(p^2 - a^2)^{1/2}]^{1/2} = (-\rho - iN\phi_1)^{1/2}$$
$$= [(R - \rho)/2]^{1/2} - i[(R + \rho)/2]^{1/2} \quad \ldots [A2c]$$

where
$$R = (\rho^2 + N^2\phi_1^2)^{1/2} \quad \ldots\ldots [A2d]$$

According to the discussion following Relation [8] the argument θ of the quantity $(-\rho - iN\phi_1)$ must lie in the range

$$-\pi < \theta < -(\pi/2) \quad \ldots\ldots [A2e]$$

Thus the signs of the real and imaginary parts of the last terms of Equations [A2c] are determined.

There now remains to determine the quantity

$$[p - N(p^2 - a^2)^{1/2}]^{1/2}$$

Equation [11] shows that it is necessary to consider the quantity

$$[(p + bi)^{1/2}(p - bi)^{1/2}]$$

first. The argument θ of the term

$$(p + bi) = (-\rho + bi)$$

is restricted by Relation [11*b*] and must therefore be in the range

$$\pi/2 < \theta < \pi$$

and may be taken as equal to $(\pi - \alpha)$, where α is an angle between zero and $\pi/2$. Similarly, the argument θ of $(p - bi)$ must be in the range

$$\pi < \theta < 3\pi/2$$

and is in fact equal to $(\pi + \alpha)$. Hence the argument θ of the product $(p + bi)(p - bi)$ is equal to 2π, and therefore

$$(p + bi)^{1/2}(p - bi)^{1/2} = -(\rho^2 + b^2)^{1/2} \quad \ldots\ldots [A3]$$

Substitution of the necessary quantities into Equation [11] gives finally

$$[p - N(p^2 - a^2)^{1/2}]^{1/2} = -[(R - \rho)/2]^{1/2} - i[(R + \rho)/2]^{1/2} \quad \ldots [A3a]$$

For this portion of the path then

$$[1/(2\pi i)]\int_{L_2} F_2(p)e^{-\lambda_2 x_1+pt_1}dp = \frac{v_0\gamma}{4B\pi}\int_0^a \frac{\rho-i\phi_1}{\phi_1(\phi_2-i\phi_2)}e^{[-\rho t_1+B(\phi_2-i\phi_2)x_1]}d\rho \quad [A4]$$

where

$$\phi_2 = [\rho(R+\rho)/2]^{1/2}, \quad \phi_3 = [\rho(R-\rho)/2]^{1/2}$$

In a similar way the integrals along L_3, L_2, l_3, and l_2 may be obtained; they give

$$[1/(\pi i)]\int_{L_3+L_2+l_3+l_2} F_2(p)e^{-\lambda_2 x_1+pt_1}dp = \frac{v_0\gamma}{B\pi}\int_0^a [1/(R\phi_1\rho)]\,[(\phi_3\rho+\phi_1\phi_3)\cosh(t_1\rho-B\phi_2 x_1)\cos B\phi_3 x_1 + (\phi_2\phi_1-\rho\phi_3)\sinh(t_1\rho-B\phi_2 x_1)\sin B\phi_3 x_1]d\rho \quad [A5]$$

In an analogous manner the result

$$\int_{L_4+L_3+l_3+l_1} F_1(p)e^{-\lambda_1 x_1+pt_1}dp = -\int_{L_4+L_3+l_3+l_2} F_2(p)e^{-\lambda_2 x_1+pt_1}dp \quad [A5a]$$

is obtained with the aid of the path of Fig. 10(*a*). Thus the integrals of the two terms of Equation [4] are equal and opposite in sign along the portion of the path indicated (which is the complete path for the $F_1(p)$ term); it should be emphasized however that these expressions must be used only in the range defined, respectively, by Equations [10] and [12] for the first and second term. The discontinuities in the solution which arise because of this have been discussed in the body of the paper.

In a similar way the integrals along l_4, l_3, L_4, and L_3 may be obtained; they give

$$[1/(2\pi i)]\int_{L_3+L_4+l_4+l_3} F_2(p)e^{-\lambda_2 x_1+pt_1}dp = \frac{v_0\gamma}{B\pi}\int_0^b \frac{\rho-(a^2+\rho^2)^{1/2}}{(a^2+\rho^2)^{1/2}\phi_4}\cosh B\phi_4 x_1\cos\rho t_1 d\rho \quad [A6]$$

The result given for $[Q/(k'AG)] = (y_1' - \psi)$ in Table 1 is found by adding this expression to those of Equations [A5] and [A5*a*], taking of course into account the ranges of validity stipulated with Equations [10] and [12]. The expression for $p\Psi$ is similarly inverted to give $\psi^{\cdot}$ as in Table 1.

The remaining desired quantities of Equations [3], namely, $y_1^{\cdot}$ and $[Mr/(EI)]$, were obtained according to Table 3 as follows: Consider, for example, the velocity $y_1^{\cdot}$; from the second of Equations [1*a*] it is

$$y_1^{\cdot} = (1/\gamma)\int_0^{t_1}(y_1' - \psi)'dt_1 \quad [A7]$$

However, a simpler method of obtaining $y_1^{\cdot}$ is as follows

$$y_1^{\cdot} = (1/\gamma)\int (y_1' - \psi)'dt_1 + f_1(x_1) \quad [A7a]$$

where $f_1(x_1)$ is an arbitrary function; and also

$$y_1^{\cdot} = \int y_1''dx_1 + f_2(t_1) = \int [(y_1' - \psi)^{\cdot} + \psi^{\cdot}]\,dx_1 + f_2(t_1) \quad [A7b]$$

where $f_2(t_1)$ is another arbitrary function. Evaluation of the integrals of Equations [A7*a*] and [A7*b*] and comparison of the resulting expressions for $y_1^{\cdot}$ showed that

$$f_1(x_1) = f_2(t_1) = \text{const.} \quad [A7c]$$

Use of the condition that

$$\left.\begin{array}{llll} y_1^{\cdot} = 0 & t_1 < 0 & \text{at } x_1 = 0 \\ y_1^{\cdot} = v_0 & t_1 > 0 & \text{at } x_1 = 0 \end{array}\right\} \quad [A7d]$$

gives the value of this constant.

Influence of Secondary Inertia Terms on Natural Frequencies of Rotating Beams

By J. L. BOGDANOFF,[1] LAFAYETTE, IND.

The equations of small motion of a straight cantilever beam attached to the rim of a rotating disk are determined assuming the Bernoulli-Euler theory of bending and the Saint Venant theory of torsion are valid, the mass and elastic axes coinciding and retaining all inertia terms. Influence of the secondary inertia terms on the fundamental torsional and lateral frequencies is then examined at two angular settings for a uniform beam having a length to disk-radius ratio in the range usually encountered in gas-turbine buckets and axial-flow compressor blades.

Introduction

IT is customary in the computation of the natural frequencies in both lateral and torsional vibration of rotating beams to assume that the rate of change of the angular momentum of the cross section due to rotation, i.e., the gyroscopic action of the cross section, can be neglected in the equations of motion (1 to 6).[2] This assumption leads to satisfactory results when considering the frequencies of the lower modes of propeller and helicopter blades, since these blades are long and slender. However, fairly short and wide compressor blades and turbine buckets occur in gas turbines, and the question naturally arises as to the accuracy of this assumption, inasmuch as very high rotational velocities are involved.

The purpose of the present paper is to determine the equations of small motion including all inertia effects for a straight cantilever beam attached at an arbitrary angular setting to the rim of a disk, which rotates with constant angular velocity, when the mass and elastic axes lie on the same radial line, the Bernoulli-Euler and Saint Venant theories of bending and torsion are valid, and the beam is very stiff in one direction; and then to determine the influence of the additional inertia terms on the fundamental lateral and torsional frequencies of a uniform beam. The equations of motion for twisted beams with noncoincident mass and elastic axes could have been written out, but were omitted here because of their considerable length. Attention has been focused on the fundamental frequencies since these appear to be of prime importance in gas-turbine application and also since it is possible to arrive at some simple, though approximate, frequency equations.

Equations of Motion

Consider the line diagram shown in Fig. 1. Let $OX_1X_2X_3$ denote rectangular Cartesian axes which are fixed in space. The unit orthogonal triad $\mathrm{II}_1, \mathrm{II}_2, \mathrm{II}_3$, with II_1 along OX_1 rotates about II_1 with angular velocity equal to $-\Omega$, where Ω is a constant. Thus II_2 and II_3 determine a rotating plane.

The undeformed central line of the cantilever beam lies along the radial line ox_3, o being at the base. The lines oX_1' and oX_2' are parallel to II_1 and II_2, respectively, and the plane $oX_1'X_2'$ contains the base of the beam. Let the principal axes of the base cross section coincide in direction with ox_1 and ox_2. The symbols i_{t_1}, i_{t_2}, i_{t_3} denote unit vectors along ox_1, ox_2, ox_3, respectively; this unit orthogonal triad has angular velocity

$$-\Omega \cos \alpha \mathrm{i}_{t_1} + \Omega \sin \alpha \mathrm{i}_{t_2} = \Omega_1 \mathrm{i}_{t_1} + \Omega_2 \mathrm{i}_{t_2}$$

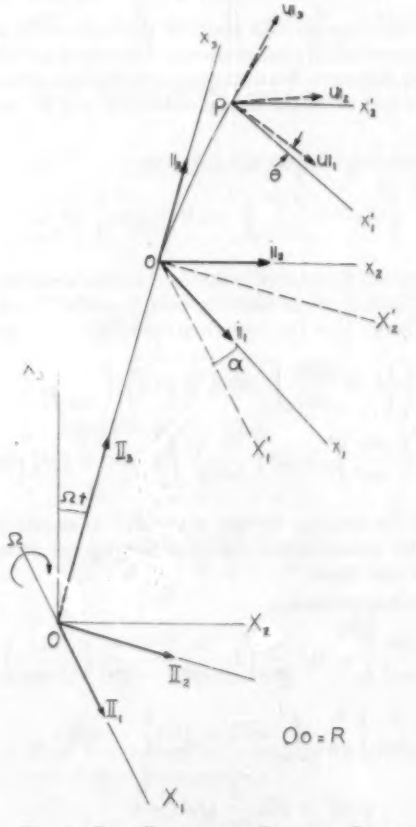

Fig. 1 Line Diagram of Rotating Beam

where α is the angle $X_1'ox_1$ which defines the setting of the beam with respect to the axis of rotation.

P represents a point on the deformed central line. The displacement of P from ox_3 is denoted by $v(x_3, t)$ and is in the i_{t_2} direction. The lines Px_1' and Px_2' are parallel to i_{t_1} and i_{t_2}, respectively. Let the unit vector u_{t_3} be tangent to the deformed central line at P; and let u_{t_1} and u_{t_2} be in the directions of the displaced principal axes of the cross section at P. The torsional

[1] Professor of Engineering Sciences, Purdue University. Mem. ASME.

[2] Numbers in parentheses refer to the Bibliography at the end of the paper.

Presented at the National Conference of the Applied Mechanics Division, Troy, N. Y., June 16–18, 1955, of The American Society of Mechanical Engineers.

Discussion of this paper should be addressed to the Secretary, ASME, 29 West 39th Street, New York, N. Y., and will be accepted until January 10, 1956, for publication at a later date. Discussion received after the closing date will be returned.

Note: Statements and opinions advanced in papers are to be understood as individual expressions of their authors and not those of the Society. Manuscript received by ASME Applied Mechanics Division, May 17, 1954. Paper No. 55—APM-17.

displacement of the cross section about ui_3 is denoted by $\theta(x_3, t)$. The velocity, q, of P is given by

$$q = \Omega_2(R + x_3)i_1 + \{\dot{v} - \Omega_1(R + x_3)\}i_2 + v\Omega_1 i_3 \ldots [1]^1$$

since the position vector, r, of P with respect to O is

$$vi_2 + (R + x_3)i_3$$

Further, one sees by inspection of Fig. 1 that the angular velocity of the unit orthogonal triad ui_1, ui_2, ui_3 is

$$(\Omega_1 - \dot{\beta})i_1 + \Omega_2 i_2 + \dot{\theta}ui_3 \ldots\ldots\ldots\ldots [2]$$

where

$$\beta = \partial v/\partial x_3$$

It then follows that the kinetic energy T of the system can be expressed by the equation

$$\begin{aligned} T = \frac{1}{2}\int_0^l [m\{&\dot{v}^2 - 2\dot{v}\Omega_1(R + x_3) + v^2\Omega_1^2 + \Omega^2(R + x_3)^2\} \\ &+ I_1\{\Omega_1^2 - 2(\Omega_1 + \theta\Omega_2)\dot{\beta} + \dot{\beta}^2 + (\Omega_2^2 - \Omega_1^2)\theta^2 \\ &+ 2\Omega_1\Omega_2\theta\} + I_2\{\Omega_2^2 + 2\Omega_2(\dot{\beta} - \Omega_1)\theta + \Omega_1^2\theta^2 \\ &- \Omega_2^2(\theta^2 + \beta^2)\} + I_3\{\Omega_2^2\beta^2 + 2\Omega_2\beta\dot{\theta} + \dot{\theta}^2\}]dx_3 \ldots [3] \end{aligned}$$

where m is the mass per unit length of the beam and $I_1\Delta x_3$, $I_2\Delta x_3$, $I_3\Delta x_3$ are the principal mass moments of inertia of a blade element of infinitesimal length Δx_3 with respect to its mass center. Equation [3] is exact to within second order of the small quantities v, β, θ.

If the torsional couple at x_3 is taken as

$$\left\{C(x_3) + \frac{J\Omega^2}{A}\int_{x_3}^l m(R + \xi)d\xi\right\}\partial\theta/\partial x_3$$

(see references 7, 8), where C is the usual torsional rigidity, and the Bernoulli-Euler theory of bending used, it can be shown that the potential energy V of the beam is given by the expression

$$\begin{aligned} 2V = \int_0^l \Bigg[&\left\{C + \frac{J\Omega^2}{A}\int_{x_3}^l m(R + \xi)d\xi\right\}\left(\frac{\partial\theta}{\partial x_3}\right)^2 \\ &+ B_1\left(\frac{\partial^2 v}{\partial x_3^2}\right)^2 + \Omega^2\left(\frac{\partial v}{\partial x_3}\right)^2\int_{x_3}^l m(R + \xi)d\xi\Bigg]dx_3 \ldots [4] \end{aligned}$$

where B_1 is the bending stiffness about ui_1. It should be pointed out that this equation and the preceding are not correct for an initially twisted beam.

The equations of motion

$$\left.\begin{aligned} &\frac{\partial^2}{\partial x_3^2}\left(B_1\frac{\partial^2 v}{\partial x_3^2}\right) + \Omega_2^2\frac{\partial}{\partial x_3}\left(I_1\frac{\partial v}{\partial x_3}\right) - \frac{\partial}{\partial x_3}\left(I_1\frac{\partial\dot{v}}{\partial x_3}\right) \\ &- \Omega^2\frac{\partial}{\partial x_3}\left\{\frac{\partial v}{\partial x_3}\int_{x_3}^l m(R + \xi)d\xi\right\} - m\Omega_1^2 v \\ &+ m\ddot{v} + 2\Omega_2\frac{\partial}{\partial x_3}(I_1\dot{\theta}) = 0 \\ &2I_1\Omega_2\frac{\partial\dot{v}}{\partial x_3} - \frac{\partial}{\partial x_3}\left[\left\{C + \frac{J\Omega^2}{A}\int_{x_3}^l m(R + \xi)d\xi\right\}\frac{\partial\theta}{\partial x_3}\right] \\ &+ (I_2 - I_1)(\Omega_2^2 - \Omega_1^2)\theta + I_3\ddot{\theta} = 0 \end{aligned}\right\} \ldots [5]$$

and the boundary conditions

$$\left.\begin{aligned} &v(0, t) = 0, \quad \left(\frac{\partial v}{\partial x_3}\right)_{x_3=0} = 0, \quad \left(\frac{\partial^2 v}{\partial x_3^2}\right)_{x_3=l} = 0 \\ &\left\{\frac{\partial}{\partial x_3}\left(B_1\frac{\partial^2 v}{\partial x_3^2}\right) + I_1\Omega_2^2\frac{\partial v}{\partial x_3}\right. \\ &\qquad \left. - I_1\frac{\partial\ddot{v}}{\partial x_3} + 2I_1\Omega_2\dot{\theta}\right\}_{x_3=l} = 0 \\ &\theta(0, t) = 0, \quad \left(\frac{\partial\theta}{\partial x_3}\right)_{x_3=l} = 0 \end{aligned}\right\} \ldots [6]$$

follow from Equation [3] and [4] on using Hamilton's principle, the nonhomogeneous term $(I_2 - I_1)\Omega_1\Omega_2$, in the second of Equations [5] being dropped. The third of Equations [6] corresponds to the vanishing at $x_3 = l$ of the transverse shear.

If we now assume that

$$\left.\begin{aligned} v(x_3, t) &= \bar{v}(x_3)e^{i\omega t} \\ \theta(x_3, t) &= i\bar{\theta}(x_3)e^{i\omega t} \end{aligned}\right\} \ldots\ldots\ldots\ldots [7]$$

where $i = \sqrt{-1}$, and that m, B_1, C, I_1, I_2, I_3, are constants and introduce the abbreviations

$$\frac{\bar{v}}{l} = \phi_1, \quad \bar{\theta} = \phi_2, \quad \frac{x_3}{l} = \zeta, \quad \frac{R}{l} = R_0, \quad M_1 = \frac{I_1}{ml^2}$$

$$M_2 = \frac{I_2}{ml^2}, \quad p_1 = \frac{I_1}{I_2}, \quad p_2 = \frac{I_3}{I_2}$$

$$\lambda^2 = \frac{ml^4\omega^2}{B_1}, \quad \Omega_1 = n_1\omega, \quad \Omega_2 = n_2\omega, \quad \Omega = n\omega$$

$n_1 = -n\cos\alpha$, $n_2 = n\sin\alpha$, n = real number, Equations [5] and [6] can be written in the forms

$$L_{ij}\phi_j = \lambda^2 M_{ij}\phi_j, \quad i, j = 1, 2 \ldots\ldots\ldots\ldots [8]$$

and

$$\left.\begin{aligned} &(\phi_1)_0 = 0, \quad (D\phi_1)_0 = 0, \quad (D^2\phi_1)_1 = 0 \\ &\{D^3\phi_1 + \lambda^2 M_1(1 + n_2^2)D\phi_1 - 2M_1 n_2\lambda^2\phi_2\}_1 = 0 \\ &(\phi_2)_0 = 0, \quad (D\phi_2)_1 = 0 \end{aligned}\right\} \ldots [9]$$

respectively, for a uniform beam, where $D = d/(d\zeta)$ and

$$L_{11} = D^4, \quad L_{12} = L_{21} = 0, \quad L_{22} = -\frac{C}{B_1}D^2$$

$$M_{11} = 1 - D\{aD\}, \quad M_{12} = 2M_1 n_2 D = -M_{21}$$

$$M_{22} = H - D\{bD\}, \quad H = M_2\{1 - (p_2 - p_1)(n_2^2 - n_1^2)\}$$

$$a = M_1(1 + n_2^2) + n^2\{R_0(\zeta - 1) + (\zeta^2 - 1)/2\}$$

$$b = \frac{J}{Al^2}n^2\{R_0(\zeta - 1) + (\zeta^2 - 1)/2\}$$

Equations [8] and [9], as well as [5] and [6], show that the lateral and torsional vibrations are coupled during rotation provided $M_1 \neq 0$ and $\sin\alpha \neq 0$. We further note from Equations [7] that the two types of motion are 90 deg out of phase in time when coupling exists.

Frequency Equations

The system defined by Equations [8] and [9] is self-adjoint. Hence the variational principle $\delta(\lambda^2) = 0$ (see reference 9) where

$$(\lambda^2) = \frac{\int_0^1 \phi_i L_{ij}\phi_j d\zeta}{\int_0^1 \phi_i M_{ij}\phi_j d\zeta} \ldots\ldots\ldots\ldots [10]$$

[1] In Equation [1] and in what follows, dots over a quantity denote differentiation with respect to time.

could be used to obtain an estimate to λ_1^2. It is difficult, however, to select trial functions ψ_i that are resonable approximations to the exact first-mode shapes $\phi_i^{(1)}$, since the $\phi_i^{(1)}$ depends upon both n and λ_1^2. For this reason an iterative scheme was adopted (9 to 12), in which the ψ_i after each iteration represents increasingly accurate approximations to the $\phi_i^{(1)}$. In principle, though not in detail, the iterative scheme proceeds as follows:

Write Equations [8] and [9] symbolically as

$$\phi(\zeta) = \lambda^2 N\phi(\zeta), \qquad 0 \leq \zeta \leq 1 \ldots\ldots\ldots [11]$$

where $\phi = (\phi_1, \phi_2)$, and the operator $N \equiv L_{ki}^{-1}M_{ij}$. Let $\psi_0(\zeta)$ denote the initial trial function, selected so as to satisfy Equations [9]. Determine ψ_1 from the equation $\psi_1(\zeta) = \lambda_{11}^2 N\psi_0$, where λ_{11}^2 is determined from the equation $\psi_0(1) = \psi_1(1)$. The first approximations to ϕ^1 and λ_1^2 are given by $\psi_1(\zeta)$ and λ_{11}^2, respectively. The function ψ_2 is next obtained from the relation $\psi_2(\zeta) = \lambda_{12}^2 N\psi_1$, and λ_{12}^2 from $\psi_2(1) = \psi_1(1)$. Continuing in this manner we find $\psi_p(\zeta) = \lambda_{1p}^2 N\psi_{(p-1)}$ where λ_{1p}^2 is obtained by means of $\psi_p(1) = \psi_{p-1}(1)$. It can be shown that

$$\lim_{p\to\infty} \psi_p(\zeta) = \phi^{(1)}(\zeta), \qquad \lim_{p\to\infty} \lambda_{1p}^2 = \lambda_1^2$$

While the process becomes tedious for $p > 2$, it is not difficult to carry out. Only one iteration was used in this paper.

Equations [8] and [9] show that if there is no coupling the procedure just described separates into two independent ones.

If α is set equal to zero in Equations [8] and [9], we find that an approximate expression for the first lateral angular frequency, ω_{1L}, can be found on eliminating the constants C_1 and C_2 from the equations

$$\left.\begin{aligned} \left(\frac{d^3\sigma}{d\zeta^3}\right)_1 = 0, \quad \left(\frac{d^3\sigma}{d\zeta^3} + M_1\lambda^2\frac{d\sigma}{d\zeta}\right)_1 = 0 \\ \sigma(1) = 6 - d_1 + d_2 \end{aligned}\right\} \ldots\ldots [12]$$

where

$$\sigma = C_1\frac{\zeta^3}{6} + C_2\frac{\zeta^2}{2} + \lambda^2\sum_{k=4}^{8}\Lambda_k\zeta^k$$

$$\lambda^2 = \frac{ml^4\omega_{1L}^2}{B_1}$$

$$-2\Lambda_4 = M_1 - n^2\left(R_0 + \frac{1}{2}\right)$$

$$-20\Lambda_5 = 4n^2R_0 - d_1\left[M_1 - n^2\left(R_0 + \frac{1}{2}\right)\right]$$

$$60\Lambda_6 = 1 - 2n^2 + \frac{3n^2d_1R_0}{2} - 2d_2\left[M_1 - n^2\left(R_0 + \frac{1}{2}\right)\right]$$

$$210\Lambda_7 = \frac{d_1(5n^2 - 1)}{4} - 4n^2d_2R_0$$

$$1680\Lambda_8 = d_2(1 - 9n^2)$$

$$d_1 = \frac{8(3 - M_1\lambda^2)}{6 - M_1\lambda^2}, \qquad d_2 = \frac{6 - 3M_1\lambda^2}{6 - M_1\lambda^2}$$

and the first torsional angular natural frequency ω_{1T} is approximately determined by

$$\omega_{1T} = 1.580\{C/I_3l^2\}^{\frac{1}{2}}\{1 - n^2(25R_0/16 + 1 - p_2 + p_1)\}^{-\frac{1}{2}} \ldots [13]$$

As was noted earlier, the two types of motion are not coupled in this case.

When $\alpha = \pi/2$, the torsional and lateral vibrations are coupled. To observe the influence on frequency of the various factors, we consider three cases. First, assume $M_1 = 0$; this also destroys the coupling. Then, from the appropriate forms of Equations [8] and [9], we find that

$$\omega_{1L} = 3.493\{B/ml^4\}^{\frac{1}{2}}\{1 - n^2(1.196 + 1.569R_0)\}^{-\frac{1}{2}} \ldots [14]$$

and

$$\omega_{1T} = 1.580\{C/I_3l^2\}^{\frac{1}{2}}\{1 - n^2(25R_0/16 + 1)\}^{-\frac{1}{2}} \ldots [15]$$

If we next take $M_1 \neq 0$ and simply ignore coupling, ω_{1L} is found from the equation which results on eliminating C_1 and C_2 from

$$\left.\begin{aligned} \left(\frac{d\sigma}{d\zeta}\right)_1 = 0, \quad \left(\frac{d^3\sigma}{d\zeta^3} + \lambda^2M_1(1 + n^2)\frac{d\sigma}{d\zeta}\right)_1 = 0 \\ 6 - g_1 + g_2 = \sigma(1) \end{aligned}\right\} \ldots [16]$$

where

$$\left.\begin{aligned} \sigma(\zeta) = C_1\frac{\zeta^3}{6} + C_2\frac{\zeta^2}{2} + \lambda^2\sum_{k=4}^{8}\pi_k\zeta^k \\ -2\pi_4 = M_1(1 + n^2) - n^2\left(R_0 + \frac{1}{2}\right) \\ -20\pi_5 = 4n^2R_0 - g_1\left[M_1(1 + n^2) - n^2\left(R_0 + \frac{1}{2}\right)\right] \\ 60\pi_6 = 1 - 3n^2 + \frac{3n^2g_1R_0}{2} \\ \qquad - 2g_2\left[M_1(1 + n^2) - n^2\left(R_0 + \frac{1}{2}\right)\right] \\ 210\pi_7 = \frac{6n^2 - 1}{4}g_1 - 4n^2g_2R_0 \\ 1680\pi_8 = g_2(1 - 10n^2) \\ g_1 = \frac{8\{3 - M_1(1 + n^2)\lambda^2\}}{6 - M_1(1 + n^2)\lambda^2} \\ g_2 = \frac{6 - 3M_1(1 + n^2)\lambda^2}{6 - M_1(1 + n^2)\lambda^2} \end{aligned}\right\} \ldots [17]$$

and

$$\omega_{1T} = 1.580\{C/I_3l^2\}^{\frac{1}{2}}\{1 - n^2(25R_0/16 + 1 + p_2 - p_1)\}^{-\frac{1}{2}} \ldots [18]$$

Finally, if $M_1 \neq 0$ and coupling is not ignored, the elimination of C_1, C_2, D, and K from the equations

$$\left.\begin{aligned} \left(\frac{d^2\sigma}{d\zeta^2}\right)_1 = 0, \quad \left\{\frac{d^3\sigma}{d\zeta^3} + M_1\lambda^2(1 + n^2)\frac{d\sigma}{d\zeta} - \kappa K\lambda^2\right\} = 0 \\ 6 - g_1' + g_2' = \sigma(1) \\ \left(\frac{d\theta}{d\zeta}\right)_1 = 0, \qquad 2\kappa = \theta(1) \end{aligned}\right\} \ldots [19]$$

where

$$\sigma(\zeta) = C_1\frac{\zeta^3}{6} + C_2\frac{\zeta^2}{2} + \lambda^2\sum_{k=4}^{8}\pi_k\zeta^k + \kappa K\lambda^2\left(\frac{\zeta^4}{8} - \frac{\zeta^6}{120}\right)$$

$$\left\{1 - M_2Sn^2\lambda^2\left[R_0(\zeta - 1) + \frac{\zeta^2 - 1}{2}\right]\right\}\theta(\zeta)$$

$$= KS\lambda^2\left\{2\zeta^3 - \frac{g_1'}{4}\zeta^4 + \frac{g_2'}{5}\zeta^5\right\} + D\zeta$$

$$-\kappa M_2Sn^2\lambda^2\left(\frac{3R_0\zeta^2}{2} + \zeta^3 - \frac{R_0\zeta^4}{4} - \frac{\zeta^5}{5}\right)$$

$$-\kappa M_2S[1 - n^2(p_2 - p_1)]\lambda^2\left(\frac{\zeta^2}{2} - \frac{\zeta^3}{20}\right)$$

$$S = B_1/C, \qquad K = 2nM_1$$

$$g_1' = \frac{2\{12 - 4M_1(1 + n^2)\lambda^2 + \kappa K\lambda^2\}}{6 - M_1(1 + n^2)\lambda^2}$$

$$g_2' = \frac{6 - 3M_1(1 + n^2)\lambda^2 + \kappa K\lambda^2}{6 - M_1(1 + n^2)\lambda^2}$$

and g_1 and g_2 in π_k of Equation [15] are replaced by g_1' and g_2', respectively, yields an algebraic equation for the determination of ω_1.

Discussion

Fig. 2 shows the influence of the angular velocity Ω on the first torsional natural frequency for $\alpha = 0$, and $\alpha = \pi/2$ with coupling ignored. Equations [13] and [18] were used and the values of the constants selected to correspond to a fairly stubby blade. The solid curves refer to the cases in which the influence of axial load and rate of change of angular momentum of section due to rotation are included. The dashed curves refer to the cases in which the influence of axial load is ignored; i.e., in Equations [13] and [18] the term $25R_0/16 + 1$ in the denominator is removed, while the influence of the rate of change of angular momentum is retained. The horizontal solid line gives the first torsional frequency as usually computed.

Referring to the dashed curves, the most striking feature is the decline in ω_{1T} with increasing Ω when $\alpha = 0$. Examination of Equation [13] for this case shows that this unusual result is due to the presence of inertia couples not ordinarily included in a torsional, vibration analysis, and these couples act to reduce the torsional stiffness. When $\alpha = \pi/2$, the couples have opposite signs, and hence act to increase the stiffness as shown. Both of the solid curves increase with increasing Ω, since the stiffening effect due to axial load dominates the inertia effect.

The influence of α on ω_{1T} for the solid curves is fairly substantial, the difference amounting to approximately 12 per cent of the lower value when $2\Omega = (\omega_{1T})_{\text{static}}$. This difference is of the same order of magnitude as that occurring in lateral vibration, Fig. 3, for the same cases.

A comparison between Equations [15] and [18] (both have $\alpha = \pi/2$) shows that ω_{1T} with rate of change of angular momentum of section due to rotation included is approximately 6 per cent larger than the ω_{1T} with this factor excluded at $2\Omega = (\omega_{1T})_{\text{static}}$.

Numerical results for other values of beam constants, within the assumption that the bending stiffness in one principal direction is much larger than in the other, can readily be found from Equations [13], [15], and [18].

In this paper, no allowance has been made for the influence of root restraint on the torsional stiffness although this factor must be important in short stubby beams.

The curves in Fig. 3 show the influence of α on the first lateral natural frequency, ω_{1L}, for $M_1 = 0.015$, $M_1 = 0.025$, and with coupling ignored; Equations [12] and [16] were used. As is well known (4), ω_{1L} for $\alpha = 0$ rises less rapidly with Ω than it does with $\alpha = \pi/2$, the difference on a percentage basis being somewhat less than that occurring in ω_{1T}, see Fig. 2, at the comparable

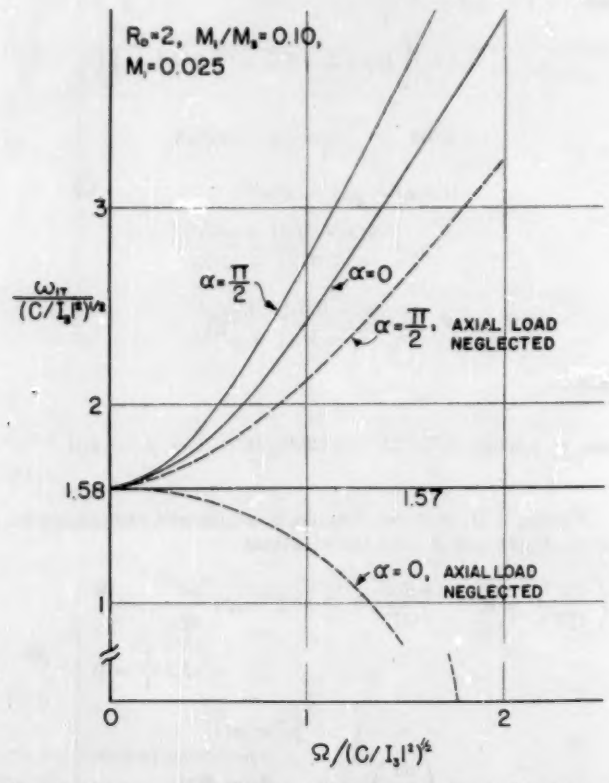

Fig. 2 Influence of Angular Setting on First Torsional Natural Frequency

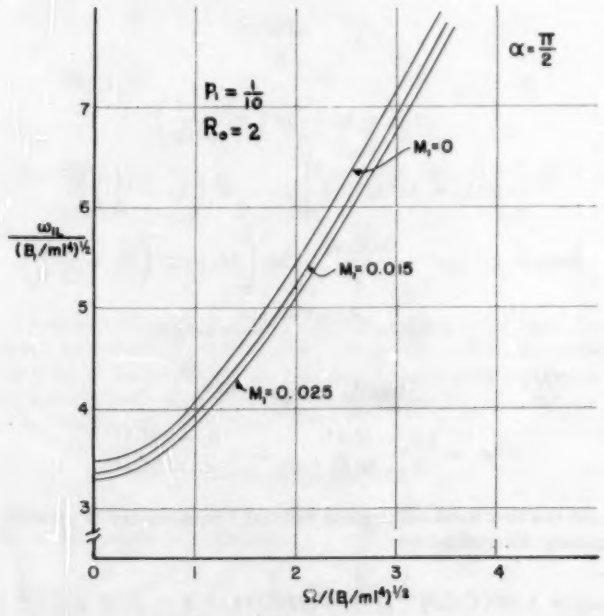

Fig. 3 Influence of M_1 on First Lateral Natural Frequency

dimensionless rotative speed. The curve of ω_{1L} versus Ω for $M_1 = 0$, $\alpha = \pi/2$, Equation [14], is given in Fig. 4. At $\Omega = 0$, $\omega_{1L} = 3.493 \{B_1/ml^4\}^{1/2}$ which is slightly below the exact value of $3.515 \{B_1/ml^4\}^{1/2}$, whereas in the case of ω_{1T}, the approximate value is slightly greater than the exact one. Thus the method used may give either high or low approximations to the exact

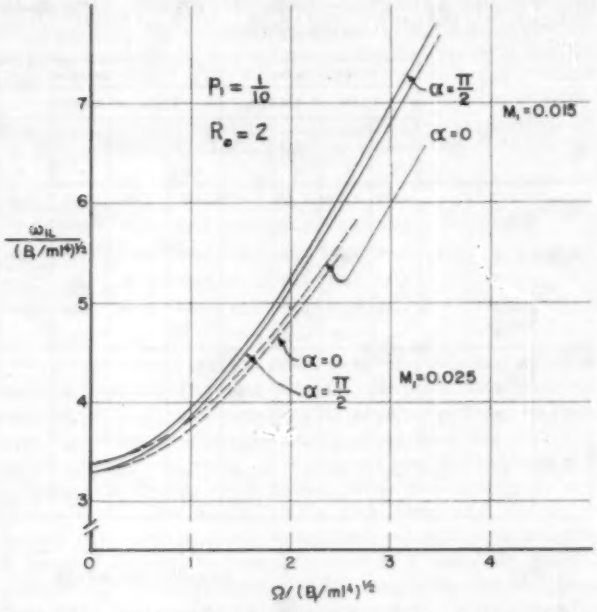

FIG. 4 INFLUENCE OF ANGULAR SETTING ON FIRST LATERAL NATURAL FREQUENCY

frequencies (11). We also see from Fig. 4 that difference between ω_{1L} with $M_1 = 0$ and ω_{1L} with $M_1 \neq 0$ and coupling ignored is only slightly influenced by Ω.

The data in the first row of Table 1 were obtained from Equation [19] with $M_1 = 0.025$, $S = 1$, $R = 2$, $p = 0.10$. A comparison of results when coupling is ignored (second row of table) indicates that even for a beam having these unusual physical constants, the influence of coupling is quite small. Hence, when dealing with the more conventional type beam, this coupling can be ignored without undue error in calculations involving the fundamental natural frequency.

TABLE 1 DATA FROM EQUATION [19]

$M_1 = 0.025$, $S = 1$

	n						
	0	0.08	0.16	0.24	0.32	0.40	0.46
ω_1 coupled	3.304	3.343	3.472	3.725	4.197	5.211	7.489
ω_{1L} uncoupled	3.304	3.344	3.476	3.736	4.223	5.284	7.794

NOTE: In Equation [4] and the preceding expression, A is the area of the cross section and J is the second moment of A about $\bar{u}_3$. For a solid cross section $mJ/A = I_3$.

BIBLIOGRAPHY

1 "Steam and Gas Turbines," by A. Stodola, translated by L. C. Loewenstein, Peter Smith, New York, N. Y., 1945, section 195.

2 "Vibration Problems in Engineering," by S. Timoshenko, D. Van Nostrand Company, Inc., New York, N. Y., second edition, 1937, section 64.

3 "Technische Dynamik," by C. B. Biezeno and R. Grammel, Julius Springer, Berlin, Germany, second edition, 1953, chapter 9.

4 "Bending Vibration of a Rotating Blade Vibrating in the Plane of Rotation," by R. L. Sutherland, JOURNAL OF APPLIED MECHANICS, Trans. ASME, vol. 71, 1949, pp. 389–394.

5 "The Vibration of Rotating, Tapered-Twisted Beams," by G. W. Jarrett and P. C. Warner, JOURNAL OF APPLIED MECHANICS, Trans. ASME, vol. 75, 1953, pp. 381–389.

6 "Free and Forced Vibrations of Rotating Blades," by R. Plunkett, *Journal of the Aeronautical Sciences*, vol. 18, no. 4, 1951, pp. 278–282.

7 "Elastic Torsion in the Presence of Initial Axial Stress," by J. N. Goodier, JOURNAL OF APPLIED MECHANICS, Trans. ASME, vol. 72, 1950, pp. 383–387.

8 "The Effect of Initial Twist on the Torsional Rigidity of Thin Prismatical Bars and Tubular Members," by Chen Chu, Proceedings of the First U. S. National Congress on Applied Mechanics, 1951, p. 265.

9 "Methods of Theoretical Physics," by P. M. Morse and H. Feshback, McGraw-Hill Book Company, Inc., New York, N. Y., part 2, 1953, chapter 9.

10 "Eigenwertprobleme," by L. Collatz, Chelsea Publishing Company, New York, N. Y., 1945, p. 116.

11 "The Computation of Characteristic Numbers and Characteristic Functions," by G. Temple, Proceedings of the London Mathematical Society, series 2, vol. 29, 1928–1929, p. 257.

12 "Mathematical Methods in Engineering," by T. von Karman and M. A. Biot, McGraw-Hill Book Company, Inc., New York, N. Y., 1940, p. 313.

Discussion

Prediction and Evaluation of Sensitivity to Transient Accelerations[1]

S. A. Granström.[2] The author has pointed out clearly the advantages of using "damage-sensitivity curves" for describing the response of structural systems under dynamic loads of different duration. On the basis of the writer's experience—structural engineering in connection with air-blast loads—he will confirm the author's statement. In order to make a certain design problem easier to handle, the writer some years ago developed a method of presenting data[3] which is surprisingly similar to that of the author. The characteristics which were called "damage curves" were represented graphically in a two-dimensional diagram with the axes "impulse" (corresponding to the author's "velocity change") and "maximum pressure" (where the author has used instead the "average acceleration"). The damage curves have been applied both to elastic and plastic systems. As our experience has been quite promising, some additional information and some comments to the author's paper may be of interest.

The author has presented the damage-sensitivity curves mainly as rather sharp set-square lines or sketched curved lines. It is true that the curves will approach their asymptotes rather rapidly in a log-log representation. There is, however, a question of ten powers until the deviation is of the magnitude of a few per cent or less and—at least in structural design—the actual values have a tendency to fall in the nonasymptotic region. The writer has found it worth while to calculate the shape of damage-sensitivity curves with about 1 per cent accuracy by solving the differential equations for the movements of undamped systems with one degree of freedom, see Table 1 and Figs. 1(*a*) and 1(*b*). The calculations cover four different types of load-time curves and two types of resistance-displacement relations for each, namely, pure elastic behavior and pure plastic behavior. The load-time curves described are: (*a*) Sudden rise and exponential fall off, (*b*) sudden rise and linear fall off, (*c*) step function, (*d*) gradual rise, smooth maximum, and return to zero as tangent to the zero line

$$\frac{p}{P} = \frac{27}{4}\frac{t}{T_1}\left(1 - \frac{t}{T_1}\right)^2$$

The results preferably can be discussed in connection with Figs. 1(*a*) and 1(*b*).

It is striking to see how similar the curves are for the elastic and the plastic systems. With the exception of type (*d*) the main difference consists in the fact that the curves in the plastic case are slightly farther from the asymptotes than in the elastic case. For type (*d*) there is a clear difference between the asymptotic value of the *P*-ratio in the plastic case, where this value is for all the types equal to 1, and in the elastic case where

[1] By M. Kornhauser, published in the December, 1954, issue of the Journal of Applied Mechanics, Trans. ASME, vol. 76, pp. 371–380.

[2] Swedish Fortification Board, Research Department, Stockholm, Sweden.

[3] "Design Method for Plates and Beams under the Action of Air Blast Loads Causing Considerable Plastic Deflection" (in Swedish), by S. A. Granström, Swedish Fortification Board, Research Department, Stockholm, Sweden, Report No. 103:9, May, 1953.

TABLE 1 REFERENCE VALUES FOR DAMAGE-SENSITIVITY CURVES. ONE-DEGREE-OF-FREEDOM SYSTEMS WITH ELASTIC AND WITH PLASTIC BEHAVIOR. FOUR TYPES OF LOAD-TIME CURVES

			Elastic Behavior				Plastic Behavior			
			Types of loading				Types of loading			
			a	b	c	d	a	b	c	d
P/P_c	100	I/I_c	1.00	1.00	1.00	1.00	1.01	1.01	1.01	1.01
	10		1.03	1.01	1.00	1.00	1.11	1.07	1.05	1.07
	5		1.08	1.02	1.01	1.01	1.28	1.17	1.12	1.17
	3		1.25	1.05	1.02	1.03	1.63	1.34	1.22	1.33
	2		1.60	1.16	1.05	1.07	2.49	1.73	1.41	1.65
	1.5		--	1.49	1.10	1.17	--	--	--	--
I/I_c	1.5	P/P_c	--	1.49	1.01	1.17	--	--	--	--
	2		1.65	1.30	1	1.10	2.37	1.77	1.33	1.65
	3		1.35	1.16	1	1.13	1.78	1.45	1.12	1.33
	5		1.19	1.09	1	1.28	1.45	1.27	1.04	1.17
	10		1.09	1.04	1	1.63	1.24	1.15	1.01	1.08
	100		1.01	1.00	1	1.90	1.09	1.03	1.00	1.01

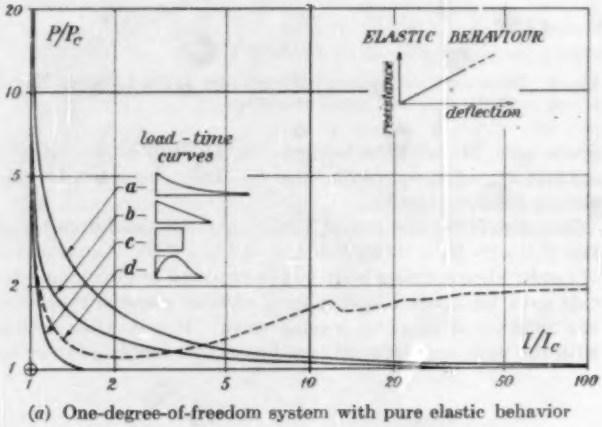

(*a*) One-degree-of-freedom system with pure elastic behavior

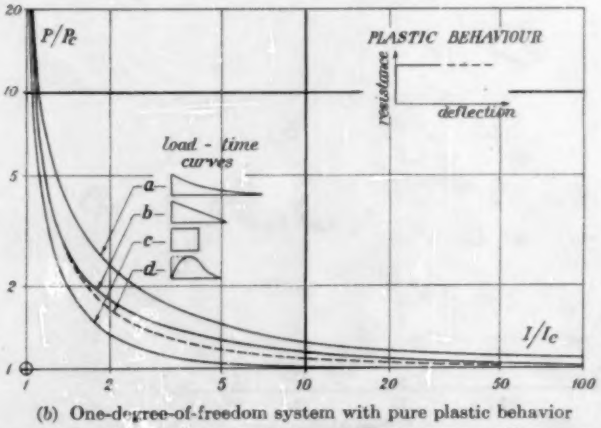

(*b*) One-degree-of-freedom system with pure plastic behavior

FIG. 1 DAMAGE-SENSITIVITY CURVES IN DIMENSIONLESS PRESENTATION. FOUR TYPES OF LOAD-TIME CURVES

this value for type (d) is equal to 2. This fact will be understood fully when considering the definitions in what follows.

The broken shape of the type (d) curve in Fig. 1(a) is due to the fact that the maximum displacement for this type does not occur continuously in the first swing (which is the case for all the other types with sudden pressure rise) but moves over from the first swing to the second swing and then to the third swing and so on as the duration increases. In this connection it may be noted that, in the author's Fig. 8(d), the sensitivity curve has some periodic property which should not be there (cf Fig. 1a, type b) of this discussion).

TABLE 2 CHARACTERISTIC VALUES FOR ONE-DEGREE-OF FREEDOM SYSTEMS WITH ELASTIC AND WITH PLASTIC BEHAVIOR

		Elastic behavior	Plastic behavior
Characteristic Pressure load	P_c	$\frac{1}{2} K_y$	K
Characteristic Impulsive load	I_c	$\sqrt{K_y M y}$	$\sqrt{2}\sqrt{K M y}$
Characteristic Time length	$T_c \left(= \frac{I_c}{P_c}\right)$	$2\sqrt{\frac{M}{K_y/y}} \left(= \frac{T}{\pi}\right)$	$\sqrt{2}\sqrt{\frac{M}{K/y}}$

To get the general problem under control it has been convenient to define three "characteristic values." These are "characteristic pressure load," P_c = external load in the shape of a step function of unlimited length which gives a certain displacement y; "characteristic impulsive load," I_c = external load in the shape of a zero-duration impulse which gives a certain displacement y; and "characteristic time length," T_c = ratio between I_c and P_c as defined. The method of calculating these values is given in Table 2, where M denotes the mass of the system, K means the internal yield force in the plastic system, and K_y means the internal spring force at the displacement y in the elastic system. K_y/y is equal to the ordinarily used spring constant k. Comments may be made as follows:

Concerning P_c. The multiplication factor $^1/_2$ connected with K_y is due to the elastic overswing. In the plastic case no such overswing exists, as the maximum resistance is supposed to act without any previous displacement. In the case of slowly rising load curves there will be no overswing even in an elastic system. This is the reason why the type (d) curve has a pressure asymptote with value 2 when the duration approaches infinity, Fig. 2(a). The comparisons refer here always to the maximum load values. This decision seems to give advantages compared with the author's mean values, at least for structural design, as the ultimate loads, and so on, are chiefly connected with the maximum values, not the mean values.

Concerning I_c. The similarity between the expressions for the elastic and the plastic cases is notable. However, it is to be observed that, in the plastic case, K has a certain constant value but in the elastic case K_y is proportional to the deflection y and constant only for a certain y. It is possible and not too complicated to find the characteristic values of both I_c and P_c, as well for all the intermediate cases of resistance-displacement curves with one pure elastic part followed by one pure plastic part by means of energy considerations.[3]

Concerning T_c. For the elastic case the value T_c is closely related to the natural period T. As the deflection time (the time from equilibrium to maximum deflection) for an elastic one-degree-of-freedom system is, for all suddenly rising load curves, $^1/_4$ to $^1/_2$ of the natural period, the value T_c will in those cases give the magnitude of the deflection time

$$T_{1/4} = \frac{\pi}{4} T_c, \qquad T_{1/2} = \frac{\pi}{2} T_c$$

For the plastic case, T_c is the same as the deflection time for a sudden pulse. For increasing duration of load, the deflection time also will increase as far as to infinite length for the characteristic pressure case. (The relations have been calculated in the reference cited.[3])

The application of the foregoing information in an "applied" case will be illustrated by means of Figs. 2(a) and 2(b). We assume one elastic and one plastic system with the calculated values of P_{c_1} and I_{c_1} corresponding to a certain displacement y. We want to plot the curves for all related values of impulse I and maximum pressure P for step-function loads which give the deflection y. We also want the similar curves to correspond to the displacements $2y$ and $4y$. The procedure is as follows:

We start with a diagram sheet containing a log-log grid with pressure units marked along the vertical axis and impulse units marked along the horizontal axis. On this diagram sheet we also have 45-deg lines which mark the ratio between the values on the horizontal and vertical axes, and accordingly get the dimension of time. When the diagram is so prepared we plot the given values

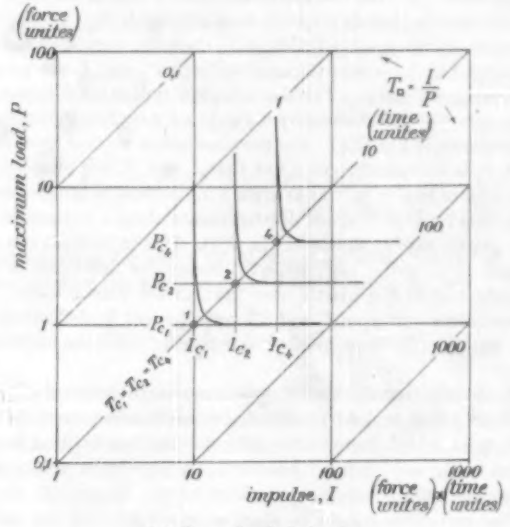

(a) Pure elastic behavior

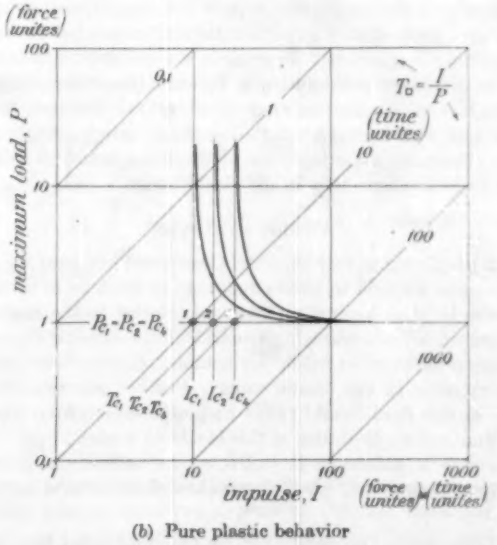

(b) Pure plastic behavior

FIG. 2 APPLICATION OF DAMAGE-SENSITIVITY CURVES TO A GIVEN SYSTEM AT THREE DIFFERENT MAGNITUDES OF DEFLECTION, y, $2y$, AND $4y$. LOAD APPLIED AS A STEP FUNCTION

of P_{c_1} and I_{c_1} along the axes and so get a "characteristic point" defined by those two co-ordinates. It is to be observed that this point could have been defined from any two of the three values P_{c_1}, I_{c_1}, and T_{c_1}. Especially for elastic systems, T_c (from the natural period) is known rather than I_c. When the characteristic point is fixed, the desired curve for simultaneous P and I values is obtained by placing the right curve (c, step function), Fig. 1, on the diagram in such a way that the intersection between $P/P_c = 1$ and $I/I_c = 1$ will fit on the characteristic point. As a multiplication is the same as a parallel translation in a logarithm diagram, there will be no change of shape of the curve, provided the curve is originally drawn to the same scale as in Fig. 2; i.e., the curve in Fig. 1 can be used as a mold.

For an arbitrary value of say I, we can now get the corresponding value of P giving the assumed deflection y. From the 45-deg line system we also get the "square-duration" $T_{\square}$, for the load in question, i.e., the duration of the actual load if transformed to a step function with the same maximum pressure and impulse as the real load. To find thereafter the corresponding curves to the displacement $2y$ and $4y$ we have to study Table 2.

For the elastic case we find that T_c does not vary with the displacement (K_y/y = const) but that both P_c and I_c are proportional to the deflection. The characteristic points for different displacements will therefore move along the 45-deg line in the elastic case as shown in Fig. 2(a). For the plastic case we find from Table 2 that P_c is independent of y but that I_c and T_c are proportional to the square root of y. That gives a movement of the characteristic points for the different displacements along a horizontal line in the plastic case as shown in Fig. 2(b). It is to be observed that the gain in carrying capacity with increasing deflection is considerably less in the plastic case than in the elastic case. The corresponding curves of P and I for the $2y$ and $4y$ deflections are easily found in the same manner as before by using the mold technique.

It is obvious that the described damage-sensitivity-curve representation is not limited to one-degree-of-freedom systems with elastic, plastic, or elastoplastic behavior but can be used in connection with any defined resistance-displacement relationship which gives a finite response to a finite input. In general, the differential equations cannot be given an exact solution but can always be solved by numerical integration. The use of the one-degree-of-freedom model for more or less complicated structures demands a great deal of experimental verification before insuring design "on the safe side." In general, one can expect the translation to the one-degree system to be satisfying, when the actual system has one dominating mode of vibration. For instance, this is the case with beams when their loadings satisfy certain conditions. From our experience the applicability seems to be rather good for beams especially in the plastic range.[4]

Author's Closure

It is gratifying to find that Dr. Granström has used the sensitivity-curve method to good advantage in the field of structural response to blast loading. Of special interest to the author are Dr. Granström's encouraging remarks on the applicability of the one-degree-of-freedom model for complex elastic structures and for structures in the plastic range. Further experimental evidence in this field should prove helpful in establishing the practical limits of applicability of this idealized model.

There is a difference in outlook (the author's approach is mainly experimental, since inertia-loaded structures are often suitable for direct experiment, with approximate formulas to be used for theoretical predictions, whereas Dr. Granström must probably depend upon design predictions) which has led to a difference in emphasis on the accuracy to be employed when working with sensitivity curves. Although the theoretical values of Fig. 8 were precisely calculated from the differential equations of motion (and the periodic property of Fig. 8(d) is also derived from careful calculation), the author purposely refrained from presenting the accurate theoretical figures, in order to help the reader avoid the temptation of applying an exact number to a physical situation which cannot be described by an accurate number.

In the author's opinion the problem of structural response to air-blast loading falls in the same category as the acceleration-loading problem, in the sense that air-blast loading curves (not the pressure-time history of the blast, but the history of the force exerted on the structure) are seldom known with precision. The structural designer should therefore attempt to design for an expected spread of pulse shapes, besides applying the usual safety factors to account for high loading amplitudes.

[4] "Approximate Design Method for Impulse-Loaded Beams With Plastic Deflection" (in Swedish), by B. Adamson, Swedish Fortification Board, Stockholm, Sweden, Technical Report No. B 12, May, 1954.

A Refinement of the Theory of Buckling Rings Under Uniform Pressure[1]

D. R. Carver.[2] The author presents a valuable contribution to the stability theory in his application of Trefftz's theory to the problem of buckling of normally and centrally loaded rings of rectangular cross sections. The results in themselves are of considerable interest and importance, and the author deserves credit for reviving and applying Trefftz's method. It is a basic tool which may be used to advantage in stability analyses of beams, columns, arches, plates, and shells.

The writer is aware of the sensitivity of buckling problems to approximations. Assumptions concerning geometry of deformations greatly affect the computed value of buckling loads and these assumptions are always open to question. But a rigorous treatment based on elasticity theory and the energy criterion of stability can hardly be questioned. The author has presented such a treatment.

C. D. Galletly[3] and R. Bart.[3] The writers wish to congratulate the author for his significant contribution to the theory of ring stability. His use of the tensor definition of strain is particularly interesting because of the light it throws on the effects of high-order terms in the strain expressions. This effect has been investigated by the writers using the following strain components

$$\left.\begin{aligned} \epsilon_r &= u_r + \frac{1}{2} v_r^2 \\ \epsilon_\theta &= \frac{u}{r} + \frac{v_\theta}{r} + \frac{1}{2}\left(\frac{u_\theta - v}{r}\right)^2 \\ \gamma_{r\theta} &= v_r + \frac{u_\theta - v}{r} + u_r\left(\frac{u_\theta - v}{r}\right) + v_r\left(\frac{u + v_\theta}{r}\right) \end{aligned}\right\} \quad \ldots [1]$$

[1] By A. P. Boresi, published in the March, 1955, issue of the Journal of Applied Mechanics, Trans. ASME, vol. 77, pp. 95–102.

[2] Head, Engineering Mechanics, Louisiana State University, Baton Rouge, La.

[3] Structural Research Engineer, David Taylor Model Basin, Navy Department, Washington, D. C.

obtained by defining strain as

$$\frac{(\text{Final length}) - (\text{original length})}{(\text{original length})}$$

It will be noted that these differ from the author's definition, Equation [1] of the paper. If the steps indicated by Equations [2] to [6] are carried out, there results, instead of Equation [6]

$$\delta^2 U = \frac{EL}{1-\nu^2}\int_0^{2\pi}\int_a^b \left\{ u_r^2 + \left[v_r^2 + \left(\frac{u_\theta - v}{r}\right)^2\right] \times \left(\frac{1-\nu}{2} + \xi_r + \frac{\xi}{r}\right) + \left(\frac{u + v_\theta}{r}\right)^2 + 2\nu u_r\left(\frac{u+v_\theta}{r}\right) + (1-\nu)v_r\left(\frac{u_\theta - v}{r}\right)\left(1 + \xi_r + \frac{\xi}{r}\right)\right\} r\, dr\, d\theta \quad [2]$$

Now, assuming that the ring buckles without shear, so that Equation [25] of the paper is satisfied, the displacements u and v become

$$\left.\begin{aligned} u &= B\cos 2\theta \\ v &= (Ar - 2B)\sin 2\theta \end{aligned}\right\} \quad [3]$$

as given by Equation [27]. With $\nu = 0$, Equation [2] of this discussion now becomes, with Equation [3], herewith and Equation [25] of the paper

$$\delta^2 U = EL\int_0^{2\pi}\int_a^b \left[\left(\frac{u+v_\theta}{r}\right)^2 + \left(\xi_r + \frac{\xi}{r}\right)\left(\frac{u_\theta - v}{r}\right)^2\right] r\, dr\, d\theta \quad [4]$$

To carry out the integration, u and v are expressed in terms of the displacements and their derivatives at the center line. Using bars to denote these special values, there follows from Equation [3]

$$\left.\begin{aligned} v &= \bar{v} + \frac{z}{R}(\bar{v} - \bar{u}_\theta) \\ u &= \bar{u} \end{aligned}\right\} \quad [5]$$

Fig. 1 shows z and R.

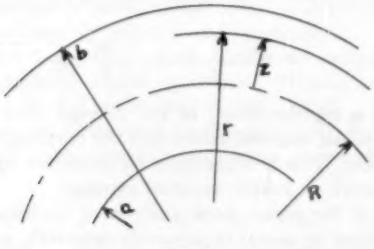

FIG. 1

Again, with $\nu = 0$, Equation [7] of the paper becomes

$$\xi = -P\left(r + \frac{a^2}{r}\right) \quad [6]$$

where

$$P = \frac{b^2 p}{E(b^2 - a^2)}$$

as given by Equation [8] with $\nu = 0$. From Equation [6] there follows

$$\xi_r + \frac{\xi}{r} = -2p \quad [7]$$

Substituting Equations [5] and [7] into [4] of this discussion, and observing from Fig. 1 that $r = R + z$, so that $dr = dz$, the limits are changed and the integration carried out across z. Setting

$$b - a = 2\lambda \quad [8]$$

there follows

$$\delta^2 U = \frac{EA}{R}\int_0^{2\pi}(\bar{u} + \bar{v}_\theta)^2 d\theta + \frac{EI}{R^2}\int_0^{2\pi}(\bar{u} + \bar{u}_{\theta\theta})^2 d\theta - pL\left[1 + \frac{2\lambda}{R} + \frac{\lambda^2}{R^2}\right]\int_0^{2\pi}(\bar{u}_\theta - \bar{v})^2 d\theta \quad [9]$$

where

$$A = L\int_{-\lambda}^{+\lambda} dz \text{ and } I = L\int_{-\lambda}^{+\lambda} z^2 dz$$

It is now desired to evaluate the second-order work. For the case of normally directed pressure, this is given by Equation [12] of the paper. Carrying out the indicated multiplication, and noting that the $\cos\theta \sin\theta$ terms vanish when integrated from 0 to 2π, Equation [12] becomes

$$\delta^2\Omega = 2pL\int_0^{2\pi}(u^2\cos^2\theta + v^2\sin^2\theta - u_\theta v\sin^2\theta + uv_\theta\cos^2\theta)d\theta \quad [10]$$

Observing from Equation [3] of this discussion that $uv_\theta = -u_\theta v$, and expanding the $\cos^2\theta$ and $\sin^2\theta$ terms, there follows

$$\delta^2\Omega = pL\int_0^{2\pi}(u^2 + v^2 - 2u_\theta v)d\theta \quad [11]$$

since the integrals of the remaining terms vanish. Since Equation [12] of the paper is defined for u and v at $r = b$, we substitute Equation [5] into Equation [11] with $z = +\lambda$ from Fig. 1, obtaining

$$\delta^2\Omega = pL\int_0^{2\pi}\left[\bar{u}^2 + \bar{v}^2 - 2\bar{u}_\theta\bar{v} + (\bar{u}_\theta - \bar{v})^2\left(\frac{2\lambda}{R} + \frac{\lambda^2}{R^2}\right)\right]d\theta \quad [12]$$

Adding Equations [9] and [12], we obtain the second variation of the total potential as

$$\delta^2 V = \frac{EA}{R}\int_0^{2\pi}(\bar{u} + \bar{v}_\theta)^2 d\theta + \frac{EI}{R^2}\int_0^{2\pi}(\bar{u} + \bar{u}_{\theta\theta})^2 d\theta - pL\int_0^{2\pi}[(\bar{u}_\theta - \bar{v})^2 - \bar{u}^2 - \bar{v}^2 + 2\bar{u}_\theta\bar{v}]d\theta \quad [13]$$

which simplifies to

$$\left.\begin{aligned} &\frac{EA}{R}\int_0^{2\pi}(\bar{u} + \bar{v}_\theta)^2 d\theta + \frac{EI}{R_2}\int_0^{2\pi}(\bar{u} + \bar{u}_{\theta\theta})^2 d\theta \\ &\qquad = pL\int_0^{2\pi}(\bar{u}_\theta^2 - \bar{u}^2)d\theta \end{aligned}\right\} \quad [14]$$

as the buckling criterion; i.e., $\delta^2 V = 0$.

Since this last equation is independent of λ, it appears that the buckling pressure does not depend on the ring thickness when the strains are defined by Equation [1] of this discussion instead of by Equation [1] of the paper.

It is also of interest to note the result obtained by von Sanden

and Tölke[4] in their study of cylindrical shells. For an infinitely long shell, they obtain the following result

$$p = \frac{\dfrac{E(2\lambda)^2}{4R^2}}{1 + \dfrac{8}{9}\dfrac{(2\lambda)^2}{R^2}} \quad \ldots\ldots [15]$$

This is their Equation [77], with $\nu = 0$, in the present notation.

The value of K_{cr} as defined in the author's Equation [33] is then obtained from Equation [15], herewith, as

$$K_{cr} = \frac{3}{1 + \dfrac{8}{9}\left(\dfrac{2}{1 + \dfrac{2a}{h}}\right)^2} \quad \ldots\ldots [16]$$

For $h/a = 0.05$, this yields $K_{cr} = 2.994$, and for $h/a = 0.10$, $K_{cr} = 2.976$. These values agree with the author's upper bounds as given in Table 1 of the paper. The writers would appreciate any comments on the results presented here.

Author's Closure

The author thanks Dr. Carver and Drs. Galletly and Bart for their comments. He agrees with Dr. Carver that Trefftz's method is a basic tool that may be used to advantage in stability analyses of structural members.

The illustration worked out by Drs. Galletly and Bart offers an interesting example of Dr. Carver's remark on the sensitivity of buckling problems to approximations. Drs. Galletly and Bart define strain as

$$\frac{\text{Final length} - \text{original length}}{\text{original length}}$$

and with this definition, they derive Equations [1] and [2] of their discussion.

However, according to classical elasticity theory, the strain-energy density is

$$V_0 = (\lambda/2 + G)J_1^2 - 2GJ_2 \quad \ldots\ldots [17]$$

In Equation [17], J_1 and J_2 are the first and second invariants of the strain tensor, defined by

$$\left.\begin{aligned} J_1 &= \epsilon_x + \epsilon_y + \epsilon_z \\ J_2 &= \epsilon_y\epsilon_z + \epsilon_z\epsilon_x + \epsilon_x\epsilon_y - (1/2)\gamma_{yz}^2 \\ &\quad - (1/2)\gamma_{zx}^2 - (1/2)\gamma_{xy}^2 \end{aligned}\right\} \quad \ldots [18]$$

in which

$$\begin{pmatrix} \epsilon_x & (1/2)\gamma_{xy} & (1/2)\gamma_{xz} \\ (1/2)\gamma_{yx} & \epsilon_y & (1/2)\gamma_{yz} \\ (1/2)\gamma_{zx} & (1/2)\gamma_{zy} & \epsilon_z \end{pmatrix} \quad \ldots\ldots [19]$$

is the classical strain tensor, defined by[5] (in cylindrical co-ordinates)

$$\left.\begin{aligned} \epsilon_x &= u_x + (1/2)(u_x^2 + v_x^2 + w_x^2) \\ \epsilon_\theta &= (v_\theta + w)/r + (1/2)[(u_\theta/r)^2 \\ &\quad + (v_\theta + w)^2/r^2 + (w_\theta - v)^2/r^2] \\ \epsilon_r &= w_r + (1/2)(u_r^2 + v_r^2 + w_r^2) \\ \gamma_{\theta r} &= (w_\theta - v)/r + v_r + (u_\theta/r)u_r \\ &\quad + \frac{(v_\theta + w)}{r}(v_r) + \frac{(w_\theta - v)(w_r)}{r} \\ \gamma_{rx} &= w_x + u_r + u_x u_r + v_x v_r + w_x w_r \\ \gamma_{x\theta} &= v_x + u_\theta/r + u_x(u_\theta/r) \\ &\quad + v_x(v_\theta + w)/r + w_x(w_\theta - v)/r \end{aligned}\right\} \quad \ldots [20]$$

where r, θ, x subscripts on u, v, w denote derivatives with respect to r, θ, x.

This is the definition of strain-energy density, Equations [17] to [20], that the author used; a definition of strain was not introduced. However, the definition of strain has no intrinsic importance; the essential things are the definition of the strain tensor, Equation [19], and the fact that the strain-energy density, Equation [20], is invariant. It is noteworthy, that by using Equation [1] of their discussion, Drs. Galletly and Bart arrive at a strain-energy density which is not invariant.

It is satisfying to note that the author's results agree with the results obtained by von Sanden and Tölke.

The Stress Problem of Vibrating Compressor Blades[1]

R. A. Arnoldi.[2] The author has presented a useful and interesting analytic representation of the aerodynamic forces acting on a stalled, vibrating airfoil. His work forms a framework for correlation of experimental data on stall flutter.

The assumption of classical (unstalled) damping forces seems perhaps an unnecessary refinement on the idealized parallelograms of the author's hysteresis loops. In the case of translational motion, the dependence of momentary angle of attack on oscillatory velocity provides a phase-lag and, consequently, a dissipative mechanism which one might expect to overshadow any classical dissipative forces. In the case of pitching, the definition of instantaneous angle of attack is a knotty question; one possible solution is the assumption of an effective angle of attack

$$\alpha_{\text{effective}} = \alpha - \frac{\dot{\alpha}b'}{V} \quad \ldots\ldots [1]$$

where b' is a representation of the average time lag between changes in actual angle of attack and the resulting effect on the airfoil surface. This is admittedly an imperfect representation, but might serve an initial empirical attempt.

The use of the phase-plane analysis of nonlinear mechanics may be avoided by means of an energy approach, providing that the inertial and elastic forces are sufficiently large to permit the assumption of harmonic motion. (This should apply well to the case of compressor blades.) If the angle of attack is represented by

$$\alpha = \alpha_0 \sin \omega t \quad \ldots\ldots [2]$$

and the hysteresis loop of Figs. 6 and 7 by

$$C = \mp \frac{C^*}{2} + \frac{dC}{d\alpha}\alpha \quad \ldots\ldots [3]$$

---

[4] "Über Stabilitätsprobleme Dünner, Kreiszylindrischer Schalen," by K. von Sanden and F. Tölke, Ingenieur-Archiv, vol. 3, 1932, pp. 24–66; also DTMB translation no. 33.

[5] "The Mathematical Theory of Elasticity," by A. E. H. Love, Cambridge University Press, fourth edition, 1934, Appendix to Chapter I, pp. 59–60; also, "Foundations of Nonlinear Theory of Elasticity," by Z. V. Novozhilov, Graylock Press, Rochester, N. Y., 1953.

[1] By Jan R. Schnittger, published in the March, 1955, issue of the Journal of Applied Mechanics, Trans. ASME, vol. 77, pp. 57–64.

[2] United Aircraft Corporation, East Hartford, Conn.

the energy loss per cycle may be evaluated by simple integrations, yielding the amplitude of the limit cycle. Equation [3] of this discussion is subject to the conditions that the minus sign applies when $\omega t_R < \omega t < \pi + \omega t_R$ and the plus sign when $\pi + \omega t_R < \omega t < 2\pi + \omega t_R$ where

$$(\alpha_1 - \alpha_2)/2 = \alpha_0 \sin \omega t_R \quad [4]$$

and the origin $C = 0$, $\alpha = 0$ has been shifted to the geometric center of the hysteresis loop.

This provides a more convenient computational procedure than that of phase-plane analysis, and lends itself readily to the inclusion of internal-friction damping in the blades. The concept of logarithmic damping discussed by the author may be replaced more accurately by an energy loss per cycle taken to be proportional to a power of the oscillation amplitude. The value of this power has recently been found to be quite large for high stress levels and temperatures. Accordingly, it is quite conceivable that internal friction may play a much greater part in limiting the amplitude of stall flutter than the use of logarithmic damping would show.

F. Sisto.[3] The author is to be congratulated for having codified, and put on a common basis, a variety of blade-excitation phenomena. It is interesting to note that none of the "stress functions" of this paper are very strong functions of the reduced frequency for the practical range of this parameter. Consequently, once the mechanism of excitation has been established in a particular instance, the maximum vibratory stress to be expected is fairly well determined (within the other requirements of the stress formulation).

The conclusion that "there are in quite a few situations no objections to the construction of slender blades" is significant. A somewhat similar conclusion was reached independently by Pearson.[4] In this reference important provisos are added: (*a*) The thicker the blades the more important material damping becomes (stall-flutter self-oscillation); and (*b*) nonresonant stresses are lower in blades of higher strength (forced vibrations). (It must be realized that the near-resonant condition, in contradistinction to precise resonance, is also of extreme practical importance.) The second proviso is contained, in substance, in Figs. 4 and 5 of the paper, so that there is unanimity of opinion on this point. This unanimity is significant since Pearson deals exclusively with quasi-steady aerodynamic forces, whereas the author has taken into account the effect of wake vortexes.

To extend this comparison a little further we confine the discussion to the bending degree of freedom. This is usually the troublesome degree of freedom in practice. Dealing first with forced vibrations, the quasi-steady approach, for example, yields a value for F_β of unity; the author's values are reproduced as follows:

k_h	0.1	0.2	0.5	1.0
F_β	1.01	1.00	0.88	0.70

These numbers imply that the quasi-steady approach gives roughly correct answers in the practical range of reduced frequency (0.1 to 0.5.) This is particularly so since any phase lag between the quasi-steady incidence and the aerodynamic reactions (the result of considering wake vortexes) is of secondary importance for a single degree of freedom as compared, for instance, to coupled bending-torsion motion. In the latter case a small change in the phase of the coupling terms may account[5] for the onset of flutter.

The quasi-steady method may be illustrated by the following example which leads to an interesting result. Except where redefined the notation is the same as the author's. Considering the case of the variations in air velocity

$$v = v_0 + dv = v_0(1 + \sigma \sin \omega t) \quad [5]$$

we expand the aerodynamic normal force, F (assumed to be an analytic function only of v and $\dot{h}$, the airfoil velocity) in Taylor series about $v = v_0$, $\dot{h} = 0$

$$F(v, \dot{h}) = F(v_0, 0) + F_v(v - v_0) + F_{\dot{h}}\dot{h} + {}^1/_2F_{vv}(v - v_0)^2 + F_{v\dot{h}}(v - v_0)\dot{h} + {}^1/_2F_{\dot{h}\dot{h}}\dot{h}^2 + \ldots \quad [6]$$

The essence of the quasi-steady approach is contained in this initial assumption of functional dependence, and in the adequacy of a normal force-coefficient representation

$$F = {}^1/_2\rho v^2 c C_F \quad [7]$$

For the linear portion of the normal force curve we have

$$C_F = \frac{dC_F}{d\alpha}\alpha = \frac{dC_F}{d\alpha}\left(\alpha_i + \frac{\dot{h}}{v}\right) \quad [8]$$

were α_i is the mean value of the angle of attack. Combining Equations [7] and [8] we obtain

$$F = {}^1/_2\rho c \frac{dC_F}{d\alpha}(\alpha_i v^2 + \dot{h}v) \quad [9]$$

Forming the partial derivatives indicated in Equation [6] and inserting therein yields the expression[6]

$$F = 1/2\rho c \frac{dC_F}{d\alpha}[\alpha_i v_0^2(1 + 2\sigma \sin \omega t + \sigma^2 \sin^2 \omega t) + \dot{h}v_0(1 + \sigma \sin \omega t)] \quad [10]$$

Applying this aerodynamic force to the simple mass-spring equation

$$m\ddot{h} + m\omega_h^2 h = F$$

we obtain, after some rearrangement

$$\ddot{h} + \frac{(2 - \epsilon)\kappa\omega_h}{k_h}(1 + \sigma \sin \omega t)\dot{h} + \omega_h^2 h = -\frac{F}{m}(1 + 2\sigma \sin \omega t + \sigma^2 \sin^2 \omega t) \quad [11]$$

where

$$\left.\begin{aligned} F &= -1/2\rho v_0^2 c \frac{dC_F}{d\alpha}\alpha_i \\ k_h &= \omega_h b/v_0 \\ \frac{dC_F}{d\alpha} &= -(2 - \epsilon)\pi \\ \kappa &= \pi\rho b^2/m \end{aligned}\right\} \quad [12]$$

Equation [11] is linear with periodic coefficients. The homo-

[3] Research Division, Wright Aeronautical Division, Curtiss-Wright Corporation, Wood-Ridge, N. J.

[4] "The Aerodynamics of Compressor Blade Vibrations," by H. Pearson, Proceedings of Fourth Anglo-American Aeronautical Conference, 1953.

[5] "Experimental Aerodynamic Derivatives of a Sinusoidally Oscillating Airfoil in Two-Dimensional Flow," by R. L. Halfman, NACA TN 2465, November, 1951.

[6] For the particular case of a linear normal force coefficient this result can be arrived at more simply by substituting Equation [5] directly in Equation [9].

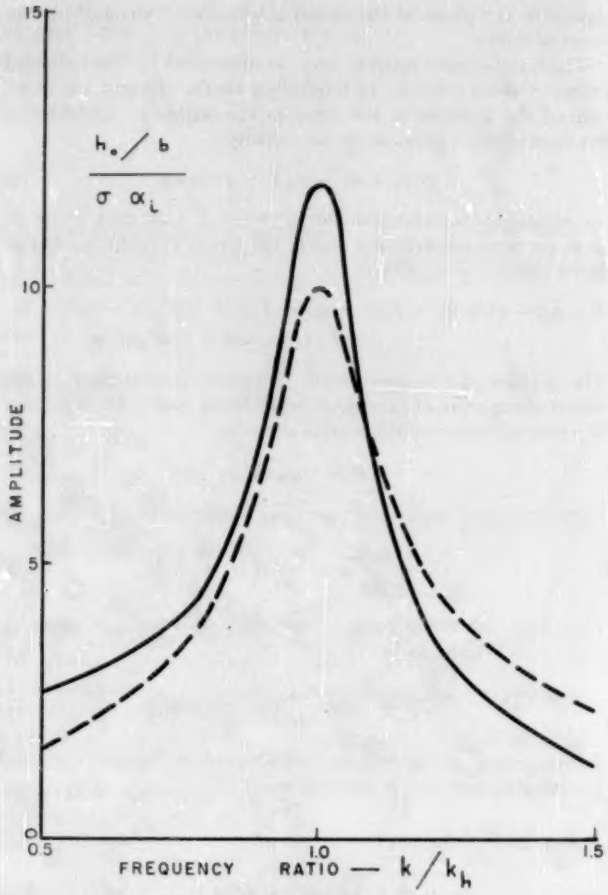

FIG. 1 AMPLITUDE OF FORCED VIBRATION, f_σ, for $\kappa = 0.02$ and $k = 0.2$.
(Author's values, solid line; quasi-steady values, dotted line.)

geneous equation may be put in the form of a Hill equation by a suitable transformation,[7] and once the homogeneous solution is known the particular integral of the original equation may be determined. Depending on the phase of the "ripple" in the periodic coefficient with respect to the free oscillation of the system, it is known[8] that the homogeneous equation may exhibit "self-excitation." Permissible frequency values for so-called "heteroparametric" self-excitation are

$$\frac{\omega_h}{\omega} = 1/2, 3/2, 5/2, \ldots;$$

$$1/4, 3/4, 5/4, \ldots; 1/6, 3/6, 5/6, \ldots, \text{etc.}$$

A further study of this equation (and others of similar type which arise in the problem of vibrating compressor blades), including the forcing terms, should prove interesting in demonstrating possible subharmonic resonances.

The quasi-steady counterpart of the function f_σ can be calculated from Equation [11] by ignoring the ripple in the damping term and suppressing the constant and second harmonic parts of the forcing term. The resulting equation gives, by conventional methods,[9] the response relation

$$\frac{h_0}{b} = \frac{2/k_h}{\sqrt{1 + [k_h(\nu - 1/\nu)/2\kappa]^2}}$$

where $\nu = k/k_h$. Precisely at resonance we have

$$\frac{h_0}{b} = f_\sigma = 2/k_h$$

or

$$F_\sigma = 2$$

The response curve for $\kappa = 0.02$ and $k_h = 0.2$ is plotted in Fig. 1 of this discussion, for comparison with the author's curve.

By similar methods the other quasi-steady "stress functions" are found to be

$$F_\sigma = 2, \quad F_\beta = 1, \quad F_p = 1/(4\pi), \quad F_{C_L}{}^* = 2/\pi^2$$

In all these expressions the slope of the normal force curve has been taken equal to -2π when necessary. In determining the amplitude of the limit cycles for self-sustained oscillations, "nearly sinusoidal" motion has been assumed and the damping work per cycle has been put equal to $8h_0bqC_L{}^*$. Some improvment in $F_{C_L}{}^*$ values could be obtained by replacing the normal force curve slope by $-2\pi F$, where F is the real part of Theodorsen's function.[10] There is some theoretical justification for this step, but since the discussion is chiefly expository there seems to be little merit in continuously refining the solution to the point where the author's (exact) values are reproduced.

In concluding this portion of the discussion it is a pleasure to commend the author for having gathered together in concise and consistent form the results of his valuable theoretical research. It is important that now cascade aerodynamics be considered[11,12] and the work be carried forward to experimental verification,[4,13] and useful semiempiricism.

A. H. STENNING.[14] It now appears that classical flutter and stall flutter are not of great importance as sources of compressor-blade failure. Whenever stall flutter might occur, rotating stall is certainly present and is accompanied by large, periodic variations in blade loading which are virtually unaffected by blade motion, since the air incidence changes induced by the propagating stall regions are of the order of 20 to 30 deg. During engine starting and acceleration, the exciting frequency of the rotating stalls will cover a wide range so that blade resonance probably will be encountered at some point during engine operation.

The author's conclusions regarding the desirability of using slender blades appear to rest entirely on the assumption that the aerodynamic damping may be predicted from classical potential-flow methods. In rotating stall, the airfoil is mostly on the stalled (or negative-slope) side of the curve of lift coefficient versus incidence, so that this assumption is a very dubious one indeed. It seems more probable that the net aerodynamic damping is small, or even negative, so that slender blades are not desirable from this standpoint.

---

[7] "Non-Linear Mechanics," by N. Minorsky, Edwards Brothers, Inc., Ann Arbor, Mich., 1947, pp. 356–357.

[8] Ibid., pp. 366–369.

[9] "Mechanical Vibrations," by J. P. Den Hartog, McGraw-Hill Book Company, Inc., New York, N. Y., third edition, 1947, p. 63.

[10] "General Theory of Aerodynamic Instability and the Mechanism of Flutter," by T. Theodorsen, NACA Report No. 496, April, 1935.

[11] "Unsteady Aerodynamic Reactions on Airfoils in Cascade," by F. Sisto, to be published in the *Journal of the Aeronautical Sciences*.

[12] "An Investigation of the Flutter Characteristics of Compressor and Turbine Blade Systems," by C. T. Wang, F. Lane, and R. J. Vaccaro, paper for delivery at the Institute of the Aeronautical Sciences Annual Meeting, New York, N. Y., 1955.

[13] "Cascade Blade Flutter and Wake Excitation," by J. F. W. Parry and H. Pearson, *Journal of the Royal Aeronautical Society*, vol. 58, July, 1954, pp. 505–508.

[14] Assistant Professor of Mechanical Engineering, Massachusetts Institute of Technology, Cambridge, Mass.

Author's Closure

The author would like to thank Dr. Arnoldi, Dr. Sisto, and Professor Stenning for the attention they gave his paper.

First, a few words about the background. At the early stage of advanced compressor design there existed in some quarters a belief that the vibration failures at "stall" might be attributed to classical two-dimensional flutter and the author therefore felt it should prove valuable to derive that this could not possibly be the case and the explanation for this was therefore shown within the realm of the classical theory itself.

Since then a great deal of research has been done, but to the best of the author's knowledge, only Mr. Pearson, quoted by Dr. Sisto, has to date published anything more detailed on blade vibrations in three-dimensional actual compressors. Because the general aerodynamics of the blade system in a two-dimensional cascade are so different from the actual case, the two-dimensional studies lead to a certain overestimation of the role of self-excitation of the blades and because of the greater capacity of the torsional mode in this respect, this type of vibration received quite an amount of attention. When the paper was written, knowledge of the rotating stall had just started to accumulate, and the fact that the torsional mode was seldom met with in actual compressors thereafter became increasingly apparent.

The author is in full agreement with Dr. Arnoldi and Professor Stenning regarding the limitations with respect to the classical aerodynamical damping and the influence of the wake vortexes. In anticipation of the full cognizance of rotating stall, the author formulated his theory in a form, where the role of self-excitation was not a crucial point. Professor Stenning's statement about rotating stall appears to fortify the view taken by the author to consider the excitation phenomena at stall as a disturbance which might have an influence somewhat similar to that appearing when a blade passes an upstream wake. If rotating stall, according to Professor Stenning, exhibits itself as large periodic disturbances, it also appears that the blades are passing in and out from regions of stalled and *unstalled* flow, the latter at least more similar to "classical" uniform flow than the stalled flow of a single blade at the same incidence as the average flow of the annular cascade. However, Mr. Pearson states, ibid, we quote: "Stress measurements showed that, in spite of the rotating stall, stalled flutter was present all the time, although evidence of variation of the flutter level at the frequency of the stall rotation was obtained." Thus, even if rotating stall is a very important factor, it appears to be a little too early to rule out entirely other excitation phenomena.

Dr. Arnoldi suggests that there exists a dissipative mechanism in translational motion because the dependence of momentary angle of attack on oscillatory velocity provides a phase lag and, consequently, a dissipative mechanism, which one might expect to overshadow any classical dissipative force. This dissipative mechanism is, however, the main damping mechanism resulting in classical theory and it is thought that Dr. Arnoldi, after our personal communications, is in full agreement with the author. The only difference between a quasisteady state theory and the classical theory is that the latter also takes into account the influence of wake vorticity by reducing the lift increment $dC_L/d\alpha$ by Theodorsen function F, which has a value between $^1/_2$ and 1. For small k_h values, the value of F is rather close to 1, as pointed out by Dr. Sisto.

The author willingly agrees with Dr. Arnoldi, however, that internal-material damping may play a much more important role in stall flutter than the author's paper has shown, whereas this is not the case with upstream wake excitation. If, as Mr. Pearson did in his paper, one makes the assumption that internal-material and blade-root damping is the *only* active damping in stall flutter and formulates the criterion for the *onset* of stall flutter vibration, one arrives at the conclusion that the aspect ratio $1/c$ but not k_h is the important parameter, a result not in disagreement with the author's conclusions as discussed by Dr. Sisto.

At the STAL Company, however, we recently found a case of stall flutter which exhibited an increased stress level but no immediate blade failure, thus emphasizing that in this case not only the *onset* but also the attained *limited stress level* is important to determine, a feature the author tried to stress in his paper. Still more, in another compressor there was a similarly located stage with much larger aspect ratio than in the first, but no similar stall-flutter vibration stresses were recorded despite similar blade loadings. The possibility that part of the blade length in the latter case is unstalled and contributes aerodynamic classical damping may not be overlooked.

The author is most grateful to Dr. Sisto for his clear perception and analysis of the concept of the stress functions, particularly so since it stresses the reasons for applying the viewpoints of nonlinear mechanics. Though not directly apparent in the author's paper, the graphical phase-plane analysis was relied upon by the author to clarify the conditions of soft and hard flutter, but Dr. Arnoldi is correct when he states that it might be better to use his approach for the simple cases discussed by the author.

Temperature Distribution and Efficiency of a Heat Exchanger Using Square Fins on Round Tubes[1]

D. H. Fax.[2] This application of the method of superposition of sources to the solution of the fin equation in a difficult geometry is ingenious and interesting. It may be worth while to point out, however, that the approximation made here becomes poor in the same range of the governing parameters as does the approximation used heretofore, that of replacing the square fin by an annular one of equal area. In the earlier method the approximation involved the distortion of the outer square adiabatic boundary into a circular one; the author, in effect, distorts the inner isothermal boundary into something approaching a curvilinear square. Either approximation becomes increasingly poor as the dimensionless parameter ac decreases toward zero and as $2p/a$ increases toward unity. Unless it can be demonstrated that the author's method has the advantage in the difficult régime, it is quite likely that the older method, involving a much simpler calculation, will continue to be used.

...

R. H. Norris.[3] Attention is hereby called to the significance of the fact that all the numerical results (Table 1 and Fig. 2 of the paper) are derived for just one particular case; namely, that where $a = 0.375$ ft and $c = 7.44$ per ft. For this one case, the agreement is found to be conveniently close (within 2 per cent) between the new results and the results obtained from the conventional approximation of a round fin of equal area.

For other cases, however, no numerical results are shown in the paper. It therefore seems appropriate to caution the reader

[1] By H. Zabronsky, published in the March, 1955, issue of the Journal of Applied Mechanics, Trans. ASME, vol. 77, pp. 119–122.

[2] Advisory Engineer, Westinghouse Electric Corporation, Pittsburgh, Pa. Assoc. Mem. ASME.

[3] Consulting Engineer, General Engineering Laboratory, General Electric Company, Schenectady, N. Y. Mem. ASME.

that the close agreement just mentioned may not necessarily apply to all cases of square fins on round tubes.

Nevertheless, the significance of the results can be generalized to a limited extent, as explained in the following:

It can be shown that for the completely general case of square fins on round tubes under the author's assumptions, the fin efficiency ϕ can be represented as a function of just two dimensionless parameters, namely, the product (ac) and the ratio a/p. The author's results in Table 1 and Fig. 2 apply to the case where the product (ac) is constant, with the value 2.79 (i.e., 0.375 times 7.44), while the ratio a/p varies from 2.5 to 200.

Accordingly, the author's results apply to other values of a and of c than those he specified provided the product (ac) is held at his chosen value of 2.79.

Author's Closure

Mr. Fax points out, quite correctly, that the approximation in the paper becomes increasingly poor as ac decreases toward zero and $2p/a$ increases toward unity. Geometrically, the condition $ac \to 0$ means that the lattice points get closer to each other; $2p/a \to 1$ means that the inner circle expands to the size of the square.

Besides verifying the "classical" approximation, in which the geometry is drastically altered, the present approximation has one great advantage; namely, the condition that the tube temperature is approximately constant on the circle is easy to verify by selecting two points of different "character," namely, for $\theta = 0$ deg, $\theta = 45$ deg. If these two points give values of the temperature which are close to each other, then the variation of the temperature all along the circle will be very small and the approximation in the paper may be used with great accuracy. Thus, for any values of the parameter of the problem, there is never a question of mutilating the problem at the outset.

The comments offered by Mr. Norris on the range of validity of the calculations in Table 1 and Fig. 2 of the paper are entirely correct. The calculation offered in the paper is an example which occurred in actual practice. It has been difficult to obtain numerical or analytical evidence comparing the two approximations. It is the author's hope to conclude this part of the problem in the near future.

Oil Streamlines in Bearings[1]

A. A. Milne.[2] The author presents an interesting method of obtaining flow streamlines in slider bearings. His solutions, however, are based merely upon the flow midway between the surfaces and are liable to be misleading. The velocity of the fluid varies continuously both in magnitude and direction across the film and the midway position has no special significance. Has the author obtained any solutions based on alternative flows, e.g., the maximum or mean velocities across the film?

Author's Closure

The author thanks Mr. Milne for his contribution, particularly for his suggestions for alternative flows, and agrees in general with his remarks. Certain simplifications are necessary and even so the labor involved is excessive. No alternative solutions have been obtained. However in order to obtain a truer picture, the author suggests that the technique be applied to a number of fractional positions between the two bearing surfaces and thus obtain the spreading effect which must actually take place.

[1] By C. F. Kettleborough, published in the March, 1955, issue of the Journal of Applied Mechanics, Trans. ASME, vol. 77, pp. 8–10.

[2] Department of Scientific and Industrial Research, Mechanical Engineering Research Laboratory, Thorntonhall, Glasgow, Scotland.

Approximate Stress Functions for Triangular Wedges[1]

G. Horvay.[2] The author's contribution is valuable both because it provides a solution—though approximate—of an important engineering problem, and because it demonstrates once again the usefulness of the variational method, in the form first used by Kantorovitch[3] and Poritsky.[4] This method which utilizes functions $g(x, y)f(y)$ where $g(x, y)$ is a chosen function adapted to certain boundary conditions, $f(y)$ a function determined by the variational principle, becomes particularly powerful,[5–11] when it is extended to include sums of functions[12]

$$\Sigma\, g_k(x, y)f_k(y)$$

It should be pointed out, however, that the stress in the corner O of the triangle, H-O-H', Fig. 1(a), of this discussion and perhaps also in the corner H' is, mathematically speaking, infinite. For it was shown by Williams[13] that when a free edge and a rigidly held edge of a plate meet in a sharp corner, the included angle exceeding 60 deg, then mathematics lead, in general, to an infinite stress in the corner. The 60 deg is no magic number; it is an approximate value, and depends somewhat on Poisson's ratio.

The infinity is not present in Silverman's solution, but neither is it present in nature. Curvature of the corner, or some flexibility, or also, some yielding, will all reduce the infinity to a finite stress, even in a mathematical sense.

[1] By I. K. Silverman, published in the March, 1955, issue of the Journal of Applied Mechanics, Trans. ASME, vol. 77, pp. 123–128.

[2] Engineer, Knolls Atomic Power Laboratory, General Electric Company, Schenectady, N. Y. Mem. ASME. The Knolls Atomic Power Laboratory is operated by the General Electric Company for the Atomic Energy Commission.

[3] "Mathematical Theory of Elasticity," by I. S. Sokolnikoff, McGraw-Hill Book Company, Inc., New York, N. Y., 1946, p. 315.

[4] "Reduction of the Solution of Certain Partial Differential Equations to Ordinary Differential Equations," by H. Poritsky, Proceedings of the Fifth International Congress of Applied Mechanics, 1938.

[5] "The End Problem of Rectangular Strips," by G. Horvay, Journal of Applied Mechanics, Trans. ASME, vol. 75, 1953, pp. 87 and 576.

[6] "Orthogonal Edge Polynomials in the Solution of Boundary Value Problems," by G. Horvay and F. N. Spiess, *Quarterly of Applied Mathematics*, vol. 12, 1954, p. 57.

[7] "The Use of Self-Equilibrating Functions in Solution of Beam Problems," by G. Horvay and J. S. Born, Second National Congress of Applied Mechanics, The American Society of Mechanical Engineers, 1954.

[8] "Thermal Stresses in Rectangular Strips—I," by G. Horvay, Second National Congress of Applied Mechanics, The American Society of Mechanical Engineers, 1954.

[9] "Thermal Stresses in Rectangular Strips—II," by J. S. Born and G. Horvay, Journal of Applied Mechanics, Trans. ASME, vol. 77, 1955, pp. 401–406.

[9] "Tables of Self-Equilibrating Functions," by G. Horvay and J. S. Born, *Journal of Mathematics and Physics*, vol. 33, 1955, p. 360.

[10] "Precise Closed-Form Solutions of Some Mixed Boundary Value Problems of Plane Elasticity," by G. Horvay and J. S. Born, submitted to the Journal of Applied Mechanics.

[11] "Biharmonic Eigenvalue Problem," by G. Horvay, in preparation.

[12] Note that in the references the role of the symbols g and f is reversed.

[13] "Stress Singularities Resulting From Various Boundary Conditions in Angular Corners of Plates in Extension," by M. L. Williams, Journal of Applied Mechanics, Trans. ASME, vol. 74, 1952, p. 526.

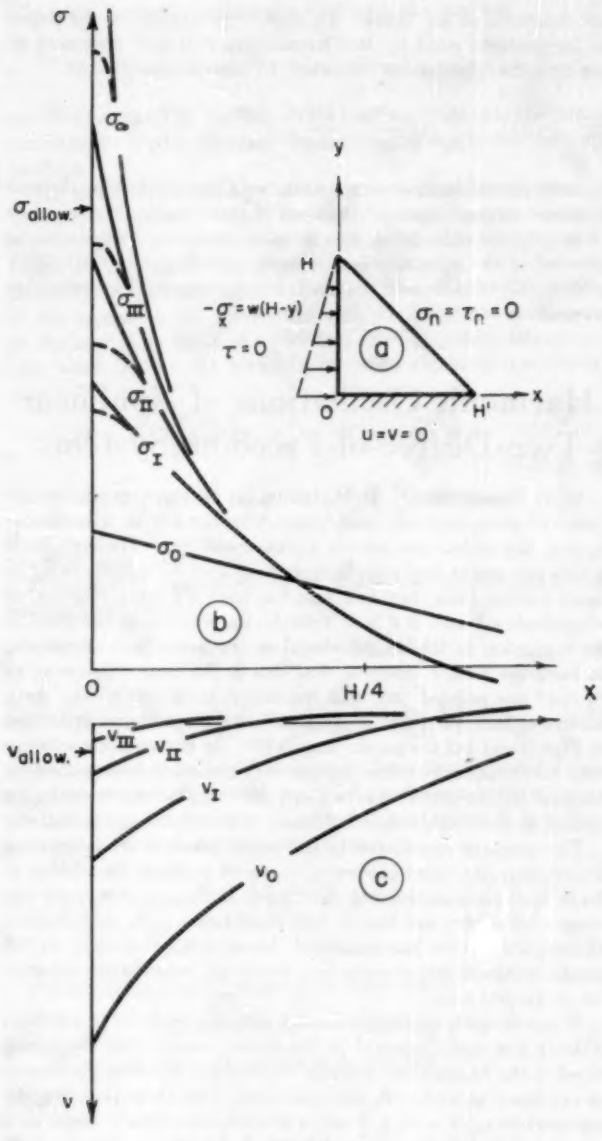

FIG. 1

If we regard the Silverman solution as essentially correct along the base O-H', except near the end points, the question still remains, what to do about the corners?

In Fig. 1(b) we drew (full-line) curves σ_∞, σ_0, and σ_I to represent, schematically, the mathematically precise solution $\sigma_y(x, 0)$ along the base near the point O, the Levy approximation based on the stress function $\varphi_0 = F_e$ and the Silverman approximation, $\varphi_I = F_e + gf$. Were we to use a 2-term variational approximation $\varphi_{II} = F_e + g_1f_1 + g_2f_2$, we would wind up with a curve σ_{II}, also illustrated, which reaches a higher ordinate at O; a 3-term approximation curve, σ_{III}, will reach still higher. Where shall we stop? The maximum allowable stress σ_{allow} which is prescribed for the structure provides a unique stopping point. Clearly, in order not to get excessive stresses we must stop (for the case illustrated) with a 2-term approximation, φ_{II}. But having thus ignored a mathematical infinity we must verify, more conscientiously than is usually done, that φ_{II} is a reasonable solution of the physical problem. This can be done by plotting the y-displacement $v(x, 0)$ along the base in the φ_0 approximation, in the φ_I approximation, in the φ_{II} approximation, etc., as indicated schematically in Fig. 1(c). If the displacement v_{II} at $x = 0$ is judged to be sufficiently small, and if noticeable departure from zero is limited to a sufficiently small vicinity of the corner, so that v_{II} may be ascribed properly to the "give" of some elastic foundation near the corner, then clearly φ_{II} provides a conservative solution of the problem. If the give is too large, then we must proceed to higher approximations φ_{III}, φ_{IV}, . . . until the give remains below the allowed limit (in Fig. 1c we illustrate the case where v_{III} stays below v_{allow}); but clearly solutions φ_{III}, φ_{IV}, . . . give, by Fig. 1(b), excessive stresses, and we conclude: The structure does not meet the stress specifications. This is the situation when only flexibility is permitted in the corner. When the corner is curved, or some plastic yielding also takes place, then there occurs a lowering of the curves σ_I, σ_{II}, . . ., σ_∞ (to, say, the dashed-line positions), so there exists the possibility that the stress σ_{III} is allowable, after all, and the structure may be judged as adequate.

The foregoing, somewhat detailed, discussion is aimed at spotlighting the two contrasting—nay, conflicting—and, yet in their respective domains, perfectly valid approaches of the engineer and the mathematician. The first ignores the infinity in the corner, and uses a solution which is essentially correct at some distance from the singular point. The second undoubtedly will start out with Williams' corner function, to get rid of the infinity, and superimpose on it correction functions which then tend to a mathematically finite limit.

While in the author's problem the calculational labor required for determining φ_{II} would probably be too great to be contemplated, and so one must forego the attempt (inviting as it is) to obtain an idea of the rapidity at which σ_0, σ_I, σ_{II}, . . . tend to infinity in the corner as more and more terms are taken, this writer believes that a quantitative determination of v_0 and v_I along O-H' is not an unreasonable task, and he would be happy if the author could furnish such a comparison of the two estimates for the displacement.

There is one more question which bothers the writer. Evidently a precise correction function φ (one which satisfies both the author's Equations [7] and $\nabla^4\varphi = 0$) is automatically self-equilibrating along the base O-H'. A brief calculation will show also that the author's function $\varphi_I - F_e$ is self-equilibrating. But is this automatic for approximate functions, or must self-equilibration be imposed independently of Equations [7], as a separate condition, when the trial function violates the biharmonic equation? (When both angles O and H' are right angles then self-equilibration is automatic. This was shown in the writer's Equations [46], [47], reference 5a.)

MAX KRONENBERG.[14] This writer's question refers to a different field of mechanical engineering than that of the author, namely, to radial stresses generated in a cutting tool. Such a tool may be considered, as a first approximation, as a triangular wedge.

Fig. 2 of this discussion shows the commonly adopted concept of a concentrated force, the resultant cutting force, acting at the apex of the wedge in any direction. In an investigation which the writer has carried out to determine the radial stresses in a cutting tool[15] he has made use of the equations originally derived by J. H. Michell[16] and has adapted them to the particular conditions of metal cutting.

The writer is wondering whether and in what respect Michell's

[14] Consulting Engineer, Cincinnati, Ohio. Mem. ASME.

[15] "Avoiding Tool Failures With Negative Rake," by Max Kronenberg, *The Tool Engineer*, vol. 34, January, 1955, pp. 83–87.

[16] J. H. Michell, Proceedings of the London Mathematical Society, vol. 34, 1902, p. 134.

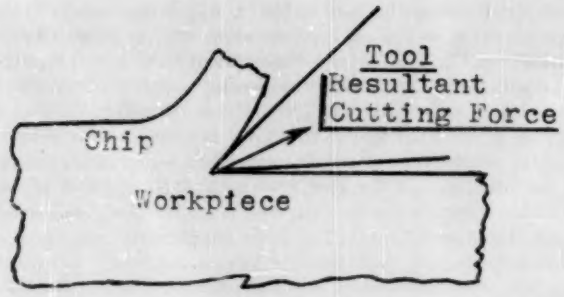

FIG. 2

formulas need a revision, how much they differ from the derivations presented by the author, and which of his formulas he suggests to use in the case of metal cutting?

AUTHOR'S CLOSURE

The problem treated in this paper deals with the encastre' beam of triangular profile. The conditions of fixity are replaced, as a result of the minimal formulation of the problem, by Equations [30], [31], and [32]. To the stresses of the infinite wedge, correction stresses are added with the resulting stresses given by Equations [41], [42], and [43]. The correction stresses are given by $F = g(x, y)f(y)$ where, in general

$$g(x, y) = \sum_{2}^{n=\alpha+1} \frac{M_n x^n (H - y)^{3-n}}{n(n-1)} \quad (\alpha = 4, 6, 8 \ldots .) \ldots [57]$$

M_n are constants determined by satisfying conditions [7]. When $\alpha = 4$, $g(x, y)$ is given by [12]. There is no reason to believe that as the number of terms used in the polynomial [57] is increased that the stresses at point O would increase as suggested by Dr. Horvay.

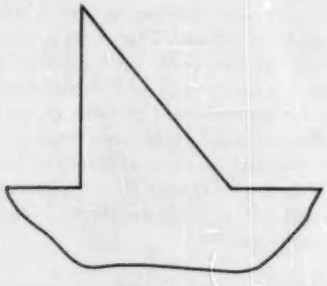

FIG. 3

Satisfaction of [7] restricts the problem to a wedge. The results obtained by the use of the approximate functions are indicative of the conditions of fixity. The stresses at re-entrant angles which may exist because of the actual support furnished to the wedge as illustrated in Fig. 1 is a separate problem and has been treated quite extensively in reference (4), page 1262.

The stress function $F = g(x, y)f(y)$ is made to yield zero stresses on the faces of the wedge by means of [7]. As a result of satisfying [7] the stresses across any section of the wedge, formed by a plane cutting the two faces, must have a resultant moment, shear, and normal force equal to zero since the unit stresses are obtained from the usual definition of $\sigma_x = F_{yy}$; $\sigma_y = F_{xx}$; $\tau = -F_{xy}$.

The left-hand sides of Equation [46], [47], [48], and [49] are functions of the geometry of the wedge while the right-hand sides are functions of the loads. To apply the method of the paper to the problem cited by Mr. Kronenberg it is only necessary to perform the integrations indicated, by substituting for

$$\frac{\partial^2 Fe}{\partial y^2}, \quad \frac{\partial^2 Fe}{\partial x^2}, \quad \frac{\partial^2 Fe}{\partial y^2}, \quad \frac{\partial^2 Fe}{\partial x^2 \partial y}, \quad \frac{\partial^2 Fe}{\partial x \partial y}$$

the corresponding expressions obtained from Michell's solutions for concentrated forces at the apex of the wedge. Having thus obtained the right-hand side of the equations, simultaneous solution of the equations furnishes the values of $f(0), f'(0), f''(0)$, and $f'''(0)$ which are required to determine the correction stresses.

Harmonic Oscillations of Nonlinear Two-Degree-of-Freedom Systems[1]

R. M. ROSENBERG.[2] In his treatment of the harmonic oscillations of some two-degree-of-freedom systems with a nonlinear spring, the author has done a workmanlike job. The only fault which one might find with his results is that he regards them as more narrow than they are. He has used a forcing function of magnitude $\epsilon_0 F$ and, if F is of order k_1, the solution is restricted to an expansion in the neighborhood of the linear free vibrations; in fact, the author observes that this is the case. However, as Stoker[3] has pointed out, this restriction is not essential. As a matter of fact, its removal would not affect the results presented in Figs. 3 and 4 of the paper. Implicitly, the author acknowledges that his results have wider applicability than indicated in the text because his computed curves reach into regions which are by no means in the neighborhood of those of the free linear vibrations.

The problem considered in the paper presents an interesting aspect from the point of view of choice of methods for solving it. In it, the spring connecting the masses is the only nonlinear element—all others are linear. In accordance with perturbation theory, the author has expanded the quantities sensitive to the nonlinearities in power series in ϵ_0, the single perturbation parameter of the problem.

It is now quite natural to inquire into the behavior of a system exactly like that discussed by the author except that the spring fixed to the support and perhaps the dashpot between the masses is nonlinear as well. In this case there arise three perturbation parameters ϵ_i; $i = 0, 1, 2$ and a second-order theory would give rise to all combinations $\epsilon_i \epsilon_j$; $i, j = 0, 1, 2$ in the equations. Evidently this complication introduces some rather profound algebraic difficulties which make the perturbation method appear unsuitable in problems with a multiplicity of nonlinearities.

Without wishing to champion a school of "iterationists" as compared to the "perturbationists" we shall now indicate the ease with which the iteration method can deal with several simultaneous nonlinearities, and also the new difficulties which arise.

Let us consider the equations

$$\left.\begin{aligned} \ddot{x} + \omega_{11}^2(x - y) + \nu_{01}^2(x - y)^3 &= F \cos \omega t \\ \ddot{y} - \omega_{12}^2(x - y) - \nu_{02}^2(x - y)^3 + \omega_{22}^2 y + \nu_{12}^2 y^3 &= 0 \end{aligned}\right\} \ldots [1]$$

[1] By T. C. Huang, published in the March, 1955, issue of the JOURNAL OF APPLIED MECHANICS, Trans. ASME, vol. 77, pp. 107–110.

[2] Acting Head of the Department of Engineering Mechanics, University of Toledo, Toledo, Ohio.

[3] "Nonlinear Vibrations," by I. J. Stoker, Interscience Publishers, Inc., New York, N. Y., 1950, p. 101.

These are the author's Equations [1] with the notation

$$k_i/m_i = \omega_{i_j}^2, \quad \epsilon_i/m_j = \nu_{i_j}^2, \quad F = F_0/m_1, \quad \nu_{12} = 0$$

and the last term on the left of the second equation is the added nonlinearity of the anchored spring, not present in the author's analysis.

The iteration method begins with the identical assumptions to the author's Equations [10] and these are adopted for the zero and first-order derivatives. A subsequent double integration of Equations [1] yields the second approximation, and the constants of integration must vanish to preserve the periodicity of the solutions. In accordance with Duffing,[4] the coefficients of the leading terms of the first and second approximations are now equated with the result (after some algebraic operations) that

$$\left.\begin{aligned} F - (\omega_{11}^2 + \omega^2)N - \frac{3}{4}\nu_{01}^2 N^3 - \omega^2 B = 0 \\ -\omega_{12}^2 N - \frac{3}{4}\nu_{02}^2 N^3 + \omega^2 B + \frac{3}{4}\nu_{12}^2 B^3 = 0 \end{aligned}\right\} \quad \ldots [2]$$

where $N = A - B$.

If the first of these is solved for B and then substituted in the second, there results

$$F - (\omega_{11}^2 + \omega_{12}^2 + \omega^2)N - \frac{3}{4}(\nu_{01}^2 + \nu_{02}^2)N^3 + \frac{3}{4}\nu_{12}^2 \left\{F - \left[\left(\frac{\omega_{11}}{\omega}\right)^2 + 1\right]N\right\} = 0 \quad \ldots [3]$$

where terms of order $(\nu_{i_j}^2)^2$ and higher have been ignored. One may now assign to N arbitrary values N_r and compute from Equation [3] the associated ω_r. The appropriate values B_r are then found from the first of Equations [2] as

$$B_r = B_r(\omega_r, N_r) = \frac{F}{\omega_r^2} - \left[\left(\frac{\omega_{11}}{\omega_r}\right)^2 + 1\right]N_r - \frac{3}{4}\left(\frac{\nu_{01}}{\omega_r}\right)^2 N_r^3 \quad \ldots [4]$$

The second approximations to the solutions are

$$\left.\begin{aligned} x_2 = P_1 \cos \omega_r t + P_3 \cos 3\omega_r t \\ y_2 = Q_1 \cos \omega_r t + Q_3 \cos 3\omega_r t \end{aligned}\right\} \quad \ldots [5]$$

where

$$P_1 = \frac{1}{\omega_r^2}\left(F - \omega_{11}^2 N_r - \frac{3}{4}\nu_{01}^2 N_r^3\right)$$

$$P_3 = -\frac{1}{36\omega_r^2}\nu_{01}^2 N_r^3$$

$$Q_1 = \frac{1}{\omega_r^2}\left(\omega_{12}^2 N_r + \frac{3}{4}\nu_{02}^2 N_r^3 - \omega_{22}^2 B_r - \frac{3}{4}\nu_{12}^2 B^3\right)$$

$$Q_3 = -\frac{1}{36\omega_r^2}(\nu_{02}^2 N_r^3 - \nu_{12}^2 B_r^3)$$

The form of Equations [5] makes it evident that one can proceed with continued iterations without any difficulties except those which arise also in the case of a single nonlinearity, because the only effect of the second nonlinearity is the presence of the last term in Q_1 and Q_3, respectively.

The grave difficulty with the foregoing development lies in the poor foundation of the iteration method. The author undoubtedly has chosen the perturbation method because the perturbation series used in his paper are known to exist under the conditions stipulated by him. However, lately a number of problems have appeared where a multiplicity of perturbation parameters makes the perturbation method unsuitable beyond a first-order approximation. This implies that the existence of the perturbation series cannot be utilized in practice and becomes primarily of academic interest. It is clear, then, that the iteration method, whose computational advantages have been demonstrated, must now be put on a sound theoretical basis.

[4] "Nonlinear Vibrations," by I. J. Stoker, Interscience Publishers, Inc., New York, N. Y., 1950, p. 85.

Author's Closure

The author wishes to express his sincere appreciation to Professor Rosenberg for his discussion. It consists of a minor point discussing the restriction due to small forcing function and a major point as to the choice of methods.

It was pointed out by Stocker[5] that the perturbation method has the advantage that it can often be applied fairly safely in the absence of foreknowledge regarding the general character of the solution, but has the disadvantage that it is often rather cumbersome for actual computation, particularly if more than one or two terms in the perturbation series are desired. Consequently, it is often advantageous to begin the attack on a new problem by the perturbation method in order to gain a first insight into the character of its solution, but to abandon this attack eventually in favor of other approaches once sufficient knowledge about the behavior of the solutions has been gained. Therefore the choice of iteration method as suggested and illustrated by Professor Rosenberg should be an appropriate supplement to the paper.

There are possibilities to apply either iteration or perturbation methods in direct operation with differential equations or in a Fourier series development with undetermined coefficients. For systems of two degrees of freedom, Professor Rosenberg's discussion illustrates iteration method for the first case, while the choice of iteration approach for the second case in determining the series coefficients has been illustrated by the author in a paper "Subharmonic Oscillations in Nonlinear Systems of Two Degrees of Freedom" on pages 95 to 100 of Proceedings of the Second U. S. National Congress of Applied Mechanics.

[5] "Nonlinear Vibration," by J. J. Stocker, Interscience Publishers, Inc., New York, N. Y., p. 99.

On Turbulent Jet Mixing of Two Gases at Constant Temperature[1]

S. Corrsin.[2] If the general continuity Equation [7] of the paper is rewritten as

$$\frac{D\rho}{Dt} + \rho\left[\frac{\partial u}{\partial x} + \frac{\partial v}{\partial y} + \frac{\partial w}{\partial z}\right] = 0 \quad \ldots [1]$$

we see that the author's use of the constant-density form, Equation [9], amounts to taking the Stokes' (substantial) derivative equal to zero

$$\frac{D\rho}{Dt} \equiv \frac{\partial \rho}{\partial t} + u\frac{\partial \rho}{\partial x} + v\frac{\partial \rho}{\partial y} + w\frac{\partial \rho}{\partial z} = 0 \quad \ldots [2]$$

This is the statement that each individual "fluid particle" keeps its density constant for all time, a restriction to immiscible fluids,

[1] By S. I. Pai, published in the March, 1955, issue of the Journal of Applied Mechanics, Trans. ASME, vol. 77, pp. 41–47.

[2] Associate Professor, Aeronautics Department, The Johns Hopkins University, Baltimore, Md.

which the author has promised to avoid (see Introduction of the paper).

In fact, the drastic nature of this simplification is emphasized by the averaged form, Equation [11]

$$\frac{\partial \bar{u}}{\partial x} + \frac{\partial \bar{v}}{\partial y} + \frac{\partial \bar{w}}{\partial z} = 0 \quad [3]$$

as the continuity equation for the mean motion. The full averaged equation follows after substitution of

$$\rho = \bar{\rho} + \rho'; \quad u = \bar{u} + u'; \quad v = \bar{v} + v'; \quad w = \bar{w} + w' \quad [4]$$

into Equation [1] of this discussion. For steady state in the mean

$$\bar{\rho}\left[\frac{\partial \bar{u}}{\partial x} + \frac{\partial \bar{v}}{\partial y} + \frac{\partial \bar{w}}{\partial z}\right] + \left[\bar{u}\frac{\partial \bar{\rho}}{\partial x} + \bar{v}\frac{\partial \bar{\rho}}{\partial y} + \bar{w}\frac{\partial \bar{\rho}}{\partial z}\right] + \left[\frac{\partial \overline{\rho' u'}}{\partial x} + \frac{\partial \overline{\rho' v'}}{\partial y} + \frac{\partial \overline{\rho' w'}}{\partial z}\right] = 0 \quad [5]$$

Presuming that the third group of terms can be neglected under the assumption of "small fluctuations," we still arrive at Equation [3] only via

$$\bar{u}\frac{\partial \bar{\rho}}{\partial x} + \bar{v}\frac{\partial \bar{\rho}}{\partial y} + \bar{w}\frac{\partial \bar{\rho}}{\partial z} = 0 \quad [6]$$

This is the statement of a constant mean density along each mean flow streamline, which hardly seems justifiable even for miscible fluids.

Other semiempirical analyses roughly predicting the effect of density difference on the spread of round turbulent jets have been published[3,4,5] and measurements in hot jets are available.[4,6]

WALTON FORSTALL.[7] This is an excellent paper and represents an important contribution to the literature on jet mixing. The neat way in which the two-dimensional and axially symmetric cases can be handled with one set of equations using the author's delta notation is particularly good.

Mixing-length theory, as a theory, has little to recommend it at the present time. By referring to it in Equations [21] and [31], the paper may tend to create an impression that the mixing-length theory is a necessary ingredient, which is not so. It would seem better to say merely that by analogy to nonturbulent flow,

where $$\frac{\tau}{\rho} = \nu \frac{\partial u}{\partial y}$$

for turbulent flow we write

$$\frac{\tau_{\text{apparent}}}{\bar{\rho}} = -\overline{u'v'} = \epsilon \frac{\partial \bar{u}}{\partial y}$$

and hence, still by analogy

$$-\overline{c'v'} = \epsilon_c \frac{\partial \bar{c}}{\partial y}$$

thus avoiding any reference to mixing length.

[3] "Field of Flow About a Jet and Effect of Jets on Stability of Jet-Propelled Airplanes," by H. S. Ribner, NACA Adv. Conf. Rep. L6C13. 1946.

[4] "Further Experiments on the Flow and Heat Transfer in a Heated Turbulent Jet," by S. Corrsin and M. S. Uberoi, NACA TN 1865, 1949 (reissued as NACA Rep. 998, 1950).

[5] "The Diffusion of a Hot Air Jet in Air in Motion," by W. Szablewski, NACA TM 1288 (translated from GCD/2460, 1946).

[6] "Die Ausbreitung heisser Gasstrahlen in bewegter Luft-II," by O. Pabst, UM 8007. 1944.

[7] Associate Professor of Mechanical Engineering, Carnegie Institute of Technology, Pittsburgh, Pa. Mem. ASME.

The value of 1.2 for E seems to be a lower limit applying to streams of the same density. Some work recently done at the Carnegie Institute of Technology with a submerged water jet into water of nearly the same density has shown a value of E approximately 1.23.

AUTHOR'S CLOSURE

In replying to Professor Corrsin's comments, the author would like to point out the following two points.

1 Since the Equation [11] of my paper

$$\frac{\partial \bar{u}}{\partial x} + \frac{\partial \bar{v}}{\partial y} + \frac{\partial \bar{w}}{\partial z} = 0$$

may be obtained from the assumption of immiscibility, it is of course possible to arrange the equation such that the immiscibility is retained. But the author does not use the assumption of immiscibility explicitly so that the present results may be easily generalized to the general case of compressible fluid which has been worked out by the author recently and which will be published in the near future.

2 The constant mean density along each mean flow streamline at constant temperature condition is a good approximation for miscible fluids of approximately the same molecular weight.

The author agrees with Professor Forstall that "mixing-length theory, as a theory, has little to recommend it at the present." The author retained the mixing length in order to show that there are two different semiempirical methods to study the jet-mixing problem, i.e., the constancy of mixing length at a given section in jet mixing region (Hu's theory) and the constancy of turbulent exchange coefficient at a given section in the mixing region (used in the present paper).

Stress Distribution in a Uniformly Rotating Equilateral Triangular Shaft[1]

H. MARCUS.[2] The analysis of the stress distribution in a rotating shaft requires the solution of two differential equations, namely

$$\nabla^4 \Phi = \frac{2(1-2\nu)}{1-\nu}\mu\omega^2 \quad [1]$$

$$\nabla^4 \Phi = 0 \quad [2]$$

The approximate solution initiated by the author is based on a combination of twelve stress polynomials expressed in cartesian co-ordinates x, y.

Equation [1] of this discussion is identical to the equation for the deflection of a triangular plate subjected to a uniform load p. In 1923 the writer[3] gave an exact solution expressed in terms of a set of three oblique co-ordinates, respectively, parallel to the three edges 1, 2, 3, of the accompanying Fig. 1. The selection of this set is justified by the symmetry conditions and by the very simple formulation of the boundary conditions. The solution does not require any development of series and is not at all laborious.

[1] By H. T. Johnson, published in the June, 1955, issue of the JOURNAL OF APPLIED MECHANICS, Trans. ASME, vol. 77, pp. 255–259.

[2] Consultant, Mechanics Division, Code 6205, Naval Research Laboratory, Washington, D. C.

[3] "Die Theorie elastischer Gewebe und ihre Anwendung auf die Berechnung biegsamer Platten," by H. Marcus, Julius Springer, Berlin, Germany, second edition, 1932.

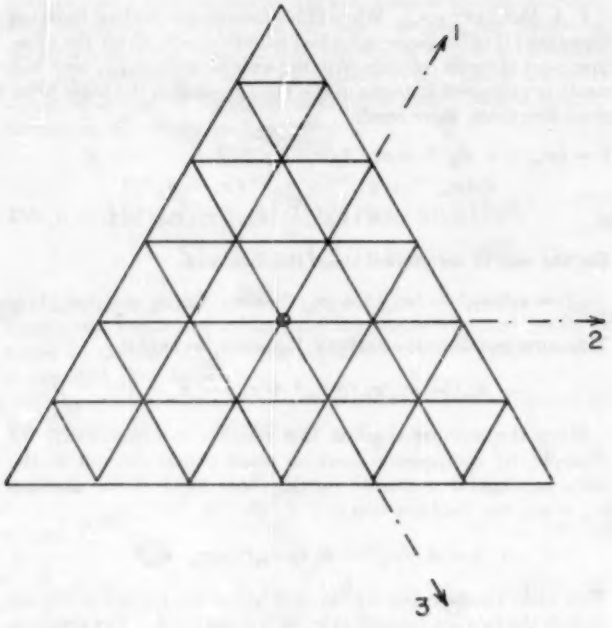

FIG. 1

A similarly simple method can be used for Equation [2].

By calling the attention to the usefulness of this type of triangular co-ordinates, the writer hopes to stimulate research on many other problems dealing with the behavior of bodies with triangular sections.

AUTHOR'S CLOSURE

The solution of the system of equations for the uniformly rotating equilateral triangular shaft by the use of the known solution for the uniformly loaded triangular plate is very interesting. The author wishes to thank Dr. Marcus for calling this to his attention.

Anisotropic Loading Functions for Combined Stresses in the Plastic Range[1]

S. B. BATDORF.[2] At the time of the inception of the slip theory (1),[3] its prediction of a yield corner in the load surface appeared both radical and improbable. Since that time the yield corner has received qualitative verification from the work of a number of investigators including Peters, Dow, and Batdorf (2), Stockton (3), Marin and Hu (4, 5, 6), and Naghdi. Marin and Hu have, in fact, verified the existence of a yield corner qualitatively for 14S-T aluminum alloy, 24S-T aluminum alloy, and mild steel. It would appear that the existence of a corner can now be considered established.

What is less clear at the present time is the nature of the yield corner. Slip theory predicted that the corner would be sharp. The consequences of the slip theory for stress-strain behavior have not yet been worked out for biaxial tension but have been for tension and shear. Consider a specimen loaded into the plastic range in tension and then subjected to increasing shear stress and simultaneously decreasing tension. If the loading path during shear is a straight line starting out approximately halfway between the elastic-plastic boundary for octahedral shear-stress theory and that for slip theory, then, according to the latter, plastic shear strains will start at the beginning of twist, while according to the former, the plastic shear strain will remain zero until the load line crosses the ellipse representing the strain-hardening elastic-plastic boundary.

Experimental data are in conflict with regard to what actually happens in this situation. The data of Budiansky, Dow, Peters, and Shepherd (7) indicate that plastic shear strains occur long before they would be predicted by octahedral shear theory but that they do not occur at the very beginning of shear as would be expected on the basis of slip theory. This has led to the hypothesis that the yield corner actually may be rounded rather than sharp. On the other hand, data obtained by Naghdi appears to support the view that the yield corner is sharp.

It would thus appear that attention should now shift from the verification of the existence of a yield corner to the investigation of its nature. The contradiction between the data of Naghdi and that of Budiansky, Dow, Peters, and Shepherd, in the case of tension and shear, needs to be resolved. Similarly, it would be desirable to work out quantitatively the predictions of slip theory for biaxial tension to see whether or not the theory is in accord with the data of the authors.

BIBLIOGRAPHY

1 "A Mathematical Theory of Plasticity Based on the Concept of Slip," by S. B. Batdorf and Bernard Budiansky, NACA TN 1871, April, 1949.

2 "Preliminary Experiments for Testing Basic Assumptions of Plasticity Theories," by R. W. Peters, N. F. Dow, and S. B. Batdorf, Proceedings of the Society of Experimental Stress Analysis, vol. 7, 1950, pp. 127–140.

3 "Experimental Evidence of Non-Linearity in Plastic Stress-Strain Relations," by F. D. Stockton, ONR Technical Report No. 88, Graduate Division of Applied Mathematics, Brown University, May, 1953.

4 "Plastic Stress-Strain Relations for Biaxial Tension and Variable Stress Ratios," by J. Marin and L. W. Hu, Proceedings of the ASTM, vol. 52, 1952, pp. 1095–1125.

5 "On the Validity of Assumptions Made in Theories of Plastic Flow for Metals," by J. Marin and L. W. Hu, Trans. ASME, vol. 75, 1953, pp. 1181–1190.

6 "Anisotropic Loading Functions for Combined Stresses in the Plastic Range," by J. Marin and L. W. Hu, ASTM Paper No. 54—A-9.

7 "Experimental Studies of Polyaxial Stress-Strain Laws of Plasticity," by B. Budiansky, N. F. Dow, R. W. Peters, and R. P. Shepherd, Proceedings of the First U. S. National Congress of Applied Mechanics, 1951.

M. W. JOHNSON.[4] In their investigation of the suitability of three yield criteria, the authors obtained maximum plastic strains of the order 0.0003 in/in. compared with maximum elastic strains of the order 0.003 in/in. The writer agrees that the results show none of the three as "the one" correct yield criterion, but believes that, since the plastic strains are relatively small compared to elastic strains, any of the three would be adequate for many problems dealing with anisotropic materials.

Some criticism of the manner of testing the maximum-shear criterion may be in order. Since these tests were run on specimens previously tested for Prager's criterion, there is a tacit as-

[1] By L. W. Hu and J. Marin, published in the March, 1955, issue of the JOURNAL OF APPLIED MECHANICS, Trans. ASME, vol. 77, pp. 77–85.

[2] Manager, Development Division, Materials Engineering Department, Westinghouse Electric Corporation, East Pittsburgh, Pa. Mem. ASME.

[3] Numbers in parentheses refer to the Bibliography at the end of this discussion.

[4] Research Assistant, Department of Mathematics, Massachusetts Institute of Technology, Cambridge, Mass.

sumption involved that the shear-yield function, if correct, will expand isotropically. Such an assumption is disproved in the second part of the experiment, however, so that this does not constitute a fair test of the shear-yield criterion.

T. H. Lin.[5] Most theories of plasticity are developed for isotropic materials. However, many thin-walled-cylinder specimens lack isotropy even after specially processed in an effort to obtain uniformity of properties (1).[6] Anisotropy develops in aluminum-alloy plate as a result of even a small amount of cold work (2). Hence a method of modifying the loading functions for isotropic materials to those for anisotropic materials is of both theoretical and practical interest.

The test results show that neither distortion energy, maximum shear, nor

$$\left(J_2^3 - \frac{9}{4}J_3^2\right)$$

criterion is adequate as a loading function. This may mainly account for the failure of the incremental theory based on distortion energy in predicting the inelastic buckling of plate under edge thrust (3). The test results also clearly show the formation of a corner in the loading surface. This agrees with the slip theory by Batdorf and Budiansky (4) and the slip theory proposed by the writer (5).

Fine-grained aggregate with crystal orientations at random will give statistical isotropy (6, 7). As the initial anisotropy of the specimens results from the previous work beyond the proportional limit during the fabrication, probably the initial isotropy may be considered as one loading surface, caused by straining in the plastic range, although the history of loading is not given. Both of these slip theories predict incremental plastic strain with incremental axial stress after the specimen is stressed tangentially in the plastic range. This agrees with the test results shown in the paper (Figs. 5, 8, 10).

Though more test data in the inelastic range with varying ratios of principal stresses were published during the last five years than in the previous similar period, more experimental data suitable for testing basic assumptions of plasticity are still needed. The present paper gives excellent data to test the existing theories and to help further development of plasticity theory.

BIBLIOGRAPHY

1 "Experimental Studies of Polyaxial Stress-Strain Laws of Plasticity," by B. Budiansky, N. F. Dow, R. W. Peters, and R. P. Shepherd, Proceedings of the First U. S. National Congress of Applied Mechanics, 1951.

2 "Dependence of the Stress-Strain Curves of Cold-Worked Metals Upon Testing," by L. J. Klingler and G. Sachs, *Journal of the Aeronautical Sciences*, March, 1948.

3 "Theory and Tests on the Plastic Stability of Plates and Shells," by P. P. Bijlaard, *Journal of the Aeronautical Sciences*, Sept., 1949.

4 "Mathematical Theory of Plasticity Based on the Concept of Slip," by S. B. Batdorf and B. A. Budiansky, NACA Tech. Note 1871, 1949.

5 "A Proposed Theory of Plasticity Based on Slips," by T. H. Lin. Proceedings of Second U. S. National Congress of Applied Mechanics, 1954.

6 "Plastic Strains in Metals," by G. I. Taylor, *Journal*, Institute of Metals, vol. 62, no. 1, 1938.

7 "The Inelastic Behavior of Engineering Materials and Structures," by A. M. Freudenthal, John Wiley & Sons, Inc., New York, N. Y., 1950.

[5] University of Detroit, Detroit, Mich.

[6] Numbers in parentheses refer to the Bibliography at the end of this discussion.

F. A. McClintock.[7] When Hill's anisotropic loading function Equation [1] of the paper is applied to problems in which the principal axes of stress coincide with the axes of anisotropy, and the result is expressed in terms of the yield stresses in the three principal directions, there results

$$1 = (\sigma_{ry}^{-2} + \sigma_{ty}^{-2} - \sigma_{ay}^{-2})(\sigma_r - \sigma_t)^2/2 + (\sigma_{ay}^{-2} + \sigma_{ry}^{-2} - \sigma_{ty}^{-2})(\sigma_a - \sigma_r)^2/2 + (\sigma_{ty}^{-2} + \sigma_{ay}^{-2} - \sigma_{ry}^{-2})(\sigma_t - \sigma_a)^2/2$$

For the case of zero radial stress this becomes

$$1 = \sigma_t^2/\sigma_{ty}^2 - (\sigma_{ay}^{-2} + \sigma_{ty}^{-2} - \sigma_{ry}^{-2})\sigma_a\sigma_t + \sigma_a^2/\sigma_{ay}^2$$

This corresponds to the authors' Equation [5] only if

$$\sigma_{ry}^2 = \sigma_{ay}^2\sigma_{ty}^2/(\sigma_{ay}^2 + \sigma_{ty}^2 - \sigma_{ay}\sigma_{ty})$$

Have the authors checked this relation experimentally, for example, by compression tests on small pellets cut out in the three principal directions? On the other hand, if one assumes $\sigma_{ry} = \sigma_{ty}$, the yield function is

$$1 = \sigma_t^2/\sigma_{ty}^2 - \sigma_a\sigma_t/\sigma_{ay}^2 + \sigma_a^2/\sigma_{ay}^2$$

This yield function lies within that given by Equation [5], although the two are tangent at $\sigma_a = 0$ and $\sigma_t = 0$. For instance, if $\sigma_{ty} = \sigma_{ry} = 30{,}000$ psi and $\sigma_{ay} = 34{,}000$ psi, then when $\sigma_t/\sigma_{ty} = \sigma_a/\sigma_{ay}$, both are equal to 0.94 rather than the value 1.0 which the authors' equation suggests.

Authors' Closure

We wish to express our appreciation to the discussers for the interest they have shown in our paper.

Dr. Batdorf's comments on the desirability of evaluating the shape of the yield corner during plastic deformation are important. As a matter of fact, some attempts have been made by the authors to determine the shape of the yield corner by a direct method,[8] but no conclusive results have been obtained. The major difficulty in such an experiment appeared to be the lack of a sensitive and accurate method to detect the initiation of plastic deformation. It is the authors' opinion that either a sensitive and reliable method for detecting the initiation of plastic deformation or some indirect method for determining the shape of the yield corner based on theory should be devised in further explorations of this subject.

As far as the relative magnitude of elastic and plastic strains is concerned, Mr. Johnson may have overlooked the purpose of this investigation. The stress levels for each test were selected such that the specimen would be still in elastic range according to the criterion under examination. Therefore the reliability of the magnitude of the observed plastic strain is determined by the accuracy and sensitivity of the measuring method rather than the magnitude of elastic components.

The comparison of the loading functions suggested in the paper with Hill's anisotropic loading function made by Professor McClintock is of great interest to us. The authors regret that they did not clarify the point that the suggested anisotropic loading functions are not exactly the same as suggested by Hill. In the paper, a procedure is suggested to convert the loading functions to dimensionless forms including the effects of anisotropy. For the distortion-energy criterion, the final expression

[7] Assistant Professor of Mechanical Engineering, Massachusetts Institute of Technology, Cambridge, Mass. Assoc. Mem. ASME.

[8] "Biaxial Plastic Stress-Strain Relations of a Mild Steel for Variable Stress Ratios," by Joseph Marin and L. W. Hu, ASME Paper No. 54—A-243.

does assume a form similar to Hill's anisotropic loading function. In other words, it was not our purpose to propose any particular form for anisotropic loading function, but to suggest a procedure by which the ratios of stress component to the yield stress in its direction instead of the stress component itself could be used to formulate anisotropic loading functions.

Bending of Orthogonally Stiffened Plates[1]

H. MARCUS.[2] The method proposed by the author for the analysis of stress and strain in orthogonally stiffened plates is based on the differential equation of the orthotropic plate with constant thickness.

This equation is presented in Timoshenko's book, "Theory of Plates and Shells," as follows

$$D_x \frac{\partial^4 w}{\partial x^4} + 2H \frac{\partial^4 w}{\partial x^2 \partial y^2} + D_y \frac{\partial^4 w}{\partial y^4} = q \quad \ldots\ldots [1]$$

where

$$D_x = E_x \frac{h^3}{12}, D_y = E_y \frac{h^3}{12}, H = \frac{h^3}{12}(E_{xy} + 2G) \ldots [2]$$

The author uses the notations

$$\left.\begin{aligned} E_x = \frac{1}{S_{1.1}}, E_y = \frac{1}{S_{2.2}}, G = \frac{1}{S_{6.6}} \\ S_{1.2} = -\nu_{xy} S_{1.1}, S_{2.1} = -\nu_{yx} S_{2.2} \end{aligned}\right\} \ldots [3]$$

Equation [1] presupposes that

$$E_{xy} = \frac{1}{S_{1.2}} = \frac{1}{S_{2.1}}$$

According to the figures given in Table 1 of the paper for grooved duralumin

$$-\frac{S_{1.2}}{h^3} \times 10^6 = 12.8, \quad -\frac{S_{2.1}}{h^3} \times 10^6 = 39.2$$

The author seems to have by-passed in this stage of hi study this great disparity between $S_{1.2}$ and $S_{2.1}$. He considers an average value of $S_{1.2}$ and $S_{2.1}$ as acceptable for the computation of the deflections because these deflections are not too much affected by the factors $S_{1.2}$ and $S_{2.1}$.

It is the opinion of the writer that the significance of this disparity should not be disregarded. Taking, for example, the figures given in reference (13 of the paper) for a paper-base laminate type $PBG_{(XX)}$

$$E_x = 2.65 \times 10^6, E_y = 1.99, \nu_{xy} = 0.31, \quad \nu_{yx} = 0.23, G = 0.665 \times 10^6$$

one obtains with

$$E_{xy} = \frac{1}{2}(E_x \nu_{xy} + E_y \nu_{yx}) = 0.6396 \times 10^6$$

$$2H = 3.9392 \times \frac{h^3}{12} \times 10^6$$

In reality, E_x, E_y, ν_{xy}, ν_{yx}, and G are not independent values. They must satisfy the equation

$$G = \frac{E_x E_y}{E_y(1 + \nu_{xy}) + E_x(1 + \nu_{yx})} = 0.9245 \times 10^6$$

With this last value

$$2H = 4.9772 \times 10^6$$

The difference between the two respective values of G and H is quite appreciable.

The writer hopes that an improvement in the method used for the experimental determination of the factors $S_{1.2}$, $S_{2.1}$, and G will eliminate the discrepancies. He wishes also that in further tests the strains in grooved or stiffened plates will be measured and that a comparison between the measured strains and those predicted by the theory of the "equivalent" orthotropic plate does corroborate the usefulness of a method of design based on that theory.

The writer wants to commend the author for his in many respects excellent work.

AUTHOR'S CLOSURE

The author appreciates the comments made by Dr. Marcus, but his commendation is too generous. With regard to specific points, however, the author considers that some clarification is necessary.

Dr. Marcus' remark that

$$E_{xy} = \frac{1}{S_{12}} = \frac{1}{S_{21}}$$

is rather confusing, possibly because he is simultaneously using his terminology, Timoshenko's terminology, and the author's terminology. The differential Equation [2] of the paper was derived using the form of stress-strain relations given by Equations [1]. If Equations [1] are solved for stress we obviously obtain

$$\sigma_1 = \frac{S_{22}}{S^*}\epsilon_1 - \frac{S_{12}}{S^*}\epsilon_2$$

$$\sigma_2 = -\frac{S_{21}}{S^*}\epsilon_1 + \frac{S_{11}}{S^*}\epsilon_2$$

where

$$S^* = |S_{ij}|$$

These may be compared with the equations given by Timoshenko in reference (10) of the paper. Equation [2] has coefficients A_x, A_y, A_{xy}, which are readily obtained in terms of the coefficient of the foregoing equations giving stress in terms of strain and constants. The assumed symmetry of the stress-strain relations makes

$$S_{12} = S_{21}$$

The author knows of no presupposition concerning E_{xy}.

The Poisson type ratios S_{12} and S_{21} are intrinsically difficult to determine in the theory because they happen to represent small differences between large numbers. On the other hand, the Young type moduli S_{11} and S_{22} are easily determined and considered to be fairly reliable. They are determined as sums of large numbers as observed in the paper. Furthermore, the shear modulus G or G_{xy}, as it is called in the paper, is determined experimentally by an independent experiment and is considered to be reliable. This fact is borne out in tests on homogeneous isotropic materials

[1] By W. H. Hoppmann, 2nd, published in the June, 1955, issue of the JOURNAL OF APPLIED MECHANICS, Trans. ASME, vol. 77, pp. 267–271.

[2] Consultant, Mechanics Division, Code 6205, Naval Research Laboratory, Washington, D. C.

for which G is known from other methods. There seems little reason to combine the moduli in the well-known fashion as indicated by Dr. Marcus in order to calculate G. There is good reason to believe that G (or G_{xy}), S_{11}, and S_{22} are satisfactorily determined and that S_{12} and S_{21} are simply inaccurate. Part of this inconsistency is thought, however, to arise because of the nature of fabricating actual plates and not entirely due to error in measurement. Until some practical suggestion is offered as to how to handle these constants, it is still considered that the best solution is to average the experimentally determined values.

It may be stated that experiments have now been performed to determine strains in orthogonally stiffened plates, and the results are given in a recent report.[3] It should be clear at the outset, however, that bending strains calculated on the basis of a flexure theory are not going to agree with strains measured in the presence of stress concentration, characteristic of stiffened plates.

In addition to interest in strains, there are physical quantities such as displacement, frequency of vibration, and buckling load which are also of importance in mechanical problems and which can be treated by this theory of orthotropic plates.

It may be of interest to Dr. Marcus that since the presentation of the paper under discussion, the author has published further work on the elastic constants, including a study of stretch of the middle surface.[4] He also has extended the theory to include bending of orthogonally stiffened shells.[5] The results seem quite encouraging with respect to solving problems of stiffened structures.

Propagation of Elastic Impact in Beams in Bending[1]

W. H. Hoppmann, 2nd.[2] In so far as matter can be represented as a mathematical continuum with elastic properties, the mathematical theory of elasticity in three dimensions provides the correct description of stress waves. The so-called dilatational and rotational waves with definite and finite velocities are characteristic of this theory. A stress-resultant theory of deformation for use with engineering structural elements may be considered as an approximation to the more general theory by deliberately introducing simplifying assumptions. However, it is interesting to note that the differential equation for the transverse vibration of a beam antedated the advent of the theory of elasticity by about 75 years. It considers only the translatory inertia of the particles of the beam and that the resultant forces act normal to the length of the beam. This particular theory was devised by D. Bernoulli and L. Euler. A modification of the theory to include the effect of rotatory inertia and shear deformation to improve the theory was introduced by Timoshenko.[3] The approach to the beam problem from the standpoint of stress-resultant theory was fully discussed in 1942 by Prescott.[4]

It is pointed out that if one considers a wave type of solution for the Bernoulli-Euler beam equation it develops that the velocity varies inversely as the wave length and hence one is faced with unbounded wave velocities which are physically absurd. If shear and rotatory inertia are considered as the present authors have done, the wave velocities become bounded and the hope is that theoretical results agree better with experimental data. So far as the writer knows, the authors are the only ones who have made calculations of strains based on the differential equation containing shear and rotatory inertia terms and an impulsive load function. Comparison was made with experimental results. Unfortunately, the authors do not compare results of calculations based on the Bernoulli-Euler equation.

Anderson[5] has given comparisons of some calculations based on both theories but the data are very sparse and to the writer they seem inconclusive. In his case it would have been useful to compare experimental results.

The writer[6] has performed experiments on 1-span, 2-span, and 3-span beams subjected to impulsive loads caused by the collision of steel spheres as shown in Fig. 1 of this discussion. The strain as a function of time was measured on the underside of the beam immediately beneath the point of impact and in the case of the multispan beams in the side spans also. He has calculated the strains using the Bernoulli-Euler beam equation and the Raman-Zener-Feschbach method of determining the force of impact. The results are shown in Figs. 2, 3, and 4, herewith. The agreement of measured and calculated strain for a short period after collision seems to be reasonably good. Dispersion as time goes on could be ascribed in the main to damping effects which are known to be present. How much agreement could be improved by adding the effect of rotatory-inertia and shear-deformation effects in the beam equation can only be a conjecture at this time.

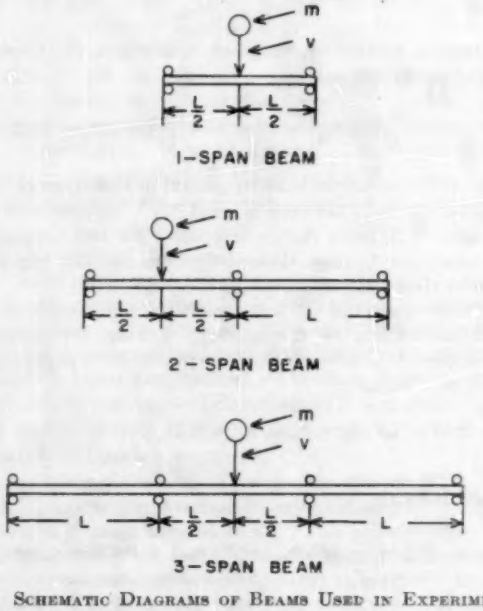

Fig. 1 Schematic Diagrams of Beams Used in Experiments

[2] "Experimental Study of a Theory of Orthogonally Stiffened Plates," by W. H. Hoppmann, 2nd, N. J. Huffington Jr., and L. S. Magness, The Johns Hopkins University, August, 1955, Contract DA-36-034-ORD-1297, Dept. of Army, Ordnance Corps.

[4] "Elastic Compliances of Orthogonally Stiffened Plates," by W. H. Hoppmann, 2nd, The Johns Hopkins University, July, 1955, Contract Nonr-248(12), Office of Naval Research. To be published in Proceedings of Society of Experimental Stress Analysis.

[5] "Bending of Orthogonally Stiffened Cylindrical Shells," by W. H. Hoppmann, 2nd, The Johns Hopkins University, September, 1955, Contract Nonr-248(12), Office of Naval Research.

[1] By Martin Goland, P. D. Wickersham, and M. A. Dengler, published in the March, 1955, issue of the Journal of Applied Mechanics, Trans. ASME, vol. 77, pp. 1–7.

[2] Associate Professor of Mechanical Engineering, The Johns Hopkins University, Baltimore, Md. Mem. ASME.

[3] "On the Transverse Vibrations of Bars of Uniform Cross-Section," by S. P. Timoshenko, *Philosophical Magazine*, 6th series, 43, 1922, p. 125.

[4] "Elastic Waves and Vibrations of Thin Rods," by John Prescott, *Philosophical Magazine*, 7th series, 33, 1942, p. 703.

[5] "Flexural Vibrations in Uniform Beams According to the Timoshenko Theory," by R. A. Anderson, Journal of Applied Mechanics, Trans. ASME, vol. 75, 1953, pp. 504–510.

[6] "Impulsive Loads on Beams," by W. H. Hoppmann, 2nd, Proceedings of Society of Experimental Stress Analysis, vol. X, 1952, p. 157.

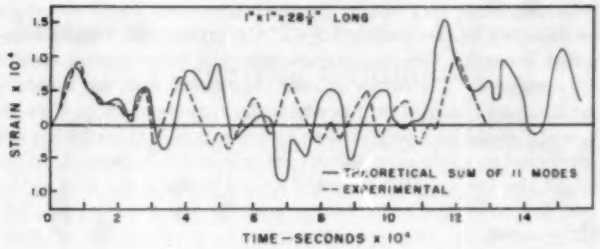

FIG. 2 SINGLE-SPAN BEAM

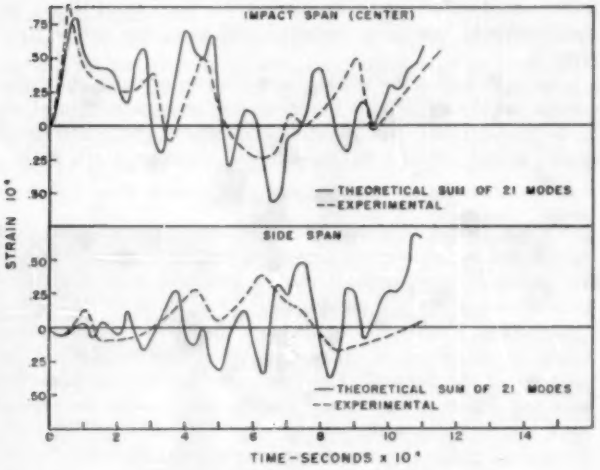

FIG. 3 TWO-SPAN 1-IN. × 1-IN. BEAM

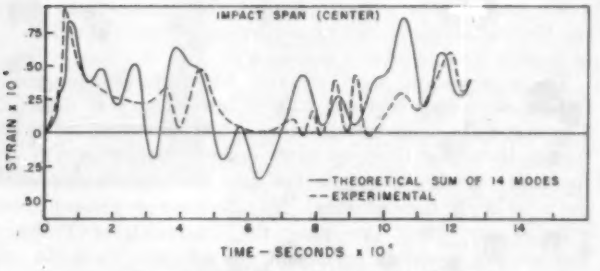

FIG. 4 THREE-SPAN 1-IN. × 1-IN. BEAM

The authors have developed an interesting method of applying an impulsive load and mensuring strains along the bar. Their experimental results appear to agree closely with strains which they calculate. It is encouraging to learn that they expect to carry their investigations further. For practical reasons it would be valuable to have comparisons of calculated strains based on the Bernoulli-Euler theory in future work. The writer will now explain why he thinks this point should be emphasized.

From recent papers on the so-called Timoshenko beam, one might obtain the impression that analysis based on the Bernoulli-Euler theory is useless. A clear understanding of the matter is important for the designer who has need of analyzing problems of dynamic loads applied to frames, trusses, columns, and thin rings. An interesting study of the dynamic response of a ring on elastic foundations was made, for example, by E. Wenk.[7] He applied what amounts to the Euler moment-change of-curvature relation in analysis of the circular ring. He calculated strains caused by an impulsive force of duration approximately equal to half the fundamental period and compared them with measured strains at many points around the ring. The agreements were excellent. What the calculated results would be if shear deformation and rotatory inertia are included is difficult to conjecture. They also would be difficult to calculate.

To sum up, it would appear that the excellent work of the authors should be extended. However, emphasis on one hand should be made on proceeding directly from the general theory of elasticity for details of wave transmission, and on the other hand should proceed to the simplest formulation acceptable from an experimental standpoint for strain and deflection studies of more complicated structures such as frames, trusses, columns, and thin rings.

R. P. N. JONES.[8] The paper shows an encouraging agreement between the authors' experimental and theoretical results. Nevertheless, the writer believes that their theoretical solution requires further examination in regard to its behavior for large values of τ.

The total energy of the beam remains constant after the application of the impulse. However, owing to the spread of the disturbance, the energy density, and therefore the stresses, must everywhere approach zero as τ tends to infinity, except possibly at a limited number of points, such as the wave fronts. For a fixed value of x the solutions given in the paper do indeed tend to zero for large values of τ. However, this consideration alone is not sufficient to show that $m(\tau, x)$ approaches zero everywhere, since the disturbance is continually spreading to fresh regions of the beam. It is necessary also to consider the behavior of $m(\tau, x)$ as both x and τ approach infinity in such a way that the ratio x/τ remains finite, and equal to a constant, V, say. In other words, we have to consider the bending moment at a point P which travels along the beam at a constant velocity V.

Taking the case when $V < C^{-1/2}$, the bending moment at P is given, for all values of τ, by setting $x = V\tau$ in Equation [3] of the paper. It is seen that the integrand now contains a term $\cos \xi\tau \cosh SV\tau$ which oscillates with increasing amplitude as $\tau \to \infty$ and it appears possible that the integral itself will show a similar trend for a certain range of values of V.

Apart from the question of the convergence of the solution as $\tau \to \infty$, the form of the integrands leads to difficulty in computation, as the authors themselves have noted. It is probable that a more convenient form would be obtained by a different choice of integration contour.

For large values of x the response becomes highly oscillatory owing to the dispersive nature of the propagation. Under these conditions a point-by-point evaluation is impracticable, and it is desirable to obtain a solution which gives directly the amplitudes and wave lengths of the predominant components of the response. Such a solution appears possible by considering the problem from the standpoint of traveling harmonic waves.

E. A. RIPPERGER.[9] In order to determine the adequacy of an approximating equation, such as the Timoshenko equation, used by the authors for representing the motion of an elastic beam, one can compare the dispersion curve, or velocity-wave-length relationship, given by the approximating equation with the dispersion curve obtained from the solution of the general equations of elasticity for waves traveling in an infinitely long beam. As the authors point out, this has been done by Cremer. Cremer's com-

[7] "Radial Impact on an Elastically Supported Ring," by E. Wenk, Jr., separate no. 157, vol. 78, ASCE, 1952.

[8] Lecturer in Applied Mechanics, University of Sheffield, England.

[9] The University of Texas, Austin, Texas. Mem. ASME.

parison, which was made on the basis of phase velocities, shows that the Timoshenko equation gives excellent agreement with the exact theory so far as the lowest branch of the dispersion curve is concerned. This lowest branch represents, in the authors' terminology, the fundamental class of beam normal modes. The agreement between the Timoshenko equation results and the exact theory in the next highest branch of the dispersion curve, representing the next highest class of modes, is not very good. For longer wave lengths the agreement might be acceptable but at the shorter wave lengths there is a disturbing and fundamental difference. The limiting velocity indicated by the exact theory is the shear velocity $\sqrt{G/\rho}$ whereas the Timoshenko equation indicates a limiting velocity of $\sqrt{E/\rho}$, the "bar velocity." The shear velocity is approximately 63 per cent of the bar velocity. The Timoshenko equation provides for only two modes of transmission and consequently two branches of the dispersion curve, while the exact theory provides an infinite number of modes and an infinite number of higher branches of the dispersion curve.

Phase velocities, in the opinion of the writer, are of less significance than group velocities in the consideration of the propagation of pulses. Consequently, a graphical comparison of group velocities given by the two solutions for the first two branches of the dispersion curves is shown in Fig. 5 of this discussion. In this figure C_g is group velocity, C_0 is the bar velocity, λ is wave length, and r is the radius of gyration of a bar with a rectangular cross section.

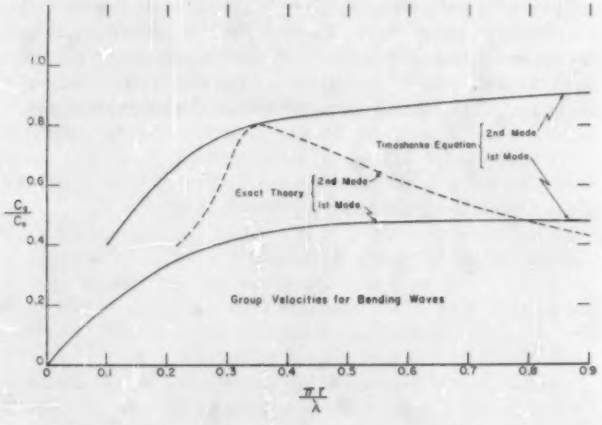

FIG. 5 GROUP VELOCITIES FOR BENDING WAVES

In this comparison the lowest branch of the dispersion curve from the Timoshenko equation has been brought into exact agreement with the lowest branch from the exact theory by proper choice of the constant C as discussed by the authors. Obviously, there is no agreement between the two theories for the second mode. These curves indicate therefore, that if, as it has been supposed, the modes of transmission higher than the second are negligible, the maximum velocity of propagation of any pulse could be no more than $0.8\sqrt{E/\rho}$. The Timoshenko equation indicates that any pulse with a steep front would have its leading edge propagated at the velocity $\sqrt{E/\rho}$. This is shown by the authors in Figs. 2 and 3.

One should expect on the basis of the exact theory that the two discontinuities corresponding to the two modes of transmission would arrive at a given point, such as station 4, almost simultaneously since the one would travel at the shear velocity and the other at the Rayleigh velocity, the difference between these two velocities being very small. Some disagreement might therefore be expected at the leading edge of the pulse when results computed from the Timoshenko equation and experimental results are compared. The rather excellent agreement between theoretical and experimental results which the authors show in Figs. 5, 6, and 7 could be interpreted as an indication that in the second transmission mode only the longer waves are important. One might also suspect that since the arrival times of the first of the two discontinuities seem to represent the bar velocity, possibly the symmetrical component generated by the impact is not completely negligible in comparison to the antisymmetrical component. This view is not supported by the results shown in Figs. 8 and 9 of the paper. Consequently, we are left with a partially unreconciled difference between what the more exact theory indicates should have been observed and what was actually observed.

This in no way detracts from the value of the paper under discussion but it does indicate that some further experimental study of the transmission of pulses of bending waves, particularly with regard to the velocities of transmission, might be worth while.

AUTHORS' CLOSURE

We are indeed indebted to the several discussers for their helpful and interesting comments. A number of interesting lines for further research are indicated, in which we hope the present authors and others will participate.

Regarding Professor Hoppmann's discussion, there is certainly no difference of opinion regarding the controlling importance of the Bernoulli-Euler concepts in studying beam impact and vibration problems. On the other hand, the present work concentrates attention on the "intermediate" stage of stress propagation due to a sharp lateral blow; this stage follows the intensely three-dimensional stress-propagation pattern induced near the load and during the loading time, and precedes the stage where a well-established Bernoulli-Euler propagation mechanism controls the system. During this intermediate stage, the Bernoulli-Euler theory introduces such severe contradictions as to make its applicability questionable.

The experimental work reported by Professor Hoppmann further emphasizes that our areas of interest may be different. The unit scale of his time-histories is 100 microseconds; in our studies, the impact times are on the order of 10 microseconds and the entire abscissa-length for the time histories reported is on the order of 100 microseconds. No reflections are present in our experiments. Even presuming the bandwidth of Professor Hoppmann's recording equipment was sufficient, his strain records probably do not possess the frequency definition considered essential for our work.

The discussion of Dr. Jones is pertinent, and an improved appreciation of our mathematical results would be worth while. It would also be helpful if alternate forms of our solutions, more amenable to calculation, could be deduced. Several other authors, all working in this same area, have not thus far been successful in simplifying the calculational problem; however, their final approaches are similar to ours.

Dr. Ripperger's discussion contains much of interest, and the authors have little to offer in the way of illuminating comment. We have thus far preferred not to deal with the problem from a wave viewpoint, but rather have derived the mathematical results, computed time-histories from them, and simply compared the end-products of analysis with the experimental records. For a thorough understanding of the problem, however, the (to us) less-direct approach of wave mechanics must, of course, be reconciled with our findings.

Determination of Thermal Stresses in Three-Ply Laminates[1]

C. Mylonas.[2] The authors deserve warm congratulations for their excellent techniques and the results obtained on a very complicated, although at first glance, simple problem. As the authors themselves point out, the state of stress in composite bodies made of dissimilar materials firmly cemented together is three-dimensional, and the results of their research obtained by two-dimensional photoelasticity are only a first approximation. The object of the discusser is to indicate how dangerous such an approximation may be under certain conditions, not necessarily those of their research.

Models similar to those of the authors were made in England in 1950, for the study of the stresses in the cement layer of joints made of thin metal sheets glued with synthetic adhesives.[3] The adherents were stainless steel or aluminum bars $^1/_4$ in. × $^1/_2$ in. in cross section cemented on their $^1/_2$ in. faces through an adhesive layer $^1/_2$ in. square in cross section, consisting of a specially made epoxy resin (Araldite) of the consistency of a medium rubber pencil eraser. These models were subjected separately to shear by displacing the adherents in opposite directions along their lengths, and in uniform compression.

Fig. 1

With a condition of plane strain the stress field away from the ends of the overlap of both shear and compression models of sufficient length should be uniform across the thickness of the adhesive. In the shear tests this is a state of pure shear, i.e., with a sum of principal stresses equal to zero, hence without any tendency for lateral contraction or expansion (in the direction of the arrow of authors' Fig. 1), independently of the values of the elastic constants of adhesive and adherents. Accordingly, the interior of the adhesive layer exhibits a uniform birefringence throughout its thickness (Fig. 1, herewith, where the opaque adherents should be imagined cemented on the sides of the shown adhesive layer and pulling upward on the right and downward on the left).

The long compression joint behaves differently. Its central area, uniformly stressed under conditions of plane strain, is also constrained from expanding longitudinally. With a Poisson's ratio $\mu = 0.5$, this will result in a hydrostatic pressure and therefore no birefringence. This condition is approximated next to the interfaces where the lateral expansion is prevented by the adhesion; these areas actually show a very small fringe order in the tests. However, some degree of freedom to expand laterally develops in areas away from the interfaces, increasing with the distance from them, so that in joints with sufficiently thick adhesive layers (as compared to their width in the direction of the light path) their middle should be in a state of plane stress (in the plane normal to the light path). If σ is the compressive stress, the longitudinal stress would then be $\mu\sigma$ and the principal stress difference $(1 - \mu)\sigma$, or $^1/_2\sigma$ for $\mu = ^1/_2$. The two values of stress difference 0 and $^1/_2\sigma$ for plane strain and plane stress, respectively, are the limits within which the stress difference can vary from the interfaces to the middle of the thickness of the layer. However, according to the proportions of the cross section of the adhesive layer the actual variation will be smaller as the existing states of stress will not reach the limits of plane strain or stress. For the square cross section of the joints investigated, the variation is sufficient to produce a great number of fringes across the thickness of the adhesive layer (Fig. 2, vertically compressed). It is obvious that the correspondence between the models used and the similar plane-strain problem is worse with the compression than with the shear joints.

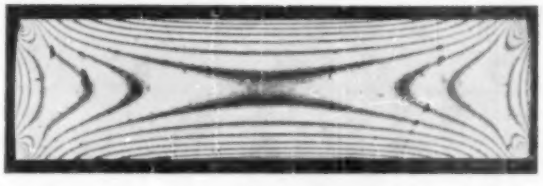

Fig. 2

The state of stress near the edges is considerably more complicated. This effect should be less pronounced in the adherents which were investigated by the authors than in the adhesive, but it is felt useful to give a strong warning of the inaccuracies that may be involved in the interpretation of the stress patterns of composite bodies.

Authors' Closure

Professor Mylonas' contribution is appreciated, but the authors feel that his comments do not disprove the correctness of the approach they have followed to study the problem, nor do they indicate any method to improve the approach.

The limitation of the two dimensional photoelastic analysis is stated in the paper. After considerable thought, the authors decided that this was the best experimental approach available at the time to obtain an approximate solution to the problem. The correlation of the photoelastic results with the location of the point at which the laminate fails and with the temperature required to produce the failure, seems to indicate that the two-dimensional analysis gives a satisfactory approximation to the three-dimensional phenomena.

The authors will highly appreciate any suggestion as to how to study experimentally, in a more accurate way, the three-dimensional stress field present at the corner region of three-ply laminates.

---

[1] By A. J. Durelli and C. H. Tsao, published in the June, 1955, issue of the Journal of Applied Mechanics, Trans. ASME, vol. 77, pp. 190–192.

[2] Associate Professor, Division of Engineering, Brown University, Providence, R. I.

[3] "Experiments With Composite Models," by C. Mylonas, Tech. Report DA-798/8, Brown University, and Proceedings of the SESA, vol. 12, no. 2, 1955.

Book Reviews

Fluid Mechanics

A SELECTION OF GRAPHS FOR USE IN CALCULATIONS OF COMPRESSIBLE AIRFLOW. Prepared on behalf of the Aeronautical Research Council by the Compressible Flow Tables Panel. L. Rosenhead, Chairman. Oxford University Press, New York, N. Y., 1954. Cloth, 15 × 11 in., x and 115 pp., $13.45.

REVIEWED by ASCHER H. SHAPIRO[1]

THIS book is a companion volume to "A Selection of Tables for Use in Calculations of Compressible Airflow," Clarendon Press, 1952 (see review in JOURNAL APPLIED MECHANICS, vol. 76, 1954, p. 97). It cannot, however, be accorded the same congratulations that the book of tables deserved.

The present book contains graphs of two types, corresponding to single and double-entry tables. Some of the graphs are on a single page, and reproduce in compact form, with accuracy suitable for rough calculations, the more important tabulations of the volume of tables. Other graphs are spread out over several pages, and, for the case of single-entry functions, permit readings with high accuracy.

All the graphs are based on a ratio of specific heats of exactly 1.4. The upper limit of the Mach number range has been arbitrarily set at 5.

There are five sets of graphs: (*a*) Isentropic flow, including the hodographic characteristic function, 42 pages; (*b*) normal shocks, 17 pages; (*c*) oblique shocks, 32 pages; (*d*) cone flow, 16 pages; (*e*) Reynolds numbers, 5 pages.

The production of the book justifies the highest praise, and it is evident that not the slightest labor was spared to obtain perfect results. Crisp and pleasing in appearance, the graphs are well labeled, easy to read, and have grids which are clear but subdued. However, there is no real excuse for the excessive size of the book (over-all dimensions 15¼ in. × 11¾ in.), which makes storage a nuisance. With little added inconvenience in use, the same accuracy could have been obtained in a volume of more normal size.

Sections A and B, involving only the single-entry functions of isentropic flow and normal shocks, do not contribute strongly to the book. The single-page graphs, giving the entire ranges of the functions in concise form, might better have appeared in the earlier volume of tables. The multiple-page graphs cannot compete with the tables either in accuracy or convenience, and have only a minor advantage in sometimes facilitating interpolation. That the graphs do not go beyond Mach number 5 is a great pity, and puts the book at a disadvantage next to some of its less handsome-looking rivals. This limitation makes the work partly obsolescent. How much better it would have been, if graphs of single-entry functions were to be included, to have extended them over an extremely broad range of Mach number, even at the expense of loss in accuracy of reading.

Sections C and D, concerned with the double-entry functions of oblique and conical-shock flows, are the real meat of the book, for it is in two-parameter representations that graphs have a real advantage over tables, in conciseness, accuracy, and ease of interpolation. These occupy about one third of the book, and are done excellently, although the comments on upper Mach number made earlier apply here as well.

There are now several good collections of tables and graphs of compressible flow functions. The present volume of graphs would have been a more useful contribution if it had been of convenient physical size, if double-entry functions were concentrated upon, and if the Mach number range were decisively extended for both single-entry and double-entry functions.

[1] Professor of Mechanical Engineering, Massachusetts Institute of Technology, Cambridge, Mass. Presently, Visiting Professor of Applied Thermodynamics, Cambridge University, Cambridge, England. Mem. ASME.

Third U. S. National Congress of Applied Mechanics
Preliminary Announcement

The Third U. S. National Congress of Applied Mechanics will be held at Brown University, Providence, Rhode Island, during June 11–14, 1958. It is hoped that the scheduling of conflicting meetings can be avoided by this early announcement of the date chosen for the Congress. Further announcements concerning the preparation of papers will be made as the Congress draws nearer.

Inquiries regarding the Congress should be addressed to one of the following members of the Organizing Committee at Brown University, Providence, R. I.:

Professor D. C. Drucker, *Secretary*
Professor E. H. Lee, *Treasurer*
Professor W. Prager, *Chairman*